



*water*

# Soil Water Conservation Dynamics and Impact

---

Edited by  
Saskia Keesstra, Simone Di Prima, Mirko Castellini and  
Mario Pirastru

Printed Edition of the Special Issue Published in *Water*

# Soil Water Conservation



# Soil Water Conservation: Dynamics and Impact

Special Issue Editors

**Saskia Keesstra**

**Simone Di Prima**

**Mirko Castellini**

**Mario Pirastru**

MDPI • Basel • Beijing • Wuhan • Barcelona • Belgrade



*Special Issue Editors*

Saskia Keesstra  
Wageningen University and Research  
The Netherlands

Simone Di Prima  
University of Sassari  
Italy

Mirko Castellini  
Council for Agricultural Research and Economics Agriculture and Environment Research Center  
CREA-AA (Bari)  
Italy

Mario Pirastru  
University of Sassari  
Italy

*Editorial Office*

MDPI  
St. Alban-Anlage 66  
4052 Basel, Switzerland

This is a reprint of articles from the Special Issue published online in the open access journal *Water* (ISSN 2073-4441) from 2017 to 2018 (available at: [https://www.mdpi.com/journal/water/special\\_issues/conservation](https://www.mdpi.com/journal/water/special_issues/conservation))

For citation purposes, cite each article independently as indicated on the article page online and as indicated below:

LastName, A.A.; LastName, B.B.; LastName, C.C. Article Title. <i>Journal Name</i> <b>Year</b> , Article Number, Page Range.
---

**ISBN 978-3-03897-852-7 (Pbk)**

**ISBN 978-3-03897-853-4 (PDF)**

Cover image courtesy of Artemi Cerdà.

© 2019 by the authors. Articles in this book are Open Access and distributed under the Creative Commons Attribution (CC BY) license, which allows users to download, copy and build upon published articles, as long as the author and publisher are properly credited, which ensures maximum dissemination and a wider impact of our publications.

The book as a whole is distributed by MDPI under the terms and conditions of the Creative Commons license CC BY-NC-ND.

# Contents

About the Special Issue Editors . . . . .	vii
Preface to "Soil Water Conservation: Dynamics and Impact" . . . . .	ix
<b>Simone Di Prima, Mirko Castellini, Mario Pirastru and Saskia Keesstra</b> Soil Water Conservation: Dynamics and Impact Reprinted from: <i>Water</i> <b>2018</b> , <i>10</i> , 952, doi:10.3390/w10070952 . . . . .	1
<b>Vincenzo Alagna, Simone Di Prima, Jesús Rodrigo-Comino, Massimo Iovino, Mario Pirastru, Saskia D. Keesstra, Agata Novara and Artemio Cerdà</b> The Impact of the Age of Vines on Soil Hydraulic Conductivity in Vineyards in Eastern Spain Reprinted from: <i>Water</i> <b>2018</b> , <i>10</i> , 14, doi:10.3390/w10010014 . . . . .	7
<b>Simone Di Prima, Laurent Lassabatere, Jesús Rodrigo-Comino, Roberto Marrosu, Manuel Pulido, Rafael Angulo-Jaramillo, Xavier Úbeda, Saskia Keesstra, Artemi Cerdà and Mario Pirastru</b> Comparing Transient and Steady-State Analysis of Single-Ring Infiltrometer Data for an Abandoned Field Affected by Fire in Eastern Spain Reprinted from: <i>Water</i> <b>2018</b> , <i>10</i> , 514, doi:10.3390/w10040514 . . . . .	18
<b>Sergio E. Lozano-Baez, Miguel Cooper, Silvio F. B. Ferraz, Ricardo Ribeiro Rodrigues, Mario Pirastru and Simone Di Prima</b> Previous Land Use Affects the Recovery of Soil Hydraulic Properties after Forest Restoration Reprinted from: <i>Water</i> <b>2018</b> , <i>10</i> , 453, doi:10.3390/w10040453 . . . . .	35
<b>Novák Petr and Hůla Josef</b> Translocation of Soil Particles during Secondary Soil Tillage along Contour Lines Reprinted from: <i>Water</i> <b>2018</b> , <i>10</i> , 568, doi:10.3390/w10050568 . . . . .	51
<b>Yu Wang, Changhong Li, Yanzhi Hu and Yonggang Xiao</b> Optimization of Multiple Seepage Piping Parameters to Maximize the Critical Hydraulic Gradient in Bimsoils Reprinted from: <i>Water</i> <b>2017</b> , <i>9</i> , 787, doi:10.3390/w9100787 . . . . .	63
<b>Cheng-Yu Ku, Chih-Yu Liu, Jing-En Xiao and Weichung Yeh</b> Transient Modeling of Flow in Unsaturated Soils Using a Novel Collocation Meshless Method Reprinted from: <i>Water</i> <b>2017</b> , <i>9</i> , 954, doi:10.3390/w9120954 . . . . .	80
<b>Xiaohua Xiang, Xiaoling Wu, Xi Chen, Qifeng Song and Xianwu Xue</b> Integrating Topography and Soil Properties for Spatial Soil Moisture Storage Modeling Reprinted from: <i>Water</i> <b>2017</b> , <i>9</i> , 647, doi:10.3390/w9090647 . . . . .	102
<b>Wenjuan Hua, Chuanhai Wang, Gang Chen, Hai Yang and Yue Zhai</b> Measurement and Simulation of Soil Water Contents in an Experimental Field in Delta Plain Reprinted from: <i>Water</i> <b>2017</b> , <i>9</i> , 947, doi:10.3390/w9120947 . . . . .	117
<b>Festo Richard Silungwe, Frieder Graef, Sonoko Dorothea Bellingrath-Kimura, Siza Donald Tumbo, Frederick Cassian Kahimba and Marcos Alberto Lana</b> Crop Upgrading Strategies and Modelling for Rainfed Cereals in a Semi-Arid Climate—A Review Reprinted from: <i>Water</i> <b>2018</b> , <i>10</i> , 356, doi:10.3390/w10040356 . . . . .	135

<b>Andrew Reid Bell, Jennifer Zavaleta Cheek, Frazer Mataya and Patrick S. Ward</b> Do As They Did: Peer Effects Explain Adoption of Conservation Agriculture in Malawi Reprinted from: <i>Water</i> <b>2018</b> , <i>10</i> , 51, doi:10.3390/w10010051 . . . . .	<b>160</b>
<b>Lina Röschel, Frieder Graef, Ottfried Dietrich, Meike Pendo Schäfer and Dagmar Haase</b> Individual Local Farmers' Perceptions of Environmental Change in Tanzania Reprinted from: <i>Water</i> <b>2018</b> , <i>10</i> , 525, doi:10.3390/w10040525 . . . . .	<b>176</b>
<b>Giovanni Rallo, Giuseppe Provenzano, Mirko Castellini and Angela Puig Sirera</b> Application of EMI and FDR Sensors to Assess the Fraction of Transpirable Soil Water over an Olive Grove Reprinted from: <i>Water</i> <b>2018</b> , <i>10</i> , 168, doi:10.3390/w10020168 . . . . .	<b>184</b>
<b>Mario Pirastru, Roberto Marrosu, Simone Di Prima, Saskia Keesstra, Filippo Giadrossich and Marcello Niedda</b> Lateral Saturated Hydraulic Conductivity of Soil Horizons Evaluated in Large-Volume Soil Monoliths Reprinted from: <i>Water</i> <b>2017</b> , <i>9</i> , 862, doi:10.3390/w9110862 . . . . .	<b>200</b>
<b>Alessandra Trinchera and Valentina Baratella</b> Use of a Non-Ionic Water Surfactant in Lettuce Fertigation for Optimizing Water Use, Improving Nutrient Use Efficiency, and Increasing Crop Quality Reprinted from: <i>Water</i> <b>2018</b> , <i>10</i> , 613, doi:10.3390/w10050613 . . . . .	<b>214</b>
<b>Akmal Akramkhanov, Muhammad Mehmood Ul Hassan and Anna-Katharina Hornidge</b> Redrawing Soil Salinity Innovation-Focused Stakeholder Interaction for Sustainable Land Management in Khorezm Province, Uzbekistan Reprinted from: <i>Water</i> <b>2018</b> , <i>10</i> , 208, doi:10.3390/w10020208 . . . . .	<b>229</b>

## About the Special Issue Editors

**Saskia Keesstra** (Dr.) main research focus revolves around understanding how soils are part of a larger system. To enable sustainable catchment management it is needed to look at the system dynamics in a holistic way. Process knowledge enables explanation of the impact of natural and human drivers on the soil system and what consequences these drivers have for water and sediment transfer (connectivity) on the human scale, both temporally and spatially. Improved understanding of the soil and water dynamics together with the development and testing practical land management tools in agricultural and forest land is one of the key topics to empower sustainable land management and mitigate soil threats like erosion and off-site water and sediment accumulation with the help of nature's forces. In my research, I focus on methodology development, specifically (i) focussing on upscaling, how point-scale methods can be used on larger spatial scales; and (ii) focussing on downscaling, from landscape to fine resolution, approaching plot scale. The last important step is to disseminate our science to other researchers and other disciplines and to the general public.

**Simone Di Prima** (Dr.) research activities focus on soil hydrology and water resources management with specific regard to laboratory and field determination of soil hydraulic properties, infiltration processes, and simulation of water flow in the vadose zone. I developed the Automat-SRI (Automated Single Ring Infiltrometer). I also contributed to developing the BEST-2K method to estimate soil hydraulic properties on dual-permeability soils.

**Mirko Castellinin** (Dr.) research activities focus on the study of soil physical and hydraulic properties. My specific research interests are i) soil physical quality; ii) soil management for sustainable agriculture; iii) land-use change impact on soil properties; iv) use of soil conditioners (e.g., amendments, composts) to improve the soil water retention; v) water fluxes in saturated and unsaturated soil conditions; vi) temporal and spatial variability of physical and hydraulic properties of the soil; vii) main factors affecting soil physical degradation processes (soil surface crusting, soil compaction, etc).

**Mario Pirastru** (Dr.) research activities focus on soil hydrology, environmental monitoring, soil water dynamics modeling, and hydrological processes in a semi-arid environment.



# Preface to "Soil Water Conservation: Dynamics and Impact"

To meet the needs of the increasing world population is one of the major challenges of our time. At the same time, the high demands for food production have major impacts on soil and water resources. Scarcity of water has been universally recognized as a global issue. Moreover, climate change has profound effects on the hydrological cycle, thus, reducing the availability of water resources in many environments. Basic human needs like food and clean water are strictly related to the maintenance of healthy and productive soils. An improved understanding of human impact on the environment is therefore necessary to preserve and manage soil and water resources. This knowledge is particularly important in semi-arid and arid regions, where the increasing demands on limited water supplies require urgent efforts to improve water quality and water use efficiency. It must be kept in mind that both soil and water are limited resources. Thus, the wise use of these natural resources is a fundamental prerequisite for the sustainability of human societies. Soil erosion is well known to be a major cause of soil degradation. Many studies have highlighted that soil erosion involves a number of processes, including land levelling, gully erosion, piping, and tillage erosion. Human activities, such as deforestation, overgrazing, road construction, and infrastructure development, have accelerated the erosion processes, causing grave negative effects over large areas. Conservation strategies are therefore essential to prevent soil degradation. Facing the problem of soil degradation also means implementing restorative measures of soil and crop management. It is now widely recognized that strategies such as zero or reduced tillage, contour farming, mulches, and cover crops may improve soil and water conservation. The development of proper conservation strategies also requires more information on how to interpret and model soil hydrological processes, such as aquifer recharge, rainfall partition into rainfall infiltration and excess runoff, and the associated transport of solutes and contaminants through the soil profile (such as nutrients, pesticides, heavy metals, radionuclides, and pathogenic microorganisms). Interpreting and modeling these processes needs the determination of the soil hydraulic characteristic curves, i.e., the relationships between volumetric soil water content, pressure head, and hydraulic conductivity. Knowledge of these properties is therefore a necessity for the sustainable management of soil and water resources. Despite the extensive literature on conservative strategies, the need for site-specific studies in different environments and socio-economic contexts still remains high. The aim of this book is to enhance our understanding on conservation strategies for effective and sustainable soil and water management.

**Saskia Keesstra, Simone Di Prima, Mirko Castellini, Mario Pirastru**  
*Special Issue Editors*



# Soil Water Conservation: Dynamics and Impact

Simone Di Prima <sup>1,\*</sup>, Mirko Castellini <sup>2</sup>, Mario Pirastru <sup>1</sup> and Saskia Keesstra <sup>3,4</sup>

<sup>1</sup> Dipartimento di Agraria, Università degli Studi di Sassari, Viale Italia 39, 07100 Sassari, Italy; mpirastru@uniss.it

<sup>2</sup> Council for Agricultural Research and Economics-Agriculture and Environment Research Center (CREA-AA), Via Celso Ulpiani 5, 70125 Bari, Italy; mirko.castellini@crea.gov.it

<sup>3</sup> Team Soil Water and Land Use, Wageningen Environmental Research, Wageningen UR, Droevendaalsesteeg 3, 6700 AA Wageningen, The Netherlands; saskia.keesstra@wur.nl

<sup>4</sup> Civil, Surveying and Environmental Engineering, The University of Newcastle, Callaghan 2308, Australia

\* Correspondence: sdiprima@uniss.it; Tel.: +39-079-229387

Received: 6 June 2018; Accepted: 17 July 2018; Published: 18 July 2018

**Abstract:** Human needs like food and clean water are directly related to good maintenance of healthy and productive soils. A good understanding of human impact on the natural environment is therefore necessary to preserve and manage soil and water resources. This knowledge is particularly important in semi-arid and arid regions, where the increasing demands on limited water supplies require urgent efforts to improve water quality and water use efficiency. It is important to keep in mind that both soil and water are limited resources. Thus, wise use of these natural resources is a fundamental prerequisite for the sustainability of human societies. This Special Issue collects 15 original contributions addressing the state of the art of soil and water conservation research. Contributions cover a wide range of topics, including (1) recovery of soil hydraulic properties; (2) erosion risk; (3) novel modeling, monitoring and experimental approaches for soil hydraulic characterization; (4) improvement of crop yields; (5) water availability; and (6) soil salinity. The collection of manuscripts presented in this Special Issue provides more insights into conservation strategies for effective and sustainable soil and water management.

**Keywords:** water and soil conservation; sustainable land management; soil erosion; soil water storage; water infiltration; water availability; crop yields

---

## 1. Introduction

To meet the needs of the increasing world population is one of the major challenges of our time [1]. At the same time, the high demands for food production have major impacts on soil and water resources [2]. Scarcity of water has been universally recognized as a global issue [3]. Moreover, climatic change has profound effects on the hydrological cycle, thus reducing the availability of water resources in many environments [4]. Basic human needs like food and clean water are strictly related to the maintenance of healthy and productive soils [5]. An improved understanding of human impact on the environment is therefore necessary to preserve and manage soil and water resources. This knowledge is particularly important in semi-arid and arid regions, where the increasing demands on limited water supplies require urgent efforts to improve water quality and water use efficiency [6]. It must be kept in mind that both soil and water are limited resources. Thus, the wise use of these natural resources is a fundamental prerequisite for the sustainability of human societies [7]. Soil erosion is well known to be a major cause of soil degradation. Many studies have highlighted that soil erosion involves a number of processes, including land levelling, gully erosion, piping and tillage erosion [8]. Human activities, such as deforestation, overgrazing, road construction and infrastructure development, have accelerated the erosion processes, causing grave negative effects over large areas [9]. Conservation strategies are

therefore essential to prevent soil degradation. Facing the problem of soil degradation also means implementing restorative measures of soil and crop management [10]. It is now widely recognized that strategies such as zero or reduced tillage, contour farming, mulches, and cover crops may improve soil and water conservation [2]. The development of proper conservation strategies also requires more information on how to interpret and model soil hydrological processes, such as aquifer recharge, rainfall partition into rainfall infiltration and excess runoff, and the associated transport of solutes and contaminants through the soil profile (such as nutrients, pesticides, heavy metals, radionuclides, and pathogenic microorganisms). Interpreting and modeling these processes needs the determination of the soil hydraulic characteristic curves, i.e., the relationships between volumetric soil water content, pressure head, and hydraulic conductivity [11–13]. Knowledge of these properties is therefore a necessity for sustainable management of soil and water resources. Despite the extensive literature on conservative strategies, the need for site-specific studies in different environments and socio-economic contexts still remains high. The aim of this Special Issue is to enhance our understanding on conservation strategies for effective and sustainable soil and water management. Contributions focus on: recovery of soil hydraulic properties [14–16]; erosion risk [17–19]; novel modeling [20–22], monitoring [23] and experimental [24] approaches for soil hydraulic characterization; improvement of crop yields [25,26]; water availability and food security [27]; and soil salinity [28]. In the following section we resume all the contributions of this Special Issue.

## 2. Overview of this Special Issue

This Special Issue collects 15 original contributions addressing the state of the art of soil and water conservation research. Three studies use infiltration experiments in order to assess the recovery of soil hydraulic properties after vineyard plantation [29], fire [15] and forest restoration [16]. With the aim of detecting the temporal variability of soil compaction and infiltration rates, Alagna et al. [29] carried out ring infiltrometer experiments in a Mediterranean vineyard planted with vines of different ages. According to these authors, planting operations caused soil compaction, which reduced the hydraulic conductivity. These modifications in the soil hydrological properties were reversed in the 24 years following planting. The rate of soil recovery was most profound immediately following the disturbance and declined thereafter, demonstrating the resilience of the considered soil to the stress induced by planting works.

Assessing the effects of fire on soil hydraulic properties in the Mediterranean area is crucial to evaluating the role of fire in land degradation and erosion processes. Among the soil hydraulic properties, field-saturated hydraulic conductivity,  $K_{fs}$ , exerts a key role in the partitioning of rainfall infiltration and excess runoff [14,30]. Therefore, estimates of  $K_{fs}$  are essential for evaluating the hydrological response of fire-affected soils. Di Prima et al. [15] determined the field-saturated soil hydraulic conductivity,  $K_{fs}$ , of an unmanaged field affected by fire by means of single-ring infiltrometer runs and the use of transient and steady-state data analysis procedures. Sampling and measurements were carried out in a fire-affected field (burnt site) and in a neighboring non-affected site (control site). The predictive potential of different data analysis procedures (i.e., transient and steady-state) to yield proper  $K_{fs}$  estimates was also investigated.

Forest cover may improve water infiltration and soil hydraulic properties, but little is known about the response and extent to which forest restoration can affect these properties. Knowledge of soil hydraulic properties after forest restoration is essential for understanding the recovery of hydrological processes, such as water infiltration. Lozano-Baez et al. [16] investigated the effect of forest restoration on surface-saturated soil hydraulic conductivity,  $K_s$ , and its recovery to the pre-disturbance soil conditions. These authors measured  $K_s$  data under three land-cover types, i.e., pasture, restored forest and a remnant forest patch. They used a simplified method based on the Beerkan infiltration experiment [31]. They found considerable differences in soil hydraulic properties between land-cover classes. The highest  $K_s$  values were observed in remnant forest sites and the lowest  $K_s$  were associated with pasture sites.

Two other papers focus on soil erosion, investigating the specific cases of tillage [18] and piping [19] erosion. In their study, Novák and Hůla [18] used aluminum cubes as tracers to investigate tillage erosion. The results demonstrated the effect of the slope gradient on the crosswise translocation of particles during secondary tillage of soil in the slope direction. The tillage equipment translocated particles in the fall line direction even if it passed along the contour line.

Many engineering geological disasters have direct relations to bimsols (block-in-matrix-soils), which are characterized by extreme non-homogeneity, environmental sensitivity, and looseness. Piping is considered to be the main mechanism leading to the failure of hydraulic structures in bimsols. Piping seepage failure in bimsols was investigated by Wang et al. [19]. The authors evaluated in the laboratory the critical hydraulic gradient on cylindrical specimens. Four different parameters: rock block percentage, soil matrix density, confining pressure and block morphology were considered.

Three studies address water flow and storage modeling [20–22]. Modeling flow processes in unsaturated soils is usually based on the numerical solutions of the Richards equation. Meshless methods are emerging tools for solving problems on complex domains. Ku et al. [21] propose a novel meshless method based on the Trefftz method for the transient modeling of subsurface flow in unsaturated soils. These authors suggest that the proposed method could be easily applied both to one-dimensional and two-dimensional subsurface flow problems.

The understanding of the temporal and spatial dynamics of soil moisture and hydraulic property is crucial to interpret several hydrological and ecological processes. A model based on topography and soil properties is proposed by Xiang et al. [22]. The model was used to describe the site-specific soil storage capacity in a sub-basin, and to simulate spatial distribution of hydrological variables of runoff, soil moisture storage and actual evapotranspiration. The proposed model yielded satisfactory predictions of daily and hourly flow discharges, and reasonable spatial variations of the considered hydrological variables.

Delta plains require special attention given their vulnerability to flooding, climatic variation and water quality deterioration. Variation in soil water content in the delta plain has its own particularity. A three-dimensional numerical model based on the Richards equation was developed by Hua et al. [20] to investigate the temporal and vertical variation of soil water content in the Yangtze River Delta (East China). The model was calibrated and validated in an experimental plot. The authors show that the variation of soil water content was mainly dependent on the groundwater table due to the significant capillary action in the delta plain.

Three studies in Sub-Saharan region are included. Declining natural resources and climate change are the major challenges to crop production and food security in Sub-Saharan African countries [32]. Silungwe et al. [25] reviewed 187 papers focused on crop upgrading strategies (UPS) for improving rainfed cereals yields in semi-arid areas. They identified four different UPS, i.e., tied ridges, microdose fertilization, varying sowing/planting dates and field scattering, as the most promising strategies to improve rainfed cereal production and reduce the risks of cereal production failure under low rainfall, high spatiotemporal variability, and poor soil fertility conditions for poor farmers.

Management of erosion in rural landscapes needs specific strategies aimed at maintaining soil cover, reducing tillage, and enhancing soil nitrogen through legumes. This set of practices is known as conservation agriculture (CA). A study concerning the adoption of specific activities of CA in Malawi was carried out by Bell et al. [17].

Röschel et al. [27] conducted a household survey of 899 farmers in a semi-arid and a sub-humid region in Tanzania. The authors examine how smallholder farmers perceived climatic and environmental changes over the past 20 years and the resulting effects on water availability and food security.

Two other papers focus on novel monitoring [23] and experimental [24] approaches for soil hydraulic characterization. With the aim of measuring and mapping the fraction of transpirable soil water, Rallo et al. [23] compared the cumulative EM38 (Geonics Ltd., Mississauga, ON, Canada) response collected by placing the sensor above ground with the corresponding soil water content obtained by integrating the values measured with a frequency domain reflectometry sensor.

Pirastu et al. [24] developed a field technique to determine spatially representative lateral saturated hydraulic conductivity,  $K_{s,l}$ , values of soil horizons of an experimental hillslope. Drainage experiments were performed on soil monoliths of about 0.12 m<sup>3</sup> volume, encased in situ with polyurethane foam. The  $K_{s,l}$  from the monoliths were in line with large spatial-scale  $K_{s,l}$  values reported for the experimental hillslope in a prior investigation based on drain data analysis. This indicated that the large-scale hydrological effects of the macropore network were well represented in the investigated soil blocks.

The remaining two investigations in the thematic issue focus on improvement of crop yields [26] and soil salinity [28]. Trinchera and Baratella [26] investigated the use of an innovative non-ionic surfactant to fertigation water in *Lactuca sativa* (var. Iceberg) production to increase water and nutrient use efficiency. Finally, Akramkhanov et al. [28] discuss the process of testing and validation of an electromagnetic induction meter, a tool for rapid salinity assessment.

### 3. Conclusions

The 15 manuscripts presented in this Special Issue contribute to enhancing our understanding of conservation strategies for effective and sustainable soil and water management. Three studies use infiltration experiments in order to assess the recovery of soil hydraulic properties. Alagna et al. [29] highlight the need to adopt effective strategies to reduce soil compaction during vineyard establishment in order to maintain the soil infiltration capacity and reducing erosion potential. Di Prima et al. [15] show a certain degree of soil degradation at the burnt site with an immediate reduction of soil organic matter and a progressive increase of soil bulk density during the five years following the fire. This general impoverishment resulted in a slight but significant decrease in the field-saturated soil hydraulic conductivity. These authors also conclude that steady-state methods are more appropriate for detecting slight changes of  $K_{fs}$  in post-fire soil hydraulic characterizations. Lozano-Baez et al. [16] suggest that soil properties and  $K_s$  recovery are affected by prior land use, and this should be taken in due account in forest management.

Two other papers focus on soil erosion. Novák and Hůla [18] show that the effect of the equipment on crosswise translocation increased with the increasing intensity of passes. Moreover, during the secondary tillage, the working tools of the equipment had an erosive effect even when the equipment moves along the contour line. Wang et al. [19] contributes to the assessment in the laboratory of the critical hydraulic gradient of bimsoils, concluding that it was mainly sensitive to the percentage of rock blocks.

Novel models are proposed by Ku et al. [21], Xiang et al. [22] and Hua et al. [20]. These contributions allow us to simulate water flow and storage in different environments.

Three studies in Sub-Saharan region are included. The conclusion drawn by Silungwe et al. [25] from the examined literature was that the most suitable models to simulate the considered UPS were the Decision Support System for Agrotechnology Transfer (DSSAT), the Agricultural Production Systems Simulator (APSIM), and the AquaCrop model. Bell et al. [17] found that farmer decisions in Malawi followed a dynamic of peer influence, with neighbors' adoption as the most effective factor. This finding might have significant implications for the overall cost of encouraging conservation agriculture as it is taken up across a landscape. Röschel et al. [27] conclude that the specific environment paired with socio-economic factors can severely increase the negative effects of water scarcity for rural farmers in Tanzania.

Two other papers focus on novel monitoring and experimental approaches for soil hydraulic characterization. The methodology proposed by Rallo et al. [23] appears usable to monitor the variations in soil water content in response to irrigation and root water uptake. Moreover, it has the practical potential to be flexible in terms of spatial and temporal sampling resolution. Pirastu et al. [24] suggest that performing drainage experiments on large-volume monoliths is a promising method for characterizing lateral conductivities over large spatial scales. This information could improve the understanding of hydrological processes and could be used to parameterize runoff-generation models at hillslope and catchment scales [33].

The remaining two investigations in the thematic issue focus on improvement of crop yields and soil salinity. Trinchera and Baratella [26] found a positive physiological response by more expanded and less thick leaves in lettuce. This finding corresponded to the lowest leaf nitrate content, indicating an improvement of the crop quality while maintaining crop production. Finally, Akramkhanov et al. [28] involved local stakeholders in Uzbekistan in a transdisciplinary and participatory approach for innovation development. From a methodological point of view, the contributions involve both field [15,16,18,23,24,29] and laboratory [19] experiments, and modeling [20–22], survey [17,27,28] and review [25] studies. The Special Issue includes studies carried out at different spatial scales, from field- to regional-scales. A wide range of geographic regions are also covered, including Brazil [16], Mediterranean basin [15,23,24,26,29], central Europe [18], China [20–22], Sub-Saharan Africa [17,25,27], and central Asia [28].

**funding:** This research received no external funding.

**Conflicts of Interest:** The authors declare no conflicts of interest.

## References

1. Blanco, H.; Lal, R. *Principles of Soil Conservation and Management*; Springer: Dordrecht, The Netherlands, 2010.
2. Godfray, H.C.J.; Beddington, J.R.; Crute, I.R.; Haddad, L.; Lawrence, D.; Muir, J.F.; Pretty, J.; Robinson, S.; Thomas, S.M.; Toulmin, C. Food security: The challenge of feeding 9 billion people. *Science* **2010**, *327*, 812–818. [[CrossRef](#)] [[PubMed](#)]
3. Vörösmarty, C.J.; Green, P.; Salisbury, J.; Lammers, R.B. Global water resources: Vulnerability from climate change and population growth. *Science* **2000**, *289*, 284–288. [[CrossRef](#)] [[PubMed](#)]
4. Groppelli, B.; Soncini, A.; Bocchiola, D.; Rosso, R. Evaluation of future hydrological cycle under climate change scenarios in a mesoscale Alpine watershed of Italy. *Nat. Hazards Earth Syst. Sci.* **2011**, *11*, 1769–1785. [[CrossRef](#)]
5. Borrelli, P.; Robinson, D.A.; Fleischer, L.R.; Lugato, E.; Ballabio, C.; Alewell, C.; Meusburger, K.; Modugno, S.; Schütt, B.; Ferro, V.; et al. An assessment of the global impact of 21st century land use change on soil erosion. *Nat. Commun.* **2017**, *8*. [[CrossRef](#)] [[PubMed](#)]
6. Scanlon, B.R.; Keese, K.E.; Flint, A.L.; Flint, L.E.; Gaye, C.B.; Edmunds, W.M.; Simmers, I. Global synthesis of groundwater recharge in semiarid and arid regions. *Hydrol. Process.* **2006**, *20*, 3335–3370. [[CrossRef](#)]
7. Keesstra, S.; Bouma, J.; Wallinga, J.; Titttonell, P.; Smith, P.; Cerdà, A.; Montanarella, L.; Quinton, J.N.; Pachepsky, Y.; van der Putten, W.H.; et al. The significance of soils and soil science towards realization of the United Nations Sustainable Development Goals. *Soil* **2016**, *2*, 111–128. [[CrossRef](#)]
8. Boardman, J.; Poesen, J.; Evans, R. Socio-economic factors in soil erosion and conservation. *Environ. Sci. Policy* **2003**, *6*, 1–6. [[CrossRef](#)]
9. Rahman, M.R.; Shi, Z.H.; Chongfa, C. Soil erosion hazard evaluation—An integrated use of remote sensing, GIS and statistical approaches with biophysical parameters towards management strategies. *Ecol. Model.* **2009**, *220*, 1724–1734. [[CrossRef](#)]
10. Lal, R.; Stewart, B.A. Need for Land Restoration. In *Soil Restoration*; Advances in Soil Science; Springer: New York, NY, USA, 1992.
11. Bagarello, V.; Di Prima, S.; Giordano, G.; Iovino, M. A test of the beerkan estimation of soil transfer parameters (BEST) procedure. *Geoderma* **2014**, *221–222*, 20–27. [[CrossRef](#)]
12. Di Prima, S. Automated single ring infiltrometer with a low-cost microcontroller circuit. *Comput. Electron. Agric.* **2015**, *118*, 390–395. [[CrossRef](#)]
13. Di Prima, S.; Concialdi, P.; Lassabatere, L.; Angulo-Jaramillo, R.; Pirastru, M.; Cerdà, A.; Keesstra, S. Laboratory testing of Beerkan infiltration experiments for assessing the role of soil sealing on water infiltration. *Catena* **2018**, *167*, 373–384. [[CrossRef](#)]
14. Alagna, V.; Bagarello, V.; Di Prima, S.; Giordano, G.; Iovino, M. Testing infiltration run effects on the estimated water transmission properties of a sandy-loam soil. *Geoderma* **2016**, *267*, 24–33. [[CrossRef](#)]
15. Di Prima, S.; Lassabatere, L.; Rodrigo-Comino, J.; Marrosu, R.; Pulido, M.; Angulo-Jaramillo, R.; Úbeda, X.; Keesstra, S.; Cerdà, A.; Pirastru, M. Comparing transient and steady-state analysis of single-ring infiltrometer data for an abandoned field affected by fire in Eastern Spain. *Water* **2018**, *10*, 514. [[CrossRef](#)]

16. Lozano-Baez, S.E.; Cooper, M.; Ferraz, S.F.B.; Ribeiro Rodrigues, R.; Pirastru, M.; Di Prima, S. Previous land use affects the recovery of soil hydraulic properties after forest restoration. *Water* **2018**, *10*, 453. [[CrossRef](#)]
17. Bell, A.R.; Zavaleta Cheek, J.; Mataya, F.; Ward, P.S. Do as they did: Peer effects explain adoption of conservation agriculture in Malawi. *Water* **2018**, *10*, 51. [[CrossRef](#)]
18. Novák, P.; Hůla, J. Translocation of soil particles during secondary soil tillage along contour lines. *Water* **2018**, *10*, 568. [[CrossRef](#)]
19. Wang, Y.; Li, C.; Hu, Y.; Xiao, Y. Optimization of multiple seepage piping parameters to maximize the critical hydraulic gradient in bimsoils. *Water* **2017**, *9*, 787. [[CrossRef](#)]
20. Hua, W.; Wang, C.; Chen, G.; Yang, H.; Zhai, Y. Measurement and simulation of soil water contents in an experimental field in delta plain. *Water* **2017**, *9*, 947. [[CrossRef](#)]
21. Ku, C.-Y.; Liu, C.-Y.; Xiao, J.-E.; Yeh, W. Transient modeling of flow in unsaturated soils using a novel collocation meshless method. *Water* **2017**, *9*, 954. [[CrossRef](#)]
22. Xiang, X.; Wu, X.; Chen, X.; Song, Q.; Xue, X. Integrating topography and soil properties for spatial soil moisture storage modeling. *Water* **2017**, *9*, 647. [[CrossRef](#)]
23. Rallo, G.; Provenzano, G.; Castellini, M.; Sirena, A.P. Application of EMI and FDR sensors to assess the fraction of transpirable soil water over an olive grove. *Water* **2018**, *10*, 168. [[CrossRef](#)]
24. Pirastru, M.; Marrosu, R.; Di Prima, S.; Keesstra, S.; Giadrossich, F.; Niedda, M. Lateral saturated hydraulic conductivity of soil horizons evaluated in large-volume soil monoliths. *Water* **2017**, *9*, 862. [[CrossRef](#)]
25. Silungwe, F.R.; Graef, F.; Bellingrath-Kimura, S.D.; Tumbo, S.D.; Kahimba, F.C.; Lana, M.A. Crop upgrading strategies and modelling for rainfed cereals in a semi-arid climate—A review. *Water* **2018**, *10*, 356. [[CrossRef](#)]
26. Trinchera, A.; Baratella, V. Use of a non-ionic water surfactant in lettuce fertigation for optimizing water use, improving nutrient use efficiency, and increasing crop quality. *Water* **2018**, *10*, 613. [[CrossRef](#)]
27. Röschel, L.; Graef, F.; Dietrich, O.; Schäfer, M.P.; Haase, D. Individual local farmers' perceptions of environmental change in Tanzania. *Water* **2018**, *10*, 525. [[CrossRef](#)]
28. Akramkhanov, A.; Ul Hassan, M.M.; Hornidge, A.-K. Redrawing soil salinity innovation-focused stakeholder interaction for sustainable land management in Khorezm Province, Uzbekistan. *Water* **2018**, *10*, 208. [[CrossRef](#)]
29. Alagna, V.; Di Prima, S.; Rodrigo-Comino, J.; Iovino, M.; Pirastru, M.; Keesstra, S.D.; Novara, A.; Cerdà, A. The impact of the age of vines on soil hydraulic conductivity in vineyards in Eastern Spain. *Water* **2018**, *10*, 14. [[CrossRef](#)]
30. Bagarello, V.; Di Prima, S.; Iovino, M.; Provenzano, G. Estimating field-saturated soil hydraulic conductivity by a simplified Beerkan infiltration experiment. *Hydrol. Process.* **2014**, *28*, 1095–1103. [[CrossRef](#)]
31. Bagarello, V.; Di Prima, S.; Iovino, M. Estimating saturated soil hydraulic conductivity by the near steady-state phase of a Beerkan infiltration test. *Geoderma* **2017**, *303*, 70–77. [[CrossRef](#)]
32. Graef, F.; Uckert, G.; Schindler, J.; König, H.J.; Mbwana, H.A.; Fasse, A.; Mwinuka, L.; Mahoo, H.; Kaburire, L.N.; Saidia, P.; et al. Expert-based ex-ante assessments of potential social, ecological, and economic impacts of upgrading strategies for improving food security in rural Tanzania using the ScalA-FS approach. *Food Secur.* **2017**, *9*, 1255–1270. [[CrossRef](#)]
33. Di Prima, S.; Marrosu, R.; Lassabatere, L.; Angulo-Jaramillo, R.; Pirastru, M. In situ characterization of preferential flow by combining plot- and point-scale infiltration experiments on a hillslope. *J. Hydrol.* **2018**, *563*, 633–642. [[CrossRef](#)]



Article

# The Impact of the Age of Vines on Soil Hydraulic Conductivity in Vineyards in Eastern Spain

Vincenzo Alagna <sup>1,\*</sup>, Simone Di Prima <sup>2</sup>, Jesús Rodrigo-Comino <sup>3,4</sup>, Massimo Iovino <sup>1</sup>, Mario Pirastru <sup>2</sup>, Saskia D. Keesstra <sup>5,6</sup>, Agata Novara <sup>1</sup> and Artemio Cerda <sup>7</sup>

<sup>1</sup> Department of Agricultural, Food and Forest Sciences, University of Palermo, Viale delle Scienze, 90128 Palermo, Italy; massimo.iovino@unipa.it (M.I.); agata.novara@unipa.it (A.N.)

<sup>2</sup> Agricultural Department, University of Sassari, Viale Italia, 39, 07100 Sassari, Italy; sdiprima@uniss.it (S.D.P.); mpirastru@uniss.it (M.P.)

<sup>3</sup> Department of Geography, Instituto de Geomorfología y Suelos, Málaga University, Campus of Teatinos s/n, 29071 Málaga, Spain; rodrigo-comino@uma.es

<sup>4</sup> Department of Physical Geography, Trier University, D-54286 Trier, Germany

<sup>5</sup> Soil Physics and Land Management Group, Wageningen University, Droevendaalsesteeg 4, 6708PB Wageningen, The Netherlands; saskia.keesstra@wur.nl

<sup>6</sup> Civil, Surveying and Environmental Engineering, The University of Newcastle, Callaghan 2308, Australia

<sup>7</sup> Soil Erosion and Degradation Research Group, Department of Geography, Valencia University, Blasco Ibáñez, 28, 46010 Valencia, Spain; artemio.cerda@uv.es

\* Correspondence: vincenzo.alagna@unipa.it; Tel.: +39-091-238-97065

Received: 2 November 2017; Accepted: 21 December 2017; Published: 25 December 2017

**Abstract:** Soil infiltration processes manage runoff generation, which in turn affects soil erosion. There is limited information on infiltration rates. In this study, the impact of vine age on soil bulk density (BD) and hydraulic conductivity ( $K_s$ ) was assessed on a loam soil tilled by chisel plough. Soil sampling was conducted in the inter row area of six vineyards, which differed by the age from planting: 0 (Age 0; just planted), 1, 3, 6, 13, and 25 years (Age 1, Age 3, Age 6, Age 13, and Age 25, respectively). The One Ponding Depth (OPD) approach was applied to ring infiltration data to estimate soil  $K_s$  with an  $\alpha^*$  parameter equal to  $0.012 \text{ mm}^{-1}$ . Soil bulk density for Age 0 was about 1.5 times greater than for Age 25, i.e., the long-term managed vineyards. Saturated hydraulic conductivity at Age 0 was 86% less than at Age 25. The planting works were considered a major factor for soil compaction and the reduction of hydraulic conductivity. Compared to the long-term managed vineyards, soil compaction was a very short-term effect given that BD was restored in one year due to ploughing. Reestablishment of  $K_s$  to the long-term value required more time.

**Keywords:** vineyards; infiltration rate; age of planting; saturated hydraulic conductivity

## 1. Introduction

Extensive research has been carried out on vineyard soils, not only due to their effect on wine quality and quantity [1,2], but also because soils in vineyards affect the environmental health, as they can be a source of pollutants [3,4], pesticides [5], sediments [5], and overland flow [6]. Also, soil management in vineyard land use is relevant for the effect that it can have on soil properties [7,8]. The recently planted vineyards require more farming operations than the older ones. These practices, which are necessary for plant growth (e.g., application of pesticides, nutrients, installation of espalier), involve the continued use of heavy machinery and, consequently, cause changes in soil physical properties. Intensive agricultural activities determine soil structure degradation, compaction, and the formation of surface crusts that in turn reduce water infiltration. If soil infiltration capacity is less than rainfall intensity, the potential risks of runoff and soil erosion are

increased. The water stored in the soil, as well sediments, nutrients, and pollutants, export out of the vineyards are also affected by infiltration.

Despite being a key to understanding the hydrological cycle, there is very limited information about the infiltration rates in vineyards. The research developed by Wainwright [9], Leonard, and Andrieux [10], and Van Dijck and Van Asch [11], are some of the most relevant studies, which have demonstrated that the infiltration process is highly variable and difficult to predict. However, nowadays, several new findings demonstrate that there are many shortcomings regarding specific information. The research of Biddoccu et al. [12], Rodrigo-Comino et al. [13], and Alagna et al. [14] showed the renewed interest in understanding the infiltration process in vineyards, as (i) during the vintage and tillage, infiltration decreases due to the compaction by trampling effect and tractor passes; (ii) after abandonment, hydrological soil properties are less variable and easy to be predicted; and (iii) there are several differences in infiltration patterns among slope positions.

Among the key parameters that indicate soil health [15], the saturated hydraulic conductivity ( $K_s$ ) is easy to measure and particularly important, because it controls several soil hydrological processes such as infiltration. Furthermore,  $K_s$  is used as runoff-model inputs to assess soil losses.

In vineyards soil redistribution by both tillage [16] and water erosion [17] contributes to high short-term [13,18] and long-term soil erosion rates [6,19,20]. However, there are few studies on seasonal and temporal changes in soil erosion and runoff generation. Recently, Rodrigo-Comino et al. [21,22] and Cerdà et al. [23] found that high erosion rates in vineyards are mainly observed during the planting period. Thus, sustainable management requires attention to erosion control some time after planting. However, the factors that determine the higher runoff and soil erosion rates during vineyard establishment were not enough investigated in prior studies.

This research focused on temporal variability of soil compaction and infiltration rates in a loam soil planted with vines of different ages. Soil cores sampling and ring infiltrometer experiments were conducted in vineyards planted 0, 1, 3, 6, 13, and 25 years prior to the survey with the aim of detecting the temporal changes in bulk density and saturated hydraulic conductivity, but also to shed light on the impact of vines planting work on soil infiltration and erosion processes.

## 2. Materials and Methods

### 2.1. Study Area

Field experiments were conducted in the Terres dels Alforins vine production area (4000 ha) in province of Valencia (Spain), a representative zone of the Mediterranean vineyards. The vineyards (40 ha) between the Pago Casa Gran and Celler del Roure farms (Figure 1) were selected that are located within the Canyoles river watershed. They were chosen because they were ploughed by the same tractor and chisel plough for 25 years at the time of vineyards planting. The selected vineyards, with a Monastrell grape variety, are from 0 to 25-year old with a plantation framework of  $3.0 \times 1.4$  m. The measurements were conducted in the south-facing slope of the Les Alcusses valley which has a slope of 5%, where the presence of colluvium from soils formed on limestone parent material is common. The soils are basic (pH = 8) and are classified as Typic Xerothent [24], with an average depth of 60 cm. The observed soil profiles were relatively homogeneous due to the tillage practices and same soil managements. The mean annual rainfall is  $350 \text{ mm year}^{-1}$ , with maximum peak intensities (higher than  $200 \text{ mm day}^{-1}$ ) occurring in the autumn season. The mean annual temperature is  $13.8 \text{ }^\circ\text{C}$ .

### 2.2. Soil Sampling

The six experimental sites were characterized by different ages of vines. Age 0 is the recently planted vineyard, and Age 1, Age 3, Age 6, Age 13, and Age 25 are vines planted 1, 3, 6, 13, and 25 years prior to field investigation. Age 25 was selected, as it corresponds to the average replanting interval in this region. For each experimental site, an area of approximately  $100 \text{ m}^2$  was chosen. Fifteen soil

samples were collected randomly from the top 5 cm of the soil with a 100 cm<sup>3</sup> steel cylinder to determine gravimetric soil water content (SWC), organic matter (OM), and bulk density (BD). Samples were weighted immediately following collection, then oven dried at 105 °C for 24 h and re-weighted at room temperature. Organic matter was measured by the dichromate method [25], and grain size distribution was measured by the pipette method [26]. Tillage is common to all the experimental sites and has been the historic management method for centuries. All samples were collected in the inter row ploughed area. Four different tractor passes are usually conducted each year to till and aerate the soil. At all sampling sites, the wheel tracks were avoided during sampling. Furthermore, the last tillage had been done more than one month before the field experiments and no rainfall occurred in this time spell. Herbicides are not applied in the study area.

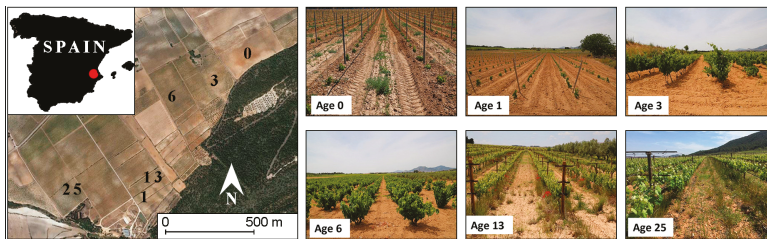


**Figure 1.** Aerial view of the studied areas with investigated vineyard sites.

### 2.3. Infiltration Measurements

At each selected site, 15 single ring infiltrometer measurements [27,28] were carried out at randomly chosen points within a 100 m<sup>2</sup> area. Field tests were conducted in summer 2014 during the typical Mediterranean drought period to limit variability in initial soil water content (SWC). A 100 mm inner-diameter steel ring was inserted vertically to a depth of about 0.01 m into the soil surface to avoid lateral loss of the ponded water. The ring was filled with fresh water and, at prescribed time intervals, the water level was measured using a ruler; then the ring was filled again. Flow rates were calculated from water level measurements at successive time steps, and steady-states were attained within 60 min for all experiments. A total of ninety experimental cumulative infiltration curves were then deduced (15 for each site (Figure 2)). The One Ponding Depth (OPD) calculation approach [28] was applied to compute field-saturated soil hydraulic conductivity,  $K_s$  (mm h<sup>-1</sup>), for each infiltration run. The OPD approach makes use of the steady-state infiltration flux,  $Q_s$  (mm<sup>3</sup> h<sup>-1</sup>), which is estimated from the cumulative infiltration vs. time plot. It also requires an estimate of the  $\alpha^*$  (mm<sup>-1</sup>) parameter, equal to the ratio between  $K_s$  and the field-saturated soil matric flux potential. In this investigation, an  $\alpha^*$  value of 0.012 mm<sup>-1</sup> was used, as it is the recommended value for the loam soil [29]. The equilibration time,  $t_s$  (min), i.e., the duration of the transient phase of the infiltration process, was estimated according to the criterion proposed by Bagarello et al. [30] for analyzing cumulative infiltration data.

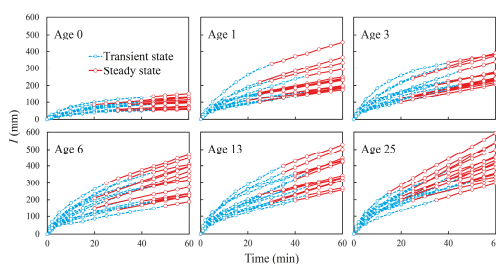


**Figure 2.** Cumulative infiltration,  $I$  (mm), vs. time (min) at the six investigated sites. Blue lines and red lines show, respectively, the transient and the steady-state conditions of infiltration process.

## 2.4. Statistical Analysis

The hypothesis of normal distribution of both the untransformed and the log-transformed  $K_s$  data was tested by the Kolmogorov–Smirnov test at  $p = 0.05$  significance level [31]. The other parameters were assumed normally distributed, and thus, no transformation was performed on these data before statistical analysis. The probability level,  $p = 0.05$ , was used for all statistical comparisons. One-way analysis of variance (ANOVA) was performed with raw and transformed data. If the ANOVA showed significant differences between the means, we used multiple comparisons to detect differences between pairs by applying the Tukey’s honestly significant difference test. Multiple comparisons analyses allowed us to group together mean values that were not statistically different. In addition, Pearson’s correlation coefficient was performed between BD and  $K_s$ . All statistical analyses were carried out using the Minitab<sup>®</sup> computer program (Minitab Inc., State College, PA, USA).

## 3. Results

### 3.1. Soil Properties

Table 1 summarizes soil physical and chemical properties of the six study sites. Organic matter content ranged from 1.2% to 1.4% and did not differ between the ninety sampling points even if relatively higher CV values were observed for Age 0 and Age 25 (respectively, 20.2% and 24.1%). The average gravimetric SWC prior to the infiltration experiments ranged from 0.051 to 0.056  $\text{g g}^{-1}$ , and the statistical comparisons did not show significant differences among the six sites. Grain size distribution was similar among ages. According to the USDA standards, the three fractions, i.e., clay (0–2  $\mu\text{m}$ ), silt (2–50  $\mu\text{m}$ ), and sand (50–2000  $\mu\text{m}$ ), were, on average, 17.9%, 38.8%, and 43.3%, and the soil of the studied area was classified as loam [24]. It was concluded that the soil properties at the six selected sites can be considered homogeneous despite the different age from vine planting.

**Table 1.** Mean values of initial soil water content ( $\text{g g}^{-1}$ ), organic matter (%), clay, silt, and sand content (%) (USDA classification system). Sample size is  $N = 15$  for each site. Coefficient of variation (%) is in brackets.

Variable	Age (Year)					
	0	1	3	6	13	25
Initial SWC	0.053 (14.9) a	0.056 (12.3) a	0.052 (15.5) a	0.055 (13.0) a	0.051 (8.8) a	0.053 (11.4) a
Organic matter	1.4 (20.2) a	1.2 (11.5) a	1.4 (16.7) a	1.3 (17.3) a	1.3 (19.0) a	1.3 (24.1) a
Clay	20.1 (17.3)	14.8 (28.3)	14.9 (26.8)	18.3 (28.2)	20.5 (18.8)	18.9 (18.1)
Silt	37.1 (9.7)	41.3 (5.9)	40.3 (8.0)	38.9 (8.1)	36.5 (10.3)	38.6 (7.4)
Sand	42.8 (6.5)	43.9 (5.8)	44.9 (6.7)	42.7 (7.9)	43.0 (6.5)	42.5 (6.6)

Note: For a given variable, mean values followed by the same lower case letter were not significantly different according to the Tukey Honestly Significant Difference test ( $p = 0.05$ ).

### 3.2. Effect of Age on Soil Bulk Density, BD

The soil bulk density ranged from 1.03 to 1.53 g cm<sup>-3</sup> (Figure 3). Within each site, the variability of BD was low (CV < 4%), confirming that this soil property generally exhibits low spatial variability [32]. The box plot comparison shows a pronounced decline of soil bulk density from Age 0 to Age 25.

Figure 4 summarizes the multiple comparison results between data pairs by using the Tukey’s honestly significant difference test. Multiple comparisons resulted in four groups (horizontal bars), whose members are not significantly different from one another. The soil bulk density is significantly higher in the Age 0 (1.53 g cm<sup>-3</sup>). In the second group (Age 1, Age 3, and Age 6), bulk density ranges from 1.07 to 1.10 g cm<sup>-3</sup>. The third group (ages from three to 12 years) shows BD = 1.05–1.08 g cm<sup>-3</sup>. The last group includes vines older than 6 years (BD = 1.03–1.07 g cm<sup>-3</sup>). From Age 0 to Age 1, BD decreases by a factor of 1.5; afterwards, it decreases more slightly, reaching the lowest value for Age 25.

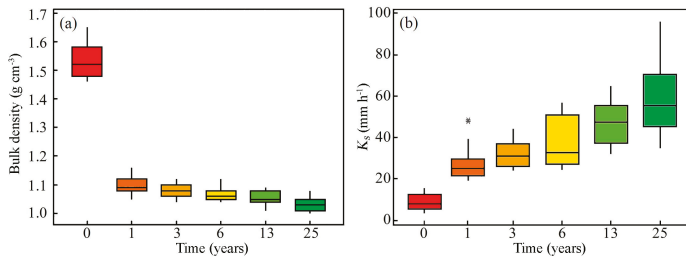


**Figure 3.** Box plots of (a) the soil bulk density (g cm<sup>-3</sup>) and (b) the field saturated soil hydraulic conductivity (K<sub>s</sub>, mm h<sup>-1</sup>) values. Boundaries indicate median, 25th, and 75th quartiles; the top and bottom whiskers indicate the minimum and maximum values. Values beyond the whiskers are outliers. Outliers are defined as data points more than 1.5 times the interquartile range away from the upper or lower quartile.

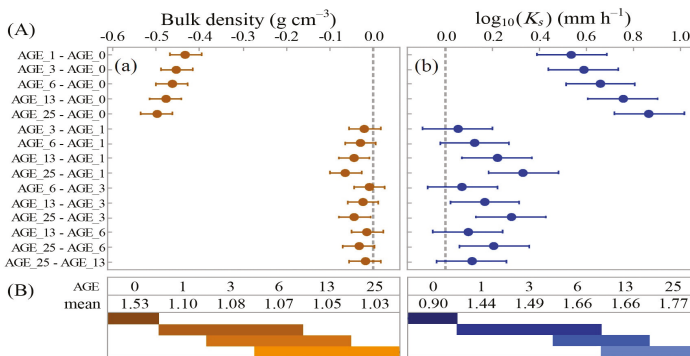


**Figure 4.** Results of the Tukey Honestly Significant Difference test for (a) the soil bulk density and (b) the log-transformed field saturated soil hydraulic conductivity (K<sub>s</sub>) values. (A) Multiple comparisons at 95% simultaneous confidence intervals of all pairs of groups. The circles represent difference between means; the confidence intervals represent the likely ranges for all the mean differences. If an interval does not contain zero, the corresponding means are significantly different. (B) The grouping information table highlights the significant and not significant comparisons. Each horizontal bar groups together members that are not statistically different.

### 3.3. Effect of Age on Infiltration and Saturated Hydraulic Conductivity, $K_s$

Figure 2 depicts cumulative infiltration curves from the 90 tests. All the curves exhibited a common shape, with a concave part corresponding to the transient stage of infiltration (blue lines) and a linear part detecting that the steady-state conditions (red lines) were achieved [33]. It should be noted that the total infiltrated depth,  $I_{end}$  (mm), increased progressively with age (Table 2). The mean  $I_{end}$  values ranged from 103 to 426 mm. Water flow reached, on average, steady-state rate after 31–38 min, depending on the site. The infiltrated depth at the equilibration time,  $I(t_s)$  (mm), also increased progressively with age.

The Kolmogorov-Smirnov test indicated that the  $K_s$  results were conformed to a log-normal distribution [32]. Therefore, statistical analyses were performed on log-transformed values. Geometric means of  $K_s$  and associated CVs corresponding to the different ages from vine planting are reported in Table 3. Similar to BD,  $K_s$  increased with time from planting by a factor of 3.4 from Age 0 to Age 1; thereafter, the differences decreased (Figure 3).

**Table 2.** Minimum, Min, maximum, Max, mean, and coefficient of variation, CV (%), of the total infiltrated depth,  $I_{end}$  (mm), infiltrated depth at the equilibration time,  $I(t_s)$  (mm), and equilibration time,  $t_s$  (min) ( $N = 15$  for each site).

Variable	$I_{end}$				$I(t_s)$				$t_s$				
	Statistic	Min	Max	Mean	CV	Min	Max	Mean	CV	Min	Max	Mean	CV
Age (Year)													
0	58	154	103 a	26.5	52	137	85 a	25.9	10	50	35 a	32	
1	175	453	250 b	31.6	102	328	176 b	33.3	20	45	31 a	27.3	
3	207	390	275 b	23.2	101	334	207 bc	32.6	20	45	36 a	27.5	
6	189	465	323 bc	27.5	143	364	239 bcd	29.7	20	50	37 a	27.6	
13	258	528	371 cd	22.1	180	399	280 d	25.7	25	45	38 a	16.5	
25	298	594	426 d	20.7	197	377	271 cd	20.6	15	50	32 a	35.8	

Note: For a given variable, mean values followed by the same lower case letter were not significantly different according to the Tukey Honestly Significant Difference test ( $p = 0.05$ ).

**Table 3.** Geometric mean, GM, and coefficient of variation, CV (%), of the saturated soil hydraulic conductivity,  $K_s$  ( $\text{mm h}^{-1}$ ), and results of the Kolmogorov-Smirnov test. Sample size,  $N = 15$  for each site.

Age (Year)	Statistic		Distribution	
	GM	CV	Normal	Log-Normal
0	8.0	51.8	not rejected	not rejected
1	27.4	29.9	rejected	not rejected
3	30.9	21.4	rejected	not rejected
6	36.4	32.9	not rejected	not rejected
13	45.4	24.3	not rejected	not rejected
25	58.7	31.3	not rejected	not rejected

Multiple comparisons resulted in four groups (Figure 4B). At Age 0, mean  $K_s$  value ( $8.0 \text{ mm h}^{-1}$ ) was significantly lower than at the other ages. There were also significant differences among the second group (Age 1, Age 3, and Age 6) with mean  $K_s$  ranging from  $27.4$  to  $36.4 \text{ mm h}^{-1}$ , the third group (Age 6 and Age 13) with  $K_s = 36.4$ – $45.4 \text{ mm h}^{-1}$ , and the last group (Age 13 and Age 25) that showed the highest  $K_s$  values ( $45.4$ – $58.7 \text{ mm h}^{-1}$ ). It is well known from previous studies that  $K_s$  is highly variable compared to other soil physical properties [32,34]. However, a relatively high variability was observed in this study only at Age 0.

A significant negative correlation was found between mean BD and  $K_s$  values ( $r = -0.677$ ,  $p < 0.001$ ) (Figure 5), highlighting that reduction in soil bulk density as a consequence of age clearly influenced the field saturated soil hydraulic conductivity.

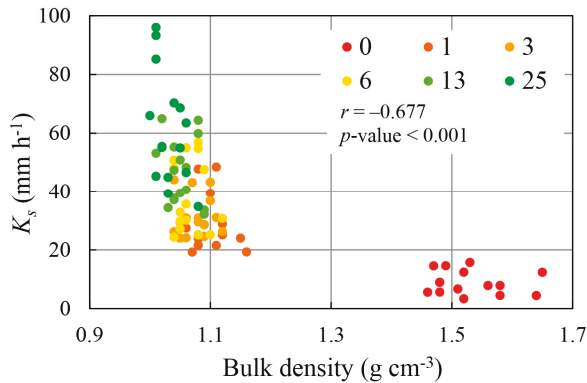


**Figure 5.** Correlation between the soil bulk density ( $\text{g cm}^{-3}$ ) and field saturated soil hydraulic conductivity,  $K_s$  ( $\text{mm h}^{-1}$ ). Pearson's correlation coefficients ( $r$ ) and probability of error ( $p$ ) are reported.

#### 4. Discussion

As is known, soil management modifies soil bulk density, pore structure and connectivity, hydraulic conductivity, and air permeability (e.g., [35,36]). Machine traffic often causes soil compaction and, consequently, a reduction of soil physical quality (e.g., [11,15,37,38]). The average initial soil bulk density (Age 0) was  $1.53 \text{ g cm}^{-3}$  for the experimental site, far greater than the optimal bulk density range ( $0.9\text{--}1.2 \text{ g cm}^{-3}$ ) suggested for a large range of agricultural soils [39,40]. Associated bulk density values up to  $1.51 \text{ g cm}^{-3}$  were observed for a loamy soil under vineyard and orchard land uses subjected to vehicle traffic [11]. In a loam soil of the Swiss Plateau, tilled with a direct drilling, Gut et al. [41] found an average BD value of  $1.47 \text{ g cm}^{-3}$  at depth  $0.1\text{--}0.16 \text{ m}$ . In an investigation conducted by Boydell and Boydell [42] in Vertisols used for grain cropping, machinery traffic determined bulk densities in the range  $1.25\text{--}1.45 \text{ g cm}^{-3}$  at depth of  $0.05\text{--}0.5 \text{ m}$ . In a sandy loam soil, machinery traffic applied when the soil was dry (mean soil moisture  $0.066 \text{ g g}^{-1}$ ) resulted in an average  $\text{BD} = 1.59 \text{ g cm}^{-3}$  at  $0.15$  to  $0.30$  depth [43]. Although care was put to avoid the wheel tracks during sampling, these results also indicate that Les Alcusses soil was throughout compacted by machinery operations due to the pass of lorries, vans, tractors, and men at the time of vineyard establishment.

During the first year from planting, the decreased BD rate was  $0.43 \text{ g cm}^{-3} \text{ year}^{-1}$ , and in the time spell between Age 1 and Age 25 it was  $0.003 \text{ g cm}^{-3} \text{ year}^{-1}$ . Assuming the value of BD at Age 25 as long-term condition for the loam soil under study, these results indicated that soil resilience determined an immediate response that allowed it to recover 86% of the final value during the first year and only 14% in the following 24 years. However, low differences between two successive ages were significant. Therefore, the routinely adopted vineyard management did not prevent recovery of the long-term bulk density conditions for this soil.

The average  $K_s$  value of  $8 \text{ mm h}^{-1}$  at Age 0 (Table 3) was approximately similar to that expected for a loam soil ( $10.4 \text{ mm h}^{-1}$ , [44]), but it was 3.4–7.3 times lower than that measured at the successive ages. Excluding this site, the average  $K_s$  values varied within a relatively narrow range ( $27.4$  to  $58.7 \text{ mm h}^{-1}$ , i.e., by a factor of 2.1), and spatial variability was very similar for the five selected sites. According to Elrick and Reynolds [29], difference in  $K_s$  by a factor of two or three can be considered negligible for practical purposes. The rate of  $K_s$  increase during the first year (Age 0 to Age 1) was equal to  $19.4 \text{ mm h}^{-1} \text{ year}^{-1}$ , whereas in the following period  $K_s$  increased at a rate of  $1.30 \text{ mm h}^{-1} \text{ year}^{-1}$ . Compared to BD, the short-term reestablishment rate of  $K_s$  is less effective given that only 38% of the final value was recovered within one year. Therefore, the saturated soil hydraulic conductivity required more time to restore its long-term condition. The significant differences in  $K_s$  highlighted by multiple comparisons among second group (Age 1, Age 3, and Age 6), third group (Age 6 and

Age 13) and fourth group (Age 13 and Age 25) can be probably explained by the fact that as vines grow, fewer and fewer farming operations are required that result in reduced soil compaction by machinery traffic. Moreover, soil tillages, performed in subsequent years in order to control weeds, destroyed the surface crust, homogenized soil properties, and led to increased  $K_s$  values.

Negative correlation between soil hydraulic conductivity and bulk density is well documented in literature (e.g., [45]). For instance, Meek et al. [46] found hydraulic conductivity of a sandy loam soil decreased by 58% when BD increased from 1.6 to 1.8 g cm<sup>-3</sup>.

In the studied area, the vines are replaced on average every 25 years; thus, attention should be paid during vineyard planting to avoid soil compaction that may have negative consequence on the hydrological processes. In this case, high intensity rainfalls, frequently occurring in Mediterranean climate, can trigger rill formation and high erosion rates [23]. Rehabilitation strategies aiming at increasing water infiltration and reducing surface runoff and soil erosion include use of cover crops [47,48], intercropping [49], and use of mulching or straw [50,51].

## 5. Conclusions

The vineyard's age affected infiltration and some soil physical properties but did not influence soil organic matter. After planting, bulk density was 1.5 times greater than the long-term bulk density corresponding to Age 25. Accordingly, field saturated soil hydraulic conductivity was 86% less than the long-term value. Planting operations caused soil compaction, which reduced hydraulic conductivity. Such modifications were reversible over 24 years following planting, notwithstanding normal machinery traffic, due to ordinary management that attended to reducing surface soil compaction and restoring the aeration of surface layer. The rate of soil recovery was greatest following disturbance and declined thereafter, demonstrating the resilience of the considered soil to the stress induced by planting works. The results of this investigation suggest that strategies to reduce soil compaction during vineyard establishment will be valuable to maintaining the soil infiltration capacity and reducing the erosion potential.

**Acknowledgments:** The research leading to these results has received funding from the European Union Seventh Framework Programme (FP7/2007-2013) under grant agreement No. 603498 (RECARE project).

**Author Contributions:** All authors equally contributed to analyse the data, discuss the results, and write the manuscript.

**Conflicts of Interest:** The authors declare no conflict of interest.

## References

1. Mackenzie, D.E.; Christy, A.G. The role of soil chemistry in wine grape quality and sustainable soil management in vineyards. *Water Sci. Technol.* **2005**, *51*, 27–37. [[PubMed](#)]
2. Reeve, J.R.; Carpenter-Boggs, L.; Reganold, J.P.; York, A.L.; McGourty, G.; McCloskey, L.P. Soil and winegrape quality in biodynamically and organically managed vineyards. *Am. J. Enol. Vitic.* **2005**, *56*, 367–376.
3. Mackie, K.A.; Müller, T.; Zikeli, S.; Kandeler, E. Long-term copper application in an organic vineyard modifies spatial distribution of soil micro-organisms. *Soil Biol. Biochem.* **2013**, *65*, 245–253. [[CrossRef](#)]
4. Pose-Juan, E.; Sánchez-Martin, M.J.; Andrades, M.S.; Rodríguez-Cruz, M.S.; Herrero-Hernández, E. Pesticide residues in vineyard soils from Spain: Spatial and temporal distributions. *Sci. Total Environ.* **2015**, *514*, 351–358. [[CrossRef](#)] [[PubMed](#)]
5. Sabatier, P.; Poulénard, J.; Fanget, B.; Reyss, J.-L.; Develle, A.-L.; Wilhelm, B.; Ployon, E.; Pignol, C.; Naffrechoux, E.; Dorioz, J.-M.; et al. Long-term relationships among pesticide applications, mobility, and soil erosion in a vineyard watershed. *Proc. Natl. Acad. Sci. USA* **2014**, *111*, 15647–15652. [[CrossRef](#)] [[PubMed](#)]
6. Biddoccu, M.; Ferraris, S.; Opsi, F.; Cavallo, E. Long-term monitoring of soil management effects on runoff and soil erosion in sloping vineyards in Alto Monferrato (North–West Italy). *Soil Tillage Res.* **2016**, *155*, 176–189. [[CrossRef](#)]

7. Morvan, X.; Naisse, C.; Malam Issa, O.; Desprats, J.F.; Combaud, A.; Cerdan, O. Effect of ground-cover type on surface runoff and subsequent soil erosion in Champagne vineyards in France. *Soil Use Manag.* **2014**, *30*, 372–381. [[CrossRef](#)]
8. Sharma, K.L.; Mandal, U.K.; Srinivas, K.; Vittal, K.P.R.; Mandal, B.; Grace, J.K.; Ramesh, V. Long-term soil management effects on crop yields and soil quality in a dryland Alfisol. *Soil Tillage Res.* **2005**, *83*, 246–259. [[CrossRef](#)]
9. Wainwright, J. Infiltration, runoff and erosion characteristics of agricultural land in extreme storm events, SE France. *Catena* **1996**, *26*, 27–47. [[CrossRef](#)]
10. Leonard, J.; Andrieux, P. Infiltration characteristics of soils in Mediterranean vineyards in Southern France. *Catena* **1998**, *32*, 209–223. [[CrossRef](#)]
11. Van Dijk, S.J.E.; Van Asch, T.W. Compaction of loamy soils due to tractor traffic in vineyards and orchards and its effect on infiltration in southern France. *Soil Tillage Res.* **2002**, *63*, 141–153. [[CrossRef](#)]
12. Biddoccu, M.; Ferraris, S.; Cavallo, E.; Opsi, F.; Previati, M.; Canone, D. Hillslope Vineyard Rainfall-Runoff Measurements in Relation to Soil Infiltration and Water Content. *Procedia Environ. Sci.* **2013**, *19*, 351–360. [[CrossRef](#)]
13. Rodrigo-Comino, J.; Seeger, M.; Senciales González, J.M.; Ruiz Sinoga, J.D.; Ries, J.B. Variación espacio-temporal de los procesos hidrológicos del suelo en viñedos con elevadas pendientes (Valle del Ruwer-Mosela, Alemania). *Cuad. Investig. Geogr.* **2016**, *42*, 281–306. [[CrossRef](#)]
14. Alagna, V.; Bagarello, V.; Di Prima, S.; Guaitoli, F.; Iovino, M.; Keestra, S.; Cerdà, A. Using beerkan experiments to estimate hydraulic conductivity of a crusted loamy soil in a Mediterranean vineyard. *J. Hydrol. Hydromech.* **2017**, under review.
15. Iovino, M.; Castellini, M.; Bagarello, V.; Giordano, G. Using Static and Dynamic Indicators to Evaluate Soil Physical Quality in a Sicilian Area. *Land Degrad. Dev.* **2016**, *27*, 200–210. [[CrossRef](#)]
16. Govers, G.; Quine, T.A.; Desmet, P.J.; Walling, D.E. The relative contribution of soil tillage and overland flow erosion to soil redistribution on agricultural land. *Earth Surf. Process. Landf.* **1996**, *21*, 929–946. [[CrossRef](#)]
17. Rodrigo-Comino, J.; Senciales, J.M.; Ramos, M.C.; Martínez-Casasnovas, J.A.; Lasanta, T.; Brevik, E.C.; Ries, J.B.; Sinoga, J.R. Understanding soil erosion processes in Mediterranean sloping vineyards (Montes de Málaga, Spain). *Geoderma* **2017**, *296*, 47–59. [[CrossRef](#)]
18. Casali, J.; Giménez, R.; De Santisteban, L.; Álvarez-Mozos, J.; Mena, J.; de Lersundi, J.D.V. Determination of long-term erosion rates in vineyards of Navarre (Spain) using botanical benchmarks. *Catena* **2009**, *78*, 12–19. [[CrossRef](#)]
19. Paroissien, J.-B.; Lagacherie, P.; Le Bissonnais, Y. A regional-scale study of multi-decennial erosion of vineyard fields using vine-stock unearthing–burying measurements. *Catena* **2010**, *82*, 159–168. [[CrossRef](#)]
20. Prosdocimi, M.; Tarolli, P.; Cerdà, A. Mulching practices for reducing soil water erosion: A review. *Earth-Sci. Rev.* **2016**, *161*, 191–203. [[CrossRef](#)]
21. Rodrigo-Comino, J.; Brings, C.; Lasso, T.; Iserloh, T.; Senciales, J.M.; Murillo, J.M.; Sinoga, J.R.; Seeger, M.; Ries, J.B. Rainfall and human activity impacts on soil losses and rill erosion in vineyards (Ruwer Valley, Germany). *Solid Earth* **2015**, *6*, 823–837. [[CrossRef](#)]
22. Rodrigo-Comino, J.; García-Díaz, A.; Brevik, E.; Keesstra, S.; Novara, A.; Pereira, P.; Jordán, A.; Cerdà, A. Role of rock fragment cover on runoff generation and sediment yield in tilled vineyards. *Eur. J. Soil Sci.* **2017**. [[CrossRef](#)]
23. Cerdà, A.; Keesstra, S.D.; Rodrigo-Comino, J.; Novara, A.; Pereira, P.; Brevik, E.; Giménez-Morera, A.; Fernández-Raga, M.; Pulido, M.; di Prima, S.; et al. Runoff initiation, soil detachment and connectivity are enhanced as a consequence of vineyards plantations. *J. Environ. Manag.* **2017**, *202*, 268–275. [[CrossRef](#)] [[PubMed](#)]
24. *Soil Survey Staff Keys to Soil Taxonomy*, 12th ed.; USDA—Natural Resources Conservation Service: Washington, DC, USA, 2014; p. 360. Available online: [https://www.nrcs.usda.gov/wps/PA\\_NRCSCconsumption/download?cid...ext=pdf](https://www.nrcs.usda.gov/wps/PA_NRCSCconsumption/download?cid...ext=pdf) (accessed on 22 December 2017).
25. Nelson, D.W.; Sommers, L.E. Total Carbon, Organic Carbon, and Organic Matter. In *Methods of Soil Analysis Part 3—Chemical Methods*; Soil Science Society of America; American Society of Agronomy: Madison, WI, USA, 1996; pp. 961–1010.

26. Day, P.R. Particle Fractionation and Particle-Size Analysis. In *Methods of Soil Analysis. Part 1. Physical and Mineralogical Properties, Including Statistics of Measurement and Sampling, Agronomy Monograph 9.1*; Soil Science Society of America; American Society of Agronomy: Madison, WI, USA, 1995; pp. 545–567.
27. Reynolds, W.D. Unsaturated hydraulic conductivity, Field measurement. In *Soil Sampling and Methods of Analysis*; Lewis Publishers: Boca Raton, FL, USA, 1993; pp. 633–644.
28. Reynolds, W.D.; Elrick, D.E. Pondered Infiltration from a Single Ring: I. Analysis of Steady Flow. *Soil Sci. Soc. Am. J.* **1990**, *54*, 1233. [[CrossRef](#)]
29. Elrick, D.E.; Reynolds, W.D. Methods for analyzing constant-head well permeameter data. *Soil Sci. Soc. Am. J.* **1992**, *56*, 320–323. [[CrossRef](#)]
30. Bagarello, V.; Iovino, M.; Reynolds, W. Measuring hydraulic conductivity in a cracking clay soil using the Guelph permeameter. *Trans. ASAE* **1999**, *42*, 957–964. [[CrossRef](#)]
31. Lilliefors, H.W. On the Kolmogorov-Smirnov test for normality with mean and variance unknown. *J. Am. Stat. Assoc.* **1967**, *62*, 399–402. [[CrossRef](#)]
32. Warrick, A.W. Spatial variability. In *Environmental Soil Physics*; Hillel, D., Ed.; Academic Press: San Diego, CA, USA, 1998; pp. 655–675.
33. Di Prima, S.; Lassabatere, L.; Bagarello, V.; Iovino, M.; Angulo-Jaramillo, R. Testing a new automated single ring infiltrometer for Beerkan infiltration experiments. *Geoderma* **2016**, *262*, 20–34. [[CrossRef](#)]
34. Aiello, R.; Bagarello, V.; Barbagallo, S.; Consoli, S.; Di Prima, S.; Giordano, G.; Iovino, M. An assessment of the Beerkan method for determining the hydraulic properties of a sandy loam soil. *Geoderma* **2014**, 235–236, 300–307. [[CrossRef](#)]
35. Osunbitan, J.A.; Oyedele, D.J.; Adekalu, K.O. Tillage effects on bulk density, hydraulic conductivity and strength of a loamy sand soil in southwestern Nigeria. *Soil Tillage Res.* **2005**, *82*, 57–64. [[CrossRef](#)]
36. Palese, A.M.; Vignozzi, N.; Celano, G.; Agnelli, A.E.; Pagliai, M.; Xiloyannis, C. Influence of soil management on soil physical characteristics and water storage in a mature rainfed olive orchard. *Soil Tillage Res.* **2014**, *144*, 96–109. [[CrossRef](#)]
37. Li, Y.X.; Tullberg, J.N.; Freebairn, D.M. Wheel traffic and tillage effects on runoff and crop yield. *Soil Tillage Res.* **2007**, *97*, 282–292. [[CrossRef](#)]
38. Li, Y.X.; Tullberg, J.N.; Freebairn, D.M.; Li, H.W. Functional relationships between soil water infiltration and wheeling and rainfall energy. *Soil Tillage Res.* **2009**, *104*, 156–163. [[CrossRef](#)]
39. Bagarello, V.; Di Prima, S.; Iovino, M.; Provenzano, G.; Sgroi, A. Testing different approaches to characterize Burundian soils by the BEST procedure. *Geoderma* **2011**, *162*, 141–150. [[CrossRef](#)]
40. Reynolds, W.D.; Drury, C.F.; Tan, C.S.; Fox, C.A.; Yang, X.M. Use of indicators and pore volume-function characteristics to quantify soil physical quality. *Geoderma* **2009**, *152*, 252–263. [[CrossRef](#)]
41. Gut, S.; Chervet, A.; Stettler, M.; Weisskopf, P.; Sturny, W.G.; Lamandé, M.; Schjonning, P.; Keller, T. Seasonal dynamics in wheel load-carrying capacity of a loam soil in the Swiss Plateau. *Soil Use Manag.* **2015**, *31*, 132–141. [[CrossRef](#)]
42. Boydell, B.; Boydell, C. A decade of directions: Trials and tribulations of precision agriculture and controlled traffic at “Marinya” (Keynote address). In Proceedings of the 16th Triennial Conference of the International Soil and Tillage Research Organisation, Brisbane, Australia, 13–18 July 2003; pp. 13–18.
43. Meek, B.D.; Rechel, E.R.; Carter, L.M.; DeTar, W.R. Bulk density of a sandy loam: Traffic, tillage, and irrigation-method effects. *Soil Sci. Soc. Am. J.* **1992**, *56*, 562–565. [[CrossRef](#)]
44. Carsel, R.F.; Parrish, R.S. Developing joint probability distributions of soil water retention characteristics. *Water Resour. Res.* **1988**, *24*, 755–769. [[CrossRef](#)]
45. Wang, T.; Wedin, D.; Zlotnik, V.A. Field evidence of a negative correlation between saturated hydraulic conductivity and soil carbon in a sandy soil. *Water Resour. Res.* **2009**, *45*, W07503. [[CrossRef](#)]
46. Meek, B.D.; Rechel, E.R.; Carter, L.M.; DeTar, W.R.; Urie, A.L. Infiltration rate of a sandy loam soil: Effects of traffic, tillage, and plant roots. *Soil Sci. Soc. Am. J.* **1992**, *56*, 908–913. [[CrossRef](#)]
47. Gristina, L.; Novara, A.; Saladino, S.; Santoro, A. Cover crops effectiveness for soil erosion control in Sicilian vineyard. In Proceedings of the EGU General Assembly Conference Abstracts, Vienna, Austria, 19–24 April 2009; Volume 11, p. 13608.
48. Kaspar, T.C.; Radke, J.K.; Laflen, J.M. Small grain cover crops and wheel traffic effects on infiltration, runoff, and erosion. *J. Soil Water Conserv.* **2001**, *56*, 160–164.

49. Sharma, N.K.; Singh, R.J.; Mandal, D.; Kumar, A.; Alam, N.M.; Keesstra, S. Increasing farmer's income and reducing soil erosion using intercropping in rainfed maize-wheat rotation of Himalaya, India. *Agric. Ecosyst. Environ.* **2017**, *247*, 43–53. [[CrossRef](#)]
50. Cerdà, A.; Rodrigo-Comino, J.; Giménez-Morera, A.; Keesstra, S.D. An economic, perception and biophysical approach to the use of oat straw as mulch in Mediterranean rainfed agriculture land. *Ecol. Eng.* **2017**, *108*, 162–171. [[CrossRef](#)]
51. Lal, R. Mulching Effects on Runoff, Soil Erosion, and Crop Response on Alfisols in Western Nigeria. *J. Sustain. Agric.* **1997**, *11*, 135–154. [[CrossRef](#)]



© 2017 by the authors. Licensee MDPI, Basel, Switzerland. This article is an open access article distributed under the terms and conditions of the Creative Commons Attribution (CC BY) license (<http://creativecommons.org/licenses/by/4.0/>).

Article

# Comparing Transient and Steady-State Analysis of Single-Ring Infiltrometer Data for an Abandoned Field Affected by Fire in Eastern Spain

Simone Di Prima <sup>1,\*</sup>, Laurent Lassabatere <sup>2</sup>, Jesús Rodrigo-Comino <sup>3</sup>, Roberto Marrosu <sup>1</sup>, Manuel Pulido <sup>4</sup>, Rafael Angulo-Jaramillo <sup>2</sup>, Xavier Úbeda <sup>5</sup>, Saskia Keesstra <sup>6,7</sup>, Artemi Cerda <sup>8</sup> and Mario Pirastru <sup>1</sup>

- <sup>1</sup> Dipartimento di Agraria, Università degli Studi di Sassari, Viale Italia 39, 07100 Sassari, Italy; rmarrosu@uniss.it (R.M.); mpirastru@uniss.it (M.P.)
  - <sup>2</sup> Université de Lyon, UMR5023 Ecologie des Hydrosystèmes Naturels et Anthropisés, CNRS, ENTPE, Université Lyon 1, 3 rue Maurice Audin, 69518 Vaulx-en-Velin, France; laurent.lassabatere@entpe.fr (L.L.); rafael.angulojaramillo@entpe.fr (R.A.-J.)
  - <sup>3</sup> Department of Geography, Instituto de Geomorfología y Suelos, Málaga University, Campus of Teatinos, 29071 Málaga, Spain; rodrigo-comino@uma.es
  - <sup>4</sup> GeoEnvironmental Research Group, Faculty of Philosophy and Letters, University of Extremadura, Avda. de la Universidad, 10071 Cáceres, Spain; mapulidof@unex.es
  - <sup>5</sup> Mediterranean Environmental Research Group (GRAM), Department of Physical Geography and Regional Geographic Analysis, University of Barcelona, Montalegre 6, 08001 Barcelona, Spain; xubeda@ub.edu
  - <sup>6</sup> Team Soil Water and Land Use, Wageningen Environmental Research, Wageningen UR, Droevendaalsesteeg 3, 6700 AA Wageningen, The Netherlands; saskia.keesstra@wur.nl
  - <sup>7</sup> Civil, Surveying and Environmental Engineering, The University of Newcastle, Callaghan 2308, Australia
  - <sup>8</sup> Soil Erosion and Degradation Research Group, Department of Geography, Valencia University, Blasco Ibáñez, 28, 46010 Valencia, Spain; artemio.cerda@uv.es
- \* Correspondence: sdiprima@uniss.it; Tel.: +39-079-229387

Received: 3 April 2018; Accepted: 18 April 2018; Published: 20 April 2018

**Abstract:** This study aimed at determining the field-saturated soil hydraulic conductivity,  $K_{fs}$ , of an unmanaged field affected by fire by means of single-ring infiltrometer runs and the use of transient and steady-state data analysis procedures. Sampling and measurements were carried out in 2012 and 2017 in a fire-affected field (burnt site) and in a neighboring non-affected site (control site). The predictive potential of different data analysis procedures (i.e., transient and steady-state) to yield proper  $K_{fs}$  estimates was investigated. In particular, the transient WU1 method and the BB, WU2 and OPD methods were compared. The cumulative linearization (CL) method was used to apply the WU1 method. Values of  $K_{fs}$  ranging from 0.87 to 4.21 mm·h<sup>-1</sup> were obtained, depending on the considered data analysis method. The WU1 method did not yield significantly different  $K_{fs}$  estimates from the sampled sites throughout the five-year period, due to the generally poor performance of the CL method, which spoiled the soil hydraulic characterization. In particular, good fits were only obtained in 23% of the cases. The BB, WU2 and the OPD methods, with a characterization based exclusively on a stabilized infiltration process, yielded an appreciably lower variability of the  $K_{fs}$  data as compared with the WU1 method. It was concluded that steady-state methods were more appropriate for detecting slight changes of  $K_{fs}$  in post-fire soil hydraulic characterizations. Our results showed a certain degree of soil degradation at the burnt site with an immediate reduction of the soil organic matter and a progressive increase of the soil bulk density during the five years following the fire. This general impoverishment resulted in a slight but significant decrease in the field-saturated soil hydraulic conductivity.

**Keywords:** post-fire soil hydraulic characterization; infiltration; bottomless bucket method; single-ring infiltrometer; field-saturated soil hydraulic conductivity; data analysis procedures

## 1. Introduction

Assessing the effects of fire on soil hydraulic properties in the Mediterranean area is crucial to evaluate the role of fire in land degradation and erosion processes. Among the soil hydraulic properties, field-saturated hydraulic conductivity,  $K_{fs}$ , exerts a key role in the partitioning of rainfall into runoff and infiltration [1]. Therefore, estimates of  $K_{fs}$  are essential for evaluating the hydrological response of fire-affected soils [2]. Soil properties are highly affected by fires due to the removal of the aboveground vegetation, the heat impact on the soil, the removal of the organic matter, the ash cover and the changes induced by rainfall on the soil surface [3–5]. Most of the research carried out on fire-affected land has paid attention to the “window of disturbance”, which is the period during which the soil losses are higher than before the fire and which lasts for a few years [6–8]. In order to understand the evolution of soil erosion after forest fires it is necessary to monitor fire-affected sites over a long period of time, in order to enable the assessment of the period affected by the window of disturbance [9]. Moreover, it is also possible to carry out measurements and experiments in areas with a different fire history. This gives information about the temporal changes in soil erosion after fire.

For this purpose, speed and ease of field procedures for soil hydraulic characterization are essential [10,11]. The single-ring infiltrometer technique [12,13] is a routinely used method for measuring  $K_{fs}$  in the field (e.g., [14–17]). With a single-ring infiltrometer, a constant or falling-head infiltration process has to be established. In the field, a constant-head single-ring infiltrometer often needs level-control setups or expensive devices with monitoring equipment containing proprietary technology with prohibitive costs [18–20]. Therefore, a falling-head experiment is preferable since it minimizes the complexity of implementation, characterizing an area of interest with minimal experimental efforts [11,21]. Recently, Nimmo et al. [11] developed the so-called bottomless bucket, named BB method hereafter, which uses a portable, falling-head, small-diameter single-ring infiltrometer. These authors adapted the Reynolds and Elrick (1990) formula to be applied instantaneously during a falling-head test. However, only few comparisons of BB estimates with other procedures can be found in the literature (e.g., [2,22]), notwithstanding that this method of soil hydraulic characterization is of noticeable practical interest. In general, establishing the reliability of new methods is not a simple task, also due to the high  $K_{fs}$  variability both in space and time [23,24]. Moreover, many other sources of variability may also arise when comparing different field measurement techniques, such as sample size [25], ring diameter [26], source shape [27] and field sampling procedure [28,29]. One could expect that considering laboratory measurements as targeted values would help to check the reliability of field data. However, this approach may be questioned due to the difficulty of representing the soil heterogeneity encountered in the field in small-scale laboratory samples (e.g., [24,30–33]). An alternative approach, considering different calculation techniques applied to the same dataset, is expected to facilitate the interpretation arising from the comparison [24]. Different methods of calculating  $K_{fs}$  from single-ring data were developed over time (e.g., [10–12,21,34–37]). Among them, the one ponding depth (OPD) calculation approach of Reynolds and Elrick [12] and Method 2 by Wu et al. [38] (WU2) have in common with the BB method that all these approaches analyze steady-state single-ring infiltrometer data, thus considering the same part of the infiltration process [24]. Moreover, they all require an estimate of the sorptive number (or macroscopic capillary length parameter),  $\alpha^*$  ( $L^{-1}$ ), expressing the relative importance of gravity and capillary forces during a ponding infiltration process [1].

The general objective of this work was to determine the  $K_{fs}$  of an abandoned unmanaged field affected by fire by means of single-ring infiltrometer runs and the use of transient and steady-state data analysis procedures. Sampling and measurements were carried out in 2012 and 2017 in a fire-affected (on 15 July) field (burnt site) and in a neighboring non-affected site (control site). The focus was put on the predictive potential of different data analysis procedures (i.e., transient and steady-state)

to yield proper  $K_{fs}$  estimates and to detect the effect of fire on saturated hydraulic conductivity. More specifically, we chose to test the bottomless bucket method by comparing the field-saturated soil hydraulic conductivity estimates with those obtained by other well-tested methods.

## 2. Theory

### 2.1. Steady-State Analysis of Single-Ring Infiltrometer Data

The bottomless bucket method of Nimmo et al. [11] considers the analysis developed by Reynolds and Elrick [12] of three-dimensional (3D), steady, ponded infiltration below a finite insertion depth, accounting for the hydrostatic pressure of the ponded water, gravity and capillarity of the unsaturated soil [1]. These authors adapted Reynolds and Elrick's (1990) formula to be applied instantaneously during a falling-head test. With this method,  $K_{fs}$  ( $L \cdot T^{-1}$ ) is calculated by the following equation:

$$K_{fs} = \frac{L_G}{t} \ln \left( \frac{L_G + \lambda_c + H_0}{L_G + \lambda_c + H} \right) \quad (1)$$

where  $H_0$  (L) is the initially established ponded depth of water,  $H(t)$  (L) is the ponded depth of water at time  $t$ ,  $\lambda_c$  (L) is the macroscopic capillary length of the soil [39], and the so-called ring installation scaling length,  $L_G$  (L), is calculated as follow:

$$L_G = 0.316\pi d + 0.184\pi r \quad (2)$$

where  $r$  (L) is the radius of the disk source and  $d$  (L) is the ring insertion depth in the soil.

The one ponding depth calculation approach by Reynolds and Elrick [12] makes use of the steady infiltrating flux,  $Q_s$  ( $L^3 \cdot T^{-1}$ ), which is estimated from the flow rate versus time plot. The following relationship is used to obtain  $K_{fs}$ :

$$K_{fs} = \frac{\alpha * \gamma_G Q_s}{r(\alpha * H + 1) + \gamma_G \alpha * \pi r^2} \quad (3)$$

where  $\gamma_G$  is a shape factor that can be estimated as follows:

$$\gamma_G = 0.316 \frac{d}{r} + 0.184 \quad (4)$$

Method 2 by Wu et al. [38] assumes steady-state infiltration. With this method,  $K_{fs}$  is calculated by the following equation:

$$K_{fs} = \frac{i_s}{af} \quad (5)$$

where  $i_s$  ( $L \cdot T^{-1}$ ) is the slope of the straight line fitted to the data describing steady-state conditions on the cumulative infiltration,  $I$  (L), versus time,  $t$  (T), relation,  $a$  is a dimensionless constant equal to 0.9084 [36], and  $f$  is a correction factor that depends on soil initial and boundary conditions and ring geometry:

$$f \cong \frac{H + 1/\alpha *}{G^*} + 1 \quad (6)$$

where the  $G^*$  (L) term is equal to:

$$G^* = d + \frac{r}{2} \quad (7)$$

### 2.2. Transient Analysis of Single-Ring Infiltrometer Data

For comparative purposes, Method 1 by Wu et al. [38] (WU1) was also applied to estimate  $K_{fs}$ . In addition, this method offered the possibility to check the assumed  $\alpha^*$  value by directly estimating this parameter from a single-ring test and a measurement of the soil water content. This method

is based on the assumption that the cumulative infiltration can be described by a relation formally identical to the two-term infiltration model by Philip [40]:

$$I = C_1\sqrt{t} + C_2t \quad (8)$$

where  $C_1$  ( $L \cdot T^{-0.5}$ ) and  $C_2$  ( $L \cdot T^{-1}$ ) are infiltration coefficients. With method 1,  $K_{fs}$  is calculated by the following equation:

$$K_{fs} = \frac{\lambda_c \Delta\theta}{T_c} \quad (9)$$

where  $\Delta\theta$  ( $L^3 \cdot L^{-3}$ ) is the difference between the saturated volumetric soil water content,  $\theta_s$  ( $L^3 \cdot L^{-3}$ ), and the initial one,  $\theta_i$  ( $L^3 \cdot L^{-3}$ ). The  $\lambda_c$  (L) and  $T_c$  (T) terms have the following expressions:

$$\lambda_c = \frac{1}{2} \left[ \sqrt{(H + G^*)^2 + 4G^*C} - (H + G^*) \right] \quad (10)$$

$$T_c = \frac{1}{4} \left( \frac{C_2 a}{b C_1} \right)^2 \quad (11)$$

where  $H$  (L) is the established ponding depth of water,  $G^*$  (L) is defined by Equation (7),  $a$  and  $b$  are dimensionless constants respectively equal to 0.9084 and 0.1682 [36], and the  $C$  (L) term is equal to:

$$C = \frac{1}{4\Delta\theta} \left( \frac{C_2}{b} \right)^2 \frac{a}{C_1} \quad (12)$$

An estimate of the sorptive number,  $\alpha^*$  ( $L^{-1}$ ), may also be obtained taking into account that:

$$\alpha^* = \frac{1}{\lambda_c} \quad (13)$$

For a given infiltration run we determined the  $C_1$  and  $C_2$  coefficients according to the fitting method referred to as cumulative linearization (CL, [41]). With the CL method, Equation (8) is linearized by dividing both sides by  $\sqrt{t}$ , giving:

$$\frac{I}{\sqrt{t}} = C_1 + C_2\sqrt{t} \quad (14)$$

Then, the  $C_1$  and  $C_2$  coefficients are determined respectively as the intercept and the slope of the  $I/\sqrt{t}$  vs.  $\sqrt{t}$  plot.

### 3. Materials and Methods

#### 3.1. Soil Sampling

We selected two study sites on abandoned fields within the “Serra de Mariola Natural Park” in Alcoi, Eastern Spain. The coordinates of the study area are  $38^\circ 43' 32.15''$  N,  $0^\circ 28' 54.70''$  W. Sampling and measurements were carried out in November 2012 and five years later, in November 2017, in a fire-affected (on 15 July) field (burnt site) and in a neighboring non-affected site (control site). The study area is characterised by typical Mediterranean climatic condition with drought from June till September, with high temperatures ( $25^\circ\text{C}$  in average), and mild spring, autumn and winter seasons. The mean annual rainfall at the nearby Cocentaina meteorological station is 480 mm, and during the study period the mean annual rainfall was 418 mm. The wettest year was 2012 with 576 mm and the driest 2014 with 209 mm. October used to be the month with the largest rainfall amount, although during the study period the wettest month was December 2015 with 295 mm, and the driest months were May 2017 and July 2014 with 0 mm of rainfall. Mean monthly rainfall data are reported in

Figure 1. The mean monthly temperature was 16.5 °C, with values in July of 28.3 °C and January with 7.0 °C. The vegetation cover was dominated by a scrubland developed after the abandonment that took place in 1950s. The main plant species were *Rosmarinus officinalis*, *Thymus vulgaris*, and *Ulex parviflorus*, and five years after the fire the vegetation was dominated by *Cistus albidus*, although *Rosmarinus officinalis* and *Ulex parviflorus* were also present.

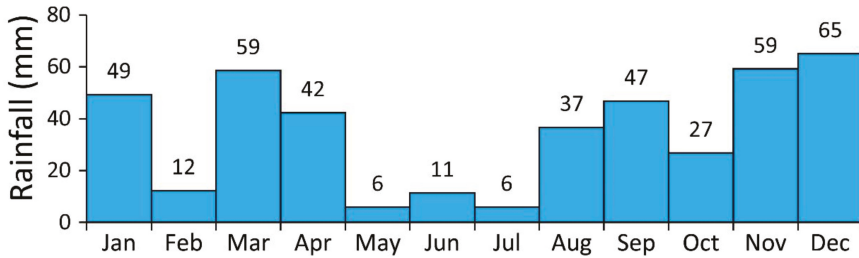


**Figure 1.** Mean monthly rainfall data recorded at the Cocentaina meteorological station during the study period (2012–2017).

The parent material is marls and the soils developed on this south-facing slope are very breakable. The soil is classified as a Typic Xerorthent [42]. According to the USDA standards, the three fractions, i.e., clay (0–2 µm), silt (2–50 µm) and sand (50–2000 µm), averaged for the two sites were 14.5%, 57.5% and 29.1%, respectively (corresponding standard deviations = 6.6, 4.3 and 5.0, respectively), and the soil of the studied area was classified as silt loam.

Plant cover was measured at each sampling point prior to infiltration experiments by measuring the presence (1) or absence (0) at 100 points regularly distributed in each 0.28 m<sup>2</sup> plot. Undisturbed soil cores were also collected at 0–60 mm soil depth. The cores were used to determine the soil bulk density,  $\rho_b$  (g·cm<sup>-3</sup>), and the initial volumetric soil water content,  $\theta_i$  (m<sup>3</sup>·m<sup>-3</sup>). According to other investigations, the saturated soil water content,  $\theta_s$  (m<sup>3</sup>·m<sup>-3</sup>), was approximated by total soil porosity, determined from bulk density  $\rho_b$  (e.g., [28,37,43–48]). Soil organic matter was determined by the Walkley-Black [49] method.

### 3.2. Single-Ring Infiltrometer

A total of forty infiltration runs (10 runs × 2 plots × 2 sampling campaigns) of the bottomless bucket type were carried out [11]. A 100-mm inner diameter ring was inserted into the soil to a depth of  $d = 50$  mm. At the start of the experiments, water was poured into the ring to establish an initial ponding depth  $H_0 = 50$  mm. In this investigation, the possible occurrence of soil water repellency was not considered, given that this phenomenon is uncommon for scrub terrain on calcareous soils in the region, even after fire [50,51]. Therefore, the use of ponding experiments, which are known to overwhelm positive soil-water-entry values induced by water repellency (e.g., [2,52–54]), was not expected to induce bias. The rate of drop of the water level was monitored by measuring the ponding depth at prescribed time intervals,  $H(t)$ . After each measurement, another volume of water was poured immediately into the ring to re-establish a ponded depth of water of 50 mm. During the first minutes, small time intervals were used. The time interval was increased up to 5 min in the late phase of the experiment. Steady-state conditions were attained within 60 min of all experiments. This procedure differs from the one proposed by Nimmo et al. [11], since these authors logged the time needed for the water to reach a minimum fixed  $H(t)$  value, thus pouring in known water volumes to re-establish the initial ponding depth. The obvious advantage to consider prescribed time intervals instead of a preselected water amount, is that monitoring time is significantly easier than monitoring water levels. Moreover, in their investigation Nimmo et al. [11] stated that the “modification of these

procedures is likely to be necessary for different soils and conditions". In our case, the sampled soils were characterized by low permeability. In such conditions, logging the time needed for the water to reach a minimum fixed  $H(t)$  value, such as the Nimmo's procedure, would imply obtaining less data points for the same duration of the experiment, or alternatively it would imply considerably extending the experiment duration to have a similar number of data points and, thus, to properly evaluate the steady-state phase of the infiltration process. Therefore, the applied criterion also allowed us to increase our confidence in the sampled data. A total of forty experimental cumulative infiltrations versus time were then deduced. Cumulative infiltration data were firstly analyzed according to the criterion suggested by Bagarello et al. [55]. Specifically, apparent steady-state infiltration rates were estimated by linear regression analysis of the last three  $(I, t)$  data points. Then, the equilibration time,  $t_s$  (min), namely the duration of the transient phase of the infiltration process, was determined as the first value for which:

$$\left| \frac{I - I_{reg}}{I} \right| \times 100 \leq E \tag{15}$$

where  $I_{reg}$  is estimated from the regression analysis of the  $I$  versus  $t$  plot, and  $E$  is a criterion to check linearity. Equation (15) is applied from the start of the experiment and progressively excludes the first data points until  $E \leq 2$  [1,24]. An illustrative example of the  $t_s$  estimation is reported in Figure 2.

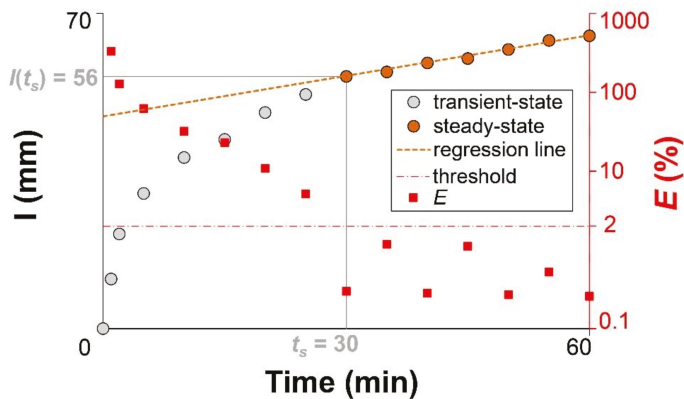


**Figure 2.** Procedure for estimating equilibration time,  $t_s$  (min), and infiltrated depth at the equilibration time,  $I(t_s)$  (mm), from cumulative infiltrations. Case of an infiltration run carried out at the burnt site in 2012.

### 3.3. Data Analysis and Calculations

The BB procedure was applied to determine  $K_{fs}$  ( $K_{fs-BB}$ ) by Equation (1), assuming  $\lambda_c = 1/\alpha^* = 0.25$  m. A value of  $\alpha^* = 4$  m<sup>-1</sup> for unstructured fine-textured soils (strong soil capillarity category) was selected from the soil texture–structure categories defined by Elrick and Reynolds [56]. The last determinations of  $K_{fs-BB}$ , representative of steady-state conditions, were averaged to obtain an estimate of  $K_{fs-BB}$  for a given test, as suggested by Angulo-Jaramillo et al. [1].

Equations (3) and (5) were applied to estimate  $K_{fs}$  data, which were denoted with the symbols  $K_{fs-WU2}$  and  $K_{fs-OPD}$ , for WU2 and OPD, respectively. It has to be noted that these latter methods are theoretically usable for a constant ponded depth of water on the infiltration surface. However, in our case, the variation of the water level during the late-phase of the infiltration process never exceeded 1–2 mm. Therefore, the ponded depth at the late-phase of the run was assumed to be practically constant.

For comparative purposes, the transient WU1 method was also applied to estimate  $K_{fs}$  and  $\alpha^*$  by Equations (9) and (13), respectively. These estimates were denoted with the symbols  $K_{fs-WU1-CL}$  and  $\alpha^*_{CL}$ . We first obtained the  $C_1$  and  $C_2$  values with the CL method by fitting Equation (14). The adequacy of the fitting procedure was evaluated by checking both the linearity of the data and the relative error defined as:

$$Er = 100 \times \sqrt{\frac{\sum_{i=1}^n (x_i^{\text{exp}} - x_i)^2}{\sum_{i=1}^n (x_i^{\text{exp}})^2}} \quad (i = 1..n) \quad (16)$$

where  $x_i^{\text{exp}}$  are the experimental data and  $x_i$  are the corresponding values deduced by fitting the functional relationship. According to the criterion proposed by Lassabatere et al. [10], values of  $Er < 5\%$  were assumed to be indicative of a satisfactory fitting ability.

The statistical frequency distributions of the  $K_{fs}$  and  $\alpha^*$  data were assumed to be lognormal, as is common for these variables (e.g., [57,58]). Therefore, geometric means and associated coefficients of variation, CV, were calculated using the appropriate “log-normal equations” [59]. The other variables considered in this investigation were summarized by calculating the arithmetic mean and the associated CV, since the characterization of an area of interest is generally based on arithmetic averages of individual determinations [60]. To compare mean values, untransformed and natural log-transformed data were used for the normal and the natural log-normal distributed variables, respectively. Different  $K_{fs}$  datasets were also compared in terms of factors of difference (FoD), calculated as the ratio between the maximum and minimum of two  $K_{fs}$  values estimated by different calculation techniques from a run [24]. Following Elrick and Reynolds [56], FoD values not exceeding a factor of two or three were considered indicative of similar estimates.

## 4. Results

### 4.1. Physical Properties

The results of the physical analysis were represented using box plot graphics (Figure 3). A major effect of fire was a consistent reduction of soil organic matter in the burnt site. SOM was measured to decrease by 22% four months after the fire, and 30% after five years. This reduction was in line with previous investigations (e.g., [3,61–63]). As a consequence, dryer conditions persisted in the burnt site, due to the known effect of a reduction of soil organic matter on soil water retention [64]. Specifically, the initial soil water content differed appreciably among the control and burnt sites, with average  $\theta_i$  values equal to 0.141 and 0.137  $\text{m}^3 \cdot \text{m}^{-3}$  at the control site and 0.096 and 0.087  $\text{m}^3 \cdot \text{m}^{-3}$  at the burnt site, for the 2012 and 2017 sampling campaigns, respectively. No significant differences in terms of soil dry bulk density were detected between the control and burnt sites four months after the fire. On the contrary, our results showed a significant increase of the bulk density five years after the fire, due probably to a progressive collapse of aggregates [9], highlighting a certain degree of soil degradation at the burnt site.

### 4.2. Performance of the Cumulative Linearization (CL) Method

The application of the transient WU1 method to determine  $K_{fs}$  and  $\alpha^*$  required the estimation of the  $C_1$  and  $C_2$  coefficients. We obtained the  $C_1$  and  $C_2$  values with the CL fitting method. This method showed general poor performance both in terms of the linearity of the data and the relative error. The  $\Delta I / \Delta \sqrt{t}$  vs.  $\sqrt{t}$  plots did not show the expected linear relationship between the considered variables for the entire infiltration run. Therefore, we progressively excluded the first data points selecting the  $C_1$  and  $C_2$  values when the following criteria were fulfilled: (i) positive values of the  $C_2$  parameter (yielding physically plausible  $K_{fs}$  estimates i.e.,  $K_{fs} > 0$ ); and (ii) a linear relationship between the considered variables. An example of the applied selection procedure for the infiltration coefficients is depicted in Figure 4. The example refers to the case of an infiltration run carried out at

the burnt site in 2017. The exclusion of no or one data point yielded negative  $C_2$  values (Figure 4a,b). The exclusion of two data points yielded a positive  $C_2$  value, but a value of  $Er = 6.6\%$  was obtained due to the departure of the first point from the general linear behaviour (Figure 4c). In this case, the  $C_2$  coefficient should make it possible to obtain an apparently physically plausible  $K_{fs}$  estimate, i.e.,  $K_{fs} > 0$ . However, given that the dataset was not linear, Equation (8) was considered inappropriate and hence the fitted parameters were considered as meaningless from a physical point of view [65]. Finally, the  $C_1$  and  $C_2$  coefficients could be properly estimated by excluding the first three data points (Figure 4d). Other investigations also suggested removing the fitting procedures the early stage of the infiltration process when a perturbation occurs (e.g., [21,38,46,66]). In contrast, the last points may be removed since the CL method mostly applies to the transient state [65,67]. Only one test never yielded positive  $C_2$  values whatever the number of data points excluded. Good fits, i.e., fitting yielding  $Er$  values lower than 5% [10], were only obtained in 23% of the cases (Figure 5).

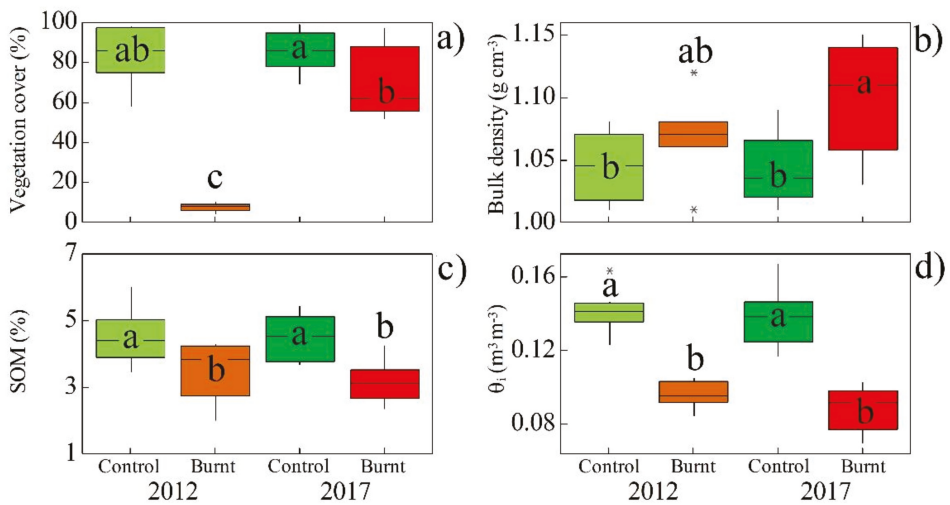


**Figure 3.** Box plots of the (a) vegetation cover (%), (b) soil bulk density ( $\text{g}\cdot\text{cm}^{-3}$ ), (c) soil organic matter, (SOM) (%), and (d) initial volumetric soil water content,  $\theta_i$  ( $\text{m}^3\cdot\text{m}^{-3}$ ), for the four scenarios. Asterisks denote outliers. Different letters represent significant differences at  $p < 0.05$ .

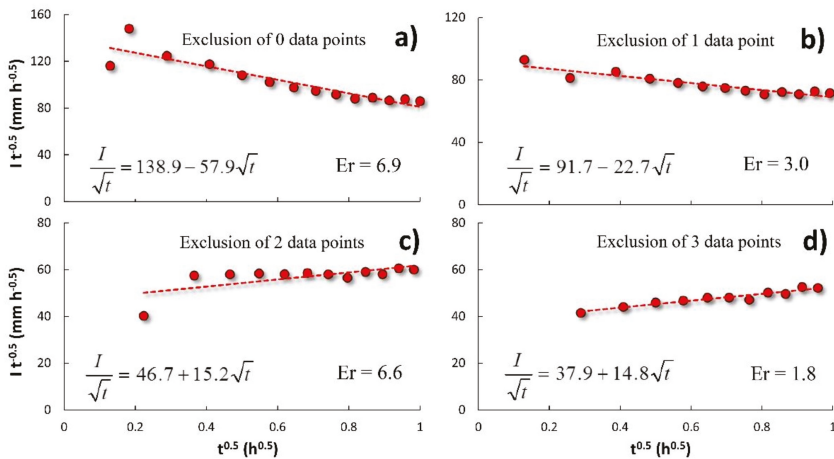


**Figure 4.** Examples of the estimation of the  $C_1$  ( $\text{mm}\cdot\text{h}^{-0.5}$ ) and  $C_2$  ( $\text{mm}\cdot\text{h}^{-1}$ ) parameters by the cumulative linearization (CL) approach excluding a different number of data points of an infiltration run carried out at the burnt site in 2017. The values of the ratio between the cumulative infiltration,  $I$  (mm), and the square root of time,  $t$  (h), are plotted against the square root of  $t$ . (a) Exclusion of zero data points:  $C_2 < 0$ . (b) Exclusion of one data point: Lower  $Er$  value (3.0%) but  $C_2 < 0$ . (c) Exclusion of two data points:  $C_2 > 0$  but  $Er = 6.6\%$ . (d) Exclusion of three data points:  $C_2 > 0$  and lowest  $Er$  value (1.8%; selected case).

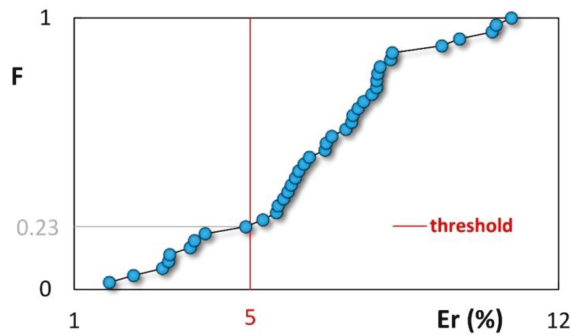


**Figure 5.** Cumulative frequency distribution of the relative errors,  $Er$  (%), of the fitting of the functional relationship (i.e., Equation (14)) for the CL method to the experimental data.  $Er$  values not exceeding 5% denote a satisfactory fitting ability of the infiltration model to the data [10].

#### 4.3. Estimation of $K_{fs}$ Data with the WU1 Method

Table 1 summarizes the field-saturated soil hydraulic conductivity obtained with the WU1 method. The average  $K_{fs-WU1-CL}$  values ranged from 0.87 to 1.50  $\text{mm}\cdot\text{h}^{-1}$ . All average  $K_{fs}$  values were lower than the expected saturated conductivity on the basis of the soil textural characteristics alone, e.g.,  $K_s = 4.5 \text{ mm}\cdot\text{h}^{-1}$  for a silt loam soil according to Carsel and Parrish [68]. This suggested that soil macroporosity in the control and burnt site did not influence the results [28]. All differences between the average  $K_{fs}$  values of different sites and sampling campaigns were not statistically significant according to the Tukey honestly significant difference test ( $p < 0.05$ ). A high variability of  $K_{fs}$  was detected in most cases, with coefficient of variations (CVs) ranging from 100.7% to 373.1% (Table 1).

The average  $\alpha^*_{CL}$  values ranged from 2.42 to 6.45  $m^{-1}$  (Table 2). We never detected extremely unreliable  $\alpha^*$  values, i.e., lower than 0.1  $m^{-1}$  and higher than 1000  $m^{-1}$  [56,69]. All differences between the average  $\alpha^*_{CL}$  values of different sites and sampling campaigns were not statistically significant according to the Tukey honestly significant difference test ( $p < 0.05$ ). Considering all the infiltration measurements, the average  $\alpha^*_{CL}$  value was equal to 3.89  $m^{-1}$ . This value was in line with the one suggested by Elrick and Reynolds [56] for strong capillarity soils ( $\alpha^* = 4 m^{-1}$ ) in their soil texture–structure categories.

**Table 1.** Summary of the field-saturated hydraulic conductivity,  $K_{fs}$  ( $mm \cdot h^{-1}$ ), values obtained by the WU1 method for each sampling campaign and site.

Variable	Year	Site	Statistic				
			N	min	max	mean	CV
$K_{sf-WU-CL}$	2012	Control	10	0.18	5.36	1.11	211.8
		Burnt	10	0.04	8.17	0.87	373.1
	2017	Control	10	0.17	2.85	0.91	100.7
		Burnt	9	0.28	7.73	1.50	158.0

All differences between two mean values were not statistically significant according to the Tukey honestly significant difference test ( $p < 0.05$ ).

**Table 2.** Summary of the  $\alpha^*_{CL}$  ( $m^{-1}$ ) values obtained by the WU1 method for each sampling campaign and site.

Variable	Year	Site	Statistic				
			N	min	max	mean	CV
$\alpha^*_{CL}$	2012	Control	10	0.90	79.99	6.45	436.8
		Burnt	10	0.74	21.29	2.94	131.7
	2017	Control	10	0.85	27.25	2.42	117.8
		Burnt	9	1.12	16.71	5.16	109.1

All differences between two mean values were not statistically significant according to the Tukey honestly significant difference test ( $p < 0.05$ ).

#### 4.4. Estimation of $K_{fs}$ Data with Steady-State Methods

We discriminated the transient and steady-state phase of the infiltration process according to the criterion suggested by Bagarello et al. [55] (Figure 2). This procedure allowed us to consider, for a given run, exactly the same final part of the curve for all the three applied methods. After a duration of 60 min, the total infiltrated depth was, on average, 64 mm. The equilibration time,  $t_s$  (min), namely the duration of the transient phase of the infiltration process, was reached, on average, after 33 min, with a mean volume of infiltrated water  $I(t_s) = 56$  mm. All the experiments exhibited a sufficiently long steady-state phase ranging from 10 to 45 min (Table 3).

**Table 3.** Summary of the equilibration time,  $t_s$  (min), and infiltrated depth at the equilibration time,  $I(t_s)$  (mm). Sample size,  $N = 10$  for each site and sampling campaign.

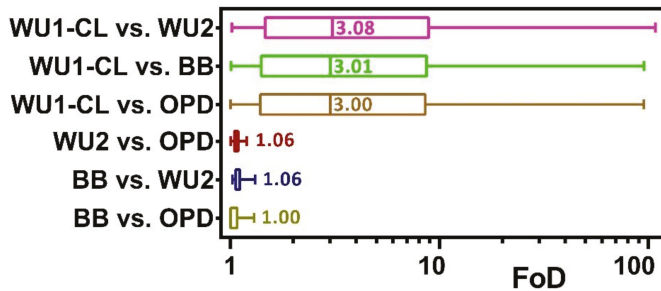
Variable	Year	Site	Statistic			
			min	max	mean	CV
$t_s$ (min)	2012	Control	25	40	30.5	12.1
		Burnt	25	45	35.0	22.3
	2017	Control	20	50	33.5	29.9
		Burnt	15	45	32.5	32.6
$I(t_s)$ (mm)	2012	Control	29	86	61.9	22.0
		Burnt	36	59	49.8	17.2
	2017	Control	53	84	64.1	17.1
		Burnt	19	71	49.3	40.6

Table 4 summarizes the field-saturated soil hydraulic conductivity,  $K_{fs}$ , obtained with the BB, OPD and WU2 methods. The average  $K_{fs-BB}$ ,  $K_{fs-OPD}$  and  $K_{fs-WU2}$  values ranged from 2.0 to 3.96, from 2.03 to 4.21 and from 1.92 to 3.91  $\text{mm}\cdot\text{h}^{-1}$ , respectively. The applied methods yielded similar information, i.e., the differences between average  $K_{fs}$  values of the control site were never statistically significant at  $p < 0.05$ . On the contrary, for the burnt site, the field campaign carried out in 2017 yielded, in all cases, two times lower  $K_{fs}$  values than the previous campaign, and the differences between sampling campaigns were always statistically significant at  $p < 0.05$  (Table 4). Figure 6 depicts the box plots of the factor of difference values, i.e., a “point-by-point” comparison between all  $K_{fs}$  datasets. FoD values never exceeded 1.3 between steady-state methods. Therefore, the three steady-state methods considered in this investigation yielded similar results, supporting the soundness of the BB analysis procedure. On the contrary, appreciably higher FoD values were obtained with the WU1 method (Figure 6). In this case, the high variability of the data affected  $K_{fs}$  comparisons between sites and sampling campaigns (Table 1).

**Table 4.** Summary of the field-saturated hydraulic conductivity,  $K_{fs}$  ( $\text{mm}\cdot\text{h}^{-1}$ ), data sets obtained by the BB, WU2, and OPD methods. Sample size,  $N = 10$  for each site and sampling campaign.

Variable	Year	Site	Statistic			
			min	max	mean	CV
$K_{sf-BB}$	2012	Control	1.52	4.99	3.04 AB	45.4
		Burnt	2.49	4.99	3.96 A	19.5
	2017	Control	2.18	5.35	3.62 A	31.6
		Burnt	0.83	8.01	2.00 B	68.7
$K_{sf-WU2}$	2012	Control	1.34	5.28	2.95 AB	59.5
		Burnt	2.64	5.16	4.21 A	20.6
	2017	Control	2.00	5.82	3.57 AB	39.1
		Burnt	0.88	8.91	2.03 B	74.7
$K_{sf-OPD}$	2012	Control	1.24	4.98	2.85 AB	56.2
		Burnt	2.49	4.98	3.91 A	19.9
	2017	Control	1.99	5.34	3.44 A	35.0
		Burnt	0.83	7.97	1.92 B	71.8

For a given method (BB, WU2 and OPD), means that do not share a letter are significantly different according to the Tukey honestly significant difference test ( $p < 0.05$ ).



**Figure 6.** Box plots of the factor of difference, FoD, between the field-saturated hydraulic conductivity,  $K_{fs}$  ( $\text{mm}\cdot\text{h}^{-1}$ ), data sets obtained by the BB, WU2, and OPD methods and the WU1 method with the cumulative linearization (CL) fitting method. The median values are also reported.

## 5. Discussion

Under the specific conditions encountered in this investigation, the transient analysis of single-ring data revealed that alternative procedures should be applied to properly analyze infiltration data, in order to avoid a misestimation of the soil hydraulic properties [66]. Specifically, the main reason for choosing other approaches was that invalid early data were detected in most cases with the CL method, and hence they were excluded from the analysis. The need to exclude the first data points when fitting the data was likely due to the highly sorptive nature of the sampled soils. Specifically, the porous media exhibited relatively low hydraulic conductivity compared to their sorptive capacity [37]. Indeed, cumulative infiltrations exhibited a marked concave part corresponding to the transient state and a linear part at the end of the curves related to the steady state [70]. This condition also made it difficult to estimate  $C_1$  values due to the importance of the lateral capillary flow [65]. As a result, a reliable estimation of  $K_{fs}$  was unlikely. In other words, the generally poor performance of the fitting method spoiled the soil hydraulic characterization, affecting the general quality of the  $K_{fs}$  estimates and, thus, the comparison between the sampled sites and field campaigns. Indeed, this method relies on an infiltration model, i.e., Equation (8), that does not account for such a time evolution of soil properties between the early- and late-time infiltration stages responsible for the observed strong concavity of cumulative curves [71]. Moreover, it has to be remarked that the transient portion of the infiltration curves is frequently not usable to estimate steady-state infiltration rates, since it could be affected by several factors, including soil permeability, antecedent soil water content, ring radius and insertion depth (e.g., [1,13,21]). Although the poor performance of the CL method likely affected the reliability of the WU1 estimates, by increasing parameter variability, it has to be noted that the WU1 method allowed at least a check of the  $\alpha^*$  value, which was selected a priori from the soil texture–structure categories to apply steady-state methods.

All steady-state methods revealed a slight but statistically significant  $K_{fs}$  decrease five years after the fire. These methods, with a characterization based exclusively on a stabilized infiltration process, yielded an appreciably lower variability of  $K_{fs}$  data compared to the WU1 method (Table 1). Steady-state methods were expected to give less variable  $K_{fs}$  estimates when compared to WU1, also as a consequence of the use of a fixed  $\alpha^*$  value for the whole field, whereas variations of this parameter exist in the field depending on the texture and structure [1]. On the other hand, this assumption substantially facilitated the hydraulic characterization, yielding at the same time a sufficient level of accuracy for determining  $K_{fs}$  (e.g., [11,15,38]).

The considered soil properties unanimously highlighted the deterioration of the soil's physical quality after the fire. The results of this study suggested that the soil was not completely recovered five years after fire, and the negative effects resulting from the vegetation burning and soil organic matter removal have not yet been mitigated. One would expect that the degraded soil, i.e., with lower organic

matter and higher bulk density, could be more prone to runoff and erosion processes than the unburned soil [72]. However, despite common perceptions, Mediterranean vegetation adapts to fire and plant recolonization in burnt areas relatively quickly (e.g., [3,73,74]). According to many authors, vegetation recovering promptly reduces post-fire runoff and soil erosion rates (e.g., [75,76]). For instance, Cerdà and Doerr [9] observed, under Mediterranean environmental conditions, a fast recovery (2–4 years) of the terrain to pre-fire erosion rates. In our investigation, vegetation recovery, reaching 70% in 2017, could have had an effective role in preventing soil erosion. In other words, the prompt recovery of the vegetation cover may have mitigated the impacts of the worsening soil quality on erosion rates. In the future, erosion-focused studies may support the above hypothesis, increasing our understanding of the effects of soil impoverishment on erosion processes at the burnt sites.

## 6. Summary and Conclusions

In this study we analyzed changes in physical and hydrological soil properties few months and five years after a fire in a semi-arid environment in Eastern Spain. With this aim, we sampled both a burned and an unburned site and compared transient and steady-state analysis of single-ring infiltrometer data. The bottomless bucket method of Nimmo et al. [11] was selected in conjunction with other well-tested methods to estimate the field-saturated soil hydraulic conductivity. Any of the tested infiltration techniques appeared usable to obtain the order of magnitude of  $K_{fs}$  at the field sites. However, with the WU1 method, the variability in  $K_{fs}$  made it difficult to draw conclusions regarding the changes in the fire-affected soil. The choice of the method of soil hydraulic characterization led to contrasting conclusions, thus highlighting the need to choose the appropriate techniques. All the applied steady-state methods appeared more appropriate to detect and quantify slight changes in  $K_{fs}$ , whereas WU1 allowed at least a check of the selected  $\alpha^*$  value. Our results showed a certain degree of soil degradation at the burnt site with an immediate reduction of the soil organic matter and a progressive increase of the soil bulk density during the five years following the fire. This general impoverishment resulted in a slight but significant decrease of the field-saturated soil hydraulic conductivity. A main implication of these results is the importance of long-term investigations of fire effects, since shorter-term studies may not always be sufficient for detecting and characterizing changes to the hydrological processes caused by a fire. This investigation also yielded encouraging signs on the applicability of the bottomless bucket method for a plausible estimation of  $K_{fs}$ . The comparison with other steady-state methods and the similarity of the results support this assessment.

**Acknowledgments:** The research leading to these results received funding from the POSTFIRE Project (CGL2013-47862-C2-1 and 2-R) and POSTFIRE\_CARE Project (CGL2016-75178-C2-2-R). S.D.P. thanks M.J.K. for his contribution to keep the spirit up.

**Author Contributions:** All authors equally contributed to analyze the data, discuss the results, and write the manuscript.

**Conflicts of Interest:** The authors declare no conflict of interest.

## References

1. Angulo-Jaramillo, R.; Bagarello, V.; Iovino, M.; Lassabatère, L. *Infiltration Measurements for Soil Hydraulic Characterization*; Springer International Publishing: New York, NY, USA, 2016; ISBN 978-3-319-31786-1.
2. Ebel, B.A.; Moody, J.A.; Martin, D.A. Hydrologic conditions controlling runoff generation immediately after wildfire. *Water Resour. Res.* **2012**, *48*, W03529. [[CrossRef](#)]
3. Certini, G. Effects of fire on properties of forest soils: A review. *Oecologia* **2005**, *143*, 1–10. [[CrossRef](#)] [[PubMed](#)]
4. Mataix-Solera, J.; Cerdà, A.; Arcenegui, V.; Jordán, A.; Zavala, L.M. Fire effects on soil aggregation: A review. *Earth-Sci. Rev.* **2011**, *109*, 44–60. [[CrossRef](#)]
5. Keesstra, S.; Wittenberg, L.; Maroulis, J.; Sambalino, F.; Malkinson, D.; Cerdà, A.; Pereira, P. The influence of fire history, plant species and post-fire management on soil water repellency in a Mediterranean catchment: The Mount Carmel range, Israel. *CATENA* **2017**, *149*, 857–866. [[CrossRef](#)]

6. Cerdà, A. Changes in overland flow and infiltration after a rangeland fire in a Mediterranean scrubland. *Hydrol. Process.* **1998**, *12*, 1031–1042. [[CrossRef](#)]
7. Novara, A.; Gristina, L.; Bodì, M.B.; Cerdà, A. The impact of fire on redistribution of soil organic matter on a mediterranean hillslope under maquia vegetation type. *Land Degrad. Dev.* **2011**, *22*, 530–536. [[CrossRef](#)]
8. Pereira, P.; Cerdà, A.; Úbeda, X.; Mataix-Solera, J.; Arcenegui, V.; Zavala, L.M. Modelling the Impacts of Wildfire on Ash Thickness in a Short-Term Period. *Land Degrad. Dev.* **2015**, *26*, 180–192. [[CrossRef](#)]
9. Cerdà, A.; Doerr, S.H. Influence of vegetation recovery on soil hydrology and erodibility following fire: An 11-year investigation. *Int. J. Wildland Fire* **2005**, *14*, 423–437. [[CrossRef](#)]
10. Lassabatere, L.; Angulo-Jaramillo, R.; Soria Ugalde, J.M.; Cuenca, R.; Braud, I.; Haverkamp, R. Beerkan estimation of soil transfer parameters through infiltration experiments—BEST. *Soil Sci. Soc. Am. J.* **2006**, *70*, 521. [[CrossRef](#)]
11. Nimmo, J.R.; Schmidt, K.M.; Perkins, K.S.; Stock, J.D. Rapid Measurement of Field-Saturated Hydraulic Conductivity for Areal Characterization. *Vadose Zone J.* **2009**, *8*, 142. [[CrossRef](#)]
12. Reynolds, W.D.; Elrick, D.E. Ponded Infiltration from a Single Ring: I. Analysis of Steady Flow. *Soil Sci. Soc. Am. J.* **1990**, *54*, 1233. [[CrossRef](#)]
13. Reynolds, W.D. Saturated hydraulic conductivity: Field measurement. In *Soil Sampling and Methods of Analysis*; Carter, M.R., Ed.; Canadian Society of Soil Science, Lewis Publishers: Boca Raton, FL, USA, 1993; pp. 599–613.
14. Ciollaro, G.; Lamaddalena, N. Effect of tillage on the hydraulic properties of a vertic soil. *J. Agric. Eng. Res.* **1998**, *71*, 147–155. [[CrossRef](#)]
15. Bagarello, V.; Iovino, M.; Elrick, D. A Simplified Falling-Head Technique for Rapid Determination of Field-Saturated Hydraulic Conductivity. *Soil Sci. Soc. Am. J.* **2004**, *68*, 66. [[CrossRef](#)]
16. Bagarello, V.; Baiamonte, G.; Castellini, M.; Di Prima, S.; Iovino, M. A comparison between the single ring pressure infiltrometer and simplified falling head techniques. *Hydrol. Process.* **2014**, *28*, 4843–4853. [[CrossRef](#)]
17. Gonzalez-Sosa, E.; Braud, I.; Dehotin, J.; Lassabatère, L.; Angulo-Jaramillo, R.; Lagouy, M.; Branger, F.; Jacqueminet, C.; Kermadi, S.; Michel, K. Impact of land use on the hydraulic properties of the topsoil in a small French catchment. *Hydrol. Process.* **2010**, *24*, 2382–2399. [[CrossRef](#)]
18. Fisher, D.K.; Gould, P.J. Open-Source Hardware Is a Low-Cost Alternative for Scientific Instrumentation and Research. *Mod. Instrum.* **2012**, *01*, 8–20. [[CrossRef](#)]
19. Di Prima, S. Automated single ring infiltrometer with a low-cost microcontroller circuit. *Comput. Electron. Agric.* **2015**, *118*, 390–395. [[CrossRef](#)]
20. Fisher, D.K.; Fletcher, R.S.; Anapalli, S.S.; Iii, H.C.P. Development of an Open-Source Cloud-Connected Sensor-Monitoring Platform. *Adv. Internet Things* **2017**, *8*, 1. [[CrossRef](#)]
21. Bagarello, V.; Di Prima, S.; Iovino, M.; Provenzano, G. Estimating field-saturated soil hydraulic conductivity by a simplified Beerkan infiltration experiment. *Hydrol. Process.* **2014**, *28*, 1095–1103. [[CrossRef](#)]
22. Alagna, V.; Bagarello, V.; Di Prima, S.; Iovino, M. Determining hydraulic properties of a loam soil by alternative infiltrometer techniques. *Hydrol. Process.* **2016**, *30*, 263–275. [[CrossRef](#)]
23. Bagarello, V.; Di Prima, S.; Iovino, M. Comparing Alternative Algorithms to Analyze the Beerkan Infiltration Experiment. *Soil Sci. Soc. Am. J.* **2014**, *78*, 724. [[CrossRef](#)]
24. Bagarello, V.; Di Prima, S.; Iovino, M. Estimating saturated soil hydraulic conductivity by the near steady-state phase of a Beerkan infiltration test. *Geoderma* **2017**, *303*, 70–77. [[CrossRef](#)]
25. Pachepsky, Y.A.; Guber, A.K.; Yakirevich, A.M.; McKee, L.; Cady, R.E.; Nicholson, T.J. Scaling and Pedotransfer in Numerical Simulations of Flow and Transport in Soils. *Vadose Zone J.* **2014**, *13*. [[CrossRef](#)]
26. Khodaverdiloo, H.; Khani Cheraghbadal, H.; Bagarello, V.; Iovino, M.; Asgarzadeh, H.; Ghorbani Dashtaki, S. Ring diameter effects on determination of field-saturated hydraulic conductivity of different loam soils. *Geoderma* **2017**, *303*, 60–69. [[CrossRef](#)]
27. Bagarello, V.; Santis, A.D.; Giordano, G.; Iovino, M. Source shape and data analysis procedure effects on hydraulic conductivity of a sandy-loam soil determined by ponding infiltration runs. *J. Agric. Eng.* **2017**, *48*, 71–80. [[CrossRef](#)]
28. Di Prima, S.; Bagarello, V.; Lassabatere, L.; Angulo-Jaramillo, R.; Bautista, I.; Burguet, M.; Cerdà, A.; Iovino, M.; Prosdocimi, M. Comparing Beerkan infiltration tests with rainfall simulation experiments for hydraulic characterization of a sandy-loam soil. *Hydrol. Process.* **2017**, *31*, 3520–3532. [[CrossRef](#)]

29. Di Prima, S.; Concialdi, P.; Lassabatère, L.; Angulo Jaramillo, R.; Pirastru, M.; Cerda, A.; Keesstra, S. Laboratory testing of Beerkan infiltration experiments for assessing the role of soil sealing on water infiltration. *CATENA* **2018**, submitted.
30. Haverkamp, R.; Bouraoui, F.; Zammit, C.; Angulo-Jaramillo, R. Soil properties and moisture movement in the unsaturated zone. In *The Handbook of Groundwater Engineering*, 3rd ed.; Taylor & Francis Group: Boca Raton, FL, USA, 1999.
31. Brooks, E.S.; Boll, J.; McDaniel, P.A. A hillslope-scale experiment to measure lateral saturated hydraulic conductivity. *Water Resour. Res.* **2004**, *40*, W04208. [[CrossRef](#)]
32. Castellini, M.; Di Prima, S.; Iovino, M. An assessment of the BEST procedure to estimate the soil water retention curve: A comparison with the evaporation method. *Geoderma* **2018**, *320*, 82–94. [[CrossRef](#)]
33. Di Prima, S.; Marrosu, R.; Lassabatere, L.; Angulo Jaramillo, R.; Pirastru, M. Determination of lateral preferential flow by combining plot- and point-scale infiltration experiments on a hillslope. *J. Hydrol.* **2018**, submitted.
34. Bagarello, V.; Castellini, M.; Di Prima, S.; Giordano, G.; Iovino, M. Testing a Simplified Approach to Determine Field Saturated Soil Hydraulic Conductivity. *Procedia Environ. Sci.* **2013**, *19*, 599–608. [[CrossRef](#)]
35. Touma, J.; Voltz, M.; Albergel, J. Determining soil saturated hydraulic conductivity and sorptivity from single ring infiltration tests. *Eur. J. Soil Sci.* **2007**, *58*, 229–238. [[CrossRef](#)]
36. Wu, L.; Pan, L. A generalized solution to infiltration from single-ring infiltrometers by scaling. *Soil Sci. Soc. Am. J.* **1997**, *61*, 1318–1322. [[CrossRef](#)]
37. Yilmaz, D.; Lassabatere, L.; Angulo-Jaramillo, R.; Deneele, D.; Legret, M. Hydrodynamic Characterization of Basic Oxygen Furnace Slag through an Adapted BEST Method. *Vadose Zone J.* **2010**, *9*, 107. [[CrossRef](#)]
38. Wu, L.; Pan, L.; Mitchell, J.; Sanden, B. Measuring Saturated Hydraulic Conductivity using a Generalized Solution for Single-Ring Infiltrometers. *Soil Sci. Soc. Am. J.* **1999**, *63*, 788. [[CrossRef](#)]
39. White, I.; Sully, M.J. Macroscopic and microscopic capillary length and time scales from field infiltration. *Water Resour. Res.* **1987**, *23*, 1514–1522. [[CrossRef](#)]
40. Philip, J. The theory of infiltration: 4. Sorptivity and algebraic infiltration equations. *Soil Sci.* **1957**, *84*, 257–264. [[CrossRef](#)]
41. Smiles, D.; Knight, J. A note on the use of the Philip infiltration equation. *Soil Res.* **1976**, *14*, 103–108. [[CrossRef](#)]
42. Soil Survey Staff. *Keys to Soil Taxonomy*, 12th ed.; USDA-Natural Resources Conservation Service: Washington, DC, USA, 2014.
43. Di Prima, S.; Rodrigo-Comino, J.; Novara, A.; Iovino, M.; Pirastru, M.; Keesstra, S.; Cerda, A. Assessing soil physical quality of citrus orchards under tillage, herbicide and organic managements. *Pedosphere*. in press.
44. Mubarak, I.; Mailhol, J.C.; Angulo-Jaramillo, R.; Ruelle, P.; Boivin, P.; Khaledian, M. Temporal variability in soil hydraulic properties under drip irrigation. *Geoderma* **2009**, *150*, 158–165. [[CrossRef](#)]
45. Xu, X.; Kiely, G.; Lewis, C. Estimation and analysis of soil hydraulic properties through infiltration experiments: Comparison of BEST and DL fitting methods. *Soil Use Manag.* **2009**, *25*, 354–361. [[CrossRef](#)]
46. Bagarello, V.; Di Prima, S.; Iovino, M.; Provenzano, G.; Sgroi, A. Testing different approaches to characterize Burundian soils by the BEST procedure. *Geoderma* **2011**, *162*, 141–150. [[CrossRef](#)]
47. Alagna, V.; Bagarello, V.; Di Prima, S.; Giordano, G.; Iovino, M. Testing infiltration run effects on the estimated water transmission properties of a sandy-loam soil. *Geoderma* **2016**, *267*, 24–33. [[CrossRef](#)]
48. Alagna, V.; Di Prima, S.; Rodrigo-Comino, J.; Iovino, M.; Pirastru, M.; Keesstra, S.D.; Novara, A.; Cerda, A. The Impact of the Age of Vines on Soil Hydraulic Conductivity in Vineyards in Eastern Spain. *Water* **2017**, *10*, 14. [[CrossRef](#)]
49. Walkley, A.; Black, I.A. An examination of the Degtjareff method for determining soil organic matter, and a proposed modification of the chromic acid titration method. *Soil Sci.* **1934**, *37*, 29–38. [[CrossRef](#)]
50. Mataix-Solera, J.; Doerr, S. Hydrophobicity and aggregate stability in calcareous topsoils from fire-affected pine forests in southeastern Spain. *Geoderma* **2004**, *118*, 77–88. [[CrossRef](#)]
51. Cerda, A.; Doerr, S.H. Soil wettability, runoff and erodibility of major dry-Mediterranean land use types on calcareous soils. *Hydrol. Process.* **2007**, *21*, 2325–2336. [[CrossRef](#)]
52. Wang, Z.; Wu, L.; Wu, Q.J. Water-entry value as an alternative indicator of soil water-repellency and wettability. *J. Hydrol.* **2000**, *231–232*, 76–83. [[CrossRef](#)]

53. Alagna, V.; Iovino, M.; Bagarello, V.; Mataix-Solera, J.; Lichner, L. Application of minidisk infiltrometer to estimate water repellency in Mediterranean pine forest soils. *J. Hydrol. Hydromech.* **2017**, *65*. [[CrossRef](#)]
54. Di Prima, S.; Bagarello, V.; Angulo-Jaramillo, R.; Bautista, I.; Cerdà, A.; del Campo, A.; González-Sanchis, M.; Iovino, M.; Lassabatere, L.; Maetzke, F. Impacts of thinning of a Mediterranean oak forest on soil properties influencing water infiltration. *J. Hydrol. Hydromech.* **2017**, *65*, 276–286. [[CrossRef](#)]
55. Bagarello, V.; Iovino, M.; Reynolds, W. Measuring hydraulic conductivity in a cracking clay soil using the Guelph permeameter. *Trans. ASAE* **1999**, *42*, 957–964. [[CrossRef](#)]
56. Elrick, D.E.; Reynolds, W.D. Methods for analyzing constant-head well permeameter data. *Soil Sci. Soc. Am. J.* **1992**, *56*, 320. [[CrossRef](#)]
57. Mohanty, B.P.; Kanwar, R.S.; Everts, C.J. Comparison of saturated hydraulic conductivity measurement methods for a glacial-till soil. *Soil Sci. Soc. Am. J.* **1994**, *58*, 672–677. [[CrossRef](#)]
58. Warrick, A.W. Spatial variability. In *Environmental Soil Physics*; Hillel, D., Ed.; Academic Press: San Diego, CA, USA, 1998; pp. 655–675.
59. Lee, D.M.; Elrick, D.E.; Reynolds, W.D.; Clothier, B.E. A comparison of three field methods for measuring saturated hydraulic conductivity. *Can. J. Soil Sci.* **1985**, *65*, 563–573. [[CrossRef](#)]
60. Reynolds, W.D.; Drury, C.F.; Tan, C.S.; Fox, C.A.; Yang, X.M. Use of indicators and pore volume-function characteristics to quantify soil physical quality. *Geoderma* **2009**, *152*, 252–263. [[CrossRef](#)]
61. García-Oliva, F.; Sanford, R.L.; Kelly, E. Effects of slash-and-burn management on soil aggregate organic C and N in a tropical deciduous forest. *Geoderma* **1999**, *88*, 1–12. [[CrossRef](#)]
62. Kane, E.S.; Kasischke, E.S.; Valentine, D.W.; Turetsky, M.R.; McGuire, A.D. Topographic influences on wildfire consumption of soil organic carbon in interior Alaska: Implications for black carbon accumulation. *J. Geophys. Res. Biogeosci.* **2007**, *112*, G03017. [[CrossRef](#)]
63. Ebel, B.A.; Moody, J.A. Rethinking infiltration in wildfire-affected soils. *Hydrol. Process.* **2013**, *27*, 1510–1514. [[CrossRef](#)]
64. Rawls, W.J.; Pachepsky, Y.A.; Ritchie, J.C.; Sobecki, T.M.; Bloodworth, H. Effect of soil organic carbon on soil water retention. *Geoderma* **2003**, *116*, 61–76. [[CrossRef](#)]
65. Vandervaere, J.-P.; Vauclin, M.; Elrick, D.E. Transient flow from tension infiltrometers I. The two-parameter equation. *Soil Sci. Soc. Am. J.* **2000**, *64*, 1263–1272. [[CrossRef](#)]
66. Vandervaere, J.-P.; Vauclin, M.; Elrick, D.E. Transient Flow from Tension Infiltrometers II. Four Methods to Determine Sorptivity and Conductivity. *Soil Sci. Soc. Am. J.* **2000**, *64*, 1272–1284. [[CrossRef](#)]
67. Lassabatere, L.; Angulo-Jaramillo, R.; Soria-Ugalde, J.M.; Šimůnek, J.; Haverkamp, R. Numerical evaluation of a set of analytical infiltration equations: EVALUATION INFILTRATION. *Water Resour. Res.* **2009**, *45*. [[CrossRef](#)]
68. Carsel, R.F.; Parrish, R.S. Developing joint probability distributions of soil water retention characteristics. *Water Resour. Res.* **1988**, *24*, 755–769. [[CrossRef](#)]
69. White, I.; Sully, M.J. On the variability and use of the hydraulic conductivity alpha parameter in stochastic treatments of unsaturated flow. *Water Resour. Res.* **1992**, *28*, 209–213. [[CrossRef](#)]
70. Di Prima, S.; Lassabatere, L.; Bagarello, V.; Iovino, M.; Angulo-Jaramillo, R. Testing a new automated single ring infiltrometer for Beerkan infiltration experiments. *Geoderma* **2016**, *262*, 20–34. [[CrossRef](#)]
71. Poulouvassilis, A.; Elmaloglou, S.; Kerkides, P.; Argyrokastritis, I. A variable sorptivity infiltration equation. *Water Resour. Manag.* **1989**, *3*, 287–298. [[CrossRef](#)]
72. Cerdà, A. The influence of aspect and vegetation on seasonal changes in erosion under rainfall simulation on a clay soil in Spain. *Can. J. Soil Sci.* **1998**, *78*, 321–330. [[CrossRef](#)]
73. Badalamenti, E.; Gristina, L.; Laudicina, V.A.; Novara, A.; Pasta, S.; Mantia, T.L. The impact of *Carpobrotus* cfr. *acinaciformis* (L.) L. Bolus on soil nutrients, microbial communities structure and native plant communities in Mediterranean ecosystems. *Plant Soil* **2016**, *409*, 19–34. [[CrossRef](#)]

74. Pasta, S.; Badalamenti, E.; Mantia, T.L. *Acacia cyclops* A. Cunn. ex G. Don (Leguminosae) in Italy: First cases of naturalization. *An. Jardín Botánico Madr.* **2012**, *69*, 193–200. [[CrossRef](#)]
75. Moody, J.A.; Martin, D.A. Initial hydrologic and geomorphic response following a wildfire in the Colorado Front Range. *Earth Surf. Process. Landf.* **2001**, *26*, 1049–1070. [[CrossRef](#)]
76. Castellini, M.; Iovino, M.; Pirastru, M.; Niedda, M.; Bagarello, V. Use of BEST Procedure to Assess Soil Physical Quality in the Baratz Lake Catchment (Sardinia, Italy). *Soil Sci. Soc. Am. J.* **2016**. [[CrossRef](#)]



© 2018 by the authors. Licensee MDPI, Basel, Switzerland. This article is an open access article distributed under the terms and conditions of the Creative Commons Attribution (CC BY) license (<http://creativecommons.org/licenses/by/4.0/>).

Article

# Previous Land Use Affects the Recovery of Soil Hydraulic Properties after Forest Restoration

Sergio E. Lozano-Baez <sup>1,\*</sup>, Miguel Cooper <sup>2</sup>, Silvio F. B. Ferraz <sup>3</sup>, Ricardo Ribeiro Rodrigues <sup>4</sup>, Mario Pirastru <sup>5</sup> and Simone Di Prima <sup>5</sup>

<sup>1</sup> Laboratory of Ecology and Forest Restoration (LERF), Department of Forest Sciences, “Luiz de Queiroz” College of Agriculture, University of São Paulo, Av. Pádua Dias 11, Piracicaba SP 13418-900, Brazil

<sup>2</sup> Department of Soil Science, “Luiz de Queiroz” College of Agriculture, University of São Paulo, Piracicaba SP 13418-900, Brazil; mcooper@usp.br

<sup>3</sup> Forest Hydrology Laboratory, “Luiz de Queiroz” College of Agriculture, University of São Paulo, Piracicaba SP 13418-900, Brazil; silvio.ferraz@usp.br

<sup>4</sup> Department of Biological Sciences, “Luiz de Queiroz” College of Agriculture, University of São Paulo, Piracicaba SP 13418-900, Brazil; rresalq@usp.br

<sup>5</sup> Agricultural Department, University of Sassari, Viale Italia, 39, 07100 Sassari, Italy; mpirastru@uniss.it (M.P.); sdiprima@uniss.it (S.D.P.)

\* Correspondence: sergio.lozano@usp.br; Tel.: +55-19-3429-4100

Received: 27 February 2018; Accepted: 6 April 2018; Published: 9 April 2018

**Abstract:** Knowledge of soil hydraulic properties after forest restoration is essential for understanding the recovery of hydrological processes, such as water infiltration. An increase of forest cover may improve water infiltration and soil hydraulic properties, but little is known about the response and extent to which forest restoration can affect these properties. The purpose of this study was to investigate the effect of forest restoration on surface-saturated soil hydraulic conductivity ( $K_s$ ), and to verify the  $K_s$  recovery to the pre-disturbance soil conditions. We sampled field  $K_s$  at the surface in Campinas municipality, São Paulo State, Brazil, at 18 plots under three land-cover types: (i) a pasture; (ii) a restored forest using a high-diversity mix of plantings (85 regional native species) of 9 years of age; and (iii) a remnant forest patch. We used the Beerkan method for soil hydraulic characterization. Bulk density ( $\rho_b$ ), soil organic carbon content (OC), soil porosity and particle size data were also sampled. We found considerable differences in soil hydraulic properties between land-cover classes. The highest  $K_s$  were observed in remnant forest sites and the lowest  $K_s$  were associated with pasture sites. The  $K_s$  recovery differs markedly between restored forests. Our results strongly suggest that soil attributes and  $K_s$  recovery are influenced by the duration and intensity of land use prior to forest restoration. Attention needs to be given to management activities before, during and after forest restoration, especially where the soil is still compacted and  $K_s$  is low.

**Keywords:** soil properties; saturated soil hydraulic conductivity; soil infiltration; Beerkan method

## 1. Introduction

The global forest restoration movement based on natural regeneration and tree plantations has increased tropical forest cover [1,2]. Nevertheless, soil hydraulic property responses in these restored forests are virtually unknown [3,4]. Soil water infiltration is a key hydrological process which, among others, influences groundwater recharge, soil erosion and surface runoff. Indeed, one of the best parameters for understanding and studying soil infiltration is the saturated soil hydraulic conductivity ( $K_s$ ) [4,5]. The  $K_s$  is a soil property with the greatest spatial and temporal variability among soil properties. The  $K_s$  variability depends on many factors, such as soil types, land uses, soil depths, landscape positions, methods of measurement and physical and chemical soil attributes [6].

Despite this variation, the  $K_s$  is a useful and sensitive indicator of the effect of land-cover change on soil hydro-physical dynamics [7], which exerts a dominating influence on the partitioning of rainfall in vertical and lateral flow paths. Therefore, estimates of  $K_s$  are essential for describing and modelling hydrological processes [8].

The Atlantic Forest is one of the most important forest biomes of Brazil that has suffered intense pressure from human occupation, with approximately 12% of the original area remaining [9]. Recently, the Atlantic Forest Restoration Pact has emerged to restore large areas of degraded land. This is the largest forest-restoration initiative in Latin America with a target of restoring 15 million hectares of forest by 2050 [10]. These efforts have a substantial impact on soil hydraulic properties and can be expected to affect the hydrological processes in the restored ecosystems. However, these hydrological implications are rarely considered in studies of forest restoration [11]. Current literature reviews in tropical landscapes suggest that forest restoration can enhance surface  $K_s$  [12,13]. However, most studies on  $K_s$  recovery after forest restoration in tropical soils emphasize areas with natural regeneration or secondary succession [4,7,14–19].

Zimmerman et al. [17] found non-significant  $K_s$  recovery at surface and near-surface (12.5 and 20 cm soil depth) levels in Brazilian Amazônia during seven years of secondary succession after pasture abandonment. Recently, Leite et al. [19] by examining four sites of different ages in the Brazilian Caatinga—an abandoned pasture, a young forest (7 years), an intermediate forest (35 years), and an older forest (more than 55 years)—observed that forest regrowth promotes surface  $K_s$  recovery, increasing progressively over time. On the other hand, the effect of active restoration on  $K_s$  has been much less studied [20]. Zwartendijk et al. [11] compared surface  $K_s$  recovery between degraded lands, semi-mature forest, 2–10-year-old naturally regenerating vegetation and fallows that were actively reforested 6–9 years ago with 120 native species in Madagascar. They found higher  $K_s$  values in the semi-mature forest, followed by the active reforested sites, suggesting that active restoration may decrease the time it takes for the soil to recover hydraulic properties. Also, the impact of afforestation on  $K_s$  has been studied in teak (*Tectona grandis*) plantations at surface and near-surface (12.5 and 20 cm soil depth) levels in Brazilian Amazônia, where after 10 years the teak plantation shows  $K_s$  recovery from pasture conditions for all soil depths, but  $K_s$  values are still distant from pre-disturbance conditions [4]. Similarly, an increase in  $K_s$  after afforestation practices has been reported by several other tropical studies [21–23].

Tree planting to restore degraded lands is conducted in the expectation that soil hydraulic properties will be improved [13]. In order to understand the effect of forest restoration on  $K_s$ , we investigated the  $K_s$  recovery by field estimation under three land covers, namely pasture, 9-year-old restored forest, and remnant forest. To the best of our knowledge, no studies have investigated the  $K_s$  recovery after planting native mixed-species in the Brazilian Atlantic Forest and compared the results with pasture and remnant forest. We hypothesized that forest restoration can recover the surface  $K_s$  to the pre-disturbance soil conditions. The following questions were addressed: (1) Does forest restoration recover top-soil  $K_s$  values that characterize the remnant forest? (2) Are the measured soil attributes between the land covers similar?

## 2. Materials and Methods

### 2.1. Field Site

This research was carried out in the county of Campinas, São Paulo State, Brazil (22°54' S, 46°54' W). The area is located inside the sub-basin of Atibaia River (2800 km<sup>2</sup>), which belongs to the Piracicaba River basin. This region has suffered over 200 years of historical landscape changes. In the Atibaia sub-basin, the main land covers are: native vegetation (33%), pasture lands (30%), and crops (17%), and the forest cover increased 5.7% in the last decade [24]. The mean annual precipitation is 1700 mm and the mean annual temperature is 20 °C, with rainy months generally concentrated between October and March. The native vegetation in the area is classified as seasonal semi-deciduous forest [25].

The two soil types found in the study sites are Ultisols and Entisols [26], related to the diverse geomorphology of the region, which is located at the transition between the Atlantic Plateau and the Peripheral Depression geomorphological provinces. The rocks in the Atlantic Plateau are mainly composed of granites and gneises, while the Peripheral Depression is characterized by sedimentary rocks. The elevation ranges from 600 m to 900 m with an undulating topography and the presence of slopes higher than 20% [27].

## 2.2. Experimental Design

The sites were selected to capture variation in soil attributes. Also, the sites' accessibility was taken into account in this selection. We examined the following land-cover classes: pasture, restored forest, and remnant forest. In each class we selected two sites or toposequences (Figure 1), under pasture (P1 and P2), under restored forest (R3 and R4), and under remnant forest (F5 and F6).

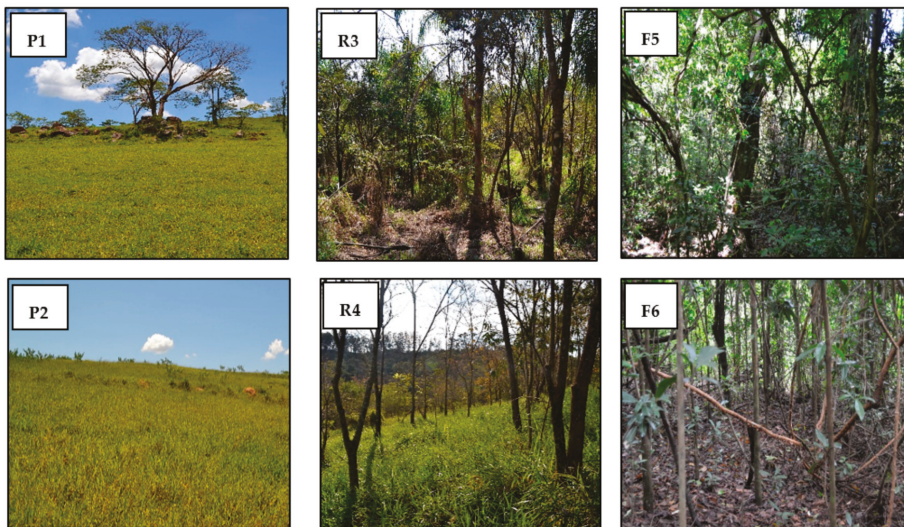


**Figure 1.** Pictures that represent the study sites in the seasonal semi-deciduous forest in Campinas, Brazil. Study sites are abbreviated with P1 and P2 for pasture, R3 and R4 for restored forest, and F5 and F6 for remnant forest.

The length of each toposequence was constrained by topography and varied between 100 m and 150 m. Each site was divided into three landscape positions (upslope (U), midslope (M) and downslope (D)). Within each landscape position, we located one plot (7 × 7 m in size), resulting in 18 plots altogether. Detailed characteristics of the three land-cover classes are as follows.

The pasture site P1 (22°49'24" S, 46°54'39" W) and P2 (22°54'38" S, 46°53'26" W) was characterised by a dense cover of grass. The dominant grass species is *Urochloa brizantha*. Information obtained from landholders revealed that the pasture sites have been heavily grazed for more than 20 years and have a stocking rate between 1 to 1.5 animal units ha<sup>-1</sup>. The measurements at these sites represent the K<sub>s</sub> and soil attributes before forest restoration actions.

The restored forest sites (R3 and R4) were 9 years old when sampled and located in Fazenda Guariroba (22°53'48" S, 46°54'28" W). The forest-restoration process of an area of 300 ha began in 2007. The mixed plantation with a high-diversity mix of seedlings (85 regional native species), aimed to provide economical insurance and ensure successional processes for landowners [28,29]. Site preparation included grass control through herbicide applications and control of leaf-cutter ants

by the distribution of insecticide baits. Direct seedling planting ( $3 \times 2$  m spacing) took place after conventional tillage. The mixed plantation also used fertilizer and irrigation at the time of planting and during the first year [28,30]. Aerial photographs and interviews with local peoples showed that land-use history differs between the restored forest sites. Both restored forests were originally deforested more than 100 years ago and planted with coffee (*Coffea arabica*) during the first decades of the 20th century. After the coffee plantation, the restored forest R3 was planted with eucalyptus (*Eucalyptus* sp.); this abandoned forest existed until 2006 without a commercial purpose, although a frequent grazing of cattle occurred, then it was harvested and grazing continued one year before the forest restoration. The eucalyptus harvest was made by motor–manual operations and a farm tractor forwarded the logs. The vegetation in the restored forest R3 prior to restoration activities consisted of low shrub and grasses. On the other hand, the restored forest R4 after the coffee plantation was used as pasture for livestock breeding until 1986, was subsequently planted again to coffee (*C. arabica*), and agricultural terraces were created with heavy track machinery. Then, the coffee plantation was replaced by pasture in 1996, which was similar to the pastures sites (P1 and P2), dominated by the grass species *U. brizantha*, and without natural regeneration.

The forest sites (F5 and F6), used as a reference for soil attributes, were located in Ribeirão Cachoeira forest ( $22^{\circ}50'13''$  S,  $46^{\circ}55'58''$  W), the second largest natural remnant forest of 245 ha in the county of Campinas. The forest presents a high tree species diversity, with an average canopy stature of 15 m and emergent trees reaching up to 35 m tall [31].

### 2.3. Soil Sampling and Measurements

The first field campaign started in February and ended in March 2017. A total of four disturbed soil samples were collected per plot to determine the soil particle size distribution (PSD) and the soil organic carbon content (OC). The PSD was determined by the hydrometer method and soil texture was classified according to the US Department of Agriculture (USDA) standards [32]. The OC was determined by the Walkley–Black method [33]. In addition, four undisturbed soil cores (0.05 m in height and 0.05 m in diameter) were also collected per plot at the depth of 0–0.05 m to determine soil macroporosity (*Mac*) and microporosity (*Mic*), using the Richards pressure chamber with the application of 6 kPa suction [34].

Soil infiltration measurements were taken in a second field campaign during the month of June 2017 (dry season). We conducted a  $K_s$  characterization using the Beerkan method [35], referred to as BEST. We chose the BEST test because it is a simple, fast and inexpensive method [36–38]. At each plot, we carried out seven infiltration runs using a steel ring with an inner diameter of 0.16 m inserted approximately 0.01 m into the soil surface, with a minimum distance between measurements of 2 m. Before the ring's insertion, the litter was removed and, if necessary, the grass and ground cover were cut in order to expose the soil surface. Sampling-point selection was influenced by suitable ground conditions for measurement and constraints such as tree roots, rocks and variations in microtopography. For each infiltration run, we collected one undisturbed soil core (0.05 m in height and 0.05 m in diameter) at the 0–0.05 m depth. We used the undisturbed soil cores to determine the initial volumetric soil water content ( $\theta_i$ ), the soil bulk density ( $\rho_b$ ) and total soil porosity ( $P_t$ ) assuming a particle density of  $2.65 \text{ g cm}^{-3}$  [39]. In each measurement, a known volume (150 mL) was repeatedly poured into the cylinder and the time needed for the complete infiltration of this volume was logged. We repeated the procedure until the difference in infiltration time between two or three consecutive trials became negligible. At the end of each infiltration test, we collected a disturbed soil sample inside the ring area to determine the saturated gravimetric water content, and thus the saturated volumetric water content ( $\theta_s$ ) was calculated using the  $\rho_b$ . A total of 126 experimental cumulative infiltrations,  $I(t)$  (L), versus time,  $t$  (T), were then deduced, 42 for each land cover, 21 for each site, and 7 for each plot.

#### 2.4. Estimating and Selecting the BEST Algorithm

The BEST-steady algorithm by Bagarello et al. [40] was used to obtain the  $K_s$  ( $K_{sB}$ , the subscript B is used to indicate BEST-steady). This choice was made since it allows a higher success percentage of the infiltration runs to be obtained compared with other possible algorithms, such as BEST-slope [41] and BEST-intercept [42], whose data require fitting to the transient stage of the infiltration run. Another expected advantage of the BEST-steady algorithm is that the possible problems associated with the use of the transient infiltration data are avoided. The BEST-steady expresses the  $K_{sB}$  with the following equation [43]:

$$K_{sB} = \frac{Ci_s}{Ab_s + C} \quad (1)$$

where  $i_s$  ( $L T^{-1}$ ) and  $b_s$  (L) are, respectively, the slope and the intercept of the regression line fitted to the data describing steady-state conditions on the cumulative infiltration  $I$  (L) versus  $t$  (T) plot. Taking into account that BEST focuses on the Brooks and Corey relationship for hydraulic conductivity [44], the  $A$  ( $L^{-1}$ ) and  $C$  constants are defined as follows [35]:

$$A = \frac{\gamma}{r(\theta_s - \theta_i)} \quad (2)$$

$$C = \frac{1}{2 \left[ 1 - \left( \frac{\theta_i}{\theta_s} \right)^\eta \right] (1 - \beta)} \ln \left( \frac{1}{\beta} \right) \quad (3)$$

where  $\gamma$  and  $\beta$  are infiltration coefficients commonly set at 0.75 and 0.6 as explained by Lassabatero et al. [3,7,16,19],  $r$  (L) is the radius of the disk source,  $\eta$  is a shape parameter that is estimated from the capillary models [45], and  $\theta_i$  and  $\theta_s$  are the initial and final water contents, respectively. Note that  $\theta_i$  should not exceed 0.25  $\theta_s$ ; however, Di Prima et al. [43] showed that BEST-steady can be applied in initially wetter soil conditions ( $\theta_i > 0.25 \theta_s$ ) without an appreciable loss of accuracy in the predictions of  $K_s$ . Therefore, as suggested by Cullotta et al. [46], the  $\theta_i$  was not considered to affect the reliability of the predicted  $K_s$ . On the other hand, the BEST-steady algorithm failed in some sampling points, providing negative  $K_s$  values and affecting the reliability of measured  $K_s$ . For this reason, we also estimated  $K_s$  for the whole data set by the near steady-state phase of a Beerkan infiltration run (SSBI— $K_{sS}$ , the subscript S is used to indicate steady-state) [47]. This method is attractive for a simple soil hydraulic characterization, but testing the ability of this procedure to estimate  $K_s$  is necessary. Indeed, in scientific literature there is no exhaustive testing of the performances of the SSBI method, notwithstanding that this method has a noticeable practical interest. This method estimates  $K_s$  through a simple Beerkan infiltration test and an estimate of the so-called sorptive parameter,  $\alpha^*$  ( $L^{-1}$ ), expressing the relative importance of gravity and capillary forces during a ponding infiltration process [48,49]. With this method  $K_{sS}$  is estimated by the following equation [47]:

$$K_{sS} = \frac{i_s}{\frac{\gamma\gamma_w}{r\alpha^*} + 1} \quad (4)$$

where  $\gamma_w$  is a dimensionless constant related to the shape of the infiltration front and is set at 1.818 [50]. In this investigation, we considered  $\alpha^*$  as a constant and equal to  $0.012 \text{ mm}^{-1}$ , since it was found to be usable in tropical soils [47,51]. The reasons for this choice was that we did not find in the literature other specific support for using a different  $\alpha^*$  value for tropical soils. Following Bagarello et al. [47], the BEST-steady algorithm was chosen to check the SSBI method by comparing  $K_{sB}$  and  $K_{sS}$  in terms of factors of difference ( $FoD$ ), calculated as the highest value between  $K_{sB}$  and  $K_{sS}$  divided by the lowest value between  $K_{sB}$  and  $K_{sS}$ . Differences between  $K_{sB}$  and  $K_{sS}$  not exceeding a factor of two were considered indicative of similar estimates [49].

## 2.5. Data Analysis

Data sets were summarized by calculating the mean and the associated coefficient of variation (CV). Following similar investigations [37,52], unique values of clay, silt, sand,  $OC$ ,  $\rho_b$ , total porosity, macroporosity, microporosity and  $\theta_i$  were determined for each plot by averaging the measured values, considering the small size of the sampled areas [52]. The hypothesis of normal distribution of both the untransformed and the log-transformed  $K_s$  data were tested by the Lilliefors test [53]. The other parameters were assumed to be normally distributed and, thus, no transformation was performed on these data before statistical analysis [54,55]. Treatment means were calculated according to the statistical distribution of the data, i.e., geometric means for  $K_s$  (log-normal distribution) and arithmetic means for all other parameters (normal distribution) [56]. According to Lee et al. [55], the appropriate CV expression for a log-normal distribution was calculated for the geometric means, and the usual CV was calculated for the arithmetic means. Statistical comparison was conducted using two-tailed  $t$ -tests, whereas the Tukey honestly significant difference test was applied to compare the data sets. The ln-transformed  $K_{sS}$  was used in the statistical comparison. A probability level,  $p = 0.05$ , was used for all statistical analyses. All analyses were carried out in the statistical programming software R [57].

## 3. Results

### 3.1. Differences in Soil Attributes among Study Sites

The PSD showed considerable differences among the soils. Most of the sampled plots presented sandy loam (P1U, P1M, P1D, R3U, R3M, RD, F5U and F5D) and sandy clay loam textures (R4U, R4M, R4D and F5M), and the rest clay loam (P2M, F6U and F6M) and loamy textures (P2U, P2D and F6D). The  $OC$  ranged from 14.76–35.37 g Kg<sup>-1</sup> under pastures (P1 and P2), from 10.46–24.60 g Kg<sup>-1</sup> under restored forests (R3 and R4), and from 17.53–48.59 g Kg<sup>-1</sup> under remnant forests (F5 and F6). The  $\rho_b$  values ranged between 1.12–1.40 g cm<sup>-3</sup> in the pastures, for the restored forests the values ranged from 1.09–1.52 g cm<sup>-3</sup>, while in the remnant forests the values ranged from 0.88–1.25 g cm<sup>-3</sup>. The  $Pt$  varied from 0.47–0.58 cm<sup>3</sup> cm<sup>-3</sup> in the pastures, from 0.43–0.59 cm<sup>3</sup> cm<sup>-3</sup> in the restored forests, and from 0.53–0.67 cm<sup>3</sup> cm<sup>-3</sup> in the remnant forests. In general, the highest soil  $Mac$  values were observed in the remnant forests, the intermediate values in restored forests, and the lowest values in the pastures. In contrast, the soil  $Mic$  was greater in the pastures, intermediate in the restored forests, and lower in the remnant forests. The mean  $\theta_i$  at the time of the Beerkan infiltration run varied between 0.16–0.37 cm<sup>3</sup> cm<sup>-3</sup> and the soil was significantly wetter in plots P2M, R4U and R4M (Table 1).

### 3.2. Estimating and Selecting the BEST Algorithm

Overall, the Beerkan method used in this study was found to be robust for measuring the  $K_s$  in the field. However, the BEST-steady algorithm yielded physically plausible estimates (i.e., positive  $K_s$  values) in 108 of 126 infiltration runs (85.7% of the cases). The percentage of successful runs was 95.2% (40 of 42 runs) both in the pasture sites and restored forest. With reference to the remnant forest (F5 and F6), BEST-steady led to a failure rate value of 33.3%, leading to a lack of estimates in 14 of 42 infiltration runs. In these cases, convex cumulative infiltration-shaped data always produced a negative intercept of the straight line fitted to the data describing steady-state conditions, which yielded negative  $K_s$  values (Figure 2). On the other hand, the SSBI method always yielded physically plausible estimates (i.e., positive  $K_s$  values) and small differences were found between the  $K_{sB}$  and  $K_{sS}$  estimates (Figure 3). The means of  $K_{sS}$  differed from the corresponding values of  $K_{sB}$ , by a factor not exceeding 1.81. The individual determination (i.e., point by point) of the factors of difference,  $FoD$ , did not exceed 2.37 (mean of  $FoD$  is equal to 1.51) and they were less than 2 and 1.5 in 90% and 53% of the cases, respectively. Therefore, it can be argued that the BEST-steady and SSBI method led to similar estimates, given that the individual  $FoD$  values were lower than two in almost all cases.

**Table 1.** Comparison between the mean and coefficient of variation (CV) of the clay (%), silt (%), sand (%), soil organic carbon content (OC in  $\text{g Kg}^{-1}$ ), soil bulk density ( $\rho_b$  in  $\text{g cm}^{-3}$ ), total porosity ( $P_t$  in  $\text{cm}^3 \text{cm}^{-3}$ ), macroporosity ( $M_{ac}$  in  $\text{cm}^3 \text{cm}^{-3}$ ), microporosity ( $M_{ic}$  in  $\text{cm}^3 \text{cm}^{-3}$ ) and initial volumetric soil water content ( $\theta_i$  in  $\text{cm}^3 \text{cm}^{-3}$ ), values for the 18 sampled plots in the landscape positions upslope (U), midslope (M) and downslope (D).

Variable	Statistic	Plots																	
		Pasture 1			Pasture 2			Restored Forest 3			Restored Forest 4			Remnant Forest 5			Remnant Forest 6		
		U	M	D	U	M	D	U	M	D	U	M	D	U	M	D	U	M	D
Clay	Mean	19.6a	10.2b	9.5b	25.0b	31.7a	21.6b	11.2b	12.1b	19.0a	26.1a	21.0b	21.9b	18.3b	23.3a	19.0b	30.2a	31.0a	24.4b
	CV	7.9	2.8	12.9	5.6	3.9	13.1	17.3	11.7	4.3	5.1	3.9	2.9	14.4	2.0	5.7	3.6	4.4	2.0
Silt	Mean	27.4a	20.2b	22.3b	30.7a	32.5a	29.9a	20.7b	21.2b	27.7a	22.7a	19.4b	19.9b	25.4a	26.3a	26.7a	34.3b	33.9b	39.7a
	CV	6.6	6.8	6.5	7.1	6.4	11.6	14.6	12.8	6.8	2.1	2.5	6.5	10.2	8.5	8.6	5.8	2.5	1.2
Sand	Mean	53.0a	69.6a	68.3a	44.4a	35.8a	48.5a	68.1b	66.8b	53.3a	51.2a	59.7b	58.3b	56.3b	50.4a	54.3b	35.6a	35.2a	35.9b
	CV	4.1	1.7	3.8	3.5	2.5	13.0	6.8	4.6	4.9	3.3	2.1	2.0	8.0	5.1	6.2	8.3	1.7	2.3
OC	Mean	30.0a	20.1b	17.8b	32.1a	32.1a	25.6b	14.5a	17.3a	21.3a	22.0a	19.0a	17.4a	30.9a	34.8a	33.8a	31.1a	34.2a	27.8a
	CV	5.9	2.4	18.6	11.7	4.9	12.7	22.6	33.7	9.8	12.2	14.8	17.0	41.4	18.5	12.6	12.3	11.0	25.4
$\rho_b$	Mean	1.27a	1.24a	1.22a	1.29a	1.18b	1.33a	1.23a	1.29a	1.22a	1.33a	1.34a	1.42a	1.05b	1.03b	1.15a	1.02a	1.05a	0.99a
	CV	5.7	5.1	3.8	5.8	4.9	5.0	7.1	3.3	5.9	3.4	6.0	5.3	5.4	7.1	7.1	9.7	7.6	8.3
$P_t$	Mean	0.53a	0.53a	0.54a	0.51a	0.55a	0.50a	0.54a	0.51a	0.54a	0.50a	0.50a	0.47a	0.60b	0.61b	0.57b	0.61b	0.60b	0.63b
	CV	4.8	4.6	3.5	6.1	4.5	4.7	6.0	3.3	5.4	4.1	6.4	6.0	3.1	4.4	5.0	6.4	5.3	4.6
$M_{ac}$	Mean	0.12b	0.18a	0.21a	0.11a	0.07b	0.06b	0.20a	0.19a	0.16b	0.18a	0.14b	0.16a	0.24a	0.26a	0.15b	0.19b	0.22a	0.18b
	CV	5.0	12.0	15.5	25.2	15.4	40.8	10.2	4.3	28.1	12.0	37.0	28.6	15.9	3.1	18.1	13.3	13.9	25.5
$M_{ic}$	Mean	0.36a	0.32b	0.32b	0.50a	0.51a	0.50a	0.28b	0.29b	0.34a	0.35a	0.33a	0.31b	0.31b	0.29b	0.37a	0.37a	0.35a	0.37a
	CV	16.8	5.7	16.5	3.7	1.1	4.8	12.1	8.4	12.3	7.7	11.4	5.9	3.1	5.1	7.8	6.5	2.3	8.0
$\theta_i$	Mean	0.32a	0.19b	0.16b	0.25b	0.37a	0.25b	0.19a	0.19a	0.19a	0.37ab	0.34a	0.23b	0.15a	0.17b	0.32a	0.21a	0.23a	0.17b
	CV	12.8	29.3	28.4	23.2	5.2	23.6	14.9	17.0	11.2	15.9	14.0	14.1	12.8	9.0	26.9	9.9	4.5	14.7

For a given variable and site (i.e., P1, P2, R3, R4, F5 and F6), means that do not share a letter are significantly different according to the Tukey test ( $p = 0.05$ ).

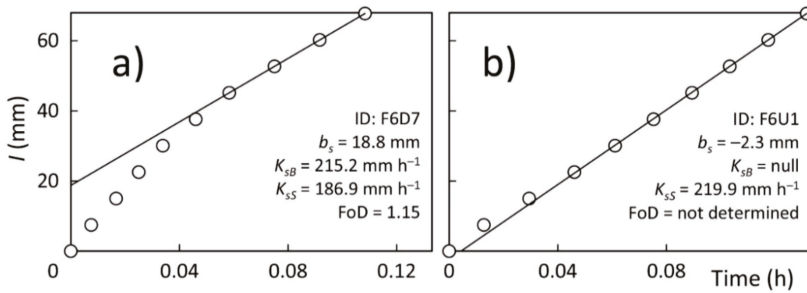


**Figure 2.** Illustrative examples of the influence of the shape of the cumulative infiltrations on the discrepancies occurring between the Beerkan method (BEST-steady) and the steady-state phase of a Beerkan infiltration (SSBI) method. (a) Concave-shaped cumulative infiltration curve in which the intercept,  $b_s$  (mm), of the straight line interpolating the last  $I$  vs.  $t$  data points is positive and the  $FoD$  between the saturated soil hydraulic conductivity values estimated with BEST-steady ( $K_{sB}$ ) and the SSBI method ( $K_{sS}$ ) is small. (b) Convex-shaped cumulative infiltration curve with a negative intercept yielding null  $K_{sB}$ .

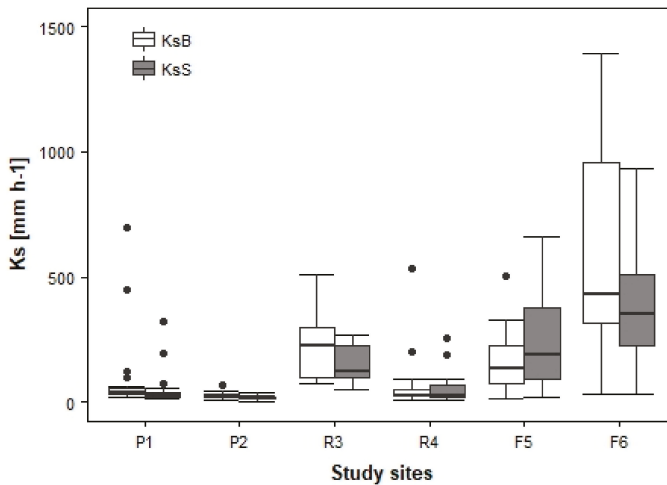


**Figure 3.** Comparison between  $K_s$  estimated with BEST-steady,  $K_{sB}$ , and the SSBI method,  $K_{sS}$ . Study sites are abbreviated with P1 and P2 for pasture, R3 and R4 for restored forest, and F5 and F6 for remnant forest.

The failure in the BEST-steady algorithm is reported by several studies in subtropical soils, where  $OC$  exceeds 5%. This failure is normally related to the occurrence of hydrophobic conditions [43,46,58]. Nevertheless, our soils showed lower  $OC$  values (less than 5%). In addition, the soil hydrophobicity is a complex property and poorly studied in tropical soils [59,60]. Other factors that probably contributed to the BEST-steady algorithm failure are the heterogeneous soil structure, changes in soil structure during measurement, initial soil moisture, and temperature [61,62]. For these reasons, the failure of the BEST-steady algorithm should be addressed in detail by future studies, considering detailed physical, chemical and mineralogical analyses. Hereafter, for the sake of reliable  $K_s$  values and comparison across study sites, only the  $K_{sS}$  values estimated using the SSBI method were considered. This choice was supported by the fact that the SSBI method allowed us to maintain the integrity of the dataset.

In addition, the  $K_{sS}$  values ranged between 3 mm h<sup>-1</sup> and 934 mm h<sup>-1</sup>, with a high variability inside all study sites.

### 3.3. Saturated Soil Hydraulic Conductivity ( $K_s$ ) Characterization

Evaluating the surface  $K_s$  values by soil texture, greater  $K_s$  variation was found in soils with higher clay content, contrasting with lower variation in soils with higher sand content. Also, soils with higher sand content did not show the higher  $K_s$ . In general, the lowest  $K_s$  values occurred in pasture plots, for example, in pasture P1 the  $K_s$  ranged from 10–320 mm h<sup>-1</sup>, and in pasture P2  $K_s$  ranged from 4–37 mm h<sup>-1</sup>, whereas the highest  $K_s$  values were observed in most remnant forest plots. The sandy loam texture highlighted the large differences between  $K_s$  in the restored forest R3 and pasture plots (P1U and P1M). In this case, the  $K_s$  in the restored forest R3 varied from 49–267 mm h<sup>-1</sup>, with the higher  $K_s$  evidenced at the restored forest plot R3D (average of 180 mm h<sup>-1</sup>); moreover, the  $K_s$  was similar to the pasture plot P1D (average of 110 mm h<sup>-1</sup>) and most remnant forest plots. For the remnant forest F5, the  $K_s$  varied from 18–660 mm h<sup>-1</sup>, showing the higher  $K_s$  at remnant forest plot F5U (average of 247 mm h<sup>-1</sup>), which differs from pasture plots (P1U and P1M) but not from restored forest R3. In contrast, the  $K_s$  at remnant forest plot F5D (average of 68 mm h<sup>-1</sup>) exhibited a similar  $K_s$  in relation to pasture and restored forest plots. For the sandy clay loam texture, the  $K_s$  in the restored forest R4 (from 6–256 mm h<sup>-1</sup>) was significantly different from the remnant forest plot F5M (average of 68 mm h<sup>-1</sup>); furthermore, all the plots in the restored forest R4 had low  $K_s$  variability, similar to the pasture land cover. Finally, clay loam and loam textures showed the same comparison among land covers, characterized by marked differences between lower  $K_s$  in pasture 2 and higher  $K_s$  in the remnant forest F6. In particular, the remnant forest F6 evidenced the higher  $K_s$  variability (from 33–934 mm) in the study sites (Figure 4).

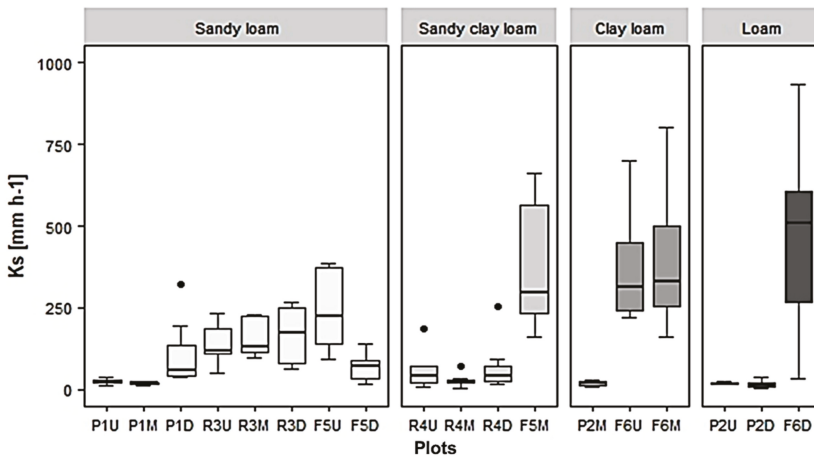


**Figure 4.**  $K_s$  estimated with SSBI method,  $K_{sS}$ , per plots and grouping by soil texture (US Department of Agriculture (USDA) classification system). Study sites are abbreviated with P1 and P2 for pasture, R3 and R4 for restored forest, and F5 and F6 for remnant forest. The subscript letter refers to the landscape position (Upslope, Middleslope and Downslope) in each site.

Statistical comparison of  $K_{sS}$  revealed no significant differences between the restored forest (R3) and the remnant forest (F5 and F6). However, significant differences between the restored forest (R4) and remnant forest were detected, indicating similarity with the pastures (P1 and P2) (Table 2).

**Table 2.** Results of the Tukey honestly significant difference test ( $p = 0.05$ ) for the ln-transformed saturated hydraulic conductivity values estimated with the SSBI method ( $K_{sS}$ ). The grouping information highlights the significant and not significant comparisons.

Variable	Grouping Information (Plots)																			
	F6M	F6U	F5M	F6D	F5U	R3D	R3M	R3U	P1D	F5D	R4D	R4U	R4M	P1U	P1M	P2U	P2M	P2D		
$K_{sS}$	a	a	a	a	a	a	a	a												
					b	b	b	b	b											
						c	c	c	c	c	c									
							d	d	d	d	d	d	d							
									e	e	e	e	e	e	e					
									f	f	f	f	f	f	f	f	f	f		
													g	g	g	g	g	g	g	g

#### 4. Discussion

##### 4.1. Effects of Land Use on Soil Attributes and $K_s$

Although the soils in the study area showed some variability, this was overcome by choosing sites and landscape positions within the different land uses that presented similar soil textural classes in the surface horizon. This approach allowed us to group and compare the soil attributes and  $K_s$  (Figure 4). In general, important differences were observed in the soil attributes and  $K_s$  between land-cover classes. These differences could be related to many factors such as intensity of past land use [4,23], spatial and topographic variations in soil types along the toposequences [63,64], density and diversity of plants, root system, vegetation type, canopy cover and soil faunal activity, among others [19]. Unfortunately, the influence of these factors on soil attributes and  $K_s$  after forest restoration is poorly understood and needs to be included in future studies.

*Pasture.* As expected,  $K_s$  was significantly lower under pasture plots than restored forest and remnant forest plots. This result was directly related to the highest  $\rho_b$  found in the study pastures, which influences the higher soil *Mic* and lower soil *Mac* values [65]. Similar findings have been reported by several authors [13–15]. An exception to this was related to pasture plot P1D, which showed similar  $K_s$  values compared to the restored forest and remnant forest in the sandy loam texture, suggesting lower soil compaction, and consequently higher soil *Mac*. Also, the highest sand content found in this plot could help to explain this result. Moreover, the present results illustrate the  $K_s$  spatial variability in two different pasture sites, characterized by a low variation in  $K_s$  values. This could be due to the soil compaction [4,13], and the duration of pasture use in the land-use history, which is one of the most important factors for  $K_s$  variability over time [15,17], as well as the cattle-grazing intensity that could have influenced the  $K_s$  variability in the pasture plots [7]. Moreover, the lower soil faunal activity and organic matter in pasture land covers are important factors when analyzing the soil attributes [15,56]. Notably, the pasture plots P1U, P2U and P2M, had OC similar to the remnant forest. These similarities are closely linked to carbon inputs in pastures sites where the root system of grasses, the animal-derived organic matter and the application of fertilizers might have increased the organic substrate [20,65]. In contrast, pasture plots P1M, P1D and P2D showed the lowest OC values in the pasture plots, which could be attributed in part to the higher sand content in these plots.

*Restored forest.* The soil texture, understory vegetation (Figure 1) and intensity of past land use were different in the restored forest sites (R3 and R4), and these are the most likely reasons for the differences in soil attributes and  $K_s$  values between both restored forests [23,66]. Also, it is important to underscore that this result could have been influenced by possible soil compaction during mechanized soil preparation during the forest restoration [67]. The most important soil attributes of the  $K_s$  differentiation between restored forest sites was the  $\rho_b$  and OC. For example, the higher  $K_s$  in the restored forest plot R3D was associated to the lowest  $\rho_b$  and higher OC values. Overall, the restored forest R3 with higher sand content (sandy loam texture) exhibited lower OC, lower soil *Mic*, lower  $\rho_b$ , higher soil *Mac* and higher  $K_s$  than restored forest R4. The higher  $K_s$  in restored forest 3, relative

to pasture plots with similar soil texture (P1U and P1M), is consistent with the results under teak plantation in Brazilian Amazônia [4] and pine plantation in Nepal [23]. Furthermore, plots in the restored forest R3 showed no significant differences in  $K_s$  from most remnant forest plots. These results can be linked to the land-use history in the restored forest R3, where the presence of an abandoned eucalyptus forest with a canopy structure of more than 50 years influenced the low trampling pressure and machinery traffic intensities, suggesting a litter accumulation that could have protected the soil surface during this period [68,69].

In the second situation, the restored forest R4 with higher clay content (sandy clay loam texture) exhibited higher  $OC$ , higher  $\rho_b$  and lower  $K_s$  than restored forest R3. In particular, the lower  $K_s$  compared to the remnant forest plot (F5M) with a similar soil texture clearly indicates that the full return to pre-disturbance conditions is still far off [22]. On the other hand, the sandy clay loam texture did not include pasture plots; however, pasture  $K_s$  in this soil texture could be assumed to be similar to the pasture sites (P1 and P2), considering the low spatial  $K_s$  variability observed in the pasture land cover. Thus, the restored forest R4 showed no significant differences in  $K_s$  with the pasture sites. This result can be related to past land-use intensity in the restored forest R4, in which the combination of coffee plantation and pastures led to greater soil exposure, and also trampling pressure and the construction of agricultural terraces could have caused erosion and soil compaction before the forest restoration. The present results agree with several studies [4,16,23], which suggest that  $K_s$  decreases with increasing land-use intensity, and that  $K_s$  recovery will be longer in view of the intensive land use. Filoso et al. [13] argued that in some cases the recovery of soil infiltration after forest restoration may be extremely difficult, because of the absence of natural understory vegetation. This research did not directly quantify the herbaceous cover, but in the field we observed that natural regeneration in the restored forest R4 is impeded by the dominance of an invasive grass species (*U. brizantha*), which is also associated with the open canopy conditions. Conversely, restored forest R3 presented visually a canopy structure with greater understory vegetation. Indeed, the canopy cover determines the interception rainfall, reducing raindrop impact and surface sealing, which could enhance the  $K_s$  [19]. Additionally, the higher  $\rho_b$  values in restored forest R4 are an indication of lower root and soil organism presence [70]; this may reduce plant seed germination, reduce root growth and decrease soil oxygen availability, becoming an ecological filter in the natural regeneration processes [71,72]. Zimmerman et al. [17] reported that invasive species could delay the  $K_s$  recovery in Brazilian Amazônia after a decade of pasture abandonment.

*Remnant forest.* Comparing remnant forest plots and pasture plots in the sandy loam, clay loam and loam textures allowed the detection of significantly higher  $K_s$  in remnant forest plots. In the case of the sandy clay loam texture, the remnant forest plot F5M showed significantly higher  $K_s$  than plots in the restored forest R4. In contrast, the sandy loam texture showed no significant differences between plots of restored forest 3 and remnant forest plot F5U. These results are related to the lowest  $\rho_b$  and higher  $Mac$  values that favor the  $K_s$ , suggesting a higher soil pore connectivity. In the specific case of remnant forest plot F5D in the sandy loam texture, no significant differences were found in relation to pasture plots (P1U and P1M). This result can be associated with the high  $\rho_b$  and a consequent increase in the soil  $Mic$  that was noted in the remnant forest plot F5D. The soil attributes and  $K_s$  values in remnant forest sites could be explained by the longer time that these forests have remained undisturbed, which allows a better soil structure to develop and the storage of more soil carbon [19,66]. These findings are in agreement with those reported by several other studies in the Atlantic Forest [63,65]. Additionally, the  $K_s$  spatial variability observed in both remnant forests is in line with previous work by Hassler et al. [7], who attributed the  $K_s$  variability in Panama forest soils to overland flows that result in erosion [19]. Other factors that might have caused the  $K_s$  spatial variability in remnant forest plots were the steepness of the sample plots and the soil distribution in the landscape positions (U, M, D) influenced by contrasting slope and topography.

#### 4.2. Management Implications

The fact that restored forests R3 and R4 showed clear differences in  $K_s$  recovery and soil attributes may provide evidence that, in some cases, simply planting trees is not, in itself, enough to recover the soil attributes to the pre-disturbance soil conditions [23]. Attention needs to be given to management activities before, during and after forest restoration, especially where the soil is still compacted and  $K_s$  is low. From this point of view, it is therefore important that monitoring forest restoration programs includes collection of soil compaction and  $K_s$  data to understand the initial compaction degree and soil infiltration, reinforcing the need to compare these values with the pre-disturbance soil conditions. After assessing soil compaction and soil infiltration at the restored forests, management practices could be implemented to alleviate soil compaction, such as mechanical loosening techniques (i.e., deep ripping and subsoiling), which may improve plant growth [73,74]. In addition, some technical methods in forest restoration that have been shown to aid natural regeneration and soil recovery are the suppression of weedy vegetation and maintenance and enrichment planting [28].

If the pasture sites (P1 and P2) presented here represent the planted pastures of the Atlantic Forest, we could observe that water infiltration is drastically affected in most cases, regardless of the soil texture. This result and the negative effects of pastures that have been heavily grazed are well documented [4,15,17] and have also been confirmed in the present research. Indeed, according to Martínez and Zinck [15] pasture degradation can be improved by rotational grazing and the introduction of silvopastoral systems during pasture management. Moreover, there is an increasing number of reports regarding different tropical land covers, suggesting that lower  $K_s$  may lead to less groundwater recharge and increases in overland flow frequency [3,7,16,19]. Thus, our results reinforce the need for better management practices in pastures and restored forests to avoid soil erosion, conserve water and create opportunities to enhance water infiltration [75].

#### 5. Conclusions

In this study, the hypothesis that forest restoration can recover the surface  $K_s$  to the pre-disturbance soil conditions was not supported for both restored forest sites (R3 and R4). We found two different situations with marked differences in soil attributes and  $K_s$  recovery between restored forest sites. Our results strongly suggest that soil attributes and surface  $K_s$  recovery are influenced by the duration and intensity of land use prior to forest restoration: while the restored forest R3 with a previous lower intensity of land use showed similar  $K_s$  to the remnant forest sites, the  $K_s$  recovery in restored forest R4 is still far-off from these remnant forest sites due to greater exposure of the soil and trampling pressure during the land-use history.

The present results further illustrate that the measured soil attributes were different between land-cover classes: pasture, restored forest and remnant forest. They also bring out the inverse relationship between  $K_s$  and  $\rho_b$ , where the  $K_s$  increases as a result of a decrease in  $\rho_b$ , and, consequently, the dominance of macropores over micropores, which facilitate soil water infiltration.

**Acknowledgments:** This research was supported by the Fundação de Amparo à Pesquisa do Estado de São Paulo (BIOTA/FAPESP Program: 2013/50718-5 and 1999/09635-0) and Conselho Nacional de Desenvolvimento Científico e Tecnológico (CNPq 561897/2010-7).

**Author Contributions:** Sergio Esteban Lozano-Baez carried out the data collection and wrote the initial draft. The other authors revised, modified and supplemented the ideas for the final draft.

**Conflicts of Interest:** The authors declare no conflict of interest.

#### References

1. Suding, K.; Higgs, E.; Palmer, M.; Callicott, J.B.; Anderson, C.B.; Baker, M.; Gutrich, J.J.; Hondula, K.L.; LaFavor, M.C.; Larson, B.M. Committing to ecological restoration. *Science* **2015**, *348*, 638–640. [[CrossRef](#)] [[PubMed](#)]

2. Chazdon, R.L.; Brancalion, P.H.S.; Lamb, D.; Laestadius, L.; Calmon, M.; Kumar, C. A Policy-Driven Knowledge Agenda for Global Forest and Landscape Restoration: A policy-driven agenda for restoration. *Conserv. Lett.* **2017**, *10*, 125–132. [[CrossRef](#)]
3. Bruijnzeel, L.A. Hydrological functions of tropical forests: Not seeing the soil for the trees? *Agric. Ecosyst. Environ.* **2004**, *104*, 185–228. [[CrossRef](#)]
4. Zimmermann, B.; Elsenbeer, H.; De Moraes, J.M. The influence of land-use changes on soil hydraulic properties: Implications for runoff generation. *For. Ecol. Manag.* **2006**, *222*, 29–38. [[CrossRef](#)]
5. Neary, D.G.; Ice, G.G.; Jackson, C.R. Linkages between forest soils and water quality and quantity. *For. Ecol. Manag.* **2009**, *258*, 2269–2281. [[CrossRef](#)]
6. Deb, S.K.; Shukla, M.K. Variability of hydraulic conductivity due to multiple factors. *Am. J. Environ. Sci.* **2012**, *8*, 489–502. [[CrossRef](#)]
7. Hassler, S.K.; Zimmermann, B.; van Breugel, M.; Hall, J.S.; Elsenbeer, H. Recovery of saturated hydraulic conductivity under secondary succession on former pasture in the humid tropics. *For. Ecol. Manag.* **2011**, *261*, 1634–1642. [[CrossRef](#)]
8. Zimmermann, A.; Schinn, D.S.; Francke, T.; Elsenbeer, H.; Zimmermann, B. Uncovering patterns of near-surface saturated hydraulic conductivity in an overland flow-controlled landscape. *Geoderma* **2013**, *195–196*, 1–11. [[CrossRef](#)]
9. Soares-Filho, B.; Rajão, R.; Macedo, M.; Carneiro, A.; Costa, W.; Coe, M.; Rodrigues, H.; Alencar, A. Cracking Brazil's forest code. *Science* **2014**, *344*, 363–364. [[CrossRef](#)] [[PubMed](#)]
10. Pinto, S.; Melo, F.; Tabarelli, M.; Padovesi, A.; Mesquita, C.; de Mattos Scaramuzza, C.; Castro, P.; Carrascosa, H.; Calmon, M.; Rodrigues, R.; et al. Governing and Delivering a Biome-Wide Restoration Initiative: The Case of Atlantic Forest Restoration Pact in Brazil. *Forests* **2014**, *5*, 2212–2229. [[CrossRef](#)]
11. Zwartendijk, B.W.; van Meerveld, H.J.; Ghimire, C.P.; Bruijnzeel, L.A.; Ravelona, M.; Jones, J.P.G. Rebuilding soil hydrological functioning after swidden agriculture in eastern Madagascar. *Agric. Ecosyst. Environ.* **2017**, *239*, 101–111. [[CrossRef](#)]
12. Ilstedt, U.; Malmer, A.; Verbeeten, E.; Murdiyarso, D. The effect of afforestation on water infiltration in the tropics: A systematic review and meta-analysis. *For. Ecol. Manag.* **2007**, *251*, 45–51. [[CrossRef](#)]
13. Filoso, S.; Bezerra, M.O.; Weiss, K.C.; Palmer, M.A. Impacts of forest restoration on water yield: A systematic review. *PLoS ONE* **2017**, *12*, e0183210. [[CrossRef](#)] [[PubMed](#)]
14. Godsey, S.; Elsenbeer, H. The soil hydrologic response to forest regrowth: A case study from southwestern Amazonia. *Hydrol. Process.* **2002**, *16*, 1519–1522. [[CrossRef](#)]
15. Martínez, L.; Zinck, J. Temporal variation of soil compaction and deterioration of soil quality in pasture areas of Colombian Amazonia. *Soil Tillage Res.* **2004**, *75*, 3–18. [[CrossRef](#)]
16. Ziegler, A.D.; Giambelluca, T.W.; Tran, L.T.; Vana, T.T.; Nullet, M.A.; Fox, J.; Vien, T.D.; Pinthong, J.; Maxwell, J.; Evett, S. Hydrological consequences of landscape fragmentation in mountainous northern Vietnam: Evidence of accelerated overland flow generation. *J. Hydrol.* **2004**, *287*, 124–146. [[CrossRef](#)]
17. Zimmermann, B.; Papritz, A.; Elsenbeer, H. Asymmetric response to disturbance and recovery: Changes of soil permeability under forest–pasture–forest transitions. *Geoderma* **2010**, *159*, 209–215. [[CrossRef](#)]
18. Nyberg, G.; Bargués Tobella, A.; Kinyangi, J.; Ilstedt, U. Soil property changes over a 120-yr chronosequence from forest to agriculture in western Kenya. *Hydrol. Earth Syst. Sci.* **2012**, *16*, 2085–2094. [[CrossRef](#)]
19. Leite, P.A.M.; de Souza, E.S.; dos Santos, E.S.; Gomes, R.J.; Cantalice, J.R.; Wilcox, B.P. The influence of forest regrowth on soil hydraulic properties and erosion in a semiarid region of Brazil. *Ecohydrology* **2017**. [[CrossRef](#)]
20. Paul, M.; Catterall, C.P.; Pollard, P.C.; Kanowski, J. Recovery of soil properties and functions in different rainforest restoration pathways. *For. Ecol. Manag.* **2010**, *259*, 2083–2092. [[CrossRef](#)]
21. Mapa, R.B. Effect of reforestation using *Tectona grandis* on infiltration and soil water retention. *For. Ecol. Manag.* **1995**, *77*, 119–125. [[CrossRef](#)]
22. Bonell, M.; Purandara, B.K.; Venkatesh, B.; Krishnaswamy, J.; Acharya, H.A.K.; Singh, U.V.; Jayakumar, R.; Chappell, N. The impact of forest use and reforestation on soil hydraulic conductivity in the Western Ghats of India: Implications for surface and sub-surface hydrology. *J. Hydrol.* **2010**, *391*, 47–62. [[CrossRef](#)]
23. Ghimire, C.P.; Bruijnzeel, L.A.; Bonell, M.; Coles, N.; Lubczynski, M.W.; Gilmour, D.A. The effects of sustained forest use on hillslope soil hydraulic conductivity in the Middle Mountains of Central Nepal: Sustained forest use and soil hydraulic conductivity. *Ecohydrology* **2014**, *7*, 478–495. [[CrossRef](#)]

24. Molin, P.G.; Gergel, S.E.; Soares-Filho, B.S.; Ferraz, S.F.B. Spatial determinants of Atlantic Forest loss and recovery in Brazil. *Landsc. Ecol.* **2017**, *32*, 857–870. [[CrossRef](#)]
25. Mello, M.H.; Pedro Junior, M.J.; Ortolani, A.A.; Alfonsi, R.R. *Chuva e Temperatura: Cem Anos de Observações em Campinas*; Boletim Técnico; IAC: Campinas, Brazil, 1994.
26. Soil Survey Staff. *Keys to Soil Taxonomy*, 12th ed.; USDA-Natural Resources Conservation Service: Washington, DC, USA, 2014.
27. De Oliveira, L.H.D.S.; Valladares, G.S.; Coelho, R.M.; Criscuolo, C. Soil vulnerability to degradation at Campinas municipality, SP. *Geogr. Londrina* **2014**, *22*, 65–79.
28. Rodrigues, R.R.; Lima, R.A.F.; Gandolfi, S.; Nave, A.G. On the restoration of high diversity forests: 30 years of experience in the Brazilian Atlantic Forest. *Biol. Conserv.* **2009**, *142*, 1242–1251. [[CrossRef](#)]
29. Rodrigues, R.R.; Gandolfi, S.; Nave, A.G.; Aronson, J.; Barreto, T.E.; Vidal, C.Y.; Brancalion, P.H.S. Large-scale ecological restoration of high-diversity tropical forests in SE Brazil. *For. Ecol. Manag.* **2011**, *261*, 1605–1613. [[CrossRef](#)]
30. Preiskorn, G.M.; Pimenta, D.; Amazonas, N.T.; Nave, A.G.; Gandolfi, S.; Rodrigues, R.R.; Belloto, A.; Cunha, M.C.S. Metodologia de restauração para fins de aproveitamento econômico (reservas legais e áreas agrícolas). In *Pacto Pela Restauração da Mata Atlântica—Referencial dos Conceitos e Ações de Restauração Florestal*; Rodrigues, R.R., Brancalion, P.H.S., Eds.; LERF/ESALQ: Instituto BioAtlântica: São Paulo, Brazil, 2009; pp. 158–175, ISBN 978-85-60840-02-1.
31. Santos, K.D.; Kinoshita, L.S.; Rezende, A.A. Species composition of climbers in seasonal semideciduous forest fragments of Southeastern Brazil. *Biota Neotropica* **2009**, *9*, 175–188. [[CrossRef](#)]
32. Gee, G.; Or, D. Particle-size analysis. In *Methods of Soil Analysis: Physical Methods*; Dane, J.H., Topp, C., Eds.; Soil Science Society of America: Madison, WI, USA, 2002; pp. 255–293, ISBN 978-0-89118-841-4.
33. Walkley, A.; Black, I.A. An examination of the degtjareff method for determining soil organic matter, and a proposed modification of the chromic acid titration method. *Soil Sci.* **1934**, *37*. [[CrossRef](#)]
34. Dane, J.H.; Hopmans, J.W. Pressure plate extractor. In *Methods of Soil Analysis: Physical Methods*; Dane, J., Topp, C., Eds.; Soil Science Society of America: Madison, WI, USA, 2002; pp. 688–690, ISBN 978-0-89118-841-4.
35. Haverkamp, R.; Ross, P.J.; Smettem, K.R.J.; Parlange, J.Y. Three-dimensional analysis of infiltration from the disc infiltrometer: 2. Physically based infiltration equation. *Water Resour. Res.* **1994**, *30*, 2931–2935. [[CrossRef](#)]
36. Alagna, V.; Bagarello, V.; Di Prima, S.; Giordano, G.; Iovino, M. A simple field method to measure the hydrodynamic properties of soil surface crust. *J. Agric. Eng.* **2013**, *44*, 74–79. [[CrossRef](#)]
37. Alagna, V.; Bagarello, V.; Di Prima, S.; Iovino, M. Determining hydraulic properties of a loam soil by alternative infiltrometer techniques: Hydraulic Properties of a Loam Soil by Infiltrometer Techniques. *Hydrol. Process.* **2016**, *30*, 263–275. [[CrossRef](#)]
38. Castellini, M.; Di Prima, S.; Iovino, M. An assessment of the BEST procedure to estimate the soil water retention curve: A comparison with the evaporation method. *Geoderma* **2018**, *320*, 82–94. [[CrossRef](#)]
39. Danielson, R.E.; Sutherland, P.L. Porosity. In *Methods of Soil Analysis. Part I. Physical and Mineralogical Methods. Agronomy Monograph No. 9*; Klute, A., Ed.; American Society of Agronomy, Soil Science Society of America: Madison, WI, USA, 1986; pp. 443–461.
40. Bagarello, V.; Di Prima, S.; Iovino, M. Comparing Alternative Algorithms to Analyze the Beerkan Infiltration Experiment. *Soil Sci. Soc. Am. J.* **2014**, *78*, 724–726. [[CrossRef](#)]
41. Lassabatere, L.; Angulo-Jaramillo, R.; Soria Ugalde, J.M.; Cuenca, R.; Braud, I.; Haverkamp, R. Beerkan estimation of soil transfer parameters through infiltration experiments—BEST. *Soil Sci. Soc. Am. J.* **2006**, *70*, 521–532. [[CrossRef](#)]
42. Yilmaz, D.; Lassabatere, L.; Angulo-Jaramillo, R.; Deneele, D.; Legret, M. Hydrodynamic Characterization of Basic Oxygen Furnace Slag through an Adapted BEST Method. *Vadose Zone J.* **2010**, *9*, 107–116. [[CrossRef](#)]
43. Di Prima, S.; Lassabatere, L.; Bagarello, V.; Iovino, M.; Angulo-Jaramillo, R. Testing a new automated single ring infiltrometer for Beerkan infiltration experiments. *Geoderma* **2016**, *262*, 20–34. [[CrossRef](#)]
44. Brooks, R.; Corey, T. *Hydraulic Properties of Porous Media*; Colorado State University: Fort Collins, CO, USA, 1964; Volume 24.
45. Haverkamp, R.; Debionne, S.; Angulo-Jaramillo, R.; Condappa, D. Soil Properties and Moisture Movement in the Unsaturated Zone. In *Groundwater Engineering*; Cushman, J.H., Tartakovsky, D.M., Eds.; CRS Press: Boca Raton, FL, USA, 1999.

46. Cullotta, S.; Bagarello, V.; Baiamonte, G.; Gugliuzza, G.; Iovino, M.; La Mela Veca, D.S.; Maetzke, F.; Palmeri, V.; Sferlazza, S. Comparing Different Methods to Determine Soil Physical Quality in a Mediterranean Forest and Pasture Land. *Soil Sci. Soc. Am. J.* **2016**, *80*, 1038–1056. [[CrossRef](#)]
47. Bagarello, V.; Di Prima, S.; Iovino, M. Estimating saturated soil hydraulic conductivity by the near steady-state phase of a Beerkan infiltration test. *Geoderma* **2017**, *303*, 70–77. [[CrossRef](#)]
48. Reynolds, W.D.; Elrick, D.E. Pondered infiltration from a single ring: I. Analysis of steady flow. *Soil Sci. Soc. Am. J.* **1990**, *54*, 1233–1241. [[CrossRef](#)]
49. Elrick, D.E.; Reynolds, W.D. Methods for analyzing constant-head well permeameter data. *Soil Sci. Soc. Am. J.* **1992**, *56*, 320–323. [[CrossRef](#)]
50. Reynolds, W.D.; Elrick, D.E. Pressure infiltrometer. In *Methods of Soil Analysis, Part 4*; Dane, J.H., Topp, G.C., Eds.; Soil Science Society of America: Madison, WI, USA, 2002; pp. 826–836.
51. Bagarello, V.; Di Prima, S.; Iovino, M.; Provenzano, G. Estimating field-saturated soil hydraulic conductivity by a simplified Beerkan infiltration experiment: Simplified determination of soil hydraulic conductivity. *Hydrol. Process.* **2014**, *28*, 1095–1103. [[CrossRef](#)]
52. Castellini, M.; Iovino, M.; Pirastru, M.; Niedda, M.; Bagarello, V. Use of BEST Procedure to Assess Soil Physical Quality in the Baratz Lake Catchment (Sardinia, Italy). *Soil Sci. Soc. Am. J.* **2016**, *80*, 742–755. [[CrossRef](#)]
53. Lilliefors, H.W. On the Kolmogorov-Smirnov test for normality with mean and variance unknown. *J. Am. Stat. Assoc.* **1967**, *62*, 399–402. [[CrossRef](#)]
54. Warrick, A.W. Spatial variability. In *Environmental Soil Physics*; Hillel, D., Ed.; Academic Press: San Diego, CA, USA, 1998; pp. 655–675.
55. Lee, D.M.; Elrick, D.E.; Reynolds, W.D.; Clothier, B.E. A comparison of three field methods for measuring saturated hydraulic conductivity. *Can. J. Soil Sci.* **1985**, *65*, 563–573. [[CrossRef](#)]
56. Reynolds, W.D.; Drury, C.F.; Yang, X.M.; Tan, C.S. Optimal soil physical quality inferred through structural regression and parameter interactions. *Geoderma* **2008**, *146*, 466–474. [[CrossRef](#)]
57. R Core Team. *R: A Language and Environment for Statistical Computing*; R Foundation for Statistical Computing: Vienna, Austria, 2014.
58. Lichner, L.; Hallett, P.D.; Drongová, Z.; Czachor, H.; Kovacic, L.; Mataix-Solera, J.; Homolák, M. Algae influence the hydrophysical parameters of a sandy soil. *Catena* **2013**, *108*, 58–68. [[CrossRef](#)]
59. Doerr, S.H.; Shakesby, R.A.; Walsh, R.P.D. Soil water repellency: Its causes, characteristics and hydro-geomorphological significance. *Earth-Sci. Rev.* **2000**, *51*, 33–65. [[CrossRef](#)]
60. Müller, K.; Deurer, M. Review of the remediation strategies for soil water repellency. *Agric. Ecosyst. Environ.* **2011**, *144*, 208–221. [[CrossRef](#)]
61. Logsdon, S.D. Transient variation in the infiltration rate during measurement with tension infiltrometers. *Soil Sci.* **1997**, *162*, 233–241. [[CrossRef](#)]
62. Kacimov, A.R.; Al-Ismaily, S.; Al-Maktoumi, A. Green-Ampt one-dimensional infiltration from a ponded surface into a heterogeneous soil. *J. Irrig. Drain. Eng.* **2009**, *136*, 68–72. [[CrossRef](#)]
63. Cooper, M.; Medeiros, J.C.; Rosa, J.D.; Soria, J.E.; Toma, R.S. Soil functioning in a toposequence under rainforest in São Paulo, Brazil. *Rev. Bras. Cienc. Solo* **2013**, *37*, 392–399. [[CrossRef](#)]
64. Zenero, M.D.O.; Silva, L.F.S.D.; Castilho, S.C.D.P.; Vidal, A.; Grimaldi, M.; Cooper, M. Characterization and Classification of Soils under Forest and Pasture in an Agroextractivist Project in Eastern Amazonia. *Rev. Bras. Cienc. Solo* **2016**, *40*. [[CrossRef](#)]
65. Nogueira, L.R.; Silva, C.F.D.; Pereira, M.G.; Gaia-Gomes, J.H.; Silva, E.M.R.D. Biological Properties and Organic Matter Dynamics of Soil in Pasture and Natural Regeneration Areas in the Atlantic Forest Biome. *Rev. Bras. Cienc. Solo* **2016**, *40*. [[CrossRef](#)]
66. Cooper, M.; Rosa, J.D.; Medeiros, J.C.; Oliveira, T.C.D.; Toma, R.S.; Juhász, C.E.P. Hydro-physical characterization of soils under tropical semi-deciduous forest. *Sci. Agric.* **2012**, *69*, 152–159. [[CrossRef](#)]
67. Löf, M.; Dey, D.C.; Navarro, R.M.; Jacobs, D.F. Mechanical site preparation for forest restoration. *New For.* **2012**, *43*, 825–848. [[CrossRef](#)]
68. Ferraz, S.F.B.; Lima, W.D.P.; Rodrigues, C.B. Managing forest plantation landscapes for water conservation. *For. Ecol. Manag.* **2013**, *301*, 58–66. [[CrossRef](#)]

69. Brockerhoff, E.G.; Jactel, H.; Parrotta, J.A.; Ferraz, S.F.B. Role of eucalypt and other planted forests in biodiversity conservation and the provision of biodiversity-related ecosystem services. *For. Ecol. Manag.* **2013**, *301*, 43–50. [[CrossRef](#)]
70. Gageler, R.; Bonner, M.; Kirchhof, G.; Amos, M.; Robinson, N.; Schmidt, S.; Shoo, L.P. Early Response of Soil Properties and Function to Riparian Rainforest Restoration. *PLoS ONE* **2014**, *9*, e104198. [[CrossRef](#)] [[PubMed](#)]
71. Holl, K.D. Factors Limiting Tropical Rain Forest Regeneration in Abandoned Pasture: Seed Rain, Seed Germination, Microclimate, and Soil. *Biotropica* **1999**, *31*, 229–242. [[CrossRef](#)]
72. Zahawi, R.A.; Augspurger, C.K. Tropical forest restoration: Tree islands as recruitment foci in degraded lands of Honduras. *Ecol. Appl.* **2006**, *16*, 464–478. [[CrossRef](#)]
73. Bassett, I.E.; Simcock, R.C.; Mitchell, N.D. Consequences of soil compaction for seedling establishment: Implications for natural regeneration and restoration. *Austral Ecol.* **2005**, *30*, 827–833. [[CrossRef](#)]
74. Hamza, M.A.; Anderson, W.K. Soil compaction in cropping systems. *Soil Tillage Res.* **2005**, *82*, 121–145. [[CrossRef](#)]
75. Latawiec, A.E.; Strassburg, B.B.; Brancalion, P.H.; Rodrigues, R.R.; Gardner, T. Creating space for large-scale restoration in tropical agricultural landscapes. *Front. Ecol. Environ.* **2015**, *13*, 211–218. [[CrossRef](#)]



© 2018 by the authors. Licensee MDPI, Basel, Switzerland. This article is an open access article distributed under the terms and conditions of the Creative Commons Attribution (CC BY) license (<http://creativecommons.org/licenses/by/4.0/>).

Article

# Translocation of Soil Particles during Secondary Soil Tillage along Contour Lines

Novák Petr \* and Hůla Josef

Faculty of Engineering, Czech University of Life Sciences Prague, Kamýcká 129, 165 21 Prague 6, Suchbát, Czech Republic; hula@tf.czu.cz

\* Correspondence: novakpetr@tf.czu.cz; Tel.: +420-224-383-133

Received: 27 March 2018; Accepted: 24 April 2018; Published: 27 April 2018

**Abstract:** A high percentage of arable land and erosion risk on agricultural land are typical of current agriculture. While tillage erosion is a less frequently studied issue, it impacts vast areas of agricultural land. Not all relationships between cultivation equipment, the gradient of the plot and other factors have been known until now. Intensive soil tillage can be a crucial erosive factor mainly when the cultivation equipment moves in a fall line direction. Nevertheless, even when the equipment moves along contour lines, soil particles can be translocated perpendicular to the direction of the equipment movement (in a fall line direction). This phenomenon has not yet been adequately studied. For measurements, a field trial with secondary tillage of soil was laid out (a seedbed preparation implement was used). The objective of the trial was to evaluate the effect of the working tools of the cultivation equipment on the crosswise and lengthwise translocation of soil particles during soil tillage. Aluminium cubes, with a side length of 16 mm, were used as tracers. Before the operation, the tracers were inserted in a row perpendicular (at a right angle) to a direction of the equipment passes. After the equipment passes, position of tracers was evaluated within a two-axis grid. The trial was performed at three gradients of the plot ( $2^\circ$ ,  $6^\circ$  and  $11^\circ$ ). For each gradient, the 1-pass, 2-pass and 3-pass treatments were tested. The equipment always moved along the plot contour line. After the equipment passes in all treatments, all tracers were localized on an orthogonal grid. The results of the trial demonstrate the effect of the slope gradient on the crosswise translocation of particles during secondary tillage of soil in the slope direction. The tillage equipment translocated particles in the fall line direction even if it passed along the contour line. With the increasing intensity of passes, the effect of the equipment on crosswise translocation increases. During secondary tillage of soil, the working tools of the equipment have an erosive effect (causing tillage erosion), even though the equipment moves along the contour line.

**Keywords:** soil tillage; tillage erosion; seedbed preparation

---

## 1. Introduction

High average gradients of plots are typical of conditions of the Czech Republic. Janeček et al. [1] and Novotný et al. [2] stated that up to a half of the farmland in the CR is exposed to erosion. In addition, a high percentage of arable land in the total agricultural land is characteristic of the CR. It is also the largest average field size in the EU. Besides water and wind erosion of soil, in Central Europe conditions, the soil quality and productivity are impaired by the operation of farm machines during soil tillage. The term ‘tillage erosion’ expresses the undesirable translocation of soil particles in the course of soil tillage. Interest in the study of tillage erosion has increased in the last fifteen years. Govers’ paper [3] was a great stimulus to begin to study tillage erosion.

There is a mutual relationship between water erosion and tillage erosion, but these processes are usually studied separately [4–6]. The translocation of soil particles during primary tillage of soil was

studied in relatively great detail, mainly during ploughing with a share plough, and during soil tillage with disk harrows and tine cultivators. Fewer experimental results of soil particle translocation by the cultivation equipment are available for secondary tillage of soil [7]. It is of note that some operations of secondary tillage have greater erosive impacts than primary tillage. The risk of tillage erosion was documented by Lobb et Kachanoski [8]. In the Ontario province in Canada, tillage erosion causes at least 70% of the total soil loss on hilltops. For the North American Great Plains and Canadian Prairies regions, Li et al. [9] used the term scalping of hilltops in relation to the use of the equipment with a large working width for soil tillage and sowing.

Van Muysen et al. [10] investigated tillage erosivity in the course of three years. Results of their evaluation were applied to determine the annual tillage transport coefficient that was associated with mechanized operations in agriculture, amounting to  $781 \text{ kg m}^{-1} \text{ year}^{-1}$ . The authors stated that this coefficient can be determined from the previously computed values of tillage transport coefficients for particular operations of soil tillage. For example, for mouldboard ploughing, Van Muysen et al. [11] reported the value of  $270 \text{ kg m}^{-1}$  per tillage pass (up and downslope tillage direction) and  $197 \text{ kg m}^{-1}$  (contour line direction). For rotary harrow and seeding equipment, the tillage transport coefficient of  $123 \text{ kg m}^{-1}$  was computed. Other authors reported lower values of the annual tillage transport coefficient:  $300 \text{ kg m}^{-1} \text{ year}^{-1}$  [12],  $523 \text{ kg m}^{-1} \text{ year}^{-1}$  [13], and  $133 \text{ kg m}^{-1} \text{ year}^{-1}$  [14]. The lowest annual tillage transport coefficient was computed for no-till drill—below  $5 \text{ kg m}^{-1}$ .

The majority of the authors documented the lower undesirable translocation of soil particles during contour tillage compared to up- and downslope tillage. Lindstrom et al. [15] believed that contour tillage can be moderately more erosive than up- and downslope tillage. This is confirmed by other results [16]. Nevertheless, there have been some objections to contour tillage: The tillage transport coefficient as an indicator of tillage erosivity was used by Van Muysen et al. [10].

$$k = -D \cdot \rho_b \cdot b$$

where  $D$  is the depth of tillage (m),  $\rho_b$  is the soil bulk density ( $\text{kg m}^{-3}$ ) and  $b$  is the slope of the linear regression equation of the relationship between soil displacement (m) and slope gradient ( $\text{m m}^{-1}$ ).

The modelling of edge effects of tillage erosion using the results from two field studies from the area of North America was done by Vieira et Dabney [17].

From the aspect of undesirable translocation of soil particles, the risk of secondary tillage is that the soil is usually loose at the time of seedbed preparation, and soil particles are translocated not only in the direction of the cultivation equipment passes but also in the downslope direction due to gravitation. Another risk is that the operations of seedbed preparation are repeated in a short time. Therefore, the undesirable gradual downslope translocation of soil particles also occurs when the equipment for seedbed preparation passes in the contour line direction, which is generally recommended. Their results lack exact measurements for repeated passes during seedbed preparation on plots of different gradients and at different directions of the equipment passes on slopes.

In general, the extent of tillage erosion is related to the erodibility of the landscape and to the erosivity of tillage operations. According to Li et al. [7], tillage erosivity is a result of the way in which the working tools are constructed and their arrangement in the equipment, while the geometry of the cutting tools is also important. Other parameters playing a role are tillage frequency, tillage speed and depth, the type of hitch for attaching the cultivation equipment to a tractor, and behaviour of the tractor driver.

According to available literature, the effect of farm machines exerted in the lengthwise direction has been solved. There is very little study on crosswise translocation, especially on slopes. However, this phenomenon occurs during soil tillage and should be further investigated. Of course, the existence of crosswise translocation has been reported by many authors [13,17–20]. However, it is difficult to find studies describing the characteristics of lengthwise and crosswise translocation of soil particles during secondary tillage. The objective of this paper is to assess the effect of the slope gradient on lengthwise and especially crosswise translocation of soil particles during secondary tillage of soil.

## 2. Materials and Methods

For the purposes of measurements, a field trial was laid out in the Nesperská Lhota locality in Central Bohemia. The altitude of the plot is 420 m a.s.l. The plot is situated on the border of the Vlašimská pahorkatina Hills (see Figure 1).

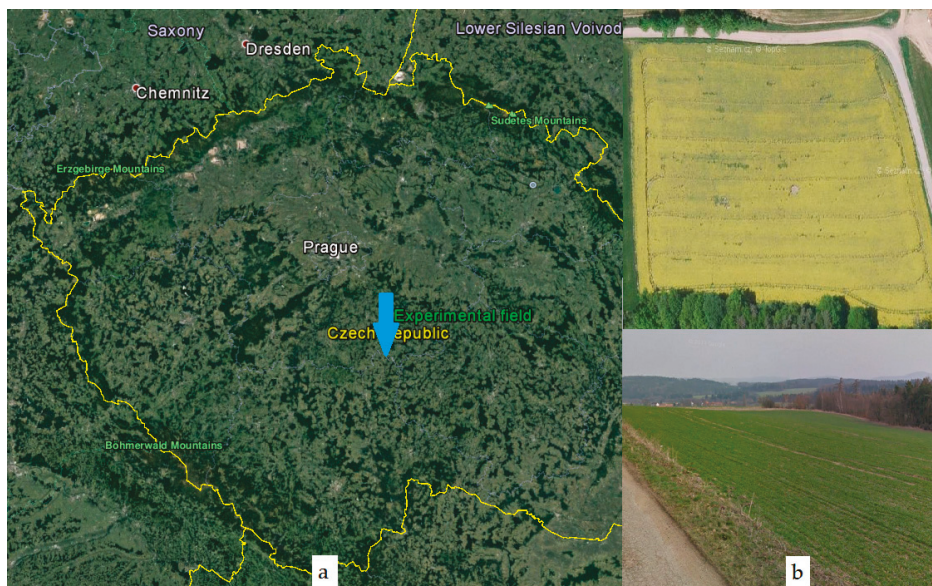


**Figure 1.** Experiment location (a) and field photo (b).

The plot has a north–south aspect. The area of the plot is 2.2 ha. Topographically, it is a slope with an average gradient of  $9.6^\circ$ . The soil on the plot is arenic cambisol. The texture class is sandy loam. Soil particle-size in topsoil is  $<0.002$  mm—8.3% weight, 0.002–0.05 mm—36.1%, 0.05–2.0 mm—55.6%;  $C_{ox}$ —1.23%;  $pH_{H_2O}$ —6.15. After the harvest of winter wheat (on 1st of August 2017), with an average yield of 5.5 t/ha, the straw was crushed and the plot was tilled with an Akpil disc harrow to a depth of 0.1 m (on 3 August 2017). In the second half of August, a nonselective herbicide (glyphosate) was applied to this plot to destroy sprouted grains. In early September, ploughing with a Ross plough was done to a depth of 0.22 m. After ploughing (direction along the contour), the plot was treated with levelling bars and harrow. The soil was left in this condition until the end of September 2017. In the meantime, natural soil subsidence was taking place. Undisturbed soil samples were taken at three depths before measurements—see Table 1. Kopecky cylinders of  $100\text{ cm}^3$  in volume were used. Soil samples were also taken after the first series of measurements (determining values after the first pass by a combinator—see Table 2). The Kopecky cylinders were analyzed in laboratories of CULS in Prague. Soil moisture was measured with a ThetaProbe sensor (Delta-T Devices, Cambridge, UK). The plot slope was measured with a digital clinometer (BMI, Hersbruck, Germany).

**Table 1.** Soil bulk density and porosity before tillage.

Depth (m)	Bulk Density ( $\text{g}\cdot\text{cm}^{-3}$ )	Porosity (%)
0.05–0.10	1.49	43.8
0.10–0.15	1.52	43.3
0.15–0.20	1.51	43.2

**Table 2.** Soil bulk density and porosity after tillage.

Depth (m)	Bulk Density ( $\text{g}\cdot\text{cm}^{-3}$ )	Porosity (%)
0.05–0.10	1.37	50.2
0.10–0.15	1.39	48.2
0.15–0.20	1.39	47.2

The trial was aimed at assessing soil dislocation during secondary tillage of soil. The average soil moisture before tillage was 12.1% volume. For measurements, a Zetor 130 HSX tractor and a Lemken Kompaktor seedbed preparation combinator were used with a working width of 6 m. The working tools of the cultivator were as follows: levelling bars, a back-up roller of 0.33 m in diameter, 2-row section with duck-foot shares (with spring protection), the second back-up roller of 0.33 m in diameter, and a Crosskill roller with cleaners (diameter 0.35 m). The tillage depth (applicable to tines) was set at 0.1 m. The working speed was  $7 \text{ km}\cdot\text{h}^{-1}$  in all cases. During measurements, this cultivation equipment always travelled along the contour line at three gradients of the plot (three treatments).

The trial had three treatments in relation to the cross slope of the plot (perpendicular to the direction of the equipment movement):

Treatment 1:  $2^\circ$

Treatment 2:  $6^\circ$

Treatment 3:  $11^\circ$  (maximum allowable tilt range of the machine).

Metallic tracers were used for the indication of soil translocation. Aluminium cubes with a side length 16 mm were used. Poesen et al. [21] used 8-mm thick steel hexagonal nuts with a diameter of 20 mm. They seemed to be the most appropriate aluminium cubes. Van Muysen et al. [10] used numbered aluminium cubes with a side length of 15 mm. The tracer technique is described by Govers et al. [14]. The advantage is that the aluminium density is similar to the density of the mineral particles in the soil. The tracers were marked with numbers and colour. At first, a furrow 0.08 m in depth was made perpendicular (at a right angle) to the direction of the equipment movement. One series of tracers (yellow colour, numbers 1–20) was inserted in this furrow. Tracer spacing was 0.2 m. The original position was plotted in an orthogonal grid for the later measurement of translocation. Then, the furrow with located tracers was refilled with soil. The other series of 20 tracers at a spacing of 0.2 m was placed on the soil surface (tracers of silver colour, numbered 1–20 again). The two series were located at the same position and in the same order, but at two depths: 0.08 m and soil surface (see Figure 2). The original position of tracers was plotted in an orthogonal grid for all treatments. The original situation was a row of tracers perpendicular to the direction of the equipment movement at two depths for each treatment of the cross slope.

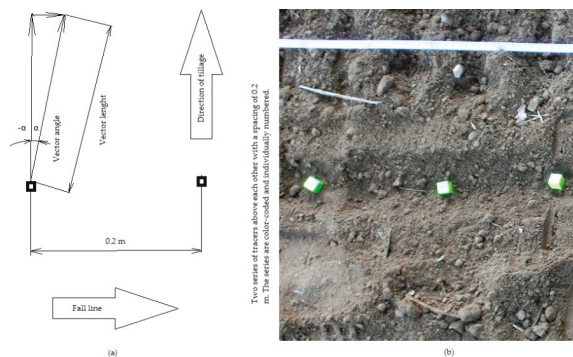


**Figure 2.** Design of tracers (location) before pass: (a) Description of measures; (b) One series of tracers.

Then, the equipment passed across all three treatments. The position of individual tracers was determined with an M6 metal detector (Whites Devices). After each tracer was detected, its lengthwise and crosswise displacement in the orthogonal grid was measured. The displacement was individually assigned to each tracer from the two series. It was possible thanks to the numbers on all tracers.

After all three treatments were assessed, the original situation was renewed. The two series of tracers were located again into two perpendicular rows to the direction of passes. Two passes of the equipment for each treatment followed. The same process was repeated for three passes of the equipment.

The repeated measurements were done because multiple passes of the equipment at the same place often occur in the field during secondary tillage of soil. These operations are performed to reach better disintegration of soil aggregates (clod size).

Data were processed using the MS Excel (Microsoft Corp., Redmond, WA, USA), Statistica 12 (Statsoft Inc., Tulsa, OK, USA) and Oriana (Kovach Computing Services, Pentraeth, UK). The following kind of statistical analyses were used: descriptive statistics, ANOVA.

### 3. Results and Discussion

Data were evaluated with respect to the length of particle translocation and direction angle of this translocation. After the first pass, the effect of the cross slope on the direction vector of particle translocation was revealed. The length of the direction vector represents the length of translocation of particular tracers from the original location. The direction vector is the angle of the vector that indicates a difference from the direction of the equipment movement. The positive value of this angle expresses translocation in a fall line direction (perpendicular to the direction of the equipment movement). The method of measurement is described in Figure 1. The results after one pass are shown in Table 3 and in Figures 3 and 4. At first, data of tracer sets from the soil surface and tracer sets located below the soil surface were compared. Tukey's HSD test did not show a statistically significant difference between the two sets. The original location of particular tracers did not significantly influence the length of the translocation vector or its angle.

Table 3 shows the negative effect of the plot's cross slope on the direction vector of translocation of particular tracers in all cases. In both sets of tracers, the angle increased along with the increasing cross slope. At the measurement of angles of particular tracers, a relatively high variance was observed in all cases, therefore the differences are below the level of statistical significance (Tukey's HSD test was used again). Nevertheless, the results demonstrate the effect of the slope on particle translocation in the slope direction, even when the cultivator equipment moved along the contour lines.

The effect of the slope on the average vector length was also observed. Such an effect is not unambiguous. In the surface set of tracers, the longest average vector was found for the medium gradient of the slope. In the set of tracers located below the soil surface, a gradual increase in the average length of the translocation vector was observed. It can probably be explained by the effect of the slope on the particular sections of the cultivation equipment. Penetration of working tools (mainly tines) to a slightly greater depth was observed due to the crosswise position of the whole equipment on the slope. It causes a larger soil layer to be carried away with tines, which is related with an increase in the translocation distance.

It was also observed that the plot slope greatly influences the direction angle of the vector. It was applicable to both sets of tracers. The angle value in both sets of tracers was found to increase in relation to the slope gradient (see Table 3). It is interesting that an opposite movement of tracers against the cross slope was recorded in the smallest slope gradient ( $2^\circ$ ). In total, it applied to three tracers out of 20 in the set located on the surface and two tracers in the set below the soil surface. It was caused by the contact of tracers with the cultivator tines. On steeper slopes ( $6^\circ$  and  $11^\circ$ ), this phenomenon was not observed in any case, which is surprising in the treatment with one pass. Each tine from the last row can move particular tracers in both directions with the same probability.

Table 3. Results obtained after one pass.

1 Passes		Below Surface		Surface	
Treatment	Length (m)	Angle (°)	Length (m)	Angle (°)	
2°	1.03 aA	4.1 bB	1.23 aA	3.9 bB	
6°	1.54 aA	6.24 bB	2.36 aA	5.9 bB	
11°	2.23 aA	7.8 bB	1.84 aA	11.2 bB	

Note: Letters denote homogeneous groups (Tukey HSD test). The lowercase letters (a, b) compare the slopes (2° / 6° / 11°); uppercase letters (A, B) represent the group of tracers (below surface / surface series).

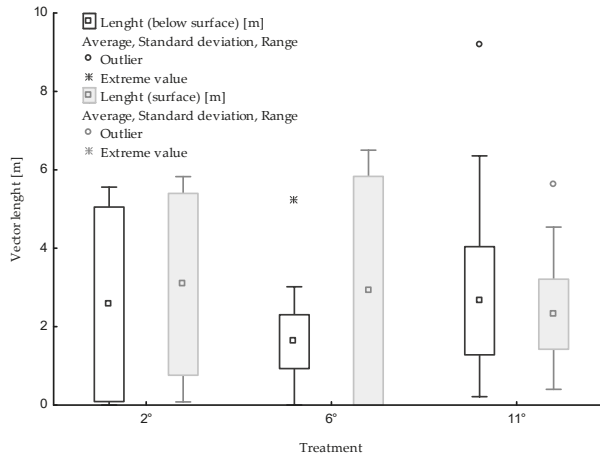


Figure 3. Vector length after one pass.

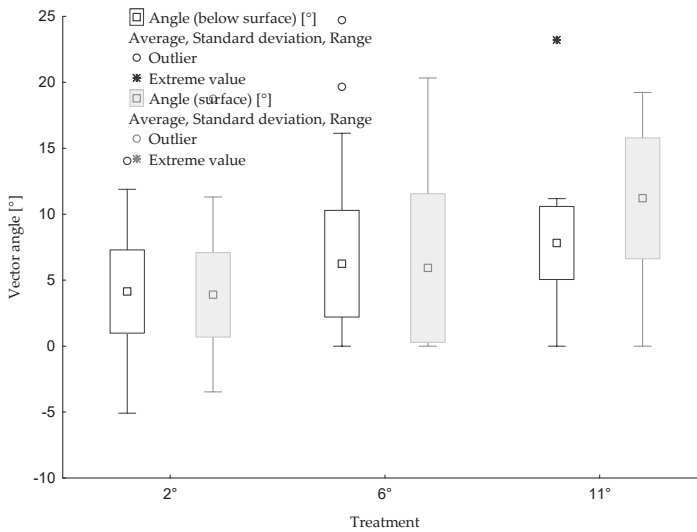


Figure 4. Vector angle after one pass.

Table 4 and Figures 5 and 6 contain the results of measurements after two passes. No statistically significant differences were revealed between both segments. It is not possible to find any relationship between the cross slope gradient and the vector length in either set of tracers. In general, there was an increase in the vector length, which was due to two passes and could be expected. However, an increase in the translocation distance was not great. It can probably be explained by the fact that the cultivator works with smaller soil aggregates during the second pass when most clods have already been disintegrated. Smaller soil aggregates are carried away by working tools of the equipment to a lesser extent.

This is consistent with the results of the vector angle evaluation. Here, a direct effect of the cross slope on the direction vector during particle translocation was confirmed again. In this case, unambiguously in both sets, an increase in the angle value in the cross slope direction was observed in the course of secondary tillage. The direction angle was generally larger in one pass of the equipment. As in the first case, a high variance of the values was found. The crosswise movement against the slope was also recorded after two passes. Such movement was recorded in one tracer during measurements on the slope of 2° and also in one tracer on the medium slope. However, the repeated pass causes a more pronounced downslope translocation of particles when the cultivator for secondary tillage moves along the contour line.

Table 4. Results obtained after two passes.

2 Passes Treatment	Below Surface		Surface	
	Length (m)	Angle (°)	Length (m)	Angle (°)
2°	2.56 <sup>aA</sup>	5.9 <sup>bB</sup>	3.08 <sup>aA</sup>	6.4 <sup>bB</sup>
6°	1.61 <sup>aA</sup>	9.3 <sup>bB</sup>	2.91 <sup>aA</sup>	10.8 <sup>bB</sup>
11°	2.66 <sup>aA</sup>	18.3 <sup>bB</sup>	2.32 <sup>aA</sup>	12.1 <sup>bB</sup>

Note: Letters denote homogeneous groups (Tukey HSD test). The lowercase letters (a, b) compare the slopes (2°/6°/11°); uppercase letters (A, B) represent the group of tracers (below surface/surface series).

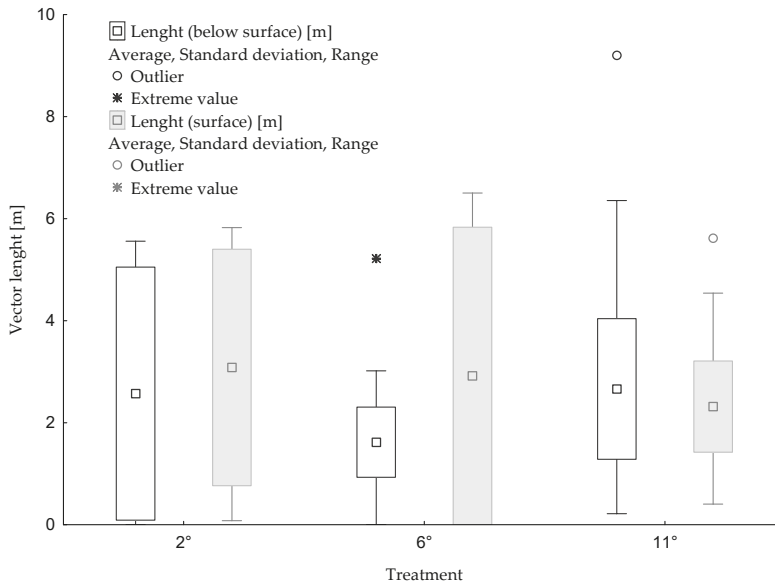


Figure 5. Vector length after two passes.

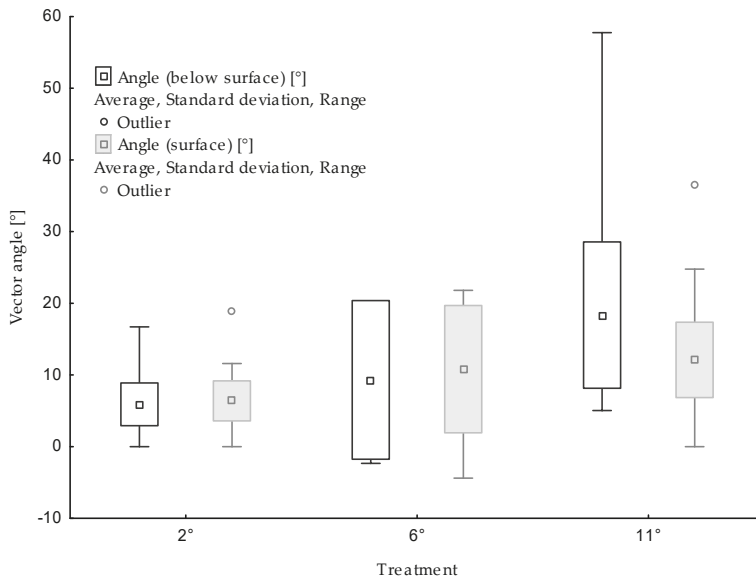


Figure 6. Vector angle after two passes.

Table 5 and Figures 7 and 8 contain the results from measuring three passes of the equipment. There were no distinct differences between the two sets of tracers, even in the third case. Relatively large differences (but below the statistical significance level) were found in the vector length. The absolutely longest average translocation of the set of tracers was observed in below-surface tracers on the smallest cross slope—on average more than 5 m. However, in three passes of the equipment, it is not possible to find a relationship between the vector length and the cross slope gradient.

The results of the evaluation of direction vectors are quite surprising. Contrary to the preceding treatment, there was a decrease in the average value of the vector angle. Such a decrease occurred in all three gradients of the cross slope. This decrease is probably caused by the disintegration of soil aggregates. During the third pass, the cultivator tills the soil without larger fractions and the soil layer is not carried away with working tools. Paradoxically, in no tracer was the crosswise translocation against the slope revealed even though the average value dropped. The variance of values was lowest for treatments with three passes.

Table 5. Results obtained after three passes.

3 Passes Treatment	Below Surface		Surface	
	Length (m)	Angle (°)	Length (m)	Angle (°)
2°	5.23 <sup>aA</sup>	3.3 <sup>bB</sup>	3.86 <sup>aA</sup>	1.4 <sup>bB</sup>
6°	2.54 <sup>aA</sup>	8.0 <sup>bB</sup>	3.06 <sup>aA</sup>	7.4 <sup>bB</sup>
11°	4.02 <sup>aA</sup>	8.4 <sup>bB</sup>	4.11 <sup>aA</sup>	9.3 <sup>bB</sup>

Note: Letters denote homogeneous groups (Tukey HSD test). The lowercase letters (a, b) compare the slopes (2°/6°/11°); uppercase letters (A, B) represent the group of tracers (below surface/surface series).

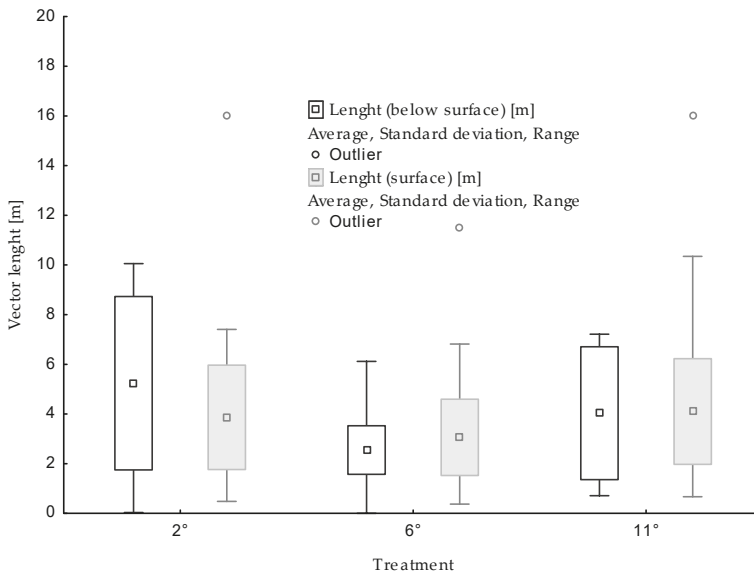


Figure 7. Vector length after three passes.

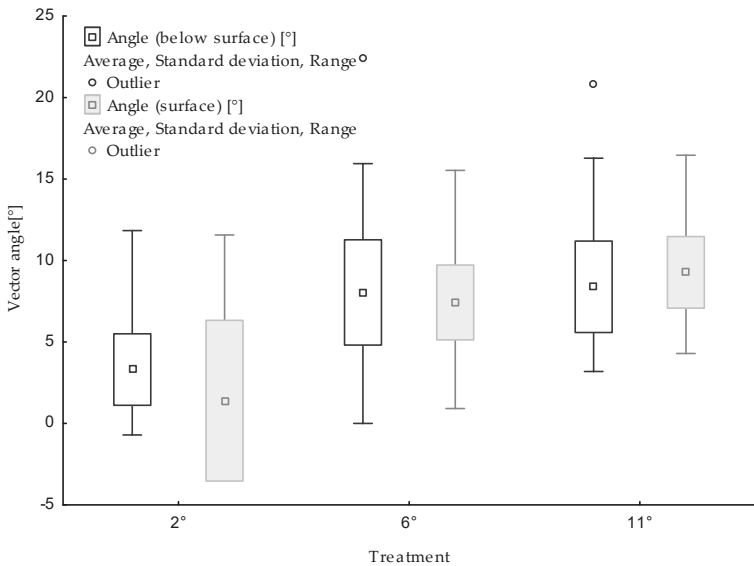


Figure 8. Vector angle after three passes.

#### 4. Discussion

Many authors have dealt with the longitudinal translocation of particles during tillage [10–13,19]. The longitudinal translocation of particles is always more significant. Studies on tillage erosion have so far been devoted to the longitudinal effects of individual machines, or their combinations [3,4,7,18]. Many studies also assess the effect of the slope on the range of particle translocation [10,11,19,20].

The influence of sloping land on the quantity of translocated particles is evident. Conclusively, downslope movement of the machine indicated a higher potential of particle translocation than movement on the flat ground or upslope. A conclusion is drawn that the upslope movement of the machine cannot be understood as a full-value corrective measure to the incorrectly chosen direction of downslope movement [20]. An optimization of the movement direction when the land topography is respected seems to be the most effective measure.

However, this recommended procedure does not involve the transverse translocation of particles. Crosswise translocation, especially on slopes, has been studied very little. However, this phenomenon occurs during soil tillage and should be further investigated. Of course, the existence of crosswise translocation has been reported by many authors [13,17–20]. Hůla et al. [22] found that the soil pollination may translocate soil particles to a different extent, both in the direction of the machine movement and in a crosswise direction. In their study, they describe the longitudinal and transverse displacement of soil particles for three basic machines of primary soil tillage (disc harrow, tine cultivator and five-share plough). However, the transverse effect was not quantified in this study. This study demonstrates the downslope translocation of particles during the work of the cultivator along the contour. Nevertheless, this study is the first step in exploring this phenomenon, and it is necessary to subdue it to further exploration for multiple soil tillage machines and technologies.

Measurement results can be affected by the properties of used tracers. In this case, aluminium cubes were used. The same material of tracers was used by Van Muysen et al. [10]. Aluminium density is greater than soil density, but the difference between is not too great. Some authors also use steel nuts for example [21]. The difference in density, in this case, is far greater. However, Rahman et al. [23] found no significant difference due to the tracer size or density. The result of this study is quite surprising. Other authors admit possible variation in size and material of tracers [20,24]. The influence of used tracers on the direction of transfer of the particles during tillage will need to be further investigated.

## 5. Conclusions

Particle translocation, particularly in the tillage direction, is evaluated in commonly available studies. Crosswise movement belongs among phenomena that have been studied very little until now. Our measurements indicate the effect of the cross slope gradient on the direction of particle translocation during secondary tillage of soil. The effect of multiple passes was not directly demonstrated. Neither was the effect of the cross slope on the average length of particle movement observed. The study of crosswise translocation phenomena is only at its beginning. It is necessary to further investigate the effect of other equipment and technologies of soil tillage. Obviously, the recommended contour farming on slopes can have impacts on downslope particle translocation. Of course, crosswise translocation and its effect will always be smaller than lengthwise movement, i.e., in the soil tillage direction.

**Author Contributions:** N.P. and H.J. designed the experiments, together performed the experiments and analyzed the data; N.P. contributed trial plot, tractor and all equipment; N.P. and H.J. wrote the paper.

**Acknowledgments:** Supported by the Ministry of Agriculture of the Czech Republic—Project No. QJ1520028.

**Conflicts of Interest:** The authors declare no conflict of interest. The funding sponsors had no role in the design of the study; in the collection, analyses, or interpretation of data; in the writing of the manuscript, and in the decision to publish the results.

## References

1. Janeček, M.; Bohuslávěk, J.; Dumbrovský, M.; Gergel, J.; Hrádek, F.; Kovář, P.; Kubátová, E.; Pasák, V.; Pivcová, J.; Tipl, M.; et al. *Anti-Erosion Protection of Agricultural Land*; ISV: Prague, Czech Republic, 2002; pp. 21–23. ISBN 85866-85-8. (In Czech)

2. Novotný, I.; Mistr, M.; Papaj, V.; Kristenová, H.; Váňová, V.; Kapička, J.; Vlček, V.; Vopravil, J.; Kulířová, P.; Kadlec, V.; et al. *Guide of Protection against Water Erosion*; Ministry of Agriculture of the Czech Republic: Prague, Czech Republic, 2014; 72p, ISBN 978-80-87361-33-7. (In Czech)
3. Govers, G.; Lobb, D.A.; Quine, T.A. Tillage erosion and translocation: Emergence of new paradigm in soil erosion research. *Soil Tillage Res.* **1999**, *51*, 167–174.
4. Wang, Y.; Zhang, J.H.; Zhang, Z.H.; Jia, L.Z. Impact of tillage erosion on water erosion in a hilly landscape. *Sci. Total Environ.* **2016**, *551*, 522–532. [[CrossRef](#)] [[PubMed](#)]
5. Morgan, R.P.C. *Soil Erosion and Conservation*; Wiley-Blackwell: Hoboken, NJ, USA, 2005; 304p, ISBN 978-1-405-11781-4.
6. Takken, I.; Govers, G.; Jetten, V.; Nachtergaele, J.; Steegen, A.; Poesen, J. Effect of tillage on runoff and erosion patterns. *Soil Tillage Res.* **2001**, *61*, 55–60. [[CrossRef](#)]
7. Li, S.; Lobb, D.A.; Lindstrom, M.J. Tillage translocation and tillage erosion in cereal-based production in Manitoba, Canada. *Soil Tillage Res.* **2007**, *94*, 164–182. [[CrossRef](#)]
8. Lobb, D.A.; Kachanoski, R.G. Modelling tillage erosion in topographically complex landscapes of southwestern Ontario, Canada. *Soil Tillage Res.* **1999**, *51*, 261–278. [[CrossRef](#)]
9. Li, S.; Lobb, D.A.; Lindstrom, M.J.; Papiernik, S.K.; Farenhorst, A. Modeling tillage-induced redistribution of soil mass and its constituents within different landscapes. *Soil Sci. Soc. Am. J.* **2008**, *1*, 167–179. [[CrossRef](#)]
10. Van Muysen, W.; Oost, K.; Govers, G. Soil translocation resulting from multiple passes of tillage under normal field operating conditions. *Soil Tillage Res.* **2006**, *87*, 218–230. [[CrossRef](#)]
11. Van Muysen, W.; Govers, G.; Van Oost, K. Identification of important factors in the process of tillage erosion: The case of mouldboard tillage. *Soil Tillage Res.* **2002**, *65*, 77–93. [[CrossRef](#)]
12. Quine, T.A.; Govers, G.; Poessen, G.; Walling, D.; van Wesemael, B.; Martinez-Fernandez, J. Fine-earth translocation by tillage in stony soils in the Guadelentín, south-east Spain: An investigation using caesium-1341. *Soil Tillage Res.* **1999**, *51*, 279–301. [[CrossRef](#)]
13. Van Oost, K.; Govers, G.; de Alba, S.; Quine, T.A. Tillage erosion: A review of controlling factors and implications for soil quality. *Prog. Phys. Geogr.* **2006**, *4*, 443–466. [[CrossRef](#)]
14. Govers, G.; Vandaele, K.; Desmet, P.; Poesen, J.; Bunte, K. The role of tillage in soil redistribution on hillslopes. *Eur. J. Soil Sci.* **1994**, *45*, 469–478. [[CrossRef](#)]
15. Lindstrom, M.J.; Nelson, W.W.; Schumacher, T.E. Quantifying tillage erosion rates due to moldboard plowing. *Soil Tillage Res.* **1992**, *24*, 243–255. [[CrossRef](#)]
16. Novák, P.; Hůla, J. Translocation of the upper soil layer in multiple operations of seedbed preparation. *Res. Agric. Eng.* **2017**, *63*, S46–S52.
17. Vieira, D.A.N.; Dabney, S.M. Modeling edge effects of tillage erosion. *Soil Tillage Res.* **2011**, *111*, 197–207. [[CrossRef](#)]
18. Tiessen, K.H.D.; Lobb, D.A.; Mehuys, G.R.; Rees, H.W. Tillage erosion within potato production in Atlantic Canada: II Erosivity of primary and secondary tillage operations. *Soil Tillage Res.* **2007**, *95*, 320–331. [[CrossRef](#)]
19. Heckrath, G.; Halekoh, U.; Djurhuus, J.; Govers, G. The effect of tillage direction on soil redistribution by mouldboard ploughing on complex slopes. *Soil Tillage Res.* **2006**, *88*, 225–241. [[CrossRef](#)]
20. Novák, P.; Hůla, J. The influence of sloping land on soil particle translocation during secondary tillage. *Agron. Res.* **2017**, *15*, 799–805.
21. Poesen, J.; Van Wesemael, B.; Govers, G.; Martinez-Fernandez, J.; Desmet, P.; Vandaele, K.; Quine, T.; Degraer, G. Patterns of rock fragment cover generated by tillage erosion. *Geomorphology* **1997**, *18*, 183–197. [[CrossRef](#)]
22. Hůla, J.; Novák, P. Translocation of soil particles during primary soil tillage. *Agron. Res.* **2016**, *14*, 392–399.

23. Rahman, S.; Lobb, D.A.; Chen, Y. Size and density of point-tracers for use in soil translocation studies. In Proceedings of the 45th Annual Meeting, Winnipeg, MB, Canada, 5–6 February 2002; Manitoba Soil Science Society: Manitoba, MB, Canada, 2002.
24. MacLeod, C.J.; Lobb, D.A.; Chen, Y. The relationships between tillage translocation, tillage depth and draught for sweeps. In Proceedings of the 43rd Annual Manitoba Soil Science Society Meeting, Winnipeg, MB, Canada, 25–26 January 2000; Manitoba Soil Science Society: Winnipeg, MB, Canada, 2000; pp. 195–199.



© 2018 by the authors. Licensee MDPI, Basel, Switzerland. This article is an open access article distributed under the terms and conditions of the Creative Commons Attribution (CC BY) license (<http://creativecommons.org/licenses/by/4.0/>).

Article

# Optimization of Multiple Seepage Piping Parameters to Maximize the Critical Hydraulic Gradient in Bimsoils

Yu Wang <sup>1,2</sup>, Changhong Li <sup>1,2,\*</sup>, Yanzhi Hu <sup>3</sup> and Yonggang Xiao <sup>1,2</sup>

<sup>1</sup> Beijing Key Laboratory of Urban Underground Space Engineering, Department of Civil Engineering, School of Civil & Resource Engineering, University of Science & Technology Beijing, Beijing 100083, China; wyzhou@ustb.edu.cn (Y.W.); xygang\_ustb@163.com (Y.X.)

<sup>2</sup> Key Laboratory of the Ministry of Education of China for High-Efficient Mining and Safety of Metal Mines, University of Science & Technology Beijing, Beijing 100083, China

<sup>3</sup> Key Laboratory of Shale Gas and Geoenvironment, Institute of Geology and Geophysics, Chinese Academy of Sciences, Beijing 100029, China; huyz\_iggcas@126.com

\* Correspondence: lch@ustb.edu.cn or lch\_ustb@126.com

Received: 2 August 2017; Accepted: 3 October 2017; Published: 15 October 2017

**Abstract:** Seepage failure in the form of piping can strongly influence the stability of block-in-matrix-soils (bimsoils), as well as weaken and affect the performance of bimsoil structures. The multiple-factor evaluation and optimization play a crucial role in controlling the seepage failure in bimsoil. The aim of this study is to improve the ability to control the piping seepage failure in bimsoil. In this work, the response surface method (RSM) was employed to evaluate and optimize the multiple piping parameters to maximize the critical hydraulic gradient (CHG), in combination with experimental modeling based on a self-developed servo-controlled flow-erosion-stress coupled testing system. All of the studied specimens with rock block percentage (RBP) of 30%, 50%, and 70% were produced as a cylindrical shape (50 mm diameter and 100 mm height) by compaction tests. Four uncertain parameters, such as RBP, soil matrix density, confining pressure, and block morphology were used to fit an optimal response of the CHG. The sensitivity analysis reveals the influential order of the studied factors to CHG. It is found that RBP is the most sensitive factor, the CHG decreases with the increase of RBP, and CHG increases with the increase of confining pressure, soil matrix density, and block angularity.

**Keywords:** bimsoils; critical hydraulic gradient (CHG); response surface methodology; multi-parameter evaluation; laboratory experiment

## 1. Introduction

Bimsoils (block-in-matrix-soils), as a kind of special geomaterial, which are characterized by the extreme nonhomogeneity, environmental sensitivity, and looseness [1–11]. Many engineering geological disasters have direct relations to the bimsoils [3–8]. As is known, piping is a very common and severe kind of seepage failure, it has been pointed out that piping is considered as the main mechanism leading to the failure of hydraulic structures in bimsoils [12–14]. It is also the primary reason resulting in the instability of landslides, dam foundation, and dyke building, which are generally composed of bimsoils. From the statistical data worldwide, for the wreckage earth-rockfill dams, about 40.5% of them are caused by seepage failure (e.g., Malpasset Arch Dam in France 1959, Balder Yamauchi dam in 1964, Tetonin USA 1976, Gouhou Reservoir Dam in China 1993, etc.). In addition, landslides composed of bimsoil material caused by seepage failure are common all over the world. Piping often occurs in loose and unstable structure of bimsoils, especially with high RBP,

part of the soil and rock units is not coupled tightly, even some soil particles are in the state of free suspension; under seepage flow, the high seepage gradient acts on soil-rock interfaces, seepage channel is easily formed in the soil-rock interfaces under the action of seepage force. Once the seepage channels are formed, these channels propagate into soil matrix under continuous water flow, small soil particles move in those channels, and seepage failure occurs accordingly.

Currently, the studies of flow characteristics of bimsoil are mainly focused on the permeable regime [10,15] and flow-stress coupling properties [16]. In addition, seepage piping erosion is almost focused on soil material (e.g., clay, silty, sand, etc.) by laboratory tests [16,17] or numerical simulation [18–20]. Up to now, from literature review, studies about the multi-parameter evolution and optimization for piping seepage failure in bimsoils are rarely reported. Under flow condition, different hydraulic properties of those components in bimsoil results in various non-linear responses [15]. The rock blocks with various size random distributes in bimsoil, change the seepage path of fluid as compared to the homogenous soil and rock material. Large seepage drop occurs at soil-rock interfaces, and contact erosion at the random interfaces is severe and at dominance. The piping characteristics of bimsoil are distinctly influenced by its complicated internal structure. Although the piping phenomenon of bimsoil has been studied through laboratory experiments [21–23], the study of the effect of multiple factors on piping evolution is rarely published. In this work, attempts are made to provide deep insights into the effective evaluation, prevention, and control of piping in bimsoils. A self-developed servo controlled flow erosion stress coupled system was used to obtain the critical hydraulic gradient. In addition, response surface methodology algorithm is used to evaluate the influential order of the studied factors, such as rock block percentage, soil matrix density, confining pressure, and block morphology. The aim of this paper is to improve the ability to control piping erosion failure, by adjusting the sensitive factors in geotechnical engineering construction composed of bimsoil.

## 2. Experimental Methods

### 2.1. Material and Sample Preparation

The sample studied here is a mixture of soil matrix and rock blocks. The soil matrix belongs to a kind of clay soil. The gradation curve of this soil is shown in Figure 1a. The clay soil contained lots of clay minerals with strong hydrophilic property. The liquid limit of the hard clay can reach 64%, while the plastic limit can reach 36%; the plasticity index was about 28 and the liquidity index was about 0.05–0.127. These indices indicated that this kind of soil belonged to a typical high plastic and high plastic clay. The saturation is about 18.5% from the lab measurement. To identify the mineral composition and mineral content, both Scanning Electron Microscope (SEM) and X-ray diffraction (XRD) tests were conducted on the clay soil. According to the results of the SEM tests, rodlike, and irregular quartz grains with a grain size of about 0.01–0.03 mm can be clearly seen that are probably surrounded by clay minerals. The XRD tests reveal that the clay soil has a higher percentage of clay minerals, such as kaolinite (26.73%), montmorillonite (61.52%), and illite (6.25%). The physical and mechanical properties of the soil matrix is listed in Table 1.

Lithology of the crushed rock blocks used in the experiment was marble, the size of rock blocks range between 2 and 5 mm (Figure 1b). According to the geotechnical test standards [24,25] and the prepared bimsoil specimen standard, the threshold value for soil particle and rock block is determined as 2 mm. Density of rock block is 2.53 g/cm<sup>3</sup>, the wet and dry uniaxial compressive strength are 43.21 and 80.75, respectively. Generally, the morphological characteristics of the rock blocks have a great effect on the geomechanical properties of bimsoils. Some quantitative morphological feature of the rock blocks with weighted average indices are obtained by digital image process [8], as listed in Table 2.

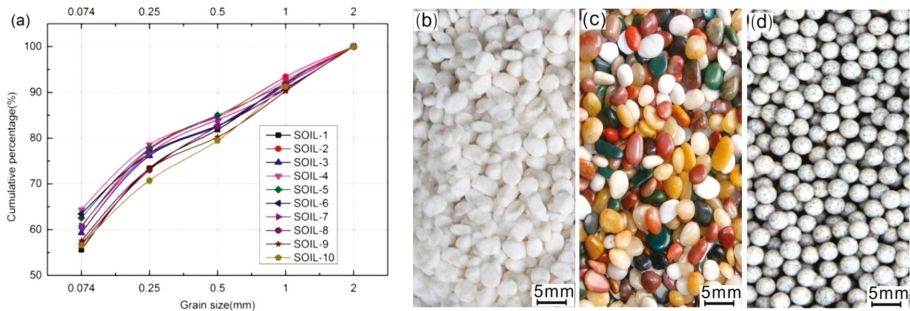


**Figure 1.** The characteristics of soil matrix and rock blocks used for bimsoils in this study. (a) Grain size distribution using sieving method for the used soil matrix; (b–d) Gravel, pebble and round rock blocks used in bimsoil specimen preparation, size range from 2 to 5 mm according to BS1377-1 (1990).

**Table 1.** Basic physical and mechanical properties of the used soil matrix and rock blocks for bimsoil samples.

Index	Soil Matrix	Rock Block
Bulk density (g/cm <sup>3</sup> )	1.64	2.53
Dryweight density (g/cm <sup>3</sup> )	2.06	/
Optimum water content (%)	9.5	/
Specific gravity (G <sub>s</sub> )	2.73	/
Effective particle size, D <sub>10</sub> (mm)	0.01	/
Coefficient of uniformity, C <sub>u</sub>	4.2	/
Coefficient of curvature, C <sub>c</sub>	1.32	/
Liquid limit (%)	64	/
plastic limit (%)	36	/
plasticity index	28	/
liquidity index	0.121	/
Wet compressive strength (MPa)	0.57	43.21
Dry compressive strength (MPa)	2.27	80.75

Note: for soil matrix, the wet state corresponds to natural state, and for rock block, the wet state corresponds to saturation state.

**Table 2.** The morphological feature of three kinds of rock blocks.

Rock Block	Outline Indices			Angularity Indices (Gradient Method)		
	Flakiness	Elongation	Sphericity	Shape Factor	Angularity	Convexity Ratio
Gravel	0.934	1.353	0.834	0.933	0.925	0.895
Pebble	0.745	1.418	0.923	0.823	0.977	0.934
Round ball	1.0	1.0	1.0	1.0	1.0	1.0

In this work, dynamic compaction was used for the preparation of the bimsoils pecimens [10–12,26,27]. The appropriate optimal hammer count was determined according to the relationship between the hammer count and the soil matrix density. Compaction was done in a split mould by applying a dynamic pressure, using a compaction test apparatus. Owing to the high difference of elastic modulus between soil matrix and rock block, compactness of bimsoil is actual the compactness of soil matrix. Soil density is a very important factor affecting the permeability of bimsoil [28]. As a result, how to control the hammer count is crucial to the sensitive analysis of piping erosion. In this work, determination of hammer count producing specimens with different soil density is from the relationship between the soil density and the optimal hammer count, as shown in Figure 2a. The soil matrix density for bimsoil with RBP of 30%, 50%, and 70% increased with the increase of hammer count. To change the soil density, three dot dash lines were drawn to intersect with the curves in Figure 2a, the corresponding of abscissa values are determined as the optimal hammer count. Figure 2b plots the relationship between different soil densities and hammer counts. When the RBP

is 70%, the soil matrix in the specimens is difficult to compacted, considering that the rock blocks in bimsoil specimens with RBP of 70% would be crushed with too much hammer counts, therefore, 12 times was determined as the optimal hammer count. All of the specimens were compacted layer by layer with three layers, as shown in Figure 3a. The length and diameter of the prepared samples were 100 and 50 mm. The prepared cylinder-shaped specimens with RBP of 30%, 50%, and 70% were shown in Figure 3b. All of the tested specimens were sealed with plastic wrap to prevent water evaporation and kept the water content constant.

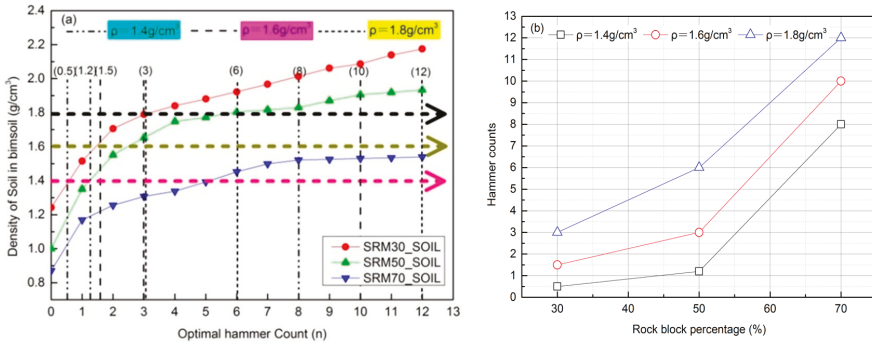


**Figure 2.** The relationships between the hammer count and soil density and the rock block percentage (a. Plot of the soil matrix density against hammer count for specimens with RBP of 30%, 50%, and 70%, respectively; b. Determination of the optimal hammer count for bimsoil specimens with different soil matrix density).



**Figure 3.** Bimsoil specimens used in the piping erosion test. (a. Compact test is used to prepare the bimsoil specimens, and the specimen was compacted with three layers; b. Partial remolded bimsoil specimens for the piping erosion test).

## 2.2. Experimental Setup

This experimental setup was previously detailed described by Wang et al. [12]. Figure 4 shows the layout of the piping test system includes the rigid specimen holder, the servo pressurized water-supply system, and the specimen chamber system. The rigid specimen holder is composed of the beams, rigid column, rigid platform, guide bar, etc. The purpose of the specimen holder is to keep the specimen chamber system steady on the platform during the whole piping test. The servo pressurized water-supply system includes the main parts of the speed feedback component, servo and drive motor, full digital servo controller, and the computer. The sample chamber system is composed of two metal seepage plates, two metal caps (upper one and lower ones), two hose clamps, and a length of heat shrink tubing accommodating the bimsoil specimen. The metal permeability caps are specially designed for the piping test; they contain the inlet valves, outlet valves, and some grooves.

The diameter of the inlet and outlet valves is 3 mm. The heat shrinks the tube and the metal cap is connected with the self-adhesive type and hose clamps. The purpose of the self-adhesive type is to prevent leakage, and its sealing hydraulic pressure can reach 1 MPa. The detailed dimensions and structure of the mental cap, and locations of the inlet and outlet valve are shown in Figure 5. The confining pressure system (Figure 6) is composed of the Hoek cell, air pump, barometer, pneumatic connector, and pneumatic pipe [12].

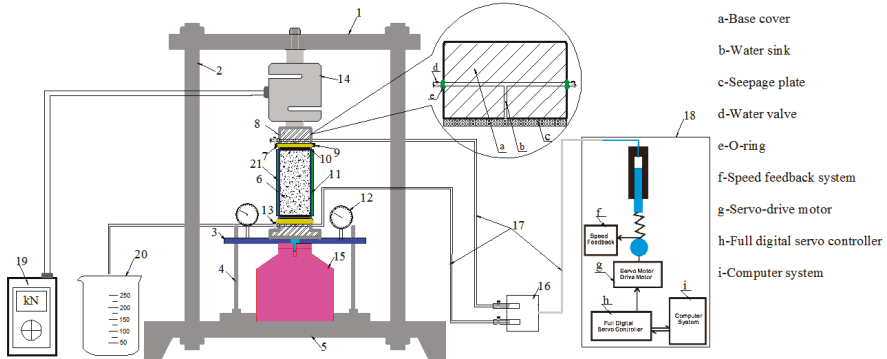


**Figure 4.** Schematic diagram of the piping testing system, which is composed of the rigid specimen holder, the servo pressurized water-supply system, and the specimen chamber system [12]. (1. Upper cross beam; 2. Rigid column; 3. Platform; 4. Guide bar; 5. Lower cross beam; 6. Binsoil specimen; 7. Self-adhesive tape; 8. Permeable cap; 9. Hose clamp; 10. Filter paper; 11. Heat shrink tubing; 12. Seconds counter; 13. Water valve; 14. Force sensor; 15. Hydraulic jack; 16. Three-way valve; 17. Water tube; 18. Servo-injection water system; 19. Force sensor and; 20. Measuring cup).

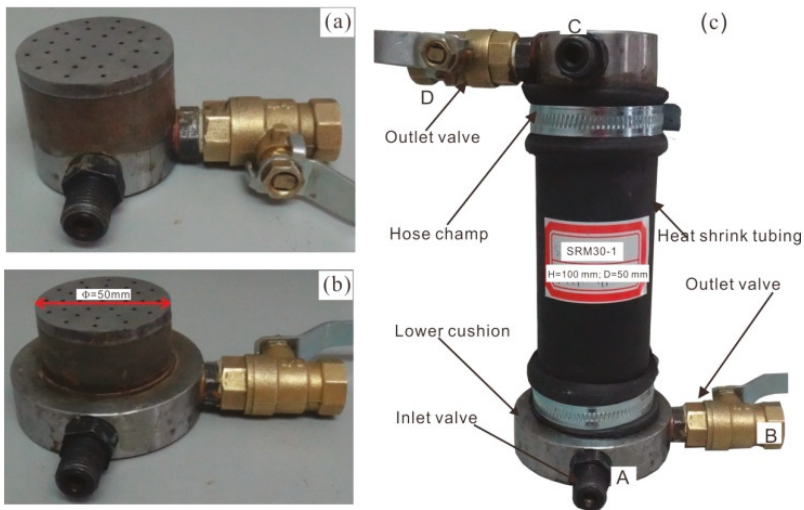


**Figure 5.** Picture of the structure of seepage cap and specimen chamber (a. the lower cap; b. the upper cap; c. specimen chamber for binsoil specimen, taking rock block percentage (RBP) of 30% for example).

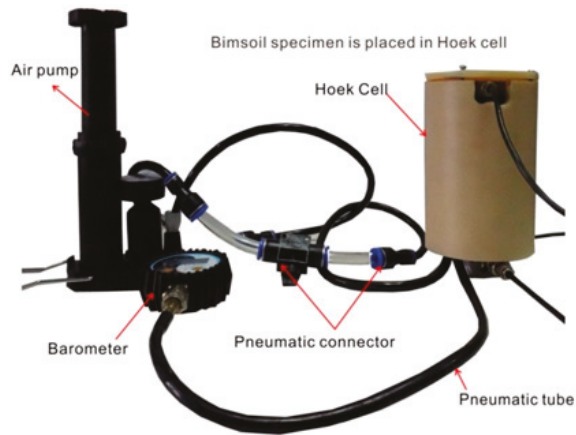


**Figure 6.** Photograph of the confining pressure system, the main components includes: air pump, hoek cell, barometer, pneumatic connector, and pneumatic tube.

### 2.3. Piping Test Procedure

To study the flow-erosion-stress coupled evolution process of bimsoil specimens with different RBPs, and obtain some important results from the piping test, the detailed technical flowchart is shown in Figure 7. The main procedures are as follows: (1) Specimen preparation and saturation. The bimsoil specimen is produced according to the method above. Saturation was performed with vacuum treatment, and then installed by the lower cap, upper cap, hose heating clamps, plastic self-adhesive tape, and shrink tube. The specimen is installed to be kept in the vertical state in order to avoid eccentric compaction. Water is injected at a low constant flow rate to saturate the specimen; (2) Formation of steady seepage field. During flow conditions, the specimen chamber system is placed on the rigid specimen holder. During the water-injection process, water is supplied by a constant pressure increment or a constant flow velocity. It is until the curve of the hydraulic pressure against time gradually became level, and the slope of the water flow curve against time is a constant value, that the steady seepage has formed in the specimen. The detail saturation process has been described by Wang et al. [12]; (3) Isotropic consolidation. The axial stress and confining pressure are exerted simultaneously, making the specimen in the state of equivalent stress; and, (4) Applying seepage pressure step by step. When water flow reaches steady state, we record the water-outflow volume, hydraulic pressure and flow time at each injection steps, and calculate the hydraulic gradient. The permeability coefficient based on the Darcy law is obtained as below:

$$k = \frac{QL}{At(P_1 - P_2)} \frac{\eta_T}{\eta_{20}} \quad (1)$$

where  $Q$  is the total amount of flow water;  $A$  is the specimen cross-section area;  $t$  is the flow time;  $L$  is flow distance (i.e., length of specimen);  $P_1$  and  $P_2$  is the hydraulic pressure of the inlet valve and outlet valve, respectively;  $\eta_T$  and  $\eta_{20}$  are the coefficient of water kinematic viscosity at  $T$  °C (the experimental temperature) and 20 °C, respectively.

Figure 7 shows the flow chart for the multiple parameters evaluation during piping test the in bimsoils. Four factors were considered in this work. Rock block percentage is an accepted factor that influences the mechanical and hydraulic properties of bimsoil, whether by numerical test or laboratory experiments, this factor is always considered [2–6]. The density of soil matrix influences the flow capacity of bimsoil. Zhou et al. [28] have conducted orthogonal test to study the effect of various factors on bimsoil permeability, and showed that soil matrix density was the first influenced factor on

the bimsoil permeability coefficient; in addition, the block morphology has effect on its permability. The stress state of the bimsoil also has an obvious effect on the evolution of piping [29–32]. Studies have shown that for an undisturbed sample, the critical hydraulic gradient is smaller than undisturbed specimen [10,11,15]; therefore, the piping test should consider the factor of stress state. Figure 8 shows the research idea of the multiparameters evaluation and optimization for piping evolution.

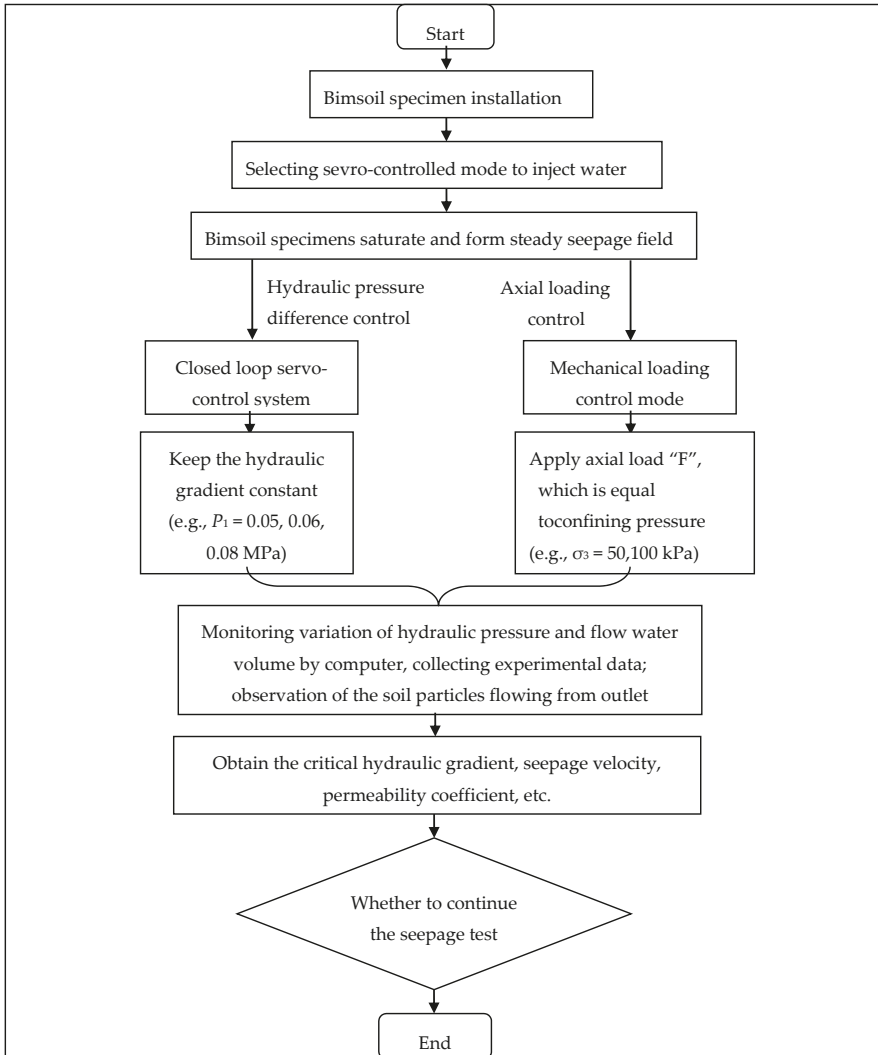
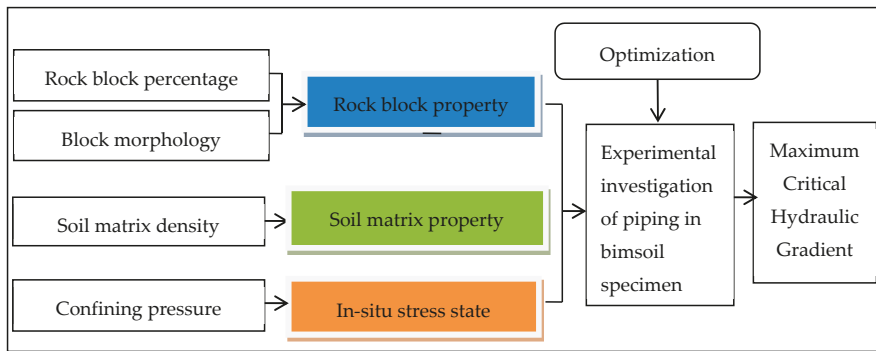


Figure 7. The flow chart of the piping test for bimsoil specimens.



**Figure 8.** The flow chart for the multiple parameters evaluation and optimization for piping in bimsoils.

### 3. Multiparameter Evaluation and Analysis

#### 3.1. Box-Behnken Design

In this work, the response surface methodology (RSM) approach is applied to the evaluation and optimization of the piping stability in the bimsoils. In this work, the RSM approach is applied to evaluate an index of critical hydraulic gradient (which is defined as the value of piping initiation) for bimsoil during piping. Based on the least squares criterion, RSM is utilized to approximate a response over a range of variability of input factors, in terms of the maximum critical hydraulic gradient. The RSM model can offer a cost-effective and efficient way to deal with the uncertain factors for piping seepage, the form of it can be linear or fully quadratic. More detailed statistical and mathematical theories of RSM can refer to studies of Myers and Montgomery [33]. Four uncertain parameters, such as rock block percentage (RBP), soil matrix density (SMD), confining pressure (CP), and block morphology (BM) are given a reasonable range with the actual minimum and maximum values or coded symbol of “−1” and “+1”, respectively, as listed in Table 3. According to the principle of the RSM method, for the four variables, a total of 27 cases were required based on the approach of Box-Behnken Design, which originated from the optimal design theory [34–36]. Table 4 lists the 27 combinations of these uncertain parameters generated by the Box-Behnken Design. After the piping experiment of each case, the results of critical hydraulic gradient are listed in column 8 in Table 4, as the response value. The critical hydraulic gradient is determined from the curves of hydraulic gradient against time. Taking the specimen with RBP of 30% and 50% for example (Figure 9), hydraulic gradient increases with the increase of flow time. When it reaches a critical value, the curve suddenly drops and fluctuates with time. The inflection point is determined as the critical hydraulic gradient. Some significant results can be drawn from Figure 9, as below:

- (1) The curves present a fluctuation trend after the critical hydraulic pressure, however, the value cannot exceed the critical peak value. This result implies that irreversible damage occurs in bimsoil during piping. During the process of piping, the erosion and movement of soil particles result in the change of permeability. When the fine soil particles during movement are clogged in the pores, leading to the increment of hydraulic gradient, seepage velocity, and the associated permeability coefficient; and when the clogged pores are broken through again, these values suddenly decrease. This non-linear multiple fluctuation always exists in the piping process.
- (2) From the curves of flow water, it can also be seen that the slope of the curve is not constant, but variational during the whole test. The non-linear fluctuation behavior of the curves shows that the evolution of piping includes a series of complex movement behaviors, such as the erosion, migration of fine soil particles; contact erosion of rock-soil interface; forming of pore channel; blocking of flow channel by fine soil particles; breakdown of the blocked flow channel; and,

re-block of the flow channel, etc. The characteristics of piping in bimsoilare progressive and repeated. The blocked flow channel can be attributed to two factors, one is the fine soil particles; the other is the movement of rock blocks, as the structure of bimsoil sample changes, the blocks would sink along the direction of water flow.

**Table 3.** The considered factors and levels for the response surface method (RSM) model.

Influential Factors	Coded Symbol	Levels		
		(-1)	(0)	(+1)
Rock block percentage (%)	A	30	50	70
Soil matrix density (g/cm <sup>3</sup> )	B	1.4	1.6	1.8
Confining pressure (kPa)	C	0	100	200
Block morphology (/)	D	0	1	2

Note: For factor of block morphology, level “0” refers to round ball; level “1” refers to pebble; level 2 refers to “gavel”.

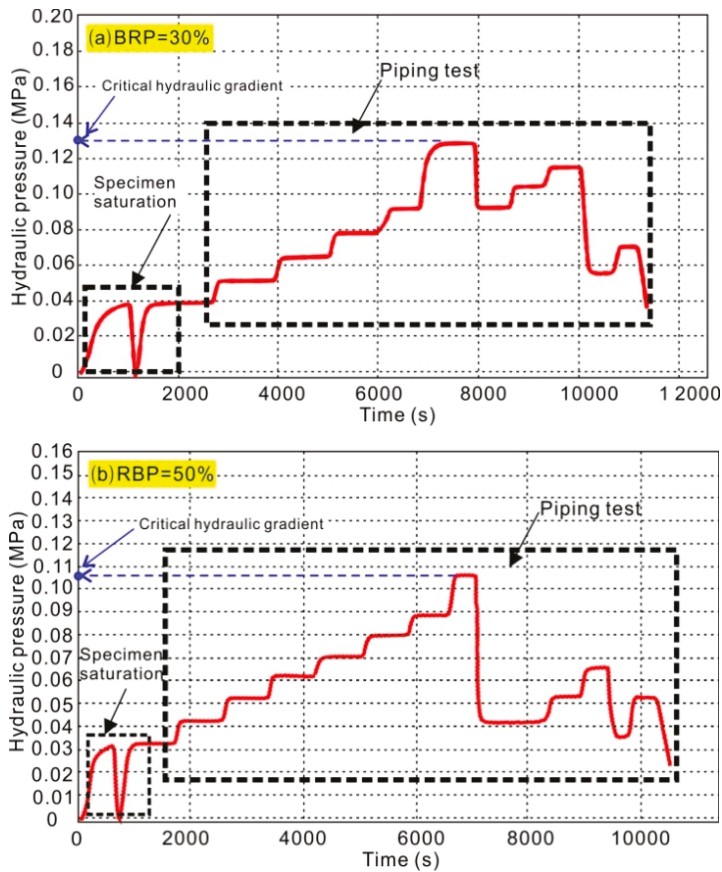


**Figure 9.** Determination of critical hydraulic gradient for bimsoil specimen with RBP of 30% and 50% (a. specimen with rock block percentage (RBP) of 30%, corresponds to the case 10 in Table 4; b. specimen with RBP of 50% corresponds to the case 16 in Table 4.

**Table 4.** Box-Behnken design table for piping erosion test.

Run	A-RBP (%)	B-SMD (g/cm <sup>3</sup> )	C-CP (kPa)	D-BM (l)	R <sup>2</sup>
1	70	1.6	100	0	88.67
2	50	1.8	200	1	120.32
3	50	1.6	200	0	127.45
4	70	1.4	100	1	80.24
5	30	1.6	0	1	135.2
6	50	1.4	100	0	109.87
7	30	1.4	100	1	138.56
8	30	1.8	100	1	177.23
9	50	1.4	100	2	98.23
10	50	1.6	100	1	107.73
11	50	1.8	0	1	115.57
12	70	1.6	200	1	105.78
13	50	1.8	100	2	106.44
14	70	1.6	100	2	86.51
15	30	1.6	100	0	160.32
16	50	1.8	100	0	118.45
17	70	1.8	100	1	90.53
18	30	1.6	200	1	156.64
19	30	1.6	100	2	147.45
20	50	1.6	0	0	108.45
21	50	1.6	100	1	107.73
22	50	1.4	0	1	100.03
23	50	1.6	0	2	102.33
24	50	1.4	200	1	110.32
25	70	1.6	0	1	78.65
26	50	1.6	100	1	107.73
27	50	1.6	200	2	116.23

### 3.2. RSM Model Analysis

From Figure 8, the onset of the steep drop in the hydraulic pressure-flow time curves was assumed to estimate the critical hydraulic gradient. Beyond this point, the seepage velocity, hydraulic gradient, and permeability fluctuate repeatedly. This method to determine the critical hydraulic gradient has also been used by other researchers, such as Das et al. [37] and Das and Viswanadham [38] during piping tests. When the critical hydraulic gradient was obtained, the RSM method is used to analyze the relationship between the response value and the four uncertain factors. In order to select the appropriate RSM model, a linear model, two factor model interaction model (2FI), quadratic model, and cubic model are selected to judge, which polynomial fits the equation based on the statistical approach, as shown in Table 5. Table 5 lists the response surface model for the critical hydraulic gradient. If the model has the highest polynomial, and the other additional terms are significant, and the model is not aliased [12,39], we choose it as the appropriate model. We would not select the cubic model, if it is aliased. Aliasing phenomenon decreases the number of experimental runs. When this appears, several groups of effects are combined into one group and the most significant effect in the group is used to represent the effect of the group. Essentially, it is important to note that the selected model should not be aliased. In addition, the model has the maximum “Predicted R-Squared” and “Adjusted R-Squared” is also important criteria to be considered [39]. From the results of Table 5, the fully quadratic model is finally selected to build the critical hydraulic gradient (CHG) response surface in the subsequent optimization process.

**Table 5.** Statistical approach to select the RSM model for critical hydraulic gradient.

Source	Std.Dev.	R-Squared	AdjustedR-Squared	PredictedR-Squared	Press	Suggestion
Linear	8.24	0.90	0.89	0.80	2280.37	-
2FI	8.81	0.92	0.87	0.75	3811.78	-
Quadratic	6.69	0.97	0.93	0.85	3093.21	Suggested
Cubic	4.02	0.99	0.97	0.40	9275.11	Aliased

The anova for the response surface quadratic model of CHG is shown in Table 6. From the result, the model F-value of 24.01 implies the model is very significant, the change is less than 0.1% that a “Model F-Value” this large could occur due to noise. Values of “Prob > F” less than 0.05 indicates that the model variations are significant. In this case, the model *p*-value prob of the studied factors is <0.0001, 0.0020, 0.013, and 0.0325; this result indicates that the factors of A, B, C, and D are all significant model terms. The smaller the *p*-value pro, the more sensitive of the factor is to the response surface. The influential order of these four factors is: A-rock block percentage > C-confining pressure > B-soil matrix density > D-block morphology. The equations fitted to the critical hydraulic gradient response surface in terms of actual factors are:

$$\text{CHG} = +119.11 - 1.73A + 50.31B + 0.12C - 12.60D - 1.77AB + 0.11A \times D - 0.07B \times C - 0.46B \times D - 0.013C \times D + 0.03A^2 + 26.19B^2 + 1.63D^2 \quad (2)$$

where A is the rock block percentage; B is the soil matrix density; C is the confining pressure; and, D is the block morphology.

**Table 6.** Anova for SRM response surface with quadratic model.

Source	Sum of Squares	df	Mean Square	F Value	<i>p</i> -Value Prob > F	Significance
Model	15,043.44	14	1074.53	24.01	<0.0001	significant
A-rock block percentage	12,353.37	1	12,353.37	276.04	<0.0001	-
B-soil matrix density	694.48	1	694.48	15.52	0.0020	-
C-confining pressure	776.18	1	776.18	17.34	0.0013	-
D-block morphology	261.52	1	261.52	5.84	0.033	-
AB	201.35	1	201.35	4.49	0.056	-
AC	8.09	1	8.09	0.18	0.68	-
AD	28.67	1	28.67	0.64	0.44	-
BC	7.67	1	7.67	0.17	0.046	-
BD	0.03	1	0.03	0.00071	0.97	-
CD	6.50	1	6.50	0.15	0.70	-
A <sup>2</sup>	650.77	1	650.77	14.54	0.0025	-
B <sup>2</sup>	5.85	1	5.85	0.13	0.72	-
C <sup>2</sup>	31.88	1	31.88	0.71	0.42	-
D <sup>2</sup>	14.06	1	14.06	0.31	0.59	-
Residual	537.01	12	44.75	-	-	-
Lack of Fit	537.01	10	53.70	-	-	-
Pure Error	0	2	0	-	-	-
Cor Total	15,580.46	26	-	-	-	-

Figure 10 shows the normal plots of residuals, which can reflect the distribution of the residuals for the response value of the critical hydraulic gradient. All of the test points in the “Normal Plot of Residuals” fall on the straight line, implying that the residuals are normally distributed, and the model is significant. Figure 11 shows the “Predicted versus Actual” for critical hydraulic gradient, illustrating whether the generated equation of gradient response surface accurately predicts the actual values. It can be seen that generated hydraulic gradient response surface models provide such reliable predicted values for hydraulic gradient, as compared to the actual values of the hydraulic gradient.

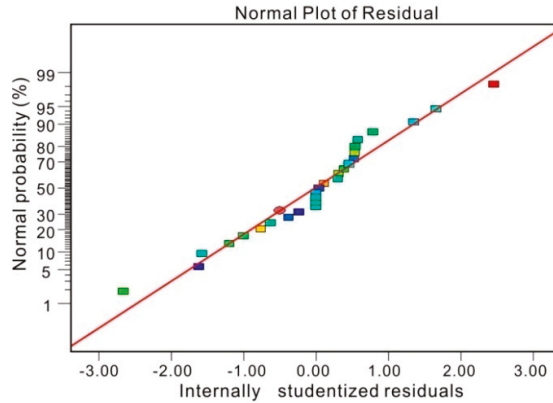


Figure 10. Normal plot of residuals for critical hydraulic gradient.

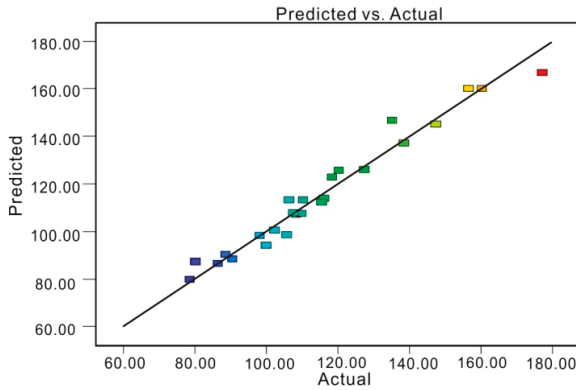
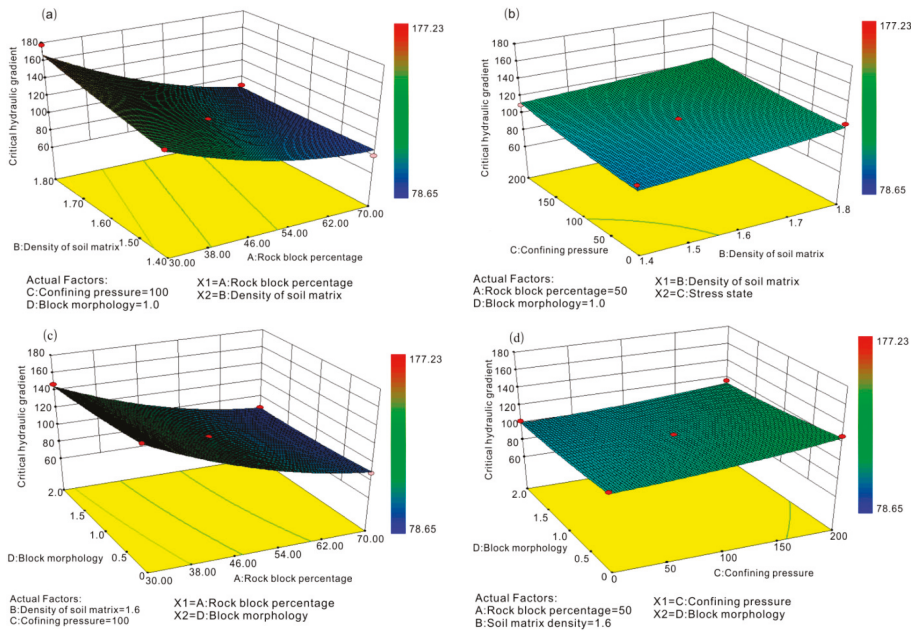


Figure 11. Predicted value versus the actual values for response surface value.

Figure 12 plots the three-dimensional (3D) response surface of the four studied factors, the response surface represents all the 27 run case. It shows the influential trend of the four factors to CHG. Figure 12a plots the influence of factor rock block percentage and soil matrix density on the CHG response. It can be clearly seen that CHG decreases with the increasing rock block percentage; Figure 12b plots the influence of soil matrix density and confining pressure on CHG response, the CHG increases with the increase of confining pressure and soil matrix density; Figure 12c plots the influence of rock block percentage and block morphology on the CHG response, the CHG increases with the increase of block angularity, this result implies the incremental compactness of soil particles and contact between soil matrix and rock blocks. The coupling degree of rock block and soil matrix improves as the confining pressure and soil density increase. Content of rock blocks increases the number of rock-soil interface, the sudden drop of seepage force at these interfaces causes the occurrence of contact erosion, and the associated seepage failure, which leads to the decrement of flow stability of bimsoil specimen.



**Figure 12.** The influential of four studied factors on critical hydraulic gradient response surface (a. influence of factor A and B on variation of the response surface; b. influence of factor B and C on variation of the response surface; c. influence of factor A and D on variation of the response surface; and, d. influence of factor C and D on variation of the response surface).

### 3.3. Critical Hydraulic Gradient Optimization

The index of CHG indicates the resistance capacity of bimsoil to seepage force, the larger the CHG value, the better capacity of bimsoil is. In this section, the RSM numerical optimization algorithm is employed to select the set of variables that leads to the maximum CHG value. A total of 54 optimal solutions are generated after the RSM numerically optimization. The desirability value ranges from 0.376 to 1.0. We select the solutions with the maximum desirability value to analyze. Figure 13 shows the relationship between the studied factors and the desirability value. The red box indicates the desirability value equal to 1.0, which are the optimist solutions. From the optimization results, the rock block percentage is about 30% if we want to obtain the maximum CHG, it corresponds to the smallest the block content. Higher soil matrix density is desirable to improve the CHG. When to get a high CHG, confining pressure ranges from 160 to 180 kPa, in-situ stress state has an important influence on the CHG. The factor of block morphology is not so sensitive to CHG, and angular rock block tends to improve CHG as compared to round block. Among the 54 solutions, we select the 20 cases when the desirability is 1, as listed in Table 7.

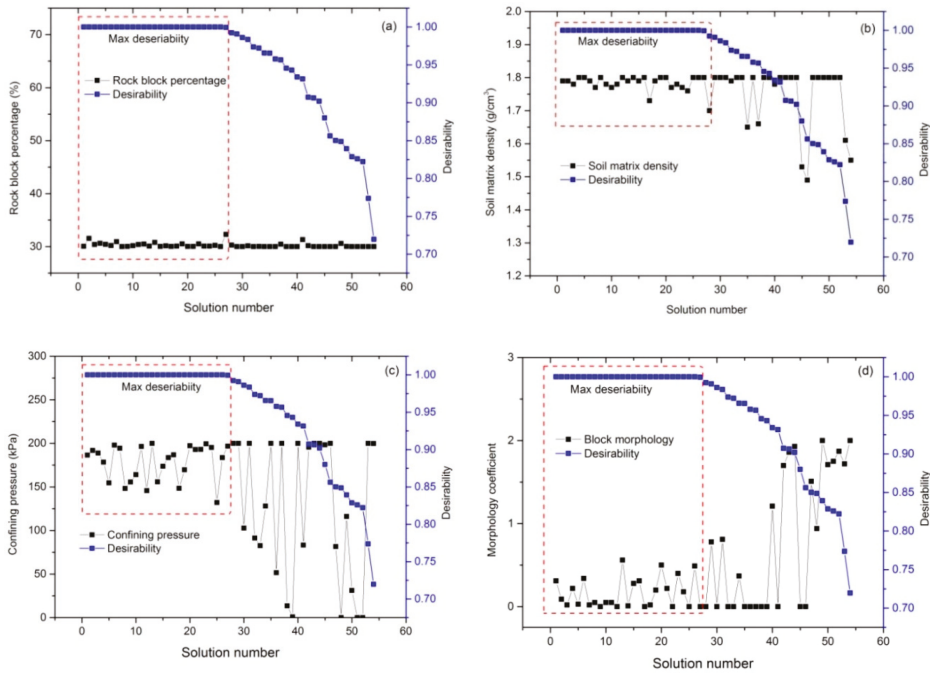


**Figure 13.** Influences of the studied factors on the optimist solutions (a–d plots the effect of rock block percentage, soil density, confining pressure, and block morphology, respectively).

**Table 7.** The optimal solutions for the maximum of critical hydraulic gradient (CHG).

Number	RBP (%)	D (g/cm3)	CP (kPa)	M (l)	CHG	Desirability
1	30.07	1.79	186.47	0.31	178.452	1
2	31.54	1.79	191.94	0.09	177.466	1
3	30.4	1.78	188.79	0.02	180.391	1
4	30.62	1.8	178.46	0.22	177.775	1
5	30.43	1.8	154.62	0.03	177.951	1
6	30.2	1.79	197.9	0.34	178.88	1
7	30.94	1.77	194.37	0.02	178.524	1
8	30.01	1.8	148.35	0.05	178.51	1
9	30.04	1.78	155.65	0	178.294	1
10	30.17	1.77	164.14	0.05	177.474	1
11	30.4	1.78	196.52	0.05	180.62	1
12	30.49	1.8	145.79	0	177.525	1
13	30.09	1.79	199.95	0.56	177.354	1
14	30.8	1.8	155.8	0.01	177.384	1
15	30.03	1.79	173.65	0.28	177.706	1
16	30.15	1.8	183.66	0.31	178.752	1
17	30.04	1.73	186.88	0	177.402	1
18	30.1	1.79	148.41	0.02	177.683	1
19	30.52	1.8	169.68	0.2	177.46	1
20	30.04	1.8	197.27	0.5	178.454	1

### 3.4. Discussions

Based on the experimental data of the piping test, we used the response surface method to conduct the sensitive analysis. The rock block percentage is the most sensitive factor influenced the seepage erosion failure. The role of rock blocks in bimsoil is always considered to be the important factor influencing the mechanical and physical properties. Xu et al. [40], Liao [41], Dan et al. [15],

and Wang et al. [10] have conducted a series of permeable test for bimsoil, they found that rock blocks in bimsoil have obvious effect on permeability coefficient. In our study, it was also found that rock blocks have an obvious influence on the critical hydraulic gradient. Although the rock blocks play a role of an impervious effect, this effect may improve the permeability in some ways, however, the contact erosion at rock-soil interface is always the decisive factor controlling the seepage failure of bimsoil. Along the seepage direction, the hydraulic pressure drops sharply at rock-soil interfaces, resulting in the formation of a great seepage force at the interfaces, flow channel of erosion first forms at these parts. Therefore, the characteristics of rock blocks (e.g., size, shape, distribution, content, etc.) control the flow life of specimens, and the critical hydraulic gradient decreases with an increasing rock block content. The factor of confining pressure reflects the in-situ stress state of bimsoil, some scholars clearly point out that when studying the permeable characteristics of bimsoil, confining pressure should not be ignored [29,42]; otherwise, most of the tests do not consider the actual stress state. Soil matrix density is also a crucial factor to the permeable characteristics of bimsoil, Zhou et al. [28] conducted orthogonal tests on the permeability of bimsoil. They found that soil density is more sensitive to other factors. Tickell and Hiatt [43] discussed the influence of granular angularity and roundness on the permeability coefficient, found that with the increasing of angularity, the permeability coefficient increases. The result implies that angularity has different degree of resistance on water flow. Our test results further prove this phenomenon and reveal some new insights on the seepage failure of bimsoils.

#### 4. Conclusions

In this work, a self-developed servo-controlled flow-erosion-stress system was used to conduct the piping experiments. By using the response surface methodology, four uncertain parameters (i.e., rock block percentage, soil matrix density, confining pressure, and block morphology) were used to evaluate and obtain the optimal solutions for the critical hydraulic gradient. The following conclusions can be drawn from this study:

- (1) By the RSM evaluation, the influential order of the studied factors to piping seepage failure is firstly obtained, rock block percentage is the most sensitive factor to the critical hydraulic gradient. The influential order is rock block percentage > confining pressure > soil matrix density > block morphology.
- (2) Confining pressure has obvious effect on the critical hydraulic gradient of bimsoil. The sensitivity of this factor is second to the rock block percentage, it is a non-negligible factor when investigating the piping erosion mechanism of bimsoil. In-situ stress state not only influences the seepage field, but also affects the degree of contact erosion among rock-soil interfaces.
- (3) Increasing soil density, confining pressure, and block angularity can improve the ability to resist piping seepage failure. In bimsoil construction, we can adjust the rock block content, compaction degree, and block morphology to improve the ability of anti-seepage erosion.

**Acknowledgments:** The authors would like to thank the editors and the anonymous reviewers for their helpful and constructive comments. This work was supported by the Beijing Natural Science Foundation of China (Grants No. 8164070), National Natural Science Foundation of China (41502294), Fundamental Research Funds for the Central Universities (2302017FRF-TP-17-027A1), and the National key technologies Research & Development program (2017YFC0804609).

**Author Contributions:** Yu Wang and Changhong Li designed the theoretical framework; Yu Wang conducted the experiment, analyzed the experimental data and wrote the manuscript; Yanzhi Hu and Yonggang Xiao corrected the figures.

**Conflicts of Interest:** The authors declare no conflict of interest.

#### References

1. Lindquist, E.S. The Strength and Deformation Properties of Melange. Ph.D. Thesis, University of California, Berkeley, Berkeley, CA, USA, March 1994.

2. Medley, E.W. Observations on tortuous failure surfaces in Bimrocks. *Felsbau Rock Soil Eng.* **2004**, *5*, 35–43.
3. Medley, E.W. Systematic characterization of mélange bimrocks and other chaotic soil/rockmixtures. *Felsbau-Rock Soil Eng.* **1999**, *17*, 152–162.
4. Goodman, R.E.; Ahlgren, C.S. Evaluating safety of concrete gravity dam on weak rock. *J. Geotech. Geoenviron. Eng.* **2000**, *126*, 429–442. [[CrossRef](#)]
5. Coli, N.; Boldin, I.D.; Bandini, A.; Lopes, D.S. Modeling of complex geological rock mixtures under triaxial testing conditions. In Proceedings of the International Symposium on Rock Engineering & Technology for Sustainable Underground Construction (Eurock), Stockholm, Sweden, 28–30 May 2012.
6. Coli, N.; Berry, P.; Boldini, D. In situ non-conventional shear tests for the mechanical characterisation of a bimrock. *Int. J. Rock Mech. Min. Sci.* **2011**, *48*, 95–102. [[CrossRef](#)]
7. Afifipour, M.; Moarefvand, P. Failure patterns of geomaterials with block-in-matrix texture: Experimental and numerical evaluation. *Arab. J. Geosci.* **2014**, *7*, 2781–2792. [[CrossRef](#)]
8. Wang, Y.; Li, X.; Zhang, B. Meso-damage cracking characteristics analysis for rock and soil aggregate with CT test. *Sci. China Technol. Sci.* **2014**, *57*, 1361–1371. [[CrossRef](#)]
9. Wang, Y.; Li, X.; Wu, Y.F.; Lin, C.; Zhang, B. Experimental study on meso-damage cracking characteristics of RSA by CT test. *Environ. Earth Sci.* **2015**, *73*, 5545–5558. [[CrossRef](#)]
10. Wang, Y.; Li, X.; Zheng, B.; Li, S.D.; Duan, Y.T. A laboratory study of the effect of confining pressure on permeable property in soil-rock mixture. *Environ. Earth Sci.* **2016**, *75*, 1–16. [[CrossRef](#)]
11. Wang, Y.; Li, X.; Zheng, B.; Ma, C.F. An Experimental Investigation of the Flow-Stress Coupling Characteristics of Soil-Rock Mixture under Compression. *Transp. Porous Media* **2016**. [[CrossRef](#)]
12. Wang, Y.; Li, C.; Zhou, X.; Wei, X. Seepage Piping Evolution Characteristics in Bimsoils—An Experimental Study. *Water* **2017**, *9*, 458. [[CrossRef](#)]
13. Estabragh, A.R.; Soltannajad, K.; Javadi, A.A. Improving piping resistance using randomly distributed fibers. *Geotext. Geomembr.* **2014**, *42*, 15–24. [[CrossRef](#)]
14. Sibille, L.; Lominé, F.; Poullain, P. Internal erosion in granular media: Direct numerical simulations and energy interpretation. *Hydrol. Process.* **2015**, *29*, 2149–2163. [[CrossRef](#)]
15. Dan, H.C.; He, L.H.; Xu, B. Experimental Investigation on Non-Darcian Flow in Unbound Graded Aggregate Material of Highway Pavement. *Transp. Porous Media* **2016**, *112*, 189–206. [[CrossRef](#)]
16. Cyril, G.; Yves-Henri, F.; Rémi, B. Contact erosion at the interface between granular coarse soil and various base soils under tangential flow condition. *J. Geotech. Geoenviron. Eng.* **2009**, *136*, 741–750. [[CrossRef](#)]
17. Richards, K.S.; Reddy, K.R. Experimental investigation of initiation of backward erosion piping in soils. *Géotechnique* **2012**, *62*, 933–942. [[CrossRef](#)]
18. Ni, X.; Wang, Y.; Dallo, Y.A.H. Discussion of Analysis of the internal stability of granular soils using different methods. *Can. Geotech. J.* **2015**, *52*, 382–384. [[CrossRef](#)]
19. Liang, Y.; Yeh, T.C.J.; Wang, J.; Liu, M.; Zha, Y.; Hao, Y. An auto-adaptive moving mesh method for the numerical simulation of piping erosion. *Comput. Geotech.* **2017**, *82*, 237–248. [[CrossRef](#)]
20. Marwan, A.; Zhou, M.M.; Abdelrehim, M.Z. Optimization of artificial ground freezing in tunneling in the presence of seepage flow. *Comput. Geotech.* **2016**, *75*, 112–125. [[CrossRef](#)]
21. Guo, Q.G. *The Engineering Properties and Application of Coarse Grained Soil*; The Yellow River Water Conservancy Press: Zhengzhou, China, 1998; pp. 286–313. (In Chinese)
22. Ge, C.; Zhang, R.T. Benxi steel NaFen dam dam foundation seepage deformation survey—On gravel seepage deformation of soil. *Oil-Gasfield Surf. Eng.* **2003**, *22*, 37–38. (In Chinese)
23. Feng, S.R.; Zhao, H.B.; Jiang, Z.M.; Zeng, X.X. Experimental study on seepage failure characteristics of broken rock mass in dam foundation at left bank of Xiangjiaba Hydropower Project. *Chin. J. Geotech. Eng.* **2012**, *34*, 600–605. (In Chinese)
24. British Standards Institution. *Methods of Test for Soils for Civil Engineering Purposes—Part 1: General Requirements and Sample Preparation*; BS1377-1 (1990) British Standard; British Standards Institution: London, UK, 1990.
25. The Ministry of Water Resources of China. *Standard for Soil Test Method*; GB/T 50123-1999 (1999); China Planning Press: Beijing, China, 1999. (In Chinese)
26. Donaghe, R.T.; Torrey, V.H. Proposed New Standard Test Method For Laboratory Compaction Testing of Soil-Rock Mixtures Using Standard Effort. *Geotech. Test. J.* **1994**, *17*, 387–392.

27. Rücknagel, J.; Götze, P.; Hofmann, B.; Christen, O.; Marschall, K. The influence of soil gravel content on compaction behavior and pre-compression stress. *Geoderma* **2013**, *209–210*, 226–232. [[CrossRef](#)]
28. Zhou, Z.; Fu, H.L.; Liu, B.C. Orthogonal tests on permeability of soil-rock mixture. *Chin. J. Rock Mech. Eng.* **2006**, *28*, 1132–1138.
29. Mao, C.X. Discussion of Seepage control of earth dam on the sand-gravel foundation. *J. Hydraul. Eng.* **1963**, *4*, 66–69. (In Chinese)
30. Cao, D.L. Cofferdam seepage control of Gezhouba Project. *J. Hydraul. Eng.* **1988**, *19*, 49–55. (In Chinese)
31. Luo, Y.L.; Wu, Q.; Zhan, M.L.; Sheng, G.C. Development of Seepage-Erosion-Stress Coupling Piping Test Apparatus and Its Primary Application. *Chin. J. Rock Mech. Eng.* **2013**, *32*, 2108–2114. (In Chinese)
32. Kenney, T.C.; Lau, D. Internal stability of granular filters. *Can. Geotech. J.* **1985**, *22*, 215–225. [[CrossRef](#)]
33. Myers, R.H.; Montgomery, D.C. *Response Surface Methodology: Process and Product Optimization Using Designed Experiments*; John Wiley and Sons: Hoboken, NJ, USA, 2002.
34. Box, G.E.P.; Wilson, K.B. On the Experimental Attainment of optimum Conditions. In *Breakthroughs in Statistics*; Springer: New York, NY, USA, 1992; pp. 270–310.
35. Kiefer, W.J. Optimum designs in regression problems. *Ann. Math. Stat.* **1999**, *30*, 271–294. [[CrossRef](#)]
36. Yu, W.; Varavei, A.; Sepehrnoori, K. Optimization of Shale Gas Production Using Design of Experiment and Response Surface Methodology. *Eng. Sour. Part A Recovery Util. Environ. Eff.* **2015**, *37*, 906–918. [[CrossRef](#)]
37. Das, A.; Jayashree, C.; Viswanadham, B.V.S. Effect of randomly distributed geofibers on the piping behaviour of embankments constructed with fly ash as a fill material. *Geotext. Geomembr.* **2009**, *27*, 341–349. [[CrossRef](#)]
38. Das, A.; Viswanadham, B.V.S. Experiments on the piping behaviour of geofiber-reinforced soil. *Geosynth. Int.* **2010**, *17*, 171–182. [[CrossRef](#)]
39. Wang, Y.; Li, X.; Hu, R.; Ma, C.F.; Zhao, Z.Z.; Zhang, B. Numerical Evaluation and Optimization of Multiple Hydraulically Fractured Parameters Using a Flow-Stress-Damage Coupled Approach. *Energies* **2016**, *9*, 325. [[CrossRef](#)]
40. Xu, W.J.; Wang, Y.G. Meso-structural permeability of S-RM based on numerical tests. *China J. Rock Mech. Eng.* **2010**, *32*, 543–550.
41. Liao, Q.L. Geological Origin and Structure model of Rock and Soil Aggregate and Study on Its Mechanical and MH Coupled Properties. Ph.D. Thesis, Institute of Geology and Geophysics, Chinese Academy of Science, Beijing, China, 2004. (In Chinese)
42. Midgley, T.L.; Fox, G.A.; Wilson, G.V.; Felice, R.M.; Heeren, D.M. In situ soil pipeflow experiments on contrasting streambank soils. *Trans. ASABE* **2013**, *56*, 479–488. [[CrossRef](#)]
43. Tickell, F.G.; Hiatt, W.N. Effect of angularity of grains on porosity and permeability of unconsolidated sands. *AAPG Bull.* **1938**, *22*, 1272–1274.



© 2017 by the authors. Licensee MDPI, Basel, Switzerland. This article is an open access article distributed under the terms and conditions of the Creative Commons Attribution (CC BY) license (<http://creativecommons.org/licenses/by/4.0/>).

Article

# Transient Modeling of Flow in Unsaturated Soils Using a Novel Collocation Meshless Method

Cheng-Yu Ku \*, Chih-Yu Liu, Jing-En Xiao and Weichung Yeih

Department of Harbor and River Engineering, National Taiwan Ocean University, Keelung 20224, Taiwan; 20452003@email.ntou.edu.tw (C.-Y.L.); 20452002@email.ntou.edu.tw (J.-E.X.); wcyeih@mail.ntou.edu.tw (W.Y.)

\* Correspondence: chkst26@mail.ntou.edu.tw; Tel.: +886-2-2462-2192 (ext. 6109)

Received: 1 November 2017; Accepted: 4 December 2017; Published: 7 December 2017

**Abstract:** In this paper, a novel meshless method for the transient modeling of subsurface flow in unsaturated soils was developed. A linearization process for the nonlinear Richards equation using the Gardner exponential model to analyze the transient flow in the unsaturated zone was adopted. For the transient modeling, we proposed a pioneering work using the collocation Trefftz method and utilized the coordinate system in Minkowski spacetime instead of that in the original Euclidean space. The initial value problem for transient modeling of subsurface flow in unsaturated soils can then be transformed into the inverse boundary value problem. A numerical solution obtained in the spacetime coordinate system was approximated by superpositioning Trefftz basis functions satisfying the governing equation for boundary collocation points on partial problem domain boundary in the spacetime coordinate system. As a result, the transient problems can be solved without using the traditional time-marching scheme. The validity of the proposed method is established for several test problems. Numerical results demonstrate that the proposed method is highly accurate and computationally efficient. The results also reveal that it has great numerical stability for the transient modeling of subsurface flow in unsaturated soils.

**Keywords:** unsaturated soil; Richards equation; the Trefftz method; transient; the meshless method

## 1. Introduction

Increasing interest has been shown in recent years in understanding the behavior of unsaturated soils. The prediction of moisture flow under transient conditions is important in engineering practice when considering such practical problems as the design of shallow foundations, pavements, and the stability of unsaturated soil slopes [1–4]. As a result, unsaturated flow has become one of the most important and active topics of research. A complete theory of subsurface flow when rainfall infiltrates unsaturated zones can be described using either the variably saturated flow equation or the generalized Richards equation [5]. The Richards equation is a highly nonlinear equation governed by nonlinear physical relationships. Nonlinear physical relationships can be described using soil–water characteristic curves [6–8]. Since the Richards equation is highly nonlinear and cannot directly provide an analytical solution, modeling flow process in unsaturated soils is usually based on the numerical solutions of the Richards equation [9–15].

Numerical approaches to the simulation of the Richards equation using the mesh-based methods, such as the finite difference method [16–19] or the finite element method [20–23], are well documented in the past. Despite the great success of the mesh-based methods as effective numerical tools for the solution of problems on complex domains, there is still growing interest in the development of new advanced computational methods [24–26]. Meshless methods emerge as a competitive alternative to discretization methods. Differing from conventional mesh-based methods, the meshless method has the advantages that it does not need the mesh generation [27]. Problems involving regions of irregular

geometry are generally intractable analytically [28]. For such problems, the use of numerical methods, especially the boundary-type meshless method, to obtain approximate solutions is advantageous [29]. A significant number of such methods have been proposed, such as the Trefftz method [30,31], the method of fundamental solution [32,33], the element-free Galerkin method [34], the reproducing kernel particle method [35], and the meshless local Petrov–Galerkin approach [36].

The Trefftz method is probably one of the most popular boundary-type meshless methods for solving boundary value problems where approximate solutions are expressed as a linear combination of functions automatically satisfying governing equations [37,38]. Li et al. [39] provided a comprehensive comparison of the Trefftz method, collocation, and other boundary methods, concluding that the collocation Trefftz method (CTM) is the simplest algorithm and provides the most accurate solutions with optimal numerical stability. Because the Trefftz method is originally developed to deal with the boundary value problems in Euclidean space, the application the Trefftz method for solving time-dependent problems is hardly found.

In this paper, we proposed a pioneering work using the CTM for transient modeling of subsurface flow in unsaturated soils. Since the Richards equation is highly nonlinear, we first proposed a linearization process for the nonlinear Richards equation using the Gardner exponential model [40,41]. To deal with the transient modeling, we adopted the coordinate system in Minkowski spacetime instead of that in the original Euclidean space [42,43]. Based on Minkowski spacetime, we assume that time is an absolute physical quantity that plays the role of the independent variable such that the spacetime coordinate system is a mathematically  $(n + 1)$ -dimensional system including  $n$ -dimensional space and one-dimensional of time [44]. In the spacetime coordinate system, both the initial and boundary conditions can be treated as boundary conditions on the spacetime domain boundary. Since the solution of final time on the other boundary of the domain is unknown, it becomes an inverse boundary value problem which is to seek an unknown boundary function on boundaries inaccessible for data measurement with the over specified boundary data on boundaries accessible for data measurement. The initial value problem for transient modeling of subsurface flow in unsaturated soils can then be transformed into the inverse boundary value problem.

A numerical solution obtained in the spacetime coordinate system was approximated by superpositioning Trefftz basis functions satisfying the governing equation for boundary collocation points on partial domain boundary in the spacetime coordinate system. As a result, the transient problems can be solved without using the traditional time-marching scheme. The validity of the proposed method is established for several test problems, including the investigation of the accuracy and the comparison of the numerical with analytical solutions. Application examples of the steady-state, the one-dimensional and two-dimensional transient problems of subsurface flow in unsaturated soils were carried out.

## 2. Trefftz Method for Modeling Subsurface Flow in Unsaturated Soils

### 2.1. The Linearized Richards Equation

For modeling subsurface flow in unsaturated soil, the Richards equation is commonly used and it may be written in three different forms such as the  $h$ -based form, the  $\theta$ -based form, and the mixed form. In this study, the  $h$ -based form is adopted. A complete three-dimensional Richards equation [5] can be expressed as

$$\frac{\partial}{\partial x} \left( K_x(h) \frac{\partial h}{\partial x} \right) + \frac{\partial}{\partial y} \left( K_y(h) \frac{\partial h}{\partial y} \right) + \frac{\partial}{\partial z} \left( K_z(h) \frac{\partial h}{\partial z} \right) + \frac{\partial K_z(h)}{\partial z} = C(h) \frac{\partial h}{\partial t} \quad (1)$$

where  $h$  is the pressure head,  $t$  is time,  $x$  points down the ground surface,  $y$  points to the tangent of the topographic contour passing through the origin,  $z$  is the vertical coordinate, normal to the  $xy$  plane,

$K_x(h)$ ,  $K_y(h)$ , and  $K_z(h)$  are the unsaturated hydraulic conductivity functions in lateral directions and the vertical direction, respectively, and  $C(h)$  is the specific moisture capacity function defined by

$$C(h) = \frac{\partial \theta_m}{\partial h} \tag{2}$$

where  $\theta_m$  is the moisture content. The Richards equation, as shown in Equation (1), is highly nonlinear because  $K_x(h)$ ,  $K_y(h)$ ,  $K_z(h)$  and  $C(h)$  are functions of  $h$ . To solve the Richards equation, three characteristic functions are required and they are the unsaturated hydraulic conductivity function, the soil–water characteristic curve, and the specific moisture capacity function [19]. Assuming that the unsaturated soils are homogeneous and isotropic, the Richards equation governing two-dimensional flow in unsaturated soils can be obtained as

$$\frac{\partial}{\partial x} \left( K \frac{\partial h}{\partial x} \right) + \frac{\partial}{\partial z} \left( K \frac{\partial h}{\partial z} + 1 \right) = \frac{\partial \theta_m}{\partial t} \tag{3}$$

It is common to normalize the hydraulic conductivity of unsaturated soil with respect to their maximum value. The normalized value can be expressed as

$$K_r = \frac{K}{K_s} \tag{4}$$

where  $K_s$  is the saturated hydraulic conductivity, and  $K_r$  is the relative hydraulic conductivity which is a function of the pressure head. The governing equation can be obtained by substituting Equation (4) into Equation (3),

$$\frac{\partial}{\partial x} \left( K_r \frac{\partial h}{\partial x} \right) + \frac{\partial}{\partial z} \left( K_r \frac{\partial h}{\partial z} \right) + \frac{\partial K_r}{\partial z} = \frac{1}{K_s} \frac{\partial \theta_m}{\partial t} \tag{5}$$

The above equation is the two-dimensional Richards equation. Gardner (1958) [40] proposed a simple one-parameter exponential model as

$$S_e = e^{\alpha_g h} \tag{6}$$

where  $\alpha_g$  is the parameter which is related to the pore size distribution of soil, and  $S_e$  is the effective saturation defined by normalizing volumetric water content with its saturated and residual values as

$$S_e = \frac{(\theta_m - \theta_r)}{(\theta_s - \theta_r)} \tag{7}$$

where  $\theta_r$  represents the residual water content, and  $\theta_s$  represents the saturated water content. Substituting Equation (7) into Equation (6), we have,

$$\theta_m = \theta_r + (\theta_s - \theta_r) e^{\alpha_g h} \tag{8}$$

Therefore, the relative hydraulic conductivity is modeled by Gardner exponential model [40,45] as

$$K_r = e^{\alpha_g h} \tag{9}$$

Using the Gardner exponential model, the linearized Richards equation for two-dimensional transient, two-dimensional steady-state and one-dimensional transient Richards equations can be derived [46] as follows, respectively.

$$\frac{\partial^2 \bar{h}}{\partial x^2} + \frac{\partial^2 \bar{h}}{\partial z^2} + \alpha_g \frac{\partial \bar{h}}{\partial z} = c \frac{\partial \bar{h}}{\partial t} \tag{10}$$

$$\frac{\partial^2 \bar{h}}{\partial x^2} + \frac{\partial^2 \bar{h}}{\partial z^2} + \alpha_s \frac{\partial \bar{h}}{\partial z} = 0 \tag{11}$$

$$\frac{\partial^2 \bar{h}}{\partial z^2} + \alpha_s \frac{\partial \bar{h}}{\partial z} = c \frac{\partial \bar{h}}{\partial t} \tag{12}$$

where  $c = \frac{\alpha_s(\theta_s - \theta_r)}{K_s}$ ,  $\bar{h}$  is the pressure head of the linearized Richards equation which can be defined as  $\bar{h} = e^{\alpha_s h} - e^{\alpha_s h_d}$ , and  $h_d$  is the pressure head when the soil is dry.

### 2.2. The Trefftz Method in Euclidean Space

The CTM begins with the consideration of T-complete functions. For indirect Trefftz formulation, the approximated solution at the boundary collocation point can be written as a linear combination of the basis functions [31,47]. For a simply connected domain, one usually locates the source point inside the domain and the number of source point is only one for in the CTM [48,49].

Considering a two-dimensional domain,  $\Omega$ , in the polar coordinate, the Laplace governing equation can be written as

$$\frac{\partial^2 h}{\partial \rho^2} + \frac{1}{\rho} \frac{\partial h}{\partial \rho} + \frac{1}{\rho^2} \frac{\partial^2 h}{\partial \theta^2} = 0 \text{ in } \Omega \tag{13}$$

with

$$h = f \text{ on } \Gamma_D \tag{14}$$

$$h_n = \frac{\partial h}{\partial n} \text{ on } \Gamma_N \tag{15}$$

where  $\rho$  and  $\theta$  are the radius and polar angle in the polar coordinate system,  $n$  denotes the outward normal direction,  $\Gamma_D$  denotes the boundary where the Dirichlet boundary condition is given,  $\Gamma_N$  denotes the boundary where the Neumann boundary condition is given, and  $f$  denotes the Dirichlet boundary condition. For the Laplace equation, the particular solutions can be obtained using the method of the separation of variables. The particular solutions of Equation (13) include the following basis functions [50].

$$1, \ln \rho, \rho^v \cos(v\theta), \rho^v \sin(v\theta), \rho^{-v} \cos(v\theta), \rho^{-v} \sin(v\theta) \tag{16}$$

If we adopt the solution of a boundary value problem and enforce it to exactly satisfy the partial differential equation with the boundary conditions at a set of points, this leads to the CTM.

Considering a simply connected domain, the CTM for the Laplace equation can be expressed as

$$h(\mathbf{x}) \approx \sum_{i=1}^m \mathbf{b}_i \mathbf{T}_i(\mathbf{x}) \tag{17}$$

where  $\mathbf{x} = (\rho, \theta)$ ,  $\mathbf{b}_i = [A_0 \ A_i \ B_i]$ , and  $\mathbf{T}_i(\mathbf{x}) = [1 \ \rho^i \cos(i\theta) \ \rho^i \sin(i\theta)]^T$ .  $m$  is the order of the T-complete basis functions for approximating the solution.  $A_0, A_i$  and  $B_i$  are unknown coefficients to be determined. The accuracy of the solution for the CTM depends on the order of the basis functions. Usually, one may need to increase the  $m$  value to obtain better accuracy. However, the ill-posed behavior may also grow up with the increase of the  $m$  value [51].

### 2.3. The T Basis Function for Steady-State Linearized Richards Equation

For modeling subsurface flow in unsaturated soils using the CTM, we first started from the derivation of the CTM for the two-dimensional steady-state linearized Richards equation. The

two-dimensional Richards governing equation can be expressed as Equation (5). Using the Gardner exponential model, the steady-state linearized Richards equation can be derived as

$$\frac{\partial^2 \bar{h}_s}{\partial x^2} + \frac{\partial^2 \bar{h}_s}{\partial z^2} + \alpha_g \frac{\partial \bar{h}_s}{\partial z} = 0 \tag{18}$$

where  $\bar{h}_s$  is the steady-state pressure head of the linearized Richards equation. The standard process of the separation of variables can now be used by taking the steady-state solution  $\bar{h}_s$  as

$$\bar{h}_s(x, z) = X(x)Z(z) \tag{19}$$

Substituting Equation (19) into Equation (18) and dividing by  $X(x)Z(z)$  gives

$$\frac{1}{X(x)} \frac{d^2 X(x)}{dx^2} + \frac{1}{Z(z)} \left( \frac{d^2 Z(z)}{dz^2} + \alpha_g \frac{dZ(z)}{dz} \right) = 0 \tag{20}$$

Each term in the above equation must be a constant for a nonzero solution, so the following are used.

$$\frac{1}{X(x)} \frac{d^2 X(x)}{dx^2} = -\lambda_i \tag{21}$$

$$\frac{1}{Z(z)} \left( \frac{d^2 Z(z)}{dz^2} + \alpha_g \frac{dZ(z)}{dz} \right) = \lambda_i \tag{22}$$

where  $\lambda_i = \frac{\pi i}{L_i}$ ,  $i$  is the positive integer, and  $L_i$  is the characteristic length. It can be found that Equations (21) and (22) are simple ordinary differential equations that have solutions as

$$X(x) = A_i \sin(\lambda_i x) + B_i \cos(\lambda_i x) \tag{23}$$

$$Z(z) = (C_i \sinh(\beta_i z) + D_i \cosh(\beta_i z)) e^{-\frac{\alpha_g z}{2}} \tag{24}$$

where  $\beta_i = \sqrt{\frac{\alpha_g^2}{4} + \lambda_i^2}$ , and  $A_i$ ,  $B_i$ ,  $C_i$  and  $D_i$  are arbitrary constants to be evaluated. If we considered a simply connected domain, the CTM for two-dimensional steady-state linearized Richards equation can be expressed as

$$\bar{h}_s(\mathbf{x}) \approx \sum_{i=1}^m \mathbf{c}_i \mathbf{J}_i(\mathbf{x}) \tag{25}$$

where  $\mathbf{x} = (x, z)$ ,  $\mathbf{c}_i = [c_{1i} \ c_{2i} \ c_{3i} \ c_{4i}]$ , and  $\mathbf{J}_i(\mathbf{x}) = [J_1 \ J_2 \ J_3 \ J_4]^T$ .  $c_{1i}$ ,  $c_{2i}$ ,  $c_{3i}$  and  $c_{4i}$  are unknown coefficients determined by the collocation method. The basis  $\mathbf{J}_i(\mathbf{x})$  for the  $T$  basis functions include four functions obtained from the separation of variables in the Cartesian coordinate system, which are listed in Table 1.

**Table 1.** T basis functions for two-dimensional linearized Richards equation.

Variable	Function	
<b>Steady-State</b>		
$J_i(\mathbf{x}) = [ J_1 \quad J_2 \quad J_3 \quad J_4 ]^T$		
$J_1$	$e^{-\frac{\alpha_g z}{2}} \sin(\lambda_i x) \sinh(\beta_i z)$	$\lambda_i = \frac{\pi i}{L_i}$
$J_2$	$e^{-\frac{\alpha_g z}{2}} \sin(\lambda_i x) \cosh(\beta_i z)$	$\beta_i = \sqrt{\frac{\alpha_g^2}{4} + \lambda_i^2}$
$J_3$	$e^{-\frac{\alpha_g z}{2}} \cos(\lambda_i x) \sinh(\beta_i z)$	$h_s = \frac{1}{\alpha_g} \ln(\bar{h}_s + e^{\alpha_g h_d})$
$J_4$	$e^{-\frac{\alpha_g z}{2}} \cos(\lambda_i x) \cosh(\beta_i z)$	
<b>Transient</b>		
$L_{ijk}(\mathbf{x}) = [ L_1 \quad L_2 \quad L_3 \quad L_4 ]^T$		
$L_1$	$e^{-\frac{\alpha_g z}{2} - \gamma_{ik} t} \sin(\lambda_i x) \sin(\lambda_k z)$	$c = \frac{\alpha_g(\theta_s - \theta_r)}{K_s}$
$L_2$	$e^{-\frac{\alpha_g z}{2} - \gamma_{ik} t} \sin(\lambda_i x) \cos(\lambda_k z)$	$\lambda_i = \frac{\pi i}{L_i}, \lambda_k = \frac{\pi k}{L_k}$
$L_3$	$e^{-\frac{\alpha_g z}{2} - \gamma_{ik} t} \cos(\lambda_i x) \cos(\lambda_k z)$	$\gamma_{ik} = \frac{1}{c} (\beta_i^2 + \lambda_k^2)$
$L_4$	$e^{-\frac{\alpha_g z}{2} - \gamma_{ik} t} \cos(\lambda_i x) \sin(\lambda_k z)$	$\bar{h}_s = (1 - e^{\alpha_g h_d}) \sin\left(\frac{\pi x}{L_i}\right) e^{\frac{\alpha_g}{2}(L_k - z)} \frac{\sinh(\beta_i z)}{\sinh(\beta_i L_k)}$
		$\bar{h} = \bar{h}_t + \bar{h}_s$
		$h = \frac{1}{\alpha_g} \ln(\bar{h} + e^{\alpha_g h_d})$

2.4. The Trefftz Method in Minkowski Spacetime

Considering a two-dimensional spacetime domain,  $\Omega^t$ , enclosed by a spacetime boundary,  $\Gamma^t$ , the linearized Richards equation for two-dimensional transient subsurface flow in homogenous and isotropic confined porous medium can be expressed as

$$\frac{\partial^2 \bar{h}}{\partial x^2} + \frac{\partial^2 \bar{h}}{\partial z^2} + \alpha_g \frac{\partial \bar{h}}{\partial z} = c \frac{\partial \bar{h}}{\partial t} \text{ in } \Omega^t \tag{26}$$

Considering the time dimension, the pressure head is the time-dependent variable. The initial condition can be described as

$$\bar{h}(x, z, t) = \bar{g} \text{ at } t = 0 \tag{27}$$

where  $\bar{g}$  denotes the distribution of the pressure head in the spacetime domain,  $\Omega^t$ , at time zero. To solve Equation (26), the boundary conditions must be given as follows.

$$\bar{h}(x, z, t) = \bar{f} \text{ on } \Gamma_D^t \tag{28}$$

$$\bar{h}_n(x, z, t) = \frac{\partial \bar{h}}{\partial n} \text{ on } \Gamma_N^t \tag{29}$$

where  $\Gamma_D^t$  denotes the spacetime boundary where the Dirichlet boundary condition is given,  $\Gamma_N^t$  denotes the spacetime boundary where the Neumann boundary condition is given, and  $\bar{f}$  denotes the Dirichlet boundary condition in the spacetime domain.

The transient pressure head of the linearized Richards equation [46,52] can be expressed as

$$\bar{h} = \bar{h}_t + \bar{h}_s \tag{30}$$

where  $\bar{h}_t$  is the transient pressure head of the linearized Richards equation. The transient linearized Richards equation is determined by substituting Equation (30) into Equation (10), which gives

$$\frac{\partial^2 \bar{h}_t}{\partial x^2} + \frac{\partial^2 \bar{h}_t}{\partial z^2} + \alpha_g \frac{\partial \bar{h}_t}{\partial z} = c \frac{\partial \bar{h}_t}{\partial t} \tag{31}$$

The standard process of the separation of variables may be used by having the transient solution  $\bar{h}_i$  as

$$\bar{h}_i(x, z, t) = P(x)Q(z)R(t) \tag{32}$$

Substituting Equation (32) into Equation (31) and dividing by  $P(x)Q(z)R(t)$  gives

$$\frac{1}{P(x)} \frac{d^2P(x)}{dx^2} + \frac{1}{Q(z)} \left( \frac{d^2Q(z)}{dz^2} + \alpha_g \frac{dQ(z)}{dz} \right) = \frac{c}{R(t)} \frac{dR(t)}{dt} \tag{33}$$

Each term in the above equation must be a constant for a nonzero solution, so the following are used.

$$\frac{1}{P(x)} \frac{d^2P(x)}{dx^2} = -\lambda_i^2 \tag{34}$$

$$\frac{1}{Q(z)} \left( \frac{d^2Q(z)}{dz^2} + \alpha_g \frac{dQ(z)}{dz} \right) = -\lambda_k^2 - \frac{\alpha_g^2}{4} \tag{35}$$

$$\frac{c}{R(t)} \frac{dR(t)}{dt} = -\left( \lambda_i^2 + \lambda_k^2 + \frac{\alpha_g^2}{4} \right) \tag{36}$$

where  $\lambda_k = \frac{\pi k}{L_k}$ ,  $k$  is the positive integer, and  $L_k$  is the characteristic length. The above equations are simple ordinary differential equations that have solutions,

$$P(x) = E_i \sin(\lambda_i x) + F_i \cos(\lambda_i x) \tag{37}$$

$$Q(z) = (G_k \sin(\lambda_k z) + H_k \cos(\lambda_k z)) e^{-\frac{\alpha_g z}{2}} \tag{38}$$

$$R(t) = I_{ik} e^{-\gamma_{ik} t} \tag{39}$$

where  $\gamma_{ik} = \frac{1}{c}(\beta_i^2 + \lambda_k^2)$ ,  $E_i, F_i, G_k, H_k$  and  $I_{ik}$  are arbitrary constants to be evaluated. If we considered a simply connected domain, the CTM for two-dimensional transient linearized Richards equation can be expressed as

$$\bar{h}_i(\mathbf{x}) \approx \sum_{k=1}^m \sum_{l=1}^o \mathbf{d}_{ik} \mathbf{L}_{ik}(\mathbf{x}) \tag{40}$$

where  $\mathbf{x} = (x, z, t)$ ,  $\mathbf{d}_{ik} = [d_{1ik} \ d_{2ik} \ d_{3ik} \ d_{4ik}]$ , and  $\mathbf{L}_{ik}(\mathbf{x}) = [L_1 \ L_2 \ L_3 \ L_4]^T \cdot d_{1ik}, d_{2ik}, d_{3ik}$  and  $d_{4ik}$  are unknown coefficients determined by the collocation method.  $m$  and  $o$  are the order of the  $T$  basis functions for approximating the solution. The basis  $\mathbf{L}_{ik}(\mathbf{x})$  for the  $T$  basis functions include four functions obtained from the separation of variables in the cartesian coordinate system, which are listed in Table 1.

Again, the CTM for one-dimensional transient linearized Richards equation can also be composed of a set of linearly independent vectors using the method of the separation of variables. Then, the solution can be derived as the linear combination of these basis functions.

$$\bar{h}_i(\mathbf{x}) \approx \sum_{k=1}^m \mathbf{f}_k \mathbf{M}_k(\mathbf{x}) \tag{41}$$

where  $\mathbf{x} = (z, t)$ ,  $\mathbf{f}_k = [f_{1k} \ f_{2k} \ f_{3k}]$ , and  $\mathbf{M}_k(\mathbf{x}) = [M_1 \ M_2 \ M_3]^T$ .  $f_{1k}, f_{2k}$  and  $f_{3k}$  are unknown coefficients determined by the collocation method. The basis  $\mathbf{M}_k(\mathbf{x})$  for the  $T$  basis functions include three functions obtained from the separation of variables in the Cartesian coordinate system, which are listed in Table 2.

The above equations can be discretized at a number of collocated points on the spacetime boundary using the initial and boundary conditions. Then, we obtained a system of simultaneous linear equations as

$$\mathbf{A}\boldsymbol{\alpha} = \mathbf{B} \tag{42}$$

where  $\mathbf{A}$  is a matrix with the size of  $aa \times bb$ ,  $\boldsymbol{\alpha}$  with the size of  $bb \times 1$  is a vector of unknown coefficients,  $\mathbf{B}$  with the size of  $aa \times 1$  is a vector of function values at collocation points,  $aa$  is the number of collocation points, and  $bb$  is the number of the order of the  $T$  basis function. For simplicity, we adopted the commercial program MATLAB backslash operator to solve Equation (42).

**Table 2.**  $T$  basis functions for one-dimensional linearized Richards equation.

Variable	Function	
<b>Transient</b>		
$\mathbf{M}_k(\mathbf{x}) = [ M_1 \quad M_2 \quad M_3 ]^T$		$c = \frac{\alpha_g(\theta_s - \theta_r)}{K_s}$
$M_1$	$e^{-\frac{\alpha_g z}{2} - \mu_k t} \sin(\lambda_k z)$	$\lambda_k = \frac{\pi k}{L_k}$
$M_2$	$e^{-\frac{\alpha_g z}{2} - \mu_k t}$	$\mu_k = \frac{1}{c} (\frac{\alpha_g^2}{4} + \lambda_k^2)$
$M_3$	$e^{-\frac{\alpha_g z}{2} - \mu_k t} \cos(\lambda_k z)$	$\bar{h}_s = (1 - e^{\alpha_g h_d}) \frac{1 - e^{-\alpha_g z}}{1 - e^{-\alpha_g L_k}}$
		$\bar{h} = \bar{h}_i + \bar{h}_s$
		$h = \frac{1}{\alpha_g} \ln(\bar{h} + e^{\alpha_g h_d})$

### 3. Numerical Examples

#### 3.1. Steady-State Modeling of Two-Dimensional Subsurface Flow in Unsaturated Soil

Meshless methods only rely on a series of random collocation points to discretize the spatial domain, which means not only onerous mesh generation is avoided, but also a more accurate description of irregular complex geometries can be achieved. Therefore, we investigated a two-dimensional steady-state unsaturated flow problem for an irregular boundary shape. With a two-dimensional simply connected domain,  $\Omega$ , enclosed by an irregular boundary, the governing equation is expressed as

$$\frac{\partial}{\partial x} (K_r \frac{\partial h}{\partial x}) + \frac{\partial}{\partial z} (K_r \frac{\partial h}{\partial z}) + \frac{\partial K_r}{\partial z} = 0 \tag{43}$$

A two-dimensional object boundary under consideration is defined as

$$\Omega = \{ (x, z) | x = \rho(\theta) \cos \theta, z = \rho(\theta) \sin \theta \} \tag{44}$$

where  $\rho(\theta) = \sqrt[1/3]{\cos 3\theta + \sqrt{2 - \sin^2 3\theta}}$ ,  $0 \leq \theta \leq 2\pi$ . The linearized governing equation is expressed as Equation (18). The boundary conditions are the Dirichlet boundary condition and the Dirichlet boundary data is applied using the following analytical solution.

$$\bar{h}_s(x, z) = x e^{-\alpha_g z} \tag{45}$$

Finally, the steady-state solution can be obtained using the following equation.

$$h_s(x, z) = \frac{1}{\alpha_g} \ln(\bar{h}_s(x, z) + e^{\alpha_g h_d}) \tag{46}$$

The soil is assumed to have the  $\alpha_g$  in the Gardner exponential model of  $2 \times 10^{-5}$ . The pressure head when the soil is dry is assumed to be  $h_d = -10^3$  (m). The Dirichlet boundary condition is given on the boundaries using the analytical solution as shown in Equation (45). There are 51 boundary collocation points and a source point. We selected  $m = 50$  and  $L_i = 180$ , and adopted the commercial

program MATLAB backslash operator to solve the system of simultaneous linear equations. Figure 1 depicts the computed pressure head distribution. Comparing with the analytical solution, it is found that highly accurate result in the order of  $10^{-15}$  can be obtained for this example, as depicted in Figure 2.

The previous example has demonstrated that the proposed method can be used to deal with the two-dimensional steady-state subsurface flow in unsaturated soils for an irregular boundary shape with very high accuracy. We further applied the proposed method to investigate the numerical solution of a two-dimensional steady-state Green–Ampt problem in the following section [53].

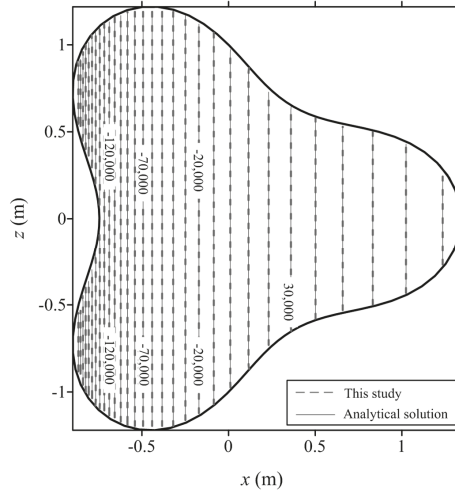


Figure 1. The computed pressure head distribution.

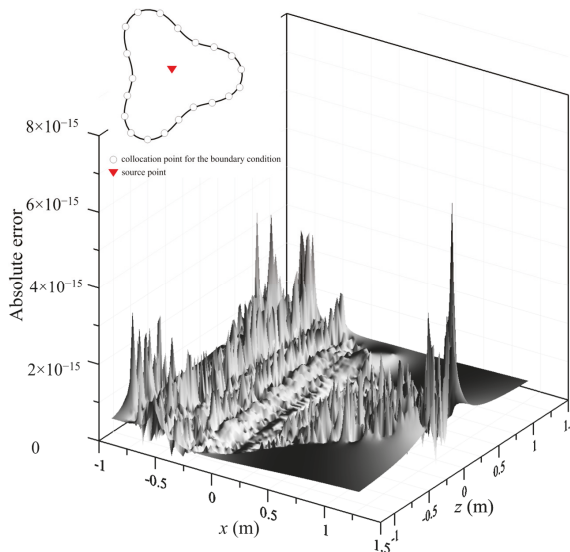


Figure 2. The absolute error of the computed results.

Figure 3 indicates a two-dimensional cross section of the soil with the dimensions of length  $a = 50$  (m) and height  $L = 10$  (m), where a two-dimensional Green–Ampt problem is investigated. A pool of water at ground surface is maintained holding the pressure head. The specified pressure head, as shown in Equation (50), is applied at the top with pressure head set to zero in the center and tapering rapidly to dry conditions at two sides of the boundary, as shown in Figure 3. The  $\alpha_g$  parameter corresponding to the soil is also used. The bottom, left and right sides of the soil are in dry condition maintained as  $h_d = -20$  (m). Therefore, the boundary conditions can be expressed as

$$h(0, z) = h_d \tag{47}$$

$$h(a, z) = h_d \tag{48}$$

$$h(x, 0) = h_d \tag{49}$$

$$h(x, L) = \frac{1}{\alpha_g} \ln \left( e^{\alpha_g h_d} + (1 - e^{\alpha_g h_d}) \left( \frac{3}{4} \sin\left(\frac{\pi x}{a}\right) - \frac{1}{4} \sin\left(\frac{3\pi x}{a}\right) \right) \right) \tag{50}$$

The analytical solution [46] of two-dimensional steady-state linearized Richards equation is given by

$$\bar{h}_s(x, z) = (1 - e^{\alpha_g h_d}) e^{\frac{\alpha_g(L-z)}{2}} \left( \frac{3}{4} \sin\left(\frac{\pi x}{a}\right) \frac{\sinh(\beta_1 z)}{\sinh(\beta_1 L)} - \frac{1}{4} \sin\left(\frac{3\pi x}{a}\right) \frac{\sinh(\beta_3 z)}{\sinh(\beta_3 L)} \right) \tag{51}$$

where  $\beta_1 = \sqrt{\frac{\alpha_g^2}{4} + \left(\frac{\pi}{a}\right)^2}$  and  $\beta_3 = \sqrt{\frac{\alpha_g^2}{4} + \left(\frac{3\pi}{a}\right)^2}$ .

The steady-state solution can then be obtained using Equation (46). There are 200 boundary collocation points uniformly distributed in the boundary. We selected  $m = 50$  and  $L_i = 50$  for solving this example. The computed results are depicted in Figure 4 which demonstrates that the process of infiltration can continue if there is a pool of water at ground surface maintained holding the pressure head for additional water at the soil surface. It is found that the best accuracy of the proposed method can reach up to  $10^{-13}$ , as shown in Figure 5.

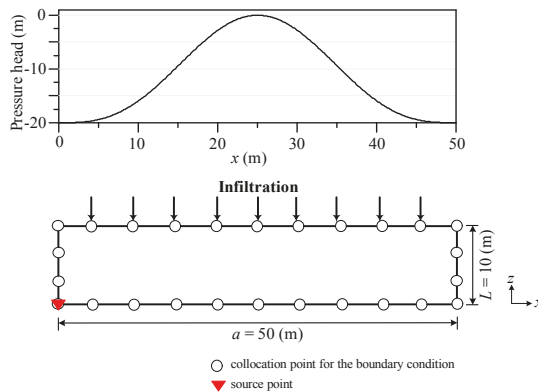
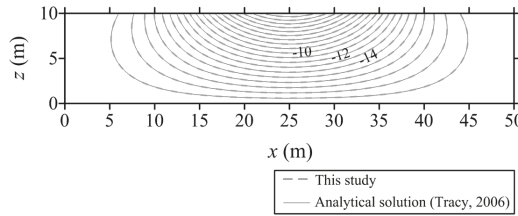
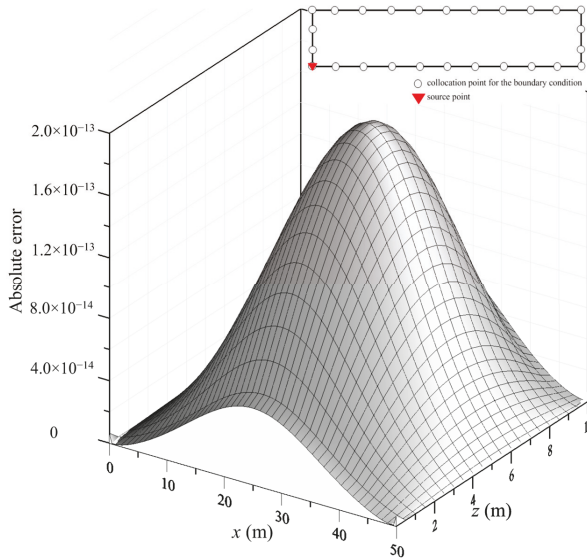


Figure 3. A view of a two-dimensional steady-state Green–Ampt problem.



**Figure 4.** Comparison of computed pressure head distribution with the analytical solution for the two-dimensional steady-state Green–Ampt problem.



**Figure 5.** The absolute error of the computed results for the two-dimensional steady-state Green–Ampt problem.

### 3.2. Transient Modeling of One-Dimensional Flow in Unsaturated Soil

The second example under investigation is the transient modeling of one-dimensional flow in unsaturated soil. The thickness of the soil ( $L$ ) is 10 (m). The soil is assumed to have the  $\alpha_g$  in the Gardner exponential model of  $2 \times 10^{-5}$ . The saturated hydraulic conductivity ( $K_s$ ), saturated water content ( $\theta_s$ ), and residual water content ( $\theta_r$ ) of this example are  $10^{-4}$  (m/h), 0.35, and 0.14, respectively [54]. The total simulation time ( $T$ ) is one hour (h). The governing equation can be expressed as follows.

$$\frac{\partial}{\partial z} \left( K_r \frac{\partial h}{\partial z} \right) + \frac{\partial K_r}{\partial z} = \frac{1}{K_s} \frac{\partial \theta_m}{\partial t} \tag{52}$$

Using the Gardner exponential model, the linearized governing equation can be expressed as Equation (12). The initial condition was the soil in dry condition maintained as  $h_d = -100$  (m). Thus,

$$h(z, 0) = h_d \tag{53}$$

The boundary conditions are the Dirichlet boundary condition. The Dirichlet boundary data are applied using the following analytical solution [46].

$$\bar{h}_t(z, t) = \frac{2(1 - e^{\alpha_g h_d})}{Lc} e^{\frac{\alpha_g(L-z)}{2}} \sum_{k=1}^m (-1)^k \left(\frac{\lambda_k}{\mu_k}\right) \sin(\lambda_k z) e^{-\mu_k t} \tag{54}$$

where  $\mu_k = \frac{1}{c} \left(\frac{\alpha_g^2}{4} + \lambda_k^2\right)$ . The  $\bar{h}(z, t)$  can be obtained using the following equations.

$$\bar{h}(z, t) = \bar{h}_t(z, t) + \bar{h}_s(z) \tag{55}$$

$$\bar{h}_s(z) = (1 - e^{\alpha_g h_d}) \frac{1 - e^{-\alpha_g z}}{1 - e^{-\alpha_g L}} \tag{56}$$

Finally, the transient solution can be obtained as follows.

$$h(z, t) = \frac{1}{\alpha_g} \ln \left( \bar{h}(z, t) + e^{\alpha_g h_d} \right) \tag{57}$$

To deal with the transient modeling, we adopted the coordinate system in Minkowski spacetime instead of that in the original Euclidean space. Based on Minkowski spacetime, we assume that time is an absolute physical quantity that plays the role of the independent variable such that the spacetime coordinate system is a n-dimensional space and one-dimensional time. In this example, there is one-dimensional space and one-dimensional time. The spacetime domain is therefore a rectangular shape, as shown in Figure 6b. We transformed the one-dimensional initial value problem, as depicted in Figure 6a, for transient modeling of subsurface flow into two-dimensional inverse boundary value problem. It should be noted that the initial and boundary conditions are both applied on the spacetime boundary. In addition, it becomes an inverse boundary value problem because the right-side boundary values in Figure 6b were not assigned.

The initial condition was applied on the left side of the spacetime domain and the boundary conditions were applied on both top and bottom sides of the domain, as shown in Figure 6b. By selecting the space interval ( $\Delta z$ ) and time interval ( $\Delta t$ ) for 0.05 (m) and 0.05 (h), there are 375 boundary collocation points and a source point. The Dirichlet boundary values were given on boundary collocation points which collocated on three sides of the domain using the analytical solution for the problem. We selected  $m = 50$  and  $L_k = 10$  for solving this example.

To obtain the computed results of the pressure head at different time, we collocated 2496 inner points which uniformly placed inside the rectangular domain. To view the results clearly, the profiles of the numerical solution on different time were selected to compare with the analytical solution. Figure 7 indicates that the computed results agreed very well with the analytical solution. Results obtained demonstrates that the accuracy of the absolute error can be reached to the order of  $10^{-12}$ . The above numerical example also illustrates that the transient problem can be solved without using the traditional time-marching scheme.

The previous example has validated the one-dimensional transient unsaturated flow problem with the analytical solution. We further investigated the application of the one-dimensional transient Green–Ampt problem using the proposed method. A column of soil is initially dry until water begins to infiltrate the soil. A pool of water at ground surface is then maintained holding the pressure head to zero. This is known as the one-dimensional Green–Ampt problem [53].

The thickness of the soil ( $L$ ) is 10 (m). The soil parameters including  $\alpha_g$ ,  $K_s$ ,  $\theta_s$  and  $\theta_r$  are the same as previous one. The total simulation time is 1 h. The governing equation is the same as shown in Equation (52). The initial condition is also the same as shown in Equation (53), where the soil is in dry condition maintained as  $h_d = -1$  (m).

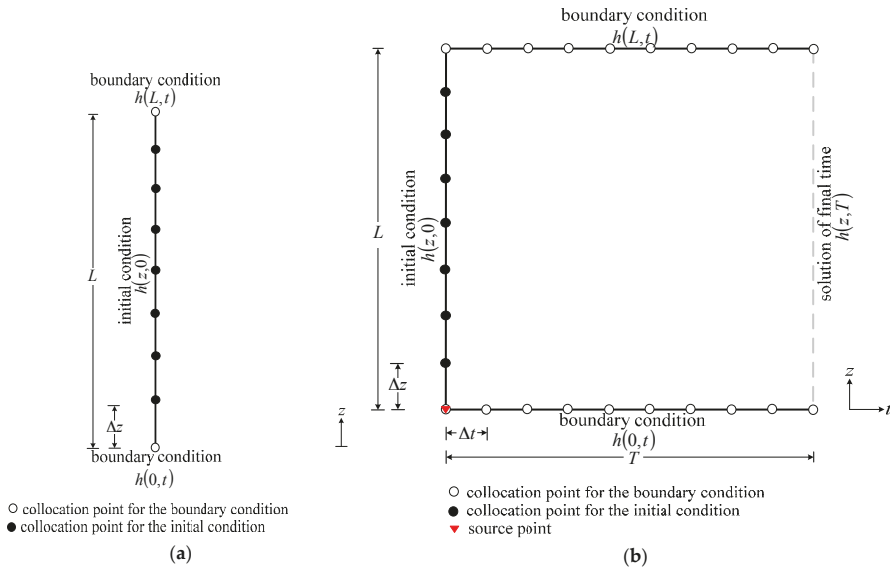


**Figure 6.** Illustration of the collocation scheme for the Trefftz method in Minkowski spacetime for the one-dimensional transient problem: (a) original one-dimensional transient problem (one-dimensional initial value problem); and (b) collocation points of one-dimensional transient problem in Minkowski spacetime domain (two-dimensional inverse boundary value problem).

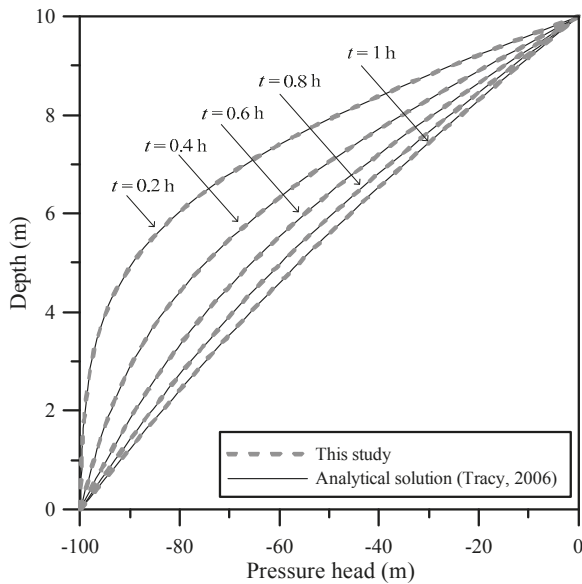


**Figure 7.** Comparison of the computed results with the analytical solution.

At time greater than zero, the boundary conditions at top and bottom of the soil can be expressed as follows.

$$h(0, t) = h_d \tag{58}$$

$$h(L, t) = 0 \tag{59}$$

The solution procedure is similar with the previous one which also adopted the coordinate system in Minkowski spacetime. The imposed initial condition was applied on the left side of the domain and the imposed boundary conditions were applied on both top and bottom sides of the domain. By selecting  $\Delta z = 0.05$  (m) and  $\Delta t = 0.05$  (h), there are 375 boundary collocation points and a source point. The Dirichlet boundary values from the given initial and boundary conditions were given on boundary collocation points which collocated on three sides of the spacetime domain. We selected  $m = 50$  and  $L_k = 10$  for solving this example.

To obtain the computed results of the pressure head at different time, we collocated 2496 inner points which uniformly placed inside the rectangular spacetime domain. Figure 8 demonstrates the absolute error of this example which demonstrates that the accuracy can be reached to the order of  $10^{-6}$ .

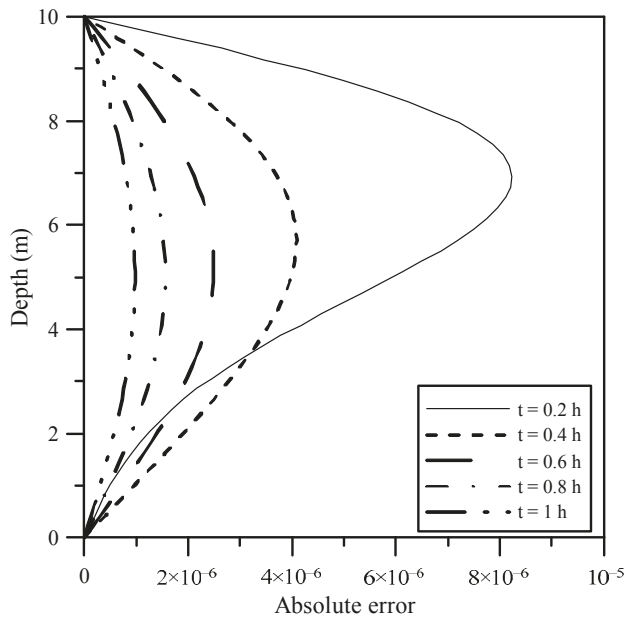


**Figure 8.** The absolute error of the computed results for the transient modeling of the one-dimensional Green-Ampt problem.

### 3.3. Transient Modeling of Two-Dimensional Flow in Unsaturated Soil

The third example under investigation is the transient modeling of two-dimensional flow in unsaturated soil. With a two-dimensional simply connected domain,  $\Omega$ , enclosed by amoeba-like boundary, as shown in Figure 9a, the governing equation can be expressed as Equation (5). The linearized Richards equation is expressed as Equation (10). The soil parameters including  $\alpha_g$ ,  $K_s$ ,  $\theta_s$  and  $\theta_r$  are the same as previous one. The total simulation time is one (h). The initial condition was the soil in dry condition maintained as  $h_d = -100$  (m). Thus,

$$h(x, z, 0) = h_d \tag{60}$$

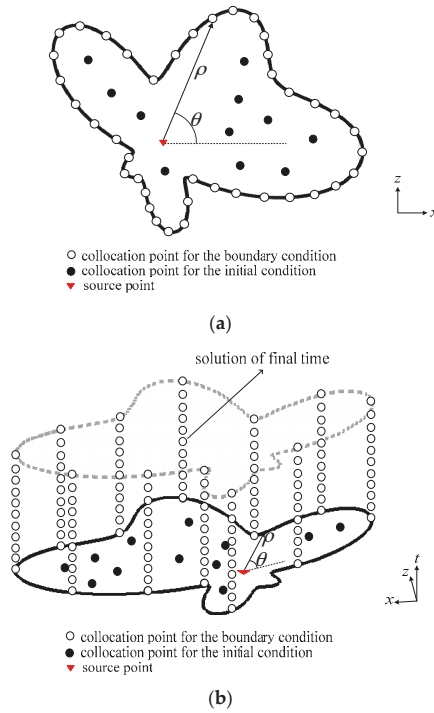


**Figure 9.** Schematic illustration of the two-dimensional transient flow in unsaturated soils for an amoeba-like boundary: (a) original two-dimensional transient problem (two-dimensional initial value problem); and (b) collocation points of two-dimensional transient problem in Minkowski spacetime domain (three-dimensional inverse boundary value problem).

A two-dimensional amoeba-like object boundary under consideration is defined as

$$\Omega = \{ (x, z, t) | x = \rho(\theta) \cos \theta, z = \rho(\theta) \sin \theta \} \tag{61}$$

where  $\rho(\theta) = e^{(\sin \theta \sin 2\theta)^2} + e^{(\cos \theta \cos 2\theta)^2}$ ,  $0 \leq \theta \leq 2\pi$ .

The boundary conditions are assumed to be the Dirichlet boundary condition. The Dirichlet boundary data are applied using the following analytical solution.

$$\bar{h}_t(x, z, t) = x e^{-\frac{\alpha_g^2 t}{4c}} e^{-\frac{\alpha_g z}{2}} \tag{62}$$

The  $\bar{h}_t(x, z, t)$  can be obtained using the following equations.

$$\bar{h}(x, z, t) = \bar{h}_t(x, z, t) + \bar{h}_s(x, z) \tag{63}$$

$$\bar{h}_s(x, z) = (1 - e^{\alpha_g h_d}) \sin\left(\frac{\pi x}{L_i}\right) e^{\frac{\alpha_g}{2}(L_k - z)} \frac{\sinh(\beta_i z)}{\sinh(\beta_i L_k)} \tag{64}$$

Finally, the transient solution can be obtained as follows.

$$h(x, z, t) = \frac{1}{\alpha_g} \ln\left(\bar{h}(x, z, t) + e^{\alpha_g h_d}\right) \tag{65}$$



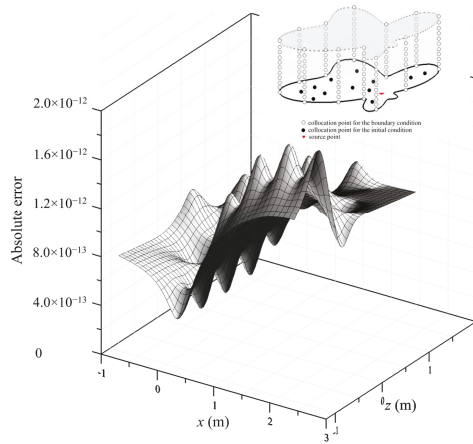


Figure 11. The absolute error of the computed results.

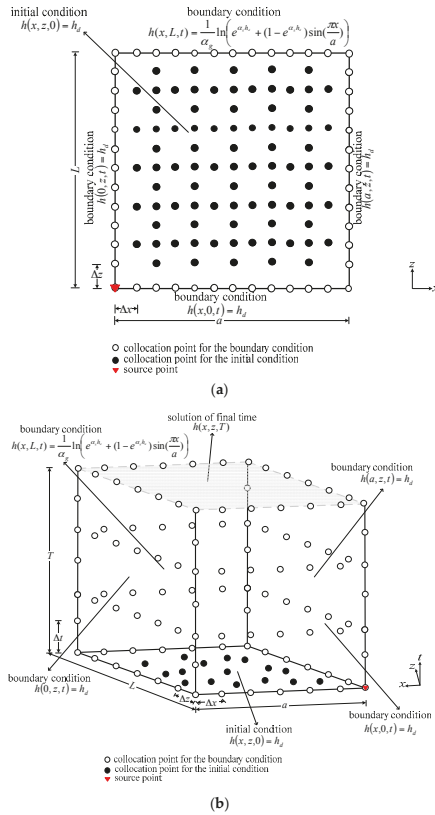


Figure 12. Schematic illustration of the two-dimensional transient Green-Ampt problem: (a) original two-dimensional transient problem (two-dimensional initial value problem); and (b) collocation points of two-dimensional transient problem in Minkowski spacetime domain (three-dimensional inverse boundary value problem).

The governing equation is the same as shown in Equation (5). The linearized Richards equation is expressed as Equation (10). The initial condition was assumed to be dry. Thus,

$$h(x, z, 0) = h_d \tag{66}$$

The boundary conditions of the soil are as follows.

$$h(0, z, t) = h_d \tag{67}$$

$$h(a, z, t) = h_d \tag{68}$$

$$h(x, 0, t) = h_d \tag{69}$$

$$h(x, L, t) = \frac{1}{\alpha_g} \ln \left( e^{\alpha_g h_d} + (1 - e^{\alpha_g h_d}) \sin \left( \frac{\pi x}{a} \right) \right) \tag{70}$$

The analytical solution [46] for  $\bar{h}_t(x, z, t)$  can be expressed as

$$\bar{h}_t(x, z, t) = \frac{2}{Lc} (1 - e^{\alpha_g h_d}) \sin \left( \frac{\pi x}{a} \right) e^{\frac{\alpha_g(L-z)}{2}} \sum_{k=1}^m (-1)^k \left( \frac{\lambda_k}{\gamma_{ik}} \right) \sin(\lambda_k z) e^{-\gamma_{ik} t} \tag{71}$$

Finally, the transient solution can be obtained using Equations (63)–(65). The solution procedure is similar with the previous one which also adopted the coordinate system in Minkowski spacetime. The imposed initial condition was applied on the bottom side of the domain and the imposed boundary conditions were applied on all four vertical sides of the domain, as shown in Figure 12b. By selecting  $\Delta z = 0.05$  (m) and  $\Delta t = 0.05$  (h), there are 736 boundary collocation points and a source point. The Dirichlet boundary values from the given initial and boundary conditions were given on boundary collocation points which collocated on five sides of the spacetime domain. We selected  $m = 10$ ,  $L_i = 1$  and  $L_k = 1$  for solving this example.

To obtain the results of the pressure head at different time, we collocated 4056 inner points which uniformly placed inside the cubic spacetime domain. Results obtained demonstrate that the numerical solution agreed very well with the analytical solution, as depicted in Figure 13. It is found that the accuracy can be reached to the order of  $10^{-5}$ . The above numerical example also illustrates that the two-dimensional transient unsaturated flow problem can be solved without using the traditional time-marching scheme.

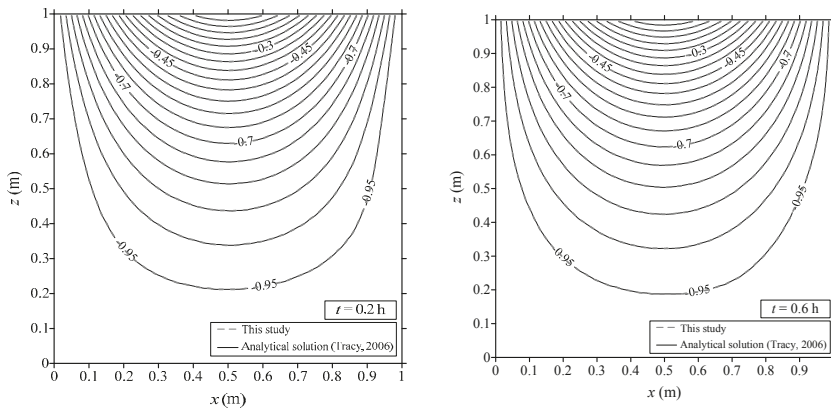
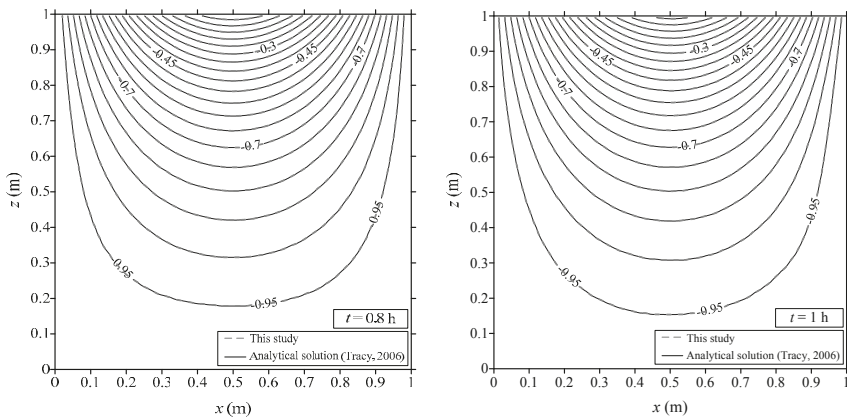


Figure 13. Cont.



**Figure 13.** Comparison of computed results with those from the analytical solution for the two-dimensional transient Green–Ampt problem.

#### 4. Conclusions

This study has proposed a novel meshless method for the transient modeling of subsurface flow in unsaturated soils. This pioneering study is based on the CTM and provides a promising solution for transient modeling of subsurface flow in unsaturated soils. The validity of the model is established for a number of test problems. Application examples of subsurface flow problems in unsaturated soils were also carried out. The fundamental concepts and the construct of the proposed method are addressed in detail. The findings are addressed as follows.

It is well known that the Richards equation is a highly nonlinear equation governed by nonlinear physical relationships. In this study, we proposed a linearization process using the Gardner exponential model for the nonlinear Richards equation to model the subsurface flow in unsaturated soils. As a result, the CTM can be applied to the numerical modeling of subsurface flow in unsaturated soils.

The CTM is originally developed to deal with the boundary value problems. The pioneering work in this study is the first successful attempt to solve the transient problem using the CTM. For the transient modeling of the subsurface flow in unsaturated soils, we proposed an innovated concept that one may adopt the coordinate system in Minkowski spacetime instead of that in the original Euclidean space. Consequently, both the initial and boundary conditions can be treated as boundary conditions on the spacetime domain boundary. The initial value problem for transient modeling of subsurface flow in unsaturated soils can then be transformed into the inverse boundary value problem. As a result, the transient problems can be solved without using the traditional time-marching scheme.

Results obtained from examples revealed that the proposed method could be easily applied to one-dimensional and two-dimensional subsurface flow problems in unsaturated soils. Since the proposed CTM is a boundary-type meshless method, it is advantageous, especially for problems involving regions of irregular geometry. In addition, the proposed method can yield highly accurate numerical solutions. The results of this study demonstrate that the applicability of the CTM may be extended to other major engineering problems in the near future.

**Acknowledgments:** This study was partially supported by the Ministry of Science and Technology of Taiwan under project grant MOST 106-2621-M-019-004-MY2. The authors thank the Ministry of Science and Technology of Taiwan for the generous financial support.

**Author Contributions:** Cheng-Yu Ku worked on the conceptualization and finalized the manuscript; Chih-Yu Liu worked on the mathematical development and numerical computations; Jing-En Xiao analyzed the data; and Weichung Yeih supervised the research.

**Conflicts of Interest:** The authors declare no conflict of interest.

## References

1. Sinai, G.; Dirksen, C. Experimental evidence of lateral flow in unsaturated homogeneous isotropic sloping soil due to rainfall. *Water Resour. Res.* **2006**, *42*, W12402. [[CrossRef](#)]
2. Ebel, B.A. Simulated unsaturated flow processes after wildfire and interactions with slope aspect. *Water Resour. Res.* **2013**, *49*, 8090–8107. [[CrossRef](#)]
3. Ku, C.Y.; Liu, C.Y.; Su, Y.; Xiao, J.E.; Huang, C.C. Transient modeling of regional rainfall-triggered shallow landslides. *Environ. Earth Sci.* **2017**, *76*, 1–18. [[CrossRef](#)]
4. Huang, F.; Luo, X.; Liu, W. Stability analysis of hydrodynamic pressure landslides with different permeability coefficients affected by reservoir water level fluctuations and rainstorms. *Water* **2017**, *9*, 450. [[CrossRef](#)]
5. Richards, L.A. Capillary conduction of liquids through porous mediums. *J. Appl. Phys.* **1931**, *1*, 318–333. [[CrossRef](#)]
6. Brooks, R.H.; Corey, A.T. *Hydraulic Properties of Porous Media*; Hydrology Paper No. 3; Colorado State University: Fort Collins, CO, USA, 1964; p. 27.
7. Van Genuchten, M.T. A closed form equation for predicting the hydraulic conductivity of unsaturated soils. *Soil Sci. Soc. Am. J.* **1980**, *44*, 892–898. [[CrossRef](#)]
8. Fredlund, D.G.; Xing, A.; Huang, S. Predicting the permeability function for unsaturated soils using the soil-water characteristic curve. *Can. Geotech. J.* **1994**, *31*, 533–546. [[CrossRef](#)]
9. Haverkamp, R.; Vauclin, M.; Touma, J.; Wierenga, P.J.; Vachaud, G. A comparison of numerical simulation models for one dimensional infiltration. *Soil Sci. Soc. Am. J.* **1977**, *41*, 285–294. [[CrossRef](#)]
10. Kavetski, D.; Binning, P.; Sloan, S.W. Noniterative time stepping schemes with adaptive truncation error control for the solution of Richards equation. *Water Resour. Res.* **2002**, *38*. [[CrossRef](#)]
11. Miller, C.T.; Abhishek, C.; Farthing, M.W. A spatially and temporally adaptive solution of Richards' equation. *Adv. Water Resour.* **2006**, *29*, 525–545. [[CrossRef](#)]
12. Li, H.; Farthing, M.W.; Dawson, C.N.; Miller, C.T. Local discontinuous Galerkin approximations to Richards' equation. *Adv. Water Resour.* **2007**, *30*, 555–575. [[CrossRef](#)]
13. Juncu, G.; Nicola, A.; Popa, C. Nonlinear multigrid methods for numerical solution of the variably saturated flow equation in two space dimensions. *Transp. Porous Media* **2012**, *91*, 35–47. [[CrossRef](#)]
14. Carbone, M.; Brunetti, G.; Piro, P. Modelling the Hydraulic behaviour of growing media with the explicit finite volume solution. *Water* **2015**, *7*, 568–591. [[CrossRef](#)]
15. Liu, X.; Zhan, H. Calculation of steady-state evaporation for an arbitrary matric potential at bare ground surface. *Water* **2017**, *9*, 729. [[CrossRef](#)]
16. Celia, M.A.; Ahuja, L.R.; Pinder, G.F. Orthogonal collocation and alternating-direction procedures for unsaturated flow problems. *Adv. Water Resour.* **1987**, *10*, 178–187. [[CrossRef](#)]
17. Celia, M.A.; Bouloutas, E.T.; Zarba, R.L. A General mass-conservation numerical solution for the unsaturated flow equation. *Water Resour. Res.* **1990**, *26*, 1483–1496. [[CrossRef](#)]
18. Chen, F.; Ren, L. Application of the finite difference heterogeneous multiscale method to the Richards' equation. *Water Resour. Res.* **2008**, *44*. [[CrossRef](#)]
19. Liu, C.Y.; Ku, C.Y.; Huang, C.C.; Lin, D.G.; Yeih, W. Numerical solutions of groundwater flow in unsaturated layered soil with extreme physical property contrasts. *Int. J. Nonlinear Sci. Numer. Simul.* **2015**, *16*, 325–336. [[CrossRef](#)]
20. Pan, L.; Warrick, A.W.; Wierenga, P.J. Finite elements methods for modeling water flow in variably saturated porous media: Numerical oscillation and mass distributed schemes. *Water Resour. Res.* **1996**, *32*, 1883–1889. [[CrossRef](#)]
21. Bergamaschi, L.; Putti, M. Mixed finite elements and Newton-type linearizations for the solution of Richards' equation. *Int. J. Numer. Methods Eng.* **1999**, *45*, 1025–1046. [[CrossRef](#)]
22. Farthing, M.W.; Kees, C.E.; Miller, C.T. Mixed finite element methods and higher order temporal approximations for variably saturated groundwater flow. *Adv. Water Resour.* **2003**, *26*, 373–394. [[CrossRef](#)]
23. Bause, M.; Knabner, P. Computation of variably saturated subsurface flow by adaptive mixed hybrid finite element methods. *Adv. Water Resour.* **2004**, *27*, 565–581. [[CrossRef](#)]
24. Katsurada, M.; Okamoto, H. The collocation points of the fundamental solution method for the potential problem. *Comput. Math. Appl.* **1996**, *31*, 123–137. [[CrossRef](#)]

25. Liu, C.S. A modified collocation Trefftz method for the inverse Cauchy problem of Laplace equation. *Eng. Anal. Bound. Elem.* **2008**, *32*, 778–785. [[CrossRef](#)]
26. Chang, Y.S.; Chang, T.J. SPH simulations of solute transport in flows with steep velocity and concentration gradients. *Water* **2017**, *9*, 132. [[CrossRef](#)]
27. Yeih, W.; Chan, I.Y.; Ku, C.Y.; Fan, C.M. Solving the inverse Cauchy problem of the Laplace equation using the method of fundamental solutions and the exponentially convergent scalar homotopy algorithm (ECSHA). *J. Mar. Sci. Technol.* **2015**, *23*, 162–171.
28. Huyakorn, P.S.; Pinder, G.F. *Computational Methods in Subsurface Flow*; Academic Press: London, UK, 1983; pp. 354–401, ISBN 978-0-12-363480-1.
29. Liu, C.S. A modified Trefftz method for two-dimensional Laplace equation considering the domain's characteristic length. *Comput. Model. Eng. Sci.* **2007**, *1*, 53–65.
30. Trefftz, E. Ein gegenstück zum ritzschen verfahren. In Proceedings of the 2nd International Congress for Applied Mechanics, Zurich, Switzerland, 12–17 September 1926; pp. 131–137.
31. Kita, E.; Kamiya, N. Trefftz method: An overview. *Adv. Eng. Softw.* **1995**, *24*, 3–12. [[CrossRef](#)]
32. Kupradze, V.D.; Aleksidze, M.A. The method of functional equations for the approximate solution of certain boundary value problems. *Comput. Math. Math. Phys.* **1964**, *4*, 82–126. [[CrossRef](#)]
33. Chen, C.S.; Karageorghis, A.; Li, Y. On choosing the location of the sources in MFS. *Numer. Algorithms* **2016**, *72*, 107–130. [[CrossRef](#)]
34. Belytschko, T.; Lu, Y.Y.; Gu, L. Element free Galerkin methods. *Int. J. Numer. Methods Eng.* **1994**, *37*, 229–256. [[CrossRef](#)]
35. Liu, W.K.; Jun, S.; Zhang, Y.F. Reproducing kernel particle methods. *Int. J. Numer. Methods Fluids* **1995**, *20*, 1081–1106. [[CrossRef](#)]
36. Lin, H.; Atluri, S.N. Meshless Local Petrov-Galerkin (MLPG) method for convection-diffusion problems. *Comput. Model. Eng. Sci.* **2000**, *1*, 45–60.
37. Kita, E.; Ikedab, Y.; Kamiya, N. Trefftz solution for boundary value problem of three-dimensional Poisson equation. *Eng. Anal. Bound. Elem.* **2005**, *29*, 383–390. [[CrossRef](#)]
38. Fan, C.M.; Chan, H.F.; Kuo, C.L.; Yeih, W. Numerical solutions of boundary detection problems using modified collocation Trefftz method and exponentially convergent scalar homotopy algorithm. *Eng. Anal. Bound. Elem.* **2012**, *36*, 2–8. [[CrossRef](#)]
39. Li, Z.C.; Lu, Z.Z.; Hu, H.Y.; Cheng, H.D. *Trefftz and Collocation Methods*; WIT Press: Southampton, UK, 2008.
40. Gardner, W.R. Some steady-state solutions of the unsaturated moisture flow equation with application to evaporation from a water table. *Soil Sci.* **1958**, *85*, 228–232. [[CrossRef](#)]
41. Srivastava, R.; Yeh, T.-C.J. Analytical solutions for onedimensional, transient infiltration toward the water table in homogeneous and layered soils. *Water Resour. Res.* **1991**, *27*, 753–762. [[CrossRef](#)]
42. Galison, P.L. Minkowski's Space-Time: From visual thinking to the absolute world. *Hist. Stud. Phys. Sci.* **1979**, *10*, 85–121. [[CrossRef](#)]
43. Naber, G.L. *The Geometry of Minkowski Spacetime*; Springer-Verlag: New York, NY, USA, 1992.
44. Catoni, F.; Boccaletti, D.; Cannata, R.; Catoni, V.; Nichelatti, E.; Zampetti, P. *The Mathematics of Minkowski Space-Time with an Introduction to Commutative Hypercomplex Numbers*; Birkhäuser Verlag: Basel, Switzerland, 2008; pp. 5–17, ISBN 978-3-7643-8613-9.
45. Segol, G. *Classic Groundwater Simulations*; Prentice Hall: Englewood Cliffs, NJ, USA, 1994.
46. Tracy, F.T. Clean two- and three-dimensional analytical solutions of Richards' equation for testing numerical solvers. *Water Resour. Res.* **2006**, *42*. [[CrossRef](#)]
47. Kita, E.; Kamiya, N.; Iio, T. Application of a direct Trefftz method with domain decomposition to two-dimensional potential problems. *Eng. Anal. Bound. Elem.* **1999**, *23*, 539–548. [[CrossRef](#)]
48. Yeih, W.; Liu, C.S.; Kuo, C.L.; Atluri, S.N. On solving the direct/inverse cauchy problems of laplace equation in a multiply connected domain, using the generalized multiple-source-point boundary-collocation Trefftz method and characteristic lengths. *Comput. Mater. Contin.* **2010**, *17*, 275–302.
49. Ku, C.Y. On solving three-dimensional Laplacian problems in a multiply connected domain using the multiple scale Trefftz method. *Comput. Model. Eng. Sci.* **2014**, *98*, 509–541.
50. Ku, C.Y.; Kuo, C.L.; Fan, C.M.; Liu, C.S.; Guan, P.C. Numerical solution of three-dimensional Laplacian problems using the multiple scale Trefftz method. *Eng. Anal. Bound. Elem.* **2015**, *50*, 157–168. [[CrossRef](#)]

51. Ku, C.Y.; Xiao, J.E.; Liu, C.Y.; Yeih, W. On the accuracy of the collocation Trefftz method for solving two and three dimensional heat equations. *Numer. Heat Transf. Part B* **2016**, *69*, 334–350. [[CrossRef](#)]
52. Logan, J.D. *Applied Mathematics*; John Wiley & Sons, Inc.: Hoboken, NJ, USA, 1987; pp. 275–360, ISBN 9780471165132.
53. Green, W.H.; Ampt, G.A. Studies on soil physics I. The flow of air and water through soils. *J. Agric. Sci.* **1911**, *4*, 1–24.
54. Lu, N.; Likos, W.J. *Unsaturated Soil Mechanics*; John Wiley & Sons, Inc.: Hoboken, NH, USA, 2004; pp. 494–527, ISBN 0-471-44731-5.



© 2017 by the authors. Licensee MDPI, Basel, Switzerland. This article is an open access article distributed under the terms and conditions of the Creative Commons Attribution (CC BY) license (<http://creativecommons.org/licenses/by/4.0/>).

Article

# Integrating Topography and Soil Properties for Spatial Soil Moisture Storage Modeling

Xiaohua Xiang <sup>1</sup>, Xiaoling Wu <sup>1</sup>, Xi Chen <sup>1,2,\*</sup>, Qifeng Song <sup>1,2</sup> and Xianwu Xue <sup>3,4</sup>

<sup>1</sup> College of Hydrology and Water Resources, Hohai University, Nanjing 210098, China; xxh\_xiang@sina.com (X.X.); freebird7237@163.com (X.W.); qfssong@sina.com (Q.S.)

<sup>2</sup> State Key Laboratory of Hydrology-Water Resources and Hydraulic Engineering, Hohai University, Nanjing 210098, China

<sup>3</sup> School of Civil Engineering and Environmental Sciences, University of Oklahoma, Norman, OK 73019, USA; xuexianwuqd@gmail.com

<sup>4</sup> Advanced Radar Research Center, National Weather Center, Norman, OK 73019, USA

\* Correspondence: xichen@hhu.edu.cn; Tel.: +86-25-8378-6981

Received: 14 July 2017; Accepted: 24 August 2017; Published: 30 August 2017

**Abstract:** The understanding of the temporal and spatial dynamics of soil moisture and hydraulic property of soil is crucial to the study of hydrological and ecological processes. The purpose of this study was to derive equations that describe spatial soil water storage deficit based on topography and soil properties. This storage deficit together with the topographical index can be used to conclude the spatial distribution curve of storage capacity in a (sub-) basin for developing hydrological model. The established model was able to match spatial and temporal variations of water balance components (i.e., soil moisture content (SMC), evapotranspiration, and runoff) over the Ziluoshan basin. Explicit expression of the soil moisture storage capacity (SMSC) in the model reduced parameters, which provides a method for hydrological simulation in ungauged basins.

**Keywords:** soil moisture storage; van Genuchten model; distributed model; Xin'anjiang model; TOPMODEL

## 1. Introduction

The understanding of the temporal and spatial dynamics of soil moisture and hydraulic property is crucial to the study of several hydrological and ecological processes. Soil moisture is a key variable in hydrological modeling. As McNamara et al. [1] pointed out that understanding soil storage and its role in regulating catchment functions should be a priority in future observation strategies and hydrological modelling. Soil moisture and hydrological routing is computed based on the saturated and unsaturated flow equations, which can be solved by finite element or difference techniques over a three dimensional grid. These models include System Hydrological European model (SHE) [2,3] and Institute of Hydrology Distributed Model (IHDM) [4,5]. While the advantages of pure, numerical simulation would seem clear, the tremendous amount of parameter evaluation required is problematic. In most cases the available data motivates the use of simple, conceptual model approaches rather than the use of a fully distributed, physically model with a large number of model parameters [6].

It is widely recognized that for saturation excess overland flow, soil storage is one of the key elements controlling runoff production in catchments in humid temperate areas. For traditionally lumped hydrological models, soil moisture is usually computed on the basis of basin average routing of unsaturated water balance, and its spatial variation is expressed in an empirical distribution curve of soil moisture storage capacity, e.g., a single parabolic curve in Xin'anjiang hydrological model [7]. The model usually lacks physical expressions and distribution functions of the hydrological processes or parameters, which solely calibrated based on observed flow discharge.

The semi-distributed models are capable to overcome shortage of the empirical models since they explicitly express watershed distribution of soil moisture storage using site-specific information of land surface features, e.g., soil properties and topography. For example, the topographic index [8] is widely used to analytically describe such distribution of soil moisture and runoff generation [9]. It is also used for improving the empirical hydrological models with a distributed function. Such as the Xin'anjiang model, the statistical curve of spatial distribution of storage capacity was directly derived from TOPMODEL's topographic index [10–12] and from catchment slopes [13] or the empirical shape parameter  $B$  of the water storage capacity of the soil non-linearly was estimated in terms of the characteristic land surface slope [14]. Some signal from the topography and soil type was used to explain the soil moisture variation [15]. These models are benefit from a combination of reasonable computation time and physically realistic hillslope simulation.

Explicitly description of storage capacity for computation of hydrological fluxes remains challenge as it relates to topography, soil, vegetation and base rock variations. In the mountainous areas, topography controls depth to groundwater table and thus distribution of soil moisture deficit. In the hilly lowland areas, near stream saturated zones will be most extensive in locations with concave hillslope profiles and wide flat valleys (Figure 1). The storage deficit in the unsaturated zone becomes small and the runoff is easily generated because the unsaturated zone for holding soil moisture is reduced due to the high groundwater table occupation or low active depth of the unsaturated zone [12].

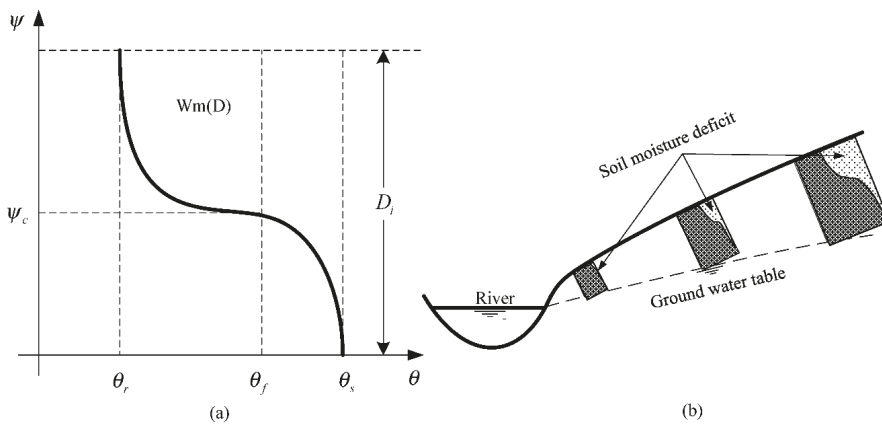


**Figure 1.** Sketch of vertical profile of soil moisture deficit  $Wm(D)$  at a specific site (a) and along hillslope (b).

The available space for moisture storage in unsaturated zone depends on not only the active depth but also the rise of the capillary fringe (Figure 1). Surface tension and soil pore capillary force lead the groundwater rise up into the soil and form a capillary fringe with a certain thickness [16], which significantly decreases soil moisture deficit. The capillary rise is associated with physical properties of soil porosity and particle diameter. For clay, where capillary is strong, a water table depth of 10 m can still be “felt” in the root zone and near surface. For sand, the water table has little role as a source if it is below the root zone [17]. It is found that low runoff potential for soils having the low rise of the capillary fringe, such as deep sand, deep loess, aggregated silts, and high runoff potential for soils having the high rise of the capillary fringe, such as heavy plastic clays, and certain saline soils [18].

The main objective of this study is to derive equations for description of the spatial soil storage capacity that can make use of topography and soil property in the humid hilly watershed. The equations were derived by combining the van Genuchten model of water retention relationship [19]

and the TOPMODEL topographic index. They can be used to describe the site specific soil storage capacity and its statistical feature in a (sub-) basin, thus to simulate spatial distribution of hydrological variables of runoff amount, evaporation and soil water storage. The model was tested on Ziluoshan basin of Huai River watershed in the humid region in China.

## 2. Materials and Methods

### 2.1. Description of Ziluoshan Basin

As one of the first tributaries in the upstream of Huai River, Shaying River originated in the western mountainous area of Henan province of China (Figure 2). The watershed area above the Ziluoshan hydrological station on Shaying River is 1800 km<sup>2</sup>, and the mountainous area accounts for 75%. These geographical and climatic features result in extremely uneven of the annual and seasonal distributions of rainfall. The annual precipitation during 1980–1996 is 900 mm, varying from the largest in the southeast to the smallest in the north. Most of annual precipitation is concentrated in the flood seasons (June–September). Nearly 60–70% of the total precipitation occurs in the months of June and August.

DEM data of 30 m grid resolution are used to describe the spatial variations of topography [20,21]. Based on the geographical map, the terrain of the catchment tilts from southwest to northeast (Figure 2). The mean elevation of topography is 820 m, varying from 284 m above the mean sea level in the downstream region to over 2122 m in the upstream mountainous areas. The topographic index in each pixel was calculated using the DTM9704 program [22,23].

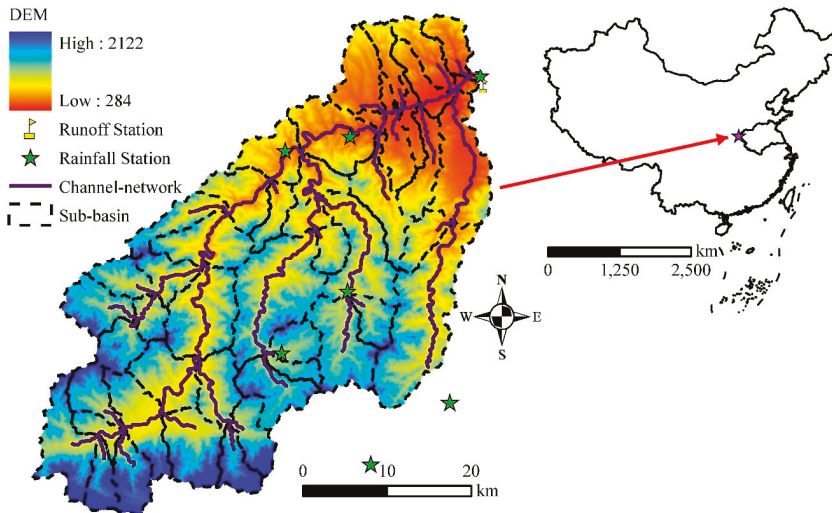


Figure 2. Location and topography in Ziluoshan basin.

Soil in the basin is primarily shallow eluvial-slope deposits consisting of sand, loam and clay (Data Center for Resources and Environmental Sciences Chinese Academy of Sciences (RESDC)). Percentage of sand and clay within the soil depth of 0–1.0 m ranges 5.3–83.0% for sand, 1.7–31.6% for clay (Figure 3), and the remaining for loam. Value of the hydraulic parameters for the three soils refers to Tuller [24] (Table 1). The mean values of soil hydraulic parameters of VG in each pixel were estimated by proportion-weighted arithmetic mean way, and the field capacity  $\theta_f$  was determined as a fraction of the saturated SMC (75% in this study [25]). The vegetation in the study region is primarily

deciduous broadleaf forest and mixed forest. The average vegetation coverage is larger than 75% [26] and average annual Normalized Difference Vegetation Index (NDVI) is larger than 0.6 [27].

**Table 1.** Van Genuchten parameters for three types of soil [24].

Parameter	Sand	Loam	Clay
$\theta_s$	0.37	0.46	0.51
$\theta_r$	0.058	0.083	0.102
$\alpha$ (cm <sup>-1</sup> )	0.035	0.025	0.021
$n$	3.19	1.31	1.2

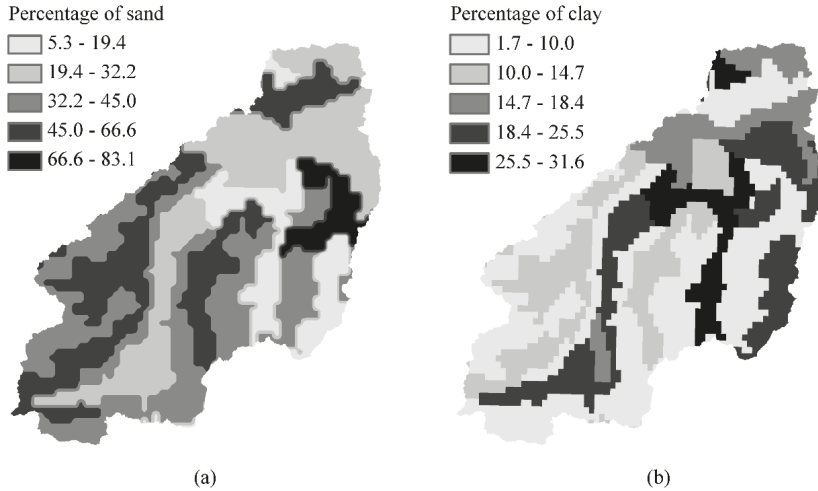


**Figure 3.** Percentage of sand and clay within the soil depth of 0–1.0 m, (a) Percentage of sand and (b) Percentage of clay.

The watershed was divided into a number of sub-basins (e.g., 50 sub-basins in this study) for describing spatial variations of runoff generation and river flow routing (Figure 4). Each sub-basin includes lots of pixels in 30 m grid resolution.

## 2.2. Outline of the Model

The soil moisture storage model was firstly introduced at site scale, and then extended to hillslope soil moisture storage capacity (SMSC) according to TOPMODEL concept. Finally, a spatial soil moisture storage curve was concluded by all sites SMSC in a statistical way to replace the traditional statistical curve in Xin’anjiang model. The detail procedure is given blow.

### 2.2.1. The Role of Soil Moisture Storage on Hydrological Fluxes

Hydrological balance on any element can be expressed as following:

$$W_t - W_{t-1} = P_t - E_t - R_t \tag{1}$$

where  $W_{t-1}$  and  $W_t$  is soil moisture storage at the time interval of  $t - 1$  and  $t$ ,  $P_t$ ,  $E_t$  and  $R_t$  is precipitation, actual evapotranspiration and runoff at the time interval of  $t - 1$  and  $t$ , respectively.

In Equation (1), computation of both actual evapotranspiration  $E$  and runoff  $R$  depends on soil storage  $W$  (SMC in this model) and its capacity  $Wm$  (SMSC in this model), e.g., for saturation excess

overland flow, runoff is generated as the soil storage reaches the capacity, which can be expressed as following:

$$R_t = \begin{cases} W_{t-1} + Pe_t - Wm & W_{t-1} + Pe_t - Wm > 0 \\ 0 & W_{t-1} + Pe_t - Wm \leq 0 \end{cases} \quad (2)$$

where  $Pe$  is net rainfall.

For distributed modeling or physical description of spatial variation function of watershed characteristics on hydrological fluxes, expression of soil spatial variation storage and its capacity in a watershed is vital.

### 2.2.2. Site Specific Soil Moisture Storage Capacity

SMSC is usually defined as the difference between the water content at field capacity and at residual multiplied by a critical depth in unsaturated zone for moisture storage and runoff generation. In humid regions, the critical depth can be regarded as unsaturated zone thickness or the depth to free water table if there is a free water table in the soil profile. In this case, vertical water content in the critical depth can be influenced by the free water table under the capillary flux from the free water to soil moisture column (Figure 1a), which results in that soil moisture seldom reach the residual water content on the groundwater table nearby. Thus, the soil moisture profile above the water table can be determined from the balance between the pressure head gradient, which tends to draw moisture up, and gravity [28].

The soil-water pressure head distribution,  $\psi(z)$ , may be modeled using Darcy’s law:

$$q = K(\psi)\left(\frac{\partial\psi}{\partial z} - 1\right) \quad (3)$$

or

$$z = \int_0^\psi \frac{K(\psi)d\psi}{K(\psi) + q} \quad (4)$$

where  $q$  is the steady state evaporation rate,  $K(\psi)$  is the unsaturated hydraulic conductivity function,  $\psi$  is the pressure head (m).

Soil moisture with depth can be described by the van Genuchten model (hereafter VG) of water retention relationship [19,29]:

$$\theta(\psi) = \theta_r + (\theta_s - \theta_r)\left(\frac{1}{1 + (\alpha\psi)^n}\right)^{1+\frac{1}{n}} \quad \psi < 0 \quad (5)$$

where  $\psi$  is the pressure head (m),  $\theta_s$  and  $\theta_r$  is saturated and residual volume water contents, respectively,  $\alpha$ ,  $n$  are fitting parameters.

Solution of Equation (3) or Equation (4) coupling with Equation (5) is a rather complicated although analytical steady state solutions can be found in the literature for some functions different with VG [30,31]. These mathematical difficulties are significantly reduced if the vertical profile of soil moisture is approximated with the profile corresponding to zero-flux conditions [32]. Under the assumption of zero vertical flux (quasi steady-state hydraulic assumption), the relationship between  $\psi$  and vertical distance above groundwater table ( $z$  is taken here to increase upwards) is that of hydraulic equilibrium:

$$\psi = z - D \quad (6)$$

where  $D$  is the depth to groundwater table.

Some comparisons between the vertical profile of soil moisture obtained with Equation (3) and the approximated profile provided by Equation (6) have been made in many literatures. It was found that difference of the soil moisture profiles between the two equations increases when the depth  $z$  increases to the nearby surface and the soil texture becomes finer. However, the difference between the

two profiles is smaller than 5–7% for a variety of soil textures [33]. For shallow water tables, the steady profile is close to hydrostatic state subject to no atmospheric forcing [34].

For the steady profile, the total profile moisture deficit will be obtained by integrating from the surface to the top of the capillary fringe. Using Equations (5) and (6), we obtain a simple mathematical expression for the unsaturated zone moisture storage  $S_f(D)$ , given the depth to groundwater table  $D$ :

$$\begin{aligned}
 S_f(D) &= \int_{\psi_c}^D \left[ \theta_r + (\theta_s - \theta_r) \left( \frac{1}{1+(\alpha z)^n} \right)^{1+\frac{1}{n}} \right] dz \\
 &= (D - \psi_c) \theta_r + \frac{D(\theta_s - \theta_r)}{[1+(\alpha D)^n]^{1/n}} - \frac{\psi_c(\theta_s - \theta_r)}{[1+(\alpha \psi_c)^n]^{1/n}}
 \end{aligned} \tag{7}$$

where  $\psi_c$  is suction pressure for the unsaturated zone storage at field capacity.

Hence, the soil moisture deficit or SMSC  $W_m(D)$  defined as the difference between the moisture content at field capacity  $\theta_f$  and at the unsaturated zone moisture profile  $S_f(D)$  in Equation (7) is given by:

$$\begin{aligned}
 W_m(D) &= (D - \psi_c) \theta_f - S_f(D) \\
 &= (D - \psi_c) (\theta_f - \theta_r) - \left[ \frac{D(\theta_s - \theta_r)}{[1+(\alpha D)^n]^{1/n}} - \frac{\psi_c(\theta_s - \theta_r)}{[1+(\alpha \psi_c)^n]^{1/n}} \right]
 \end{aligned} \tag{8}$$

Equation (8) explicitly expresses the storage capacity in terms of the site specific depth to groundwater table and hydraulic parameters of soil. A large storage capacity corresponds to low groundwater table and low capillary fringe.

### 2.2.3. Hillslope SMSC

In a hilly mountain area, the topographic index is widely used to represent the influences of terrain on the spatial variations of soil wetness. In TOPMODEL, the large topographic index always being obtained in the local valley area, where happened to be the saturated zone. So a larger topographic index in a local area means less soil moisture deficit or easier runoff generation in response to rainfall input [12]. Figure 1b illustrates that the local moisture deficit varies significantly along the catchment slope, with low values where the water table is near the surface (at the bottom of hills) and high values where the water table is deeper (at the top of hills) [35].

According to TOPMODEL concept, the depth to groundwater table at any location is given in terms of the watershed average depth to the water table and local topography wetness index [8]:

$$D_i = \bar{D} - S_{zm}(tp_i - \bar{\lambda}) \tag{9}$$

where  $D_i$  is the depth to groundwater table at the location  $i$ ,  $\bar{D}$  is the watershed-average depth to the water table,  $S_{zm}$  is a scaling parameter, known as the ‘effective depth’ that determines the decay of hydraulic conductivity with depth,  $tp_i$  is local topography wetness index ( $tp_i = \ln(\frac{a}{\tan \beta})$ ), where  $a$  is the cumulative area draining through a unit length of contour line,  $\beta$  is the slope of the unit area,  $\bar{\lambda}$  is the areal average of  $tp_i$ .

Equation (9) is written in the form:

$$D_i = -S_{zm}tp_i + C \tag{10}$$

Equation (10) is substituted into Equation (8) to get:

$$\begin{aligned}
 W_m(D_i) &= (-S_{zm}tp_i + C - \psi_c) (\theta_f - \theta_r) \\
 &\quad - \left[ \frac{(-S_{zm}tp_i + C)(\theta_s - \theta_r)}{[1+(\alpha(-S_{zm}tp_i + C))^n]^{1/n}} - \frac{\psi_c(\theta_s - \theta_r)}{[1+(\alpha \psi_c)^n]^{1/n}} \right]
 \end{aligned} \tag{11}$$

Equation (11) explicitly expresses soil moisture deficit at any location influenced by integration of soil properties, topography and depth to groundwater table.

The local storage capacity  $W_m(D_i)$  and its basin mean value  $WM$  solely depend on the effective soil depth  $S_{zm}$  if other parameters in the van Genuchten model in Equation (11) are measured or given according to available investigations. Beven et al. [36] described that larger value of the parameter  $S_{zm}$  means increase of active soil depth for water storage and runoff generation. Habets and Saulnier [37] stated that the parameter  $S_{zm}$  can be defined as one quarter of the maximum storage deficit.

In some humid area like Ziluoshan basin, streams are typically gaining streams (gaining water by drainage of baseflow from the groundwater into the stream). For the perennial rivers, the groundwater table near the surface is coincident or close to the stream water surface elevation [18,38]. Thus  $D_i$  and  $W_m(D_i)$  approach zero in the areas nearby the stream water surface where  $tp_i$  reaches its maximum value. Then, coefficient  $C$  in Equation (10) is:

$$C = S_{zm} \max(tp_i) \tag{12}$$

Equation (12) is substituted into Equation (11) to get:

$$W_m(D_i) = (S_{zm}(\max(tp_i) - tp_i) - \psi_c)(\theta_f - \theta_r) - \left[ \frac{S_{zm}(\max(tp_i) - tp_i)(\theta_s - \theta_r)}{[1 + (\alpha(S_{zm}(\max(tp_i) - tp_i))^n]^{1/n}} - \frac{\psi_c(\theta_s - \theta_r)}{[1 + (\alpha\psi_c)^n]^{1/n}} \right] \tag{13}$$

Thus, spatial variation of topographic index and soil properties in Table 1 are used to compute the curves of  $W_m$  versus  $f/F$  for all sub-basins as shown in Figure 4.

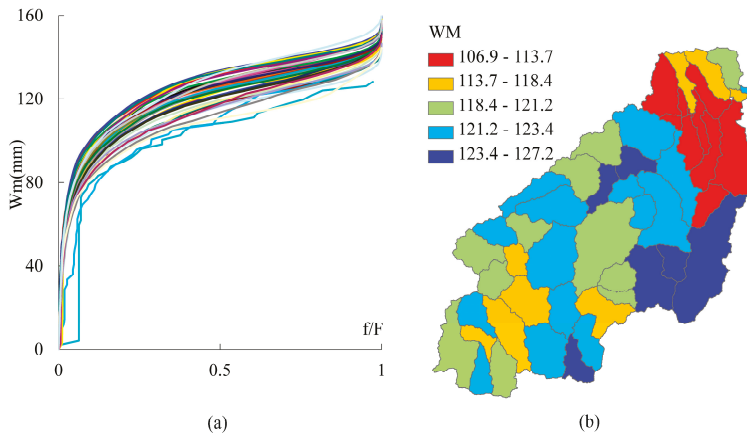


**Figure 4.** Spatial distribution of storage capacity  $WM$  (basin mean value of local storage capacity). (a) Cumulative frequency (cumulative proportion of partial basin area versus total basin area) of  $W_m \sim f/F$  in terms of Equation (13) for the 50 sub-basins, (b) sub-basin mean  $WM$ .

### 2.2.4. The Watershed Model Development

The model can be executed at each grid based on storage capacity  $W_m(D_i)$  at any local area calculated in terms of Equation (11). For runoff generation, grid runoff depth for a specific precipitation amount can be calculated based on saturation overland flow concept that runoff occurs where soil moisture reaches storage capacity (Equation (2)).

The site-specific storage capacity can be grouped into a number of intervals, each representing that fraction of the watershed with similar water table depth and soil moisture characteristics [39]. Water balance equations (Equation (2)) are applied at each interval, which separate estimates of unsaturated zone soil moisture, evapotranspiration and runoff for the whole intervals [40–42].

The individual fluxes in every interval are then really weighted and combined to obtain the water balance for the entire watershed. This modeling method is efficient in computation of flow routing and parameter calibration of the model.

For a large watershed, the model can be executed at each sub-basin based on distribution curve of  $W_m \sim f/F$  ( $f/F$  represents proportion of  $W_m$  value in a specific interval with an area  $f$  to the total (sub-) basin area  $F$ , the ratio value is between 0 and 1.) and its average value  $WM$  in a (sub-) basin. This modeling method becomes lumped structure like Xin'anjiang model, but it physically interprets the field capacity curve that allows for application in ungauged basins and consecutive routing in the large watershed.

Computations of actual evaporation, separation of runoff components and flow routing in the watershed and rivers are same as Xin'anjiang model in this study. The calibrated parameter meaning was listed in Table 2. A spatial distribution curve of free water storage capacity with a catchment average  $SM$  and an exponent of the spatial distribution curve,  $EX$ , is used to represent regulation of catchment heterogeneity on free water  $R$ . For thin soils,  $SM$  is around 10 mm, and  $EX$  is between 1.0 and 1.5 [43]. The free water  $R$  is then separated into overland flow  $R_s$ , subsurface flow  $R_i$ , and deep layer flow (groundwater)  $R_g$ .  $KI$  and  $KG$  are the outflow coefficients of the free water storage to interflow and groundwater. It is suggested that the sum  $KI + KG$  may be taken as 0.7–0.8 and the ratio of the three runoff components will be changed by altering the ratio of  $KG/KI$  [43].

**Table 2.** Calibrated parameter values of the modified Xin'anjiang model [43].

Parameter	Explanation	Unit	Lower Bound	Upper Bound	Value
Runoff Generation Calculation					
$KC$	Ratio of potential evapotranspiration to pan evaporation		0.6	1.2	0.7
$WM$	Areal mean tension water capacity	mm			92–127
$S_{zm}$	Scaling parameter based on soil properties	mm	10	1000	42.8
$C$	Deeper evapotranspiration coefficient		0.08	0.18	0.17
Water Source Separation					
$SM$	Free water storage capacity	mm	5	50	5/15
$EX$	Exponential of the distribution of water capacity		1	1.5	1.5
$KG$	Outflow coefficient of free water storage to the groundwater flow		0.2	0.6	0.4
$KI$	Outflow coefficient of free water storage to the interflow		0.2	0.6	0.3
Concentration Calculation					
$CS$	Recession constant of surface water storage		0	0.7	0.1/0.2
$CI$	Recession constant of interflow storage		0.5	0.9	0.5/0.7
$CG$	Recession constant of groundwater storage		0.5	0.998	0.995/0.98
$KE$	Residence time of water	h	0.5	1.5	1
$XE$	Muskingum coefficient		0	0.5	0.3

Note: for \*/\*, the upper and lower values represent calibrated parameter values for daily and hourly simulations in the following verification, respectively.

For application of the model in a large watershed, the whole watershed can be divided into a lot of sub-basins. These sub-basins are linked with the river channel system. The flow hydrograph at a point on the watershed from a known hydrograph of upstream or sub-basin is routed by the Muskingum method. Small tributaries of sub-basins merge to form larger stream which ultimately lead to outlet of the watershed.

### 2.3. Model Verification

Within the study area, daily and hourly observed precipitation data at 7 rainfall stations, pan evaporation and streamflow at the outlet of watershed were used for model testing (Figure 2). The largest and smallest streamflow discharges during 1979 and 1995 are 2080.0 and 1.0 m<sup>3</sup>/s, respectively. Daily and hourly rainfall in each of the watershed was interpolated by the Thiessen polygon method from observation data of rainfall stations. The model is calibrated and validated based on daily and hourly observed streamflow discharges at the whole watershed outlet in calibration and validation periods, respectively. The calibration period is 10 years from 1979 to 1988, and the validation period is 7 years from 1989 to 1995. Twelve and seven flood events with hourly observation

data in calibration and validation periods, respectively, are further selected for model calibration and validation.

The calibration procedures followed the Xin’anjiang model calibration proposed by Zhao et al. [43]: (1) giving initial values of the parameters suggested; (2) calibrating the parameters of runoff generation processes to test annual water balance, e.g., KC in Table 2, by comparing totals of the simulated and observed runoff; (3) calibrating other parameters of water source separation and flow routing in Table 2 to test flow discharges by comparing the simulated and observed runoff. Model performance is evaluated with respect to the objective function of maximizing Nash–Sutcliffe efficiency coefficient (NSC) between observed and simulated runoff. Another measure of model performance used in the study is the root mean squared error (RMSE) of flow discharge. The calibrated parameters and values were listed in Table 2. The calibrated value of  $S_{zm}$  is 42.8 mm. It is used to calculate mean value of storage capacity  $WM$  in each sub-basin and in whole watershed. The sub-basin mean  $WM$  for the 50 sub-basins ranges 107–127 mm, and whole watershed  $WM$  is 120 mm.

### 3. Result and Discussion

The calibration and validation results of flow discharges for daily and hourly data are listed in Tables 3 and 4, respectively. For daily simulation during the calibration period (Table 3), mean NSC value is 0.73, annually ranging 0.47–0.91; mean RMSE is 1.6 mm, annually ranging 0.6–4.4 mm. The daily simulation results during the validation period are even better than those in the calibration period, e.g., mean NSC value is 0.77, ranging 0.67–0.87; mean RMSE is 1.0 mm, ranging 0.6–1.4 mm.

**Table 3.** Results of model calibration and validation using daily data.

Period	Year	Annual P (mm)	Annual E (mm)	R (mm)		RE (%)	RMSE (mm)	NSC
				Obs	Sim.			
Calibration	1979	898.3	542.3	227	226.1	−0.42	1.1	0.77
	1980	792	470.6	188.1	196.1	4.24	1.0	0.73
	1981	653.6	464.4	94.6	98.4	3.99	0.6	0.58
	1982	1096.3	435.3	551.1	523.1	−5.06	4.4	0.91
	1983	1222.8	519.1	644.3	607.1	−5.78	2.8	0.87
	1984	984.6	557	362.1	337.9	−6.69	1.5	0.78
	1985	873.5	489.5	296.4	298.4	0.68	1.5	0.78
	1986	596.1	433.4	80.9	79.5	−1.73	0.6	0.47
	1987	736.6	469.4	146.4	153.2	4.64	1.1	0.56
	1988	803.3	380.3	224.4	233.2	3.92	1.6	0.85
	Mean	865.7	476.1	281.5	275.3	−0.22	1.6	0.73
Validation	1989	854.6	408.6	257.9	268.8	4.23	1.4	0.74
	1990	870.3	554.5	258.8	257.7	−0.44	1.4	0.87
	1991	605.5	475.7	120.1	109.2	−9.1	0.7	0.67
	1992	741.7	467.5	108.1	104	−3.85	0.7	0.75
	1993	647.8	492.2	95.1	99.8	4.93	0.6	0.83
	1994	867.3	473.4	155.3	166	6.94	1.4	0.73
	1995	731.4	407.8	151.3	153.2	1.27	1.1	0.81
	Mean	759.8	468.5	163.8	165.5	0.57	1.0	0.77

The model captured the flood processes (Table 4 and Figure 5) as well. During the calibration and validation periods, respectively, mean NSC value of all flood events is 0.85 and 0.83; the relative error of the simulated and observed peak discharges is 3.70% and 2.26%; mean RMSE is 44.5 and 35.6 m<sup>3</sup>/s. For illustrative purpose, hourly simulated and observed flood discharges are shown in Figure 5. These results demonstrated that the model is capable of reproducing both the magnitude and the dynamics of the daily and hourly flow discharges.

**Table 4.** Results of model calibration and validation using hourly data.

	Flood No.	P (mm)	E (mm)	Flood Volume ( $10^6 \text{ m}^3$ )			Peak Discharge ( $\text{m}^3/\text{s}$ )			RMSE ( $\text{m}^3/\text{s}$ )	NSC
				Vobs	Vsim	RE (%)	Qobs	Qsim	RE (%)		
Calibration	1980070219	32.4	5.7	41.6	39.4	-5.28	408.0	407.3	-0.18	30.9	0.94
	1980082320	26.3	4.4	23.4	24.9	6.31	245.0	227.2	-7.26	37.5	0.71
	1981062405	30.0	4.7	15.4	14.2	-7.85	174.0	175.2	0.66	7.9	0.87
	1981071510	12.7	4.3	13.2	13.3	0.88	154.0	146.4	-4.94	25.3	0.79
	1982081309	31.7	0.9	57.3	52.8	-7.82	619.0	591.6	-4.43	42.1	0.89
	1983073021	68.7	4.7	119.3	126.3	5.89	1180.0	1153.3	-2.26	121.6	0.83
	1984090820	49.1	4.9	52.6	62.2	18.34	483.0	481.2	-0.37	68.8	0.80
	1984092320	41.9	0.9	53.8	60.8	13.07	838.0	827.5	-1.26	71.1	0.92
	1985091415	82.5	5.2	91.3	86.8	-4.97	524.0	496.5	-5.26	22.9	0.98
	1986090922	7.0	0.9	12.9	14.5	12.73	258.0	249.5	-3.31	36.8	0.81
	1987060101	27.5	4.1	16.3	14.9	-8.61	260.0	233.0	-10.40	33.3	0.87
1987051201	47.2	3.3	18.0	19.8	10.06	270.0	255.6	-5.35	36.1	0.84	
Mean	38.1	3.7	42.9	44.2	2.73	451.1	437.0	-3.70	44.5	0.85	
Validation	1989081615	111.0	13.7	116.9	110.3	-5.71	402.0	408.1	1.51	29.7	0.93
	1989081122	11.1	1.3	13.8	15.5	12.29	242.0	229.1	-5.34	31.9	0.80
	1990061915	33.2	10.7	50.9	40.2	-21.16	524.0	517.6	-1.23	41.6	0.95
	1991053120	45.8	28.8	41.5	46.8	12.79	266.0	269.7	1.37	24.6	0.89
	1991061412	18.5	11.4	16.9	19.5	15.50	155.0	155.9	0.56	23.4	0.72
	1993051220	19.8	5.9	18.7	17.6	-6.08	103.0	99.0	-3.90	15.6	0.78
	1995072422	52.7	3.5	36.1	38.2	5.98	775.0	706.2	-8.88	85.0	0.74
Mean	41.7	10.8	42.1	41.2	1.94	352.4	340.8	-2.27	35.6	0.83	

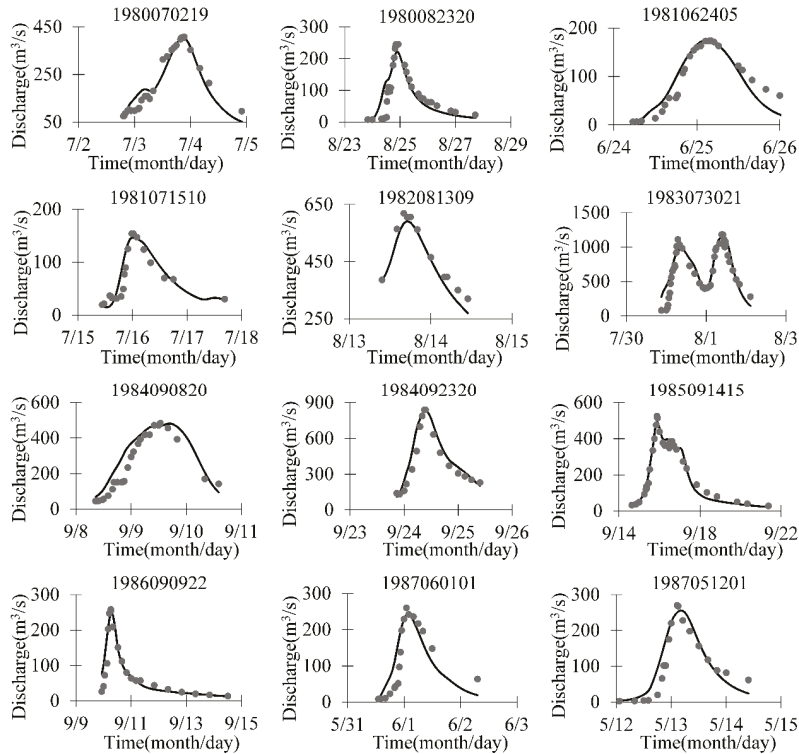


**Figure 5.** Cont.

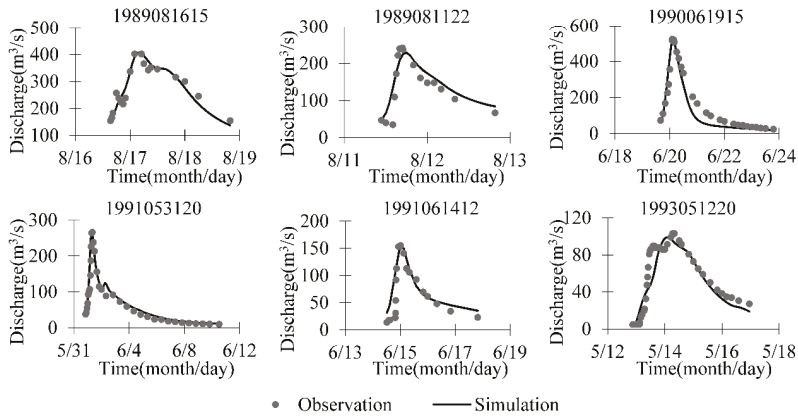


Figure 5. Hourly simulated and observed runoff in the watershed for the selected flooding events.

3.1. Sensitivity Analysis

In this study, sensitivity analysis of parameters for the effective depth  $S_{zm}$  and soil properties was carried out to evaluate and quantify the effect of the parameter variations on model output. Curves of  $W_m \sim f/F$  for  $S_{zm}$  values within 10–50 mm in the whole watershed were shown in Figure 6a. Sensitive analysis was executed by simulating changes of streamflow in response to these curves. For the specific soil distribution in the study watershed (Figure 3), change of mean annual streamflow for the flood period 11 May–23 September 1985 responded to changes in  $S_{zm}$  and WM are shown in Figure 6b. Increase of  $S_{zm}$  significantly increased WM and thus decreased runoff. Simulated results indicate that as  $S_{zm}$  increased from 10 to 50 mm, WM increased from 12.6 to 143.8 mm, resulting in 70.0% decrease of runoff from 251.5 to 75.4 mm.

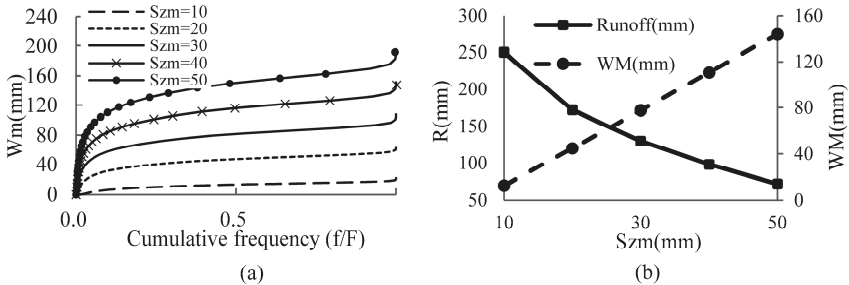
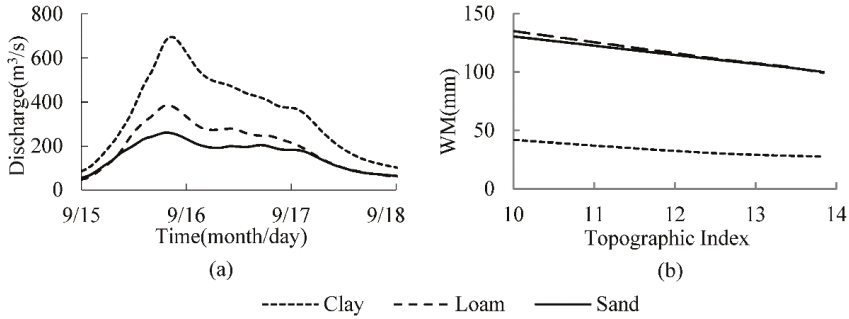


Figure 6. Distribution of soil moisture storage capacity  $W_m$  related to  $S_{zm}$  ('effective depth' that determines the decay of hydraulic conductivity with depth) in the whole watershed (a) and sensitivity of parameter  $S_{zm}$  to runoff  $R$  and watershed mean storage capacity  $WM$  (basin mean value of local storage capacity) for the flood period during 11 May–23 September, 1985 (b).

Sensitivity of soil properties on model output was executed for the rainfall. If the soils in the whole watershed were replaced by one of the three soils (silt, sandy loam and clay), the analysis results of relationship between  $WM$  and topographic index in 50 sub-basins indicated that sub-basin mean  $WM$  decreased with the topographic index increase (Figure 7a). Because of high residual moisture content  $\theta_r$  and capillary rise for clay, the storage capacity  $WM$  for clay was much smaller than that of sand and sandy loam. Therefore, precipitation on the clay soil generates much more runoff than that on sand and sandy loam. As an example, simulated flood discharges for the precipitation of 81.9 mm

during 15–18 September 1985 for sand, sandy loam and clay are shown in Figure 7b. This amount of precipitation generates runoff of 55.8 mm for clay, 42% and 52% larger than the generated runoff of 32.4 and 26.6 mm for sandy loam and sand, respectively. For the simulated flood events, the peak discharge generated on clay is 696.0 m<sup>3</sup>/s, 44% and 63% larger than the peak discharges of 386.0 and 260.0 m<sup>3</sup>/s on sandy loam and sand, respectively.



**Figure 7.** Relationship between sub-basin mean WM (basin mean value of local storage capacity) and topographic index for 50 sub-basins with soil types of silt, sandy loam and clay, respectively. (Note: catchment mean  $S_{zm}$  (‘effective depth’ that determines the decay of hydraulic conductivity with depth) is assumed as 42.8 mm in the figure). (a) And simulated flood discharges for sand, sand loam and clay in 1985 (b).

### 3.2. Spatial Variation of Hydrological Components

For hydrological modeling, distribution of the three components, soil moisture content, actual evapotranspiration and runoff, are vital for water resources management, environmental protection and assessment of land use and climate change impacts on hydrology. A major strength of the model is its capability to describe the spatial variations of such components.

The developed model was executed in each of sub-basins with rainfall input and  $W_m \sim f/F$  curves (Figure 4). The hydrological components, i.e., soil moisture content, actual evapotranspiration and runoff were calculated in each sub-basin and their spatial variations were then described. For illustrative purposes, spatial variations of mean annual precipitation and runoff during 1980–1996 simulated by the model are shown in Figure 8a,b and soil moisture content and actual evapotranspiration on 1 October 1987 after a non-rainfall period of 20 days are shown in Figure 8c,d.

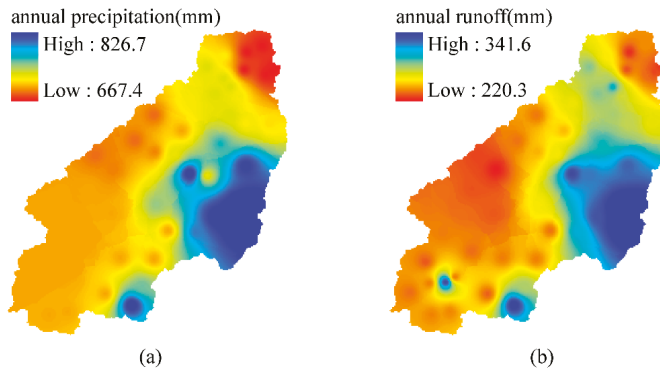


**Figure 8.** Cont.

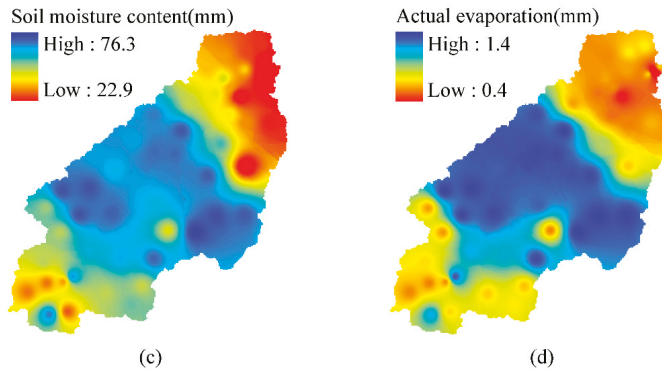


**Figure 8.** Spatial variation of mean annual precipitation (a) and runoff (b) during 1980–1996 and spatial variation of soil moisture content (c) and actual evaporation (d) on 1 October 1987.

Figure 8 demonstrates that for the multi-year average, runoff distribution (Figure 8b) agrees with precipitation distribution (Figure 8a), larger in south and southwest of the high mountain area and smaller in the north and north east. Simulated results in Figures 8a and 8b indicate that actual evaporation distribution generally corresponds to soil moisture content distribution, and both components are controlled by storage capacity for a specific time. As shown in Figure 8c, soil moisture content on 1 October 1987 is larger in the middle areas of watershed with a high value of WM (mostly higher than 120 mm in Figure 4b), and smaller in the north and south areas of the watershed with a low value of WM (mostly lower than 120 mm in Figure 4b). Larger soil moisture offers more water for evaporation (Figure 8d).

#### 4. Conclusions

For the saturation excess overland flow modeling, the critical spatial soil moisture distribution was usually represented either by a grid by grid method or a distribution curve based on the controlling component, such as soil moisture (deficit). The latter method was generally more efficient, but such curve was traditionally empirical and lacked of directly physical interpretation, which did not allow for the extended application in ungauged basins. In order to overcome the limitations, the storage capacity distribution curve in a (sub-) basin was explicitly expressed by the van Genuchten model and topographic index in TOPMODEL on the basis of digital elevation and soil map. Because the new model had capacity in describing soil moisture deficit at a grid scale or its statistical curve in a sub-basin, the model could be used to simulate temporal and spatial distributions of hydrological components, and to investigate their relation with precipitation, topography and soil variations.

The model had been proven to be a reliable and flexible tool for rainfall-runoff modelling in Ziluoshan basin. The results demonstrated that the model was not only capable of reproducing daily and hourly flow discharges, but also able to produce reasonable spatial variations of hydrological components such as runoff, soil moisture storage and actual evapotranspiration. Sensitivity analysis showed effect of the soil effective depth and soil properties on runoff. This study helped us to understand scale effects of land surface characteristics on hydrological processes.

**Acknowledgments:** This research is supported by the National Key R&D Programme of China (No. 2016YFA0601000) and the Fundamental Research Funds for the Central Universities (Grant No. 2015B20314).

**Author Contributions:** Xiaohua Xiang contributed to the experiment design; Xiaoling Wu contributed to the data analysis and manuscript review; Xi Chen contributed to the experiment design, manuscript preparation and editing; Qifeng Song contributed to the data analysis and manuscript review; Xianwu Xue contributed to the manuscript review.

**Conflicts of Interest:** The authors declare no conflict of interest.

## References

1. McNamara, J.P.; Tetzlaff, D.; Bishop, K.; Soulsby, C.; Seyfried, M.; Peters, N.E.; Aulenbach, B.T.; Hooper, R. Storage as a metric of catchment comparison. *Hydrol. Process.* **2011**, *25*, 3364–3371. [[CrossRef](#)]
2. Abbott, M.B.; Bathurst, J.C.; Cunge, J.A.; O’Connell, P.E.; Rasmussen, J. An introduction to the European Hydrological System-Systeme Hydrologique Europeen, SHE. 1. History and philosophy of a physically-based distributed modelling system. *J. Hydrol.* **1986**, *87*, 45–59. [[CrossRef](#)]
3. Abbott, M.B.; Bathurst, J.C.; Cunge, J.A.; O’Connell, P.E.; Rasmussen, J. An introduction to the European Hydrological System-Systeme Hydrologique Europeen, SHE. 2 Structure of a physicallybased distributed modelling system. *J. Hydrol.* **1986**, *87*, 61–77. [[CrossRef](#)]
4. Beven, K.J.; Calver, A.; Morris, E.M. *The Institute of Hydrology Distributed Model*; Report 98; The Institute of Hydrology: Wallingford, UK, 1987.
5. Binley, A.; Elgy, J.; Beven, K.J. A physically based model of heterogeneous hillslopes: 1. Runoff Production. *Water Resour. Res.* **1989**, *25*, 1219–1226. [[CrossRef](#)]
6. Seibert, J.; Bishop, K.; Rodhe, A.; McDonnell, J.J. Groundwater dynamics along a hillslope: A test of the steady state hypothesis. *Water Resour. Res.* **2003**, *39*, 1014. [[CrossRef](#)]
7. Zhao, R.J.; Zhuang, Y.L.; Fang, L.R.; Liu, X.R.; Zhang, Q.S. The Xin’anjiang model. In *Hydrological Forecasting*; IAHS Publication No. 129; IAHS Press: Wallingford, UK, 1980; pp. 351–356.
8. Beven, K.J.; Kirkby, M.J. A physically based variable contributing area model of basin hydrology. *Hydrol. Sci. Bull.* **1979**, *24*, 43–69. [[CrossRef](#)]
9. Pellenq, J.; Kalma, J.; Boulet, G.; Saulnier, G.M.; Wooldridge, S.; Kerr, Y.; Chehbouni, A. A disaggregation scheme for soil moisture based on topography and s O’Kane oil depth. *J. Hydrol.* **2003**, *276*, 112–127. [[CrossRef](#)]
10. Bell, V.A.; Moore, R.J. A grid-based distributed flood forecasting model for use with weather radar data: Part 1. *Hydrol. Earth Syst. Sci.* **1998**, *2*, 265–281. [[CrossRef](#)]
11. Guo, F.; Liu, X.R.; Ren, L.L. Topography based watershed hydrological model-TOPOMODEL and its application. *Adv. Water Resour.* **2000**, *11*, 296–301. (In Chinese)
12. Chen, X.; Chen, Y.D.; Xu, C.Y. A distributed monthly hydrological model for integrating spatial variations of basin topography and rainfall. *Hydrol. Process.* **2007**, *21*, 242–252. [[CrossRef](#)]
13. Kong, F.Z.; Song, X.M. A Computation Method for Spatial Distribution of Soil Moisture Storage Capacity in Xin’anjiang Model. *J. China Hydrol.* **2011**, *31*, 1–14. (In Chinese)
14. Dumenil, L.; Todini, E. A rainfall-runoff scheme for use in the Hamburg climate model. In *Advances in Theoretical Hydrology, A Tribute to James Dooge*; O’Kane, J.P., Ed.; Elsevier Science Publishers B.V.: Amsterdam, The Netherlands, 1992; pp. 129–157.
15. Blyth, E.M.; Finch, J.; Robinson, M.; Rosier, P. Can soil moisture be mapped onto the terrain? *Hydrol. Earth Syst. Sci.* **2004**, *8*, 923–930. [[CrossRef](#)]
16. Carman, P.C. Capillary rise and capillary movement of moisture in fine sands. *Soil Sci.* **1941**, *52*, 1–14. [[CrossRef](#)]
17. Fan, Y.; Miguez-Macho, G.; Weaver, C.P.; Walko, R.; Robock, A. Incorporating water table dynamics in climate modeling: 1. Water table observations and equilibrium water table simulations. *J. Geophys. Res.* **2007**, *112*, D10125. [[CrossRef](#)]
18. Todini, E. The ARNO rainfall-runoff model. *J. Hydrol.* **1996**, *175*, 339–382. [[CrossRef](#)]
19. Van Genuchten, M.Th. A closed-form equation for predicting the hydraulic conductivity of unsaturated soils. *Soil Sci. Soc. Am. J.* **1980**, *44*, 892–898. [[CrossRef](#)]
20. ASTER GDEM Readme File-ASTER GDEM Version1. Available online: [http://www.jspacesystems.or.jp/ersdac/GDEM/E/image/ASTER%20GDEM%20Readme\\_Ev1.0.pdf](http://www.jspacesystems.or.jp/ersdac/GDEM/E/image/ASTER%20GDEM%20Readme_Ev1.0.pdf) (accessed on 30 June 2009).
21. ASTER GDEM Validation Summary Report. Available online: [https://lpdaac.usgs.gov/sites/default/files/public/aster/docs/ASTER\\_GDEM\\_Validation\\_Summary\\_Report.pdf](https://lpdaac.usgs.gov/sites/default/files/public/aster/docs/ASTER_GDEM_Validation_Summary_Report.pdf) (accessed on 30 June 2009).
22. Beven, K.J. *TOPMODEL User Notes (Windows Version 1997)*; Lancaster University Centre for Research on Environmental Systems and Statistics: Lancaster, UK, 1998.
23. Beven, K.J. TOPMODEL: A critique. *Hydrol. Process.* **1997**, *11*, 1069–1085. [[CrossRef](#)]

24. Tuller, M.; Or, D. Water Retention and Soil Water Characteristics Curve. In *Encycl. Soil. Environ*; Hillel, D., Ed.; Elsevier: Oxford, UK, 2005; pp. 278–289.
25. Grewal, K.S.; Buchan, G.D.; Tonkin, P.J. Estimation of field capacity and wilting point of some New Zealand soils from their saturation percentages, New Zealand. *N. Z. J. Crop. Hort.* **1990**, *18*, 241–246. [[CrossRef](#)]
26. Liu, Y.A.; Huang, B.; Cheng, T. Vegetation coverage in upper Huaihe River Basin based on binary pixel model of remote sensing. *Bull. Soil Water Conserv.* **2012**, *1*, 93–97. (In Chinese)
27. Wang, Q.; Liu, X.H.; Lv, B.L. Dynamic changes and spatial patterns of vegetation cover in a river basin based on SPOT-VGT data: A case study in the Huaihe River Basin. *Prog. Geogr.* **2013**, *32*, 270–277. (In Chinese)
28. Ducharne, A.; Koster, R.D.; Suarez, M.J.; Stieglitz, M.; Kumar, P. A catchment-based approach to modeling land surface processes in a GCM, Part 2, Parameter estimation and model demonstration. *J. Geophys. Res.* **2000**, *105*, 24823–24838. [[CrossRef](#)]
29. Troch, P. Conceptual Basin-Scale Runoff Process Models for Humid Catchments: Analysis, Synthesis and Applications. Ph.D. Thesis, Ghent University, Gent, Belgium, 1993.
30. Gardner, W. Some steady-state solutions of the unsaturated moisture flow equation with application to evaporation from a water table. *Soil Sci.* **1958**, *85*, 228–232. [[CrossRef](#)]
31. Salvucci, G.D. An approximate solution for steady vertical flux of moisture through an unsaturated homogeneous soil. *Water Resour. Res.* **1993**, *29*, 3749–3753. [[CrossRef](#)]
32. Hilberts, A.G.J. Low-Dimensional Modeling of Hillslope Subsurface Flow Processes, Developing and Testing the Hillslope-Storage Boussinesq Model. Ph.D. Thesis, Wageningen Universiteit, Wageningen, The Netherlands, 2006; pp. 25–48.
33. Ridolfi, L.; D’Odorico, P.; Laio, F.; Tamea, S.; Rodriguez-iturbe, I. Coupled stochastic dynamics of water table and soil moisture in bare soil conditions. *Water Resour. Res.* **2008**, *44*, W01435. [[CrossRef](#)]
34. Salvucci, G.D.; Entekhabi, D. Equivalent steady soil moisture profile and time compression approximation in water balance modeling. *Water Resour. Res.* **1994**, *30*, 2737–2750. [[CrossRef](#)]
35. Koster, R.D.; Suarez, M.J.; Ducharne, A.; Kumar, P. A Catchment-Based Approach to Modeling Land Surface Processes in a GCM. Part 1: Model Structure. *J. Geophys. Res.* **2000**, *105*, 24823–24838. [[CrossRef](#)]
36. Singh, V.P. *Computer Models of Watershed Hydrology*; Water Resources Publications: Littleton, CO, USA, 1995.
37. Habets, F.; Saulnier, G.M. Subgrid runoff parameterization. *Phys. Chem. Earth Part B* **2001**, *26*, 455–459. [[CrossRef](#)]
38. Marani, M.; Eltahir, E.; Rinaldo, A. Geomorphic controls on regional base flow. *Water Resour. Res.* **2001**, *37*, 2619–2630. [[CrossRef](#)]
39. Stieglitz, M.; Rind, D.; Famiglietti, J.; Rosenzweig, C. An efficient approach to modeling the topographic control of surface hydrology for regional and global climate modeling. *J. Clim.* **1997**, *10*, 118–137. [[CrossRef](#)]
40. Famiglietti, J.S.; Wood, E.F. Multiscale modeling of spatially variable water and energy balance processes. *Water Resour. Res.* **1994**, *30*, 3061–3078. [[CrossRef](#)]
41. Famiglietti, J.S.; Wood, E.F. Effects of spatial variability and scale on areally averaged evapotranspiration. *Water Resour. Res.* **1994**, *30*, 3079–3093. [[CrossRef](#)]
42. Wolock, D.M.; Price, C.V. Effects of digital elevation model map scale and data resolution on a topography-based watershed model. *Water Resour. Res.* **1994**, *30*, 3041–3052. [[CrossRef](#)]
43. Zhao, R.J.; Liu, X.R. The Xinanjiang model. In *Computer Models of Watershed Hydrology*; Singh, V.P., Ed.; Water Resources Publications: Littleton, CO, USA, 1995; pp. 215–232.



Article

# Measurement and Simulation of Soil Water Contents in an Experimental Field in Delta Plain

Wenjuan Hua <sup>1,2,\*</sup>, Chuanhai Wang <sup>1,2</sup>, Gang Chen <sup>1,2</sup>, Hai Yang <sup>1,2</sup> and Yue Zhai <sup>2</sup>

<sup>1</sup> State Key Laboratory of Hydrology-Water Resources and Hydraulic Engineering, Hohai University, Nanjing 210098, China; wangchuanhai@vip.sina.com (C.W.); gangchen@hhu.edu.cn (G.C.); yhasan@163.com (H.Y.)

<sup>2</sup> College of Hydrology and Water Resources, Hohai University, Nanjing 210098, China; partychai2014@hotmail.com

\* Correspondence: huawenjuan0106@126.com; Tel.: +86-159-9623-8960

Received: 8 October 2017; Accepted: 2 December 2017; Published: 6 December 2017

**Abstract:** Variation in soil water content in the delta plain has its own particularity and is significant for agricultural improvement, the utilization of water resources and flood risk mitigation. In this study, experimental data collected from a plot of farmland located in the Taihu Basin were used to investigate the temporal and vertical variation of soil water content, as well as the effects of individual rainfall on soil water and shallow groundwater and their interaction. The results showed that the variation of soil water content is dependent on the comprehensive influence of soil hydraulic properties, meteorological factors and shallow groundwater and the correlation to the groundwater table is the strongest due to the significant capillary action in the delta plain. A saturated-unsaturated three-dimensional soil water numerical model was developed for the study area in response to rainfall and evapotranspiration. Scenario simulations were performed with different soil depths for soil water content and the error source was analyzed to improve the model. The average RMSE, RE and  $R^2$  values of the soil water content at the five depths between the measured and simulated results were  $0.0192 \text{ cm}^3 \cdot \text{cm}^{-3}$ , 2.09% and 0.8119, respectively. The results indicated that the developed model could estimate vertical soil water content and its dynamics over time at the study site at an acceptable level. Moreover, further research and application to other sites in delta plains are necessary to verify and improve the model.

**Keywords:** soil water content; field observation; three-dimensional model; numerical model; delta plain; shallow groundwater

## 1. Introduction

Most delta plains are lowlands, which are often densely populated and form centers of agricultural production, economic activity and transportation [1] such as the Taihu Basin in the Yangtze River Delta, East China, approximately 30% of which are lowland polders [2]. However, these areas are characterized by low elevation, flat topography, a shallow groundwater table, extensive river networks and uncertain catchment boundaries [3–5]. Therefore, delta plains require more attention to keep out natural hazards given their vulnerability to flooding, climatic variation and water quality deterioration. To avoid and mitigate the effects of natural and artificial disasters, exploring and simulating the specific hydrologic processes of delta plains are quite important for regional risk assessment and water resource engineering design.

Soil water content is a key state variable in the terrestrial system as it interacts with various system components [6,7] and is of great importance in many investigations and applications pertaining to agriculture, hydraulic engineering, hydrology, meteorology and soil mechanics [8–10]. Climatic conditions [11], vegetation types [12–14], topography [15], soil properties [16,17], antecedent soil water

content [18] and hysteresis [19,20] determine the spatio-temporal variability of soil water content [21], which in turn affects the exchange of energy and water in the unsaturated zone of the hydrological system [22]. These exchange processes are characterized by high nonlinearity and complex feedback mechanisms [6]. Consequently, different measurement technologies (e.g., sensor technologies and distributed sensor networks [23–25]) and simulation models have been used to study the importance of soil water content for describing and understanding vadose zone processes [26], climate and atmospheric processes [27], soil moisture estimation [28] and so on.

There are two main approaches for soil water study and prediction: field observation-based and modeling-based methods. As one of the dielectric-based techniques to determine soil water content at the local scale, the well-known time domain reflectometry (TDR) was introduced by Topp et al. [29] and has developed into a standard method to measure soil water content. It provides the apparent relative dielectric permittivity of soil determined by monitoring the travel time of a fast-rise-step voltage pulse along a transmission line connected to a suitable probe placed in the soil at the required measuring depth [8]. Nevertheless, observations of shallow groundwater and meteorology (e.g., temperature, rainfall and evaporation) should also be considered and applied to models when simulating soil water content. Two of the most widespread soil water models are the Richards equation-based models and the Bucket model. HYDRUS [30,31], which numerically solves the Richards equation for saturated–unsaturated water flow and convection–dispersion type equations for heat and solute transport, has been widely used to analyze the multi-layer soil water flow for preferential flow [32–35], transport domains for both laboratory [36,37] and field-scale applications [38,39]. However, it is not recommended to use HYDRUS for very large 3D domains such as entire catchments [40]. For certain types of applications, a successful synopsis of both monitoring and modeling issues was presented by Morbidelli et al. [41] that referred to the experimental field campaigns carried out to measure the soil water content with the TDR method in the vertical soil profiles of five different plots. However, it was not designed for delta plains with shallow groundwater. Some models coupling surface water to groundwater can also be used for soil water dynamics analysis or simulation. The SWATMOD model [42] is the coupling of the SWAT model and the MODFLOW model but tends to simulate soil percolation which skips unsaturated soil water. The MODBRNCH model [43] develops a pattern to connect the MODFLOW model and the BRNCH model where Saint-Venant equations need to be solved with much shorter steps than in the former. There are other models, like the HSPF-MODFLOW model, GSFLOW model, MODFLOW-DAFLOW model, IFM Mike model, IGSM model [44], etc., where most of these models are the direct coupling of two mature models referring to saturated and understanding the soil water, respectively, which saves much work but also has their own shortages and limitations. Furthermore, the two sub models are in an unconsolidated couple by infiltration but with independent processes and calculations. Comparatively, the Mike-SHE model [45] developed by the Danish Institute of Water Conservancy is complete with different functions but it is a model based on the actual physical process which needs a large amount of hydrologic data, topographic map and parameters. Therefore, a simplified specific model is required for conducting research in a particular location to greatly improve work efficiency, especially as the basis for an upscaling model in further work. Meanwhile, field observation is an important and pervasive way to support analysis and verification.

In this study, an experimental field was introduced in detail and measured data were analyzed in different ways. A three-dimensional numerical model was built up, calibrated and validated for the soil water flow at the study site based on the Richards equation. The basic research into soil water and addressing this as a backbone for specific model development will help us understand various hydrological processes, provide reference to improving agricultural planning and more accurate hydrological prediction. Three objectives of this study are proposed: (1) Construct a special experimental field with necessary instruments in the Yangtze River Delta to make future experiments more targeted, operable and flexible; (2) Explore the temporal and vertical variations of soil water content, the effects of individual rainfall on soil water and shallow groundwater and their interaction;

(3) Seek a simplified special model for soil water estimation in the delta plain. In this paper, the field experiments and the numerical methods are provided in Section 2. The data analyses and modeling results for soil water are presented in Section 3. Several significant points are discussed in Section 4. Conclusions are made in Section 4.

## 2. Materials and Methods

### 2.1. Site, Soil Sampling and Instrumentation

The study site for the hydrological observation and field experiment is located in ZhuLin, Changzhou City in China (Figure 1a). It is part of the Taihu Basin in the Yangtze River Delta and is characterized by flat terrain and a river network. The region has a subtropical monsoon climate with 900–1100 mm annual rainfall and 1000–1500 mm annual evaporation. The soil consists of a 30 m deposit of Quaternary. The upper 0.55–0.6 m soil layer is plain fill with high clay and the lower 0.7–0.9 m consists of silty clay. From 1.9 to 3.2 m below the ground surface, the third layer is mainly composed of silt and silty sand. The phreatic water table level is located at approximately 1 m in depth. The saturated hydraulic conductivity ( $K$ ) is around  $3 \times 10^{-4}$  m/s according to testing results.

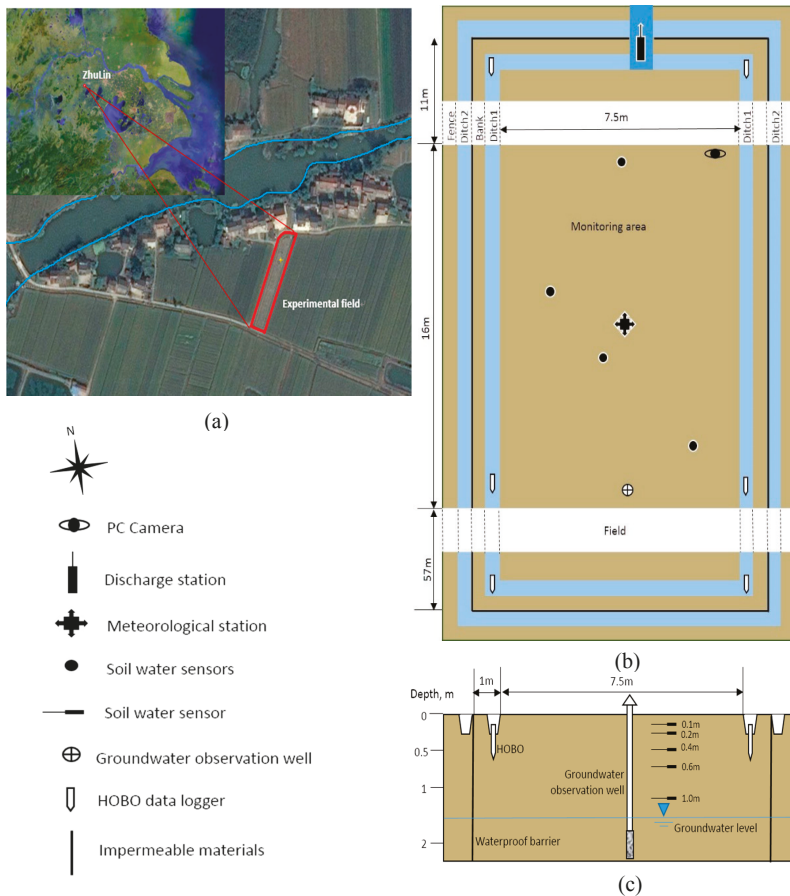


**Figure 1.** Field tests: (a) Site of the study in Taihu Basin; (b) layout of the experimental field; and (c) vertical layout of the field (0.0–2.0 m depth).

The experimental field is isolated from the surrounding surface water with a waterproof barrier. Two drainage ditches inside and outside the impermeable materials are linked at the outlet leading to a river. Figure 1b shows the layout of the field, which has an area of 798 m<sup>2</sup> with a length of 84 m and width of 9.5 m. Measuring instruments installed there included a video camera, a discharge meter next to a V-notch weir, a meteorological station, four soil water profiles, a groundwater observation well and some HOBO data loggers (Figure 2). Meteorological factors such as rainfall, evaporation, temperature, wind speed and direction were measured by the meteorological station. The measurements of soil water content at different depths (10, 20, 40, 60 and 100 cm) of soil profile were performed by the soil water sensors (TDR100, Campbell Scientific) and were recorded at intervals of 10 min in terms of volumetric water content obtained from the TDR signal through the universal calibration curve of Topp et al. [29]. The phreatic water table was recorded continuously with a time step of 5 min by the groundwater observation well. The HOBO data loggers recorded the water table and temperature in the ditch with a time step of 5 min. Detailed information on the vertical layout of the field is shown in Figure 1c.

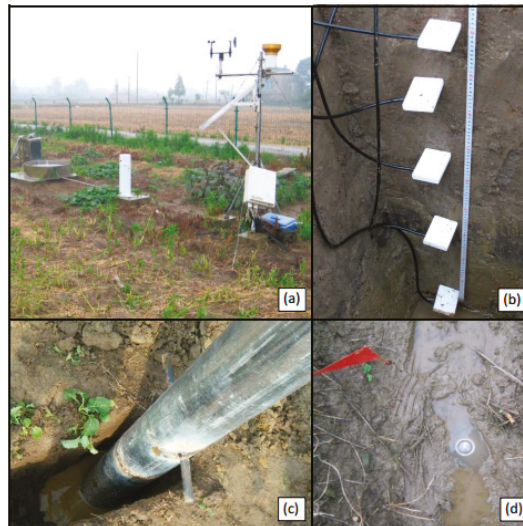


**Figure 2.** View of the some measuring instruments installed in the experimental field: (a) meteorological station; (b) soil water profile and sensors; (c) groundwater observation well; and (d) HOBO data logger.

Soil samples were collected using a corer with a 100 cm<sup>3</sup> volume sample ring at 0.10, 0.20, 0.40, 0.60 and 1.00 m depths near the sensor probe below the ground surface in the experimental field. First, the oven-drying method was used to verify the accuracy of the soil water content measured by the sensor. The results indicated that the value measured by the sensor was systematically higher than by the oven-drying method. The range of calibrated soil water content was further determined by the membrane pressure gauge method. The soil water content at a pressure of 0 kPa and 30 kPa was determined as the saturated value (maximum) and the field capacity (minimum), respectively. The rest of the soil water content data were calibrated in proportion. Pan evaporation measured by the evaporation gauge (255-100 Novalynx Analog Output Evaporation Gauge, Campbell Scientific, Inc., Logan, UT, USA) was used to calculate potential evapotranspiration. The physical properties and grain composition of soil samples at 10, 20, 40, 60 and 100 cm depths in the north, center and south of the experimental field were measured by certified professionals. Some of the results are shown in Table 1, which can presumably reflect the spatial heterogeneity of soil.

**Table 1.** Physical properties and grain composition of soil samples at different depths in the north, center and south of the experimental field.

Soil Sample at Different Depths	Unit Weight (g/cm <sup>3</sup> )	Saturated Hydraulic Conductivity (10 <sup>-4</sup> cm/s)	Grain Composition (Particle Diameter)		
			<0.002 (%)	0.002–0.05 (%)	>0.05 (%)
N10 cm	1.24	7.44	29.87	57.07	13.07
N20 cm	1.13	13.08	27.20	60.80	12.00
N40 cm	1.44	17.71	27.73	65.07	7.20
N60 cm	1.43	23.60	33.60	59.73	6.67
N100 cm	1.48	5.24	42.13	52.80	5.07
C10 cm	1.12	21.98	30.40	58.67	10.93
C20 cm	1.35	2.49	29.87	61.87	8.27
C40 cm	1.50	8.89	28.80	61.33	9.87
C60 cm	1.47	14.98	33.60	61.33	5.07
C100 cm	1.43	7.10	39.47	56.53	4.00
S10 cm	1.24	31.11	32.00	54.40	13.60
S20 cm	1.21	22.14	30.40	60.27	9.33
S40 cm	1.46	8.05	31.47	63.47	5.07
S60 cm	1.47	9.27	32.00	62.40	5.60
S100 cm	1.48	1.23	40.53	53.33	6.13

2.2. Mathematic Model and Parameters

2.2.1. Equations of Saturated-Unsaturated Soil Water Flow

Water moves from where the soil water potential is higher to where it is lower. The soil water potential in the unsaturated zone is constructed of gravitational potential and matric potential, while the saturated zone is composed of gravitational potential and pressure potential. Gravitational potential is expressed as the pressure head of vertical position, *z*; pressure potential shows as the positive pressure head, *h*; and matric potential is represented as the negative pressure head, *h*, based on the assumption of a 0 air pressure. Soil water potential,  $\psi$ , is expressed as pressure head, *h*.

The Darcy Buckingham equation [46] is substituted into the continuity equation based on the principle of mass conservation and the storage term is modified to construct saturated-unsaturated flow conditions, then the 3D Richards equation in partial differential form expressed by the pressure head *h* is as follows:

$$\frac{\partial}{\partial x} \left[ K_x(h) \frac{\partial h}{\partial x} \right] + \frac{\partial}{\partial y} \left[ K_y(h) \frac{\partial h}{\partial y} \right] + \frac{\partial}{\partial z} \left[ K_z(h) \left( \frac{\partial h}{\partial z} + 1 \right) \right] + W = \left[ S_f u_s + C(h) \right] \frac{\partial h}{\partial t} \tag{1}$$

where  $K_x(h)$ ,  $K_y(h)$  and  $K_z(h)$  are the hydraulic conductivities in the *x*, *y* and *z* directions, respectively; *h* is the pressure head (L); and *W* is a volumetric source or sink term (L<sup>3</sup>·L<sup>-3</sup>·T<sup>-1</sup>) including rainfall infiltration, evapotranspiration and so on. *C(h)* is the specific moisture capacity (L<sup>-1</sup>); *S<sub>f</sub>* is the saturation ratio (=θ/η); θ is the moisture content; η is the porosity; and *u<sub>s</sub>* is the specific storage (L<sup>-1</sup>). Equation (1) involving the saturated zone is called the modified Richards equation [47].

Hydraulic conductivity can be calculated from this empirical equation by the Van Genuchten [48] parametric functions:

$$K(h) = K_s \frac{\left[ 1 - \frac{|\alpha h|^{n-1}}{(1+|\alpha h|^n)^m} \right]^2}{(1+|\alpha h|^n)^{\frac{m}{2}}} \quad h < 0$$

$$K(h) = K_s \quad h \geq 0 \tag{2}$$

where *K<sub>s</sub>* is the saturated hydraulic conductivity; *h* is the pressure head; α and *n* are fitting parameters in the soil water retention curve; and *m* = 1 - 1/*n*, *n* > 1.

Paniconi et al. [49] modified van Genuchten and Nielsen’s [48] closed-form equation for hydraulic conductivity using the moisture retention curve. Thus, the specific moisture capacity *C(h)* can be calculated by:

$$C(h) = \frac{(n-1)(\theta_s - \theta_r)|h|^{m-1}}{|h_s|^n(1+\beta)^{m+1}} \quad h \leq h_0 \quad (3)$$

$$C(h) = 0 \quad h > h_0$$

where  $\theta_r$  is the residual water content;  $\theta_s$  is the saturated soil water content;  $\beta = (|h/h_s|)^n$ ;  $h_s$  is the air entry pressure head (L);  $n$  is a fitting parameter in the soil water retention curve;  $m = 1 - 1/n$ ; and  $h_0$  is a parameter solved on the basis of a given value of  $C(h) = u_s$ .

### 2.2.2. Rainfall Infiltration

Rainfall and evapotranspiration are treated as the volumetric source or sink term ( $W$ ) in the modified 3D Richards equation. The rainfall is going down and up is taken to be the positive direction for the  $z$ -axis, so the infiltration rate of the land surface is defined as  $I_{z2}$ . The value of  $I_{z2}$  is dependent on the magnitude relationship between rainfall intensity and infiltration capacity, which is equal to the smaller one. The volumetric source from rainfall can be calculated as follows:

$$W = I_{z2}\Delta x\Delta y \quad (4)$$

where  $\Delta x\Delta y$  is the area of the grid cell.

### 2.2.3. Potential Evapotranspiration

Evapotranspiration in this model is treated as a combination of transpiration and evaporation. Potential evapotranspiration (PET) can be calculated using two different options. The first option is the pan evaporation technique, which requires daily measured pan evaporation values and pan coefficients. In this method, PET is calculated as:

$$PET = C_{pan}E_{pan} \quad (5)$$

where  $C_{pan}$  is the pan coefficient, which is generally equal to approximately 0.7; and  $E_{pan}$  is the measured pan evaporation [50]. Actual evaporation ( $E_a$ ) is assumed to be equal to  $PET$  in the moist areas empirically and applied to the land surface as a negative flux boundary condition.

## 2.3. Boundary Conditions

In this model, variable boundary conditions are used to describe rainfall (infiltration) and evapotranspiration processes. The rainfall reaching the land surface is treated as a specified flux boundary condition. If the total head on the land surface is greater than the maximum ponding depth, this means that the infiltration capacity has been reached and the boundary condition is changed to a specified head boundary condition. Similarly, the evapotranspiration is applied to an outward flux boundary at the surface (i.e., a Neumann boundary) until water arrives at the top surface of the soil. Then, if the soil water content is reduced to a specified minimum water content, the boundary conditions are set to a prescribed minimum pressure (i.e., a Dirichlet boundary), which infrequently occurs considering the climate characteristics in this region. The maximum potential evapotranspiration is first calculated [22].

The boundary condition at the bottom was specified as a free drainage condition and the water flux through the bottom was considered as an approximation of groundwater recharge due to the soil water contents in the deep (more than 100 cm) being relatively steady. The soil water pressure and pressure head at the water table at the beginning of each simulation period were used to characterize the initial condition. The soil water pressures can be calculated by the van Genuchten model with the soil water content measured by the soil water content sensor. The measured value of the pressure head at the water table is zero.

### 2.4. Model Calibration

Relative error (*RE*), root-mean squared error (*RMSE*) and the coefficient of correlation ( $R^2$ ) between the simulated and observed soil water content were calculated to evaluate the accuracy of the model [51,52]:

$$RE = \left| \frac{\sum_{i=1}^n S_i}{\sum_{i=1}^n O_i} - 1 \right| \tag{6}$$

$$RMSE = \sqrt{\frac{1}{n} \sum_{i=1}^n (S_i - O_i)^2} \tag{7}$$

where  $O_i$  is the observed;  $S_i$  the simulated soil water content and  $n$  is the sample size. The match between the model prediction and observation increased as the relative error and root-mean squared error decreased.

## 3. Results and Discussion

### 3.1. Data Set Analysis

Figure 3 presents several meteorological elements and volumetric soil water content observed at the experimental field during 2014. Rainfall was mostly concentrated between April and September, with the maximum appearing in July reaching about 100 mm a day. The evaporation had roughly same tendency as the daily mean temperature. The trend of soil water content of the topsoil at the depth of 10 cm resembled that of the daily mean temperature and rainfall [53]. It changed less than the daily mean temperature but had large fluctuations (the greatest variation was about 37%) with rainfall. The soil water content at five depths had similar varying tendency, while the fluctuation range became smaller and values gradually increased from a depth of 10 cm to 100 cm. Higher values of soil water content appeared between the depths of 60 cm and 100 cm, ranging from 0.44–0.563.

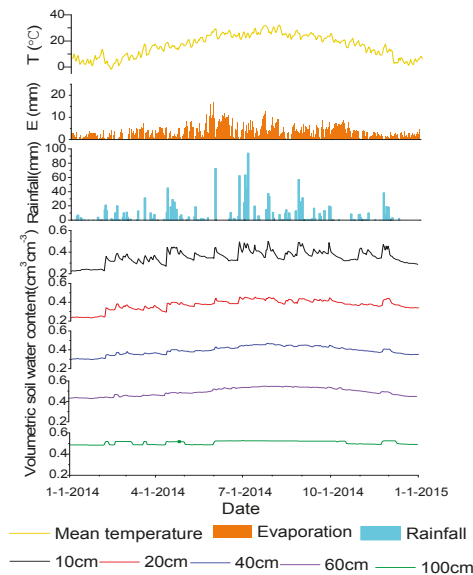


**Figure 3.** Daily mean temperature (°C), evaporation (mm), rainfall (mm) and volumetric soil water contents ( $\text{cm}^3 \cdot \text{cm}^{-3}$ ) at five depths of soil layers: 10, 20, 40, 60 and 100 cm at the experimental field, from 1 January 2014 to 31 December 2014.

### 3.1.1. Effect of Rainfall on the Soil Water Content

To investigate the impact of rainfall on soil water content at different depths, a representative rainfall event was selected to record the soil water content in a soil profile before, during and after it with a time step of one hour (Figure 4a). Before the rain, the soil water content first increases, then decreases with increasing soil depth, where the maximum was 0.458 at a depth of 60 cm. This difference may be caused by the combined effect of evapotranspiration, the supply of shallow groundwater and disparities in soil property at different depths. The increasing soil depth produced a mild drag on the increase of soil water content with the rainfall, which may be due to different field capacities. The soil water content of the topsoil increased greatly at a depth of less than 40 cm and the maximum increment at 0.2 appeared at a 10 cm depth. The soil water content at the depths of 60 cm and 100 cm were similarly always the maximum, while producing relative minimum increments of 0.03 with the rainfall. The soil water content at the depths of 10 cm and 20 cm stopped increasing and at 20 cm and 40 cm depths tended to be the same after the rainfall process.

In comparison, the decrease of soil water content is mainly caused by evapotranspiration without human activity. The pan evaporation measured in this experimental field was used to calculate potential evapotranspiration in the model. A 12-day evaporation period is shown in Figure 4b, which indicated that the soil water content decreased mostly at a depth of less than 20 cm, particularly in the topsoil at a 10 cm depth with the evaporation. The differences between Figure 4a,b suggested that the soil water content was more sensitive to rainfall than evapotranspiration and that the effects of rainfall could reach deeper soil layers. Therefore, soil water contents above the 20 cm depth are essentially controlled by rainfall and evapotranspiration [20] and those below the 40 cm depth are mainly controlled by rainfall and shallow groundwater in this field.

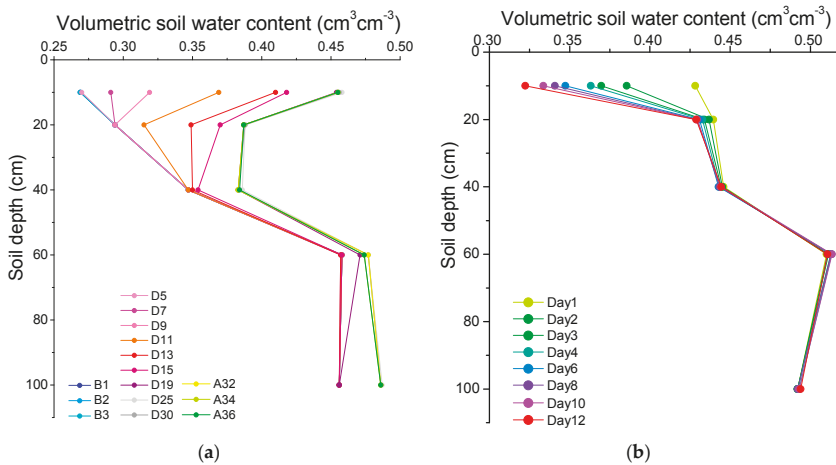


**Figure 4.** Soil water content at different depths of a soil profile: (a) during a rainfall event; and (b) during the 12-day evaporation period. Lines B1 to B3, D5 to D30 and A32 to A36 represent the soil water content before, during and after a rainfall event, respectively; the numbers represent the number of hours. Lines Day1 to Day12 show the soil water content from the first day to the twelfth day and the numbers represent the number of days.

### 3.1.2. Combined Effects of Rainfall and Water Table Depth on Soil Water Content

The experimental field where the study was conducted is a typical site in the Taihu Basin with a river network. Figure 5b–f show the variations in shallow groundwater table (depth: 0.237–1.491 m) and soil water contents ( $\theta$ : 0.266–0.563) at the depths of 10, 20, 40, 60 and 100 cm during different

rainfalls. The annual dynamic changes in Figure 5a presents a positive correlation between the water table depth and soil water content between depths from 10 cm and 60 cm. The soil water content increases with increasing soil depth when the shallow groundwater table falls and is at a relatively low level with no rainfall. However, when the water table starts to rise, the distribution rule begins to be broken due to the rainfall. The soil water content at a depth less than 10 cm can usually go beyond that at depths between 20 cm and 40 cm under rainfall, while the soil water content at depths of 60 cm and 100 cm ( $\theta$ : 0.44–0.563) are always much greater than the others ( $\theta$ : 0.266–0.492). Soil water content at a depth of 100 cm is relatively stable with values around 0.513 and its slight increase appears earlier than the rising of the water table. This indicates that the soil water and groundwater are mainly supplied by rainfall and the soil water content at the depths of more than 100 cm can obtain enough recharge from the groundwater [54] by capillary pressure to remain fairly constant when there is little or no rain. However, the soil water content at depths less than 60 cm can increase considerably and quickly with rainfall and decrease gradually with evaporation as it is too far relatively to receive enough groundwater recharge.

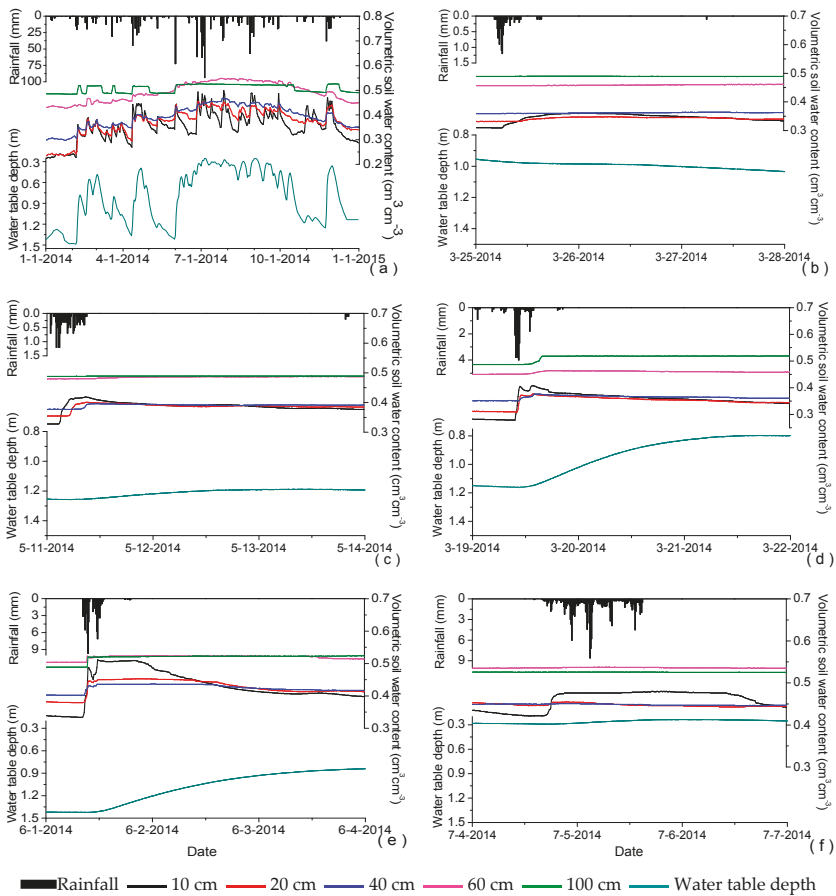


**Figure 5.** Rainfall conditions: (a) Shallow water table and soil water contents at 0.10, 0.20, 0.40, 0.60 and 1.00 m soil depths during 2014; (b–f) changes under five different rainfall conditions.

Furthermore, the soil water content at a depth of 100 cm decreases when the water table falls to where it is still above the depth of 1 m. This may be due to the falling water table decreasing the pressure on the residual gas in the soil pore, so that the volume of gas becomes relatively greater and the soil water content decreases. Similarly, the special stage where soil water content at a depth of 60 cm exceeds that at a depth of 100 cm occurs when the shallow groundwater table is above a depth of 60 cm for a fairly long period of time. This may be caused by the difference of soil properties [55] at the two depths and the rising water table above a depth of 60 cm increases the pressure on the gas in the soil pore at a depth of 60 cm, which makes the volume of gas relatively smaller and the soil water content greater.

The rainfall conditions and details of shallow groundwater table for Figure 5b–f are given in Table 2. When the rainfall was as small as 9.3 mm (Figure 5b), only the soil water content at depths of 10 cm and 20 cm increased by 0.051 (16.5%) and 0.017 (5.1%), respectively. Instead of rising after the rain, the shallow groundwater table fell by 0.079 m (8.3%). This was because the long period of rainfall before had allowed the water table to rise significantly and then began to fall with evaporation, despite this small rain. At the same time, the soil water content of the deep layers remained relatively stable for capillary rise [56,57]. When the rainfall increased to 17.5 mm (Figure 5c) and 30.8 mm (Figure 5d), the water table rose by 0.065 m (5.2%) and 0.360 m (31.0%), respectively. This difference was caused by a relatively high-intensity rainfall and a low initial water table for the latter. During these two rainfall events, the soil water content at depths of 10, 20 and 40 cm all increased and the increment decreased with the increase of depth, which ranged from 0.091–0.019 (27.7–5.0%) for the former and 0.129–0.025 (46.2–7.1%) for the latter. The difference was that, in the former case, the value of the soil water content at a depth of 60 cm approached that of a depth of 100 cm and remained increasing, while in the latter case, the soil water content at a depth of 100 cm was 0.06 greater and increased much more than that at a depth of 60 cm. This indicates that only when the rainfall intensity is high enough can the soil water content at depths of more than 100 cm increase remarkably or quickly. Additionally, the soil water content at a depth of 60 cm in May was generally greater than that in March, which suggested that evaporation was less able to influence the deep soil layer with the onset of the rainy season and intermittent rains could make the soil water content at depths less than 60 cm change with the seasons [20,53], forming an annual cycle similar to a cosine curve (Figure 5a). However, soil water content and shallow groundwater table tend to be steady values when the rainfall was more intense or heavier. Figure 5e,f show that under rainfalls of 72.3 mm and 138.6 mm, respectively, the rainfall intensity of the former was nearly three times higher than the latter. The soil water content at a depth of 10 cm increased 0.118 more under conditions of higher intensity than a larger amount of rainfall. Although the soil water content at the other depths in the former case all increased normally, only that at a depth of 20 cm increased by 2.7% in the case of the latter. Furthermore, the water table rose by only 0.056 m with the largest amount of rainfall in this study, which was only one tenth that of the former. The differences indicate that the shallow groundwater table is greatly controlled by rainfall and evaporation and the initial depth of the water table decides the sensitivity.

**Table 2.** Variation of shallow groundwater table under different rainfall conditions.

Figure 5	Rainfall Amount (mm)	Rainfall Intensity (mm/h)	Rainfall Duration (mm)	Water Table Depth 1 (m)	Water Table Depth 2 (m)	Water Table Variation (m)
(b)	9.3	1.47	6.33	0.955	1.034	−0.079
(c)	17.5	2.19	8.0	1.255	1.190	0.065
(d)	30.8	6.16	5.0	1.160	0.800	0.360
(e)	72.3	16.07	4.5	1.423	0.840	0.583
(f)	138.6	5.78	24.0	0.290	0.238	0.052

The maximum soil water content varied at different depths and the natural minimum of shallow groundwater table depth was around 0.2 m in the field. Soils were wetted to the degree of saturation from 26.6 to 56.3%. This was closely associated with the soil properties, soil hydraulic properties,

capillary action and hydrologic characteristics of the plain river network in this region [57–59]. Therefore, it was significant to calculate or calibrate the values of the hydraulic parameters for the five soil zones separately in the model. The ranges of several hydrological factors were accepted by experimental data analysis and provide reference for inputting the model parameters and validating the model.

The relationship between the soil water content ( $\theta$ ) and rainfall ( $P$ ) or water table depth ( $H$ ) were analyzed using the Pearson correlation analysis method [60] (Table 3). The soil water contents were positively correlated with rainfall in topsoil, while there was weak correlation between them below the depth of 20 cm as only topsoil water can be replenished when there is not much rainfall. However, the soil water contents were all negatively correlated with the shallow groundwater table to varying degrees and the correlation between the water table and soil water content was relatively strong in the deep soil layers, which was strongest at a depth of 100 cm. The results indicated that the soil water contents in the topsoil at depths between 10 cm and 20 cm were much more affected by meteorological factors than groundwater, while those below depths of 40 cm were related to the shallow groundwater table in the field. High values of soil water content were observed at the deeper soil layers and strong correlation between soil water content and the water table were found at a depth of around 100 cm. The capillary action is significant in this region and the height of this capillary rise can be quite substantial [56,57].

**Table 3.** Pearson correlation analysis between daily soil water content ( $\theta$ ) and rainfall ( $P$ ) or water table depth ( $H$ ) at different soil depths.

Soil Depths(cm)	Pearson Correlation Coefficient	
	$P-\theta$	$H-\theta$
10 cm	0.327	-0.680
20 cm	0.202	-0.785
40 cm	0.179	-0.811
60 cm	0.151	-0.759
100 cm	0.175	-0.925

### 3.2. Parameter Calibration and Model Validation

Based on the field observations and laboratory experiment results, the numerical model was calibrated to identify reasonable values of the parameters. The experimental field was divided into a  $98 \times 14 \times 200$  three-dimensional grid of cuboid cells with corresponding measured elevations. The time step-size used in the computation was one hour. Model calibration was based on the data obtained from 1 January to 30 June 2014 using the measured soil moisture contents at various depths (10 cm, 20 cm, 40 cm, 60 cm and 100 cm) as the initial condition. It was found that the change rule of soil water contents at different depths were various when simulating the soil water with observed data as the boundary conditions. Accordingly, each soil layer was independently given hydraulic parameters.

The parameters  $\theta_r$ ,  $\theta_s$ ,  $\alpha$ ,  $n$ ,  $K_s$  and  $l$  at the study site were finally identified by calibration and the results are shown in Table 4. To illustrate the performance of the model, comparisons between the simulated and observed values of the soil water content at five depths from 1 January to 30 June 2014 are shown in Figure 6. The agreement of the results is indicated by the relatively large values of  $R^2$  and the comparatively small values of RE and RMSE, which are listed in Figure 7 and Table 5.

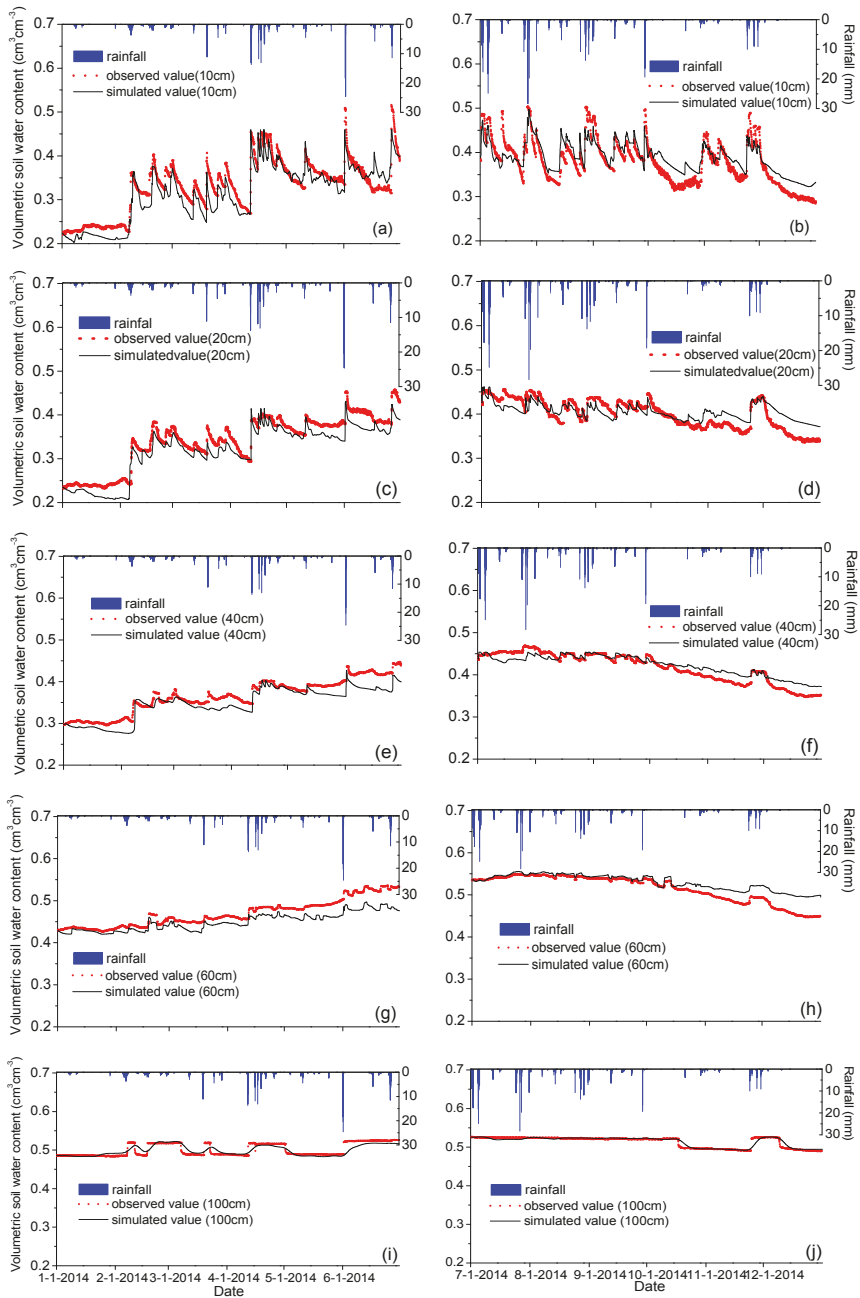


**Figure 6.** Simulated results (curves) versus observed (dots) soil water contents at different depths from 1 January 2014 to 30 June 2014 for calibration (a,c,e,g,i) and from 1 July 2014 to 31 December 2014 for validation (b,d,f,h,j). Daily rainfall measurements were also plotted.

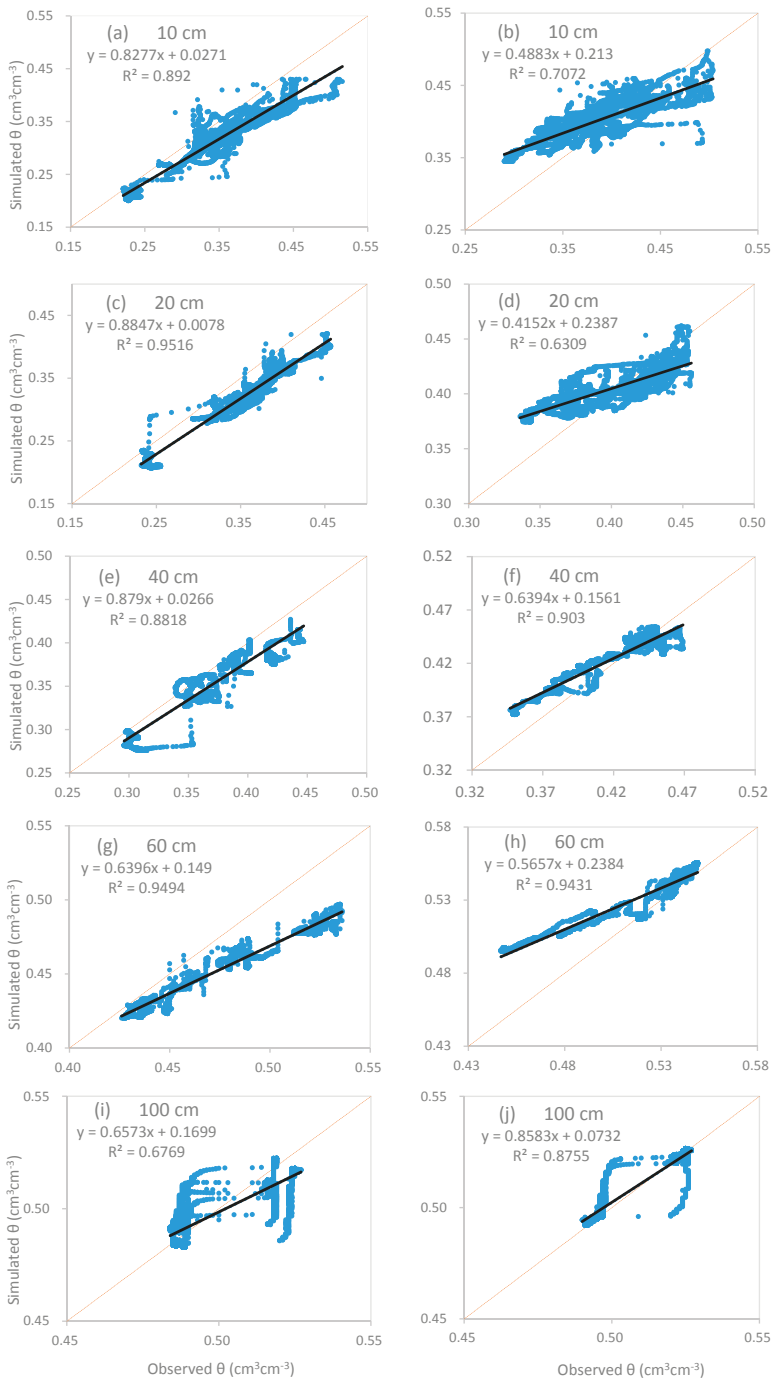


**Figure 7.** Correlation of simulated vs. observed volumetric soil water content ( $\theta$ ) at different depths. Results of the calibration (a,c,e,g,i) and validation (b,d,f,h,j) for the model are shown.

**Table 4.** Calibrated hydraulic parameters for the five soil zones in the model.

Depth	$\theta_r$	$\theta_s$	$\alpha$ (1/cm)	$n$	$K_s$ ( $10^{-4}$ cm/s)	$l$
0~15 cm	0.10	0.46	0.013	1.48	2.6	0.5
15~30 cm	0.10	0.42	0.0116	1.35	1.7	0.5
30~55 cm	0.10	0.42	0.009	1.38	0.8	0.5
55~80 cm	0.10	0.50	0.010	1.43	0.4	0.5
80~200 cm	0.10	0.49	0.010	1.42	0.5	0.5

**Table 5.** The root mean square error (*RMSE*), mean relative error (*RE*) and coefficient of correlation ( $R^2$ ) between the simulated and observed soil water contents.

	Soil Depths (cm)	Volumetric Soil Water Content		
		<i>RMSE</i> ( $\text{cm}^3 \cdot \text{cm}^{-3}$ )	<i>RE</i> (%)	$R^2$
Model calibration	10	0.0363	9.03	0.8920
	20	0.0343	9.25	0.9516
	40	0.0225	4.84	0.8818
	60	0.0239	4.34	0.9494
	100	0.0094	0.35	0.6769
Model validation	10	0.0348	5.13	0.7072
	20	0.0216	1.09	0.6309
	40	0.0152	1.28	0.9030
	60	0.0198	2.87	0.9431
	100	0.0047	0.08	0.8755

The model provided good simulations of hourly soil water content compared to the hourly soil water sensor measurements with relatively small *RMSE* values that were less than 0.05 and comparatively large  $R^2$  values of more than 0.6. The values of *RE* at depths less than 20 cm were over 9%, which were much bigger than those below a 40 cm depth. These discrepancies may be related to uncertainties in the estimation of potential evapotranspiration, which was calculated using pan evaporation data measured out of the experimental field. Additionally, the runoff and discharge in the field deserve further investigation to improve the simulation results [61].

The observed soil water contents increased and decreased more slowly than the simulated values after most rainfall events in the upper layers of soil, while a contrary relationship appeared in the deeper soil layers. A tendency of overall increasing of soil water contents from winter to summer was more obvious in the measurements than simulation. These may be caused by the shallow groundwater table in the field being connected to the water table of the whole plain. Many influential factors can make the shallow groundwater table change out of the control of the direct atmospheric boundary such as irrigations for huge regions of farmland and irregular precipitation in space and time [20,53].

The previously calibrated model was further validated based on the observation data from 1 July to 31 December 2014, using the measured soil volumetric water contents of different soil layers at depths of 10 cm, 20 cm, 40 cm, 60 cm and 100 cm to construct the initial condition. Results are shown in Figure 6. On the whole, the simulated results were close to the observations, especially for the soil water contents in deep soil. The average *RMSE* and *RE* values of the soil water content at the five depths were  $0.0192 \text{ cm}^3 \cdot \text{cm}^{-3}$  and 2.09%, respectively. The coefficient of correlation ( $R^2 = 0.8119$ ) showed an acceptable correlation between the measured and simulated hourly soil water contents. As indicated in Figure 6, the modeling simulation slightly overestimated the soil water contents at soil depths less than 100 cm, which was the opposite of calibration results. This difference may be caused by the seasonal changes as the observations from summer to winter had the opposite tendency of those from winter to summer, being affected by seasonal variations of several meteorological elements. Moreover, the shallow groundwater table in the study site is controlled by the water table of the whole area and is influenced by anthropogenic recharge and discharge and the temporal and spatial

variations of rainfall. Therefore, further investigation will take the problems of a series of uncertain factors and scale in consideration to illustrate the changes in soil water content and improve the model [62–64].

#### 4. Conclusions

Soil water is a determinant part in the interaction between surface water and groundwater, both of which are important for crop growth and for farm planning decisions. Furthermore, it affects flood risk mitigation and increases in productivity.

In the present study, to research the temporal and vertical change rule of soil water contents as a typical example for delta plains, two approaches were combined: First, a special experimental field was set up in a delta plain and targeted observations for soil water content were conducted where a series of analyses of soil water content data indicated that soils in this field were wetted to the degree of saturation from 26.6–56.3% and the maximum soil water contents varied at different depths. The capillary action was significant in this region and the height of this capillary rise could be quite substantial and the soil water contents at depths of more than 100 cm could obtain enough recharge from the groundwater to remain fairly constant. Second, a simplified 3D soil water numerical model, especially for delta plains was built, which treated the complete subsurface space as a unified whole and the soil water in the unsaturated zone was integrated with the saturated flow. The simulation results were close to the field observations and followed short-term responses to hydrological events, although the longer-term seasonal trend needed to be improved. The results indicated that the model could be used to calculate soil water content in three dimensions based on the given rainfall data, especially for where the capillary rise of the soil is significant. Temporal and spatial expansion should be the orientation of future research activities. The model should be further improved for long-term simulation suitability and be applied in basin scale.

**Acknowledgments:** This research is supported by the National Key R&D Programme of China (2016YFA0601000), the Postgraduate Research & Practice Innovation Program of Jiangsu Province (KYCX17\_0411), the state major project of water pollution control and management (2014ZX07101-011), the Fundamental Research Funds for the Central Universities (2017B608X14 and 2017B05814) and Jiangsu water conservancy science and technology project (SLT-KY-2015007). We also wish to thank the students who contributed to the field work including Shipeng Du, Liguo Zhu and Jingbo Chen.

**Author Contributions:** The field work was conducted by Wenjuan Hua, Chuanhai Wang, Hai Yang and Yue Zhai; the paper was written by Wenjuan Hua; Chuanhai Wang and Gang Chen reviewed and improved the manuscript with comments; and the data compilation and statistical analyses were completed by all authors.

**Conflicts of Interest:** The authors declare no conflict of interest.

#### References

1. Brauer, C.C.; Teuling, A.J.; Torfs, P.J.J.F.; Uijlenhoet, R. The wageningen lowland runoff simulator (walrus): A lumped rainfall-runoff model for catchments with shallow groundwater. *Geosci. Model Dev.* **2014**, *7*, 2313–2332. [[CrossRef](#)]
2. Yan, R.; Gao, J.; Dong, C.; Huang, J. Assessment of ecosystem services for polder terrestrial ecosystem in the Taihu Basin. *Res. Environ. Sci.* **2015**, *28*, 393–400.
3. Wandee, P. Optimization of Water Management in Polder Areas: Some Examples for the Temperate Humid and the Humid Tropical Zone. Ph.D. Thesis, Wageningen University, Wageningen, The Netherlands, 2005.
4. Koch, S.; Bauwe, A.; Lennartz, B. Application of the swat model for a tile-drained lowland catchment in north-eastern Germany on subbasin scale. *Water Resour. Manag.* **2013**, *27*, 791–805. [[CrossRef](#)]
5. Northcott, W.J.; Cooke, R.A.; Walker, S.E.; Mitchell, J.K.; Hirschi, M.C. Modeling flow on tile-drained watershed using a GIS-integrated DRAINMOD. *Trans. ASAE* **2002**, *45*, 1405–1423. [[CrossRef](#)]
6. Vereecken, H.; Huisman, J.A.; Pachepsky, Y.; Montzka, C.; Kruk, J.V.D.; Bogaen, H.; Weihermüllera, M.; Herbsta, M.; Martinezb, G.; Vanderborghta, J.; et al. On the spatio-temporal dynamics of soil moisture at the field scale. *J. Hydrol.* **2014**, *516*, 76–96. [[CrossRef](#)]

7. Cornelissen, T.; Diekkrüger, B.; Bogena, H.R. Significance of scale and lower boundary condition in the 3D simulation of hydrological processes and soil moisture variability in a forested headwater catchment. *J. Hydrol.* **2014**, *516*, 140–153. [[CrossRef](#)]
8. Romano, N. Soil moisture at local scale: Measurements and simulations. *J. Hydrol.* **2014**, *516*, 6–20. [[CrossRef](#)]
9. Servadio, P. Applications of empirical methods in central Italy for predicting field wheeled and tracked vehicle performance. *Soil Tillage Res.* **2010**, *110*, 236–242. [[CrossRef](#)]
10. Servadio, P.; Bergonzoli, S.; Beni, C. Soil tillage systems and wheat yield under climate change scenarios. *Agronomy* **2016**, *6*, 43. [[CrossRef](#)]
11. Western, A.W.; Zhou, S.L.; Grayson, R.B.; McMahon, T.A.; Blöschl, G.; Wilson, D.J. Spatial correlation of soil moisture in small catchments and its relationship to dominant spatial hydrological processes. *J. Hydrol.* **2004**, *286*, 113–134. [[CrossRef](#)]
12. Schwärzel, K.; Menzer, A.; Clausnitzer, F.; Spank, U.; Häntzschel, J.; Grünwald, T.; Köstner, B.; Bernhofer, C.; Feger, K.H. Soil water content measurements deliver reliable estimates of water fluxes: A comparative study in a beech and a spruce stand in the Tharandt forest (Saxony, Germany). *Agric. For. Meteorol.* **2009**, *149*, 1994–2006. [[CrossRef](#)]
13. Schume, H.; Jost, G.; Hager, H. Soil water depletion and recharge patterns in mixed and pure forest stands of European beech and Norway spruce. *J. Hydrol.* **2004**, *289*, 258–274. [[CrossRef](#)]
14. Jost, G.; Schume, H.; Hager, H. Factors controlling soil water-recharge in a mixed European beech (*Fagus sylvatica* L.)–Norway spruce [*Picea abies* (L.) Karst.] stand. *Eur. J. For. Res.* **2004**, *123*, 93–104. [[CrossRef](#)]
15. Grayson, R.B.; Western, A.W.; Chiew, F.H.S.; Böschl, G. Preferred states in spatial soil moisture patterns: Local and nonlocal controls. *Water Resour. Res.* **1997**, *33*, 2897–2908. [[CrossRef](#)]
16. Vereecken, H.; Kamaï, T.; Harter, T.; Kasteel, R.; Hopmans, J.; Vanderborght, J. Explaining soil moisture variability as a function of mean soil moisture: A stochastic unsaturated flow perspective. *Geophys. Res. Lett.* **2007**, *34*, 315–324. [[CrossRef](#)]
17. Beni, C.; Servadio, P.; Marconi, S.; Neri, U.; Aromolo, R.; Diana, G. Anaerobic digestate administration: Effect on soil physical and mechanical behavior. *Commun. Soil Sci. Plant Anal.* **2012**, *43*, 821–834. [[CrossRef](#)]
18. Pan, F.; Peters-Lidard, C.D. On the relationship between mean and variance of soil moisture fields. *J. Am. Water Resour. Assoc.* **2008**, *44*, 235–242. [[CrossRef](#)]
19. Ivanov, V.Y.; Fatichi, S.; Jenerette, G.D.; Espeleta, J.F.; Troch, P.A.; Huxman, T.E. Hysteresis of soil moisture spatial heterogeneity and the “homogenizing” effect of vegetation. *Water Resour. Res.* **2010**, *46*. [[CrossRef](#)]
20. Rosenbaum, U.; Bogena, H.R.; Herbst, M.; Huisman, J.A.; Peterson, T.J.; Weuthen, A.; Western, A.W.; Vereecken, H. Seasonal and event dynamics of spatial soil moisture patterns at the small catchment scale. *Water Resour. Res.* **2012**, *48*, 3472–3476. [[CrossRef](#)]
21. Servadio, P.; Bergonzoli, S.; Verotti, M. Delineation of management zones based on soil mechanical-chemical properties to apply variable rates of inputs throughout a field (VRA). *Eng. Agric. Environ. Food* **2017**, *10*, 20–30. [[CrossRef](#)]
22. Motz, L.H.; Dogan, A. Saturated-unsaturated 3D Groundwater Model. I: Development. *J. Hydrol. Eng.* **2005**, *10*, 492–504.
23. Fares, A.; Temimi, M.; Morgan, K.; Kelleners, T.J. In-situ and remote soil moisture sensing technologies for vadose zone hydrology. *Vadose Zone J.* **2013**, *12*, 332–338. [[CrossRef](#)]
24. Robinson, D.A.; Binley, A.; Crook, N.; Day-Lewis, F.D.; Ferré, T.P.A.; Grauch, V.J.S.; Knight, R.; Knoll, M.; Lakshmi, V.; Miller, R.; et al. Advancing process-based watershed hydrological research using near-surface geophysics: A vision for and review of, electrical and magnetic geophysical methods. *Hydrol. Process.* **2008**, *22*, 3604–3635. [[CrossRef](#)]
25. Robinson, D.A.; Campbell, C.S.; Hopmans, J.W.; Hornbuckle, B.K.; Jones, S.B.; Knight, R.; Ogden, F.; Selker, J.; Wendroth, O. Soil moisture measurement for ecological and hydrological watershed-scale observatories: A review. *Vadose Zone J.* **2008**, *7*, 358–389. [[CrossRef](#)]
26. Vereecken, H.; Huisman, J.A.; Bogena, H.; Vanderborght, J.; Vrugt, J.A.; Hopmans, J.W. On the value of soil moisture measurements in vadose zone hydrology: A review. *Water Resour. Res.* **2008**, *44*, 253–270. [[CrossRef](#)]
27. Seneviratne, S.I.; Corti, T.; Davin, E.L.; Hirschi, M.; Jaeger, E.B.; Lehner, I.; Orlowsky, B.; Teuling, A.J. Investigating soil moisture–climate interactions in a changing climate: A review. *Earth Sci. Rev.* **2010**, *99*, 125–161. [[CrossRef](#)]

28. Zhu, Q.; Liao, K.; Xu, Y.; Yang, G.; Wu, S.; Zhou, S. Monitoring and prediction of soil moisture spatial-temporal variations from a hydropedological perspective: A review. *Soil Res.* **2012**, *50*, 625–637. [[CrossRef](#)]
29. Topp, G.C.; Davis, J.L.; Annan, A.P. Electromagnetic determination of soil water content: Measurements in coaxial transmission lines. *Water Resour. Res.* **1980**, *16*, 574–582. [[CrossRef](#)]
30. Simunek, J.; Sejna, M.; van Genuchten, M.T. The HYDRUS-1D software package for simulating the one-dimensional movement of water, heat and multiple solutes in variably-saturated media. In *Version 4.0. HYDRUS*; University of California Riverside: Riverside, CA, USA, 2008.
31. Šimunek, J.; Genuchten, M.T.V.; Šejna, M. Recent developments and applications of the HYDRUS computer software packages. *Vadose Zone J.* **2016**, *6*. [[CrossRef](#)]
32. Dash, C.J.; Sarangi, A.; Singh, D.K.; Singh, A.K.; Adhikary, P.P. Prediction of root zone water and nitrogen balance in an irrigated rice field using a simulation model. *Paddy Water Environ.* **2015**, *13*, 281–290. [[CrossRef](#)]
33. Garg, K.K.; Das, B.S.; Safeeq, M.; Bhadoria, P.B.S. Measurement and modeling of soil water regime in a lowland paddy field showing preferential transport. *Agric. Water Manag.* **2009**, *96*, 1705–1714. [[CrossRef](#)]
34. Sander, T.; Gerke, H. Modelling field-data of preferential flow in paddy soil induced by earthworm burrows. *J. Contam. Hydrol.* **2009**, *104*, 126–136. [[CrossRef](#)] [[PubMed](#)]
35. Tan, X.; Shao, D.; Liu, H. Simulating soil water regime in lowland paddy fields under different water managements using HYDRUS-1D. *Agric. Water Manag.* **2014**, *132*, 69–78. [[CrossRef](#)]
36. Rühle, F.A.; Klier, C.; Stumpp, C. Changes in water flow and solute transport pathways during long-term column experiments. *Vadose Zone J.* **2013**, *12*, 918–924. [[CrossRef](#)]
37. Rühle, F.A.; Netzer, F.V.; Lueders, T.; Stumpp, C. Response of transport parameters and sediment microbiota to water table fluctuations in laboratory columns. *Vadose Zone J.* **2015**, *10*, 1623–1636. [[CrossRef](#)]
38. Yakirevich, A.; Gish, T.J.; Imunek, J.; Genuchten, M.T.V.; Pachepsky, Y.A.; Nicholson, T.J.; Cady, R.E. Potential impact of a seepage face on solute transport to a pumping well. *Vadose Zone J.* **2010**, *9*, 686–698. [[CrossRef](#)]
39. Pachepsky, Y.A.; Guber, A.K.; Yakirevich, A.M.; Mckee, L.; Cady, R.E.; Nicholson, T.J. Scaling and pedotransfer in numerical simulations of flow and transport in soils. *Vadose Zone J.* **2014**, *13*. [[CrossRef](#)]
40. Šimunek, J.; Van Genuchten, M.T.; Šejna, M. HYDRUS: Model use, calibration and validation. *Trans. ASABE* **2012**, *55*, 1561–1574.
41. Morbidelli, R.; Saltalippi, C.; Flammini, A.; Rossi, E.; Corradini, C. Soil water content vertical profiles under natural conditions: Matching of experiments and simulations by a conceptual model. *Hydrol. Process.* **2013**, *28*, 4732–4742. [[CrossRef](#)]
42. Sophocleous, M.A.; Koelliker, J.K.; Govindaraju, R.S.; Birdie, T.; Ramireddygar, S.R.; Perkins, S.P. Integrated numerical modeling for basin-wide water management: The case of the rattlesnake creek basin in south-central Kansas. *J. Hydrol.* **1999**, *214*, 179–196. [[CrossRef](#)]
43. Zhang, B.; Lerner, D.N. Modeling of ground water flow to adits. *Groundwater* **2010**, *38*, 99–105. [[CrossRef](#)]
44. Labolle, E.M.; Ahmed, A.A.; Fogg, G.E. Review of the integrated groundwater and surface-water model (IGSM). *Groundwater* **2003**, *41*, 238–246. [[CrossRef](#)]
45. Demetriou, C.; Punthakey, J.F. Evaluating sustainable groundwater management options using the mike she integrated hydrogeological modelling package. *Environ. Model. Softw.* **1998**, *14*, 129–140. [[CrossRef](#)]
46. Narasimhan, T.N. Something to think about . . . Darcy-Buckingham’s law. *Groundwater* **1998**, *36*, 194–195. [[CrossRef](#)]
47. Celia, M.A.; Bouloutas, E.T.; Zarba, R.L. A general mass-conservative numerical solution for the unsaturated flow equation. *Water Resour. Res.* **1990**, *26*, 1483–1496. [[CrossRef](#)]
48. Genuchten, M.T.V.; Nielsen, D.R. On describing and predicting the hydraulic properties of unsaturated soil. *Ann. Geophys.* **1985**, *3*, 615–628.
49. Paniconi, C.; Aldama, A.A.; Wood, E.F. Numerical evaluation of iterative and noniterative methods for the solution of the nonlinear Richards equation. *Water Resour. Res.* **1991**, *27*, 1147–1163. [[CrossRef](#)]
50. Fares, A. Environmental Impact of Unharvested Forest Buffer Zones upon Cypress-Pond System in Coastal Plains Regions: Modeling Analyses. Ph.D. Thesis, University of Florida, Gainesville, FL, USA, 1996.
51. Hou, L.; Wang, X.S.; Hu, B.X.; Shang, J.; Wan, L. Experimental and numerical investigations of soil water balance at the hinterland of the Badain Jaran Desert for groundwater recharge estimation. *J. Hydrol.* **2016**, *540*, 386–396. [[CrossRef](#)]

52. Schwen, A.; Bodner, G.; Loiskandl, W. Time-variable soil hydraulic properties in near-surface soil water simulations for different tillage methods. *Agric. Water Manag.* **2011**, *99*, 42–50. [[CrossRef](#)]
53. Geris, J.; Tetzlaff, D.; McDonnell, J.J.; Soulsby, C. Spatial and temporal patterns of soil water storage and vegetation water use in humid northern catchments. *Sci. Total Environ.* **2017**, *595*, 486–493. [[CrossRef](#)] [[PubMed](#)]
54. Schindler, U.; Müller, L.; Behrendt, A. Field investigations of soil hydrological properties of fen soils in North-East Germany. *J. Plant Nutr. Soil Sci.* **2003**, *166*, 364–369. [[CrossRef](#)]
55. García, G.M.; Pachepsky, Y.A.; Vereecken, H. Effect of soil hydraulic properties on the relationship between the spatial mean and variability of soil moisture. *J. Hydrol.* **2014**, *516*, 154–160. [[CrossRef](#)]
56. Wang, N.Q.; Wang, Q.T.; Liu, X.L.; Pang, Q. Prediction study of capillary rise height on unsaturated soil. *Adv. Mater. Res.* **2013**, *860–863*, 1260–1264. [[CrossRef](#)]
57. Al-Samahiji, D.; Houston, S.; Houston, W. Degree and extent of wetting due to capillary rise in soils. *Transp. Res. Rec.* **2000**, *1709*, 114–120. [[CrossRef](#)]
58. Amer, A.M. Water flow and conductivity into capillary and non-capillary pores of soils. *J. Soil Sci. Plant Nutr.* **2012**, *12*, 99–112. [[CrossRef](#)]
59. Huza, J.; Teuling, A.J.; Braud, I.; Grazioli, J.; Melsen, L.A.; Nord, G.; Raupach, T.H.; Uijlenhoet, R. Precipitation, soil moisture and runoff variability in a small river catchment (Ardèche, France) during hymex special observation period 1. *J. Hydrol.* **2014**, *516*, 330–342. [[CrossRef](#)]
60. Lin, G.; Wang, T.; Zheng, X. Assessing effects of soil hydraulic properties on the temporal stability of absolute soil moisture content and soil moisture anomaly under different climatic conditions. *Environ. Earth Sci.* **2016**, *75*, 143. [[CrossRef](#)]
61. Brocca, L.; Ciabatta, L.; Massari, C.; Camici, S.; Tarpanelli, A. Soil moisture for hydrological applications: Open questions and new opportunities. *Water* **2017**, *9*, 140. [[CrossRef](#)]
62. Dogan, A.; Motz, L.H. Saturated-unsaturated 3D groundwater model. II: Verification and application. *J. Hydrol. Eng.* **2005**, *10*, 505–515. [[CrossRef](#)]
63. Porporato, A.; Daly, E.; Rodrigueziturbe, I. Soil water balance and ecosystem response to climate change. *Am. Nat.* **2004**, *164*, 625–632. [[CrossRef](#)] [[PubMed](#)]
64. Ojha, R.; Morbidelli, R.; Saltalippi, C.; Flammini, A.; Rao, S.G. Scaling of surface soil moisture over heterogeneous fields subjected to a single rainfall event. *J. Hydrol.* **2014**, *516*, 21–36. [[CrossRef](#)]



© 2017 by the authors. Licensee MDPI, Basel, Switzerland. This article is an open access article distributed under the terms and conditions of the Creative Commons Attribution (CC BY) license (<http://creativecommons.org/licenses/by/4.0/>).

Review

# Crop Upgrading Strategies and Modelling for Rainfed Cereals in a Semi-Arid Climate—A Review

Festo Richard Silungwe<sup>1,2,\*</sup>, Frieder Graef<sup>1</sup>, Sonoko Dorothea Bellingrath-Kimura<sup>1,2</sup>, Siza Donald Tumbo<sup>3</sup>, Frederick Cassian Kahimba<sup>3</sup> and Marcos Alberto Lana<sup>1,4</sup>

<sup>1</sup> Leibniz Center for Agricultural Landscape Research (ZALF), Institute of Land Use Systems, Eberswalder Straße, 84, 15374 Müncheberg, Germany; graef@zalf.de (F.G.); belks@zalf.de (S.D.B.-K.); marcos.lana@zalf.de (M.A.L.)

<sup>2</sup> Faculty of Life Sciences, Humboldt Universität zu Berlin, Unter den Linden 6, 10099 Berlin, Germany

<sup>3</sup> Department of Engineering Sciences and Technology, Sokoine University of Agriculture, P.O. Box 3003, CHUO KIKUU, Morogoro 3003, Tanzania; siza.tumbo@gmail.com (S.D.T.); fredkahimba@suanent.ac.tz (F.C.K.)

<sup>4</sup> Crop. Production Ecology, Swedish University of Agricultural Sciences, Ulls väg 16, 75007 Uppsala, Sweden

\* Correspondence: festo.richard@zalf.de; Tel.: +49-157-8482-5561

Received: 30 November 2017; Accepted: 16 March 2018; Published: 22 March 2018

**Abstract:** Spatiotemporal rainfall variability and low soil fertility are the primary crop production challenges facing poor farmers in semi-arid environments. However, there are few solutions for addressing these challenges. The literature provides several crop upgrading strategies (UPS) for improving crop yields, and biophysical models are used to simulate these strategies. However, the suitability of UPS is limited by systemization of their areas of application and the need to cope with the challenges faced by poor farmers. In this study, we reviewed 187 papers from peer-reviewed journals, conferences and reports that discuss UPS suitable for cereals and biophysical models used to assist in the selection of UPS in semi-arid areas. We found that four UPS were the most suitable, namely tied ridges, microdose fertilization, varying sowing dates, and field scattering. The DSSAT, APSIM and AquaCrop models adequately simulate these UPS. This work provides a systemization of crop UPS and models in semi-arid areas that can be applied by scientists and planners.

**Keywords:** The Agricultural Production Systems sIMulator (APSIM) software; AquaCrop; cereals; DSSAT; field scattering; food security; microdose fertilization; rainfall variability; tied ridges; upgrading strategies

## 1. Introduction

Food security refers to physical and economic access to sufficient, safe, and nutritious food that meets people's dietary requirements and food preferences for an active and healthy life [1,2]. Despite efforts from 1990 to 2012 to reduce the number of people suffering from hunger, the hungry population in Sub-Saharan African (SSA) countries was reduced by only 5%. Millions of people in this region are still not able to meet food demand for their families due to land degradation, land use pressures, and climate change [3]. Other causes include population growth, poverty, weak institutions and infrastructure, high dependency on rainfed agriculture, unequal global trade relationships, and poor soil fertility [4–6]. There are also constraints related to the production value chain in general, food access [5,7] due to geographical locations and associated eating behaviors [8], socio-economic status [9], technology adoption [10,11], and sustainable production [12–14].

A total of 57% of the population in East African countries (Tanzania, Kenya, Uganda, Rwanda and Burundi) experienced food insecurity during 2015–2016, which is only a slight decrease from 59% during 1990–1992 [15]. The future status of food security of East African countries requires an

integrated, long-term hunger mitigation plan to protect vulnerable households. The plan should involve governments in collaboration with civil society and international partners [16]. The responses may include the introduction of new technologies, extension of local expertise, and active involvement of the vulnerable households and communities suffering from hunger [16]. A previous study in Ethiopia emphasized the importance of investing in agricultural research of major staple foods to improve food security [11]. Kassie et al. [17] suggested the importance of formulating policies that target sustainable agricultural practices. These efforts can stimulate the adoption of crop upgrading strategies [18] and, thus, improve crop production and food security. Actually, enhancing agricultural production has improved food security and resulted in greater yields for many agricultural products since 2000 in Nigeria, Uganda, Tanzania and Kenya [19].

Food security upgrading strategies (UPS) can be defined as a set of good practices to secure food across local to regional food value chains [20]. They are designed to raise the sustainability of agricultural production of crops under rainfed conditions in semi-arid areas. Normally, UPS are adapted to a particular location depending on the local conditions of the soil, weather, culture, and socio-economic status. The UPS that enhance crop production include farm water ponds [21,22], irrigation [23,24], mulching [25,26], tied ridges [27,28], field scattering and shifting of planting/sowing dates [29,30]. While UPS are useful in enhancing agricultural production in general; their impacts are more visible for poor smallholder farmers who have a limited capacity to obtain the inputs for their farms such as irrigation and soil nutrients. The process of designing the UPS and testing them for adoption in different environments is the first step of a continuous process involving the creation and diffusion of new knowledge. There is a strong negative relationship between the number of food-deficient households and innovations in their farming practices [31], meaning that the households with the lowest food security are the ones adopting the fewest UPS. Encouraging farmers to use affordable UPS is vital for increasing harvests and reducing hunger in general. However, there is limited understanding of the roles that different UPS can play in securing harvests for farms that are limited by high rainfall variability and poor soil nutrients. Modelling approaches can provide such understanding, leading to recommendations for the implementation of UPS in different areas.

To understand crop production and associated management strategies at the local level and to expand the results to obtain an overview at the regional level, software crop simulation models such as Decision Support System for Agrotechnology Transfer (DSSAT) are useful [32]. Models can consider the interaction between UPS and weather parameters (such as rainfall and temperature) [24,33,34]. Thus, crop models are useful tools for researchers, academics, scientists, extension educators, policymakers, and planners in supporting the implementation and evaluation of the sustainability of UPS [35,36]. Models are very useful as they can provide prior sensitive information to reduce the risk of crop failure in rainfed cereal production systems. However, there is limited systemization of the information gathered on biophysical models that can be used to model the UPS that secure the optimum possible harvest of cereals under limited rainfall and soil nutrient conditions.

The objectives of this review were to (i) collect and systemize the scientific results on the performance of different UPS in reducing the risks related to rainfed cereal production in semi-arid environments; (ii) identify the biophysical models used to study selected UPS; and (iii) evaluate the strengths and limitations of the models in enhancing rainfed cereal production.

## 2. Materials and Methods

We collected papers from different literature repositories that describe the roles of upgrading strategies in the production of cereals (Table 1). The search keywords that were used and the examples of combinations are presented in Table 1. The papers were screened in succession starting from a global context, then in arid and semi-arid climate countries and finally to the topic of this study. A total of 187 papers were relevant to this review from more than 1000 papers. The papers covered broadly the roles of UPS for cereal production in arid and semi-arid regions. In addition, the papers described the

usefulness of modelling UPS for enhancing cereal production under low and highly variable rainfall and poor soil fertility conditions.

**Table 1.** Keywords and some of the combinations used to search the literature in the Web of Science, Directory of Open Access Journals (DOAJ), Google Scholar and ResearchGate.

Keywords	Combinations Used
Upgrading strategies	Upgrading strategies for cereals
Cereals	Cereal crop management
Crop management	Rainfall in arid and semi-arid
Arid	Drought and harvest risk
Semi-arid	Adoption of crop management
Modelling	Spatiotemporal rainfall variability
Rainfall variability	Spatial plot distribution
Drought	Modelling tied ridges
Adoption	Food security and hunger for poor farmers
Food security	Food security in semi-arid areas
Climate change	Crop management strategies
Hydrology	Temporal rainfall variability
Tied ridges	Spatiotemporal rainfall variability in semi-arid areas
Planting dates	Crop management strategies for rainfall variability
Agricultural water	Crop management in poor soils
Spatiotemporal	Fertilizer management in drought areas
Spatial	Crop management strategies for poor farmers
Temporal	Spatiotemporal rainfall variability and crop yield
Plot scattering	Modelling of crop management
Microdose fertilization	Biophysical models for cereals in arid and semi-arid
Hunger	Rainfall variability and harvest risk of cereals
Risk	Simulation of cereals growth in semi-arid
Harvest Soil fertility	Arid-semi-maize-rainfall-variability-management-yield

The other conditions for the inclusion of papers in this review were the following:

- i. Peer-reviewed articles on crop UPS and modelling in English published in 1990 and after. The UPS that were included were categorized as rainwater harvesting, soil moisture conservation, means of water application and productivity, nutrient addition to the soil, soil conservation, drought coping measures and measurements of rainfall variability.
- ii. Reports with qualitative or quantitative empirical findings and perceptions and views discussed in relation to UPS and modelling.
- iii. Conference proceedings papers related to UPS and modelling.

All the UPS identified in the selected papers were ranked according to importance, affordability, possibility, and effectiveness (Table 2). The authors arbitrarily defined these criteria in terms of UPS adequacy to address the rainfall variability and soil fertility conditions faced by farmers in semi-arid areas.

The constraints categories for the UPS were scored by six experts, ranging from 1 (highest constraining potential), 2 (medium constraining potential) to 3 (lowest constraining potential). These experts were familiar with UPS and were capable of making informed judgements about them. Using the experts' results, the constraint with highest scores was regarded as having the least constraining potential. The authors of this study then scored the UPS using the scores given by the experts. The UPS with the highest efficiency in overcoming the stated constraint in each criterion as judged by expert scores was given a score of 3, the medium efficient was given a score of 2 and the least efficient was given a score of 1. If half or more of the six experts gave a score of 3 to the constraint (i.e., expert one score = 3, expert two score = 3, expert three score = 1, expert 4 score = 3, expert 5 score = 2, expert 6 score = 1) then we picked 3 as a score. If the scores tied, for instance, three experts gave a score

of 3 and two experts gave a score of 2, then we picked the highest score, which is 3. Similarly, if two experts each gave similar scores we picked the highest score of the three given (i.e., two experts gave 1, the other two gave a score of 2 and the other gave a score of 3, then we picked 3). For example, for the criterion “importance” the constraint social acceptance was given a score of 1 because four experts gave a score of 1, for constraint “labor” the score was 2 because three out of six experts gave a score of 2 and for constraint “sustainability” the score was 2 since four experts gave a score of 2. In the next step, all constraints of a given criterion were averaged, producing suitability scores ranging from 1 to 3, with 3 being the highest suitability, while 1 means low suitability. Finally, all criteria scores for a given UPS were averaged to form a final score.

**Table 2.** Four criteria used to select the most suitable upgrading strategies in semi-arid areas.

Criteria	Criteria Definition	Constraints	Constraint Definition (Questions)
Importance	It significantly improves production in semi-arid environments under production constraints, has high social acceptance, is easy to implement and is sustainable	Social acceptance	Is it likely to be adopted by most people?
		Labor	Does it involve much labor to implement?
		Sustainability	Can it be maintained easily?
		Environment	Will it have a reduced effect or no harm to the environment?
		Rainfall variability	Does it reduce the effect of rainfall variability?
		Soil fertility	Can it enhance soil fertility?
Affordability	It should be less limited by financial constraints, labor and is easily purchased	Land availability	Does it require much land for its implementation?
		Productivity	Does it enhance crop productivity?
		Costs	Can it be implemented with a minimum cost?
		Labor	Is there a cheap labor available for its implementation?
Possibility	It should be possible to implement with less difficulty and is socially and culturally acceptable	Availability/easy to implement	Are there cheap materials available for its implementation?
		Easy to implement	Does it require much knowledge in implementing?
		Social acceptance	Are there any traditional limitations in implementing?
		Labor	Does it involve much labor in implementing?
Effectiveness	It should be effective in reducing the risk of rainfall variability (prolongs soil moisture) and preserving soil nutrients	Land availability	Is it limited by land availability?
		Rainfall variability	Does it prolong crop growth under rainfall variability?
		Soil fertility	Does it conserve soil fertility?
		Productivity	Can it increase crop yield?

Once the four UPS with the highest overall average scores according to the criteria in Table 2 were selected, we searched for literature that described the biophysical models able to simulate them. The main criterion for model selection was that the reported models must have been used to adequately simulate the selected UPS. The models that were the most robust in simulating these UPS were further described and analyzed. Depending on the number of the UPS simulated by the biophysical models, we ranked the models from those that simulated all the four selected UPS to those which simulated at least one UPS. We described three of the most frequently used models pertaining to the four selected crop UPS. We used the FAO database (FAOSTAT) (<http://www.fao.org/faostat/en/#data>, accessed on 7 July 2017) to extract information on cereals’ global harvested area and production. We then computed the relationship between the model coverage of the four UPS by counting the number of papers from our collection under each cereal and the global harvested area of the cereals to determine whether there was any association. In addition, we analyzed the relationship between the global harvested area of different cereals and the usage of the four UPS.

### 3. Results

#### 3.1. Roles of Crop Upgrading Strategies for Cereal Production

We identified 13 UPS that are useful for cereal crop production (Table 3).

**Table 3.** Reported upgrading strategies used for enhancing and securing cereal crop production.

UPS	Countries and References	General Results	Challenges for Adoption
On-farm pond/well management	China [37], India [38–40], Ethiopia [22]	Prolonged water availability for crops, leaching requirements and crop productivity	Farm size limitations and costs of excavation
Irrigation	Tunisia [41], India [42], Iran [43], China [44–47], Benin [48]	Irrigation provides water for crop requirements at all stages of plant growth and increases crop yield	Availability of a reliable source of water
Mulching	China [44,49,50], Zambia [51], Zimbabwe [52]	Enhance infiltration rate of rainfall and reduces evaporation of moisture from soil	Availability of mulch to cover large fields
Crop rotation, and intercropping	Ohio [53], China [54], Turkey [55], Spain [56], Iran [57], India [58,59], Burkina Faso [60], Zimbabwe [61]	Crop rotation enhances soil structure and hence reduces runoff and soil erosion	Enough land is needed to allow the rotation of the same amount of land for cultivation
Reservoir tillage or Pit cultivation	Tanzania [62], Zimbabwe [63,64]	Potential for improved soil water availability and crop productivity. Additionally, reservoir tillage of sandy loam is effective for the infield harvesting of high-intensity rainfall	Care should be given to harvest rainwater so as not to destruct the water balance of the catchment, especially groundwater storage
Micro-dose fertilization	Iran [65], China [66–68], Nepal [69]	Micro-dose fertilization improves nutrient availability to the soil and grain yield and provides income for poor communities	Limited by availability of sufficient soil moisture
Crop substitution	Iran [70], Canada [71]	Substitution of maize with pearl millet was found as the best option in future climates for the production of fodder	Traditional and cultural practice challenges
Varying planting/sowing dates	India [72,73], Brazil [32], Nigeria [74], Burkina Faso [75], Tanzania [74], South Africa [74,76], Zimbabwe [77], Egypt [78], Hungary [79], Syria [80], Lebanon [81], Nepal [69], Iran [82]	Reduces the effects of yield loss due to temporal rainfall variability	Timing of the start of planting dates
Use of groundwater	Oman [83], Iran [84], China [85–87]	Adds to the fresh water that can be made available for agriculture	Requires energy to lift water from below ground to the fields
Spatial plot distribution	Niger [88], [29], Greece [89], Kazakhstan [90], Benin [91]	Reduces the risk of complete production failure	Requires ownership of spatially distinct land
Change of cultivars	Ethiopia [92], Iran [84,93,94], India [95], China [96,97], Italy [98], Brazil [99], Tanzania [100]	Reduce the risk of complete production failure	Social preferences and fear of loss of indigenous species
Contour strips (ridges) and tied ridges	Kenya [27,101], Gambia [102], Tanzania [103], Ethiopia [92,104], Nigeria [105]	Contour strips and tied ridges decrease soil erosion, enhance groundwater recharge and prolong soil moisture availability	Requires labor and is not easily mechanized
Reduced tillage and zero tillage	India [106,107], Ethiopia [108], Mexico [109,110], Canada [111], Pakistan [112–114]	It may be applied when onset is uncertain and for conserving soil moisture and nutrients	Reduced yield due to a less favorable crop growth environment

Determining the balance between the strengths and limitations of the UPS is important because these will respectively encourage and discourage farmers during the adoption stages. For instance, in the study on the suitability of on-farm ponds (irrigation), Roost et al. [37] had to analyze soil characteristics in order to understand water dynamics, of which deep percolation was a concern. This implied that even if on-farm ponds are suitable for improving yields, they may work better when soils have a robust ability to retain the stored water. In addition, land availability that can be reserved for ponds within farmers' fields will be a challenge as most poor farmers' landholdings in semi-arid areas have small plot sizes [3]. Thus, sustainability of these practices becomes a challenge since it largely depends on the type of soil. Ponds primary purpose is to supplement a soil moisture deficit through irrigation. Other operational costs such as pumping or intensive labor for water lifting may be needed. Under high rainfall variability water storage for supplemental irrigation is important; the main challenge remains to be affordability and possibility.

Similar concerns arise when we examine the use of groundwater as an alternative source of water for supplemental irrigation [84]. This UPS, despite being important and effective, also faces challenges

of affordability and possibility as it requires an initial investment for boreholes or a large amount of labor for hand dug wells. Additionally, during irrigation, the operational costs of lifting water via pumping are untenable for most poor farmers. Raising water for irrigation by hand is unattractive due to drudgery work involved. In general, this makes the UPS difficult to implement and labor intensive, and it may also face the challenge of availability of groundwater, hence jeopardizing its adoption possibilities.

Mulching helps to prolong soil moisture by protecting it from excessive evaporation [115], and in that regard is reported as an important strategy by many authors (Table 3). It is socially acceptable, sustainable, environmentally friendly, not constrained by land availability, and helps improving microbial activities in the soil, and productivity. Mulch also is well suited with zero tillage. However, when rainfall is minimal mulch may obstruct rainfall from falling directly on the soil. Under high rainfall variability, mulch works better when combined with a field scattering strategy and it may work with irrigation to improve water use efficiency [49]. The main challenge is mulch availability, and the labor involved in laying down the mulch. Some authors did not find significant advantage for yields when mulch was used [51], and farmers are reluctant to practice mulching [52]. Other UPS such as crop rotation, crop substitution, reservoir/pit tillage, and irrigation using surface water, all have their strengths and weaknesses (Table 3). In our analysis, we found four UPS to be the most suitable for boosting cereal production in semi-arid areas.

In Table 4, the experts' scores for each constraint and criterion related to individual UPS are presented. The results indicate the amplitude of scores but also show that this procedure can identify the most suitable UPS for the target region. For example, irrigation is among the most important and effective UPS to improve crop performance; however, considering the context in which this assessment is done, it is very costly and requires extensive knowledge, thus, scoring very low in affordability and possibility. When considering the four UPS with higher overall scores (Figure 1), the strategies were shift planting/sowing dates, contour strips and tied ridges, spatial plot distribution and micro-fertilization.

Table 4. Experts' scores for each constraint and criterion related to individual UPS.

Criteria	On-Farm Pond/Wells Management	Irrigation	Mulching	Crop rotation, and Intercropping	Reservoir Tillage or Pit Cultivation	Micro-Fertilization	Crop Substitution	Shift Planting/Sowing Dates	Use of Groundwater	Spatial Plot Distribution	Change of Cultivars	Contour Strip and Tied Ridges	Reduced Tillage and Zero Tillage	
Importance	Social acceptance	1	3	3	2	3	2	3	1	3	2	3	2	
	Labor	2	1	2	2	1	3	3	1	3	3	2	2	
	Sustainability	2	2	3	3	2	1	3	1	3	2	3	3	
	Environment	2	2	3	3	3	2	3	1	3	2	3	3	
	Rainfall variability	2	2	1	2	3	2	3	3	3	2	3	2	
	Soil fertility	2	2	2	2	2	3	2	3	2	1	2	2	
	Land availability	1	1	2	2	2	3	3	1	1	3	3	3	
	Productivity	3	3	2	2	2	3	2	3	3	3	2	2	
	<b>Average</b>	<b>2.1</b>	<b>2.0</b>	<b>2.3</b>	<b>2.3</b>	<b>2.3</b>	<b>2.6</b>	<b>2.1</b>	<b>2.9</b>	<b>1.5</b>	<b>2.6</b>	<b>2.1</b>	<b>2.8</b>	<b>2.4</b>
	Affordability	Costs	1	1	2	2	2	2	2	1	3	2	2	2
Labor		1	1	1	2	2	3	2	1	1	1	2	2	
Availability/easy to implement		1	1	1	2	2	1	3	2	3	2	3	3	
<b>Average</b>		<b>1.0</b>	<b>1.0</b>	<b>1.3</b>	<b>2.0</b>	<b>2.0</b>	<b>2.0</b>	<b>2.0</b>	<b>2.7</b>	<b>1.3</b>	<b>2.3</b>	<b>2.0</b>	<b>2.3</b>	
Possibility	Easy to implement	1	1	1	2	2	2	1	3	3	2	3	3	
	Social acceptance	2	3	1	2	2	3	1	3	1	3	2	3	
	Labor	1	1	1	2	2	2	3	1	1	2	2	2	
	Land availability	1	1	3	2	3	3	3	2	2	3	3	3	
<b>Average</b>	<b>1.3</b>	<b>1.5</b>	<b>1.5</b>	<b>2.0</b>	<b>2.3</b>	<b>2.5</b>	<b>2.0</b>	<b>2.5</b>	<b>1.5</b>	<b>2.3</b>	<b>2.0</b>	<b>2.8</b>	<b>2.5</b>	
Effectiveness	Rainfall variability	2	3	1	2	3	2	2	3	3	2	3	2	
	Soil fertility	2	2	2	2	2	3	1	2	1	2	1	2	
	Productivity	3	3	2	2	2	3	2	3	3	2	3	2	
	<b>Average</b>	<b>2.3</b>	<b>2.7</b>	<b>1.7</b>	<b>2.0</b>	<b>2.3</b>	<b>2.7</b>	<b>1.7</b>	<b>2.7</b>	<b>2.3</b>	<b>2.7</b>	<b>1.7</b>	<b>2.0</b>	

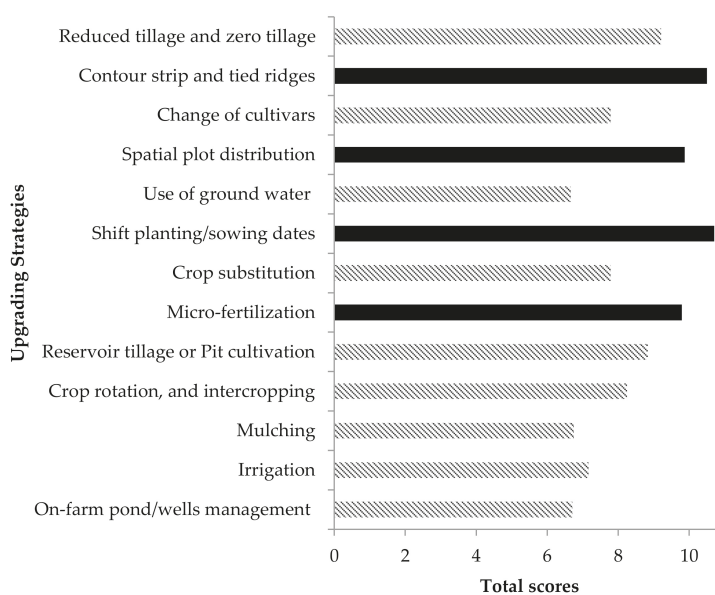


Figure 1. Ranking of UPS using total average scores from Table 4.

### 3.2. Modelling Cereal Crops UPS for Enhancing Production

Many models have successfully simulated the four selected crop UPS and have suggested methods to tackle the production challenges of cereal crops in semi-arid areas. Examples of these models include DSSAT, APSIM, AquaCrop, HYDRUS-2D, EPICSEAR, MSM and others (Table 5).

Table 5. Different models reported for simulating UPS in semi-arid areas.

UPS	Models and Authors	Country	Crops
Contour strip and tied ridges	ACRU [116], SWAT [117], AquaCrop model [118], HYDRUS-2D Software [119], APSIM [120]	Zimbabwe, Kenya, Ethiopia, China	Maize
Micro-fertilization	APSIM [121–123], EPICSEAR [124], MSM [125], DSSAT [126–131], AquaCrop [132]	Zimbabwe, Kenya, Madagascar, Niger, Brazil, China, Canada, Korea, Pakistan	Maize, Wheat, Rice, Pearl, Millet, Barley
Shifting planting/sowing dates	APSIM [121,133], GIS-based EPIC [74], DSSAT [134], AquaCrop model [135,136], CropSyst model [73], Soil moisture model [137]	Zimbabwe, Mozambique, Morocco, Botswana, Malawi, China, India, Iran, Jordan	Maize, Wheat, Rice, Sorghum, Barley
Spatial plot distribution	DSSAT [73,138], APSIM [142]	Brazil, Jordan, India, Timor-Leste	Maize, Sorghum, Rice, Wheat, Barley

Definitions of the model acronyms: ACRU—Agricultural Research Unit simulation model; SWAT—Soil and Water Assessment Tool; AquaCrop—crop-water productivity model; HYDRUS-2D—a software package for simulating water, heat, and solute movement in two- and three-dimensional variably saturated media; APSIM—Agricultural Production Systems Simulator model; MSM—An integrated water and N Maize Simulation Model; DSSAT—Decision Support System for Agrotechnology Transfer; EPIC—Environmental Policy Integrated Climate; EPICSEAR—newly developed version derived from the Erosion Productivity Impact Calculator model for simulating crop production and nutrient uptake on highly weathered, acidic soils; CropSyst—Cropping Systems Simulation Model; Soil moisture model—a continuous soil water balance model for the simulation of soil moisture temporal evolution.

In general, the simulations of UPS for semi-arid climates are reported by only a few papers compared to the multitude of papers available on modelling/simulation. We found that 30 out of the 187 papers contained in this review specifically covered the modelling of at least one of the four selected

UPS in semi-arid areas. One strong reason for such a shortage is the limitation in the availability of, and access to, quality data [100,143,144]. Maize was covered by 51% of the papers reviewed. The other cereal crops that were covered were wheat (23%), rice (10%), barley (8%), sorghum (5%) and pearl millet (3%), (Figure 2). We found a strong positive correlation ( $r$ ) between the global harvested area and the frequency of crop coverage by the models in the papers that simulated the four crop UPS in semi-arid regions (Figure 2). Thus, the cereals with large global harvest areas not only possess a good chance to be cultivated with UPS but also attract more modelling studies to improve their production. This is evident because the three major cereal crops (wheat, rice, and maize), which occupy more than 80% of the global area of harvest for cereals, show a high frequency of usage of models and UPS (Figure 2) compared to millet sorghum and barley. We also found a relationship between the productivity of global cereals (Table 6) and their frequency of model coverage for the UPS in the reviewed papers, which may best be represented by a quadratic model (Figure 3).

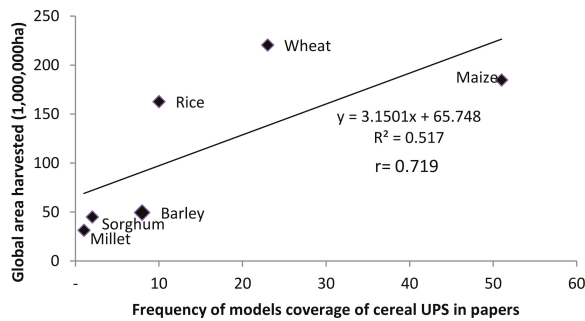


Figure 2. Relationship between global harvested area and frequency of the model coverage of cereal UPS in papers (number of papers), data from FAOSTAT, 2014 accessed on 7 July 2017.

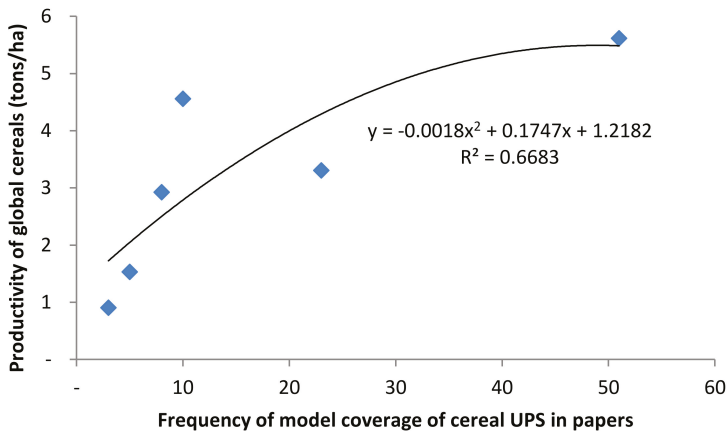


Figure 3. Relationship between the productivity of global cereals and frequency of the model coverage of cereal UPS in papers (number of papers), data from FAOSTAT, 2014 accessed on 7 July 2017.

**Table 6.** Global productivity area of cereals (FAOSTAT, 2014 accessed on 7 July 2017).

Crop	Production tons/ha
Barley	2.92
Maize	5.62
Millet	0.90
Rice	4.56
Sorghum	1.53
Wheat	3.31

Crops such as pearl millet and sorghum, which are among the major staple food crops in semi-arid areas, especially in Africa, have gained less modelling attention. This lack of attention could be due to the disadvantage related to global harvest area, as explained by the relationship in Figure 2. This disadvantage is also due to the population that consumes these crops which is small when compared to other cereals. The relationship can be associated with the analysis of White [145]. However, these crops can be of major importance locally as they represent large potential for reducing food insecurity and poverty in semi-arid areas.

From our review, we selected three models to describe and discuss; these are DSSAT, APSIM and AquaCrop. These models cover the four UPS adequately. In summary, in this paper's framework, the DSSAT model dominated the studies, followed by APSIM and AquaCrop. The reason for the dominance of these models can be understood further through their descriptions and discussion, which is also presented in this paper.

#### 4. Discussion

The choice of UPS depends on the involvement of stakeholders and their knowledge of labor limitations, financial constraints, restrictive governmental policies, environmental and climatic conditions, social and cultural conditions and related food security risks [20]. Thus, UPS are important to sustainable crop production and food security. In our review, all 13 UPS were found to be suitable for improving production; however, they all had constraints in their adoption. In Tables 2 and 4 we have identified the constraints, assigned a score as supported by the literature and ranked the UPS according to the average scores of the constraints. The scores of the constraints were given by experts as a result of the understanding found in the literature describing the ability of the UPS to overcome these constraints. We have picked the four highest ranked UPS and described them below.

##### 4.1. Contour Ridges and Tied Ridges

"A ridge is a long, narrow, elevated strip of land or any raised strip or band. A ridge is called a contour ridge when it is created along the upslope furrow to accommodate runoff from a catchment strip between the ridges that are 15 to 20 cm high" [146]. "These ridges may be 1.5 to 10.0 m apart depending on the microcatchment system, as the catchment is a function of the distance between ridges. The precise distance should be calculated according to the expected rainfall and the soil texture of the region" [146]. When a ridge is crossed by the ridge of another perpendicular earthen band, it is called a tied ridge (Figure 4). "Small earthen ties are made within the furrows at 4 to 5 m intervals to prevent the lateral flow of water. The main objective of a tied ridge system is to collect local water runoff and store it within the soil profile in the vicinity of the plant roots" [146].

Tied ridges prolong the retention of soil moisture and enhance nutrient uptake by crops [101,104,147]. Tied ridges provide a better crop growth environment [102,148,149] in areas where the temporal rainfall variability is a challenge. Evidence of higher cereal yields and increased rain water use efficiency [27,101], and even better income [92,104], have been reported. Tied ridges can be improved to be more effective, for instance by combining tied ridges with microdosage techniques [147]. This UPS is found to be the most useful in reducing the acuteness of temporal rainfall variability.



**Figure 4.** Examples of tied ridges planted with pearl millet in Idifu-Dodoma, Tanzania.

Araya and Stroosnijder [104] report that tied ridging and mulching can increase soil water availability in the root zone by more than 13% and crop grain yield (barley) by at least 44% during below average rainfall years. Other evidence shows that tied ridges are beneficial in drought-prone areas. Arid and semi-arid areas can benefit from enhanced production, up to five times greater, of sorghum yields grown in loamy soils [103].

Care should be taken when farming using tied ridges, and it is advised to carefully open the ridges when excess water is expected to cause waterlogging [104]. Thus, when rainfall is well distributed during the cropping season, tied ridging is not a necessary tillage alternative for cereals such as maize on flat land. However, when tied ridges are used in areas with modest slopes, they markedly increase soil water reserves at 0.15 to 0.60 m depths after maize harvest [102]. This strategy is limited by the difficulties related to mechanization [150] and excess rainfall. The limitations necessitate “an assessment of the major agro-meteorological challenges, existing tillage, hoeing and associated land management practices” [150].

#### 4.2. Micro-Fertilization

After water availability, soil nutritional status is the greatest constraint to food production across the arid and semi-arid SSA countries [105,151,152]. When soil moisture is adequate for plant growth, the crop will reach its maximum growth potential if nutrient supply is adequate. Several authors have reported a challenge of poor soil fertility that farmers in semi-arid areas are facing [153–155]. The problem is acute for poor farmers in semi-arid Sub-Saharan Africa countries [151,156,157]. The precision-farming technique referred to as “microdosing” has been developed by experts [158–160]. It “involves the application of small quantities of fertilizer with the seed at the time of planting or as top dressing three to four weeks after emergence” [161]. This method enhances the efficiency of fertilizer use when compared to the broadcasting application method. Micro-fertilization helps poor farmers increase the returns on small initial investments [160,162].

In agreement with Biielders and Gerard [162], farmers have to develop the capacity to apply recommended amounts of fertilizer over time. The best option could be the application of manure or organic fertilizers. However, manure availability can be a challenge for farmers who are not livestock keepers. In such conditions, microdose fertilization remains an important option to these farmers. So far, microdosing has been introduced in Zimbabwe, Mozambique, and South Africa, which are in the southern part of the African continent [151,157]. Farmers apply fertilizer in small quantities (micro-fertilization) to cover large areas of their farms, and this method has helped them increase crop yields [163]. The results from Niger and Mali show a yearly average of 20 kg P<sub>2</sub>O<sub>5</sub> ha<sup>-1</sup> and 30 kg N ha<sup>-1</sup> increased stover yields by 400 to 1500 kg ha<sup>-1</sup>, and the stover yield was not further increased with higher application rates of 40 kg P<sub>2</sub>O<sub>5</sub> ha<sup>-1</sup> and 60 kg N ha<sup>-1</sup> [164]. Similar reports of millet yield success have been reported in Niger [162]. Other promising results from initial on-farm trials in Zimbabwe show increases in yield by 30–100% when microdoses, as little as 10 kgN ha<sup>-1</sup> [151] were applied.

Thus, micro-fertilization UPS are recommended in low-yielding plots, as microdosing in plots with minimum yield bears a non-negligible financial risk [151]. Twomlow et al. [151] reported that micro-fertilization was an effective strategy to counteract the disadvantages of late sowing, and it better suited as a means of famine mitigation [151]. They provided yield data that smallholder farmers could increase their yields by 30–100% through application of micro-fertilization as little as 10 kg Nitrogen ha<sup>-1</sup> [151]. However, these experiences from West Africa have shown that the adoption of micro-fertilization technology requires supportive and complementary institutional innovation [151]. The major constraints to the adoption of this strategy are the initial access to fertilizer, access to credit, insufficient flows of information and training to farmers, and inappropriate policies [151]. Of much interest is what additional benefits can be obtained by combining microdose fertilization with other UPS, such as varying planting dates, tied ridges and field scattering.

#### 4.3. Varying Sowing/Planting Dates as a Measure to Counteract Rainfall Uncertainties

Varying planting dates increases the efficiency of the use of available water or rainfall and it has the potential to reduce the risk of temporal rainfall variability [29]. Under current climate change and variability, the onset of seasonal rainfall is uncertain for most years [76,165–167]. Therefore, farmers cannot rely on the planting dates they previously used. To reduce the risk of total production failure, farmers are advised to vary planting dates to capture the best planting date for the season. This method guarantees the probability of at least one planting date secures a harvest. In this case, the timing of the start of planting dates is crucial and very challenging [74].

In addition, a challenge related to the affordability remains, as poor farmers have a limited capacity to purchase enough seeds to cover several planting dates. A study in Southern Africa established optimum planting dates for six locations. These dates were from the 5 to 27 December, 26 December to 7 January, and 4 to 7 December for Malawi, Mozambique, and Zimbabwe, respectively [76]. Sacks et al. [168] discovered that maize planting dates might vary more widely in tropical regions. The findings reflected that sowing time can be optimized for stable rainfed maize yields, but the effect of sowing dates on rainfed maize yield is modified by both soil depth and soil fertility.

In general, varying sowing/planting dates increases the chance of crop production under high temporal rainfall variability; for some cereal crops, this strategy has significantly influenced seed germination, plant height, tillering, total biomass, and overall grain yield and water productivity under rainfed conditions. Such cereals include wheat [168,169], rice [170,171], maize [172,173] and sorghum [174–176]. The weakness of the method is related to the difficulties in controlling the harvest loss for all dates combined. Thus, this strategy provides an opportunity for farmers to have a wide range of planting date options that can help them secure a possible optimum harvest for the season. The timing of planting should be adjusted based on the forecast of the onset of seasonal rainfall to harness the maximum potential of available seasonal rainfall.

#### 4.4. Spatial Plot Distribution as a Measure to Combat Spatial Rainfall Variability

Rainfall can vary over a spatial distance as small as 800 m [29]. Efforts to protect crop yields from the impacts of climate change should, therefore, consider spatial rainfall variations [177]. Spatial plot distribution (cultivating fields at different locations within a few kilometers) reduces the risk of complete production failure when there is less rainfall and high spatial variability in the area; however, fields cannot avoid production losses altogether [29,30]. The spatial plot distribution strategy has been successfully used in Niger [29] and Nigeria [30]. Spatial plot distribution is limited by land and financial resources of farmers to be able to farm fields in different locations. The strategy is useful in areas that are not constrained by land resources and have low rainfall with high spatial variability [29,30].

#### 4.5. Roles of Models for Cereal UPS

The models are good at exploring different questions that arise from the limitations of UPS at the field level and extrapolating the results to a large scale that allows for more informed decision making [178]. Modelling and simulation studies help in making more sensible decisions for the current climatic status and the future production of cereals. They provide an alert for the measures to take in case food security is at risk. The models should subsequently be improved as they have several limitations, as described below.

##### 4.5.1. Description of DSSAT-Models

The “decision support system for agrotechnology transfer” (DSSAT) encompasses 16 different crop models for different evaluation purposes [179]. The models in DSSAT integrate the effects of soil, crop phenotype, management options and weather. A DSSAT model has been adopted in a wide range of countries and continents (Table 5), which indicates its strength in accommodating a wide range of climatic and agricultural conditions. For instance, one simulation study found clear signs of decline in the future production of maize and rice in India [73]. Additionally, they determined that shifting planting dates would have a positive impact on production. Rezaei et al. [70] used the DSSAT model and found that maize crops could be substituted by pearl millet to counter yield reduction in the future, while other studies have suggested that a change of cultivar would be an option to sustain food production in the future [32,180].

In this survey, we found that the models have satisfactorily explained farmers’ attitudes to planting/sowing time, microdosage under nutrient management, and scattered field or spatial field dispersion. In most of the papers, data used for calibration were daily weather records, measured physical, chemical, and morphological characteristics of the soils as model inputs, and crop genetic coefficients that are specific to each cultivar of interest. In a study by Jagtap and Abamu [127], DSSAT model used farmers’ planting dates to simulate maize growth and found that “early planting together with manure from cattle allowed to graze on crop residues increased yield response to fertilizer N” [127]. The results also showed that changing the planting date by 30 days (more or less) had minimal effect on obtainable maize grain yields in production systems characterized by high N inputs (120–150 kg/ha) [127].

DSSAT offers nutrient management functions, where fertilizer application can be varied from optimum to minimum applications (micro-fertilization). Nutrient management has been simulated extensively and reported by many authors. For example, Gerardeaux et al. [129] used the DSSAT 4.5 cropping system model (DSSAT-CSM) to explain the impact of various climate changes on rice productivity in Madagascar using two tillage strategies and two fertilization rates: low and high nitrogen. They used a locally cultivated rice cultivar to calibrate and validate the model, with a 6-year experimental data set. Nitrogen was found to be a major constraint while zero tillage demonstrated no advantage in addressing impacts of climate change. Another study by Jeong et al. [130] using DSSAT found that adjusting the split N fertilizer application rate was enough to attain a satisfactory yield of rice, providing an additional 10–20 kg/ha. Other studies also done on wheat [126], pearl millet [131] and maize [32,125] demonstrated the potential of using DSSAT in simulating fertilizer microdosage.

DSSAT has also been reported to simulate field scattering as an UPS for improving cereal yields in semi-arid areas. In a study by Jalota and Vashisht [73], they found that “in the future, the magnitude of climate change and variability would vary with agro-climatic zone” as well as the yields of maize and rice [73]. A simulation of wheat at different locations using a DSSAT model [140] also recorded different yields, which were a result of different agro-climatic zones within India. Hurtado et al. [138] also reported that the DSSAT was able to simulate corn yields related to field spatial variability. The authors used data of “maximum and minimum temperatures, rainfall and solar radiation; soil data in the 0–27, 27–45, 45–68, 68–80 and 80–100 cm layers to each experimental plot, management information of corn crop and genetic parameters of the corn hybrid” [138]. The authors reported that the DSSAT was able to simulate yields as related to the spatial variables of the soil attribute base saturation.

Although DSSAT models are reported to adequately simulate planting dates, micro-fertilization and spatial plot distribution UPS, we found no evidence that DSSAT models were used to simulate tied ridges strategies. This is a gap that crop modelers may be required to fill as this UPS is among the four prioritized UPS found to be effective in reducing the adverse effects of rainfall variability and in conserving soil fertility and moisture during crop growth in semi-arid areas. Another summary of the strengths and weaknesses of DSSAT models is presented by Brillì et al. [181]. The limitations reported include overestimation or underestimation of soil organic carbon and soil nitrogen.

#### 4.5.2. Description of APSIM Model

“The Agricultural Production Systems Simulator (APSIM)” [182] simulates several systems and addresses the interactions among plants, animals, soil, climate, and management. The model allows for the analysis of a whole-farm system, including crop and pasture sequences and rotations, and livestock [182]. Maize was found to be a dominant crop simulated by the APSIM model followed by wheat and sorghum. For example, Ngugi et al. [120] adopted the APSIM model for a scenario analysis of the effect of tied ridges on maize yield in two study sites in Kenya and found different responses to tied ridges and fertilizer application. In general, when combined, tied ridges and fertilizer application boosted the maize yield significantly [120]. This provides evidence for the concept of combining different UPS to counteract the effect of rainfall variability and poor soil fertility. In this study, the combined UPS increased yields of maize grain between 507–3370 kg/ha [120].

In Zimbabwe, the APSIM model was used to explore the “risk associated with N fertilizer use by smallholder farmers and management strategies to minimize that risk” [121]. They used long term data from Nitrogen fertilizer maize trials for calibration and validation of the model before using it in their exploration. In their results, they found moderate fertilizer application rates and early sowing will give economic benefits to farmers [121,122]. Kisaka et al. [122] found similar results in Kenya and recommended that “for subsistence farming, low-cost recommendations are geared towards some ‘guaranteed’ yield stability each cropping season” [122]. Ahmed et al. [123] also calibrated and validated the APSIM model and used it to predict nitrogen use efficiency of wheat under rain-fed conditions for the Pothwar region of Pakistan. The simulation revealed the potential of the APSIM model to provide fertilizer recommendation rates that may achieve agricultural production and economic benefits, a finding that is in agreement with [142].

In the study by Ngugi et al. [120], the authors reported the potential of the APSIM model to inform the planting dates UPS. They found that timing of planting was key in improving yields. The results are in agreement with Heng et al. [133] who reported that “early sowing is important for achieving high yields by avoiding terminal water deficit” [133]. The algorithm for simulating planting dates in the model provides opportunities to determine optimum planting dates, which can help farmers to avoid total crop failure. The model, in addition, could “simulate maize yields at four locations with 8 years of reliable weather records” [142], which highlights the potential of the model in determining the effect of spatial plot distribution UPS. Under high spatial rainfall variability, the model can help in predetermining the potential positions of fields where farmers can expect to obtain optimum yields.

Some of the weaknesses of the model have been summarized by [181], which include underestimation of soil nitrogen and soil organic component, overestimation of annual leaching, and underestimation/overestimation of N<sub>2</sub>O emissions. In this regard, the APSIM model still requires periodic improvements so that it can be used with more certainty. In addition, [181] provides a detailed summary and review of the strengths and weaknesses of the APSIM model.

#### 4.5.3. Description of the AquaCrop Model

“The AquaCrop model simulates major herbaceous crops as a function of water consumption under rainfed, supplemental, deficit, and full irrigation conditions” [183]. It also simulates evapotranspiration as separately soil evaporation and crop transpiration. The model also simulates the biomass accumulated each day using crop specific parameters that are normalized for reference

evapotranspiration [183–185], which makes the model useful to in different climates [132,186,187]. The model has been successfully used to simulate different cereal UPS in semi-arid areas. We found six papers that discussed planting dates for maize [77,184], barley [136,186], winter wheat [135], and varying nitrogen levels (microdose fertilization) for maize [132]. We found the model to have the potential for extrapolating successful cereal UPS in arid and semi-arid areas. Expansion of the usage of the model for simulating tied ridges and modifying the model to accommodate spatial field dynamics will be of importance for its robust usage.

Most of the weaknesses of the AquaCrop model are mentioned on the FAO website for land and water (<http://www.fao.org/aquacrop/overview/limitations/en/>). Our overview finds that the weaknesses resemble the limitations of DSSAT and APSIM. These limitations include the following: (i) AquaCrop simulates a single growth cycle only; (ii) the model predicts crop yields at a single point in its simulations [183] and assumes that the field is uniform without spatial differences in crop development, transpiration, soil characteristics or management [183]; and (iii) the AquaCrop model considers only incoming vertical (irrigation capillary and rainfall rise) and outgoing (transpiration, deep percolation and evaporation) water fluxes in its simulations [183].

## 5. Conclusions

Four UPS were identified as the most promising to improve rainfed cereal production for poor farmers in semi-arid areas. These UPS are tied ridges, microdose fertilization, varying sowing/planting dates and field scattering. These strategies are suitable for reducing the risks of cereal production failure under low rainfall, high spatiotemporal variability, and poor soil fertility conditions.

Among the different biophysical models, three of them—namely, DSSAT, APSIM and AquaCrop—have more frequently studied the four selected UPS. We found that both the strengths and the weaknesses of these models were comparable. In general, the models have performance weaknesses when temporal and spatial variations in soil moisture, soil temperature and aeration are considered. In addition, they do not include algorithms for each UPS or for soil organic content and they consider only vertical water fluxes. The frequency of the use of models is an important proxy for their robustness. This assessment also identified the main points necessary to improve the selected UPS's. Despite their limitations, we encourage researchers and decision makers to use these models since they have been instrumental in research and decision-making.

**Acknowledgments:** The research conducted in this study has received funding from the German Federal Ministry of Agriculture and Food (BMEL) in the frame of PhD program by the Federal Office of Agriculture and Food (BLE). The preparation and publication of this article is funded by Leibniz Center for Agricultural Landscape Research (ZALF).

**Author Contributions:** Festo Richard Silungwe conceived, designed, and drafted the paper, Frieder Graef and Marcos Alberto Lana revised the design of the paper, contributed to its writing, and provided additional literature, Sonoko Dorothea Bellingrath-Kimura revised the paper and contributed substantially to its writing, Frederick Cassian Kahimba and Siza Donald Tumbo contributed to revision and supplementing text.

**Conflicts of Interest:** The authors declare no conflict of interest.

## References

1. World Food Summit. *World Food Summit in FAO, Volume 1*; World Food Summit: Rome, Italy, 1996; pp. 23–30.
2. Bawadi, H.A.; Tayyem, R.F.; Dwairy, A.N.; Al-Akour, N. Prevalence of Food Insecurity among Women in Northern Jordan. *J. Health Popul. Nutr.* **2012**, *30*, 49–55. [[CrossRef](#)] [[PubMed](#)]
3. Food and Agriculture Organization. *Comprehensive Food Security & Vulnerability Analysis (CFSVA), Tanzania*; FAO: Rome, Italy, 2013.
4. Brown, M.E.; Hintermann, B.; Higgins, N. Markets, Climate Change, and Food Security in West Africa. *Environ. Sci. Technol.* **2009**, *43*, 8016–8020. [[CrossRef](#)] [[PubMed](#)]
5. Haug, R.; Hella, J. The art of balancing food security: Securing availability and affordability of food in Tanzania. *Food Secur.* **2013**, *5*, 415–426. [[CrossRef](#)]

6. Webber, H.; Gaiser, T.; Ewert, F. What role can crop models play in supporting climate change adaptation decisions to enhance food security in Sub-Saharan Africa? *Agric. Syst.* **2014**, *127*, 161–177. [[CrossRef](#)]
7. Hussein, K. Food security: Rights, livelihoods and the World Food Summit—Five years later. *Soc. Policy Adm.* **2002**, *36*, 626–647. [[CrossRef](#)]
8. Paul, K.H.; Muti, M.; Khalfan, S.S.; Humphrey, J.H.; Caffarella, R.; Stoltzfus, R.J. Beyond food insecurity: How context can improve complementary feeding interventions. *Food Nutr. Bull.* **2011**, *32*, 244–253. [[CrossRef](#)] [[PubMed](#)]
9. McCoy, S.I.; Ralph, L.J.; Njau, P.F.; Msolla, M.M.; Padian, N.S. Food Insecurity, Socioeconomic Status, and HIV-Related Risk Behavior among Women in Farming Households in Tanzania. *Aids Behav.* **2014**, *18*, 1224–1236. [[CrossRef](#)] [[PubMed](#)]
10. Asfaw, S.; Shiferaw, B.; Simtowe, F.; Lipper, L. Impact of modern agricultural technologies on smallholder welfare: Evidence from Tanzania and Ethiopia. *Food Policy* **2012**, *37*, 283–295. [[CrossRef](#)]
11. Shiferaw, B.; Kassie, M.; Jaleta, M.; Yirga, C. Adoption of improved wheat varieties and impacts on household food security in Ethiopia. *Food Policy* **2014**, *44*, 272–284. [[CrossRef](#)]
12. Lal, R. Sustainable horticulture and resource management. In *Proceedings of the International Symposium on Sustainability through Integrated and Organic Horticulture*; Prange, R.K., Bishop, S.D., Eds.; International Society for Horticultural Science: Leuven, Belgium, 2008; pp. 19–43.
13. Bakewell-Stone, P.; Lieblein, G.; Francis, C. Potentials for organic agriculture to sustain livelihoods in Tanzania. *Int. J. Agric. Sustain.* **2008**, *6*, 22–36. [[CrossRef](#)]
14. Berry, E.M.; Dermiri, S.; Burlingame, B.; Meybeck, A.; Conforti, P. Food security and sustainability: Can one exist without the other? *Public Health Nutr.* **2015**, *18*, 2293–2302. [[CrossRef](#)] [[PubMed](#)]
15. FAO. *Regional Overview of Food Insecurity: African Food Security Prospects Brighter Than Ever*; FAO: Accra, Ghana, 2015.
16. Baro, M.; Deubel, T.F. Persistent hunger: Perspectives on vulnerability, famine, and food security in Sub-Saharan African. In *Annual Review of Anthropology*; Annual Reviews: Palo Alto, CA, USA, 2006; pp. 521–538.
17. Kassie, B.T.; van Ittersum, M.K.; Hengsdijk, H.; Asseng, S.; Wolf, J.; Rotter, R.P. Climate-induced yield variability and yield gaps of maize (*Zea mays* L.) in the Central Rift Valley of Ethiopia. *Field Crops Res.* **2014**, *160*, 41–53. [[CrossRef](#)]
18. Kassie, M.; Jaleta, M.; Shiferaw, B.; Mmbando, F.; Mekuria, M. Adoption of interrelated sustainable agricultural practices in smallholder systems: Evidence from rural Tanzania. *Technol. Forecast. Soc. Chang.* **2013**, *80*, 525–540. [[CrossRef](#)]
19. Akinyoade, A.; Dietz, T.; Leliveld, A. Agricultural Pockets of Effectiveness in Africa: A Comparative Inventory of Nigeria, Kenya, Tanzania and Uganda since 2000. In *Digging Deeper: Inside Africa's Agricultural, Food and Nutrition Dynamics*; Akinyoade, A., Klaver, W., Soeters, S., Foeken, D., Eds.; Brill: Leiden, The Netherlands, 2014; pp. 55–82.
20. Graef, F.; Schneider, I.; Fasse, A.; Germer, J.U.; Gevorgyan, E.; Haule, F.; Hoffmann, H.; Kahimba, F.C.; Kashaga, L.; Kissoly, L.; et al. Assessment of upgrading strategies to improve regional food systems in Tanzania: Food processing, waste management and bioenergy, and income generation. *Outlook Agric.* **2015**, *44*, 179–186. [[CrossRef](#)]
21. Martinez-Alvarez, V.; Garcia-Bastida, P.A.; Martin-Gorriiz, B.; Soto-Garcia, M. Adaptive strategies of on-farm water management under water supply constraints in south-eastern Spain. *Agric. Water Manag.* **2014**, *136*, 59–67. [[CrossRef](#)]
22. Dile, Y.T.; Karlberg, L.; Daggupati, P.; Srinivasan, R.; Wiberg, D.; Rockstrom, J. Assessing the implications of water harvesting intensification on upstream-downstream ecosystem services: A case study in the Lake Tana basin. *Sci. Total Environ.* **2016**, *542*, 22–35. [[CrossRef](#)] [[PubMed](#)]
23. Wichelns, D.; Qadir, M. Achieving sustainable irrigation requires effective management of salts, soil salinity, and shallow groundwater. *Agric. Water Manag.* **2015**, *157*, 31–38. [[CrossRef](#)]
24. Zhang, B.B.; Feng, G.; Kong, X.B.; Lal, R.; Ouyang, Y.; Adeli, A.; Jenkins, J.N. Simulating yield potential by irrigation and yield gap of rainfed soybean using APEX model in a humid region. *Agric. Water Manag.* **2016**, *177*, 440–453. [[CrossRef](#)]
25. Yan, N.N.; Wu, B.F.; Perry, C.; Zeng, H.W. Assessing potential water savings in agriculture on the Hai Basin plain, China. *Agric. Water Manag.* **2015**, *154*, 11–19. [[CrossRef](#)]

26. Guo, K.; Liu, X.J. Infiltration of meltwater from frozen saline water located on the soil can result in reclamation of a coastal saline soil. *Irrig. Sci.* **2015**, *33*, 441–452. [[CrossRef](#)]
27. Njeru, P.N.M.; Mugwe, J.; Maina, I.; Mucheru-Muna, M.; Mugendi, D.; Lekasi, J.K.; Kimani, S.K.; Miriti, J.; Oeba, V.O.; Esilaba, A.O.; et al. Integrating Farmers and Scientific Methods for Evaluating Climate Change Adaptation Options in Embu County. In *Adapting African Agriculture to Climate Change: Transforming Rural Livelihoods*; Filho, W.L., Esilaba, A.O., Rao, K.P.C., Sridhar, G., Eds.; Springer: Cham, Switzerland, 2015; pp. 185–197.
28. Hunink, J.E.; Contreras, S.; Soto-Garcia, M.; Martin-Gorriz, B.; Martinez-Alvarez, V.; Baille, A. Estimating groundwater use patterns of perennial and seasonal crops in a Mediterranean irrigation scheme, using remote sensing. *Agric. Water Manag.* **2015**, *162*, 47–56. [[CrossRef](#)]
29. Graef, F.; Haigis, J. Spatial and temporal rainfall variability in the Sahel and its effects on farmers' management strategies. *J. Arid Environ.* **2001**, *48*, 221–231. [[CrossRef](#)]
30. Babatolu, J.S.; Akinnubi, R.T. Smallholder Farmers Perception of Climate Change and Variability Impact and Their Adaptation Strategies in the Upper and Lower Niger River Basin Development Authority Areas, Nigeria. *J. Petroleum Environ. Biotechnol.* **2016**, *7*, 279.
31. Kristjansson, P.; Neufeldt, H.; Gassner, A.; Mango, J.; Kyazze, F.B.; Desta, S.; Sayula, G.; Thiede, B.; Forch, W.; Thornton, P.K.; et al. Are food insecure smallholder households making changes in their farming practices? Evidence from East Africa. *Food Secur.* **2012**, *4*, 381–397. [[CrossRef](#)]
32. Lana, M.A.; Eulenstein, F.; Schlindwein, S.; Guevara, E.; Meira, S.; Wurbs, A.; Sieber, S.; Svoboda, N.; Bonatti, M. Regionalization of climate scenarios impacts on maize production and the role of cultivar and planting date as an adaptation strategy. *Reg. Environ. Chang.* **2016**, *16*, 1319–1331. [[CrossRef](#)]
33. Liu, S.; Yang, J.Y.; Zhang, X.Y.; Drury, C.F.; Reynolds, W.D.; Hoogenboom, G. Modelling crop yield, soil water content and soil temperature for a soybean-maize rotation under conventional and conservation tillage systems in Northeast China. *Agric. Water Manag.* **2013**, *123*, 32–44. [[CrossRef](#)]
34. Gautam, S.; Mbonimpa, E.G.; Kumar, S.; Bonta, J.V.; Lal, R. Agricultural Policy Environmental eXtender model simulation of climate change impacts on runoff from a small no-till watershed. *J. Soil Water Conserv.* **2015**, *70*, 101–109. [[CrossRef](#)]
35. Nasim, W.; Ahmad, A.; Beihouchette, H.; Fahad, S.; Hoogenboom, G. Evaluation of the OILCROP-SUN model for sunflower hybrids under different agro-meteorological conditions of Punjab-Pakistan. *Field Crops Res.* **2016**, *188*, 17–30. [[CrossRef](#)]
36. Nasim, W.; Belhouchette, H.; Ahmad, A.; Habib-ur-Rahman, M.; Jabran, K.; Ullah, K.; Fahad, S.; Shakeel, M.; Hoogenboom, G. Modelling climate change impacts and adaptation strategies for sunflower in Pakistan. *Outlook Agric.* **2016**, *45*, 39–45. [[CrossRef](#)]
37. Roost, N.; Cai, X.L.; Turrall, H.; Molden, D.; Cui, Y.L. Adapting to intersectoral transfers in the Zhanghe Irrigation System, China—Part II: Impacts of in-system storage on water balance and productivity. *Agric. Water Manag.* **2008**, *95*, 685–697. [[CrossRef](#)]
38. Samuel, M.P.; Satapathy, K.K. Concerted rainwater harvesting technologies suitable for hilly agro-ecosystems of Northeast India. *Curr. Sci.* **2008**, *95*, 1130–1132.
39. Das, A.; Munda, G.C.; Thakur, N.S.A.; Yadav, R.K.; Ghosh, P.K.; Ngachan, S.V.; Bujarbaruah, K.M.; Lal, B.; Das, S.K.; Mahapatra, B.K.; et al. Rainwater harvesting and integrated development of agri-horti-livestock-cum-pisciculture in high altitudes for livelihood of Tribal farmers. *Indian J. Agric. Sci.* **2014**, *84*, 643–649.
40. Tuppad, P.; Santhi, C.; Wang, X.; Williams, J.R.; Srinivasan, R.; Gowda, P.H. Simulation of conservation practices using the apex model. *Appl. Eng. Agric.* **2010**, *26*, 779–794. [[CrossRef](#)]
41. Zairi, A.; el Amami, H.; Slatni, A.; Pereira, L.S.; Rodrigues, P.N.; Machado, T. Coping with drought: Deficit irrigation strategies for cereals and field horticultural crops in Central Tunisia. In *Tools for Drought Mitigation in Mediterranean Regions*; Rossi, G., Cancelliere, A., Pereira, L.S., Oweis, T., Shatanawi, M., Zairi, A., Eds.; Springer: Dordrecht, The Netherlands, 2003; pp. 181–201.
42. Singh, R.; van Dam, J.C.; Feddes, R.A. Water productivity analysis of irrigated crops in Sirsa district, India. *Agric. Water Manag.* **2006**, *82*, 253–278. [[CrossRef](#)]
43. Koocheki, A.; Seyyedi, S.M.; Eyni, M.J. Irrigation levels and dense planting affect flower yield and phosphorus concentration of saffron corms under semi-arid region of Mashhad, Northeast Iran. *Sci. Hortic.* **2014**, *180*, 147–155. [[CrossRef](#)]

44. Zhou, L.F.; Feng, H.; Zhao, Y.; Qi, Z.J.; Zhang, T.B.; He, J.Q.; Dyck, M. Drip irrigation lateral spacing and mulching affects the wetting pattern, shoot-root regulation, and yield of maize in a sand-layered soil. *Agric. Water Manag.* **2017**, *184*, 114–123. [[CrossRef](#)]
45. Yang, Y.H.; Watanabe, M.; Zhang, X.Y.; Zhang, J.Q.; Wang, Q.X.; Hayashi, S. Optimizing irrigation management for wheat to reduce groundwater depletion in the piedmont region of the Taihang Mountains in the North China Plain. *Agric. Water Manag.* **2006**, *82*, 25–44. [[CrossRef](#)]
46. Fan, Z.B.; Lin, S.; Zhang, X.M.; Jiang, Z.M.; Yang, K.C.; Jian, D.D.; Chen, Y.Z.; Li, J.L.; Chen, Q.; Wang, J.G. Conventional flooding irrigation causes an overuse of nitrogen fertilizer and low nitrogen use efficiency in intensively used solar greenhouse vegetable production. *Agric. Water Manag.* **2014**, *144*, 11–19. [[CrossRef](#)]
47. Meng, W.W.; Yu, Z.W.; Zhang, Y.L.; Shi, Y.; Wang, D. Effects of supplemental irrigation on water consumption characteristics and grain yield in different wheat cultivars. *Chil. J. Agric. Res.* **2015**, *75*, 216–223.
48. Bouraima, A.K.; Zhang, W.H.; Wei, C.F. Irrigation water requirements of rice using Cropwat model in Northern Benin. *Int. J. Agric. Biol. Eng.* **2015**, *8*, 58–64.
49. Wang, Y.J.; Xie, Z.K.; Malhi, S.S.; Vera, C.L.; Zhang, Y.B.; Wang, J.N. Effects of rainfall harvesting and mulching technologies on water use efficiency and crop yield in the semi-arid Loess Plateau, China. *Agric. Water Manag.* **2009**, *96*, 374–382. [[CrossRef](#)]
50. Yeboah, S.; Zhang, R.; Cai, L.; Li, L.; Xie, J.; Luo, Z.; Liu, J.; Wu, J. Tillage effect on soil organic carbon, microbial biomass carbon and crop yield in spring wheat-field pea rotation. *Plant Soil Environ.* **2016**, *62*, 279–285. [[CrossRef](#)]
51. Corbeels, M.; Chirat, G.; Messad, S.; Thierfelder, C. Performance and sensitivity of the DSSAT crop growth model in simulating maize yield under conservation agriculture. *Eur. J. Agron.* **2016**, *76*, 41–53. [[CrossRef](#)]
52. Baudron, F.; Delmotte, S.; Corbeels, M.; Herrera, J.M.; Titttonell, P. Multi-scale trade-off analysis of cereal residue use for livestock feeding vs. soil mulching in the Mid-Zambezi Valley, Zimbabwe. *Agric. Syst.* **2015**, *134*, 97–106. [[CrossRef](#)]
53. Nielsen, D.C.; Vigil, M.F. Intensifying a semi-arid dryland crop rotation by replacing fallow with pea. *Agric. Water Manag.* **2017**, *186*, 127–138. [[CrossRef](#)]
54. Jiang, J.S.; Guo, S.L.; Zhang, Y.J.; Liu, Q.F.; Wang, R.; Wang, Z.Q.; Li, N.N.; Li, R.J. Changes in temperature sensitivity of soil respiration in the phases of a three-year crop rotation system. *Soil Tillage Res.* **2015**, *150*, 139–146. [[CrossRef](#)]
55. Gozubuyuk, Z.; Sahin, U.; Adiguzel, M.C.; Ozturk, I.; Celik, A. The influence of different tillage practices on water content of soil and crop yield in vetch-winter wheat rotation compared to fallow-winter wheat rotation in a high altitude and cool climate. *Agric. Water Manag.* **2015**, *160*, 84–97. [[CrossRef](#)]
56. Fernandez-Getino, A.P.; Santin-Montanya, M.I.; Zambrana, E.; de Andres, E.F.; Tenorio, J.L. The response of barley to rainfall and temperature in different tillage and crop rotation systems in semi-arid conditions. *Ann. Appl. Biol.* **2015**, *166*, 143–153. [[CrossRef](#)]
57. Sarani, M.; Oveysi, M.; Mashhadi, H.R.; Alizade, H.; Gonzalez-Andujar, J.L. Interactions between the tillage system and crop rotation on the crop yield and weed populations under arid conditions. *Weed Biol. Manag.* **2014**, *14*, 198–208. [[CrossRef](#)]
58. Srinivasarao, C.; Venkateswarlu, B.; Lal, R.; Singh, A.K.; Kundu, S.; Vittal, K.P.R.; Ramachandrapa, B.K.; Gajanan, G.N. Long-term effects of crop residues and fertility management on carbon sequestration and agronomic productivity of groundnut-finger millet rotation on an Alfisol in southern India. *Int. J. Agric. Sustain.* **2012**, *10*, 230–244. [[CrossRef](#)]
59. Aulakh, M.S.; Manchanda, J.S.; Garg, A.K.; Kumar, S.; Dercon, G.; Nguyen, M.L. Crop production and nutrient use efficiency of conservation agriculture for soybean-wheat rotation in the Indo-Gangetic Plains of Northwestern India. *Soil Tillage Res.* **2012**, *120*, 50–60. [[CrossRef](#)]
60. Soler, C.M.T.; Bado, V.B.; Traore, K.; Bostick, W.M.; Jones, J.W.; Hoogenboom, G. Soil organic carbon dynamics and crop yield for different crop rotations in a degraded ferruginous tropical soil in a semi-arid region: A simulation approach. *J. Agric. Sci.* **2011**, *149*, 579–593. [[CrossRef](#)] [[PubMed](#)]
61. Gwenzi, W.; Gotosa, J.; Chakanetsa, S.; Mutema, Z. Effects of tillage systems on soil organic carbon dynamics, structural stability and crop yields in irrigated wheat (*Triticum aestivum* L.)-cotton (*Gossypium hirsutum* L.) rotation in semi-arid Zimbabwe. *Nutr. Cycl. Agroecosyst.* **2009**, *83*, 211–221. [[CrossRef](#)]

62. Malley, Z.J.U.; Kayombo, B.; Willcocks, T.J.; Mtakwa, P.W. Ngoro: An indigenous, sustainable and profitable soil, water and nutrient conservation system in Tanzania for sloping land. *Soil Tillage Res.* **2004**, *77*, 47–58. [[CrossRef](#)]
63. Mupangwa, W.; Twomlow, S.; Walker, S. Dead level contours and infiltration pits for risk mitigation in smallholder cropping systems of southern Zimbabwe. *Phys. Chem. Earth* **2012**, *47–48*, 166–172. [[CrossRef](#)]
64. Nyakudya, I.W.; Stroosnijder, L.; Nyagumbo, I. Infiltration and planting pits for improved water management and maize yield in semi-arid Zimbabwe. *Agric. Water Manag.* **2014**, *141*, 30–46. [[CrossRef](#)]
65. Gheysari, M.; Miriatifi, S.M.; Bannayan, M.; Homaae, M.; Hoogenboom, G. Interaction of water and nitrogen on maize grown for silage. *Agric. Water Manag.* **2009**, *96*, 809–821. [[CrossRef](#)]
66. Li, W.L.; Li, W.D.; Li, Z.Z. Irrigation and fertilizer effects on water use and yield of spring wheat in semi-arid regions. *Agric. Water Manag.* **2004**, *67*, 35–46. [[CrossRef](#)]
67. Wen, J.L.; Li, J.S.; Li, Y.F. Response of maize growth and yield to different water and nitrogen schemes on very coarse sandy loam soil under sprinkler irrigation in the semi-arid region of china. *Irrig. Drain.* **2015**, *64*, 619–636. [[CrossRef](#)]
68. Jia, X.C.; Shao, L.J.; Liu, P.; Zhao, B.Q.; Gu, L.M.; Dong, S.T.; Bing, S.H.; Zhang, J.W.; Zhao, B. Effect of different nitrogen and irrigation treatments on yield and nitrate leaching of summer maize (*Zea mays* L.) under lysimeter conditions. *Agric. Water Manag.* **2014**, *137*, 92–103. [[CrossRef](#)]
69. Devkota, K.P.; McDonald, A.J.; Khadka, L.; Khadka, A.; Paudel, G.; Devkota, M. Fertilizers, hybrids, and the sustainable intensification of maize systems in the rainfed mid-hills of Nepal. *Eur. J. Agron.* **2016**, *80*, 154–167. [[CrossRef](#)]
70. Rezaei, E.E.; Gaiser, T.; Siebert, S.; Ewert, F. Adaptation of crop production to climate change by crop substitution. *Mitig. Adapt. Strateg. Glob. Chang.* **2015**, *20*, 1155–1174. [[CrossRef](#)]
71. Biederbeck, V.O.; Janzen, H.H.; Campbell, C.A.; Zentner, R.P. Labile soil organic-matter as influenced by cropping practices in an arid environment. *Soil Biol. Biochem.* **1994**, *26*, 1647–1656. [[CrossRef](#)]
72. Balwinder, S.; Humphreys, E.; Sudhir, Y.; Gaydon, D.S. Options for increasing the productivity of the rice-wheat system of north-west India while reducing groundwater depletion. Part 1. Rice variety duration, sowing date and inclusion of mungbean. *Field Crops Res.* **2015**, *173*, 68–80. [[CrossRef](#)]
73. Jalota, S.K.; Vashisht, B.B. Adapting cropping systems to future climate change scenario in three agro-climatic zones of Punjab, India. *J. Agrometeorol.* **2016**, *18*, 48–56.
74. Folberth, C.; Gaiser, T.; Abbaspour, K.C.; Schulin, R.; Yang, H. Regionalization of a large-scale crop growth model for sub-Saharan Africa: Model setup, evaluation, and estimation of maize yields. *Agric. Ecosyst. Environ.* **2012**, *151*, 21–33. [[CrossRef](#)]
75. Waongo, M.; Laux, P.; Kunstmann, H. Adaptation to climate change: The impacts of optimized planting dates on attainable maize yields under rainfed conditions in Burkina Faso. *Agric. For. Meteorol.* **2015**, *205*, 23–39. [[CrossRef](#)]
76. Nyagumbo, I.; Mkuhlani, S.; Mupangwa, W.; Rodriguez, D. Planting date and yield benefits from conservation agriculture practices across Southern Africa. *Agric. Syst.* **2017**, *150*, 21–33. [[CrossRef](#)]
77. Nyakudya, I.W.; Stroosnijder, L. Effect of rooting depth, plant density and planting date on maize (*Zea mays* L.) yield and water use efficiency in semi-arid Zimbabwe: Modelling with AquaCrop. *Agric. Water Manag.* **2014**, *146*, 280–296. [[CrossRef](#)]
78. Abou-Hadid, A.F. The agro-climate application information system for crop production and protection in Egypt. In *Proceedings of the International Symposium on Mediterranean Horticulture: Issues and Prospects*; Sansavini, S., Janick, J., Eds.; ISHS Acta Horticulturae: Leuven, Belgium, 2002; pp. 41–51.
79. Sarvari, M.; Futo, Z.; Zsoldos, M. Effect of sowing date and plant density on maize yields in 2001. *Novenytermeles* **2002**, *51*, 291–307.
80. Oweis, T.; Hachum, A.; Pala, M. Water use efficiency of winter-sown chickpea under supplemental irrigation in a mediterranean environment. *Agric. Water Manag.* **2004**, *66*, 163–179. [[CrossRef](#)]
81. Yau, S.K.; Nimah, M.; Farran, M. Early sowing and irrigation to increase barley yields and water use efficiency in Mediterranean conditions. *Agric. Water Manag.* **2011**, *98*, 1776–1781. [[CrossRef](#)]
82. Moradi, R.; Koocheki, A.; Mahallati, M.N.; Mansoori, H. Adaptation strategies for maize cultivation under climate change in Iran: Irrigation and planting date management. *Mitig. Adapt. Strateg. Glob. Chang.* **2013**, *18*, 265–284. [[CrossRef](#)]

83. Al Khamisi, S.A.; Prathapar, S.A.; Ahmed, M. Conjunctive use of reclaimed water and groundwater in crop rotations. *Agric. Water Manag.* **2013**, *116*, 228–234. [[CrossRef](#)]
84. Ghamarnia, H.; Farmanifard, M. Yield production and water-use efficiency of wheat (*Triticum aestivum* L.) cultivars under shallow groundwater use in semi-arid region. *Arch. Agron. Soil Sci.* **2014**, *60*, 1677–1700.
85. Wu, Y.; Liu, T.X.; Paredes, P.; Duan, L.M.; Pereira, L.S. Water use by a groundwater dependent maize in a semi-arid region of Inner Mongolia: Evapotranspiration partitioning and capillary rise. *Agric. Water Manag.* **2015**, *152*, 222–232. [[CrossRef](#)]
86. Liu, Z.; Huang, W.C. Drought early warning in irrigation area by integrating surface water and groundwater. *Paddy Water Environ.* **2015**, *13*, 145–157. [[CrossRef](#)]
87. Wu, X.; Zheng, Y.; Wu, B.; Tian, Y.; Han, F.; Zheng, C.M. Optimizing conjunctive use of surface water and groundwater for irrigation to address human-nature water conflicts: A surrogate modeling approach. *Agric. Water Manag.* **2016**, *163*, 380–392. [[CrossRef](#)]
88. Brouwer, J.; Fussell, L.K.; Herrmann, L. Soil and crop growth microvariability in the West-African semiarid tropics—A possible risk-reducing factor for subsistence farmers. *Agric. Ecosyst. Environ.* **1993**, *45*, 229–238. [[CrossRef](#)]
89. Filintas, A.; Dioudis, P.; Prochaska, C. GIS modeling of the impact of drip irrigation, of water quality and of soil's available water capacity on *Zea mays* L. biomass yield and its biofuel potential. *Desalination Water Treat.* **2010**, *13*, 303–319. [[CrossRef](#)]
90. Anzai, T.; Kitamura, Y.; Shimizu, K. The influence of seepage from canals and paddy fields on the groundwater level of neighboring rotation cropping fields: A case study from the lower Ili River Basin, Kazakhstan. *Paddy Water Environ.* **2014**, *12*, 387–392. [[CrossRef](#)]
91. Schmitter, P.; Zwart, S.J.; Danvi, A.; Gbaguidi, F. Contributions of lateral flow and groundwater to the spatio-temporal variation of irrigated rice yields and water productivity in a West-African inland valley. *Agric. Water Manag.* **2015**, *152*, 286–298. [[CrossRef](#)]
92. Bayu, W.; Rethman, N.F.G.; Hammes, P.S. Effects of tied-ridge, nitrogen fertilizer and cultivar on the yield and nitrogen use efficiency of sorghum in semi-arid Ethiopia. *Arch. Agron. Soil Sci.* **2012**, *58*, 547–560. [[CrossRef](#)]
93. Bijanzadeh, E.; Emam, Y. Evaluation of assimilate remobilization and yield of wheat cultivars under different irrigation regimes in an arid climate. *Arch. Agron. Soil Sci.* **2012**, *58*, 1243–1259. [[CrossRef](#)]
94. Haghshenas, A.; Emam, Y.; Ghadiri, H.; Kazemeini, S.A.; Kamgar-Haghighi, A.A. Effect of Mixed Cropping of an Early- and a Middle-ripening Wheat Cultivar on Mitigation of Competition during Post-anthesis Moisture Stress. *J. Agric. Sci. Technol.* **2013**, *15*, 491–503.
95. Meena, L.R.; Meena, S.L. Production potential, nutrient uptake, economics and soil properties as influenced by fodder sorghum (*Sorghum bicolor*) cultivars, nitrogen levels and FYM under semi-arid condition of Rajasthan. *Range Manag. Agrofor.* **2012**, *33*, 171–176.
96. Fan, F.; Spiertz, J.H.J.; Han, L.P.; Liu, Z.X.; Xie, G.H. Sweet sorghum performance under irrigated conditions in north-west China: Biomass and its partitioning in inbred and hybrid cultivars at two nitrogen levels. *Res. Crops* **2013**, *14*, 459–470.
97. Wang, X.L.; Chen, Y.L.; Zhang, S.Q. Cultivar mixture improved yield and water use efficiency via optimization of root properties and biomass distribution in maize (*Zea mays* L.). *Emir. J. Food Agric.* **2017**, *29*, 264–273. [[CrossRef](#)]
98. Patane, C.; Saita, A.; Sortino, O. Comparative Effects of Salt and Water Stress on Seed Germination and Early Embryo Growth in Two Cultivars of Sweet Sorghum. *J. Agron. Crop Sci.* **2013**, *199*, 30–37. [[CrossRef](#)]
99. Perazzo, A.F.; de Carvalho, G.G.P.; Santos, E.M.; Pinho, R.M.A.; Campos, F.S.; Macedo, C.H.O.; Azevedo, J.A.G.; Tabosa, J.N. Agronomic evaluation of 32 sorghum cultivars in the Brazilian semi-arid region. *Rev. Bras. Zootecnia Braz. J. Anim. Sci.* **2014**, *43*, 232–237. [[CrossRef](#)]
100. Mourice, S.K.; Rweyemamu, C.L.; Tumbo, S.D.; Amuri, N. Maize Cultivar Specific Parameters for Decision Support System for Agrotechnology Transfer (DSSAT) Application in Tanzania. *Am. J. Plant Sci.* **2014**, *5*, 821–833. [[CrossRef](#)]
101. Miriti, J.M.; Kironchi, G.; Esilaba, A.O.; Heng, L.K.; Gachene, C.K.K.; Mwangi, D.M. Yield and water use efficiencies of maize and cowpea as affected by tillage and cropping systems in semi-arid Eastern Kenya. *Agric. Water Manag.* **2012**, *115*, 148–155. [[CrossRef](#)]

102. Wright, J.P.; Posner, J.L.; Doll, J.D. The effect of tied ridge cultivation on the yield of maize and a maize cowpea relay in the Gambia. *Exp. Agric.* **1991**, *27*, 269–279. [[CrossRef](#)]
103. Kabanza, A.K.; Rwehumbiza, F.B.R. Assessment of the contribution of tied ridges and farmyard manure application to sorghum production in semi-arid areas of Tanzania. In *Advances in Integrated Soil Fertility Management in Sub-Saharan Africa: Challenges and Opportunities*; Bationo, A., Waswa, B., Kihara, J., Kimetu, J., Eds.; Springer: Dordrecht, The Netherlands, 2007; pp. 723–729.
104. Araya, A.; Stroosnijder, L. Effects of tied ridges and mulch on barley (*Hordeum vulgare*) rainwater use efficiency and production in Northern Ethiopia. *Agric. Water Manag.* **2010**, *97*, 841–847. [[CrossRef](#)]
105. Odunze, A.C.; Mando, A.; Sogbedji, J.; Amapu, I.Y.; Tarfa, B.D.; Yusuf, A.A.; Sunday, A.; Bello, H. Moisture conservation and fertilizer use for sustainable cotton production in the sub-humid Savanna zones of Nigeria. *Arch. Agron. Soil Sci.* **2012**, *58*, S190–S194. [[CrossRef](#)]
106. Saha, S.; Chakraborty, D.; Sharma, A.R.; Tomar, R.K.; Bhadraray, S.; Sen, U.; Behera, U.K.; Purakayastha, T.J.; Garg, R.N.; Kalra, N. Effect of tillage and residue management on soil physical properties and crop productivity in maize (*Zea mays*)-Indian mustard (*Brassica juncea*) system. *Indian J. Agric. Sci.* **2010**, *80*, 679–685.
107. Choudhury, S.G.; Srivastava, S.; Singh, R.; Chaudhari, S.K.; Sharma, D.K.; Singh, S.K.; Sarkar, D. Tillage and residue management effects on soil aggregation, organic carbon dynamics and yield attribute in rice-wheat cropping system under reclaimed sodic soil. *Soil Tillage Res.* **2014**, *136*, 76–83. [[CrossRef](#)]
108. Temesgen, M.; Savenije, H.H.G.; Rockstrom, J.; Hoogmoed, W.B. Assessment of strip tillage systems for maize production in semi-arid Ethiopia: Effects on grain yield, water balance and water productivity. *Phys. Chem. Earth* **2012**, *47–48*, 156–165. [[CrossRef](#)]
109. Verhulst, N.; Sayre, K.D.; Vargas, M.; Crossa, J.; Deckers, J.; Raes, D.; Goyaerts, B. Wheat yield and tillage-straw management system × year interaction explained by climatic co-variables for an irrigated bed planting system in northwestern Mexico. *Field Crops Res.* **2011**, *124*, 347–356. [[CrossRef](#)]
110. Verhulst, N.; Nelissen, V.; Jespers, N.; Haven, H.; Sayre, K.D.; Raes, D.; Deckers, J.; Govaerts, B. Soil water content, maize yield and its stability as affected by tillage and crop residue management in rainfed semi-arid highlands. *Plant Soil* **2011**, *344*, 73–85. [[CrossRef](#)]
111. Malhi, S.S.; Soon, Y.K.; Brandt, S. Effect of growing season rainfall and tillage on the uptake and recovery of (15)N-labelled urea fertilizer by spring wheat in a semi-arid environment. *Can. J. Soil Sci.* **2009**, *89*, 403–411. [[CrossRef](#)]
112. Iqbal, M.; Anwar-Ul-Hassan; Lal, R. Nutrient content of maize and soil organic matter status under various tillage methods and farmyard manure levels. *Acta Agric. Scand. Sect. B Soil Plant Sci.* **2007**, *57*, 349–356.
113. Iqbal, M.; Anwar-Ul-Hassan; Ibrahim, M. Effects of tillage systems and mulch on soil physical quality parameters and maize (*Zea mays* L.) yield in semi-arid Pakistan. *Biol. Agric. Horticult.* **2008**, *25*, 311–325. [[CrossRef](#)]
114. Iqbal, M.; Anwar-Ul-Hassan; van Es, H.M. Influence of Residue Management and Tillage Systems on Carbon Sequestration and Nitrogen, Phosphorus, and Potassium Dynamics of Soil and Plant and Wheat Production in Semi-arid Region. *Commun. Soil Sci. Plant Anal.* **2011**, *42*, 528–547. [[CrossRef](#)]
115. Scopel, E.; da Silva, F.A.M.; Corbeels, M.; Affholder, F.O.; Maraux, F. Modelling crop residue mulching effects on water use and production of maize under semi-arid and humid tropical conditions. *Agronomie* **2004**, *24*, 383–395. [[CrossRef](#)]
116. Mugabe, F.T.; Chitata, T.; Kashaigili, J.; Chagonda, I. Modelling the effect of rainfall variability, land use change and increased reservoir abstraction on surface water resources in semi-arid southern Zimbabwe. *Phys. Chem. Earth* **2011**, *36*, 1025–1032. [[CrossRef](#)]
117. Shao, H.; Baffaut, C.; Gao, J.E.; Nelson, N.O.; Janssen, K.A.; Pierzynski, G.M.; Barnes, P.L. Development and application of algorithms for simulating terraces within swat. *Trans. Asabe* **2013**, *56*, 1715–1730.
118. Biazin, B.; Stroosnijder, L. To tie or not to tie ridges for water conservation in Rift Valley drylands of Ethiopia. *Soil Tillage Res.* **2012**, *124*, 83–94. [[CrossRef](#)]
119. Iqbal, S.; Guber, A.K.; Khan, H.Z. Estimating nitrogen leaching losses after compost application in furrow irrigated soils of Pakistan using HYDRUS-2D software. *Agric. Water Manag.* **2016**, *168*, 85–95. [[CrossRef](#)]

120. Ngugi, L.W.; Rao, K.P.C.; Oyoo, A.; Kwena, K. Opportunities for Coping with Climate Change and Variability through Adoption of Soil and Water Conservation Technologies in Semi-arid Eastern Kenya. In *Adapting African Agriculture to Climate Change: Transforming Rural Livelihoods*; Filho, W.L., Esilaba, A.O., Rao, K.P.C., Sridhar, G., Eds.; Springer: Cham, Switzerland, 2015; pp. 149–157.
121. Shamudzarira, Z.; Robertson, M.J. Simulating response of maize to nitrogen fertilizer in semi-arid Zimbabwe. *Exp. Agric.* **2002**, *38*, 79–96. [[CrossRef](#)]
122. Kisaka, M.O.; Mucheru-Muna, M.; Ngetich, F.K.; Mugwe, J.N.; Mugendi, D.N.; Mairura, F.; Muriuki, J. Using apsim-model as a decision-support-tool for long-term integrated-nitrogen-management and maize productivity under semi-arid conditions in Kenya. *Exp. Agric.* **2016**, *52*, 279–299. [[CrossRef](#)]
123. Ahmed, M.; Aslam, M.A.; Ul, H.F.; Asif, M.; Hayat, R. Use of APSIM to Model Nitrogen Use Efficiency of Rain-fed Wheat. *Int. J. Agric. Biol.* **2014**, *16*, 461–470.
124. Gaiser, T.; de Barros, I.; Lange, F.M.; Williams, J.R. Water use efficiency of a maize/cowpea intercrop on a highly acidic tropical soil as affected by liming and fertilizer application. *Plant Soil* **2004**, *263*, 165–171. [[CrossRef](#)]
125. Azizian, A.; Sepaskhah, A.R.; Zand-Parsa, S. Modification of a maize simulation model under different water, nitrogen and salinity levels. *Int. J. Plant Prod.* **2015**, *9*, 609–632.
126. Anwar, M.R.; Takahashi, S.; Itoh, S.; Nakatsuji, T. Modeling yield and grain protein of Japanese wheat by DSSAT cropping system model. In *Plant Growth Modeling and Applications*; Hu, B.G., Jaeger, M., Eds.; Liama, Chinese Agricultural University: Beijing, China, 2003; pp. 312–320.
127. Jagtap, S.S.; Abamu, F.J. Matching improved maize production technologies to the resource base of farmers in a moist savanna. *Agric. Syst.* **2003**, *76*, 1067–1084. [[CrossRef](#)]
128. Liu, H.L.; Yang, J.Y.; Drury, C.F.; Reynolds, W.D.; Tan, C.S.; Bai, Y.L.; He, P.; Jin, J.; Hoogenboom, G. Using the DSSAT-CERES-Maize model to simulate crop yield and nitrogen cycling in fields under long-term continuous maize production. *Nutr. Cycl. Agroecosyst.* **2011**, *89*, 313–328. [[CrossRef](#)]
129. Gerardeaux, E.; Giner, M.; Ramanantsoanirina, A.; Dusserre, J. Positive effects of climate change on rice in Madagascar. *Agron. Sustain. Dev.* **2012**, *32*, 619–627. [[CrossRef](#)]
130. Jeong, H.; Jang, T.; Seong, C.; Park, S. Assessing nitrogen fertilizer rates and split applications using the DSSAT model for rice irrigated with urban wastewater. *Agric. Water Manag.* **2014**, *141*, 1–9. [[CrossRef](#)]
131. Rezaei, E.E.; Gaiser, T.; Siebert, S.; Sultan, B.; Ewert, F. Combined impacts of climate and nutrient fertilization on yields of pearl millet in Niger. *Eur. J. Agron.* **2014**, *55*, 77–88. [[CrossRef](#)]
132. Abedinpour, M.; Sarangi, A.; Rajput, T.B.S.; Singh, M.; Pathak, H.; Ahmad, T. Performance evaluation of AquaCrop model for maize crop in a semi-arid environment. *Agric. Water Manag.* **2012**, *110*, 55–66. [[CrossRef](#)]
133. Heng, L.K.; Asseng, S.; Mejahed, K.; Rusan, M. Optimizing wheat productivity in two rain-fed environments of the West Asia-North Africa region using a simulation model. *Eur. J. Agron.* **2007**, *26*, 121–129. [[CrossRef](#)]
134. Soltani, A.; Meinke, H.; de Voil, P. Assessing linear interpolation to generate daily radiation and temperature data for use in crop simulations. *Eur. J. Agron.* **2004**, *21*, 133–148. [[CrossRef](#)]
135. Toumi, J.; Er-Raki, S.; Ezzahar, J.; Khabba, S.; Jarlan, L.; Chehbouni, A. Performance assessment of AquaCrop model for estimating evapotranspiration, soil water content and grain yield of winter wheat in Tensift Al Haouz (Morocco): Application to irrigation management. *Agric. Water Manag.* **2016**, *163*, 219–235. [[CrossRef](#)]
136. Abrha, B.; Delbecque, N.; Raes, D.; Tsegay, A.; Todorovic, M.; Heng, L.; Vanutrecht, E.; Geerts, S.; Garcia-Vila, M.; Deckers, S. Sowing strategies for barley (*Hordeum vulgare* L.) Based on modelled yield response to water with aquacrop. *Exp. Agric.* **2012**, *48*, 252–271. [[CrossRef](#)]
137. Alemaw, B.F.; Chaoka, T.R.; Totolo, O. Soil moisture modeling and application in agricultural water management. In *Proceedings of the IASTED International Conference on Environmentally Sound Technology in Water Resources Management: Science and Technology for Development in the 21st Century*; Totolo, O., Ed.; ACTA Press: Calgary, AB, Canada, 2006; pp. 120–125.
138. Hurtado, S.M.C.; Paglis, C.M.; von Pinho, R.G. Ceres-Maize model efficiency in corn yield prediction within spatial variable areas. *Cienc. Agrotecnol.* **2005**, *29*, 1153–1160. [[CrossRef](#)]
139. Al-Bakri, J.; Suleiman, A.; Abdulla, F.; Ayad, J. Potential impact of climate change on rainfed agriculture of a semi-arid basin in Jordan. *Phys. Chem. Earth* **2011**, *36*, 125–134. [[CrossRef](#)]

140. Sandhu, S.S.; Prabhjyot, K.; Tripathi, P.; Patel, S.R.; Prasad, R.; Solanki, N.S.; Kumar, R.; Singh, C.B.; Dubey, A.P.; Rao, V.U.M. Effect of intra-seasonal temperature on wheat at different locations of India: A study using CERES-Wheat model. *J. Agrometeorol.* **2016**, *18*, 222–233.
141. MacCarthy, D.S.; Adiku, S.G.K.; Freduah, B.S.; Gbefo, F.; Kamara, A.Y. Using CERES-Maize and ENSO as Decision Support Tools to Evaluate Climate Sensitive Farm Management Practices for Maize Production in the Northern Regions of Ghana. *Front. Plant Sci.* **2017**, *8*, 31. [[CrossRef](#)] [[PubMed](#)]
142. Bacon, S.A.; Mau, R.; Neto, F.M.; Williams, R.L.; Turner, N.C. Effect of climate warming on maize production in Timor-Leste: Interaction with nitrogen supply. *Crop Pasture Sci.* **2016**, *67*, 156–166.
143. Manfreda, S.; Scanlon, T.M.; Caylor, K.K. On the importance of accurate depiction of infiltration processes on modelled soil moisture and vegetation water stress. *Ecohydrology* **2010**, *3*, 155–165. [[CrossRef](#)]
144. Prucha, B.; Graham, D.; Watson, M.; Avenant, M.; Esterhuysen, S.; Joubert, A.; Kemp, M.; King, J.; le Roux, P.; Redelinghuys, N.; et al. MIKE-SHE integrated groundwater and surface water model used to simulate scenario hydrology for input to DRIFT-ARID: The Mokolo River case study. *Water SA* **2016**, *42*, 384–398. [[CrossRef](#)]
145. White, J.W.; Hoogenboom, G.; Kimball, B.A.; Wall, G.W. Methodologies for simulating impacts of climate change on crop production. *Field Crops Res.* **2011**, *124*, 357–368. [[CrossRef](#)]
146. Critchley, W.; Reij, C.; Seznec, A. *Water Harvesting for Plant Production, Volume II: Case Studies and Conclusions for Sub-Saharan Africa*; World Bank Technical Paper No. 157; Africa Technical Department Series 134; The World Bank: Washington, DC, USA, 1992.
147. Nyamangara, J.; Nyagumbo, I. Interactive effects of selected nutrient resources and tied-ridging on plant growth performance in a semi-arid smallholder farming environment in central Zimbabwe. *Nutr. Cycl. Agroecosyst.* **2010**, *88*, 103–109. [[CrossRef](#)]
148. Patrick, C.; Kechavarzi, C.; James, I.T.; O'Dogherty, M.; Godwin, R.J. Developing reservoir tillage technology for semi-arid environments. *Soil Use Manag.* **2007**, *23*, 185–191. [[CrossRef](#)]
149. Hunink, J.E.; Droogers, P.; Kauffman, S.; Mwaniki, B.M.; Bouma, J. Quantitative simulation tools to analyze up- and downstream interactions of soil and water conservation measures: Supporting policy making in the Green Water Credits program of Kenya. *J. Environ. Manag.* **2012**, *111*, 187–194. [[CrossRef](#)] [[PubMed](#)]
150. Biazin, B.; Sterk, G.; Temesgen, M. Participatory Planning of Appropriate Rainwater Harvesting and Management Techniques in the Central Rift Valley Dry Lands of Ethiopia. *Environ. Nat. Resour. Res.* **2014**, *4*. [[CrossRef](#)]
151. Twomlow, S.; Rohrbach, D.; Dimes, J.; Rusike, J.; Mupangwa, W.; Ncube, B.; Hove, L.; Moyo, M.; Mashingaidze, N.; Mahposa, P. Micro-dosing as a pathway to Africa's Green Revolution: Evidence from broad-scale on-farm trials. *Nutr. Cycl. Agroecosyst.* **2010**, *88*, 3–15. [[CrossRef](#)]
152. Sankar, G.R.M.; Sharma, K.L.; Dhanapal, G.N.; Shankar, M.A.; Mishra, P.K.; Venkateswarlu, B.; Grace, J.K. Influence of Soil and Fertilizer Nutrients on Sustainability of Rainfed Finger Millet Yield and Soil Fertility in Semi-arid Alfisols. *Commun. Soil Sci. Plant Anal.* **2011**, *42*, 1462–1483. [[CrossRef](#)]
153. Tan, Z.X.; Lal, R.; Wiebe, K.D. Global soil nutrient depletion and yield reduction. *J. Sustain. Agric.* **2005**, *26*, 123–146. [[CrossRef](#)]
154. Wickama, J.; Okoba, B.; Sterk, G. Effectiveness of sustainable land management measures in West Usambara highlands, Tanzania. *Catena* **2014**, *118*, 91–102. [[CrossRef](#)]
155. Gessesse, B.; Bewket, W.; Brauning, A. Model-Based Characterization and Monitoring of Runoff and Soil Erosion in Response to Land Use/Land Cover Changes in the Modjo Watershed, Ethiopia. *Land Degrad. Dev.* **2015**, *26*, 711–724. [[CrossRef](#)]
156. Bationo, A.; Mokwunye, A.U. Alleviating soil fertility constraints to increased crop production in West Africa—The experience in the Sahel. *Fertil. Res.* **1991**, *29*, 95–115. [[CrossRef](#)]
157. Mashingaidze, N.; Belder, P.; Twomlow, S.; Hove, L.; Moyo, M. Improving maize (*Zea mays* L.) performance in semi-arid zimbabwe through micro-dosing with ammonium nitrate tablets. *Exp. Agric.* **2013**, *49*, 179–196. [[CrossRef](#)]
158. Ibrahim, A.; Abaidoo, R.C.; Fatondji, D.; Opoku, A. Integrated use of fertilizer micro-dosing and *Acacia tumida* mulching increases millet yield and water use efficiency in Sahelian semi-arid environment. *Nutr. Cycl. Agroecosyst.* **2015**, *103*, 375–388. [[CrossRef](#)]

159. Ibahim, A.; Pasternak, D.; Fatondji, D. Impact of depth of placement of mineral fertilizer micro-dosing on growth, yield and partial nutrient balance in pearl millet cropping system in the Sahel. *J. Agric. Sci.* **2015**, *153*, 1412–1421. [[CrossRef](#)]
160. Ibrahim, A.L.I.; Abaidoo, R.C.; Fatondji, D.; Opoku, A. Determinants of Fertilizer Microdosing-Induced Yield Increment of Pearl Millet on an Acid Sandy Soil. *Exp. Agric.* **2015**, *52*, 562–578. [[CrossRef](#)]
161. ICRISAT. *Fertilizer-Microdosing: Boosting Production in Unproductive Lands*; Institute for Semi-Arid Tropics: Patancheru, India, 2009.
162. Biielders, C.L.; Gerard, B. Millet response to microdose fertilization in south-western Niger: Effect of antecedent fertility management and environmental factors. *Field Crops Res.* **2015**, *171*, 165–175. [[CrossRef](#)]
163. Lamers, J.P.A.; Bruentrup, M.; Buerkert, A. Financial performance of fertilization strategies for sustainable soil fertility management in Sudano-Sahelian West Africa. 2: Profitability of long-term capital investments in rockphosphate. *Nutr. Cycl. Agroecosyst.* **2015**, *102*, 149–165. [[CrossRef](#)]
164. Bagayoko, M.; Maman, N.; Palé, S.; Sirifi, S.; Taonda, S.J.B.; Traore, S.; Mason, S.C. Microdose and N and P fertilizer application rates for pearl millet in West Africa. *Afr. J. Agric. Res.* **2011**, *6*, 1141–1150.
165. Kijazi, A.L.; Reason, C.J.C. Analysis of the 1998 to 2005 drought over the northeastern highlands of Tanzania. *Clim. Res.* **2009**, *38*, 209–223. [[CrossRef](#)]
166. Flaounas, E.; Bastin, S.; Janicot, S. Regional climate modelling of the 2006 West African monsoon: Sensitivity to convection and planetary boundary layer parameterisation using WRF. *Clim. Dyn.* **2011**, *36*, 1083–1105. [[CrossRef](#)]
167. Recha, C.W.; Makokha, G.L.; Traore, P.S.; Shisanya, C.; Lodoun, T.; Sako, A. Determination of seasonal rainfall variability, onset and cessation in semi-arid Tharaka district, Kenya. *Theor. Appl. Climatol.* **2012**, *108*, 479–494. [[CrossRef](#)]
168. Sacks, W.J.; Deryng, D.; Foley, J.A.; Ramankutty, N. Crop planting dates: An analysis of global patterns. *Glob. Ecol. Biogeogr.* **2010**, *19*, 607–620. [[CrossRef](#)]
169. Nasim, W.; Ahmad, A.; Wajid, S.A.; Usman, M.; Hussain, A.; Khaliq, T.; Sultana, S.R.; Muddasir, M.A.; Ahmad, S. Modeling the Effect of Climate Change on Sowing Dates, Yield and Yield Components in Various Wheat Cultivars under Different Agro-ecological Zones of Punjab-Pakistan. In *Progress in Environmental Science and Technology, Vol. II, Parts A and B*; Li, S.C., Wang, Y.J., Cao, F.X., Huang, P., Zhang, Y., Eds.; Science Press, Cop.: Beijing, China, 2009; pp. 69–74.
170. Kalita, H.; Bora, P.C.; Debnath, M.C. Effect of sowing date and tillage on soil properties, nutrient uptake and yield of linseed (*Linum usitatissimum*) grown in winter rice (*Oryza sativa*)-fallow. *Indian J. Agron.* **2005**, *50*, 70–72.
171. Bashir, M.U.; Akbar, N.; Iqbal, A.; Zaman, H. Effect of different sowing dates on yield and yield components of direct seeded coarse rice (*Oryza sativa* L.). *Pak. J. Agric. Sci.* **2010**, *47*, 361–365.
172. Futo, Z.; Sarvari, M. Effect of sowing date on the yield of maize (*Zea mays* L.) in different years. *Novenytermeles* **2003**, *52*, 543–558.
173. Yamusa, A.M.; Abubakar, I.U.; Falaki, A.M. Rainfall Variability and Crop Production in the Northern-Western Semi-arid Zone of Nigeria. *J. Soil Sci. Environ. Manag.* **2015**, *6*, 125–131.
174. Almodares, A.; Darany, S.M.M. Effects of planting date and time of nitrogen application on yield and sugar content of sweet sorghum. *J. Environ. Biol.* **2006**, *27*, 601–605. [[PubMed](#)]
175. Teetor, V.H.; Duclos, D.V.; Wittenberg, E.T.; Young, K.M.; Chawhuaymak, J.; Riley, M.R.; Ray, D.T. Effects of planting date on sugar and ethanol yield of sweet sorghum grown in Arizona. *Ind. Crops Prod.* **2011**, *34*, 1293–1300. [[CrossRef](#)]
176. Nafchi, M.A.M.; Golparvar, A.R. Effect of planting dates on protein percentage and yield components of sorghum cultivars grown in Isfahan province of Iran. *Res. Crops* **2012**, *13*, 1023–1025.
177. Akossou, A.Y.J.; Attakpa, E.Y.; Fonton, N.H.; Sinsin, B.; Bosma, R.H. Spatial and temporal analysis of maize (*Zea mays*) crop yields in Benin from 1987 to 2007. *Agric. For. Meteorol.* **2016**, *220*, 177–189. [[CrossRef](#)]
178. Rowe, E.C.; van Wijk, M.T.; de Ridder, N.; Giller, K.E. Nutrient allocation strategies across a simplified heterogeneous African smallholder farm. *Agric. Ecosyst. Environ.* **2006**, *116*, 60–71. [[CrossRef](#)]
179. Jones, J.W.; Keating, B.A.; Porter, C.H. Approaches to modular model development. *Agric. Syst.* **2001**, *70*, 421–443. [[CrossRef](#)]

180. Ahmed, M.; Akram, M.N.; Asim, M.; Aslam, M.; Hassan, F.U.; Higgins, S.; Stockle, C.O.; Hoogenboom, G. Calibration and validation of APSIM-Wheat and CERES-Wheat for spring wheat under rainfed conditions: Models evaluation and application. *Comput. Electron. Agric.* **2016**, *123*, 384–401. [[CrossRef](#)]
181. Brilli, L.; Bechini, L.; Bindi, M.; Carozzi, M.; Cavalli, D.; Conant, R.; Dorich, C.D.; Doro, L.; Ehrhardt, F.; Farina, R.; et al. Review and analysis of strengths and weaknesses of agro-ecosystem models for simulating C and N fluxes. *Sci. Total Environ.* **2017**, *598*, 445–470. [[CrossRef](#)] [[PubMed](#)]
182. Keating, B.A.; Carberry, P.S.; Hammer, G.L.; Probert, M.E.; Robertson, M.J.; Holzworth, D.; Huth, N.L.; Hargreaves, J.N.G.; Meinke, H.; Hochman, Z.; et al. An overview of APSIM, a model designed for farming systems simulation. *Eur. J. Agron.* **2003**, *18*, 267–288. [[CrossRef](#)]
183. Steduto, P.; Hsiao, T.C.; Raes, D.; Fereres, E. AquaCrop-The FAO Crop Model to Simulate Yield Response to Water: I. Concepts and Underlying Principles. *Agron. J.* **2009**, *101*, 426–437. [[CrossRef](#)]
184. Hsiao, T.C.; Heng, L.; Steduto, P.; Rojas-Lara, B.; Raes, D.; Fereres, E. AquaCrop-The FAO Crop Model to Simulate Yield Response to Water: III. Parameterization and Testing for Maize. *Agron. J.* **2009**, *101*, 448–459. [[CrossRef](#)]
185. Raes, D.; Steduto, P.; Hsiao, T.C.; Fereres, E. AquaCrop-The FAO Crop Model to Simulate Yield Response to Water: II. Main Algorithms and Software Description. *Agron. J.* **2009**, *101*, 438–447. [[CrossRef](#)]
186. Araya, A.; Habtu, S.; Hadgu, K.M.; Kebede, A.; Dejene, T. Test of AquaCrop model in simulating biomass and yield of water deficient and irrigated barley (*Hordeum vulgare*). *Agric. Water Manag.* **2010**, *97*, 1838–1846. [[CrossRef](#)]
187. Wellens, J.; Raes, D.; Traore, F.; Denis, A.; Djaby, B.; Tychon, B. Performance assessment of the FAO AquaCrop model for irrigated cabbage on farmer plots in a semi-arid environment. *Agric. Water Manag.* **2013**, *127*, 40–47. [[CrossRef](#)]



© 2018 by the authors. Licensee MDPI, Basel, Switzerland. This article is an open access article distributed under the terms and conditions of the Creative Commons Attribution (CC BY) license (<http://creativecommons.org/licenses/by/4.0/>).

Article

# Do As They Did: Peer Effects Explain Adoption of Conservation Agriculture in Malawi

Andrew Reid Bell <sup>1,\*</sup>, Jennifer Zavaleta Cheek <sup>2</sup>, Frazer Mataya <sup>3</sup> and Patrick S. Ward <sup>4</sup>

<sup>1</sup> Department of Environmental Studies, New York University, New York, NY 10003, USA

<sup>2</sup> School of Environment and Sustainability, University of Michigan, Ann Arbor, MI 48109, USA; zavaleta@umich.edu

<sup>3</sup> National Smallholder Farmers' Association of Malawi, Lilongwe 3, Malawi; fmataya@nasfam.org

<sup>4</sup> International Food Policy Research Institute, Washington, DC 20006, USA; p.ward@cgiar.org

\* Correspondence: ab6176@nyu.edu; Tel.: +1-212-998-8899

Received: 7 October 2017; Accepted: 17 November 2017; Published: 10 January 2018

**Abstract:** Adoption of the trinity of practices known commonly today as conservation agriculture (CA)—maintaining soil cover, reducing tillage, and enhancing soil nitrogen through legumes—is a critical process to the management of erosion in rural landscapes, and maintenance of aquatic habitats and hydropower potential. However, the large literature on the benefits and risks of CA fails to find any universal determinants of adoption, with competing uses for crop residues, availability of labor, and access to physical inputs common constraints appearing in different contexts. We conduct a study in the specific context of Malawi, using ethnographic interviewing to draw out possible decision criteria and machine learning to identify their explanatory power. This study is structured to inform the question: “How do farmers decide to adopt the specific activities of CA in Malawi?” We find that more than any other factor, adoption by neighbors (i.e., peer effects) matters, with possible implications for the overall cost of encouraging CA (e.g., through subsidies) as it is taken up across a landscape. Further, we note that little else within our household survey (save for more detailed articulation of neighbor and neighborhood characteristics) offers greater explanatory power than those factors identified by farmers themselves. Finally, we note that decisions made in the presence of an incentive are structurally different than those made without incentives, validating previous concerns in the literature regarding the basis most CA adoption studies, within CA promotion interventions.

**Keywords:** Malawi; conservation agriculture; peer effects; decision tree modeling

## 1. Introduction

Careful management of erosion is critical to maintaining aquatic habitat and long-term hydropower potential in the Shire River Basin of Malawi [1]. As a means to reduce sediment loads to the Shire Basin system, the Government of Malawi encourages adoption of conservation agriculture (CA), a trinity of agricultural practices that, while taking various forms across the globe [2], generally encourages farmers to avoid tilling soil, to keep soil covered with mulch or cover crops, and to introduce a (usually nitrogen-fixing) intercrop or rotation. In Malawi, CA is written into the country's Agricultural Sector Wide Approach (ASWAp) as (i) crop residue mulching (CR); (ii) zero tillage (ZT); and (iii) legume intercropping or rotation (IC) [3]. Several different approaches to financing incentives for CA adoption are under design and evaluation in Malawi, including the UNDP's Green Water Credit Scheme [4] and a private trust for promoting CA in riparian micro-catchments developed by the MCC [5]. The role of CA in reducing sediment loading to surface waters is fairly well characterized in the literature at around 65% [6,7], but the calculus of adoption for households (e.g., constraints and net benefits) is much murkier, highlighting the need for context-specific assessments. In the current

study we present a method for allowing farmers themselves to provide key criteria in their decisions to adopt or not, and evaluate the importance of these criteria in a large-*n* study.

Examination of the factors shaping uptake and diffusion of CA, which is acknowledged across Southern Africa to be generally low overall [8], is an area of active research [9–12]. So far, the findings can be well described as “mixed”; in the words of one research group reviewing this literature, “There are few if any universal variables that regularly explain the adoption of conservation agriculture” [13]. Giller (2009) notes, for example, that in many contexts, competing uses for crop residues, availability of labor, and access to physical inputs can restrict adoption of CA [14]. Pannell (2014) notes crop residues as well, pointing additionally to short-term yield gaps and farmers’ general aversion to uncertainty [15]. Although researchers frequently point to the competing uses for crop residues (e.g., animal fodder) as a constraint to the diffusion of CA [16,17], it is also observed that—for Malawi in particular—the low density of grazers makes this less likely to be a constraint [17]. Summarizing the challenge of understanding and encouraging CA adoption, we suggest that various factors including costs, agronomic knowledge, and production risks in the early stages of CA adoption discourage farmers from sustained adoption of CA, misaligning their actions with the longer-term needs of their communities.

Andersson and D’Souza (2014) note that many of the studies within this literature are conducted in the context of an intervention promoting CA, so their results are largely limited to revealing “general characteristics of CA (component) adopters, rather than revealing farmers’ resource allocation strategies that underpin adoption and non-adoption” [17]. The present study also examines CA from within the context of an intervention promoting CA, and it also employs tools to compare decision-making across both our treatment and control groups in order to look more closely at the structure of CA adoption decisions and how they are shaped by the presence of incentives. That is, our study design allows us to look at whether incentives re-organize decision-making in a meaningful way, such that different factors matter, which might offer some explanation as to why there is little clear consistency across different contexts in terms of which factors shape adoption.

Specifically, we draw from the ethnographic decision tree modeling (EDTM) work pioneered by Christina Gladwin (in Malawi, largely) in the 1980s and conduct interviews in which key points in respondents’ decision processes (specifically those pertaining to farmers’ decisions to adopt each of the three constituent practices of CA) are identified and articulated, and subsequently applied to construct classification trees whose terminal nodes best classify the order of factors that affect the decision taken by participants [18]. This technique has enjoyed continued use through recent decades with continued application to agricultural decisions, such as farm planning [19] and weed management [20], as well as in other contexts, such as counselling psychology [21]. By asking farmers directly about how they make decisions, as compared to traditional models where researchers provide potentially relevant variables *a priori* as is the case in household surveys, we are better able to capture and characterize the issues that matter most to farmers. Our study contributes and expands this methodology by combining ethnographic methods with machine learning, which can more efficiently determine decision trees and discover complex structures that were not specified in advance [22]. Bootstrap aggregating (or bagging) is a popular ensemble learning method for statistical classification. Compared with other meta-algorithms for data classification, bagging has been shown to be a stable, accurate, and easy-to-implement algorithm for data classification [23]. Bagging generates multiple versions of a predictor and then uses model averaging to arrive at an aggregated predictor. In our study, we depart from the typical small-*n* approach to building trees by re-applying our identified key decision criteria in a large-*n* endline survey. This allows us (i) to make use of machine learning tools (specifically the random forest and bootstrap aggregation algorithms) to identify structure in farmer decision-making; (ii) to examine the explanatory power of farmer-identified factors for the adoption of CA alongside that of other sets of variables commonly solicited in a household survey; and (iii) to compare differences in decision structure across groups who have (treatment) and have not (control) been offered incentives to adopt CA.

This study is structured to inform the question: “How do farmers decide to adopt the specific activities of CA?” Within this broader question, we also wish to understand how decisions to adopt each of the different practices may differ, and how these decisions may differ in the presence of an incentive, with the goal of informing the behavioral response side of potential soil and water conservation programs. Through our novel integration of ethnography and machine learning, we find that more than any other factor, adoption by neighbors (i.e., peer effects) matters, with possible implications for the overall cost of encouraging CA (e.g., through subsidies) as it is taken up across a landscape. Further, we note that little else within our household survey (save for more detailed articulation of neighbor and neighborhood characteristics) offers greater explanatory power than those factors identified by farmers themselves. Finally, we note that decisions made in the presence of an incentive are structurally different than those made without incentives, validating previous concerns in the literature regarding the basis most CA adoption studies, within CA promotion interventions.

## 2. Materials and Methods

Our primary data collection occurred via two activities within a larger project evaluating the impact of different incentive structures [24] on the adoption of the three practices of conservation agriculture in the Shire River Basin, Malawi. This larger project includes a random sample of 63 villages selected from the pooled sampling frame of the 5 extension planning areas (EPAs) riparian to the upper Shire River Basin, including Balaka and Machinga districts and a portion of Zomba district (Figure 1). The work presented in the current paper does not draw on distinctions across treatments, and rather focuses on the aggregate effect of having been offered an incentive or not, but the interested reader is directed to [25] or to Appendix A for further details on project design. The two activities whose data we draw on in the current study include a small-n ethnographic exercise ( $n = 96$  respondents) conducted in a selection of project villages between the end of the intervention and the endline study, as well as a survey module within the project’s endline study ( $n = 1923$  respondents).

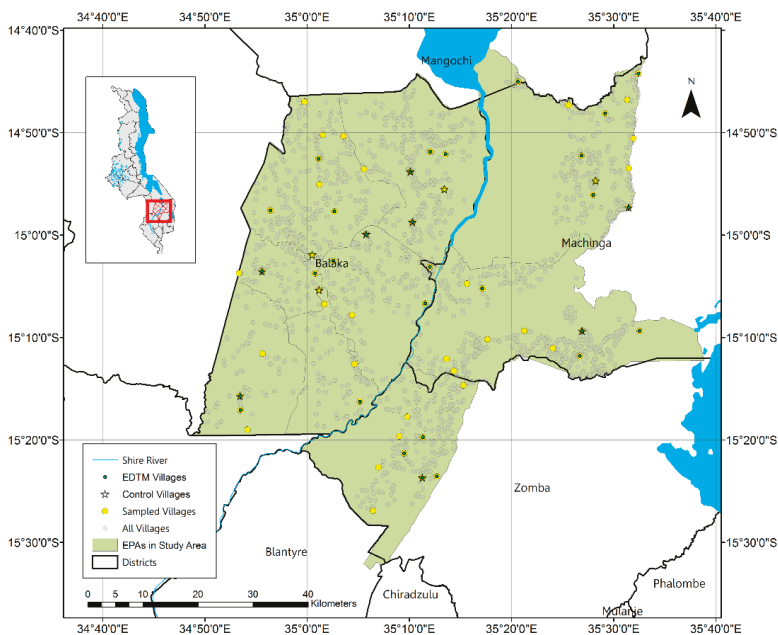


Figure 1. Study Area.

The ethnographic exercise drew a clustered, quota sample of participants from within the larger project's sample. Specifically, we visited a random selection of 8 of the 12 control villages and 24 of the 48 treatment villages, and in each village identified three participants for interviews: one who was practicing intercropping/rotation (irrespective of whether they also practiced zero tillage or mulching); one who was practicing zero tillage or mulching (irrespective of whether they practiced intercropping/rotation); and one participant who was practicing none of these three CA practices. Following the method of ethnographic decision tree modeling (EDTM) of [18], our team of interviewers from the National Smallholder Farmers' Association of Malawi (NASFAM) conducted face-to-face interviews with 96 participants to probe for key factors shaping the decision whether to adopt the three constituent practices of CA. Coding of the interviews yielded 26 unique criteria from across the set of interviews (summarized in our results section as Table 1). In the traditional EDTM espoused by [18], these decision criteria would be used to manually construct decision trees that could then be quantitatively analyzed to assess the predictive accuracy of the decision tree. In our analysis, we departed from Gladwin's method in two distinct ways. First, rather than construct decision trees from this relatively small sample of 96 interviews, we instead leveraged the knowledge gleaned from these interviews to design a household survey module (consisting of a series of binary response items) to be included in the larger project's endline survey ( $n = 1923$  respondents). Additionally, for each item we added a follow-up question that asked explicitly whether the respondent believed that factor had shaped their choice to adopt or not any of the three CA practices. Second, rather than constructing the decision trees manually based on the ethnographic interviews, we applied machine learning tools to this large- $n$  dataset (from the endline survey) to identify structure in farmers' decision-making using decision trees (and forests) as described below.

We used the TreeBagger package in Matlab's Machine Learning Toolbox to train a "forest" of 100 classification trees to predict farmers' adoption of each of the three CA practices using data from the EDTM module, separately for both (i) responses from respondents in control villages (hereafter, "control") and (ii) responses from respondents in treatment villages (hereafter, "treatment"). Each forest is generated using 10-fold cross validation, meaning that the available data are sliced into 10 parts, with a part excluded from a set of trees trained on the remaining nine parts, and repeated 10 times. The trained trees are then validated on the excluded part, generating an estimate of "out of bag" (OOB) prediction error. TreeBagger also generates an estimate of predictor importance, by estimating the relative OOB prediction error when individual predictors are excluded from the trees. To compare the predictive capacity of the EDTM module with that of other survey modules common to household surveys, we incorporated other modules from the endline survey (treatment characteristics, household characteristics, neighborhood characteristics, farm characteristics, and risk perceptions; a list of included items as well as our complete Android ODK protocol is attached as supplementary information) and repeated the above TreeBagger exercise, giving us estimates of predictor importance as well as average prediction error for forests of trees (and predictors within them) built from pooling the EDTM module with these additional modules.

Following this exercise, we selected "best fit" trees for each case by identifying the tree structure that minimized OOB prediction error, using the `fitcree.m` and `cvloss.m` functions in the Machine Learning Toolbox and following Matlab's "Classification" example [26]. There are several options for selecting a best fit, with MathWorks suggesting both (i) choosing the tree that gives an absolute minimum in prediction error (without considering tree complexity) and (ii) finding an optimum that identifies the simplest tree structure whose OOB prediction error is within one standard error of the absolute minimum; we select the latter approach for selecting trees.

**Table 1.** Survey items in EDTM Module identified from ethnographic interviews, including authors’ tags for categorization and counts of online respondents perceiving an influence on the decision to adopt intercropping (IC), zero tillage (ZT), or crop residue mulching (CR). Items were tagged as relating to any of the categories physical environment, climate, social, economic, risk, and governance; and then sorted per their memberships in those categories, in that order.

Names	Survey Item	Physical Env	Climate	Social	Economic	Risk	Governance	IC	ZT	CR
‘soil erosion’	Do you consider the levels of soil erosion your soils undergo to be problematic?	x	x			x		22	123	75
‘soil moisture’	Do you consider the moisture levels of your soils to be problematic?	x	x					24	74	206
‘weed growth’	Do you consider the level of weed growth on your plots to be problematic?	x	x					20	219	251
‘hard pans’	Would you say that you have hard pans in the soils of any of your plots?	x	x					10	164	67
‘crop residues’	Do you feel that you have sufficient crop residues that you would be willing to use as mulch in your plots?	x			x			27	18	831
‘enough land’	Do you feel that you have an amount of land for which CA would be valuable?	x			x			100	29	52
‘animal pests’	Do you feel that any of your plots are at risk of damage from animal pests?	x				x		118	17	87
‘insect pests’	Do you feel that any of your plots are at risk of damage from insect pests?	x				x		149	25	217
‘waterlogging’	Do you feel that any of your plots are at risk of damage from waterlogging?	x				x		7	111	153
‘crop failure concern’	Are you concerned about failure of any one of your crops?		x		x	x		469	45	46
‘rainfall’	During [this past season/the season before this one], would you describe the rainfall as having been below average, average, or above average? **		x			x		81	61	98
‘planting’	Were you able to plant your crops [last year/the year before last year] at the time you wanted to? **		x			x		173	33	30
‘household labor’	Would you say that your household could handle the labor requirements of CA?		x		x			46	36	226
‘vandalism’	Do you feel that your plots are at risk of vandalism (i.e., arson, theft)?			x		x		63	17	109
‘neighbors CA’	Do any of your neighbors practice CA?			x				36	49	58
‘community position’	Do you feel that your position in the community makes it important for you to practice CA, to NOT practice CA, or does it not matter?			x				16	27	27
‘CA incentive’	Have you been offered incentives to adopt CA?				x		x	36	15	33
‘crops for own’	Do you feel that you would want to grow more crops for your own consumption on the same amount of land?				x			661	19	37
‘crops for sale’	Do you feel that you would want to grow more crops for sale on the same amount of land?				x			623	20	37
‘market for crops’	Do you feel that you could sell more crops profitably, if you wanted to?				x			540	16	29
‘can buy fertilizer’	Are you able to purchase fertilizer for your crops?				x			90	15	80
‘can buy herbicide’	Are you able to purchase herbicides for your crops?				x			32	187	110
‘willing to try new’	Do you feel that you are willing and able to try new or different practices?					x		26	56	69
‘extension CA’	Have you been able to learn about CA from extension agents or lead farmers?						x	40	21	50

Note: \*\* These items were asked for each of the last two seasons, as two separate items.

### 3. Results

#### 3.1. Key Decision Criteria and Perceived Relevance

We identified 26 different criteria from our ethnographic interviews that farmers mentioned as shaping their decisions to adopt any of the agricultural practices within CA; these are summarized in Table 1 in the question form through which they were verified in return interviews and included in our endline survey. These criteria span a range of different factors, and we have tagged them (for organization and visualization only) based on our judgments as belonging to social, physical environment, climatic, economic, risk perception, and governance themes. In-depth descriptions of these criteria, along with supporting quotations from ethnographic interviews, are included as Appendix B.

We asked respondents in our endline survey about each of the 26 decision criteria (Table 1), and whether they felt that particular criteria influenced their decisions regarding each of the three CA practices individually. The endline survey encompassed 1923 respondents, in which 1669 (87 percent) respondents reported practicing intercropping, 961 (50 percent) reported practicing crop residue mulching, and 750 (39 percent) reported practicing zero tillage; 535 (28 percent) respondents reported practicing all three. In general, respondents reported that the choice to intercrop was based on economic motivations such as improving yields or reducing the risk of food insecurity (in the case of intercropping) or economic constraints such as the limited availability of inputs (in the case of mulching residues and practicing zero tillage). In addition to these economic factors, the decision(s) to mulch crop residues and practice zero tillage were also influenced by the environmental conditions of their agricultural land (Table 1).

Specifically, farmers identified that their decision of whether to intercrop was based on their perception that they would have more crops to consume (661) or to sell (623), indicating that people intercrop because they think it will increase their total output. Similarly, whether there was a market for the crop was an identified decision criterion (540). In addition to market forces, farmers were influenced to do intercropping in order to mitigate risks to yields like crop failure (469), planting delays (173), and concerns of pests whether insect (149) or other animals (118).

Farmers most often explained their choice of whether to retain crop residues in terms of the inputs required like sufficient access to crop residues (831) and sufficient labor to apply them (226). They also explained that they were influenced by the competing benefits and drawbacks of crop residue application. Farmers may be influenced to adopt crop residues because they are concerned with weed growth (251), which can be stifled with crop residue application and of soil moisture (206). However, they also may be discouraged from adopting it since they are concerned with increased insect pests (217), which may increase when residues are transferred across fields.

Farmers indicated that their choice to adopt zero tillage was influenced (either positively or negatively) by the conditions of their plots like if they had soil erosion problems (123), waterlogging issues (111), which are associated with hard pans (164)—a condition of the soil that makes it compact and more difficult for plant roots to establish. Farmers were also influenced by their concern of weed growth (219) and if they could buy herbicide (187) to address it.

In sum, across our ethnographic surveys and in the perceptions reported by respondents in our endline survey, different factors shape decisions for the different CA practices. In particular, farmers link the decision to intercrop most commonly with crop performance and market opportunities, while they link the decisions for zero tillage and crop residue mulching more commonly with physical constraints such as access to residues, labor constraints, and weed issues. Our next analyses draw on machine learning tools to examine whether these same reported factors also help to predict adoption within our sample.

#### 3.2. Random Forest Results

We analyzed “forests” of classification trees trained on the dataset of adoption decisions and the 26 criteria from Table 1, and found that the variables that explain the most variation in farmers’ choices

to adopt were different than what farmers self-reported (Figures 2 and 3). Additionally, the factors that influenced farmers’ decisions to adopt intercropping were different between control and treatment groups. However, the decision criteria for applying crop residues and zero tillage were similar for each activity and between treatment and control groups.

In ensemble predictions for the control samples, the choice to intercrop was driven by a number of variables, but the top decision criterion was concern about soil erosion (Figure 2), along with the perception that there would be a market and the ability to sell the leguminous crop, or that they could be consumed by the household. The choice to do intercropping within the treatment group was also driven by market factors, as well as concerns about pests, and the ability to purchase herbicides.

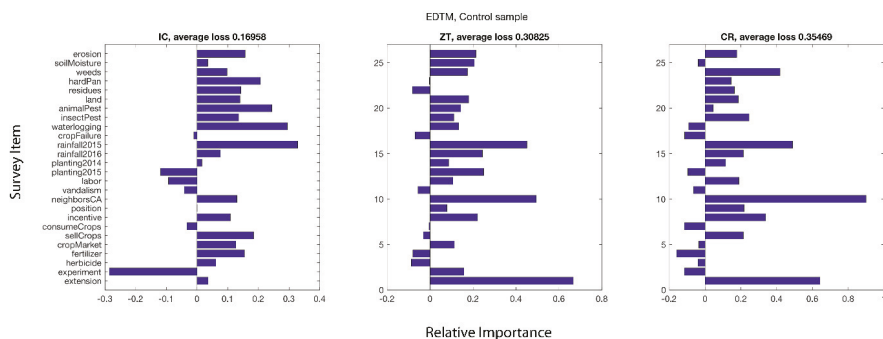


**Figure 2.** Relative variable importance in predicting intercropping (IC), zero tillage (ZT), or crop residue mulching (CR) within the Control sample from the EDTM module, based on change in OOB prediction error across a forest of trained classification trees. Variables ordered as in Table 1.

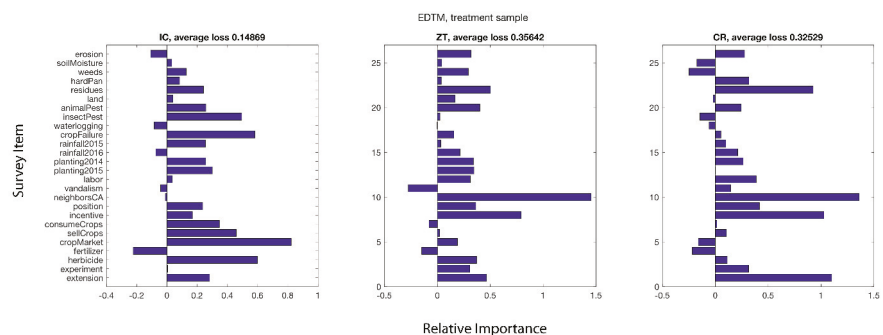


**Figure 3.** Relative variable importance in predicting intercropping (IC), zero tillage (ZT), or crop residue mulching (CR) within the Treatment sample from the EDTM module, based on change in OOB prediction error across a forest of trained classification trees. Variables ordered as in Table 1.

The ensemble predictions for the decision to adopt crop residues were generally most influenced by whether people had been exposed to the practice. In control groups people were most influenced by whether their neighbors did it and if they had access to extension and, to a lesser extent, whether they were concerned with weed growth. The main factor for applying crop residues for the treatment group was the monetary incentive, along with whether they had exposure to it either through extension or if their neighbors did it, and also if crop residues were available to them.

Similar to crop residue application, the decision to do zero tillage, in both control and treatment groups, was driven by whether or not people had exposure to it. In the control group people adopted

zero tillage when they had access to extension or if their neighbors did it. To a lesser extent, people in the control group were influenced by whether there was sufficient rain in the previous year. Those in the treatment group were most influenced by whether their neighbors did zero tillage (Figure 3). To a much lesser extent the treatment group was also influenced by the monetary incentive and whether they had access to residues.

### 3.3. Expanded Ensemble Predictions

As a means of comparing how well the set of criteria outlined by farmers (in the EDTM module) performed as predictors relative to the kinds of variables commonly identified in standard agricultural household surveys, we trained additional forests using the EDTM module, plus one of the following sets of variables also included in our endline survey: treatment characteristics, household characteristics, neighborhood characteristics, farm characteristics, and risk perceptions (list of survey items included in these modules, along with full survey protocol, is included as supplementary information). Additionally, we trained one final forest on the combined set of all modules.

Prediction error is reduced in most cases by inclusion of neighborhood characteristics; inclusion of risk variables offers some improvement to explaining crop residue mulching and zero tillage in the treatment group; inclusion of farm characteristics improves prediction of IC in both the treatment and control groups. It is notable that the module with the greatest additional impact on prediction, neighborhood characteristics, is captured coarsely by the EDTM module (“Do any of your neighbors practice ...”); and it is possible that more detailed probing of this topic in the interviews may have yielded additional criteria to capture the variability explained by the neighborhood module. Additional points to draw from Figure 4, reinforcing the message from other results in this study are that (i) the prediction of intercropping and the factors that improve prediction of intercropping are distinct from those which predict crop residue mulching and zero tillage and (ii) the factors that improve prediction in the treatment group appear to be different from those that improve prediction in the control group. Finally, it is noteworthy that in most cases, the reduction in prediction error with additional modules is modest, highlighting that the criteria outlined by farmers themselves were able to explain variability in adoption nearly as well as would the items in a larger household survey.

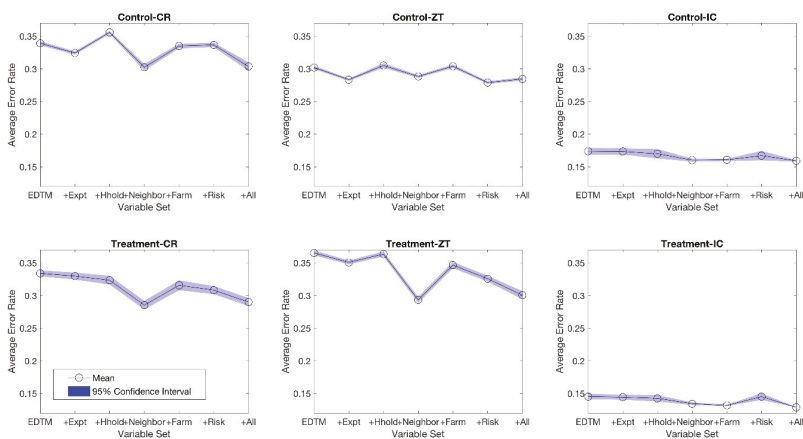


**Figure 4.** Average out-of-bag prediction error from ensembles of classification trees (“forests”) trained on data from the EDTM variables (farmer-identified criteria for adoption), as well as additional modules of experimental conditions (Expt), household characteristics (Hhold), neighborhood characteristics (neighbor), farm characteristics (farm), and risk perceptions (risk); for each of the three CA practices (intercropping (IC), zero tillage (ZT), or crop residue mulching (CR)) within both the control and treatment groups.

### 3.4. Decision Tree Results

Finally, we present individual trees for each of the three practices across treatment and control (Figure 5), whose structure was selected as optimal (the simplest tree structure whose cross-validation prediction error falls within one standard error of the minimum prediction error across all trees—see Methods). Once again, the decision trees for each of the CA activities are different, which indicates that farmers use different decision criteria when deciding to do a particular CA practice. In addition, the availability of an incentive changes the way farmers structure decisions to adopt CA. In the case of intercropping, for both treatment and control groups, there is no decision “tree,” in large part because rates of intercropping are simply very high across both samples (>80%) and there are no variables that improve upon the simple prediction that a farmer will intercrop.

The choice to apply crop residues is best explained in the dataset by whether or not one’s neighbor does it, regardless of treatment. Within the control group the decision is straightforward: if your neighbors apply cover crops, you likely will too and if they do not, you likely will not. The treatment group is similar in that if your neighbors are doing it, you likely will too, but there are additional factors that explain variability. Where their neighbors are not mulching residues, farmers in treatment villages who have residues and are offered an incentive are likely to adopt as well. For those in treatment villages whose neighbors are practicing zero tillage, but who have not received extension training on zero tillage, a lack of labor or a lack of residues are the key things that keep them from also adopting. Interestingly, the presence of neighbors practicing mulching makes the availability of residues a much lower-order factor than when such role models are absent.

Like the case for intercropping, there is no decision “tree” for farmers to adopt zero tillage in the control group. Most simply do not do zero tillage (>70%); and of those that are doing it, their decision criteria are not held enough in common to structure a tree. The tree for the treatment group is more complex, and like the decision to apply crop residues, is most strongly influenced by neighbors’ practices. Those whose neighbors have not adopted, most likely will also not adopt. Those whose neighbors have adopted and who were offered an incentive most likely will also adopt. Where farmers have neighbors who have adopted and were not offered an incentive are more likely to adopt if the last year’s planting went as planned and if they feel they have available crop residues for residue mulching. Though of minor importance to the zero tillage decision, the presence of crop residues in this tree supports the idea that these two decisions are linked.

As a last note on the importance of neighbors, we note that the importance of neighbors transcends both the availability of an incentive (i.e., neighbors matter in both control and treatment groups) as well as the structure of incentive. The “neighbors CA” variable remains the most important (top node) variable in the optimal trees for adoption of crop residues and zero tillage in the data subsets for both payment structures offered in our main intervention (standard subsidy, and agglomeration payment; see Methods) (additional trees included as supplementary information). As outlined in the Methods section, the “agglomeration payment” structure offers bonuses to adoptees whose neighbors also adopt, creating a network externality in which neighborhood adoption should matter [26]. Our analysis in the current paper does not focus on the agglomeration payment directly but only on the broader effect of having been offered an incentive. However, the importance of the neighbor effect across all treatments as well as the control highlights that there are clear peer effects latent in the system that incentives like the agglomeration payment can be designed to harness.

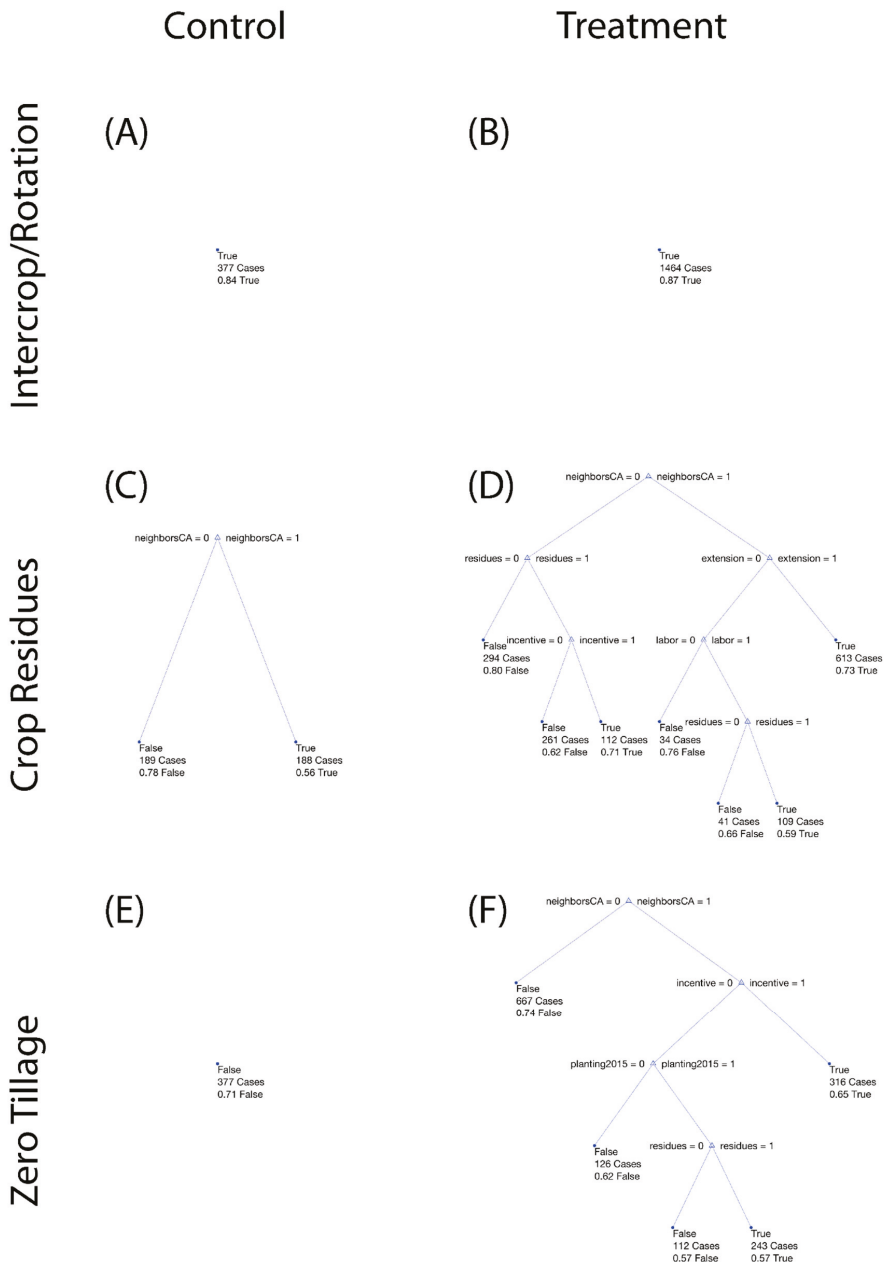


Figure 5. Decision trees for farmers’ choices to adopt treatment for intercropping, crop residue, and zero tillage in control (A,C,E) and payment (B,D,F) treatment groups.

#### 4. Discussion

We have presented results from two data collection efforts: (i) a set of ethnographic interviews in which respondents identified a set of key criteria shaping their decisions to adopt the different practices

that comprise conservation agriculture (CA), and (ii) a large-scale endline survey in which farmers from both treatment and control villages were asked to report on these same criteria, as well as the role they perceived them to have in their CA decision-making. In our analysis we examined farmers' own perceptions of which factors shaped their decision-making; which factors better explained variability in adoption of CA within the sample; and how the set of factors identified by farmers themselves compared with other common household survey items in predicting adoption.

Most notably the set of factors explaining adoption of intercropping differs sharply from the factors that explain adoption of zero tillage or crop residue mulching (between which there is much overlap), a finding that is consistent across both the farmers' perceived factors of importance, as well as the factors identified as important by our random forest approach. This finding supports the findings of [27], who characterized the adoption of CA not as one decision nor three but closer to two; one regards intercropping and a second regards the mulching of crop residues over (generally) untilled soil. The second finding of interest is that the set of factors emerging as important, as perceived by the farmers, is different from the set of factors identified as important within the decision tree and random forest approaches (i.e., explaining variation in adoption within the dataset).

More specifically, variation in adoption of zero tillage and crop residue mulching is explained by a small number of variables, most notably adoption by neighbors and the presence of incentives. Though adoption by neighbors emerged as perhaps the most important factor in shaping adoption, it was perceived by only a handful of respondents as having shaped their decisions (2–3%; Table 1). At least in the case of crop residue mulching, early adopters might feel otherwise; one interviewee noted, "People used to laugh at us when we adopted ground cover, but now the same people are coming to me asking for assistance on how they can also do it".

A unique element of our study is that we examined the structure of decision-making across farmers both inside and outside of an intervention. Our decision tree analysis demonstrated that, while neighbor effects seem to matter both inside and outside the intervention, decisions on CA practices within the treatment may be structured differently. That is, variation in adoption by members of the treatment group could be better explained (in terms of cross-validated errors) by additional factors such as the presence of incentives and access to factors such as crop residues, extension, and labor, while variation in adoption within the control group could not. One implication of the appearance of crop residues in the trees for both zero tillage and crop residue mulching is that access to sufficient crop residues may be a key entry point to shifting adoption of both CA practices.

#### *Implications for Programmatic Soil and Water Conservation*

Our analysis shows that, within our sample and timeframe, neighbors and incentives emerge as the key factors shaping adoption. An implication of this is that in the absence of neighbors as role models, incentives are likely necessary to encourage initial adopters in a region. However, the importance of neighbors in our results suggests that once some adoption has been achieved, further adoption may be more likely, rather than less. Additionally, the incentives necessary to encourage further adoption may be lower (rather than higher), as farmers need less of an encouragement to follow in the footsteps of their peers. Though the role of peer effects to encourage adoption and diffusion is nothing new [28], it is by no means universal, nor are there generally universal factors shaping adoption in CA contexts [13]. Identifying neighbors' adoption as a clear driver of new adoption in the Shire Basin context has clear application in the design of new research and development programs in the region aimed at improving livelihoods, landscapes, and water systems. We mean to suggest that, based on our findings in this paper, the CA adoption problem may have a tipping point (beyond which further adoption is self-reinforcing as people observe their neighbors also adopting). This kind of system behavior supports the argument that payments need to be high upfront, but may not need to stay that way—as neighbors adopt, and as the private benefits of CA accrue to the adopter (reduced input costs, improved soil structure yields, etc.), payments can be phased out. In the sustainable land management context, demonstrated reduction in sedimentation could even provide the basis for

payments for ecosystem services (PES) program [29,30], with a direct beneficiary willing to take over any provision of encouragement. Though adoption of CA is generally low across Southern Africa [8], we suggest the importance of research that identifies landscapes within the region where CA adoption is comparatively high, in order to better test the potential for tipping point behavior in the addressing the challenge of land degradation.

**Supplementary Materials:** The following are available online at [www.mdpi.com/2073-4441/10/1/51](http://www.mdpi.com/2073-4441/10/1/51), Spreadsheet S1: Item list and Survey Protocol; Binder S1: Additional Classification Trees.

**Acknowledgments:** This work is part of the project entitled Agglomeration Payments for Catchment Conservation in Malawi-NE/L001624/1, which is partly funded with support from the Ecosystem Services for Poverty Alleviation (ESPA) program. The ESPA program is funded by the Department for International Development, the Economic and Social Research Council, and the Natural Environment Research Council. This work was further supported through a grant from the Feed the Future Innovation Lab for Collaborative Research on Assets and Market Access, funded by the United States Agency for International Development. Additional support was provided by the CGIAR Research Program on Policies, Institutions, and Markets (PIM), led by IFPRI.

**Author Contributions:** A.R.B., J.Z.C., and P.S.W. conceived and designed the experiments; F.M. performed the experiments; A.R.B., J.Z.C. and F.M. analyzed the data; A.R.B., J.Z.C., F.M. and P.S.W. wrote the paper.

**Conflicts of Interest:** The authors declare no conflict of interest. The founding sponsors had no role in the design of the study; in the collection, analyses, or interpretation of data; in the writing of the manuscript, and in the decision to publish the results.

## Appendix A. Description of Methods in Larger Project Intervention

Our primary data collection occurred via two activities within a larger project evaluating the impact of different incentive structures on the adoption of the three practices of conservation agriculture in the Shire River Basin, Malawi. This larger project includes a random sample of 63 villages selected from the pooled sampling frame of the 5 extension planning areas (EPAs) riparian to the upper Shire River Basin, including Balaka and Machinga districts and a portion of Zomba district (Figure 1). The sample was originally designed as 12 control villages and 48 treatment villages—6 treatments each with 8 villages—with 3 additional villages added incidentally as intervention teams visited accidentally visited villages close to the true sampled village with similar names. The project collected baseline data from a clustered sample of 30 households in each of the sampled villages; implemented a two-year, opt-in intervention at the village level in each of the 48 treatment villages (plus the 3 accidental inclusions); followed by an endline panel survey with respondents from the baseline survey, adding in additional households from the original sampling frame to replace households that had left the village or were otherwise unable or unwilling to participate. With additional villages and new responses to account for attrition, our final endline survey was given to 1923 respondents.

The interventions in each village varied in structure, following a  $2 \times 3$  design of (i) payment structure and (ii) monitoring level. Payments took one of two structures—a standard subsidy, and an “agglomeration payment” [22], which included a smaller standard subsidy along with bonus payments given for participation by neighboring farmers. All payments were calibrated to have a value on the order of 30 USD per acre (up to a maximum of one acre, in increments of 0.1 acres) for complete adoption of all three CA practices. Monitoring levels varied from (i) high (all participants); (ii) reduced (half of participants); to (iii) low (no participants). In “high” monitoring treatments, all registered plots were visited at the end of the season to verify compliance, while in “reduced” monitoring treatments, a random selection of half of the participants had a plot visit while others merely self-reported. In “low” monitoring treatments, all participants self-reported.

## Appendix B. Ethnographic Results—Thick Descriptions

We identified 26 different criteria from our ethnographic interviews that farmers mentioned as shaping their decisions to adopt any of the agricultural practices within CA; these are summarized in Table 1 in the main paper, in the question form through which they were verified in return interviews and included in our endline survey. The reasoning behind the adoption (or not) of

each of the three practices differs, and in the text below we draw supporting quotations from our interviews to provide a thicker description of farmer thinking than is provided by Table 1. Across our 96 interviews, 73 respondents (76 percent) reported practicing intercropping (or leguminous crop rotations), 56 (58 percent) reported mulching crop residues, and 23 (24 percent) reported practicing zero tillage; only 12 (13 percent) practiced all three.

#### *Appendix B.1. Intercropping*

Farmers reported choosing to intercrop because they believed that it would increase their food supplies and incomes through mitigating the risk of crop failure and by maximizing the number of crops planted, especially when land is limited. Farmers also reported choosing to intercrop because it improved their food security through increasing the amount and diversity of food that they could access. Lastly, people adopted intercropping because they thought it would improve their soil fertility, which would lead to improved yields and profits.

Some farmers viewed intercropping as a strategy to reduce the potentially negative impacts of drought and flooding that could lead to crop failure, which could result in both food insecurity and income loss. An adopter explains, “When we plant maize with pigeon peas and the maize does not do well, we are able to sell the pigeon peas and buy maize”. Another adopter emphasized how intercropping (though not of a legume) allowed her to overcome a climatic shock: “If it were not for sorghum, I would have died from hunger as my maize crop was washed away by floods”. Not only did people intercrop to buffer against risks, they did so to increase their yields. Many farmers attribute their decision to intercrop to seeing that their neighbors harvest higher yields and even bumper harvests. Increased yields can improve food security through increasing the amount of food produced, expanding dietary diversity, and increasing income (e.g., through sales of marketable surpluses). An adopter explained, “Low maize yields prompted me to start intercropping maize with cowpeas, so that I have food and can also sell”. Also, an adopter explained how intercropping leads to more dietary diversity, “When we plant maize, cowpeas and pigeon peas and it is time to harvest, we have more food. It is like we have planted both food and relish”.

Farmers also adopted intercropping in order to maximize the use of their limited space and increase income. Another respondent elucidates, “Since my piece of land is small, I have always been forced to practice intercropping so that I can harvest more crops on this small piece of land”. Another furthers that intercropping can be profitable: “I plan to continue growing maize with pigeon peas because the pigeon peas are bringing me money after selling”. Farmers also consider that intercropping will lead to future improved yields by improving soil fertility. A respondent explains, “I realized that there was rampant soil degradation and felt the need to intercrop the maize with legumes to improve the fertility of the soil”. Another farmer adds, “The leaves of the pigeon pea plants shed off and improve the fertility of the soil so we obtain food ... and also income when we sell the pigeon pea”. Even though most farmers thought that intercropping would improve soil and yields, others explained that concerns about yield were why they did not adopt intercropping: “Planting more crops in the same field results in poor performance of maize, which is the main crop here”.

#### *Appendix B.2. Crop Residues*

Among farmers who mulched crop residues, the most commonly cited reasons were the perceived environmental benefits of retained soil moisture, improved soil fertility, and reduced soil erosion. People also mulched crop residues because of the reduced labor requirements (e.g., to remove stubble) and as a means of limiting termites, though some people think that crop residues can actually increase pest problems. Those who did not apply crop residues explained that they did not do so because they did not have the stalks, were concerned about arson, or did not have access to extension to learn how to do it.

These farmers often explain their primary reason for mulching residues as being improved soil moisture. A respondent explains, “In this type of farming, when I cover the field with maize stalks,

even when rainfall is low, the crop does not wilt, it still grows and the harvest is good". Also, another farmer adds the increasing important benefits of soil moisture: "I noticed some time back that climate was changing because we were receiving inconsistent rainfall. Therefore, I decided to use the husks to preserve moisture in the soil, which helps the crops to grow". Farmers also explained that they adopted it because they thought it improved the soil quality. One said, "This ground cover helps to prevent loss of nutrients by reducing soil erosion when we have floods". Another perceived benefit of retaining crop residues is the reduced labor inputs required. One farmer explained, "Before I started this type of farming, I used to face problems especially tilling of the field and I had to weed more than twice. However, now, I am able to rest and I simply go and remove the weeds by hand". Some farmers were additionally persuaded to do cover cropping because they thought it would reduce termite damage. "Due to the prolonged dry spells, there was a termite attack but the damage was minimal as the pests were busy feeding on the ground cover". Though others did not adopt it for the same reason. "Much as [ground cover] is good, the main challenge that I am facing is that termites tend to cut down the crops on the areas which I have put much covering materials".

For those that do not adopt, the main reported reason was that they did not have access to inputs like maize stalks and others worried that applying maize stalks would increase the chances of arson on their property. A respondent explains, "For me to start, I will need organic manure and maize stalks". Obtaining maize stalks can be difficult because they are also used as fodder for livestock. In some cases, farmers must choose between using them for livestock or improved soil moisture on their farm and, in other cases, there are few stalks left after it is consumed by livestock in the community. A farmer explains, "In this village there are some rich people who have cattle and these cattle destroy the materials I used for ground cover practice and other selfish young people just set fire on the ground cover materials, which discourages many people from practicing [it]".

### *Appendix B.3. Zero Tillage*

Farmers who adopted zero tillage (23 of 96 interviewees) reported that they chose to do so because they thought it would increase their yields and food security as well as improve soil health. Many people lamented that they were not able to adopt zero tillage because it required too much labor, they did not have the inputs required, and that there was little extension training on the zero tillage practice. At times, the choice to do zero tillage was associated with their willingness to apply crop residues, which is evidenced by people complaining that they could not do zero tillage because "they did not have enough maize stalks which are also needed for this type of farming".

Farmers chose to adopt zero tillage after they were told by extension agents or saw from their neighbors that would be able to increase yields, especially when coupled with applying crop residues. "At first I was only trying the practice after the extension agent told me about this ground cover farming, but now I have seen the yields have improved and I plan on increase the land under this practice". Part of the reason that farmers adopted this practice was because they recognized the potential benefit of their soil and, consequently, their yield. A farmer explains, "It is not good to till the land every year because that degrades the soil. By tilling the soil every year, there used to be emergence of red weeds resulting in wilting of maize". Though other people explained that soil concerns were why they did not adopt: "The soil type in this area is hard, and when we tried it we realized we were better off [just] doing ground cover". To some extent, farmers were able to see some of the agronomic benefits of CA emerging, as another explained, "I have benefited a lot from this type of farming as the field was not infested with weeds and that germination was good since the basins were able to retain moisture".

Those that did not adopt zero tillage said that it was because they did not have extra labor and inputs required, nor did they have sufficient access to extension agents. People choose not to do zero tillage because "digging the basins is quite laborious and time consuming". A couple of different women explained that they were not able to do it without additional male labor, which was not always available. One woman whose husband migrates explained, "I do farm activities alone ... and I can only

do minimum tillage if we could be two with my husband". Beyond labor, which was a major concern for many, few people also complained that they did not have inputs like maize stalks and fertilizer, which they said were required to do zero tillage. Last, farmers indicated that of all the CA practices taught by extension agents, zero tillage was the least accessible. A farmer explained, "We were only trained on [applying crop residues] and intercropping, therefore, I am unable to practice this farming". Another suggested, "There's need of more agricultural extension workers so that we keep up the momentum. That way more people in the village will adopt these methods".

## References

1. Kumambala, P. *Sustainability of Water Resources Development for Malawi with Particular Emphasis on North and Central Malawi*; University of Glasgow: Glasgow, UK, 2010.
2. Scopel, E.; Triomphe, B.; Affholder, F.; Da Silva, F.A.M.; Corbeels, M.; Xavier, J.H.V.; Lahmar, R.; Recous, S.; Bernoux, M.; Blanchart, E.; et al. Conservation agriculture cropping systems in temperate and tropical conditions, performances and impacts. A review. *Agron. Sustain. Dev.* **2013**, *33*, 113–130. [CrossRef]
3. Government of Malawi. *Malawi the Agriculture Sector Wide Approach (ASWAp): Malawi's Prioritised and Harmonised Agricultural Development Agenda*; Government of Malawi: Lilongwe, Malawi, 2010.
4. Fleskens, L.; Chilima, C. *Development of a Green Water Credit Scheme in the Shire River Basin*; UNDP: Lilongwe, Malawi, 2013.
5. Campbell, B.; Pierson, O. Creating a Market Mechanism to Keep the Lights on in Malawi. Available online: <https://www.mcc.gov/resources/story/story-kin-apr-2015-creating-a-market-mechanism-to-keep-the-lights-on> (accessed on 10 October 2016).
6. Araya, T.; Cornelis, W.M.; Nyssen, J.; Govaerts, B.; Bauer, H.; Gebreegziabher, T.; Oicha, T.; Raes, D.; Sayre, K.D.; Haile, M.; et al. Effects of conservation agriculture on runoff, soil loss and crop yield under rainfed conditions in Tigray, Northern Ethiopia. *Soil Use Manag.* **2011**, *27*, 404–414. [CrossRef]
7. Mchuru, C.N.; Lorentz, S.; Jewitt, J.; Manson, A.; Chaplot, V. No-Till Impact on Soil and Soil Organic Carbon Erosion under Crop Residue Scarcity in Africa. *Soil Sci. Soc. Am. J.* **2011**, *75*, 1503–1512. [CrossRef]
8. Ndah, H.T.; Schuler, J.; Uthes, S.; Zander, P.; Traore, K.; Gama, M.-S.; Nyagumbo, I.; Triomphe, B.; Sieber, S.; Corbeels, M. Adoption potential of conservation agriculture practices in sub-Saharan Africa: Results from five case studies. *Environ. Manag.* **2014**, *53*, 620–635. [CrossRef] [PubMed]
9. Friedrich, T.; Derpsch, R.; Kassam, A. Overview of the global spread of conservation agriculture. *Field Actions Sci. Rep.* **2012**, *6*. Available online: <http://journals.openedition.org/factsreports/1941> (accessed on 8 January 2018).
10. Kassam, A.; Friedrich, T. Conservation Agriculture: Concepts, worldwide experience, and lessons for success of CA-based systems in the semi-arid Mediterranean environments. *Opt. Méditerranéennes* **2010**, *96*, 11–51.
11. Brouder, S.M.; Gomez-macpherson, H. Agriculture, Ecosystems and Environment The impact of conservation agriculture on smallholder agricultural yields: A scoping review of the evidence. *Agric. Ecosyst. Environ.* **2014**, *187*, 11–32. [CrossRef]
12. Brown, B.; Nuberg, I.; Llewellyn, R. Stepwise frameworks for understanding the utilisation of conservation agriculture in Africa. *Agric. Syst.* **2017**, *153*, 11–22. [CrossRef]
13. Knowler, D.; Bradshaw, B. Farmers' adoption of conservation agriculture: A review and synthesis of recent research. *Food Policy* **2007**, *32*, 25–48. [CrossRef]
14. Giller, K.; Witter, E.; Corbeels, M.; Tittonell, P. Conservation agriculture and smallholder farming in Africa: The heretics' view. *Field Crop. Res.* **2009**, *114*, 23–34. [CrossRef]
15. Pannell, D.J.; Llewellyn, R.S.; Corbeels, M. The farm-level economics of conservation agriculture for resource-poor farmers. *Agric. Ecosyst. Environ.* **2014**, *187*, 52–64. [CrossRef]
16. Arslan, A.; McCarthy, N.; Lipper, L.; Asfaw, S.; Cattaneo, A. Adoption and intensity of adoption of conservation farming practices in Zambia. *Agric. Ecosyst. Environ.* **2014**, *187*, 72–86. [CrossRef]
17. Andersson, J.A.; D'Souza, S. From adoption claims to understanding farmers and contexts: A literature review of Conservation Agriculture (CA) adoption among smallholder farmers in southern Africa. *Agric. Ecosyst. Environ.* **2014**, *187*, 116–132. [CrossRef]
18. Gladwin, C.H. *Ethnographic Decision Tree Modeling*; Sage: Thousand Oaks, CA, USA, 1989, ISBN 9780803934863.

19. Roth, H.; Conference, T.; Nelson, C.; August, N.Z. Using Ethnographic Decision Tree Modelling to Explore Farmers' Decision-making Processes: A Case Study Paper. In Proceedings of the 2009 NZARES Conference, Nelson, New Zealand, 27–28 August 2009.
20. Orr, A.; Mwale, B.; Saiti, D. Modelling agricultural “performance”: Smallholder weed management in Southern Malawi. *Int. J. Pest Manag.* **2002**, *48*, 265–278. [[CrossRef](#)]
21. Beck, K.A. Ethnographic decision tree modeling: A research method for counseling psychology. *J. Couns. Psychol.* **2005**, *52*, 243–249. [[CrossRef](#)]
22. Mullainathan, S.; Spiess, J. Machine Learning: An Applied Econometric Approach. *J. Econ. Perspect.* **2017**, *31*, 87–106. [[CrossRef](#)]
23. Bauer, E.; Kohavi, R.; Chan, P.; Stolfo, S.; Wolpert, D. An Empirical Comparison of Voting Classification Algorithms: Bagging, Boosting, and Variants. *Mach. Learn.* **1999**, *36*, 105–139. [[CrossRef](#)]
24. Parkhurst, G.M.; Shogren, J.F. Smart Subsidies for Conservation. *Am. J. Agric. Econ.* **2008**, *90*, 1192–1200. [[CrossRef](#)]
25. Ward, P.S.; Bell, A.R.; Parkhurst, G.M.; Droppelmann, K. Heterogeneous Preferences and the Effects of Incentives in Promoting Conservation Agriculture in Malawi. *Agric. Ecosyst. Environ.* **2016**, *222*, 67–79. [[CrossRef](#)]
26. Mathworks Classification—MATLAB & Simulink Example. Available online: <https://www.mathworks.com/help/stats/examples/classification.html?requestedDomain=www.mathworks.com> (accessed on 5 July 2017).
27. Ward, P.S.; Bell, A.R.; Droppelmann, K.; Benton, T. Early adoption of conservation agriculture practices: Understanding partial compliance in programs with multiple adoption decisions. *Land Use Policy* **2018**, *70*, 27–37. [[CrossRef](#)]
28. Rogers, E.M.; Shoemaker, F.F. *Communication of Innovations: A Cross-Cultural Approach*; Free Press: New York, NY, USA, 1971.
29. Engel, S.; Schaefer, M. Ecosystem services—A useful concept for addressing water challenges? *Curr. Opin. Environ. Sustain.* **2013**, *5*, 696–707. [[CrossRef](#)]
30. Bell, A.; Matthews, N.; Zhang, W. Opportunities for improved promotion of ecosystem services in agriculture under the Water-Energy-Food Nexus. *J. Environ. Stud. Sci.* **2016**, *6*, 183–191. [[CrossRef](#)]



© 2018 by the authors. Licensee MDPI, Basel, Switzerland. This article is an open access article distributed under the terms and conditions of the Creative Commons Attribution (CC BY) license (<http://creativecommons.org/licenses/by/4.0/>).

Communication

# Individual Local Farmers' Perceptions of Environmental Change in Tanzania

Lina Röschel <sup>1</sup>, Frieder Graef <sup>2</sup>, Ottfried Dietrich <sup>2</sup>, Meike Pendo Schäfer <sup>2,\*</sup> and Dagmar Haase <sup>3</sup>

<sup>1</sup> Ecologic Institute Berlin, 10717 Berlin, Germany; l.roeschel@googlemail.com

<sup>2</sup> Leibniz Centre for Agricultural Landscape Research (ZALF), 15374 Müncheberg, Germany; graef@zalf.de (F.G.); dietrich@zalf.de (O.D.)

<sup>3</sup> Geographic Department of Humboldt, University of Berlin, 12489 Berlin, Germany; dagmar.haase@geo.hu-berlin.de

\* Correspondence: meike.schaefer@zalf.de; Tel.: +49-(0)33432-82-310

Received: 7 February 2018; Accepted: 20 April 2018; Published: 22 April 2018

**Abstract:** Climatic and environmental changes are expected to affect in particular those regions where the economy is primarily based on the agricultural sector and where the dependency on water availability is high. This study examines how smallholder farmers in rural Tanzania perceived climatic and environmental changes over the past 20 years and the resulting effects on water availability and food security. The study is based on a household survey of 899 farmers in a semi-arid and a sub-humid region in Tanzania. It was found that (a) significant differences in perceptions of the environment by farmers can be attributed to agro-climatic location, while the distance to a water source has less impact on individual perception; (b) differently perceived changes affect individual water availability and food security; and (c) the farm level adaptation methods applied are linked to vulnerability to changes and the household dependence on the immediate environment. The authors conclude that the specific environmental surroundings paired with socio-economic factors can severely compound the negative effects of water scarcity on rural farmers.

**Keywords:** environmental change; local perception; food security; adaptation

## 1. Introduction

Changes in water availability can be quantified by advanced technology as well as individual perception. People whose livelihoods directly depend on water resources, such as farmers, are likely to perceive changes in water availability and their environment. However, there is mixed scientific evidence regarding the accuracy of this evidence [1–3]. Therefore, human perceptions of environmental changes are useful to supplement current environmental data methods and add a qualitative perspective regarding the effects of the changes [4,5].

Perception of the environment describes how a person perceives the environment through the brain's and their senses' ability to process and store information. The perceptual process is highly complex, but broken down it consists of six steps: the presence of objects, observation, selection, organization, interpretation, and response [6]. The selection, organization, and interpretation is personalized and driven by internal and external factors. For example, the motivation, personality, or experience of an individual plays a role in how they perceive their surroundings, but also a continued repetition of being exposed to an object or a situation can alter their personal perception. Observers are often very poor at reporting changes to their visual environment, but sensitivity to change does still occur in the absence of awareness and does not rely on the redeployment of attention. The more acute the change occurs, the more likely it will be perceived by the individual [6].

Perception of the environment as a diagnostic tool was first declared by the UNESCO's Man and the Biosphere program, stating that the study of perception of the environment is a fundamental tool

for the management of places and landscapes [7]. Other studies have shown that perceived changes in the environment are instrumental towards policy design and sustainable resource management, as they may detect socio-environmental issues and interlinkages which other methods neglect [8–10]. Thus, an inconsistency between individual perception and scientific “measured” data can be utilized to critically review results and to guide interpretation and management methods [11].

Individual perception is an especially effective diagnostic tool for the review of regional environmental deviances on a small scale as present scientific measuring techniques may be too imprecise for a detailed and in particular for an individual analysis [4,12,13]. The effects of change in water availability can be highly succinct in terms of regional deviations and are subject to environmental as well as socio-economic conditions [3,12]. Accordingly, an analysis of the link between distance to water sources, the resulting amount of time spent outdoor in the environment, and perceived related environmental change grants insight on why some perceive environmental change more strongly than others.

This research on individual perceptions of water availability and food security in two study areas, in rural semi-arid and in sub-humid Tanzania, investigates the discrepancies between perceived changes in the environment and location across to regions. The objective is to discriminate perceptions between the two study regions and explore the importance of agro-climatic location in terms of the effects of environmental change on the individual perception. Furthermore, it aims to detect differences in perceived changes in water availability and food security based on the time needed by an individual to reach a drinking water source. We hypothesized that both agro-climatic location and distance from water source would influence individual perception insofar that harsher environmental surroundings stimulate sensitivity to change within those surroundings. Furthermore, it was expected that if environmental changes are perceived, measures would be put in place to prevent or reduce expected risks, which in turn could increase long-term water availability and food security.

## 2. Materials and Methods

### 2.1. Study Area

The Wami River drainage basin constitutes the hydrological unit encompassing the selected case study regions in Tanzania (Figure 1). Water availability in this area partly depends on the state of the Wami River basin’s water resources, which have been and continue to be affected by strong hydrological changes due to population growth, agricultural sector development, and climate change [14–16].

This study was carried out in two agro-ecologically differing regions in Tanzania. The predominantly sub-humid Morogoro case study region (600–800 mm annual rainfall) features flat plains, highlands, and dry alluvial valleys [17]. The diverse food systems are based on maize, sorghum, legumes, rice, and horticulture, with livestock being only marginally integrated in the livelihood system. The semi-arid Dodoma case study region (350–500 mm annual rainfall) is predominantly characterized by flat plains. The food system is primarily based on sorghum and millet with a strong integration of livestock [17–19]. Morogoro contains areas with different levels of sensitivity concerning food security, while the areas in Dodoma are usually characterized by high food insecurity.

### 2.2. Data Collection

The study uses the findings of empirical qualitative research conducted in 2014 from six villages (Changarawe, Idifu, Ilakala, Ilolo, Ndebwe, Nyali; case study sites in Figure 1) in two rural regions in Tanzania. A baseline household survey (Faße, et al. [20]) interviewed 899 household heads to describe the climatic and environmental changes in their immediate surroundings over the past 20 years, in case they had perceived any. The surveyed households were selected randomly from a list of household heads’ names and the corresponding sub-villages they lived in. From each village, 150 households were randomly selected, collectively adding up to 900 surveyed parties in total from both districts.

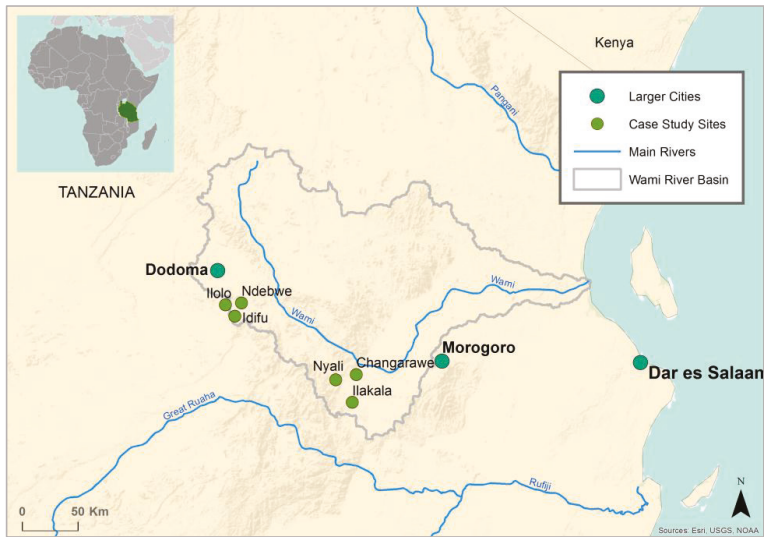


**Figure 1.** Location of case study sites, larger neighboring cities, major rivers and corresponding river basin in Tanzania.

### 2.3. Quantitative Analysis

A selected number of information from the survey sections regarding climatic changes, environmental changes, water sources and water availability were used for this study. Additionally, information on the location as well as the distance to cover to reach the main source of drinking water was extracted. After the data was collected, it was entered into a database and later exported to the statistical software STATA 13 for data cleaning. The data was cleaned in terms of income and consumption aggregation. The data was then analysed with IBM SPSS Statistics Version 16.0, using the Mann–Whitney-U test for testing regionally differing perceptions of the environment and using the Kruskal–Wallis-H test for verifying a possible relationship between distance categories to the water source and their perceptions of the environment.

## 3. Results

### 3.1. Region-Specific Perceptions

The results of the statistical analysis shows that perceptions of change related to climate (Table 1) and environment (Table 2) were significantly different between the two regions. While 97% of all farmers from both regions perceived climatic changes over the past 20 years, highly significant differences in perceptions became apparent for changes in temperature, forest, grazing lands, soil fertility, river water levels, food security and coping activities.

The perception of interviewees from Dodoma in regards to changes in temperature revealed that individuals felt less affected by potential changes than interviewees from Morogoro. Individuals from Dodoma more often expressed that they had not perceived any change in temperature as well as lower temperatures during the summer season. Interviewees from Morogoro reported to have suffered more heat days and extreme temperatures than those from Dodoma.

**Table 1.** Perceptions of climatic change in Dodoma and Morogoro (Mann–Whitney-U Test).

Parameter	Semi-Arid Dodoma	Sub-Humid Morogoro
<b>Climatic Change</b>	<b>n.Sign.</b>	<b>n.Sign.</b>
-No change	2.7%	3.1%
-Change	97.3%	96.9%
<b>Rainfall</b>	<b>n.Sign.</b>	<b>n.Sign.</b>
-Less annual rainfall	43.2%	46.2%
-Less rainy days	13.4%	13.1%
-Rainy season shorter	10.1%	8.0%
-Other <sup>b</sup>	33.3%	32.7%
<b>Temperature</b>	<b>**</b>	<b>**</b>
-No change	5.6%	1.8%
-Less hot in summer	5.0%	1.6%
-Hotter in summer	25.0%	17.8%
-Extreme temperatures	32.2%	41.9%
More heat days	23.4%	27.8%
Other <sup>b</sup>	8.8%	9.1%

\*\* significance level  $\alpha \leq 0.01$ ; <sup>b</sup> 'Other': answer categories that were selected by less than 10% of interviewees in both regions were aggregated.

**Table 2.** Perceptions of environmental change in Dodoma and Morogoro (Mann–Whitney-U Test).

Parameter	Semi-Arid Dodoma	Sub-Humid Morogoro
<b>Environment</b>	<b>n.Sign.</b>	<b>n.Sign.</b>
-No change	4.2%	5.6%
-Change	95.8%	94.4%
<b>Forest</b>	<b>**</b>	<b>**</b>
-No change	2.5%	9.4%
-Less forest area	40.6%	34.1%
-Less trees	20.3%	18.5%
-Less dense forest	17.2%	11.4%
-No more big trees	10.8%	17.6%
-Other <sup>b</sup>	11.1%	18.4%
<b>Grazing Land</b>	<b>***</b>	<b>***</b>
-No change	3.2%	23.5%
-Less grazing lands	35.9%	41.9%
-Less pasture	30.3%	8.8%
-Grazing lands degraded	22.7%	15.0%
-Other <sup>b</sup>	7.9%	10.8%
<b>Soil Fertility</b>	<b>**</b>	<b>**</b>
-No change	6.3%	16.2%
-Lower yields	85.2%	75.1%
-Other <sup>b</sup>	8.5%	8.7%
<b>River Water Level Wet Season</b>	<b>***</b>	<b>***</b>
-No change	37.7%	17.3%
-Lower water level	20.2%	63.7%
-Higher water level	16.1%	13.1%
-Other <sup>b</sup>	26.0%	5.9%
<b>River Water Level Dry Season</b>	<b>n.Sign.</b>	<b>n.Sign.</b>
-No change	31.3%	12.1%
-Lower water level	24.0%	14.5%
-Higher water level	20.4%	67.5%
-Other <sup>b</sup>	24.3%	5.8%

\*\* significance level  $\alpha \leq 0.01$ ; \*\*\* significance level  $\alpha \leq 0.001$ ; <sup>b</sup> 'Other': answer categories that were selected by less than 10% of interviewees in both regions were aggregated.

People from Dodoma perceived more severe negative changes in forests and were more likely to notice a negative change in pasture compared to interviewees from Morogoro. While a higher percentage of people from Morogoro found no changes in soil fertility in comparison to those of Dodoma, the survey concludes that populations from both case studies have largely suffered lower yields, suggesting a cause for the extensive negative effects on food security in both regions. In terms of food security, respondents from Dodoma indicated to have suffered negative impacts more frequently, which is in line with their perception of climatic and environmental changes.

Coping activities to approach the declining food security varied strongly between the two regions. While nearly one fifth of interviewees from Dodoma chose to undergo no adjustment in the face of environmental change, even twice as many refrained from doing so in Morogoro. Many interviewees from Dodoma chose to take up non-farm employment. In Morogoro, popular coping mechanisms included growing more crop varieties, taking up non-farm employment, and saving money. Hardly any interviewees coped by migrating to another village or region or by investing in irrigation to cope with the changing circumstances.

### 3.2. Perception Based on Distance to Water Source

Perceptions based on individual household distances to the closest water source did not show any significant differences between water source distance classes (short distances less than 30 min by foot, long distances between 30 and 240 min' walk), except for soil fertility. Interviewees from longer distance households tended not to perceive changes in soil fertility compared to shorter distances. Though not significant, we found more rainfall in the early season and longer rainy seasons to be solely perceived by interviewees who only had to overcome short to medium distances to their next source of drinking water, while none of the interviewees with a journey longer than 30 min had noticed a positive change.

## 4. Discussion

### 4.1. Region-Specific Perceptions

Our aim was to discriminate between different perceptions on environmental change and the resulting effects on water availability and food security between (a) two agro-climatically differing regions and (b) households with differing distances to water sources. The study results proved that region-specific environmental variables affect individuals' perception of environmental changes [21–24], with highly significant perception differences on the regional level regarding changes in temperature, forest, grazing lands, soil fertility, river levels, food security, and coping activities. Region-specific environmental settings and possibly the associated social and economic circumstances [25–27] are predominant reasons for these differences. The interviewees of the semi-arid Dodoma region perceived negative climatic changes less than those from Morogoro region; they were, however, more likely to perceive changes within their environment, suggesting a linkage between perception of environmental changes and vulnerability to these changes [28]. Due to the unimodal and low annual rainfall within only few and erratic events, and high spatial variability in distribution, food insecurity is higher throughout Dodoma region. This places higher pressure on households to adjust their situation by applying coping mechanisms such as non-farm employment [29], even if they entail higher uncertainty [30].

Present environmental risks within a region increase the individual's perception of other environmental changes when the respective livelihoods highly depend on water availability and stability [31]. Greater changes in river water levels were perceived year-round in Morogoro in comparison to Dodoma, where surface water plays a minor role and is only available in the rainy season. Agricultural communities of Morogoro mainly live off of soils that are subject to seasonal flooding, intensifying their perception of changes in river water levels. The dependency on surface water increases vulnerability to environmental changes and in turn increases the likeliness for perception of

changes to natural surroundings. However, even though the low annual precipitation entails higher water and food insecurity in the Dodoma region, adoption of adaptation measures there is low amongst interviewees, even if somewhat higher than in Morogoro.

Perceived changes on a local and individual level may trigger community-level adaptation. Without the support of community-based mechanisms, however, individual coping strategies are limited and subject to risk. As this study shows, a high number of interviewees decided to refrain from action even though high-impact environmental changes were perceived (Table 3). Farmers may be constrained in undertaking adaption measures due to lack of funds, poor planning, or due to the environmental changes themselves, for instance, shortage of water [30]. Others may perceive changes, but not fully realize the culminating associated risks.

**Table 3.** Perceptions of impact on food security and utilized coping activities in Dodoma and Morogoro (Mann–Whitney–U Test).

Parameter	Semi-Arid Dodoma	Sub-Humid Morogoro
<b>Food Security</b>	<b>***</b>	<b>***</b>
-Highly negative impact	49.3%	30.4%
-Medium negative impact	13.7%	17.2%
-Medium positive impact	5.9%	11.1%
-Highly positive impact	14.4%	16.8%
-Other <sup>b</sup>	16.7%	5.7%
<b>Coping Activities</b>	<b>***</b>	<b>***</b>
-No adjustment	17.7%	37.4%
-Non-farm employment	17.3%	9.7%
-Grow more varieties	5.9%	11.4%
-Save money	4.8%	8.4%
-Migrate to another village/region	0.2%	0.9%
-Invest more in irrigation	1.1%	0.9%
-Other <sup>b</sup>	53.0%	31.3%

\*\*\* significance level  $\alpha \leq 0.001$ ; <sup>b</sup> 'Other': answer categories that were selected by less than 10% of interviewees in both regions were aggregated.

In line with Iqbal et al.'s findings, our results suggest that those farmers located further away from a major city or core village perceive environmental changes more [31]. The Dodoma region case studies are geographically clustered closely together in a notable distance to the next larger city, so perceptions were very similar amongst the villagers. However, in the Morogoro region, Changanawe and Nyali are notably closer to Kilosa town than Ilakala, whose inhabitants strongly perceived a highly negative impact of environmental changes on food security. Possible reasons may be a lack of interest, information and resources that farmers living in close proximity to a city have access to, as well as the availability of off-farm work.

#### 4.2. Perception Based on Distance to Water Source

Unexpectedly, few significant differences were found in perceived environmental changes based on the time needed by an individual to reach the source of drinking water, except for perception on soil fertility. The time needed and the associated physical burden directly affects the volume of water consumed by households using non-networked sources [32]. Previous research also affirmed that households with water sources located more than 30 min away collect less water than is believed necessary for basic need [33]. It was expected that a higher distance to a water source encourages perception of environmental and climatic changes, as extended walks increases exposure. However, our study indicates a weak relation between walking time, the implied increased environmental exposure and the individuals' perception of change in water availability. Even more and to our assumption, those households with longer walking distances tended to be less likely to adapt to water

scarcity and food insecurity. It is suggested that those households who are currently accessing long distance water sources are also those with the least opportunities for incremental change. Ongoing further correlation analysis and synchronization of findings with regional expert interviews should deepen the understanding of these complex interactions.

## 5. Conclusions and Recommendations

The results of this study show that environmental surroundings paired with socio-economic factors affect the perception of climatic and environmental changes by rural farmers. Even though perceptions of changes and their effects on water availability and food security were very high, farm level adaptation measures were not applied by a large percentage of interviewees. The type of applied coping mechanism was especially dependent on the respective region of the individual. The lack of utilized adaptation methods underlines the present margin between perception and action. Alerting individuals for early warning signs of adverse environmental changes may be part of the solution. In addition to external activities such as financial aid, social learning activities and policy action, individuals could profit from being informed of cost-effective, long-term adaptation measures that they can implement themselves and that respond best to the mentioned changes of the environment. While farmers with access to urban centers or institutional services are more likely to implement adaptation measures, especially remote locations most vulnerable to environmental changes should be supported with targeted outreach programs with clear targets that need to be regularly monitored.

**Acknowledgments:** This publication is a product of the Trans-SEC project ([www.trans-sec.org](http://www.trans-sec.org)) and was funded by the German Federal Ministry of Education and Research (BMBF) and the German Federal Ministry for Economic Cooperation and Development (BMZ) under grant number 031A249A. The views expressed are purely those of the authors and may not under any circumstances be regarded as stating an official position of the BMBF or BMZ.

**Author Contributions:** Frieder Graef, Ottfried Dietrich and Meike Pendo Schäfer were part of the team who conceived and designed the field data collection survey; Lina Röschel analyzed relevant sections of collected data and wrote the paper; Frieder Graef, Ottfried Dietrich, Meike Pendo Schäfer and Dagmar Haase contributed analysis tools, background information, and edited the paper; Meike Pendo Schäfer formatted the paper.

**Conflicts of Interest:** The authors declare no conflict of interest. The founding sponsors had no role in the design of the study; in the collection, analyses, or interpretation of data; in the writing of the manuscript, and in the decision to publish the results.

## References

1. Codjoe, S.N.A.; Owusu, G.; Burkett, V. Perception, experience, and indigenous knowledge of climate change and variability: The case of accra, a sub-saharan African city. *Reg. Environ. Chang.* **2014**, *14*, 369–383. [[CrossRef](#)]
2. Yaro, J.A. The perception of and adaptation to climate variability/change in ghana by small-scale and commercial farmers. *Reg. Environ. Chang.* **2013**, *13*, 1259–1272. [[CrossRef](#)]
3. Below, T.B.; Schmid, J.C.; Sieber, S. Farmers' knowledge and perception of climatic risks and options for climate change adaptation: A case study from two Tanzanian Villages. *Reg. Environ. Chang.* **2015**, *15*, 1169–1180. [[CrossRef](#)]
4. Boyd, D.; Crawford, K. Critical questions for big data: Provocations for a cultural, technological, and scholarly phenomenon. *Inf. Commun. Soc.* **2012**, *15*, 662–679. [[CrossRef](#)]
5. Li, Y.; Urban, M.A. Water resource variability and climate change. *Water* **2016**, *8*, 348. [[CrossRef](#)]
6. LumenLearning. Individual Perceptions and Behavior. Available online: <https://courses.lumenlearning.com/boundless-management/chapter/individual-perceptions-and-behavior/> (accessed on 25 March 2018).
7. UNESCO. *Perception of Environmental Quality*; UNESCO: Paris, France, 1973; p. 76.
8. GESAMP. *The Contributions of Science to Integrated Coastal Management*; FAO: Rome, Italy, 1996; p. 66.
9. Weber, E.U. Experience-based and description-based perceptions of long-term risk: Why global warming does not scare us (yet). *Clim. Chang.* **2006**, *77*, 103–120. [[CrossRef](#)]
10. Whyte, A.V.T. Guidelines for field studies in environmental perception. In *MAB Technical Notes No. 5*; UNESCO: Paris, France, 1977; p. 118.

11. Elliot, A.J.; McGregor, H.A.; Gable, S. Achievement goals, study strategies, and exam performance: A mediational analysis. *J. Educ. Psychol.* **1999**, *91*, 549–563. [[CrossRef](#)]
12. Ayeni, A.O.; Olorunfemi, F. Reflections on environmental security, indigenous knowledge and the implications for sustainable development in Nigeria. *J. Res. Natl. Dev.* **2014**, *12*, 46–57.
13. Maddison, D. *The Perception of and Adaptation to Climate Change in Africa*; The World Bank: Washington, DC, USA, 2007; p. 51.
14. Schäfer, M.P.; Dietrich, O. *Water Resources Situation in CSS—General Conditions of Water Resources in Kilosa and Chamwino District and Expected Implications for Agricultural and Food Security Strategies*; Institute of Landscape Hydrology, Leibniz Centre for Agricultural Landscape Research (ZALF): Müncheberg, Germany, 2015; p. 28.
15. Wambura, F.J.; Ndomba, P.M.; Kongo, V.; Tumbo, S.D. Uncertainty of runoff projections under changing climate in wami river sub-basin. *J. Hydrol. Reg. Stud.* **2015**, *4*, 333–348. [[CrossRef](#)]
16. Wambura, F.; Dietrich, O.; Lischeid, G. Evaluation of spatio-temporal patterns of remotely sensed evapotranspiration to infer information about hydrological behaviour in a data-scarce region. *Water* **2017**, *9*, 333. [[CrossRef](#)]
17. GLOWS-FIU. *Water Atlas of Wami/Ruvu Basin, Tanzania*; GLOWS-FIU: North Miami, FL, USA, 2014; p. 120.
18. Mnenwa, R.; Maliti, E. *A Comparative Analysis of Poverty Incidence in Farming Systems of Tanzania*; Research on Poverty Alleviation: Dares Salaam, Tanzania, 2010; p. 37.
19. Liwenga, E.T. *Food Insecurity and Coping Strategies in Semiarid Areas: The Case of Mvumi in Central Tanzania*. Ph.D Thesis, University of Stockholm, Stockholm, Sweden, 21 March 2003.
20. Faße, A.; Kissoly, L.; Brüßow, K.; Grote, U. *Household Survey Wave I: Baseline*; Institute for Environmental Economics and World Trade (IUW) at the Leibniz University of Hannover (LUH)ermany; Leibniz University of Hannover: Hannover, Germany, 2014.
21. Aretano, R.; Petrosillo, I.; Zaccarelli, N.; Semeraro, T.; Zurlini, G. People perception of landscape change effects on ecosystem services in small mediterranean islands: A combination of subjective and objective assessments. *Landsc. Urban Plan.* **2013**, *112*, 63–73. [[CrossRef](#)]
22. Brehm, J.M.; Eisenhauer, B.W.; Stedman, R.C. Environmental concern: Examining the role of place meaning and place attachment. *Soc. Nat. Resour.* **2013**, *26*, 522–538. [[CrossRef](#)]
23. Ndamani, F.; Watanabe, T. Determinants of farmers’ climate risk perceptions in agriculture—A rural Ghana perspective. *Water* **2017**, *9*, 210. [[CrossRef](#)]
24. Dobbie, M.; Green, R. Public perceptions of freshwater wetlands in Victoria, Australia. *Landsc. Urban Plan.* **2013**, *110*, 143–154. [[CrossRef](#)]
25. Röschel, L. *Perception of Environmental Changes and Its Effects on Food Security and Water Availability*. Master’s Thesis, Humboldt University of Berlin, Berlin, Germany, 19 May 2016.
26. Bogner, F.X. The influence of a residential outdoor education programme to pupil’s environmental perception. *Eur. J. Psychol. Educ.* **2002**, *17*, 19–34. [[CrossRef](#)]
27. Huang, C.H.; Yu, S.C. A study of environmental perception patterns of the visually impaired and environmental design. *Indoor Built Environ.* **2013**, *22*, 743–749. [[CrossRef](#)]
28. O’Brien, K.L.; Leichenko, R.M. Double exposure: Assessing the impacts of climate change within the context of economic globalization. *Glob. Environ. Chang.* **2000**, *10*, 221–232. [[CrossRef](#)]
29. Van de Walle, D.; Cratty, D. Is the emerging non-farm market economy the route out of poverty in Vietnam? *Econ. Transit.* **2004**, *12*, 237–274. [[CrossRef](#)]
30. Imai, K.S.; Gaiha, R.; Thapa, G. Does non-farm sector employment reduce rural poverty and vulnerability? Evidence from Vietnam and India. *J. Asian Econ.* **2015**, *36*, 47–61. [[CrossRef](#)]
31. Stern, P.C.; Dietz, T.; Guagnano, G.A. The new ecological paradigm in social-psychological context. *Environ. Behav.* **1995**, *27*, 723–743. [[CrossRef](#)]
32. Pickering, A.J.; Davis, J. Freshwater availability and water fetching distance affect child health in sub-Saharan Africa. *Environ. Sci. Technol.* **2012**, *46*, 2391–2397. [[CrossRef](#)] [[PubMed](#)]
33. Cairncross, S. The benefits of water supply. In *Developing World Water 2*; Pickford, J., Ed.; Grosvenor Press: London, UK, 1987; pp. 30–34.



Article

# Application of EMI and FDR Sensors to Assess the Fraction of Transpirable Soil Water over an Olive Grove

Giovanni Rallo <sup>1,\*</sup>, Giuseppe Provenzano <sup>2</sup>, Mirko Castellini <sup>3</sup> and Àngela Puig Sirera <sup>1</sup>

<sup>1</sup> Dipartimento Scienze Agrarie, Alimentari e Agro-Ambientali, Università di Pisa, Via del Borghetto 80, 56124 Pisa, Italy; a.puigsirera@studenti.unipi.it

<sup>2</sup> Dipartimento Scienze Agrarie, Alimentari e Forestali, Università degli Studi di Palermo, Viale delle Scienze 12 Ed. 4, 90128 Palermo, Italy; giuseppe.provenzano@unipa.it

<sup>3</sup> Council for Agricultural Research and Economics-Agriculture and Environment Research Center (CREA-AA), Via Celso Ulpiani 5, 70125 Bari, Italy; mirko.castellini@crea.gov.it

\* Correspondence: giovanni.rallo@unipi.it; Tel.: +39-050-221-6158

Received: 27 November 2017; Accepted: 5 February 2018; Published: 8 February 2018

**Abstract:** Accurate soil water status measurements across spatial and temporal scales are still a challenging task, specifically at intermediate spatial (0.1–10 ha) and temporal (minutes to days) scales. Consequently, a gap in knowledge limits our understanding of the reliability of the spatial measurements and its practical applicability in agricultural water management. This paper compares the cumulative EM38 (Geonics Ltd., Mississauga, ON, Canada) response collected by placing the sensor above ground with the corresponding soil water content obtained by integrating the values measured with an FDR (frequency domain reflectometry) sensor. In two field areas, characterized by different soil clay content, two Diviner 2000 access tubes (1.2 m) were installed and used to quantify the dimensionless fraction of transpirable soil water (*FTSW*). After the calibration, the work proposes the combined use of the FDR and electromagnetic induction (EMI) sensors to measure and map *FTSW*. A strong correlation ( $R^2 = 0.86$ ) between *FTSW* and EM38 bulk electrical conductivity was found. As a result, field changes of *FTSW* are due to the variability of soil water content and soil texture. As with the data acquired in the field, more structured patterns occurred after a wetting event, indicating the presence of subsurface flow or root water uptake paths. After assessing the relationship between the soil and crop water status, the *FTSW* domain includes a critical value, estimated around 0.38, below which a strong reduction of relative transpiration can be recognized.

**Keywords:** olive grove; sap flow; relative transpiration; FDR sensor; EM38; fraction transpiration soil water

## 1. Introduction

Accurate measurements of soil water status across different spatial and temporal scales are a challenging task, especially at intermediate spatial (0.1–10 ha) and temporal (minutes to days) scales. There is still a gap in knowledge related to the reliability of the spatial measurements of soil water content (SWC) and their practical applicability for irrigation scheduling [1].

In micro-irrigated heterogeneous crop systems, such as Mediterranean arboreal crops, field variability of SWC depends on the spatial distribution of the roots and the localized water supply. However, the physical characteristics of the soil can be responsible for SWC field variability, which in turn affects the spatial distribution of root density. These factors are, in fact, tightly interconnected: roots are not uniformly distributed in the soil and water availability is heterogeneous in space and time. Consequently, such heterogeneity affects the crop water status and management strategies. Moreover, it has been observed that plants, including tree crops, can take up soil water, even when

the SWC is lower than the theoretical wilting point, which corresponds to a soil matric potential of  $-1.5$  MPa [2]. These behaviors need to be accounted for in precision irrigation scheduling and ecophysiological research [3].

The fraction of transpirable soil water (*FTSW*) [4] has been frequently used to monitor crop water status and as an indicator of soil water deficit [4–6]. *FTSW* can be computed as the ratio between available soil water (*ASW*) and total transpirable soil water (*TTSW*) for a given crop in a given soil [7]. Furthermore, *TTSW* is defined as the difference between soil water content at field capacity and a minimum value that, depending on crop species, is obtained when plants are no longer able to extract water from the soil. These two values can be directly estimated in the field and not in the laboratory by analyzing the temporal dynamics of the soil water content [8].

*TTSW* is frequently lower than the theoretical soil water availability, mainly when root density becomes limiting for water extraction [4,9]. However, *TTSW* may exceed the theoretical value in the upper soil layer, probably due to the loss of water by evaporation at the soil surface. Research results evidenced that for sparse crops, such as vineyards [10] and olive groves [11], at the end of the cropping season the minimum soil water content resulted in a lower level than the wilting point in the upper soil layers (above 0.3 m). Additionally, the minimum soil water content was higher than the wilting point when considering the deeper soil layers with low root density.

*FTSW* allows the plant water stress to be estimated through the reductions in root water uptake and/or flux transpiration, both representing natural responses of the plant to drought [3]. Such reductions are usually schematized based on the macroscopic approach. This method represents the root water uptake by a sink term in the volumetric mass balance. The microscopic approach, on the other hand, requires detailed knowledge of the roots' characteristics, which is difficult to evaluate.

Using the macroscopic approach, it is possible to assess empirical functions (i.e., crop water deficit response). This procedure is able to describe the plant's response to *FTSW*, which includes parameters depending on soil or crop water status [3]. Therefore, actual transpiration fluxes can be determined by multiplying the maximum crop transpiration for the relative transpiration, which depends on the soil/plant water status, and environmental variables.

Measurements of tree transpiration fluxes are required to calibrate the crop water deficit response function. For this reason, innovative monitoring technologies, such as micrometeorological techniques, allow distributed values of actual evapotranspiration fluxes to be measured. These techniques coupled with tree sap flow measurements permit soil evaporation and plant transpiration fluxes to be evaluated separately [12,13]. At the same time, micrometeorological approaches can be used to validate the tree flux upscaling procedures [14].

Due to the high sensitivity of *FTSW* to variations in the soil water content in the rooting domain, only downhole soil moisture sensors have been established. These sensors measure the dynamics of soil volumetric water content in depth and time. As a consequence, this tool is desirable to monitor soil water status indicators, such as *FTSW*. Generally, this instrument uses the FDR (frequency domain reflectometry) technique to estimate the volumetric soil water content (*SWC*) ( $\text{m}^3 \text{m}^{-3}$ ) on the basis of a calibration equation provided by the manufacturer. Nonetheless, this calibration equation cannot provide accurate measurements of volumetric soil water content for all soil types due to the dependence of the soil dielectric properties on its texture and structure.

In addition, agricultural activities alter soil properties, such as the bulk density and organic matter content, with consequent effects on water storage capacity. Consequently, site-specific calibration equations have been recommended when an accuracy of the actual volumetric soil water content is requested [15–17]. Thus, a network of downhole sensors is necessary to explore the spatial variability of *SWC* at the field level. However, this solution requires high investment for the installation and maintenance of sensors.

In precision agriculture, electromagnetic induction (EMI) represents an efficient method for accurately monitoring variations at field level of the physical and chemical properties of the soil [18]. This method of soil water monitoring does not use radioactive sources, is non-invasive, allows

quick acquisitions, and is easy to use. Moreover, this technique does not require field installation of ancillary devices.

EMI sensors measure the bulk electrical conductivity (EC) profiles of soil, which are strongly influenced by soil water content. Due to this fact, the technique has also been applied to investigate the spatiotemporal variability of soil water content at a field scale [18]. According to the EM38 sensor (Geonics Ltd., Mississauga, ON, Canada), several authors have suggested the use of a linear combination of punctual measurements that are acquired by placing the sensor in a horizontal and a vertical mode [19]. Moreover, Huth and Poulton [19] showed that when the effects of seasonal fluctuations in soil temperatures are accounted for, the variations of EMI measurements are strongly correlated with soil water content. Thus, EMI sensors can be effectively used for quick monitoring of the soil water content at the field scale.

The main objective of this research was to verify whether combining the measurements acquired with the EM38 and FDR (Diviner 2000, Sentek Pty Ltd., Stepney, Australia) probes are able to provide quick and suitable data of soil water status in the root zone of an olive orchard. After identifying the EM38 calibration equation to predict the fraction of the transpirable soil water (*FTSW*), the ordinary Kriging procedure was used. This methodology maps the spatial changes of *FTSW* fixed in the EM38 monitoring during two irrigation seasons (2008 and 2009). Finally, the relationship between *FTSW* and the relative transpiration,  $\alpha$ , was assessed based on the values of actual crop transpiration,  $T_a$ , obtained by upscaling sap flow measurements.

## 2. Materials and Methods

The study area (Figure 1) was located in the southwest of Sicily (Italy) next to the town of Castelvetrano (TP) on the commercial olive farm “Tenute Rocchetta” (Lat: 37°38’35” N; Lon: 12°50’50” E). The olive orchard (cv. Nocellara del Belice) has an extension of 13 ha and it is planted according to a regular grid of 8 m × 5 m (~250 trees/ha). The orchard is irrigated with a micro-irrigation system with drip laterals along the tree rows. Each lateral contains four 8 L/h emitters per tree, placed on both sides of each plant at a distance of one and two meters. The fraction of wetted soil after an irrigation event was generally equal to 0.2, while the fraction of canopy cover was about 0.3.

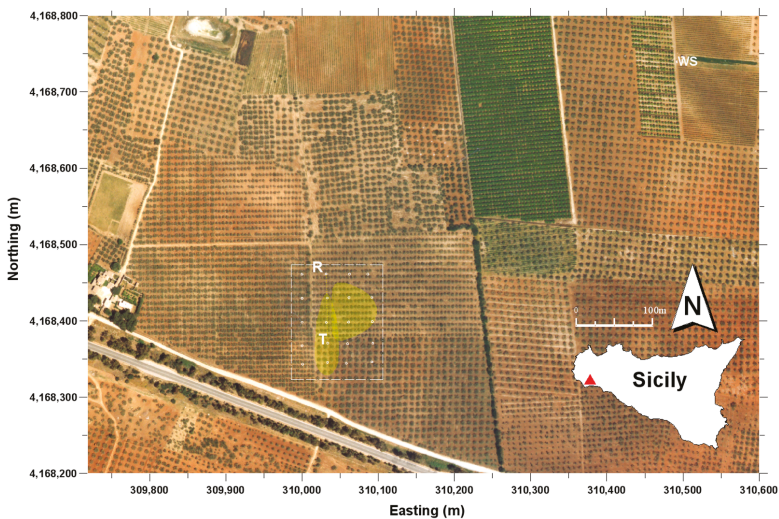


**Figure 1.** Location of the experimental farm with the sampling zone (dashed box) and the measurement points (dots). Scintillometric footprints (yellow shaded area) along two wind directions are also indicated. WS: weather station; R: scintillometer receiver unit; T: scintillometer transmission unit.

The experimental activities were conducted during two irrigation seasons in 2008 and 2009. The irrigation scheduling followed the ordinary management practised in the surrounding area [20]. In 2008, the total irrigation depth provided by the farmer was equal to 122 mm divided into four watering events, whereas in 2009 it resulted in 127 mm distributed into five events.

Previous research activities [3,12,14,21] on the farm have investigated different monitoring techniques for crop water requirements. These have been done at different spatial scales and acquisition platforms: ground-based sensing [3], micrometeorology [12,14], and remote sensing acquisitions [21]. During 2008, a scintillometric application [14] addressed quantifying crop water requirements at the field scale. This process validated an upscaling procedure of the tree fluxes based on measurements of the leaf area index by remote sensing.

Because the upscaling procedure [13] was calibrated with reference to the sensing surface (footprint) investigated by the scintillometer, our research used variables collected in a sampling area covering this sensing surface. In particular, according to a preliminary footprint analysis (Figure 1), sampling points for the physical analysis and bulk electrical conductivity measurements of the soil were chosen inside the area where the “relative normalized contribution” to actual evapotranspiration,  $ET_r$ , was on average close to the daily maximum. The footprint reference area was marked by considering the wind direction acting along and perpendicular to the scintillometer path in order to be sure that the location of the source area was always inside the sampling grid (Figure 1).

The soil’s electrical conductivity and texture and bulk electrical conductivity were evaluated on a surface of 1.25 ha in which 20 measurements were selected according to a 25 m × 25 m square grid. In each point, soil texture analysis and six EM38 measurements (three with horizontal and three with a vertical dipole) were collected. The EM38 sensor was in particular placed at ground level and (i) at the center of four trees, (ii) in the middle between two trees along the row and (iii) below an emitter.

In 2008, an irrigation event of about 33 mm distributed over two days was monitored with EM38, while in 2009 two events were observed. For each wetting event, EM38 measurements were executed immediately before and after irrigation until the following watering based on a weekly time-step. Furthermore, additional measurements of soil water status were collected during and after rain events.

### 2.1. Soil Physical Characterization and EM38 Calibration Procedure

A preliminary analysis determined the soil salinity on sieved soil randomly collected in the topsoil (0–0.3 m). Soil electrical conductivity was determined on 1:5 soil-water extract with a conductivity meter (microCM 2200, Crison Instruments, Barcelona, Spain) by a standard procedure [22]. These results showed the absence of salt accumulation since the electrical conductivity ranged from 0.11 to 0.36 dS m<sup>-1</sup> [23].

A texture analysis was performed on the soil samples collected on the grid to determine the spatial variability of the clay content in the area. At each sampling point, around 1 kg of topsoil (0–0.3 m) was collected and the sample positions (Universal Transverse Mercator, UTM, coordinates system) detected with a differential GPS (Global Positioning System). The textural distribution of the soil samples was determined in the laboratory by the hydrometer method. The percentage of clay content (diameter lower than 2 µm) was used as a proxy variable to investigate the spatial variability of both the EM38 response and the fraction of transpirable soil water (FTSW).

Due to the considerable variability of the soil clay content, two sites (A and B) were selected to calibrate the EM38 sensor. At each site, a more detailed soil textural analysis was carried out on disturbed soil samples collected every 0.15 m up to 1.2 m depth. After analyzing each sample, the data was aggregated in layers of 0.3 m depth. At each site, a Diviner 2000 access tube, 1.2 m long, was installed. This technique permitted pairing the measurements of soil bulk electrical conductivity and SWC along the soil profile. The Diviner 2000 [16] is a handheld monitoring device for soil water content. It consists of a portable display/logger unit connected to an automatic depth-sensing probe in which two electric rings, forming a capacitor, are installed at its extremity. The capacitor and the oscillator represent a circuit that generates an oscillating electrical field into the soil through the wall

of the access tube. Consequently, the sensor's output is represented by the resonant frequency of the circuit (raw count) that depends on the dielectric properties of the soil surrounding the access tube. The resonant frequency detected by the sensor in the soil ( $F_s$ ) is scaled to a value,  $SF$ , ranging between 0 and 1 on the basis of the frequency readings obtained in air ( $F_a$ ) and water ( $F_w$ ). At the same time, the site-specific calibration equations proposed by Provenzano et al. [17] were used to transform the scaled frequency measured by the Diviner 2000 probe and to obtain accurate SWC estimations for the investigated sites.

The EM38 sensor (Geonics Ltd., Mississauga, ON, Canada) consists of a transmitter and a receiver coil, installed 1.0 m apart at the opposite ends of a bar, and operating at a frequency of 14.6 kHz. The investigated depth range depends on the coil configuration, as well as on the distance between coils [24]. While the distance is fixed, the coils can be oriented in a vertical mode with the magnetic dipole maintained perpendicular to the soil surface, or in a horizontal mode with the dipole parallel to the soil surface. In the horizontal mode, the highest sensitivity is at the soil surface, while in the vertical mode the maximum is approximately 0.3–0.4 m below the instrument. The measurement unit of the bulk electrical conductivity ( $EC$ ) is in milliSiemens per meter ( $mS\ m^{-1}$ ).

The calibration procedure was carried out during the irrigation season of 2008. It was based on 47 profiles of soil water content and contextual readings of the soil bulk electrical conductivity in the vertical ( $EC_V$ ) and horizontal ( $EC_H$ ) dipole orientations. EM38 measurements were acquired around the Diviner 2000 access tubes in different periods to explore at both sites a wide range of soil water status conditions.

The EM38 was calibrated and nulled according to the manufacturer's instruction before each measurement. Vertical ( $EC_V$ ) and horizontal ( $EC_H$ ) readings were weighted in order to obtain a single value of the total soil electrical conductivity ( $EC_t$ ) as suggested by Cook and Walker [25]. A linear combination of vertical and horizontal readings was particularly used to assess a single depth response function that better matches the portion of the investigated soil profile ( $EC_t$ ):

$$EC_t = 0.77EC_V + 0.23EC_H \quad (1)$$

Following the approach suggested by Lacape et al. [4], at each site the total transpirable soil water ( $TTSW$ ) was calculated by summing the differences over the explored soil depth (1.2 m) between the soil water content at field capacity ( $SWC_{fc}$ ) (upper limit) and the minimum soil water content ( $SWC_{min}$ ) (lower limit):

$$TTSW = \sum_0^{1.2} (SWC_{fc} - SWC_{min}) \quad (2)$$

In addition, the available soil water at a given time ( $ASW$ ) was calculated by summing the differences between the actual ( $SWC_d$ ) and minimum ( $SWC_{min}$ ) soil water content over the same soil depth:

$$ASW = \sum_0^{1.2} (SWC_d - SWC_{min}) \quad (3)$$

Soil water content at a field capacity ( $SWC_{fc}$ ), as well as the lower limit ( $SWC_{min}$ ), was directly obtained by examining the temporal dynamics of SWC along the soil profile, following the assumptions of Polak et al. [8]. Immediately after a wetting event, a sharp decrease in SWC occurs, mainly due to the free drainage in which the root water uptake can be neglected. After that, the reductions in SWC are due to the combination of free drainage and root water uptake. This takes place until a period in which free drainage ceases and SWC reaches its minimum ( $SWC_{min}$ ). Below this value, the roots cannot extract more water from the soil [4].

As suggested by Polak et al. [8], SWC can be considered "close to" field capacity ( $SWC_{fc}$ ) when most of the free water has drained. In irrigation science, this value is considered the upper limit of available soil water, while, as suggested by Lacape et al. [4],  $SWC_{min}$  can be placed instead of the ordinary wilting point.

## 2.2. Transpiration Fluxes and Relative Transpiration Measurements

The standard meteorological variables were provided by the SIAS (Servizio Informativo Agrometeorologico Siciliano) weather station n. 302, located about 500 m northeast of the experimental site (Figure 1). The weather station is equipped with sensors for hourly measurements of air temperature at a 2-m height, precipitation, relative air humidity, wind speed and direction at 2- and 10-m heights, air pressure, and global incoming solar radiation. The net radiation  $R$  and its components were measured with a four-component net radiometer (NR01, Hukseflux, Delft, The Netherlands).

The macroscopic approach was used to quantify the water status of the olive trees, defined as a reduction term ( $\alpha$ ) of maximum crop transpiration:

$$\alpha = \frac{T_a}{T_p} \quad (4)$$

where  $T_a$  and  $T_p$  are the actual and maximum transpiration, respectively. Once the latter is determined, the knowledge of  $\alpha$  allows the estimation of actual transpiration  $T_a$ . The maximum transpiration ( $T_p$ ), was estimated by following the procedure suggested by Jarvis and McNaughton [26]:

$$T_p = \frac{\Delta R + \frac{\rho C_p VPD}{r_a}}{\lambda \left[ \Delta + \gamma \left( \frac{r_a + r_{c,min}}{r_a} \right) \right]} \quad (5)$$

where  $\Delta$  ( $\text{kPa } ^\circ\text{C}^{-1}$ ) is the slope of the saturation vapor pressure curve,  $R$  ( $\text{W m}^{-2}$ ) is the net radiation,  $\rho$  ( $\text{Kg m}^{-3}$ ) is the air density,  $C_p$  ( $\text{J Kg}^{-1} \text{K}^{-1}$ ) is the air specific heat at constant pressure,  $\gamma$  ( $\text{kPa K}^{-1}$ ) is the psychrometric constant,  $VPD$  ( $\text{kPa}$ ) is the air vapor pressure deficit,  $\lambda$  ( $\text{J Kg}^{-1}$ ) is the latent heat of vaporization, and  $r_a$  and  $r_{c,min}$  are the aerodynamic and the minimum canopy resistance ( $\text{s m}^{-1}$ ), respectively. All the variables in Equation (5) were obtained from the recorded meteorological data, except  $r_a$  and  $r_c$ , determined as indicated in Rallo and Provenzano [3].

The actual transpiration  $T_a$  was measured hourly on three olive trees by using two standard thermal dissipation probes (TDPs) [27] per tree. These trees were chosen based on a preliminary biometric analysis addressed to quantify the spatial distribution of leaf area index (LAI) in the study area. The measurements of LAI were performed with the LAI 2000 (Li-Cor Inc., Lincoln, NE, USA) by following a standard protocol for tree crops [28]. Considering that LAI was distributed according to a normal distribution with average  $\mu = 1.55 \text{ m}^2 \text{ m}^{-2}$  and standard deviation  $\sigma = \pm 0.4$ , trees with LAI between  $\mu - \sigma$  and  $\mu + \sigma$  were chosen to install the TDPs. At the end of the experiments, the sapwood area was determined by a colorimetric method on a total of six wood cores extracted with a Pressler gimlet from the same three trees and between each couple of sap flow probes.

Daily values of actual transpiration were obtained by integrating the instantaneous sap flux, following the hypothesis of neglecting tree capacitance. Daily transpiration depth ( $\text{mm day}^{-1}$ ) was obtained by dividing the daily flux ( $\text{L day}^{-1}$ ) for the pertinence area of the plant, equal to  $40 \text{ m}^2$ .

Afterwards, to evaluate a representative value of the stand transpiration for the entire field, it was necessary to upscale the plant fluxes. This was done by considering, as a proximal variable, the ratio between the average leaf area index ( $\text{LAI}_{\text{field}}$ ) and the value ( $\text{LAI}_{\text{plant}}$ ) measured on the plant in which sap fluxes were monitored. The up-scaling factor for each plant was derived by the remotely sensed LAI maps, as described in Cammalleri et al. [13], and validated by comparison with micrometeorological observed data [13,21].

## 2.3. Data Analysis and Pre-Processing

In 2008, a calibration model to estimate indirectly  $FTSW$  in the soil profile (1–2 m depth) was derived from the paired FDR and EM38 measurements. The  $EC_V$  and  $EC_H$  values were used to obtain the total electrical conductivity,  $EC_t$  (Equation (1)). The root mean square error (RMSE) was used to quantify the performance of the relationship between  $FTSW$  and  $EC_t$ .

A geostatistical analysis allowed the spatialization of both the clay content and the *FTSW* by means of ordinary Kriging [29].

Meteorological and sap flow data were pre-processed in order to create a database of daily values of maximum crop transpiration  $T_p$ , actual transpiration  $T_a$ , and relative transpiration  $\alpha$ . During 2008, the  $T_a$  dataset comprehended the period from the first decade of June, corresponding to the initial fruit development stage, to the first decade of September, at the crop maturity stage.

XLSTAT statistical software and data analysis (Addinsoft XLSTAT, Paris, France) was used for the relationship between *FTSW* and relative transpiration  $\alpha$ . Each  $\alpha$  value was plotted as a function of the average value of *FTSW* retrieved on the corresponding day. The threshold at which the relative transpiration begins to decline was determined by using a logistic regression analysis, as described in [30].

### 3. Results and Discussion

#### 3.1. Soil Surface Texture and Spatial Analysis

High variability of clay content was observed in the investigated area with values ranging between 15% and 40%. Sand content, on the other hand, was characterized by a maximum of 75% and a minimum of 41%. According to the USDA (United States Department of Agriculture) classification, the most frequent textural classes are represented by sandy-clay-loam and clay-loam (Figure 2).

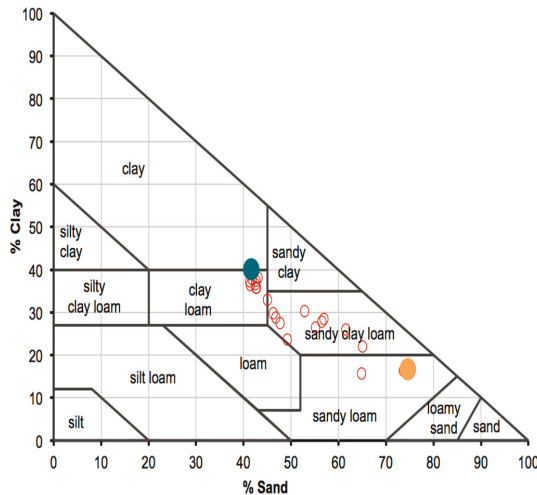
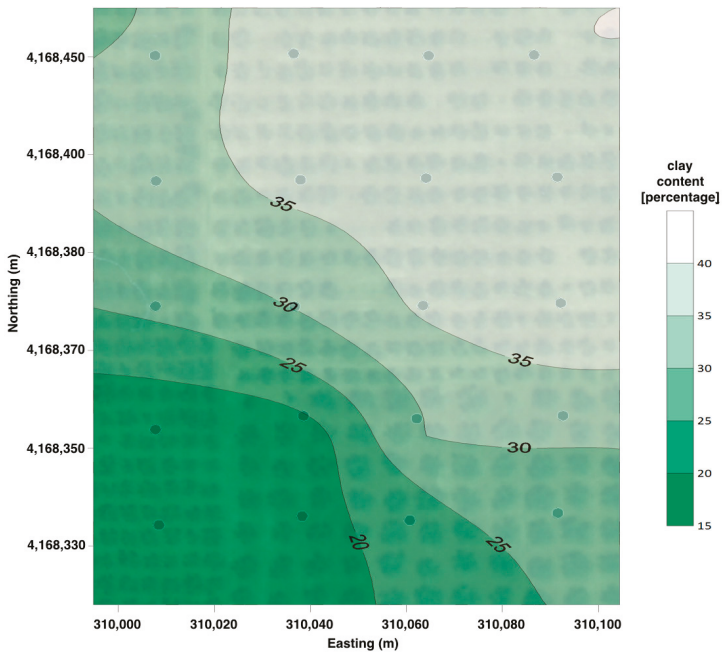


Figure 2. USDA soil texture triangle and texture of topsoil samples collected at EM38 measurement points.

The Kriging analysis of the spatialized clay content data showed a linear variogram and, consequently, it did not present range and sill parameters. However, a nugget variance effect (nugget = 17.8) was observed, which is imputable to measurement errors and/or to spatial sources of variation at distances smaller than the sampling interval. Thus, Figure 3 shows the map of measured clay percentage. As it can be observed, the coarsest texture (clay  $\leq$  20%) is mainly located in the southwest side of the study area.



**Figure 3.** Map of the topsoil clay percentage. North and East coordinates are referred to UTM ED50 system. The sampling points (dots) and a transparent image of the field are also shown.

According to the wide variability of soil clay content, two Diviner 2000 access tubes were installed in the NE (site A) and SW (site B) sides of the field. At both sites, the EM38 sensor had been preliminarily calibrated. Moreover, a detailed soil textural analysis was performed on disturbed soil samples collected every 0.15 m, up to 1.2 m depth. Table 1 shows the vertical distribution of clay content on layers of 0.3 m depth for sites A and B. Each value was obtained as the average of two measurements from each 0.15 m depth layer.

**Table 1.** Vertical distribution of clay percentages in sites A and B.

Soil Layer (m)	Clay Content [%]	
	Site A	Site B
0–0.3	42.4	28.4
0.3–0.6	43.3	27.8
0.6–0.9	39.1	27.3
0.9–1.2	27.9	26.0

As it can be observed, site A is characterized by higher clay content than site B at all depths. Moreover, the percentage of clay decreased with soil depth in site A, whereas site B was more uniform.

### 3.2. Evaluation of Total Transpirable Soil Water (TTSW)

A wide range of soil water content was considered for calibrating the EM38 sensor. Figure 4 shows the maximum profiles, the average and the minimum SWC. The variability of SWC at site A was more marked than at site B due to the higher clay content. Additionally, the variability in the soil water content along the profile ensured that the collected dataset encompassed most of the soil water status occurring during the investigated irrigation season.

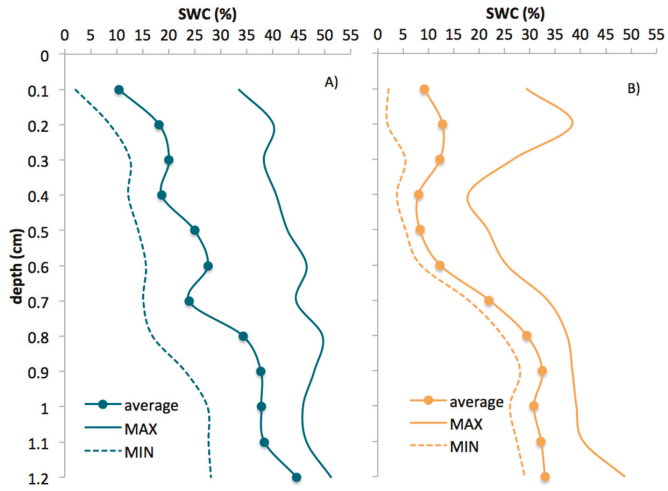


**Figure 4.** Maximum, minimum, and average profiles of soil water content observed at **A)** sites A and **B)** site B.

Figure 5 displays the temporal dynamics of the measured SWCs for sites A and B, respectively, during the 2008 irrigation season. In the same graphs, the transitory of SWCs among the three stages described by Polak et al. [8] are also shown. Measurements were collected from May 20th, about 10 days after the rainy events registered in the first decade of the month. According to the low transpiration activity and the limited rainfall of the period, it is plausible to hypothesize that the initial SWCs were acquired in the absence of free drainage when only root water uptake occurred. In agreement with Polak and Wallach [8], this SWC corresponds to the field capacity of the layer. Practically, we considered  $SWC_{fc}$  as the average value of SWC data collected from 1 June to 19 June.

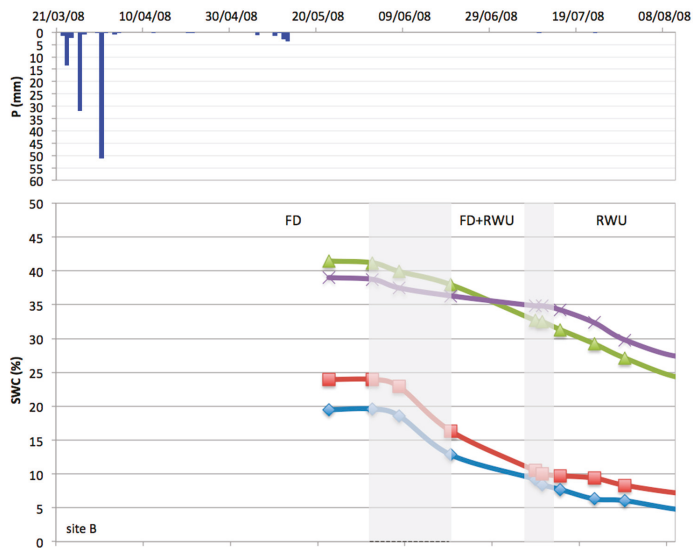


**Figure 5.** Cont.

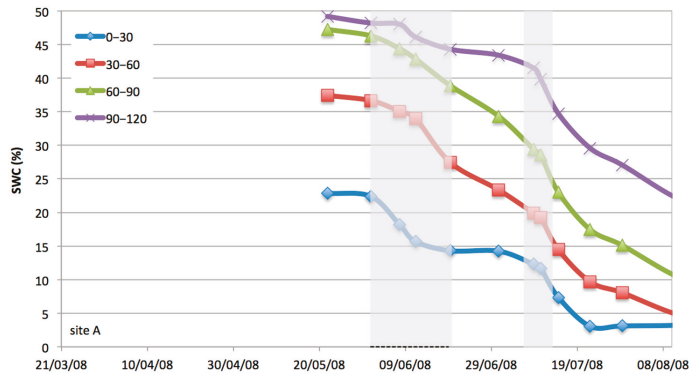


**Figure 5.** Temporal dynamics of SWC observed at different soil layers at sites A and B. Shaded zones represent the transitory phases of SWCs between the stages of free drainage (FD), free drainage and root water uptake (FD + RWU), and root water uptake (RWU).

The analysis of SWC acquired over the whole season allowed, as well, the evaluation of the minimum soil water content  $SWC_{min}$ .

Based on the above-mentioned analysis, the upper ( $SWC_{fc}$ ) and the lower ( $SWC_{min}$ ) limits used to evaluate  $TTSW$  were obtained for both sites at the investigated soil layers. Figure 6 shows the values of  $SWC_{fc}$  and  $SWC_{min}$  for the four soil layers, as well as the corresponding  $TTSW$ .

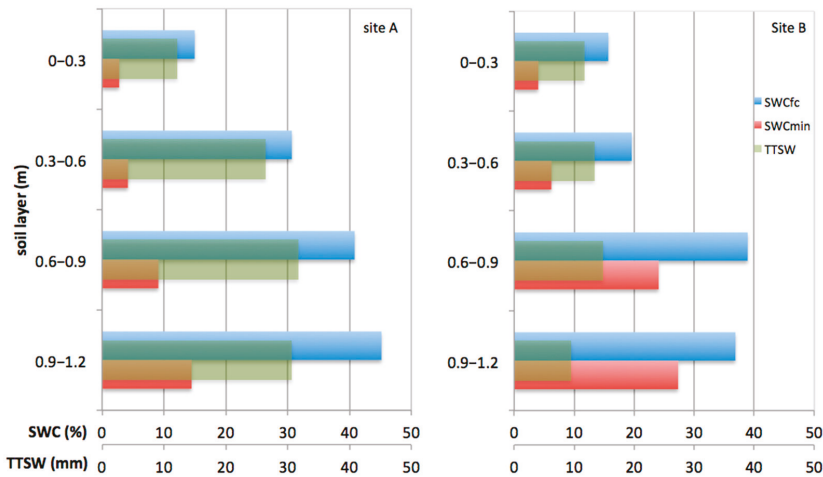


**Figure 6.** Upper ( $SWC_{fc}$ ) and lower ( $SWC_{min}$ ) limits of  $TTSW$  obtained for the four soil layers at sites A (left) and B (right).

When considering the upper soil layer (0–0.3 m),  $TTSW$  values were similar at sites A and B, whereas these values were higher at site A than at B when the higher depths are considered. The  $SWC_{min}$  at A was lower than at B for all investigated depths while, on the contrary, the  $SWC_{fc}$  was generally higher. These limits depend on soil texture, as well as on the root water uptake ability [9]. At both sites, the differences in  $TTSW$  were consistent with the recognized soil textures.

### 3.3. EM38 Model to Predict the Fraction of Transpirable Soil Water

As illustrated in Figure 7, a strong correlation was observed between  $EC_t$  measured with EM38 and the corresponding  $FTSW$  values obtained with the Diviner 2000 measurements. Experimental  $FTSW$  and  $EC_t$  data obtained at sites A and B were linearly correlated with  $R^2$  and RMSE equal to 0.86 and 0.10, respectively.

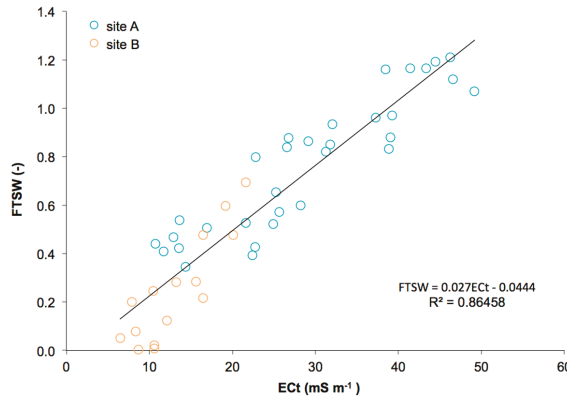


Figure 7. Values of  $FTSW$  versus EM38 readings for sites A and B and their corresponding fitting equation.

Huth and Poulton obtained similar results [19], which evidenced that the term  $SWC_{min}$  used to evaluate  $FTSW$  accounts for the electrical conductivity of the solid phase. Consequently, it reduces the effects of the different clay content that characterizes these two sites. Even the term  $SWC_d - SWC_{min}$  accounts for the effects of both the electrical conductivity of the liquid phase and of the soil pore space.

### 3.4. Temporal and Spatial Variability of Soil Bulk Electrical Conductivity and Plant Water Status

Figure 8 depicts the temporal dynamics of the soil bulk electrical conductivity  $EC_t$  measured with the EM38 sensor during the irrigation seasons of 2008 and 2009, as well as the irrigation and precipitation events occurring in the examined periods. As it can be observed, the temporal dynamics of  $EC_t$  are sensible to changes in the soil water status. In fact,  $EC_t$  values increased after the wetting events and decreased during soil drying processes.

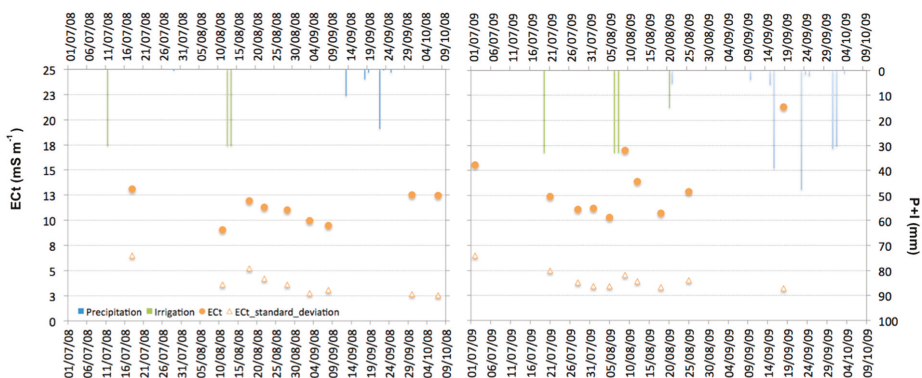
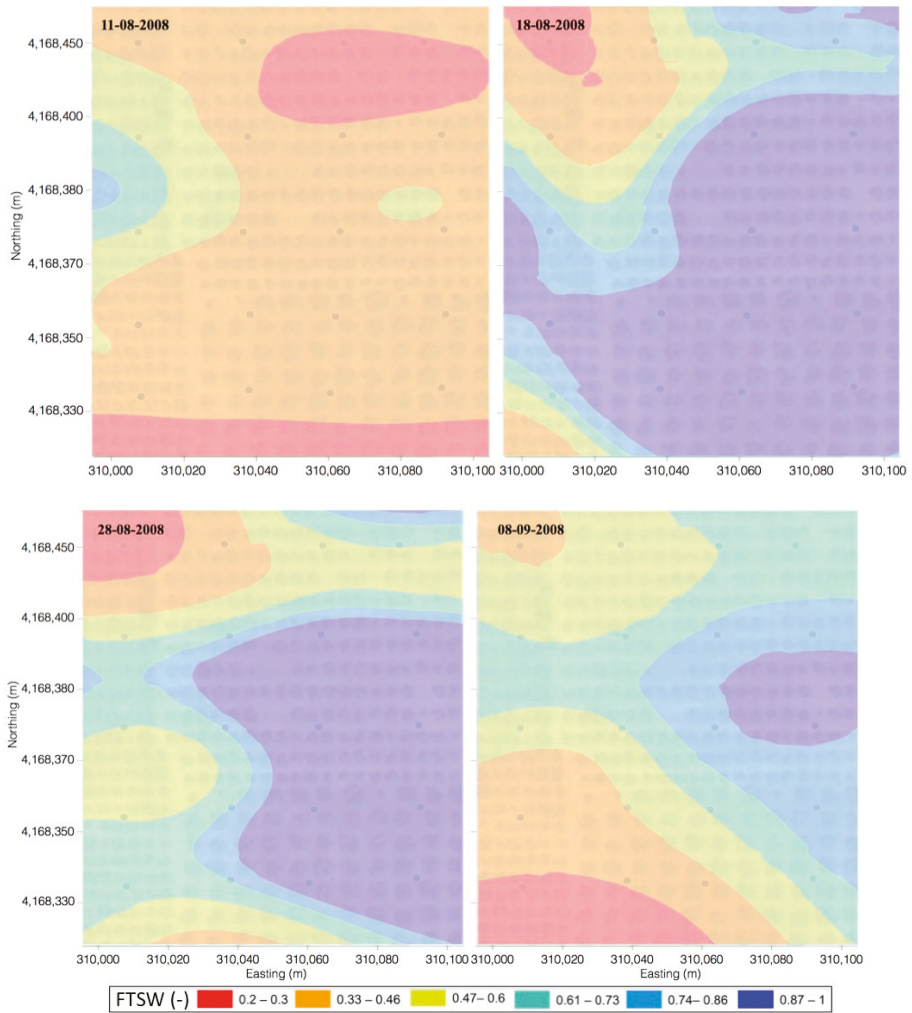


Figure 8. Temporal dynamics of  $EC_t$  values and the corresponding standard deviation during the irrigation seasons of 2008 and 2009. Irrigation and precipitation events are also represented.

Even the standard deviation associated with  $EC_t$  was higher after irrigation and lower when the soil was dry. This higher standard deviation observed after irrigation events is mainly due to the localized irrigation system. In fact, EM38 readings, collected at the center of four trees, did not detect any change in soil water content, contrary to the readings collected below the emitters.

Relative to the 2008 season, the spatiotemporal variability of  $FTSW$  values was investigated before and after the irrigation event of 14 August. Figure 9 shows for some of these days the spatial distributions of  $FTSW$  indirectly estimated on the basis of the EM38 survey. In the same manner, more structured patterns occurred after irrigation as a possible consequence of subsurface flow, soil evaporation, and root water uptake processes. It is possible to assume that the combination of these hydrological processes affects the soil bulk electrical conductivity and therefore the fraction of water available to the plants.



**Figure 9.** Maps of transpirable soil water ( $FTSW$ ) fraction before and after the irrigation event of 14 August 2008. The sampling points (dots) and the field image are also shown.

According to the spatial variability of the soil texture (Figure 3), the fastest drying processes occurred in the east side of the area where the sand percentage is relatively higher. On the other hand, the west side, characterized by clay percentages higher than 30–35%, showed high values of *FTSW* even one month after irrigation.

### 3.5. Relations between Relative Transpiration and the Fraction of Transpirable Soil Water

Figure 10 displays the values of measured relative transpiration ( $\alpha$ ) as a function of the fraction of transpirable soil water (*FTSW*) estimated in 2008 and 2009. Moreover, this figure performs the logistic model used to fit the experimental data. As it can be observed for any fixed *FTSW*, the variability of the corresponding  $\alpha$  depends on the atmospheric water demand [3]. Despite the limited number of measurements related to the high water content, the values of the relative transpiration,  $\alpha$ , were practically constant when the soil water content was higher than a threshold, below which it decreased drastically. The statistical analysis evidenced a critical threshold of *FTSW*, approximately equal to 0.38, below which the reduction of relative transpiration is recognizable.

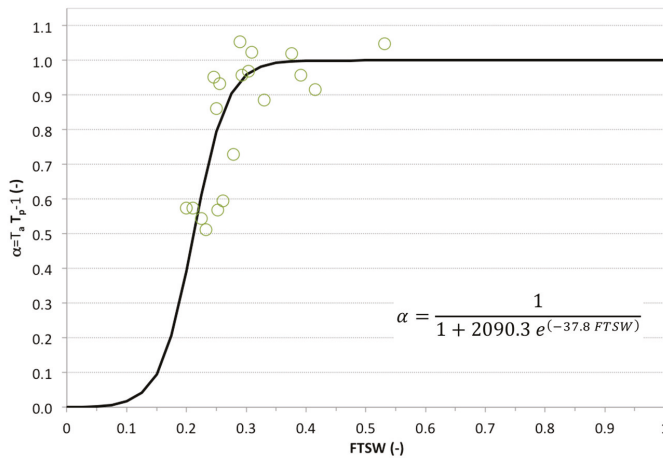


Figure 10. Relationship between relative transpiration and the fraction of transpirable soil water.

A more detailed analysis of the data evidenced that, despite a large variability of  $\alpha$ , the corresponding changes of *FTSW* were almost limited. Relative transpiration was more or less constant and equal approximately to 1 for a higher *FTSW* than the critical value, whereas the measured relative transpiration dropped off to a minimum value of about 0.5 for lower *FTSW*.

Unfortunately, the absence of  $T_a / T_p - 1$  measurements lower than 0.5 did not permit to clearly identify the best shape of the curve under more severe water stress conditions than those observed. In fact, it was very difficult to reach  $\alpha$  values lower than 0.5 for the examined situation, considering that (i) the high capacitance characterizing the olive plants allows a certain adaptation to water stress conditions; (ii) the investigated field is characterized by high values of soil water retention; and (iii) due to the relatively high plant spacing a large soil volume is available for root water uptake.

## 4. Conclusions

The measurements acquired in an olive orchard with the EM38 ground conductivity meter (Geonics Ltd., Mississauga, ON, Canada) combined with Diviner 2000 probe (Sentek Pty Ltd., Stepney, Australia) can provide quick and suitable monitoring of the fraction of transpirable soil water (*FTSW*). Moreover, the relationship between *FTSW* and the relative transpiration,  $\alpha$ , was assessed based on the

values of actual crop transpiration,  $T_a$ . These data were measured with sap-flow sensors and up-scaled through the leaf area index (LAI).

A strong linear relationship ( $R^2 = 0.86$ ) was found between the fraction of transpirable soil water (FTSW), integrated to a depth of 1.2 m, and the total bulk electrical conductivity ( $EC_t$ ). This last value was obtained by combining EM38 readings at the soil surface in the vertical and horizontal dipole orientations. Despite the different soil clay content characterizing the area, a single model was found to describe the variability of FTSW with  $EC_t$ . These results are in line with those of other authors who evidenced that the term  $SWC_{min}$ , used to evaluate FTSW, accounts for the conductivity of the solid phase. Consequently, it reduces the effects of the different clay contents characterizing the investigated sites.

More structured patterns of FTSW occurred after the irrigation events because of the occurrence of water redistribution, soil evaporation, and root water uptake processes. The high standard deviation, mainly observed after irrigation, was due to the localized irrigation system. This water distribution method determines extensive gradients of soil water content around the trees and through the soil depth.

In fact, EM38 readings collected at the center of four trees did not detect any change in soil water content, contrary to the readings collected below emitters. Therefore, to account for the large variability in root density and water uptake in arboreal crop systems, it is necessary to increase the temporal frequency of acquisition, as well as the number of spatial acquisitions. This procedure could be faced by means of a vehicular-based sampling.

The macroscopic approach was followed to assess the empirical function able to describe the plant water status response and to correlate the relative transpiration to the FTSW. Despite the limited number of measurements, a value of  $FTSW = 0.38$  was found as a critical threshold below which a strong reduction of relative transpiration can be recognized.

The research indicates the effectiveness of EMI techniques in monitoring the variations of soil water content in response to irrigation and root water uptake. This technique allows a great degree of flexibility in terms of spatial and temporal sampling resolution. This is possible mainly when precise knowledge of the vertical distribution of soil water content is not as important as its variation in time and space. The availability for using FDR measurements to calibrate EMI acquisitions in areas characterized by different soil properties has concrete advantages, even in precision agriculture, when accurate monitoring of soil water content is necessary. Furthermore, once performed, a suitable  $\alpha = f(FTSW)$  model for actual field transpiration fluxes could be determined by multiplying the maximum crop transpiration to the relative transpiration coefficient estimated by the proposed methodology. Further research will be carried out to extend the domain of explored FTSW values, and with a more detailed scheme of sampling.

**Acknowledgments:** Data analyses have been partly funded by the Università di Pisa (Fondi di Ateneo, 2016) and MIUR (Finanziamento delle attività base di ricerca, 2017-Rallo). Experimental data were collected in the frame of research projects co-financed by the University of Palermo.

**Author Contributions:** G.R. and G.P. designed the experimental layout and analyzed the data. Field experiments were carried out by G.R. All authors contributed to the final editing of the manuscript.

**Conflicts of Interest:** The authors declare no conflict of interest. The founding sponsors had no role in the design of the study; in the collection, analyses, or interpretation of data; in the writing of the manuscript; or in the decision to publish the results.

## References

1. Costantini, E.A.C.; Pellegrini, S.; Bucelli, P.; Storchi, P.; Vignozzi, N.; Barbetti, R.; Campagnolo, S. Relevance of the Lin's and Host hydroopedological models to predict grape yield and wine quality. *Hydrol. Earth Syst. Sci.* **2009**, *13*, 1635–1648. [[CrossRef](#)]
2. Xiloyannis, C.; Dichio, B.; Nuzzo, V.; Celano, G. Defence strategies of olive against water stress. *Acta Hort.* **1999**, *474*, 423–426. [[CrossRef](#)]

3. Rallo, G.; Provenzano, G. Modelling eco-physiological response of table olive trees (*Olea europaea* L.) to soil water deficit conditions. *Agric. Water Manag.* **2013**, *120*, 79–88. [CrossRef]
4. Lacape, M.J.; Wery, J.; Annerose, D.J.M. Relationships between plant and soil water status in five field-grown cotton (*Gossypium hirsutum* L.) cultivars. *Field Crop. Res.* **1998**, *57*, 29–43. [CrossRef]
5. Lecoeur, J.; Guilioni, L. Rate of leaf production in response to soil water deficits in field pea. *Field Crop. Res.* **1998**, *57*, 319–328. [CrossRef]
6. Wery, J.; Lecoeur, J. Learning crop physiology from the development of a crop simulation model. *J. Nat. Resour. Life Sci. Educ.* **2000**, *29*, 1–7.
7. Sinclair, T.; Ludlow, M. Influence of Soil Water Supply on the Plant Water Balance of Four Tropical Grain Legumes. *Aust. J. Plant Physiol.* **1986**, *13*, 329–341. [CrossRef]
8. Polak, A.; Wallach, R. Analysis of soil moisture variations in an irrigated orchard root zone. *Plant Soil* **2001**, *233*, 145–159. [CrossRef]
9. Cabelguenne, M.; Debaeke, P. Experimental determination and modelling of the soil water extraction capacities of crops of maize, sunflower, soya bean, sorghum and wheat. *Plant Soil* **1998**, *202*, 175–192. [CrossRef]
10. Trambouze, W.; Voltz, M. Measurement and modelling of the transpiration of a Mediterranean vineyard. *Agric. For. Meteorol.* **2001**, *107*, 153–166. [CrossRef]
11. Rallo, G.; Agnese, C.; Blanda, F.; Minacapilli, M.; Provenzano, G. Agro-Hydrological models to schedule irrigation of Mediterranean tree crops. *Ital. J. Agrometeorol.* **2010**, *1*, 11–21.
12. Motisi, A.; Consoli, S.; Papa, R.; Cammalleri, C.; Rossi, F.; Minacapilli, M.; Rallo, G. Eddy covariance and sap flow measurement of energy and mass exchanges of woody crops in a Mediterranean environment. *Acta Hortic.* **2012**, *951*, 121–127. [CrossRef]
13. Cammalleri, C.; Rallo, G.; Agnese, C.; Ciraolo, G.; Minacapilli, M.; Provenzano, G. Combined use of eddy covariance and sap flow techniques for partition of et fluxes and water stress assessment in an irrigated olive orchard. *Agric. Water Manag.* **2013**, *120*, 89–97. [CrossRef]
14. Cammalleri, C.; Agnese, C.; Ciraolo, G.; Minacapilli, M.; Provenzano, G.; Rallo, G. Actual evapotranspiration assessment by means of a coupled energy/hydrologic balance model: Validation over an olive grove by means of scintillometry and measurements of soil water contents. *J. Hydrol.* **2010**, *392*, 70–82. [CrossRef]
15. Starr, J.L.; Rowland, R. Soil Water Measurement Comparisons between Semi-Permanent and Portable Capacitance Probes. *Soil Sci. Soc. Am. J.* **2007**, *71*, 51–52. [CrossRef]
16. Evett, S.R.; Tolk, J.A.; Howell, T.A. Soil Profile Water Content Determination: Sensor Accuracy, Axial Response, Calibration, Temperature Dependence, and Precision. *Vadose Zone J.* **2006**, *5*, 894–907. [CrossRef]
17. Provenzano, G.; Rallo, G.; Ghazouani, H. Assessing Field and Laboratory Calibration Protocols for the Diviner 2000 Probe in a Range of Soils with Different Textures. *J. Irrig. Drain. Eng.* **2016**, *142*, 4015040. [CrossRef]
18. Corwin, D.L.; Plant, R.E. Applications of apparent soil electrical conductivity in precision agriculture. *Comput. Electron. Agric.* **2005**, *46*, 1–10. [CrossRef]
19. Huth, N.I.; Poulton, P.L. An electromagnetic induction method for monitoring variation in soil moisture in agroforestry systems. *Aust. J. Soil Res.* **2007**, *45*, 63–72. [CrossRef]
20. Rallo, G.; Agnese, C.; Minacapilli, M.; Provenzano, G. Comparison of SWAP and FAO agro-hydrological models to schedule irrigation of wine grapes. *J. Irrig. Drain. Eng.* **2012**, *138*, 581–591. [CrossRef]
21. Cammalleri, C.; Ciraolo, G.; Minacapilli, M.; Rallo, G. Evapotranspiration from an Olive Orchard using Remote Sensing-Based Dual Crop Coefficient Approach. *Water Resour. Manag.* **2013**, *27*, 4877–4895. [CrossRef]
22. Carter, M.R.; Gregorich, E.G.; Pennock, D.; Yates, T.; Braidek, J. Electrical Conductivity and Soluble Ions. In *Soil Sampling and Methods of Analysis*, 2nd ed.; CRC Press: Boca Raton, FL, USA, 2007; Volume 44, p. 3.
23. Ditzler, C.; Scheffe, K.; Monger, H.C. Examination and Description of Soil Profiles. In *Soil Survey Manual (SSM)—Soil Science Division Staff*; USDA Handbook 18; Government Printing Office: Washington, DC, USA, 2017. Available online: [https://www.nrcs.usda.gov/wps/portal/nrcs/detailfull/soils/ref/?cid=nrcs142p2\\_054262](https://www.nrcs.usda.gov/wps/portal/nrcs/detailfull/soils/ref/?cid=nrcs142p2_054262) (accessed on 21 January 2018).
24. McNeill, J.D. *Electromagnetic Terrain Conductivity Measurement at Low Induction Numbers*; Technical Note TN-6; Geonics Ltd.: Mississauga, ON, Canada, 1980; p. 13. Available online: <http://www.geonics.com/pdfs/technicalnotes/tm6.pdf> (accessed on 21 January 2018).

25. Cook, P.G.; Walker, G.R. Depth Profiles of Electrical Conductivity from Linear Combinations of Electromagnetic Induction Measurements. *Soil Sci. Soc. Am. J.* **1992**, *56*, 1015–1022. [[CrossRef](#)]
26. Jarvis, P.G.; Mcnaughton, K.G. Stomatal Control of Transpiration: Scaling Up from Leaf to Region. *Adv. Ecol. Res.* **1986**, *15*, 1–49.
27. Granier, A. Evaluation of transpiration in a Douglas-fir stand by means of sap flow measurements. *Tree Physiol.* **1987**, *3*, 309–320. [[CrossRef](#)] [[PubMed](#)]
28. Villalobos, F.J.; Orgaz, F.; Mateos, L. Non-destructive measurement of leaf area in olive (*Olea europaea* L.) trees using a gap inversion method. *Agric. For. Meteorol.* **1995**, *73*, 29–42. [[CrossRef](#)]
29. Jin, L.; Heap, A.D. A review of comparative studies of spatial interpolation methods in environmental sciences: Performance and impact factors. *Ecol. Inform.* **2011**, *6*, 228–241.
30. Ahuja, L.R.; Reddy, V.R.; Saseendran, S.A.; Yu, Q. Response of Crops to Limited Water: Understanding and Modeling Water Stress Effects on Plant Growth Processes. In *Advances in Agricultural Systems Modeling*; American Society of Agronomy, Crop Science Society of America, Soil Science Society of America: Madison, WI, USA, 2008; Volume 11.



© 2018 by the authors. Licensee MDPI, Basel, Switzerland. This article is an open access article distributed under the terms and conditions of the Creative Commons Attribution (CC BY) license (<http://creativecommons.org/licenses/by/4.0/>).

Article

# Lateral Saturated Hydraulic Conductivity of Soil Horizons Evaluated in Large-Volume Soil Monoliths

Mario Pirastru <sup>1,\*</sup>, Roberto Marrosu <sup>1</sup>, Simone Di Prima <sup>1</sup>, Saskia Keesstra <sup>2</sup>,  
Filippo Giadrossich <sup>1</sup> and Marcello Niedda <sup>1</sup>

<sup>1</sup> Agricultural Department, University of Sassari, Viale Italia, 39, 07100 Sassari, Italy; rmarrosu@uniss.it (R.M.); simoedg@gmail.com (S.D.P.); fgiadrossich@uniss.it (F.G.); niedda@uniss.it (M.N.)

<sup>2</sup> Soil Physics and Land Management Group, Wageningen University, Droevendaalsesteeg 4, 6708PB Wageningen, The Netherlands; saskia.keesstra@gmail.com

\* Correspondence: mpirastru@uniss.it

Received: 26 September 2017; Accepted: 2 November 2017; Published: 6 November 2017

**Abstract:** Evaluating the lateral saturated hydraulic conductivity,  $K_{s,l}$ , of soil horizons is crucial for understanding and modelling the subsurface flow dynamics in many shallow hill soils. A  $K_{s,l}$  measurement method should be able to catch the effects of soil heterogeneities governing hydrological processes at the scale of interest, in order to yield  $K_{s,l}$  representative values over large spatial scales. This study aims to develop a field technique to determine spatially representative  $K_{s,l}$  values of soil horizons of an experimental hillslope. Drainage experiments were performed on soil monoliths of about 0.12 m<sup>3</sup> volume, encased in situ with polyurethane foam. Median  $K_{s,l}$  of 2450 mm·h<sup>-1</sup> and 552 mm·h<sup>-1</sup> were estimated in the A and B horizon, respectively. In the upper part of the B horizon, the median  $K_{s,l}$  was 490 mm·h<sup>-1</sup>, whereas it mostly halved near the underlying restricting layer. The decline of  $K_{s,l}$  values with depth was consistent with the water-table dynamics observed at the same site in previous studies. Moreover, the  $K_{s,l}$  from the monoliths were in line with large spatial-scale  $K_{s,l}$  values reported from the hillslope in a prior investigation based on drain data analysis. This indicated that the large-scale hydrological effects of the macropore network were well represented in the investigated soil blocks. Our findings suggest that performing drainage experiments on large-volume monoliths is a promising method for characterizing lateral conductivities over large spatial scales. This information could improve our understanding of hydrological processes and can be used to parameterize runoff-generation models at hillslope and catchment scale.

**Keywords:** soil block; subsurface flow; macropore network; spatial scale; polyurethane foam; hillslope

## 1. Introduction

In many hillslopes with shallow steep soils, the spatial and temporal dynamics of the perched water table are dominated by the lateral (namely slope-parallel) saturated subsurface flow. These water tables often originate from infiltrated precipitation that is hindered from further downwards percolation by restrictive layers beneath soils, e.g., fragipan in [1], argillic Bt horizon in [2], and weathered granite in [3]. Then, the water flows towards the footslope, where it can reach the surface once again and produces runoff [4–6]. In most cases, the preferential flow via macropores controls this runoff-generation process [1,3,7,8]. The lateral saturated hydraulic conductivity,  $K_{s,l}$ , is the soil property that influences transmission rate of the lateral subsurface water flow [9,10].

In layered soils on hillslopes, soil horizons can differ in hydraulic conductivity by orders of magnitude [9–11]. Evaluating the hydraulic conductivity of each soil horizon is fundamental to understanding the subsurface flow dynamics of these hillslopes. Moreover, it is necessary to

characterize the vertical variability of the hydraulic conductivity in order to model consistently the spatial and temporal soil hydrological dynamics. The vertical architecture of the permeability also controls the dynamics of nutrients and pollutants, as revealed by a number of tracer experiments in natural and agricultural landscapes [12–14]. Many modelling applications assume saturated hydraulic conductivities exponentially declining with depth [15]. As reported by Ameli et al. [16] changing the rate of the exponential  $K_{s,l}$  decline significantly affects model simulation of soil water and solute storage, mixing, and releasing in hillslopes. Hence, the lack of information about the vertical variability of the hydraulic conductivity in soils can be one of the major limitations in the numerical modelling of the hydrological behaviour of hillslopes.

Despite the acknowledged importance of a detailed hydraulic characterization of the soils, few methods have been specifically developed to assess  $K_{s,l}$  values in the field, particularly for steep soils. Therefore, in most cases only laboratory-derived conductivity values are available. Furthermore, it is difficult to obtain  $K_{s,l}$  data that can be representative of large spatial scales, from tens to hundreds of square meters, as the typical cell extents of the grid-based hydrological models. Consequently, some modelers consider the  $K_{s,l}$  as a calibration parameter, without any experimental evaluation (as for example in [17]). In other cases (e.g., [18,19]) runoff-generation models use  $K_{s,l}$  values obtained through methodologies inducing flow processes mainly vertically oriented. Instead, the hydraulic conductivity should be determined in agreement with the modelled flow direction. In fact, anisotropy can cause saturated conductivity to greatly differ with flow direction (e.g., [20,21]).

A useful approach for determining representative  $K_{s,l}$  values of macroporous soil is to perform drainage experiments in large-volume soil blocks, or monoliths, encased in situ with impermeable material. These experiments constrain the water flow along a prescribed direction through the soil, in order to define unambiguously the terms of Darcy's law [22,23]. Field procedures for evaluating the  $K_{s,l}$  in large soil samples are reported, among others, by Blanco-Canqui et al. [24] and Mendoza and Steenhuis [23]. The latter described a device called a "hillslope infiltrometer" by which the lateral drainage from each horizon of a layered soil was collected. The drainage rates were used to compute specific  $K_{s,l}$  values of the soil horizons.

Both Blanco-Canqui et al. [24] and Mendoza and Steenhuis [23] in their field applications used steel plates to enclose and hydraulically isolate the soil blocks. In some cases, metal-sheet insertion may be too cumbersome, especially in stony soils. Expandable polyurethane foam can be more conveniently used in situ as material encasing the soil blocks. The foam is used as waterproof material to obtain soil bulk density data with the excavation method [25–27], and to study the hydraulic soil anisotropy by measuring hydraulic conductivities in the laboratory on small cubes [28,29] or on large soil cores [30]. To our knowledge, the suitability of the expandable polyurethane foam for support in situ  $K_{s,l}$  experimental investigations has not been tested until now. The foam is purchased in pressurized cans, which are easy to transport to the field. It is waterproof, fast to apply, and it adheres to the irregular soil surfaces preventing bypass flow at the edges of the samples.

This paper focuses on field experiments aimed at evaluating the  $K_{s,l}$  of the shallow soil of a steep hillslope. The measurements were carried out on monoliths encased in situ with expandable polyurethane foam. The soil surface and volume of the monoliths were on average about 0.4 m<sup>2</sup> and 0.12 m<sup>3</sup>, respectively. Hence, the sample soil sizes were larger than the commonly sampled sizes through laboratory and field methods, with the exception of studies based on either drain or trench measurements. By saturating decreasing soil thicknesses during each experiment, the  $K_{s,l}$  for each soil horizon was detected. Using the method illustrated in this paper, we aim to obtain, with a sustainable effort, field soil data that are useful for interpreting the hydrological response of hillslopes, and that can be used to parameterize hydrological models. The specific objectives of the research are: (1) to design a method to determine in field soil  $K_{s,l}$  values; (2) to assess the  $K_{s,l}$  variability in the soil vertical profile, in order to obtain  $K_{s,l}$  values for each soil horizon; (3) to evaluate spatially representative  $K_{s,l}$  values for the soil horizons in the studied hillslope.

## 2. Material and Methods

### 2.1. Location

The experiments were carried out in the Baratz Lake watershed, in north-west Sardinia, Italy. The study site (Figure 1a) is the steep side of a hill (40°41'53.36" N, 8°14'4.15" E) with elevations ranging from 50 m to 65 m a.s.l. and mean slope of 30%. The area is a firebreak about 60 m long and 15 m wide with a mainly herbaceous coverage, bounded by Mediterranean maquis [31]. The soil is a sandy loam Lithic Haploxerepts, ranging in depth from 30 cm to 40 cm. The soil horizons are Ap (0–15 cm), BW and C [32]. The latter is a dense altered Permian sandstone acting as restrictive layer. In the remainder of the text, A, B and “restrictive layer” are substituted for the Ap, BW and “C horizon”, respectively. The climate is semiarid Mediterranean, with mild winters, warm summers and high water deficit from April to September. The average annual precipitation is about 600 mm, mainly falling from autumn to spring. The potential evapotranspiration is around 1000 mm per year [33].



**Figure 1.** (a) Field equipment to determine lateral saturated soil hydraulic conductivities in the monoliths MA, MB and MC; (b) soil monolith encased with polyurethane foam, with signed inflow (IP) and outflow (OP) pits; (c) spillway pipes inserted in the OP foam of the monolith MD to set the water level and collect the drainage.

### 2.2. Soil Monolith Preparation

In winter 2017 four soil monoliths, represented by letters MA, MB, MC and MD, were carved on selected locations on the hillslope. Soil blocks, each approximately 50 cm wide, 105 cm long and 70 cm deep (Figure 1b), extending for about 40 cm within the restrictive layer, were obtained by hand digging 20 cm-wide enclosing trenches. Vegetation at the monolith surfaces was preserved and the roots spreading out from the exposed faces were gently cut. Expandable polyurethane foam was injected to fill about 70% of the trench volume. Pressurized cans of 750 mL, each providing 0.05 m<sup>3</sup> of expanded foam, were used. Wooden boards were placed on top of the trenches to constrain the foam expansion. The boards forced the foam expansion towards the trench and monolith sides in order to achieve a tight contact between the foam and the irregular block surfaces. This was essential for minimizing leakages between the soil and the foam at the monolith edges during the drainage experiments. After 24 h, the expanded foam completely backfilled the trenches, and any foam excess was cut off. Consequently, two 16 cm-wide pits were excavated to the depth of the restrictive layer at the uphill and downhill internal sides of the foam barriers. Inflow and outflow pits were, therefore, created, hereby noted as IP and OP respectively (Figure 1b). At the end, the resulting monoliths had soil volumes ranging from 0.1 m<sup>3</sup> to 0.16 m<sup>3</sup>. Table 1 reports the dimensions of each sampled monolith.

**Table 1.** Dimensions of the soil monoliths sampled in the drainage experiments.

Monolith	Length (cm)	Width (cm)	Soil Depth (cm)	Soil Volume (m <sup>3</sup> )	Surface Slope
MA	80	52.5	31	0.13	0.27
MB	69	50.0	29	0.10	0.35
MC	68	50.0 </td <td>30</td> <td>0.10</td> <td>0.42</td>	30	0.10	0.42
MD	85	54.0	35	0.16	0.36

2.3. Instrumentation

A custom-built Mariotte bottle supplied water and regulated the water level in the IP during the experiments (Figures 1a and 2). It was a 2 m-high PVC pipe with the capacity of about 0.06 m<sup>3</sup>. The water level in the IP was set by adjusting in height the air-entry tube inlet of the bottle. The bottle discharged into the IP within a fissured PVC pipe wrapped with geotextile to minimize flow turbulence when the bottle outlet-tap was turned on. The discharged volume was computed from the lowering water level measured in the transparent level gauge of the bottle, which had a resolution of 1 mm (28.6 mL·mm<sup>-1</sup>). Accuracy of the Mariotte device was tested for several discharge rates (from 0.6–4.1 L·min<sup>-1</sup>, the maximum discharge allowed by the bottle) by measuring the water volumes flowing from the bottle outlet. The mean relative error among the collected volumes and the estimated ones with the readings taken at the bottle was 0.6%, which was considered acceptable for the purposes of this study.

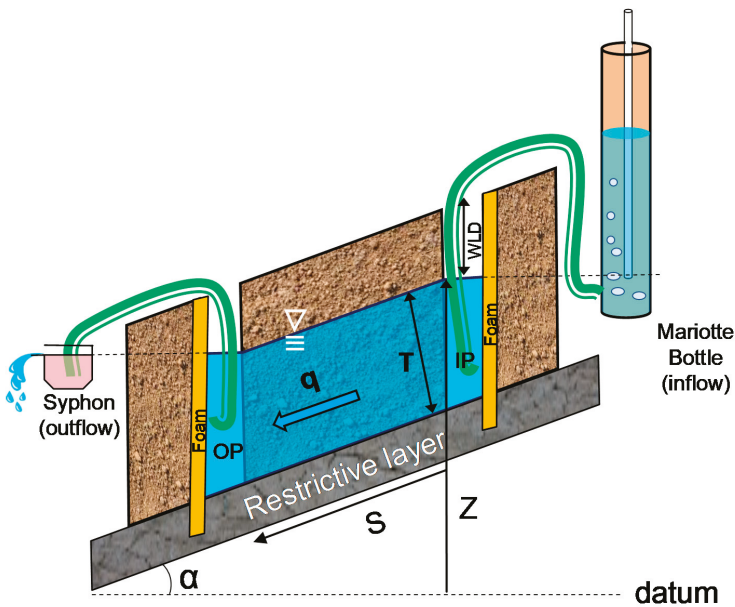


**Figure 2.** Experimental design to estimate the lateral saturated hydraulic conductivity of soil horizons from drainage of large-volume soil monoliths. The sketch represents the syphon system used in the MA, MB and MC monoliths to set the water levels and collect the drainage.

At the MA, MB and MC monoliths, a syphon system was used both to maintain the prescribed water levels into the OP and to measure the outgoing drainage. The syphon system consisted of a vacuum tube connecting the pit to a small water tank with spillway. The tank hung from a tripod by a rope and pulley, so as to finely tune the reservoir elevation and the water level within the OP

accordingly. For a prescribed elevation, the outflow from the spillway was the drainage through the soil monoliths. The outgoing flow discharged into a bucket and was weighted with a scale (5 g of resolution). In monolith MD, the system was slightly different as for the water level control and the collection of the drainage, since pipes through the foam were inserted as spillways in OP (Figure 1c). This was done by removing the resting soil from the outside-down foam wall of the OP. The foam was holed in order to place three spillway pipes at prescribed levels, then any gap between the pipes and foam was resealed.

#### 2.4. Drainage Experiments

At first, water was poured into the IP from a storage reservoir located at the top of the hillslope. The water level was slowly increased until it reached the depth of 5 cm below the soil surface. The same water-level depth (WLD) was achieved in the OP by the water that flowed through the soil monolith. At the WLD of 5 cm in the OP, water started flowing in the vacuum tube of the syphon system (monoliths MA to MC), or through the spillway inserted in the foam at that depth (MD). At that moment, we started to feed the IP through the Mariotte bottle and to measure the flow rates. This procedure of soil saturation from below was chosen because it was similar to the bottom-up saturation process that took place during the natural rainfall events, as reported in Pirastru et al. [32] for the same area. Moreover, visual inspection of the exposed seepage soil face in the OP at the beginning of the drainage reveals the dominant flow processes, i.e., preferential or uniform flows, which helps data interpretation.

For each monolith, the WLDs of 5 cm, 15 cm and 25 cm in both inflow and outflow pits were sequentially imposed. The top 5 cm of soil was excluded to avoid water-table cross depressions at the soil surface. The water levels were changed when either the flows became steady or the time of the stage with a prescribed level lasted over 1.5 h. The inflows and outflows were considered steady once the rate variations were below the instrumental resolutions for more than at least 30 min. The WLD transitions were achieved by first lowering the level in the OP, then waiting for equilibration in the IP until the prescribed depth, over which the bottle restarted supplying water. To measure the low flow rates accurately, the inflows and outflows were monitored by increasing time intervals, namely every 5 min, 10 min and 15 min for WLDs of 5 cm, 15 cm and 25 cm.

#### 2.5. $K_{s,l}$ Calculation

The  $K_{s,l}$  of the saturated soil layers were estimated by Darcy's formula:

$$K_{s,l} = -\frac{q}{T \text{ grad } \phi} \quad (1)$$

where  $q$  [ $L^2 \cdot T^{-1}$ ] was the outflow rate per unit width of the monoliths, computed as the mean of the rates over the last half-hour of a stage with a prescribed water level;  $T$  was the thickness of the saturated layers, measured perpendicularly to the sloping restrictive layer; and  $\text{grad } \phi$  was the total hydraulic gradient, negative along the flow direction.

The  $K_{s,l}$  value determined by Equation (1) represented the average value of lateral saturated hydraulic conductivities,  $K_s(z)$ , at a specific elevation  $z$  within the soil profile that was saturated [9]. By definition,  $K_{s,l}$  is related to  $K_s(z)$  by the following relation:

$$K_{s,l} = \frac{\int_{z_0}^Z K_s(z) dz}{Z - z_0} \quad (2)$$

where  $z_0$  and  $Z$  are, respectively, the elevation of the restrictive layer and of the water table above an arbitrary datum. The numerator of Equation (2) is the transmissivity of the saturated layer above the restrictive layer, and the denominator is the saturated thickness.

By imposing decreasing water levels in the monolith pits during the drainage experiments, the  $K_{s,l}$  values of three decreasing saturated soil thicknesses on the restrictive layer were computed for each monolith by using Equation (1). These values are denoted by  $K_{s,l WLD5}$ ,  $K_{s,l WLD15}$  and  $K_{s,l WLD25}$  with reference to the water-level depths sequentially applied. These  $K_{s,l}$  values are then used to calculate the specific  $K_{s,l}$  values of the individual soil layers in each monolith: (i) A horizon, approximately as large as the root zone, from 5 cm to 15 cm of depth; (ii) upper layer of the B horizon, from 15 cm to 25 cm of soil depth; (iii) lower layer of the B horizon profile, from 25 cm to the depth of the restrictive layer. Differentiation in the B horizon was done in order to detect the  $K_{s,l}$  changes in proximity of the restrictive layer. For computing the specific  $K_{s,l}$  of the A horizon, both  $K_{s,l WLD5}$  and  $K_{s,l WLD15}$  were used. By denoting with  $z_{WLD5}$  and  $z_{WLD15}$  the elevations above the datum of the water levels 5 cm and 15 cm deep, respectively, the  $K_{s,l}$  of the A horizon was:

$$K_{s,l}(A) = \frac{\int_{z_{WLD15}}^{z_{WLD5}} K_s(z) dz}{z_{WLD5} - z_{WLD15}} = \frac{K_{s,l WLD5} \cdot (z_{WLD5} - z_0) - K_{s,l WLD15} \cdot (z_{WLD15} - z_0)}{z_{WLD5} - z_{WLD15}} \quad (3)$$

The same procedure was applied to compute the specific  $K_{s,l}$  for the upper part of the B profile, but for this layer the  $K_{s,l WLD15}$  and  $K_{s,l WLD25}$  values and the proper water-level elevations were used. Finally, the specific  $K_{s,l}$  for the lower part of the B horizon profile was  $K_{s,l WLD25}$ .

### 3. Results

#### 3.1. Observed Inflow and Outflow Rates

The mean inflow and outflow rates computed over the last 30 min of stages with the three prescribed water levels are shown in Table 2. The greatest decrease in drainage rates with depth was recorded in MC, varying by about two orders of magnitude when it was going from a WLD of 5 cm to 25 cm. For this monolith in particular, we observed quick flow through macropores at the seepage face in the OP when the water level was near the soil surface during the saturation stage, whereas uniform matrix flow dominated the drainage for small saturated soil thicknesses on the restrictive layer (WLD > 15 cm). This was different in MB, where for the same water level variation the outflow decreased by 79%. This monolith gave the highest outflow rates among the monoliths for each set WLD. During the saturation stage, we observed a macropore gushing copiously at the interface between the soil and the restrictive layer. This contributed to sustaining a high soil water transmissivity, despite the lowering of water level.

**Table 2.** Arithmetic means of the outflow and inflow rates calculated over the last 30 min of the stages for each prescribed water-level depth. Inflows are in parentheses. The rates are in  $\text{mL} \cdot \text{min}^{-1} \cdot \text{m}^{-1}$ .

Monolith	Water-Level Depth (WLD)		
	5 cm	15 cm	25 cm
MA	810 (838)	218 (236)	42 (47)
MB	2660 (2671)	851 (864)	565 (565)
MC	1581 (1595)	273 (272)	21 (15)
MD	307 (2308)	98 (867)	23 (286)

In the monolith MD, the removal of soil from the downhill foam wall of the outflow pit to permit the spillways insertion caused water leakage below the lower end of the foam, from the OP reservoir towards the surrounding soil. This resulted in a poor outflow collection, although the leakage did not hinder setting of the prescribed water levels throughout the experiment time. At the end of the run, the soil resting against the external walls of the foam was removed, in order to check for traces of leakages around the monolith. Signs of water leakage were not found along the external sides,

except for the lower foam edge of the OP. This suggested that the supplied water flowed unaffected through the whole soil sample. Therefore, in the monolith MD the measured inflow was used in place of the outflow in Equation (1) for computing  $K_{s,l}$ .

Figure 3a,b show two representative examples of the temporal dynamics of the inflow and outflow rates measured during the drainage experiments. In MA (Figure 3a), the inflows for the water-level depths of 5 cm, 15 cm and 25 cm were almost immediately stable at the beginning of the measurement. The same was true for the outflow rates, except for the imposed WLD of 25 cm. In MC (Figure 3b), for WLD = 5 cm the flows were nearly stable at the start of the measurement, but approximately 140 min after the start of the experiment linearly decreased, and became 3% lower than the initial values after half an hour. A decreasing rate was observed with WLD set to 15 cm as well. Declining flow rates were also observed in MB and MD monoliths when WLD was 5 cm, and in the MD trough at the stage with WLD set to 15 cm. In this last case, a steady-state condition was reached at the end of the stage.

Initially in all the drainage experiment stages with WLD set to 25 cm, the outflow was observed to be in excess of inflow and progressively was converging towards these latter, as shown in Figure 3a,b for MA and MC. This was because the outflow included inflow and vertical drainage from the upper unsaturated soil. The vertical drainage decreased over time due to the progressive desaturating of the unsaturated zone until this approached the hydrostatic equilibrium state.

The differences between the mean rates of outflows and inflows at each end stage of the drainage runs and for the three imposed water levels (Table 2) were on average  $11 \text{ mL}\cdot\text{min}^{-1}\cdot\text{m}^{-1}$  for monoliths MA, MB and MC. The partials of the differences between outflows and inflows through drainage experiments were at the maximum at the start of the runs, and decreased with time, as illustrated in Figure 3c,d for MA and MC, respectively. The scattering of the outflow/inflow difference data points was caused by measuring errors due to both the instrument resolutions and the difficulty of taking accurate readings at the bottle level gauge, particularly when high water rates were supplied.

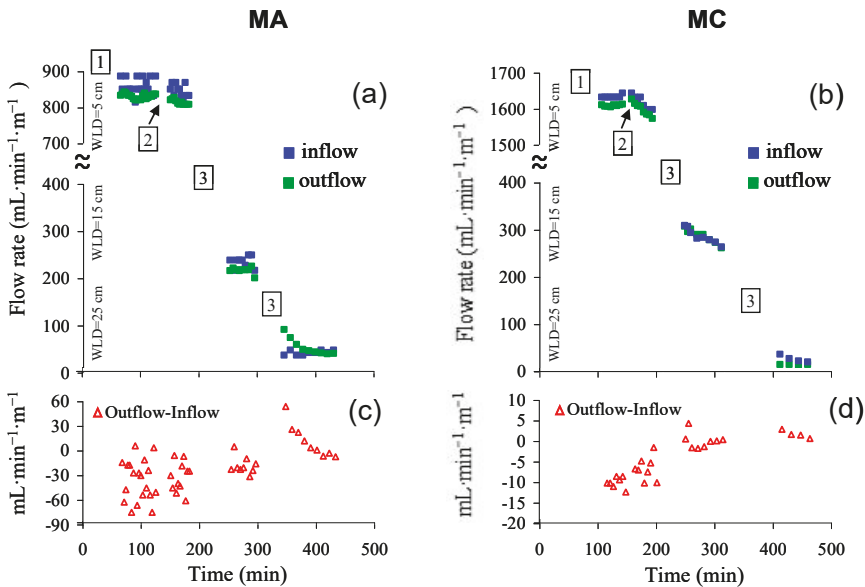


**Figure 3.** (a,b) Time series of the inflow and outflow rates measured during the experiments in the soil monoliths MA and MC; (c,d) computed differences between outflows and inflows. Note the difference in flow rate scale in the graphics. Numbers in squares indicate the following experiment stages: (1) soil saturation; (2) Mariotte bottle refilling; (3) water-level depth transition.

### 3.2. Lateral Saturated Soil Hydraulic Conductivities

The estimated  $K_{s,l}$  values in the soil monoliths for WLD of 5 cm, 15 cm and 25 cm are reported in Table 3. In MC the  $K_{s,l}$  decreased by 15 times in the passage from WLD of 5 cm to 25 cm. Smaller reductions with depth were found in the other monoliths, with the exception of MB, where at 25 cm the  $K_{s,l}$  increased to 2750  $\text{mm}\cdot\text{h}^{-1}$ . This was the highest value found among all the experiments. The variability of the  $K_{s,l}$  estimates (Table 3) increased with depth, because soil heterogeneity effects were averaged over progressively smaller soil volumes. The median values roughly halved going from 5 cm to 15 cm. At WLD of 25 cm, the median  $K_{s,l}$  value reduced further, and was 40% lower than the median determined at 15 cm of depth. However, this result was largely affected by very high  $K_{s,l}$  found in MB. As can be seen in Table 3 and in Figure 4, it clearly appeared as an outlier in comparison to the rest of the  $K_{s,l}$  assessments. Without considering this monolith, the median  $K_{s,l}$  at WLD = 25 cm became about 70% lower than that estimated at the depth of 15 cm.

**Table 3.** Lateral saturated soil hydraulic conductivities,  $K_{s,l}$  ( $\text{mm}\cdot\text{h}^{-1}$ ), estimated from the drainage experiments in the five soil monoliths for the water-level depths (WLD) of 5 cm, 15 cm and 25 cm from the soil surface.

Monolith	Water-Level Depth		
	5 cm	15 cm	25 cm
MA	724	313	153
MB	2157	1184	2750
MC	1066	307	70
MD	1416	791	509
Median	1241	552	331

The specific  $K_{s,l}$  values calculated for the A horizon in the soil monoliths, and for the upper and lower layers of the B horizon, are shown in Figure 4. The median value of the specific  $K_{s,l}$  was around 2450  $\text{mm}\cdot\text{h}^{-1}$  in the A horizon. This value reduced by 80% in the upper layer of the B horizon. The ratio of the median  $K_{s,l}$  of the lower and upper B layers was 0.67 or 0.31, depending on whether or not the monolith MB was included in the calculation.

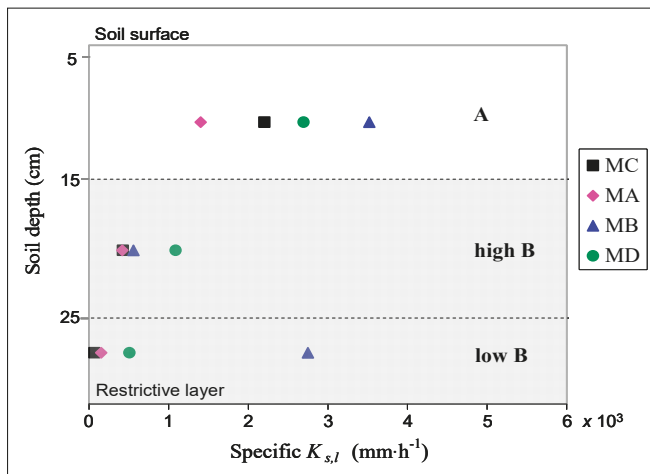


**Figure 4.** Computed specific  $K_{s,l}$  values in the A horizon and in the upper and lower layers of the B horizon. The shaded area is the soil B horizon.

## 4. Discussion

### 4.1. Benefits of the Proposed Field Soil $K_{s,l}$ Assessment Tool

The soil block methodology employed by Blanco et al. [24] to assess the soil  $K_{s,l}$  was modified in order to obtain accurate conductivity values of individual layers in a vertical soil profile, as well as to simplify field procedures. The self-built Mariotte bottle and the syphon system allowed easy and accurate setting of the sequence of descending water levels within the inflow and outflow pits, respectively. The developed procedure appeared simpler than lateral flow collectors embedded in the soil profile in order to yield separately the drainage from each horizon, as undertaken, for instance, by Mendoza and Steenhuis [23]. The procedure illustrated is certainly more practical for investigations in soils with widespread stoniness, where the rock fragments could prevent the collectors from being placed correctly (e.g., in [34]).

The water heads overlying the restrictive layer in both up and downhill pits of the monoliths defined first-type, or Dirichlet, boundary conditions to the flow spatial domain. The positive pressure diagrams at the monolith faces were like those determined by groundwater that built up on the restrictive layer when the soil was saturated by rainfall. Mainly for the downhill seepage face of the monoliths, digging pits to store water has advantages in comparison with other drainage-collecting systems, such as the aforementioned insertion of lateral flow collectors in the soil profile. In fact, from the latter, water had to be quickly removed to allow measurement, in this way establishing an atmospheric pressure boundary condition at the exfiltration surface.

All the hydrological processes of water leakage, vertical unsaturated flow and air spilling determined the temporal dynamics of the differences between outflows and inflows observed during the drainage experiments. Water leakages were due to percolation in the low-permeable subsoil and leakage at the bottom foam edges. These two processes were expected to decrease sharply over time with progressive subsoil saturation and for the lowering of the hydraulic head settings throughout the experiments. For WLDs set to 5 cm leakages in particular, we expected to account for the greatest part of the differences between outflows and inflows. Water movement from the unsaturated soil zone towards the water table in the monoliths increased the lateral saturated flow. The rates of vertical flow were related to the unsaturated zone thicknesses, and thus were lower at the starting WLD of 5 cm as compared to the other WLDs. Furthermore, at a prescribed WLD, the decrease over time of unsaturated drainage was due to unsaturated zone depletion, as can be deduced from Figure 3a,b for WLDs of 25 cm. The soil–air spill process, which was caused by the air–water dissolution and by the drag forces induced by the lateral water flow, contributed to reducing the differences between outflow and inflow during the experiments. However, this process was expected to have the least effect as compared with the water leakages and unsaturated vertical flow. In fact, the initial procedure of soil saturation by slowly increasing the water table level from below, without water ponding on the soil surface, should have facilitated the upward spilling of most entrapped soil air.

The  $q$  term of Equation (1) was the flow that perpendicularly was crossing the saturated soil sections throughout the monolith's extent. Hence, in order to obtain reliable estimates of  $q$ , the groundwater equipotential lines had to be kept as parallel as possible in the flow spatial domain. First, this was done by imposing equal water-level depths in the pits, which also allowed evaluation with sufficient certainty the flow cross sections and hydraulic gradients to be used in Equation (1). However, within the monoliths, water leakages and unsaturated vertical drainages could have caused deviations from the right conditions, so that both processes had to be minimized in order to apply Darcy's law properly. In the monoliths MA, MB and MC for the WLDs of 5 cm and 15 cm, and in MB for WLD = 25 cm, at the end of the stages outflows differed negligibly from inflows (Table 2). This indicated that the restrictive layer limited the deep-water percolation in a satisfactory way and the polyurethane expandable foam sufficiently sealed all sides of the monoliths. Furthermore, at the end of the stage, the unsaturated vertical drainage rates were negligible in comparison with the high lateral saturated flow rates. Consequently, the  $q$  flow terms were evaluated accurately in all the cases

we referred to above. The recorded outflows in monolith MD, which were much lower than inflows (Table 2), did not account for a fair picture of the flow dynamics within the monolith. In this case, there was field evidence of localized water leakage at the bottom foam edge at the OP, while the hydraulic sealing was preserved in the inflow pit and at the lateral sides of the monolith. Furthermore, the encouraging results from the experiments in MA, MB and MC provided more weight to the idea that, in MD also, the restrictive layer and the undisturbed polyurethane foam efficiently encased the soil block. In addition, the unsaturated vertical flow was also expected to be a negligible fraction of the outflow rate in this monolith at all the investigated WLDs. Therefore, to use inflow instead of outflow in Equation (1) was a reasonable assumption in order to obtain reliable determinations of  $K_{s,l}$ . Very slow lateral flows were measured in monoliths A and C during the experimental stages with a WLD of 25 cm. In these cases, it could not be excluded that both leakages and unsaturated vertical flows had affected the final outflow values. Therefore, in these experiments, the  $K_{s,l}$  evaluations for the highest imposed WLD should be less certain in percentage terms compared to the remaining cases.

Steady-state flows were not achieved in some stages of the experiments with WLD set to 5 cm and 15 cm. In the illustrated case of the MC monolith for WLD = 5 cm (Figure 3b), transient ending flows were measured despite the fact that in an early stage of the process steady-state conditions were detected. Similar circumstances were reported in Alagna et al. [35] for the recorded infiltration rates during prolonged runs. The same behavior also was pointed out by Bagarello et al. [29] in long-time drainage experiments on small (0.001 m<sup>3</sup>) undisturbed soil samples. Dikinya et al. [36] observed that when water moved in two repacked soil columns, the hydraulic conductivities decreased up to one order of magnitude from the start until the shutdown of the flow experiments. These authors argued that this was due to particle mobilization and pore-clogging processes. It is probable that in the monoliths, the observed decline of flow rates revealed pore-structure rearrangements, as plausibly caused by the high drainage rates in the soil layers close to the surface. In fact, the fast flow in macropores might have weakened the bonds of fine soil particles. This resulted in the detachment and delivery of particles through the soil, and clogging in the flow path. The choice to vary the water level, despite the fact that the steady-state flow was not always reached, was made in order to limit the ongoing soil rearrangement processes during the experiments. The  $K_{s,l}$  values computed for the WLDs of 5 cm and 15 cm by the mean flow measurements from the first half-hour of the experiment stages were on average 12% greater than  $K_{s,l}$  calculated from the final mean flow measurements (Table 2). This suggested that the soil rearrangement processes did not have significant impacts on the results of the experiments.

#### 4.2. $K_{s,l}$ Values of Individual Soil Horizons

Median  $K_{s,l}$  of 2450 mm·h<sup>-1</sup> was computed for the A soil horizon averaging the specific  $K_{s,l}$  values determined through Equation (3) for each soil monolith (Figure 4). The high median  $K_{s,l}$  indicated that macropores governed the lateral drainage processes in this horizon. Decayed roots and micro- and mesofauna activities were probably most responsible for the slope-parallel macropore network, which was observed close to the soil surface. Similar findings were reported by Brooks et al. [9], which estimated  $K_{s,l}$  values up to 600 mm·h<sup>-1</sup> in the macro-porous A horizon of their study site. Also Appels et al. [37] measured topsoil  $K_{s,l}$  values over 1900 mm·h<sup>-1</sup>. Dusek et al. [3] used  $K_{s,l}$  values of several thousands of mm·h<sup>-1</sup> to simulate water flow in macropores in the superficial soil layers in an experimental hillslope. The median  $K_{s,l}$  value, 552 mm·h<sup>-1</sup> (Table 3), of the B horizon of the monoliths (from 15 cm of depth to the restrictive layer), was about 78% lower than that of the A horizon. In particular, in the upper layer of the B horizon (15–25 cm of depth) specific  $K_{s,l}$  values spanning from around 400–1000 mm·h<sup>-1</sup> indicated that macropores here dominated the flow processes. In the lower B layer, estimated specific  $K_{s,l}$  values ranging from tens to thousands of mm·h<sup>-1</sup> suggested that, in some cases, the flow was dominated by the soil matrix and in the rest by macropore flow. Overall, median specific values of  $K_{s,l}$  were reduced by a factor of 0.20 passing from the A to the upper B layer, and further decreased in the lower B horizon compared to the upper B. This indicated that there was a

vertical gradient of macropore density. Instead, the increase of matrix porosity with depth could be excluded, based on a previous investigation in the same site [32] reporting the invariance of the bulk density along the vertical soil profile.

Pirastu et al. [32] determined average soil vertical hydraulic conductivities of  $139 \text{ mm}\cdot\text{h}^{-1}$  and  $94 \text{ mm}\cdot\text{h}^{-1}$  in the A and B horizons, respectively, with a single-ring infiltrometer (see Table 2 in [32], winter measurements). Therefore, the saturated soil hydraulic conductivities were much greater in the sub-horizontal direction compared to the vertical conductivity. Pirastu et al. [32] and Pirastu et al. [38] observed, in piezometers augered to the restrictive layer, the water table rapidly depleted when it rose in the A horizon. Even under the heaviest rainfall, the water table never reached the soil surface, with the exception of the wells located at the foot slope, close to the stream. Conversely, the water table persisted in the lower part of the B soil profile throughout the inter-storm periods during the rainy winters, and completely ran out from the hillslope only at the beginning of the dry periods in spring. The hydromorphic signs as greyish, brown and reddish soil color anomalies, commonly found in this part of the profile, also confirm that here the soil is prone to waterlogging. The very high  $K_{s,l}$  values computed for the near soil surface in the monoliths can explain the reported groundwater hydrological dynamics in the A horizon of the hill. In fact, the high lateral permeability of this horizon caused the swift downslope delivery of the soil water, resulting in the rapid depletion of the water table when it approached the soil surface. This hindered the saturation of the whole soil profile, even during intense precipitation. In the lower B horizon, the persistence of the water table for long periods across the hillslope indicated the lower permeability of the soil near the restrictive layer. This hydrological behavior, which was in contrast to that observed in the A horizon, was consistent with the remarkable decreasing of the median  $K_{s,l}$  value along the vertical soil profile, as determined through the drainage experiments in the soil monoliths.

Another objective of the research was to investigate the effectiveness of the drainage experiments in large soil-volume monoliths in order to evaluate spatially representative  $K_{s,l}$  values for the soil horizons in the analysed hillslope. For this reason, we took the relationship between  $K_{s,l}$  and water-table depths reported in Pirastu et al. [38] for the same site as a benchmark. The authors estimated soil average  $K_{s,l}$  by combining measurements of drainage rates from a 2.5 m-long drain and water-table levels from two well transects extending 10 m upslope of the drain. Therefore, this relationship was considered representative for the soil over a large area of the hillslope. Although specific  $K_{s,l}$  values for soil horizons are not shown in Pirastu et al. [38], these can easily be gathered by applying Equation (3) with the  $K_{s,l}$  values of the large-scale relationship coupled with the prescribed soil depths and the corresponding water-table elevations. Having done this, mean specific large-scale  $K_{s,l}$  values of  $8000 \text{ mm}\cdot\text{h}^{-1}$ ,  $780 \text{ mm}\cdot\text{h}^{-1}$  and  $180 \text{ mm}\cdot\text{h}^{-1}$  were calculated for the A, upper B and lower B soil layers, respectively. Compared to these values, the median  $K_{s,l}$  values of the same soil layers in the monoliths differed by factors of 0.3, 0.6 and 1.8, respectively. Hence, the  $K_{s,l}$  values in the soil monoliths were similar in magnitude to the large-scale  $K_{s,l}$  determinations. Brooks et al. [9] reported hillslope-scale estimations in soil horizons within one and two orders of magnitude greater than the available values from Guelph permeameter measurements. Montgomery and Dietrich [10] evaluated the  $K_{s,l}$  of an A horizon both by falling-head tests in wells and by yielding discharge from a gully cut, which had shown evidence of macropore flow. They estimated  $K_{s,l}$  values from the falling-head tests ranging between  $10^{-1} \text{ cm}\cdot\text{s}^{-1}$  to  $10^{-2} \text{ cm}\cdot\text{s}^{-1}$ , and large-scale  $K_{s,l}$  values comparable only with the high end of the range of conductivities obtained in the wells. Chappell and Lancaster [39] reported large-scale  $K_{s,l}$  values by trench percolation tests on average 37 times larger than the mean conductivity obtained by slug tests made in piezometers adjacent to their trenches. Therefore, in comparison to these studies, in our investigation we detected a more satisfactory agreement between the estimated  $K_{s,l}$  in the monoliths and the values available from the large spatial scale investigation.

For the lower B soil layer, the median  $K_{s,l}$  value measured in soil monoliths is more consistent with the large-scale value from the drain when the high  $K_{s,l}$  value estimated in MB ( $2750 \text{ mm}\cdot\text{h}^{-1}$ ) is excluded from the computation. In fact, in this case the median  $K_{s,l}$  value of the lower B layer

was just 15% lower than the large-scale value. This result suggested that in the monolith MB the characteristics of lateral drainage for small-saturated soil thicknesses of the hillslope were probably not fairly represented. Also, the water-table dynamics reported for the B horizon of this site by Pirastru et al. [32] and Pirastru et al. [38] further supported the idea that in MB the characteristics of soil lateral drainage were misrepresented. During the saturation phase of the experiment, we observed that an isolated, large pore located at the soil-restrictive layer interface quickly drained when water was initially supplied to the inflow pit. We assume that this macropore ran through the entire length of the sample. Instead, such macropores in the field are commonly constrained in their extent by the surrounding soil matrix. By converting this macropore into a continuous pipe within the sample, the soil  $K_{s,l}$  may have been significantly overestimated.

In a modeling study assessing the climate and land-use change effects in the water balance at the Baratz lake catchment, Niedda et al. [40] used a maximum value of the  $K_{s,l}$  parameter of  $1000 \text{ mm} \cdot \text{h}^{-1}$  at the soil surface, then it decreased in depth. They efficiently simulated the discharge at the catchment outlet. The median  $K_{s,l}$  values (Table 3) found in the soil monoliths were in line with the parameter values used in simulations. This suggests that drainage experiments in large-volume soil monoliths can potentially be used to obtain parameter values for the hydrological models, in order to simulate the runoff-generation processes at catchment scale.

## 5. Conclusions

The lateral saturated hydraulic conductivities in the soil horizons of the shallow steep soil of a hillslope was evaluated in situ by drainage experiments in monoliths ranging in volume from  $0.1 \text{ m}^3$  to  $0.16 \text{ m}^3$ . The expandable polyurethane foam used to encase the samples on the field made the hydraulic isolation of the soil blocks easy. Moreover, the removal of the foam from the field was easy, allowing a reduction of the impact on the experimental area. Minimizing leakages along the sides of the foam barriers allowed evaluation of the flow rate, cross-section area and hydraulic gradient terms of Darcy's law, in order to obtain reliable  $K_{s,l}$  values. Thanks to the large volume sampled in each experiment, soil macropores were included in the measurements and sufficiently characterized. The information about the lateral permeability of the soil horizons that was obtained was consistent with the groundwater dynamics observed during previous investigations in the hillslope studied. Likewise, the median values of the  $K_{s,l}$  obtained in the soil horizons of monoliths were comparable with large spatial-scale  $K_{s,l}$  values computed through drain flow measurements in the same site. This indicated that the hydrological large-scale effects of the soil macropore network of the hillslope were sufficiently represented in the large-volume soil samples. Currently, drainage measurements are ongoing at an 8.5 m-long drain, in order to yield  $K_{s,l}$  values that could be more representative for the hillslope scale. A future comparison with these values will give us further indications about the suitability of the drainage experiments in the soil monoliths for characterizing hydrological processes and determining hydraulic conductivities at the hillslope-scale.

It took four days to prepare the setup and perform the drainage experiment on each soil monolith in order to determine the  $K_{s,l}$ . Considering the effort required and the need to maintain a field campaign of reasonable duration, a limited number of samples were investigated. Despite this,  $K_{s,l}$  values sufficiently representative for the soil in the hillslope were achieved. The  $K_{s,l}$  discrepancies between the monoliths and the drain were smaller in comparison with those reported by other authors who have compared small- and large-scale  $K_{s,l}$  values. Therefore, the methodology described in this study appears to represent a step forward in the possibility of detecting, through a low number of experiments, representative hydraulic conductivities of soil horizons over large spatial scales. Hence, such experimentation will allow, through a sustainable effort, valuable information for interpreting hydrological processes and parameterizing runoff-generation models both at the hillslope and catchment scale to be obtained.

**Acknowledgments:** This research was funded by the program: “Promotion of the scientific research and technological innovation in Sardinia (IT), RL7/2007”, specific project “Anthropogenic and climate impacts in the hydrologic cycle at basin and hillslope scales”.

**Author Contributions:** M.P., R.M. and S.D.P. carried out the experimental work and write the paper. All authors designed the work and analyzed the results.

**Conflicts of Interest:** The authors declare no conflict of interest.

## References

1. McDaniel, P.A.; Regan, M.P.; Brooks, E.; Boll, J.; Barndt, S.; Falen, A.; Young, S.K.; Hammel, J.E. Linking fragipans, perched water tables, and catchment-scale hydrological processes. *CATENA* **2008**, *73*, 166–173. [[CrossRef](#)]
2. Du, E.; Rhett Jackson, C.; Klaus, J.; McDonnell, J.J.; Griffiths, N.A.; Williamson, M.F.; Greco, J.L.; Bitew, M. Interflow dynamics on a low relief forested hillslope: Lots of fill, little spill. *J. Hydrol.* **2016**, *534*, 648–658. [[CrossRef](#)]
3. Dusek, J.; Vogel, T.; Dohnal, M.; Gerke, H.H. Combining dual-continuum approach with diffusion wave model to include a preferential flow component in hillslope scale modeling of shallow subsurface runoff. *Adv. Water Resour.* **2012**, *44*, 113–125. [[CrossRef](#)]
4. Alaoui, A.; Caduff, U.; Gerke, H.H.; Weingartner, R. A Preferential Flow Effects on Infiltration and Runoff in Grassland and Forest Soils. *Vadose Zone J.* **2011**, *10*, 367. [[CrossRef](#)]
5. Van Schaik, N.L.M.B.; Schnabel, S.; Jetten, V.G. The influence of preferential flow on hillslope hydrology in a semi-arid watershed (in the Spanish Dehesas). *Hydrol. Process.* **2008**, *22*, 3844–3855. [[CrossRef](#)]
6. Wienhöfer, J.; Zehe, E. Predicting subsurface stormflow response of a forested hillslope—The role of connected flow paths. *Hydrol. Earth Syst. Sci.* **2014**, *18*, 121–138. [[CrossRef](#)]
7. Schmocker-Fackel, P.; Naef, F.; Scherrer, S. Identifying runoff processes on the plot and catchment scale. *Hydrol. Earth Syst. Sci.* **2007**, *11*, 891–906. [[CrossRef](#)]
8. Weiler, M.; McDonnell, J.J.; Tromp-van Meerveld, I.; Uchida, T. Subsurface Stormflow. In *Encyclopedia of Hydrological Sciences*; Anderson, M.G., McDonnell, J.J., Eds.; John Wiley & Sons, Ltd.: Chichester, UK, 2006. ISBN 0471491039, 9780471491033, 0470848944, 9780470848944.
9. Brooks, E.S.; Boll, J.; McDaniel, P.A. A hillslope-scale experiment to measure lateral saturated hydraulic conductivity. *Water Resour. Res.* **2004**, *40*, W04208. [[CrossRef](#)]
10. Montgomery, D.R.; Dietrich, W.E. Hydrologic Processes in a Low-Gradient Source Area. *Water Resour. Res.* **1995**, *31*, 1–10. [[CrossRef](#)]
11. McGuire, K.J.; McDonnell, J.J. Hydrological connectivity of hillslopes and streams: Characteristic time scales and nonlinearities. *Water Resour. Res.* **2010**, *46*. [[CrossRef](#)]
12. Starr, J.L.; Sadeghi, A.M.; Pachepsky, Y.A. Monitoring and Modeling Lateral Transport through a Large In Situ Chamber. *Soil Sci. Soc. Am. J.* **2005**, *69*, 1871. [[CrossRef](#)]
13. Stutter, M.I.; Deeks, L.K.; Billett, M.F. Transport of conservative and reactive tracers through a naturally structured upland podzol field lysimeter. *J. Hydrol.* **2005**, *300*, 1–19. [[CrossRef](#)]
14. Van Verseveld, W.J.; McDonnell, J.J.; Lajtha, K. The role of hillslope hydrology in controlling nutrient loss. *J. Hydrol.* **2009**, *367*, 177–187. [[CrossRef](#)]
15. Ambrose, B.; Beven, K.; Freer, J. Toward a Generalization of the TOPMODEL Concepts: Topographic Indices of Hydrological Similarity. *Water Resour. Res.* **1996**, *32*, 2135–2145. [[CrossRef](#)]
16. Ameli, A.A.; Amvrosiadi, N.; Grabs, T.; Laudon, H.; Creed, I.F.; McDonnell, J.J.; Bishop, K. Hillslope permeability architecture controls on subsurface transit time distribution and flow paths. *J. Hydrol.* **2016**, *543*, 17–30. [[CrossRef](#)]
17. Matonse, A.H.; Kroll, C.N. Applying hillslope-storage models to improve low flow estimates with limited streamflow data at a watershed scale. *J. Hydrol.* **2013**, *494*, 20–31. [[CrossRef](#)]
18. Maneta, M.; Schnabel, S.; Jetten, V. Continuous spatially distributed simulation of surface and subsurface hydrological processes in a small semiarid catchment. *Hydrol. Process.* **2008**, *22*, 2196–2214. [[CrossRef](#)]
19. Van Schaik, N.L.M.B.; Bronstert, A.; De Jong, S.M.; Jetten, V.G.; Van Dam, J.C.; Ritsema, C.J.; Schnabel, S. Process-based modelling of a headwater catchment in a semi-arid area: The influence of macropore flow: Process-based modelling of a headwater catchment. *Hydrol. Process.* **2014**, *28*, 5805–5816. [[CrossRef](#)]

20. Bathke, G.R.; Cassel, D.K. Anisotropic Variation of Profile Characteristics and Saturated Hydraulic Conductivity in an Ultisol Landscape. *Soil Sci. Soc. Am. J.* **1991**, *55*, 333. [[CrossRef](#)]
21. Beckwith, C.W.; Baird, A.J.; Heathwaite, A.L. Anisotropy and depth-related heterogeneity of hydraulic conductivity in a bog peat. I: Laboratory measurements. *Hydrol. Process.* **2003**, *17*, 89–101. [[CrossRef](#)]
22. Vepraskas, M.J.; Williams, J.P. Hydraulic Conductivity of Saprolite as a Function of Sample Dimensions and Measurement Technique. *Soil Sci. Soc. Am. J.* **1995**, *59*, 975. [[CrossRef](#)]
23. Mendoza, G.; Steenhuis, T.S. Determination of hydraulic behavior of hillsides with a hillslope infiltrometer. *Soil Sci. Soc. Am. J.* **2002**, *66*, 1501. [[CrossRef](#)]
24. Blanco-Canqui, H.; Gantzer, C.J.; Anderson, S.H.; Alberts, E.E.; Ghidey, F. Saturated Hydraulic Conductivity and Its Impact on Simulated Runoff for Claypan Soils. *Soil Sci. Soc. Am. J.* **2002**, *66*, 1596. [[CrossRef](#)]
25. Brye, K.R.; Morris, T.L.; Miller, D.M.; Formica, S.J.; Van Eps, M.A. Estimating Bulk Density in Vertically Exposed Stoney Alluvium Using a Modified Excavation Method. *J. Environ. Qual.* **2004**, *33*, 1937. [[CrossRef](#)] [[PubMed](#)]
26. Muller, R.N.; Hamilton, M.E. A simple, effective method for determining the bulk density of stony soils. *Commun. Soil Sci. Plant Anal.* **1992**, *23*, 313–319. [[CrossRef](#)]
27. Page-Dumroese, D.S.; Brown, R.E.; Jurgensen, M.F.; Mroz, G.D. Comparison of Methods for Determining Bulk Densities of Rocky Forest Soils. *Soil Sci. Soc. Am. J.* **1999**, *63*, 379. [[CrossRef](#)]
28. Bagarello, V.; Sgroi, A. Testing Soil Encasing Materials for Measuring Hydraulic Conductivity of a Sandy-Loam Soil by the Cube Methods. *Soil Sci. Soc. Am. J.* **2008**, *72*, 1048. [[CrossRef](#)]
29. Bagarello, V.; Sferlazza, S.; Sgroi, A. Testing laboratory methods to determine the anisotropy of saturated hydraulic conductivity in a sandy-loam soil. *Geoderma* **2009**, *154*, 52–58. [[CrossRef](#)]
30. Germer, K.; Braun, J. Determination of Anisotropic Saturated Hydraulic Conductivity of a Macroporous Slope Soil. *Soil Sci. Soc. Am. J.* **2015**, *79*, 1528. [[CrossRef](#)]
31. Castellini, M.; Iovino, M.; Pirastru, M.; Niedda, M.; Bagarello, V. Use of BEST Procedure to Assess Soil Physical Quality in the Baratz Lake Catchment (Sardinia, Italy). *Soil Sci. Soc. Am. J.* **2016**, *80*, 742. [[CrossRef](#)]
32. Pirastru, M.; Niedda, M.; Castellini, M. Effects of maquis clearing on the properties of the soil and on the near-surface hydrological processes in a semi-arid Mediterranean environment. *J. Agric. Eng.* **2014**, *45*, 176. [[CrossRef](#)]
33. Giadrossich, F.; Niedda, M.; Cohen, D.; Pirastru, M. Evaporation in a Mediterranean environment by energy budget and Penman methods, Lake Baratz, Sardinia, Italy. *Hydrol. Earth Syst. Sci.* **2015**, *19*, 2451–2468. [[CrossRef](#)]
34. Day, R.L.; Calmon, M.A.; Stiteler, J.M.; Jabro, J.D.; Cunningham, R.L. Water balance and flow patterns in a fragipan using in situ soil block. *Soil Sci.* **1998**, *163*, 517–528. [[CrossRef](#)]
35. Alagna, V.; Bagarello, V.; Di Prima, S.; Giordano, G.; Iovino, M. Testing infiltration run effects on the estimated water transmission properties of a sandy-loam soil. *Geoderma* **2016**, *267*, 24–33. [[CrossRef](#)]
36. Dikinya, O.; Hinz, C.; Aylmore, G. Decrease in hydraulic conductivity and particle release associated with self-filtration in saturated soil columns. *Geoderma* **2008**, *146*, 192–200. [[CrossRef](#)]
37. Appels, W.M.; Graham, C.B.; Freer, J.E.; McDonnell, J.J. Factors affecting the spatial pattern of bedrock groundwater recharge at the hillslope scale: Spatial Patterns of Bedrock Groundwater Recharge. *Hydrol. Process.* **2015**, *29*, 4594–4610. [[CrossRef](#)]
38. Pirastru, M.; Bagarello, V.; Iovino, M.; Marrosu, R.; Castellini, M.; Giadrossich, F.; Niedda, M. Subsurface flow and large-scale lateral saturated soil hydraulic conductivity in a Mediterranean hillslope with contrasting land uses. *J. Hydrol. Hydromech.* **2017**, *65*. [[CrossRef](#)]
39. Chappell, N.A.; Lancaster, J.W. Comparison of methodological uncertainties within permeability measurements. *Hydrol. Process.* **2007**, *21*, 2504–2514. [[CrossRef](#)]
40. Niedda, M.; Pirastru, M.; Castellini, M.; Giadrossich, F. Simulating the hydrological response of a closed catchment-lake system to recent climate and land-use changes in semi-arid Mediterranean environment. *J. Hydrol.* **2014**, *517*, 732–745. [[CrossRef](#)]



Article

# Use of a Non-Ionic Water Surfactant in Lettuce Fertigation for Optimizing Water Use, Improving Nutrient Use Efficiency, and Increasing Crop Quality

Alessandra Trinchera \* and Valentina Baratella

Council for Agricultural Research and Economics, Research Center for Agriculture and Environment (CREA-AA), Via della Navicella 2-4, 00184 Rome, Italy; valentina.baratella@crea.gov.it

\* Correspondence: alessandra.trinchera@crea.gov.it; Tel.: +39-06-7005413-222

Received: 26 February 2018; Accepted: 4 May 2018; Published: 8 May 2018

**Abstract:** The use of water surfactants in fertigation constitutes a viable approach to increase soil wetting, potentially improving crop nutrient uptake and quality. An in-field demonstration test was carried out by applying an innovative, eco-friendly, non-ionic surfactant to fertigation water in *Lactuca sativa* (var. Iceberg) production to increase nutrient use efficiency and improve the crop's access to water. A non-ionic methyl-oxirane surfactant (methyl-oxirane + 2-methyl-oxirane) was added at an increasing rate to the fertigation solution (Hoagland). Upon harvesting, the main growth and nutritional parameters were determined on the aboveground and belowground portions of the lettuce. Leaf nitrate content, water, and nitrogen use efficiency were recorded; the relationship of lettuce aboveground dry biomass with nutrient uptake was evaluated using vectorial analysis; and ultrastructural analysis of lettuce roots was performed by scanning electron microscopy. The surfactant, applied by fertigation at the rate of  $1.0 \text{ mL} \times L_{\text{Hoagland}}^{-1}$ , improved crop P, K, Mn, and Fe use efficiency. When applied by fertigation, although the surfactant did not increase the water use efficiency index, it induced a significant decrease of the specific leaf water content (−8.8%) and an increase of the leaf area (+13.3%). By comparison with the recent literature, we inferred a positive physiological response by more expanded and less thick leaves in lettuce, likely by the optimization of the crop water and nutrient root uptakes mediated by the abundant but shortest lateral roots. This finding corresponded to the lowest leaf nitrate content, indicating an improvement of the lettuce quality without losing the crop yield.

**Keywords:** water infiltration; nitrogen use efficiency; specific leaf water content; vegetable production; soil; yield

## 1. Introduction

Under the effects of climate change, high temperatures and extreme weather events occurring within a short period of time, especially in areas with poor vegetation cover or bare soil, lead to soil erosion, aridity, and loss of organic matter. As a result, the supply of adequate water and nutrients to crops is becoming an issue [1]. In the Mediterranean region, water scarcity and the increasing pressure over water availability coming from other productive sectors urge farmers to find alternative solutions to improve the water and nutrient uptake by crops, exploiting all technical innovations available on the market [2]. Moreover, even if excessive fertilization does encourage great yields, at the same time it results in water and soil pollution; the possibility of reducing nutrient inputs and improving crop nutrient use efficiency may instead reduce the amount of fertilizers employed by farmers.

Among other solutions, the use of water surfactants in fertigation could constitute a viable approach to increase crops nutrient use efficiency and quality [3] by reducing soil water repellency [4], increasing water infiltration rate, and limiting runoff in Pacific Northwest soils [5]. This would indicate

an improvement of the water use efficiency, guaranteeing that an adequate amount of nutrients reaches the crops.

The adjuvants comprise a broad range of substances, of which solvents and surfactants are the major types [6]. In particular, surfactants are organic molecules, containing both hydrophobic and hydrophilic groups, which act at the interface between two different phases by lowering the surface tension of a liquid. Among them, the non-ionic, modified methyl co-polymers constitute a class of wetting agents where the molecular structure was modified by replacing terminal hydroxyl groups with methyl caps. As  $-OH$  is a hydrophilic group while  $-CH_3$  is typically hydrophobic, these molecular changes modify the hydrophilic properties of the surfactant, thus modulating its water repellency and wettability [7].

Their mode of action allows liquid solutions to penetrate and wet agricultural soils more easily, potentially improving water use efficiency and crop quality [3,8]. This behavior has been demonstrated for hydrophobic soils [6,9] and in recent years has received attention for hydrophilic soils [10–12]. The properties of surfactants seem to be correlated with their intrinsic strength and the concentration of the solution [11]. Moreover, it has been demonstrated that their characteristic properties markedly change when reaching a critical concentration of the surfactant solutions (CMC, critical micelle concentration) [9]. At the CMC, surface active ions or molecules in the solution (such as the available nutrients in soil) associate to form larger units (micelles) in the presence of the surfactant. The CMC corresponds to the concentration of surfactants above which micelles form, constituting a key parameter able to interact with their super-spreading effect [9–11]. The possibility of using this kind of surfactant as adjuvants in the irrigation water to be applied on agricultural land has been poorly investigated so far, with contrasting results. Their potential effects on crops uptake and growth is currently being explored [13], and a first theoretical model of their mechanism of action in soil was recently provided [11]. McCauley [14] evaluated the effect of a non-ionic surfactant on soybean (*Glycine max* L.), and found that yield increased with surfactant application to the irrigation water. Other authors reported no effects on plant growth after surfactant application by fertigation to corn (*Zea mays* L.), soybean, wheat (*Triticum aestivum* L.), and potato [15–17]. Preliminary research has shown that non-ionic surfactants added to the irrigation water may increase root growth [3,18]. Another study on turf grass revealed neither positive nor negative effects on macronutrient and micronutrient uptake due to fertigation with surfactant application [19]. Similar results were obtained by Banks [20], who observed no consistent effects on nutrient uptake after surfactant application to corn in different soils. Surfactant application at planting is considered a management technique that may reduce nitrate leaching from potato fields [13]. As far as the nitrogen is concerned, Arriaga et al. [21] found that the use of a non-ionic surfactant may reduce nitrogen leaching and improve nitrogen utilization in potatoes. A recent work showed that the application of a non-ionic surfactant to irrigation water in corn production under a Mediterranean climate gave a net increase of water use efficiency and, in parallel, a high corn yield and dry matter. This testified an undoubted economic advantage to farmers by saving water and reducing fertilizer inputs; in fact, even if the surfactant application increased the irrigation costs by 4.7%, it increased the profit by 19.7% [22].

The potential advantages for water conservation deriving from surfactants application to soil could be profitably exploited by Mediterranean farmers involved in vegetable production, which suffer due to scarce rainfalls in spring and summer cropping seasons [22–24]. Since in many countries, such as Italy, Greece, and Spain, vegetable production represents a relevant commercial sector and water availability is becoming an issue, all technical-agronomical strategies to reduce water input and improve nutrient use efficiency by increasing soil wettability are considered valuable alternatives to the indiscriminate use of such precious resources that are often dispersed inefficiently in the environment [25]. At the moment, very little information is available about the potential synergistic or antagonistic effects of surfactants addition to irrigation water on broad-leaved vegetable production as well as its interaction with mineral fertilization. A recent experimental trial on lettuce after the addition of a non-ionic surfactant to the irrigation water in the absence of fertilization gave positive

results on water and soil nutrient uptake [11]. However, it is not yet clear if and how these types of non-ionic surfactants, added to mineral fertilizers in fertigation, are able to interact and thus modulate the translocation of the macro, meso, and micronutrients from the root to the vegetable leaves.

The objective of the present research was to verify whether the addition of an eco-friendly, non-ionic surfactant to fertigation could improve the nutrient use efficiency and quality of lettuce via the optimization of crop water uptake. The final purpose was to reduce the water supply in broad-leaved vegetable production while guaranteeing the same crop yield. Since different surfactants were available on the market, our choice in surfactant selection was guided by its molecular structure, chemical properties, and biodegradability in the environment [26,27].

## 2. Materials and Methods

**Water surfactant characteristics and use**—The tested surfactant (methyl oxirane surfactant, MOS) was a non-ionic fluid material, composed of 80% *w/w* methyl-oxirane and 20% *w/w* of 2-methyloxirane, and produced by a patented industrial process. The chemical structure of this surfactant consisted in a hydrophilic head group (2-methyl-oxirane) and hydrophobic tails  $[-O-Si-(CH_3)_3]_n$ , which gave it a typical water repelling property. It was defined as an eco-friendly compound, since its final biodegradability was >80% under aerobic conditions in 28 days, on the basis of the application of the eco-toxicity testing methods reported in the Council Regulation (EC) No 440/2008 (EC method C.4-D, 440/2008/EEC) and the Organisation for Economic Co-operation and Development (OECD) guideline 301 F (1992) [28,29]. In order to define the best application dose of MOS as a fertigation surfactant in crop production, it was added to the fertigation solution at two different doses:  $0.2 \text{ mL}_{\text{MOS}} \times L_{\text{Hoagland}}^{-1}$  (F S0.2 solution) or  $1.0 \text{ mL}_{\text{MOS}} \times L_{\text{Hoagland}}^{-1}$  (F S1.0 solution). The control treatment (F CNT) was fertilized with the same fertigation solution without the addition of MOS.

**Experimental site and design**—A one-year in-field demonstration test was carried out on a broad-leaved vegetable crop to evaluate the influence of MOS used in fertigation on crop nutrient uptake by changes in water use by the crop. The research was conducted in open field, at the experimental site of the Council for Agricultural Research and Economics, Research Center for Agriculture and Environment (CREA-AA) in Rome (Central Italy), (N 41°53'7.475"; E 12°29'43.464" 42 m a.s.l.) with a typical thermo-Mediterranean climate. The absolute annual temperatures ranged between 0 °C in winter and 40 °C in summer. The field test lasted 40 days, from April to May 2015; in this period, temperatures ranged between 16 and 28 °C and no rainfalls were recorded during the trial.

Soil was characterized in relation to texture, pH, organic C ( $C_{\text{org}}$  %), total nitrogen ( $N_{\text{tot}}$  %), cation exchange capacity (CEC,  $\text{meq } 100 \text{ g}^{-1}$ ), organic matter (%), available phosphorous ( $P_{\text{Olsen}}$ ,  $\text{mg kg}^{-1}$ ), total potassium ( $K_2O$ ,  $\text{mg kg}^{-1}$ ), exchangeable calcium (Ca,  $\text{meq } 100 \text{ g}^{-1}$ ), potassium (K,  $\text{meq } 100 \text{ g}^{-1}$ ), sodium (Na,  $\text{meq } 100 \text{ g}^{-1}$ ), magnesium (Mg,  $\text{meq } 100 \text{ g}^{-1}$ ), and cadmium (Cd), copper (Cu), iron (Fe), nickel (Ni), lead (Pb), and zinc (Zn) ( $\text{mg kg}^{-1}$ ). The soil chemical-physical properties are reported in Table 1.

**Table 1.** Main soil physicochemical parameters [30]. CEC: cation exchange capacity.

Soil Parameter			
Silt (%)	47.6	Ca ( $\text{meq } 100 \text{ g}^{-1}$ )	24.3
Sand (%)	24.4	K ( $\text{meq } 100 \text{ g}^{-1}$ )	1.3
Loam (%)	28.0	Na ( $\text{meq } 100 \text{ g}^{-1}$ )	3.2
pH	7.6	Mg ( $\text{meq } 100 \text{ g}^{-1}$ )	0.7
$C_{\text{organic}}$ (%)	1.21	Cd ( $\text{mg kg}^{-1}$ )	<0.05
$N_{\text{tot}}$ (%)	0.12	Cu ( $\text{mg kg}^{-1}$ )	1.0
CEC ( $\text{meq } 100 \text{ g}^{-1}$ )	29	Fe ( $\text{mg kg}^{-1}$ )	401.1
Organic matter (%)	1.79	Ni ( $\text{mg kg}^{-1}$ )	0.6
$P_{\text{Olsen}}$ ( $\text{mg kg}^{-1}$ )	25.2	Pb ( $\text{mg kg}^{-1}$ )	2.1
$K_2O$ ( $\text{mg kg}^{-1}$ )	598.1	Zn ( $\text{mg kg}^{-1}$ )	1.3

Lettuce (*Lactuca sativa* var. "Iceberg") seedlings, grown in 2 cm × 2 cm × 4 cm of 60% perlite + 40% peat growing media, were transplanted in soil at about a height of 6 cm (three fully expanded leaves). In a randomized three-block designed system of 18 m<sup>2</sup>, 60 plants per block (20 plants per treatment) were transplanted, for a total of 180 plants. The treatments were the fertigated control (F CNT) and two different doses of surfactant (F S0.2 and F S1.0) added to the fertigation solution. An additional non-fertilized control (NF CNT) (20 plants per block) was additionally considered only for calculations on the Nitrogen Uptake Efficiency:  $NUpE = (N_F - N_{NF})/N_F$ , where  $N_{NF}$  was the N uptake of the unfertilized plot (NF CNT) and  $N_F$  were those of fertilized plots. Data on NF CNT were reported exclusively for calculating the  $NUpE$ , since the aim of this research was to evaluate the effect of MOS application on nutrient availability supplied by fertigation.

Fertigation was performed by applying a half-strength (50%) Hoagland solution to the lettuce, in order to emphasize the effect of the surfactant addition in suboptimal nutrient supply. The 50% Hoagland solution was prepared by diluting 0.25 g L<sup>-1</sup> KNO<sub>3</sub>, 0.068 g L<sup>-1</sup> KH<sub>2</sub>PO<sub>4</sub>, 0.59 g L<sup>-1</sup> Ca(NO<sub>3</sub>)<sub>2</sub>·4 H<sub>2</sub>O, and 0.25 g L<sup>-1</sup> MgSO<sub>4</sub>·7 H<sub>2</sub>O in 1 L of distilled water. Drip-fertigation was carried out by administering 50 mL per plant of the nutrient solution after 1, 3, 8, and 16 days from transplanting (with a total of 200 mL/plant of fertilized solution). The Hoagland solution was added to the fertilized control (F CNT). To supply the surfactant by fertigation, MOS was added in the Hoagland solution at a concentration of 0.2 mL<sub>MOS</sub> × L<sub>Hoagland</sub><sup>-1</sup> for the treatments F S0.2 and 1.0 mL<sub>MOS</sub> × L<sub>Hoagland</sub><sup>-1</sup> for the treatments F S1.0. During experimental trial, each plant was irrigated with 50 mL of distilled water on alternate days, strictly avoiding subirrigation. During the whole lettuce cropping cycle, the total amount of water was 600 mL water per plant.

At harvest, multiple parameters were determined for the crop: (i) crop growth and leaf water content; (ii) crop water and nutrient use efficiency; (iii) plant root growth and morphology.

Crop growth and leaf water content—In order to evaluate the effect of the application of MOS by fertigation on crop growth and water uptake by lettuce, at harvest, five plants/treatment/block, for a total of 15 plants/treatment, were collected and separated into aboveground and belowground portions, then dried in a forced-air oven at 80 °C for 72 h in order to determine the dry biomass and leaf water content. The following data were collected, separately for the aboveground and belowground lettuce: fresh (FW) and dry (DW) weight (g plant<sup>-1</sup>); leaf area (LA, cm<sup>2</sup> plant<sup>-1</sup>), dry matter (DM, total dry weight/fresh weight); number of leaves (N, leaves plant<sup>-1</sup>); specific leaf fresh (LFW) and dry (LDW) weight (mg cm<sup>-2</sup>), specific leaf water content (SLWC, as LFW – LDW, mg cm<sup>-2</sup>); root fresh (RF, g plant<sup>-1</sup>) and dry weight (RD, g plant<sup>-1</sup>), root dry matter (RDM), and root to shoot ratio (RS). Leaf area (LA) was measured using an electronic area meter (LI-COR Model 3100, Delta-T Devices Ltd., Cambridge, UK).

Crop water and nutrient use efficiency—To assess the potential benefit of the surfactant treatments, the water use efficiency (WUE, in g L<sup>-1</sup>) was calculated on lettuce fresh (FWUE) and dry (DWUE) biomass, as the ratio between the aboveground fresh (FW) or dry (DW) weight (g) and the applied amount of irrigation water [11,22].

Crop nutrient use efficiency was evaluated by applying the vector analysis to all nutrients (N, P, K, Ca, Mg, Na, Fe, Mn, Zn, Cu, B) [31] and by calculating the nitrogen uptake efficiency ( $NUpE$ ) [32]. For the mineral analysis, dried leaf tissues, taken at the end of the experiment, were ground separately in a Wiley mill (20-mesh screen). Then, 1.0 g of the dried plant tissues were analyzed for the following elemental content: P, K, Ca, Mg, Na, Fe, Mn, Zn, Cu, B. The related concentrations were determined by dry ashing at 400 °C for 24 h, dissolving the ash in 1:25 HCl, and assaying the solution obtained using an inductively coupled plasma emission spectrophotometer (ICP-AES Thermo Optek, Milano, Italy) [33]. The N content (%) of both the aboveground lettuce ( $N_P$ ) and the belowground portions ( $N_R$ ) was determined on a dry-weight basis, using a nitrogen analyzer (FP-528; Leco Corp-USA) to calculate the lettuce N uptake. The leaf nitrate concentration (NO<sub>3</sub>, in mg/kg) was determined by a nitrate test (116995-Reflectoquant, Merck, Darmstadt, Germany). On the basis of the amount of N supplied by the half-strength Hoagland solution, equal to 21 mg of N per plant, the N

uptake efficiency (NUpE) was calculated as the ratio:  $((U_F - U_{NF})/N_F)$ , where  $N_F$  was the N supplied by fertigation,  $U_F$  the N uptake when  $N_F$  was given, and  $U_{NF}$  the N uptake in the control plot that was not fertilized (NF CNT) [26].

**Root growth and morphology**—On the basis of previous research, where the role of different agronomic strategies on roots development in horticultural and tree crops was evaluated by scanning electron microscopy (SEM) [34,35], in the present work the effect of MOS on lettuce root morphology was evaluated by visual observation and SEM analysis, by selecting three roots fragments per plant and collecting three plants per treatment. In particular, secondary lateral roots were cut with a razor blade from 5 mm to 15 mm from the root tip to assess the potential effect induced by the surfactant on the turgidity of the meristematic cells. The fresh root fragments were observed by SEM (Carl Zeiss A.G., Oberkochen-Germany) under variable pressure equipped with a tungsten (W) electron source, using the backscattered electrons detector (SEM-BSE), which is able to improve the resolution so as to optimize the visualization of the biological ultra-structural root morphology.

**Statistical analysis**—All data were statistically analyzed by ANOVA with post hoc Tukey's HSD test or Duncan's multiple-range test for means comparison using the SPSS software package (IBM Corp., Armonk, NY, USA). We applied Tukey's HSD test (checking that the model assumptions were met), as it exhibited a greater power than the other tests under most circumstances (e.g., Bonferroni tends to lack power overcorrecting for Type I error). The method of Duncan, which is less conservative, was applied as alternative test when the data showed some tendency to be not significant with Tukey's test (i.e.,  $p \approx 0.05$ ), since Tukey pays the price of a greatly increased Type II error rate. Bi-dimensional vector analysis was then applied for the simultaneous comparison of plant growth and nutrient content [3,31]. Under vector analysis, changes in nutrient content, nutrient concentration, and dry weight were plotted as vectors in a bi-dimensional graph, with each point representing the combination of these three parameters within four Cartesian subplots. Nutrient content obtained under the different treatments were compared after normalization, while changes in dry weight and concentration were plotted with curved content isoclines included for interpretation. Dry weights were displayed in relation to the nutrient content of plant tissue; the abscissas represented the dry weight (x-axis) and the ordinates represented the nutrient concentration (y-axis) [3,31].

### 3. Results

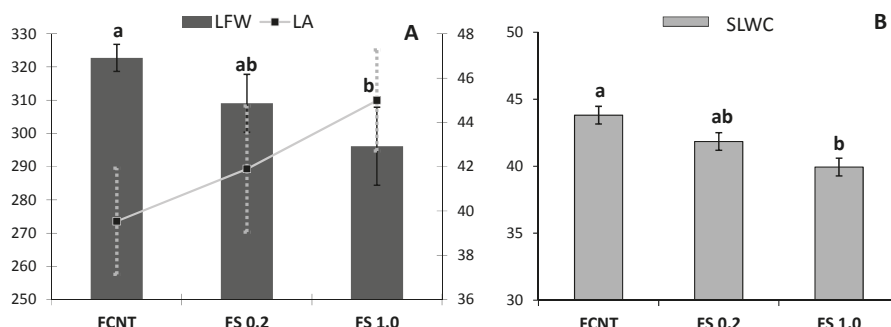
**Crop growth and leaf water content**—Results showed that fertigation with MOS application at both the doses did not affect the considered aboveground (FW, DW, DM, N leaves, LA) and belowground (RF, RD, RDM, R:S) parameters (Table 2 and Figure 1), with the exception of LFW, which was lower in presence of the surfactant at both the concentrations ( $p \leq 0.05$ , Figure 1). MOS application also determined a slight, but not significant increase of the aboveground DM values (Table 2).

**Table 2.** Surfactant and fertigation effects on aboveground and belowground biometric parameters: fresh (FW) and dry (DW) weight (g plant<sup>-1</sup>), dry matter (DM), number of leaves (N. leaves plant<sup>-1</sup>), specific dry (LDW) weight (leaf weight/leaf area, mg cm<sup>-2</sup>), root fresh (RF) and dry (RD) weight (g plant<sup>-1</sup>), root dry matter (RDM), root:shoot ratio (RS). F CNT = fertigation control, F S0.2 and F S1.0 = surfactant application by fertigation at 0.2 mL<sub>MOS</sub> × L<sub>Hoagland</sub><sup>-1</sup> and 1.0 mL<sub>MOS</sub> × L<sub>Hoagland</sub><sup>-1</sup>, respectively. Data are reported as mean ± standard error (SE). Significant differences at *p* < 0.05 (Tukey’s HSD post hoc test). <sup>a</sup>: \*, \*\*, \*\*\* = significant at *p* ≤ 0.05, 0.01, and 0.001, respectively; NS = not significant.

Treatment	Aboveground Biometric Parameters									
	FW (g)		DW (g)		DM (%)		N. Leaves		LDW (mg/cm <sup>2</sup> )	
	SE	SE	SE	SE	SE	SE	SE	SE	SE	SE
F CNT	15.58	1.37	1.02	0.08	6.63	0.30	14.00	0.70	3.10	0.19
F S0.2	11.91	1.37	0.89	0.07	6.89	0.30	13.60	0.70	3.01	0.19
F S1.0	13.56	1.23	1.01	0.08	7.09	0.33	14.20	0.70	2.98	0.17
Significance <sup>a</sup>	NS		NS		NS		NS		NS	

Treatment	Belowground Biometric Parameters							
	RF (g)		RD (g)		RDM (%)		RS	
	SE	SE	SE	SE	SE	SE	SE	
F CNT	4.13	0.38	0.36	0.03	90.96	10.95	0.34	0.06
F S0.2	3.20	0.38	0.27	0.03	84.91	10.95	0.28	0.06
F S1.0	3.67	0.38	0.29	0.03	85.85	10.95	0.32	0.06
Significance <sup>a</sup>	NS		NS		NS		NS	



**Figure 1.** (A) Specific leaves fresh weight (LFW, mg cm<sup>-2</sup>), leaf area (LA, cm<sup>2</sup> plant<sup>-1</sup>); (B) specific leaf water content (SLWC, mg cm<sup>-2</sup>). F CNT = fertigation control, F S0.2 and F S1.0 = surfactant application by fertigation at 0.2 mL<sub>MOS</sub> × L<sub>Hoagland</sub><sup>-1</sup> and 1.0 mL<sub>MOS</sub> × L<sub>Hoagland</sub><sup>-1</sup>, respectively. Different letters represent significant differences, mean separation at *p* < 0.05 with Tukey’s HSD post hoc test.

The LFW, which expresses the fresh weight of the surface unit of the lettuce leaf (cm<sup>2</sup>), was significantly higher (*p* = 0.0012) in the control (46.9 mg cm<sup>-2</sup>) with respect to that recorded after MOS application by fertigation at 1.0 mL L<sup>-1</sup> (42.9 mg cm<sup>-2</sup>). The increasing trend of LA (+13.3% at 1.0 mL<sub>MOS</sub> × L<sub>Hoagland</sub><sup>-1</sup>, *p* = 0.094, Figure 1A) that was recorded for MOS-fertilized lettuce seem to suggest that the lower specific fresh weight of MOS-fertilized lettuce could be due to a major expansion of the leaf area, or to an increased evapotranspiration, or both (Figure 1A). Furthermore, the SLWC, i.e., the water content of the leaf surface unit, decreased significantly (*p* = 0.042, Figure 1B) at increasing doses of the MOS application, being about 7% lower in F S1.0 with respect to F CNT.

Crop water and nutrient use efficiency—Results related to the lettuce FWUE and DWUE are reported in Figure 2. The FWUE of F CNT was significantly higher than that of F S0.2, but it did not differ from that of F S1.0; otherwise, the DWUE was the same in F CNT and F S1.0, and again the lowest under F S0.2 treatment.

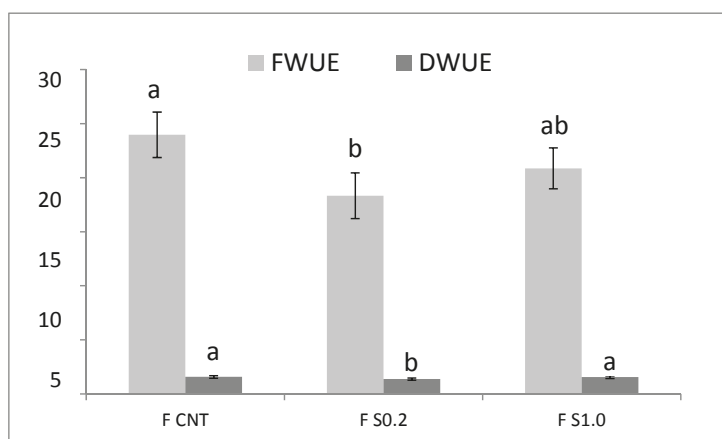


**Figure 2.** Water use efficiency for lettuce fresh (FWUE, g L<sup>-1</sup>) and dry (DWUE, g L<sup>-1</sup>) yield. F CNT = fertigation control, F S0.2 and F S1.0 = surfactant application by fertigation at 0.2 mL<sub>MOS</sub> × L<sub>Hoagland</sub><sup>-1</sup> and 1.0 mL<sub>MOS</sub> × L<sub>Hoagland</sub><sup>-1</sup>, respectively. Error bars represent standard error. Different letters represent significant differences, mean separation at *p* < 0.05 with Tukey’s HSD.

Regarding the nutrient uptake of lettuce, the concentrations of macro, meso, and microelements in leaves, as affected by MOS addition by fertigation, are reported in Table 3.

**Table 3.** Surfactant effects on macro (g kg<sup>-1</sup>) and microelements (mg kg<sup>-1</sup>) concentration of lettuce leaves: F S0.2 and F S1.0 = surfactant application by fertigation at 0.2 mL<sub>MOS</sub> × L<sub>Hoagland</sub><sup>-1</sup> and 1.0 mL<sub>MOS</sub> × L<sub>Hoagland</sub><sup>-1</sup>, respectively; F CNT = fertigation only. Data are reported as mean ± standard error (SE). Different letters represent significant differences across surfactant treatments, mean separation at *p* < 0.05 with Duncan’s multiple-range test. <sup>a</sup>, \*\*, \*\*\* = significant at *p* ≤ 0.05, 0.01, and 0.001, respectively; NS = not significant.

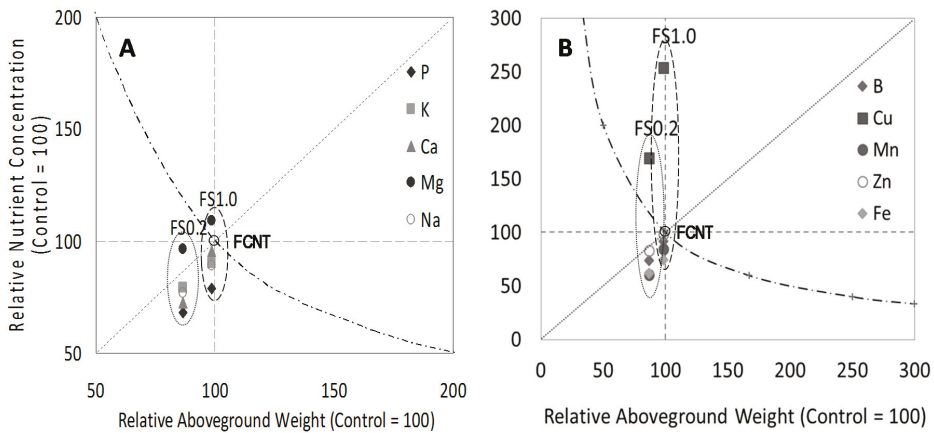
Treatment	Macro and Mesonutrients (g kg <sup>-1</sup> )										
	P		K		Ca		Mg		Na		Fe
F CNT	2.28 a	±0.12	44.36	±2.06	4.45	±0.34	1.08	±0.08	1.07	±0.08	0.09 ±0.03
F S0.2	1.79 b	±0.12	40.66	±2.06	3.73	±0.30	1.20	±0.08	0.95	±0.08	0.06 ±0.03
F S1.0	1.82 b	±0.15	40.49	±2.06	4.31	±0.30	1.20	±0.08	0.97	±0.08	0.07 ±0.03
Significance <sup>a</sup>	*		NS		NS		NS		NS		NS

Treatment	Micronutrients (mg kg <sup>-1</sup> )							
	B		Cu		Mn		Zn	
F CNT	11.50	±0.72	0.77 b	±0.30	62.13 a	±5.50	14.97	±1.15
F S0.2	9.76	±0.72	1.51 ab	±0.30	43.50 b	±5.50	14.34	±1.03
F S1.0	10.74	±0.72	1.99 a	±0.27	53.09 ab	±5.50	14.95	±1.03
Significance <sup>a</sup>	NS		*		*		NS	

Significant differences were found in the elemental concentration of lettuce leaves for P, Mn, and Cu. The P concentration decreased from 2.2 g kg<sup>-1</sup> in the untreated lettuce (F CNT) to 1.8 g kg<sup>-1</sup> in the MOS-fertilized lettuce (Table 3). Likewise, Mn decreased from 62.13 (F CNT) to 53.09 (F S0.2) and 43.50 mg kg<sup>-1</sup> (F S1.0). In contrast, Cu concentrations significantly increased from 0.77 mg kg<sup>-1</sup> in F CNT to 1.51 and 1.99 mg kg<sup>-1</sup> when the surfactant was administered at increasing doses by fertigation.

The bi-dimensional vector analysis, which allows for the simultaneous comparison of plant growth (i.e., lettuce aboveground dry weight) and nutrient content [3,11,31] is reported in Figure 3, showing the effect of MOS application by fertigation on lettuce nutrient use efficiency.



**Figure 3.** Vector analysis of aboveground macro (P, K) and meso (Ca, Mg, Fe, Na) nutrient (A), and micronutrient (B, Cu, Mn, Zn) (B) contents in lettuce. Each colored point is a vector, where plant aboveground weight is the x-value and the relative concentration of each nutrient is the y-value, under F S0.2 (dotted ellipse:  $0.2 \text{ mL}_{\text{MOS}} \times \text{L}_{\text{Hoagland}}^{-1}$ ) or F S1.0 (dashed ellipse:  $1.0 \text{ mL}_{\text{MOS}} \times \text{L}_{\text{Hoagland}}^{-1}$ ) surfactant application by fertigation. Concentration and plant aboveground dry weight of F CNT (O) were used as reference points, normalized to 100%. The content isolines in vector nomograms represent combinations of dry weight and concentration, giving the constant contents per unit of dry weight.

When administering the surfactant by fertigation at the lowest dose ( $0.2 \text{ mL L}^{-1}$ ), both the nutrient concentration and the total content of macro (Figure 3A) and micronutrients (Figure 3B) declined, with an insignificant decrease in plant dry weight when compared to the control, giving an indication of a lowered nutrient availability that may compromise the lettuce yield. On the contrary, at the highest surfactant dose ( $1.0 \text{ mL L}^{-1}$ ), even if the total content of macro, meso (Figure 3A), and micronutrients such as Mn and Fe (Figure 3B) decreased, no appreciable decrease in lettuce dry weight was found. At the highest rate of surfactant, the decline in P and K uptake were not a limiting factor for lettuce growth. Different behavior was noticed for Cu, which significantly increased in both of the surfactant treatments, regardless of the crop growth response.

In relation to nitrogen uptake and use efficiency, the lettuce N content of the whole plant and, separately, of the aboveground and belowground portions are reported in Table 4, together with nitrate content and NUpE, as affected by MOS applications by fertigation at both doses.

**Table 4.** Surfactant effects on nitrogen uptake of lettuce: F S0.2 and F S1.0 = surfactant application by fertigation at  $0.2 \text{ mL-MOS} \times \text{L-Hoagland}^{-1}$  and  $1.0 \text{ mL-MOS} \times \text{L-Hoagland}^{-1}$ , respectively; F CNT = fertigation only.  $N_{\text{TOT}}$  = lettuce total N content, mg/kg;  $\text{NO}_3$  = aboveground lettuce nitrate content, %;  $N_{\text{P}}$  = aboveground lettuce N content, %;  $N_{\text{R}}$  = root lettuce N content, %; and NUpE (nitrogen uptake efficiency). Data are reported as mean  $\pm$  standard error (SE). Statistical analysis performed only on fertilized treatments. For fertilized treatment only: different letters represent significant differences across surfactant treatments, mean separation at  $p < 0.05$  with Duncan’s multiple-range test. <sup>a</sup>: \*, \*\*, \*\*\* = significant at  $p \leq 0.05, 0.01,$  and  $0.001,$  respectively; NS = not significant.

Treatment	Nitrogen Crop Uptake						Nitrogen Use			
	Lettuce $N_{\text{TOT}}\%$	Plant				Root	NupE <sup>c</sup>			
		$\text{NO}_3$ (mg/kg)		$N_{\text{P}}\%$		$N_{\text{R}}\%$				
F CNT	1.63 ab	$\pm 0.07$	21.37	$\pm 4.06$	1.06 ab	$\pm 0.05$	0.55	$\pm 0.090$	0.46	$\pm 0.183$
F S0.2	1.55 b	$\pm 0.15$	21.77	$\pm 2.04$	1.01 b	$\pm 0.05$	0.56	$\pm 0.106$	0.49	$\pm 0.106$
F S1.0	1.83 a	$\pm 0.13$	17.31	$\pm 2.97$	1.17 a	$\pm 0.08$	0.61	$\pm 0.093$	0.56	$\pm 0.044$
Significance <sup>a</sup>	**		NS		**		NS		NS	
NF CNT <sup>b</sup>	<b>0.83</b>	<b><math>\pm 0.11</math></b>	<b>19.88</b>	<b><math>\pm 4.08</math></b>	<b>0.78</b>	<b><math>\pm 0.06</math></b>	<b>0.39</b>	<b><math>\pm 0.094</math></b>	-	

Note: <sup>b</sup> = unfertilized control data for the calculation of NUpE. <sup>c</sup> = calculated as the ratio:  $(U_{\text{F}} - U_{\text{NF}})/N_{\text{F}}, U_{\text{NF}}$  being the N uptake in NF CNT unfertilized plot [32].

Overall, the uptake of N was evidently strongly influenced by MOS addition in fertigation at the highest rate of application, giving the highest nitrogen content of lettuce both for the whole plant ( $N_{\text{TOT}}$ , Table 4) and for the marketable fraction ( $N_{\text{P}}$ , Table 4). In contrast, we did not find significant differences for the nitrate content, even if a tendency to decrease was evident under the F S1.0 treatment. This is a positive result, since a reduction of leaf nitrates is considered a key parameter of crop safety. Similarly, the NUpE was not significantly affected by surfactant additions; nonetheless, a slight increasing trend was observed at increasing applications (Table 4). These results can be better highlighted by analyzing the lettuce N content by means of bi-dimensional vector analysis [11,36]. Actually, the NUpE indicates the N uptake from aboveground lettuce minus the N uptake from the soil, normalized against the N supplied by fertigation. In other words, it solely expresses the ability of the crop to take up N from the fertilized system. To investigate the use efficiency of the absorbed N, that is, the efficiency by which the crop was able to utilize the N taken up from the substrate (i.e., the fertilized soil) to grow, we analyzed the N content of the aboveground lettuce in the bi-dimensional vector plane. In Figure 4, the  $N_{\text{P}}$  content of lettuce leaves under F S0.2 and F S1.0 treatments was normalized to that of F CNT (control = 100) and then expressed in relation to the lettuce aboveground dry weight to emphasize the effect of the surfactant on fertigation. When MOS was added to the fertigation solution, the marketable lettuce showed a lower N relative to the unit weight under F S0.2, and an unchanged one under F S1.0, which indicates better nitrogen use efficiency in MOS-treated lettuce when compared to the F-CNT lettuce (Figure 4).

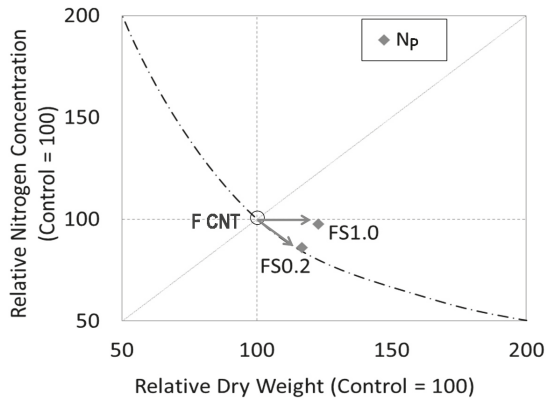


**Figure 4.** Vector analysis of aboveground nitrogen ( $N_p$ ) content. Each colored point is a vector, where plant aboveground weight is the x-value and the relative concentration of  $N_p$  is the y-value, under F S0.2 ( $0.2 \text{ mL}_{\text{MOS}} \times L_{\text{Hoagland}}^{-1}$ ) or F S1.0 ( $1.0 \text{ mL}_{\text{MOS}} \times L_{\text{Hoagland}}^{-1}$ ) surfactant application by fertigation. Concentration and plant aboveground dry weight of F CNT (O) were used as reference points, normalized to 100%. The content isolines in vector nomograms represent combinations of dry weight and concentration, giving the constant contents per unit of dry weight.

Root growth and morphology—Root apparatus of lettuce under the different treatments was visually observed (Figure 5(A1–A3)) and then evaluated by scanning electron microscopy under variable pressure, giving a comparison of root meristematic cells (Figure 5(B1–B3)) and root apex (Figure 5(C1–C3)).

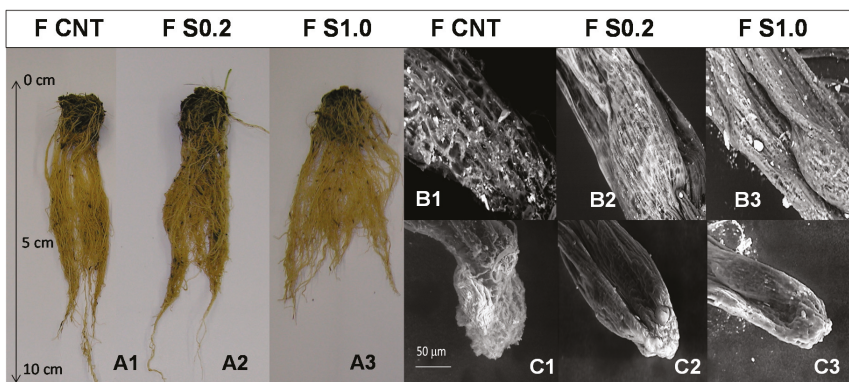


**Figure 5.** (A1–A3) Visual image of lettuce root apparatus. (B1–B3) Mag.  $200\times$  SEM analysis of root meristematic cells. (C1–C3) Mag.  $200\times$  SEM analysis of root apex. F CNT= control; F S0.2 and F S1.0 = MOS application by fertigation at  $0.2 \text{ mL}_{\text{MOS}} \times L_{\text{Hoagland}}^{-1}$  and  $1.0 \text{ mL}_{\text{MOS}} \times L_{\text{Hoagland}}^{-1}$ , respectively.

Even if the RF, RD, and root DM values were the same in samples with surfactant addition with respect to F CNT (Table 2), it was evident that the root apparatus in F S0.2 and F S1.0 (Figure 5(A2,A3)) treatments were different compared to that of F CNT (Figure 5(A1)), as they were less elongated in the lettuce treated with the highest dose of surfactant. In fact, the majority of F S1.0 roots (Figure 5(A3)) had an average length of about 5.5–6.0 cm, compared to the length of 7.5–8.0 cm recorded in F CNT and F S0.2 treatments (Figure 5(A1,A2)). The SEM analysis gives evidence of a higher regularity of the

meristematic cells (Figure 5(B2,B3)) and a greater turgidity of root apex (Figure 5(C2,C3)) in both the roots of F S0.2 and F S1.0 samples in comparison to the untreated control (Figure 5(B1,C1)).

#### 4. Discussion

To evaluate the potential agronomical advantages on lettuce production deriving from the application of non-ionic surfactants by fertigation, in our demonstration tested we measured the crop yield, a set of morphological aboveground and belowground data, the FWUE/DWUE, the  $NU_pE$ , and, at the end, we applied vector analysis to compare the actual aboveground lettuce dry weight and the related nutrient uptake to the theoretical crop yield and nutrient concentration (i.e., isolines). This multi-approach evaluation helped to reveal whether the application of MOS by fertigation was able to improve the lettuce quality in terms of nutritional content, ensuring the same yield, by the optimization of the crop root uptake of irrigation water.

The surfactant did not increase nor decrease the lettuce yield. In any case, due to the reduced LFW, SLWC and the increased LA, we inferred that the use of the surfactant in fertigation apparently determined a positive physiological response by inducing more expanded and thinner leaves in lettuce. In the literature, several ecophysiological studies [11,37–40] identified the leaf thickness as an index of sclerophylly that may respond to resource gradients. In fact, the lignification or suberisation of cell walls in parenchyma tissues can occur in natural environments in response to biotic and abiotic stresses, in particular to low water availability [37]. High levels of sclerophylly and increased tissue density are associated in nature with the acquisition of leaf resistance to many environmental factors, e.g., high temperature, high irradiance, and low water availability [38–40]. In our test, the recorded reduction of LFW when the surfactant was added at the highest rate could be explained by the higher leaf expansion (i.e., increased LA, +13.3% at  $1.0 \text{ mL}_{MOS} \times L_{Hoagland}^{-1}$ ) and likely by the increase of evapotranspiration, with the consequent lower values of SLWC, which were  $-4.5\%$  in F S0.2 and  $-8.8\%$  in F S1.0 with respect to F CNT [37]. The LDW was almost constant among the considered treatments, while the DWUE did not decrease with the increase of MOS, confirming the positive effect of the surfactant in optimizing the use of water by the crop. The change in leaf morphology induced by the use of MOS in fertigation was then evaluated in relation to the lettuce nutrient uptake and root morphology. According to Scagel [31], when the content of some nutrients is lower and the plant dry weight is the same when compared to the control, the system is characterized by a higher use efficiency of such nutrients, which corresponds to lower nutritional absorption [3,11,36,41]. The slight tendency for a reduction of FW recorded in F S0.2 could be related to a reduced nutrient availability, as showed in the vector analysis. In particular, the K, Ca, and Mg content of F S0.2 (under the isoline with respect to F CNT in Figure 3), being correlated to a decrease in the aboveground dry weight, showed a less efficient use of such nutrients. On the other hands, since the lettuce  $N_p$  of F S0.2 was not located in the “deficiency” vector space (under the isoline in Figure 4), the nitrogen was evidently not a limiting factor for F S0.2 lettuce growth. When MOS was added at the highest rate, it determined the reduction of P ( $-20\%$ ) and, to a lesser extent, of Mn concentration ( $-14.6\%$ ) in lettuce tissues with respect to F CNT. This indicated that, at the rate of  $1.0 \text{ mL L}^{-1}$ , the soil nutrient availability was enough to reduce the uptake of some nutrients and increase others’ (i.e., Cu: +158%) without compromising the crop yield. While the concentration and the total content of macro and micronutrients decreased, the higher dose of MOS lead to no appreciable increases in plant weight. In this case, the nutrients uptake could be considered either luxury consumption or storage [31,42]. Since the reduction of the nutrient content in lettuce was observed only on selected nutrients, we hypothesized a different attitude of the surfactant molecules in their interaction with each ion, consequently modifying their availability to the crop into the soil in a positive (i.e., Cu) or in negative (i.e., P and Mn) way. This behavior could be due a different chemical affinity between those elements and the water surfactant molecule, which could act as a complexing agent towards certain elements in relation to their mass/charge ratio, consequently rendering them more or less available to plant roots [43].

The surfactant addition at the highest rate increased the lettuce quality. The strong decrease of leaf nitrate content (−19%) in F S1.0 with respect to F CNT, despite the corresponding increase of  $N_P$  (+10%), suggested that the water surfactant was capable to limit the nitrate accumulation in lettuce leaf. These results are partially in line with the work of Baratella et al. [3], which highlighted a dose-related detrimental effect of a non-ionic surfactant formulation (45% fatty acid ester, 45% sorbitan sesqui-octanoate, and 10% propylene glycol) as an irrigation adjuvant in the absence of N fertilization. Qiu and colleagues [44] found a highly linear relationship between nitrate accumulation and water content in different vegetable tissues, indicating that the proper soil water content in agronomic practice is essential for decreasing leaf nitrate content [45]. In our findings,  $N_{TOT}$  and  $N_P$  were higher and  $N_R$  was the same in F S1.0 with respect to F CNT; the surfactant was able to modulated lettuce N uptake in favor of the ammonium form, without incurring any negative effect to the N nutritional status of the plant. Apparently, both  $NO_3^-$  and  $H_2PO_4^-$  anions exhibited reduced absorbance by F S1.0 lettuce in favor of  $NH_4^+$  or  $Cu^{2+}$  cations. We hypothesized that their positive charges interacted with the proton-acceptor sites of the surfactant (i.e., the oxirane groups), which probably prevented their soil immobilization and made them more available to plant root uptake. In contrast, the nitrates and phosphates, as negative ions, were repelled by the surfactant, a mechanism which potentially decreased their crop availability in the short term and thus justified the decreased uptake of nitrate, P, and Mn by lettuce.

In terms of root morphology, even if no differences of RF and RD were recorded, when compared to that of F CNT, the F S1.0 root showed more organized meristem cells, a highest turgidity of the root apex, and abundant but shorter lateral roots to better intercept water and nutrients, probably localized in the upper soil layer where the surfactant was administered. Actually, at the dose of F S1.0, the root apparatus did not need to elongate more than 5.5–6.0 cm to suitability intercept the water and nutrients, while in the F CNT and F S0.2 treatments the roots grew to an 8-cm depth. Many authors argued that extensive root systems are vital when plants are grown in soils containing insufficient supplies of water or nutrients [46]. The same increased leaf expansion recorded under F S1.0 could be also correlated to a higher soil softness [47], as the consequence of the direct signaling between root and shoot was associated with the reduction of soil mechanical impedance after MOS addition [48]. It was supposed that the non-ionic surfactant, by modifying the water repellency, was able to change the water tension of the circulating solution in the soil, thus improving the wettability and spreading into the soil micropores [11–15] and reducing the depth of the soil wetted front. As a consequence, when MOS was applied by fertigation, the soil water was mainly localized in the soil volume not deeper than 5.5–6.0 cm, where lettuce roots developed. Moreover, this non-ionic surfactant led to surfactant-induced capillary pressure gradients [11] within the wetting front, which indirectly increased the lettuce roots' accessibility to nutrients [3–11].

## 5. Conclusions

The non-ionic surfactant MOS, applied to lettuce by fertigation at the dose of  $1.0 \text{ mL}_{MOS} \times L_{Hoagland}^{-1}$ , did not significantly affect the vegetable yield nor the water use efficiency index. Nonetheless, it was able to improve the nutrient use efficiency by the crop. Likely, the surfactant acted at the soil/root interface, modulating the water and nutrient uptake on the basis of their soil nutrient availability and the availability of nutrients in the soil, as well as their mutual chemical affinity with the surfactant. Since a theoretical model recently explained how non-ionic organosilicone surfactants affect soil capillary and adsorption processes in horticultural systems [11], we may correctly refer to the MOS ability to optimize lettuce water uptake and specific nutrients assimilation, in particular that of P, K, Fe, and Mn. Moreover, unexpectedly, the application of the surfactant at the highest dose strongly increased the quality of lettuce by significantly reducing the nitrate accumulation in lettuce leaves.

The obtained results should be considered to be preliminary, as they refer to an in-field demonstration test. Still, given the marketable parameters of lettuce recorded in this study,

we inferred that the non-ionic surfactant, used at the highest dose, offered the possibility to: (i) guarantee the adequate rate of nutrient inputs; (ii) maintain a good standard quality of the crop in vegetable production; and (iii) potentially increase farmers' income by reducing the amount of fertigation water for vegetable production by 5–8%, without detrimental effect on crop yield. However, supplementary multi-year field trials are needed to further validate the positive feedback obtained from our demonstration experiment.

**Author Contributions:** A.T. conceived the hypothesis of the research. V.B. determined the plant parameters. A.T. carried out the SEM analysis on plant roots. V.B. performed the analysis. A.T. and V.B. wrote the manuscript.

**Funding:** This research was funded by Evonik Industries AG—Essen (Germany).

**Conflicts of Interest:** The authors declare no conflict of interest.

## References

1. European Environment Agency. Climate Change, Impacts and Vulnerability in Europe 2012—Soil Erosion. 2012. Available online: <http://www.eea.europa.eu/publications/climate-impacts-and-vulnerability-2012/> (accessed on 12 September 2017).
2. Rockström, J.; Karlberg, L.; Wani, S.P.; Barron, J.; Hatibu, N.; Oweis, T.; Bruggeman, A.; Farahani, J.; Qiang, Z. Managing water in rainfed agriculture—The need for a paradigm shift. *Agric. Water Manag.* **2010**, *97*, 543–550. [[CrossRef](#)]
3. Baratella, V.; Renzaglia, M.; Trinchera, A. Effect of Surfactant as Adjuvant for Irrigation/Fertigation in Vegetable Production: Preliminary Results on Lettuce. *Acta Hort.* **2016**, *1123*, 157–164. [[CrossRef](#)]
4. Blackwell, P.S. Management of water repellency in Australia, and risks associated with preferential flow, pesticide concentration and leaching. *J. Hydrol.* **2000**, *231–232*, 384–395. [[CrossRef](#)]
5. Lehrsch, G.A.; Sojka, R.E.; Reed, J.L.; Henderson, R.A.; Kostka, S.J. Surfactant and irrigation effects on wettable soils: Runoff, erosion, and water retention responses. *Hydrol. Process.* **2011**, *25*, 766–777. [[CrossRef](#)]
6. Krogh, K.A.; Halling-Sorensen, B.; Mogensen, B.B.; Vejrup, K.V. Environmental properties and effects of non-ionic surfactant adjuvants in pesticides: A review. *Chemosphere* **2003**, *50*, 871–901. [[CrossRef](#)]
7. Zontek, S.J.; Kostka, S.J. Understanding the different wetting agent chemistries. *USGA Green Sec. Rec.* **2012**, *50*, 15.
8. Lowery, B. The potential for wetting agents as soil additives. In *Proceedings of the Fertilizer, Aglime, and Pest Management Conference*; Univ. of Wisconsin-Extension: Madison, WI, USA, 1981; Volume 20, pp. 86–90.
9. Karagunduz, A.; Pennell, K.D.; Young, M.H. Influence of a non-ionic surfactant on the water retention properties of unsaturated soils. *Soil Sci. Soc. Am. J.* **2001**, *65*, 1392–1399. [[CrossRef](#)]
10. Wiel-Shafran, A.; Ronen, Z.; Weisbrod, N.; Adar, E.; Gross, A. Potential changes in soil properties following irrigation with surfactant-rich greywater. *Ecol. Eng.* **2006**, *26*, 348–354. [[CrossRef](#)]
11. Baratella, V.; Trinchera, A. Organosilicone surfactants as innovative irrigation adjuvants: Can they improve water use efficiency and nutrient uptake in crop production? *Agric. Water Manag.* **2018**, *204C*, 149–161. [[CrossRef](#)]
12. Baurle, S.A.; Kroener, J. Modeling effective interactions of micellar aggregates of ionic surfactants with the Gauss-Core potential. *J. Math. Chem.* **2004**, *36*, 409–421. [[CrossRef](#)]
13. Kelling, K.A.; Speth, P.E.; Arriaga, F.J.; Lowery, B. Use of non-ionic surfactant to improve nitrogen use efficiency of potato. *Acta Hort.* **2003**, *619*, 225–232. [[CrossRef](#)]
14. McCauley, G.N. Non-ionic surfactant and supplemental irrigation of soybean on crusting soils. *Agron. J.* **1993**, *85*, 17–21. [[CrossRef](#)]
15. Fenster, W.; Randall, G.; Nelson, W.; Evans, S.; Schoper, R. Effect of WEX on nutrient uptake and crop yields, 1976–1977. In *Compendium of Research Reports on the Use of Non-Traditional Materials for Crop Production*; NCR-103 Committee on Non-Traditional Soil Amendments and Growth Stimulants, E.3.1.1–13; Iowa State Press: Ames, Iowa, 1978.
16. Laughlin, W.M.; Smith, G.R.; Peters, M.A. A multipurpose wetting agent, WEX, and a cultured biological product, Agrispon, leave potato yields unchanged. *Am. Potato J.* **1982**, *59*, 87–91. [[CrossRef](#)]
17. Wolkowski, R.P.; Kelling, K.A.; Oplinger, E.S. Evaluation of three wetting agents as soil additives for improving crop yield and nutrient availability. *Agron. J.* **1985**, *77*, 695–698. [[CrossRef](#)]

18. Brumbaugh, E.; Peterson, M. The use of a non-ionic surfactant to alleviate the effects of compacted soil on corn (*Zea mays* L.) yield and root growth. In Proceedings of the Sixth International Symposium on Adjuvants for Agrochemicals, Amsterdam, The Netherlands, 13–17 August 2001.
19. Walworth, J.; Kopec, D. *Response and Nutrient Uptake in Bermudagrass Treated with Aquatrols Surfactant ACA 1848 in the Desert Southwest*. AZ 1359 Series. 2004. Available online: [www.arizona.openrepository.com/handle/10150/216539](http://www.arizona.openrepository.com/handle/10150/216539) (accessed on 22 July 2017).
20. Banks, M.L.; Kremer, R.J.; Eivazi, F.; Motavalli, P.P.; Nelson, K.A. Effects of Selected Surfactants on Nutrient Uptake in Corn (*Zea Mays* L.). *J. Plant Nutr.* **2015**, *38*, 1036–1049. [[CrossRef](#)]
21. Arriaga, F.J.; Lowery, B.; Kelling, K.A. Surfactant Impact on Nitrogen Utilization and Leaching in Potatoes. *Am. J. Potato Res.* **2009**, *86*, 383–390. [[CrossRef](#)]
22. Chaichi, M.R.; Nurre, P.; Slaven, J.; Rostamza, M. Surfactant Application on Yield and Irrigation Water Use Efficiency in Corn under Limited Irrigation. *Crop Sci.* **2015**, *55*, 386–393. [[CrossRef](#)]
23. Yang, H.; Wang, L.; Zehnder, A.J.B. Water scarcity and food trade in the Southern and Eastern Mediterranean countries. *Food Policy* **2007**, *32*, 585–605. [[CrossRef](#)]
24. Directorate-General for Environment—European Commission. *Mediterranean Water Scarcity and Drought—Technical Report*; Mediterranean Water Scarcity and Drought Working Group: Brussels, Belgium, 2011.
25. Trinchera, A.; Allegra, M.; Rocuzzo, G.; Rea, E.; Rinaldi, S.; Sequi, P.; Intrigliolo, F. Organo-mineral fertilizers from glass-matrix and organic biomasses. A new way to release nutrients. *J. Sci. Food Agric.* **2011**, *91*, 2386–2393. [[CrossRef](#)]
26. Hazra, G. Different Types of Eco-Friendly Fertilizers: An Overview. *Sustain. Environ.* **2011**, *1*, 54–70. [[CrossRef](#)]
27. Lee, S.; Lee, J.Y.; Yu, H.P.; Lim, J.C. Synthesis of environment friendly non-ionic surfactants from sugar base and characterization of interfacial properties for detergent application. *J. Ind. Eng. Chem.* **2016**, *38*, 157–166. [[CrossRef](#)]
28. Council Regulation (EC). *Ecotoxicity Testing Methods to Be Used by the REACH Regulation. Evaluation, Authorisation and Restriction of Chemicals (REACH)*; No. 440/2008; EC: Brussels, Belgium, 2008.
29. OECD Guideline for Testing of Chemical, Method OECD 301F. 1992. Available online: <https://www.oecd.org/chemicalsafety/risk-assessment/1948209.pdf> (accessed on 14 June 2016).
30. Italian Official Methods for Soil Analysis. *Official Italian Gazette*, 21 October 1999; n. 248.
31. Scagel, C.F. Growth and nutrient use of ericaceous plants grown in media amended with sphagnum moss peat or coir dust. *HortScience* **2003**, *38*, 46–54.
32. Benincasa, P.; Guiducci, M.; Tei, F. The Nitrogen Use Efficiency: Meaning and Sources of Variation—Case Studies on Three Vegetable Crops in Central Italy. *HortTechnology* **2011**, *21*, 266–273.
33. Isaac, R.A.; Johnson, W.C. Elemental determination by inductively coupled plasma atomic emission spectrometry. In *Handbook and Reference Methods for Plant Analysis*; Kalra, Y., Ed.; CRC Press: New York, NY, USA, 1998; Volume 21, pp. 165–170. ISBN 1-57444-124-8.
34. Trinchera, A.; Torrisi, B.; Allegra, M.; Rinaldi, S.; Rea, E.; Intrigliolo, F.; Rocuzzo, G. Effects of Organic Fertilization on Soil Organic Matter and Root Morphology and Density of Orange Trees. *Acta Hort.* **2015**, *1065*, 1807–1814. [[CrossRef](#)]
35. Trinchera, A.; Testani, E.; Ciaccia, C.; Campanelli, G.; Leteo, F.; Canali, S. Effects induced by living mulch on rhizosphere interactions in organic artichoke: The cultivar's adaptive strategy. *Renew. Agric. Food Syst.* **2016**, *32*, 214–223. [[CrossRef](#)]
36. Trinchera, A.; Baratella, V.; Rinaldi, S.; Renzaglia, M.; Marcucci, A.; Rea, E. Greenhouse Lettuce: Assessing Nutrient Use Efficiency of Digested Livestock Manure as Organic N-Fertiliser. *Acta Hort.* **2013**, *1041*, 63–69. [[CrossRef](#)]
37. Bacelar, E.A.; Correia, C.M.; Moutinho-Pereira, J.M.; Goncalves, B.C.; Lopes, J.I.; Torres-Pereira, G.M.G. Sclerophylly and leaf anatomical traits of five field-grown olive cultivars growing under drought conditions. *Tree Physiol.* **2004**, *24*, 233–239. [[CrossRef](#)] [[PubMed](#)]
38. Read, J.; Sanson, G.D. Characterising sclerophylly: The mechanical properties of a diverse range of leaf types. *New Phytol.* **2003**, *160*, 81–99. [[CrossRef](#)]
39. Press, M.C. The functional significance of leaf structure: A search for generalizations. *New Phytol.* **1999**, *143*, 213–219. [[CrossRef](#)]

40. Groom, P.K.; Lamont, B.B. Which common indices of sclerophylly best reflect differences in leaf structure? *Environ. Sci. Ecol.* **1999**, *6*, 471–474. [[CrossRef](#)]
41. De Lucia, B.; Vecchiatti, L.; Rinaldi, S.; Rivera, C.M.; Trinchera, A.; Rea, E. Effect of Peat-Reduced and Peat-Free Substrates on Rosemary Growth. *J. Plant Nutr.* **2013**, *36*, 863–876. [[CrossRef](#)]
42. Trinchera, A.; Rivera, C.M.; Rea, E.; Intrigliolo, F.; Rocuzzo, G.; Salerno, A. Nutritional Response of *Zea mais* L. Seedlings to “On Plant Demand” Fertilizer: A Vector Analysis Approach. *J. Plant Nutr.* **2016**, *39*, 895–903. [[CrossRef](#)]
43. Singh, Z.; Khan, A.S. Surfactant and Nutrient Uptake in Citrus. *Adv. Citr. Nutr.* **2012**, 157–167. [[CrossRef](#)]
44. Qiu, W.; Wang, Z.; Huang, C.; Chen, B.; Yang, R. Nitrate Accumulation in Leafy Vegetables and Its Relationship with Water. *J. Soil Sci. Plant Nutr.* **2014**, *14*, 761–768. [[CrossRef](#)]
45. Silber, A.; Xu, G.; Levkovitch, I.; Soriano, S.; Bilu, A.; Wallach, R. High fertigation frequency: The effects on uptake of nutrients, water and plant growth. *Plant Soil* **2003**, *253*, 467–477. [[CrossRef](#)]
46. Bengough, A.G.; McKenzie, B.M.; Hallett, B.D.; Valentine, T.A. Root elongation, water stress, and mechanical impedance: A review of limiting stresses and beneficial root tip traits. *J. Exp. Bot.* **2011**, *62*, 59–68. [[CrossRef](#)] [[PubMed](#)]
47. Masle, J.; Passioura, J.B. The effect of soil strength on the growth of young wheat plants. *Aust. J. Plant Physiol.* **1987**, *14*, 643–656. [[CrossRef](#)]
48. Taylor, H.M.; Ratliff, L.H. Root elongation rates of cotton and peanuts as a function of soil strength and water content. *Soil Sci.* **1969**, *108*, 113–119. [[CrossRef](#)]



© 2018 by the authors. Licensee MDPI, Basel, Switzerland. This article is an open access article distributed under the terms and conditions of the Creative Commons Attribution (CC BY) license (<http://creativecommons.org/licenses/by/4.0/>).

Article

# Redrawing Soil Salinity Innovation-Focused Stakeholder Interaction for Sustainable Land Management in Khorezm Province, Uzbekistan

Akmal Akramkhanov <sup>1,\*</sup>, Muhammad Mehmood Ul Hassan <sup>2</sup> and Anna-Katharina Hornidge <sup>3,4</sup>

<sup>1</sup> International Centre for Agricultural Research in Dry Areas, PO Box 4375, Tashkent 100000, Uzbekistan

<sup>2</sup> World Agroforestry Centre, United Nations Avenue, Nairobi 30677 00100, Kenya; m.hassan@cgiar.org

<sup>3</sup> Leibniz Centre for Tropical Marine Research, Fahrenheitstr. 6, Bremen 28359, Germany; anna-katharina.hornidge@leibniz-zmt.de

<sup>4</sup> Institute of Sociology, University of Bremen, Mary-Somerville-Str. 9, Bremen 28359, Germany; hornidge@uni-bremen.de

\* Correspondence: a.akramkhanov@cgiar.org

Received: 15 September 2017; Accepted: 29 December 2017; Published: 15 February 2018

**Abstract:** Addressing soil salinity in irrigated drylands is tightly linked with water and land management decisions thus requiring interdisciplinary engagement. The salinity mapping approaches in Central Asia are undertaken through field sampling and laboratory analysis, which is a time consuming process. As a consequence, salinity maps are not available on time to estimate water requirements to cope with varying levels of soil salinity. Reducing the time lag between assessment and delivery of such maps would enable authorities to determine in advance appropriate water volumes for leaching the salts before and during the growing season. Research initiated in Uzbekistan context explored transdisciplinary and participatory approach to innovation development with local stakeholders. As one of the innovations, an electromagnetic induction meter (EM), a tool for rapid salinity assessment, was chosen and jointly with local salinity mapping related institutions tested, validated, and local capacities for its use developed. This paper redraws this process of innovation-focused stakeholder interaction and transdisciplinary research and discusses it with reference to ongoing debates on participatory and/or transdisciplinary innovation research. The existence of strong path dependencies within implementation oriented organizations could be observed, meaning that the innovation demands many changes to the existing system. Furthermore, the encountered challenges of participatory, transdisciplinary research in the hierarchically shaped setting of post-soviet Uzbekistan are illustrated in selected qualitative field notes and assessed. For improved joint learning and research in a transdisciplinary team, feedback cycles of mutual learning and critical reflection of how to theoretically and practically work in a transdisciplinary manner turned out to be crucial and not to be underestimated.

**Keywords:** transdisciplinary research; Follow-the-Innovation; innovation development; electromagnetic induction meter (EM)

## 1. Introduction

Land degradation due to increased soil salinity in the Aral Sea Basin has become widespread [1,2]. Globally, salt-induced land degradation is common in arid and semi-arid regions where agriculture is not viable without irrigation. Over-irrigation, as well as insufficient and ill functioning drainage in irrigation schemes are among often mentioned factors causing salt accumulation in the upper soil layer that negatively affects soil properties as well as crop productivity [1]. Resulting secondary salinization also triggered by other forms of poor agricultural management affects large areas worldwide, estimated

figures reach millions of hectares with varying levels of soil salinity. In some countries salt-affected area consists of over half of the total irrigated land [2].

Among those countries with a large share of salinized land is Uzbekistan. Although the share of salinized land differs within the country, provinces located in the lower reaches of the Amudarya river are the most salinized, salinity affected areas exceed 90% of the total irrigated land [1]. Such difference is attributed to hydrogeological features of downstream areas of the Amudarya river, particularly of Khorezm and Karakalpakstan that are located in low accumulative plains characterized by poorly drained alluvial lowlands making these areas prone to salinization (Figure 1).

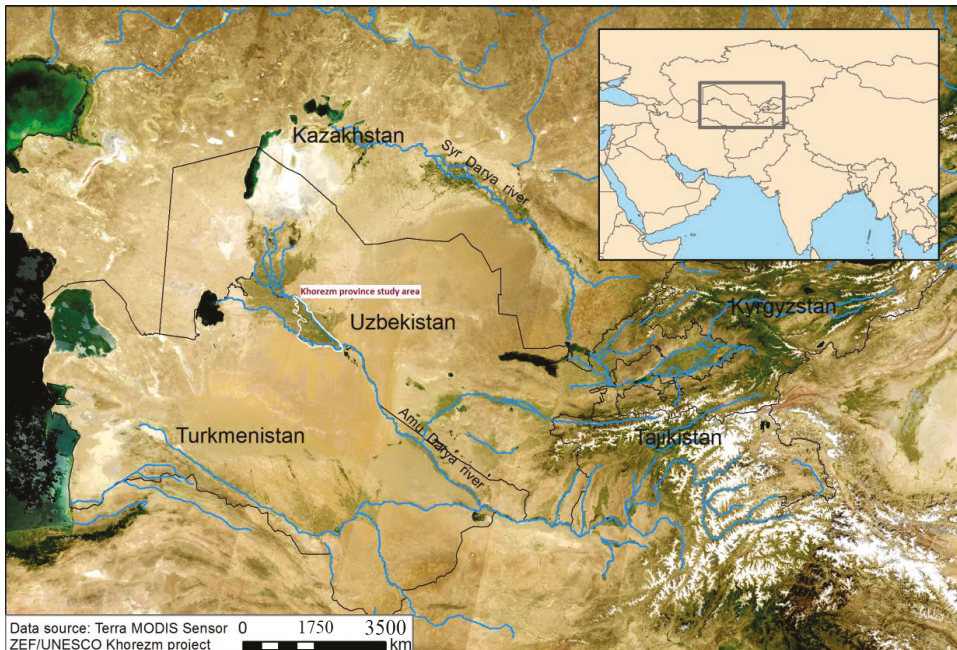


**Figure 1.** Map of Uzbekistan and the irrigated areas in the southern parts along the Amudarya river [2] (note: Khorezm province is delineated with a white boundary).

To reclaim soils that accumulated excessive amounts of salts in the root zone, water is applied to leach the salts out of the intended soil layer. Leaching of the salts in the lower reaches of the Amudarya river is a common practice, consuming around 25%–30% of the water diverted for irrigation, to keep the soils suitable for crop growth [2] and is carried out under the blanket norms specified at the provincial level without much reference to actual salinity levels due to inadequate soil salinity mapping and monitoring. Field studies [3] demonstrate that water for leaching applications rather excessive and wasteful.

The salinity mapping approaches in Uzbekistan are undertaken through field sampling and laboratory analysis, and results are then transferred to salinity maps at district, regional, and national scales, which is a time consuming process. As a consequence, the salinity maps are not available on time to estimate water requirements to cope with varying levels of soil salinity [2,3]. Reducing the time lag between assessment and delivery of such maps would enable authorities to determine in advance appropriate water volumes for leaching the salts before and during the growing season.

With the aim to improve the current methods of salinity assessment in Uzbekistan, the Center for Development Research (ZEF) of the University of Bonn under its project “Restructuring Land

and Water Use in Khorezm Province, Uzbekistan” in 2008 started a transdisciplinary process of innovation testing and adaptation. As a part of the Follow-the-Innovation (FTI) component, together with stakeholders [4,5] an electromagnetic device for rapid salinity mapping was tested. The technique had not been used in Uzbekistan so far. The key objectives of this process were: (i) to create awareness among selected stakeholders about the methods; (ii) to validate the use of the device as an express method for salinity assessment and mapping with stakeholders; and (iii) to assist in capacity building of the relevant stakeholders for wider outscaling.

This paper aims to redraw this process of innovation-focused stakeholder interaction and joint transdisciplinary research and to assess it with reference to ongoing debates on participatory and/or transdisciplinary innovation research. Taking into account that effective researcher-stakeholder collaborations are challenging to establish, develop only over a period of at least few years, and require substantial investments of energy and time to maintain [6], the presented process of research jointly with local stakeholders was one of four transdisciplinary innovation development processes [5,7]. While all four approaches were designed as ‘transdisciplinary’ research approaches, the line between transdisciplinary and participatory innovation research with local stakeholders in the fostering of the actual, practical processes was not always clear. However, instead it was regularly, mostly implicitly, debated and the theory redefined through practice. As such, this paper aims to empirically contribute to respective ongoing debates on transdisciplinarity.

Methodologically this paper is based on the empirical experience of fostering a transdisciplinary innovation research process for salinity measuring from early 2008 to early 2011. It thus draws on the personal experiences of the authors, researchers, driving or accompanying the process as well as a stock of over 20 documents such as workplans, minutes of the meetings, and capturing the steps taken during this time.

## 2. ‘Transdisciplinary’ versus ‘Participatory’ Research with Stakeholders

The study, in designing the overall transdisciplinary research component FTI explicitly rejected linear approaches to innovation diffusion such as the ‘Transfer of Technology’ (ToT) approach [8] or ‘Diffusion of Innovations’ [9]. Linear approach here means developed by one actor group and scaled out to others, often in a top down manner. Instead, the ‘Follow-the-Technology’ (FTT) framework [10] was chosen as starting point. FTT as a participatory approach to innovation development, is composed of a set of steps assuming that once there is an innovation with a ‘plausible promise’ that may work and raise interest of users, innovators engage in a process in which the innovation is experimented with, in real-life situations by users [11]. The process itself is one of trial and selection, leading finally to a point where the innovation is sufficiently robust to be released more widely or abandoned because it has proven to be unsuitable for the region. The methodology FTT, uses this intervention as the entry point into a complex situation, and then allows what is discovered to determine what is important [10,12]. Douthwaite’s idea to ‘follow the technology’ was then adapted to include both technical and institutional innovation packages.

With the aim with stakeholders to jointly test the innovation packages and adapt them to the actual real-life situations of potential users, the so far interdisciplinary team opened and included stakeholders into the innovation development processes. The actual interaction between researchers and stakeholders consequently was hoped to be one of equal partnership and respect and therefore be fostered through participatory approaches. Reference to participatory approaches as methods and tools for facilitating transdisciplinary interaction and research can be found in many definitions of transdisciplinarity [13–15]. Wiesman [13] states: “Collaboration between science and society in transdisciplinary research implies participatory processes”. Häberli [16] underlines the involvement of local stakeholders and state: “The core idea of transdisciplinarity is, different academic disciplines working jointly with practitioners to solve a real-world problem. It can be applied in a great variety of fields.” Hoffmann-Riem [17] points to this aim of transdisciplinarity to produce solutions to real-life problems and distinguish four aspirations: “Transdisciplinary research, therefore aims at identifying,

structuring, analyzing and handling issues in problem fields with the aspiration (a) to grasp the relevant complexity of a problem, (b) to take into account the diversity of the lifeworld and scientific perceptions of problems, (c) to link abstract and case-specific knowledge, and (d) to develop knowledge and practices that promote what is perceived to be the common good". Overall, transdisciplinary and participatory approaches in general are bottom up in character and thus are more likely to be accepted and taken up by larger groups of people.

Gibbons [18] and others distinguish Mode 1 (or disciplinary and interdisciplinary science) and Mode 2 (or transdisciplinary science) knowledge production [18–20]. According to the authors, Mode 1 knowledge production is characterized by the search for universal explanations, a hierarchically higher valued rationality, as organized within the science system and a largely Western definition of the moral values of intellectual ideals. In contrast to this, Mode 2 knowledge production is socially contextualised research with the research questions being generated from the research problem itself, leading to the production of heterogeneous knowledge, heterarchically organized and based on new forms of relation between scientific and non-scientific organizations.

For fostering these new forms of relation between scientific and non-scientific stakeholders, leading to heterarchically organizations, heterogeneous knowledge participatory approaches are commonly applied. Elzinga [21] points to the diversity of reasons, leading to the adoption of participatory approaches. The range of reasons is quite broad, those that are relevant in the here assessed Follow-the-Innovation approach are to access and include tacit knowledge of local stakeholders in the process of testing and adapting innovations. This of course entails the critical question of the participatory approach being instrumentalized by the researcher for merely sending a message, or actually for inspired communication and enhanced creativity [22]. A basic condition for participatory (and at the same time also transdisciplinary) research to work, based on the experiences presented in Cleaver [23], is that trust has to exist, or to be built, between the participants involved. This trust forms the fundamental basis for the mutual exchange of knowledge [5]. In order to avoid the development of mistrust, which is highly counterproductive to any form of participatory process, Elzinga [21] points to the importance of three criteria: the participant should be independent, involved in the research process as early as possible, and be given resources to effectively influence decision-making.

Critical literature on participatory approaches such as by Cleaver [23], Shutt [24] or Mosse [25], amongst many others, repeatedly point to the important aspect of participatory (and the same holds true for transdisciplinary) processes being significantly driven by the stakeholder him/herself, rather than dominantly by the researchers or donor-funded programs. There is strong dependence of outlined transdisciplinary and participatory processes to innovation testing and further development on the stakeholders' interest. Innovation-focused interaction taken in this study reflect the stakeholder's interest, however, the process has been challenged in many other aspects. In the following, we assess these challenges and discuss the positive and negative outcomes and lessons learnt.

### 3. Materials and Methods

#### 3.1. Study Area and Context

Stakeholders engaged in the study are located in the Khorezm province which is part of Uzbekistan, situated in the upper delta plain of the Amudarya river. Agriculture as the major sector in Khorezm provides 40% of employment. The modern landscape of the province has been heavily altered by men harnessing the river water to cultivate 270,000 ha of irrigated land. Waterlogging and salinity affect almost all of the area that is under irrigation due to seepage losses from earthen canals and inadequate drainage infrastructure. Major crops grown in the area are cotton, winter wheat, and rice that altogether occupy around 70%–80% of irrigated land.

The province is located on alluvial lowlands with elevations ranging from 77 to 132 m. Khorezm experiences a continental climate, average annual temperature is around 12–15 °C, however, hot and

dry summer temperatures reach 45 °C, and cold winter minimum temperatures reach −20 °C. Annual precipitation is around 100 mm. Most of the soils are loamy soils, about 80% of soils consist of silt loams (USDA soil texture classification), sandy loams, and loams [26].

The conventional method of soil salinity assessment in Uzbekistan based on soil sampling at different depths and subsequent analysis to determine total dissolved solids (TDS) was described by [27]. As an alternative to TDS, the electrical conductivity (EC) meter and a method developed by local stakeholder was also included in the evaluation matrix. The method refers to EC of 1:1 ratio of soil:water solution measured directly in the soil solution by EC meter. Both, TDS and EC, are considered as destructive soil salinity testing.

The area for evaluation of salinity assessment methods conducted by local stakeholder was located in Khanka district, experimental farm comprised of 60 ha of irrigated land. Soils were predominantly of silt loam texture and 20 locations were randomly sampled over the study site. Samples for TDS and EC analyses were collected at 30 cm increments down to a depth of 150 cm. Evaluation and reflections provided by the stakeholder were based on comparing TDS and EC with the proposed innovation.

### 3.2. Electromagnetic Induction Meter—The Innovation

Several techniques, such as soil electrical resistivity [28], time domain reflectometry (TDR) [29], and electromagnetic induction (EM) [30] have been deployed elsewhere to rapidly assess and map salinity. The electromagnetic induction meter (EM) is considered as a non-destructive soil salinity monitoring method that measures bulk apparent electric conductivity ( $EC_a$ ) [28], and has been introduced from geophysical applications. These provide an effective measuring depth of up to 1.5 m, suitable for both, deep- and shallow-rooted crops [28]. Furthermore, the calibrations of EM devices to transfer readings into commonly used indicators of electrical conductivity of the saturation extract ( $EC_e$ ) or TDS have already been conducted [27,28].

EM could potentially offer greater advantage in terms of speedily mapping the salinity without inducing non-sampling errors [31]. The devices can be easily mounted on vehicles equipped with storage, connected to a computer, and used with geographic information systems (GIS) to rapidly and frequently map salinity for various spatial scales. Besides, EM surveys allow for the identification of fine-scale spatial variation because they offer continuous measurements.

Studies conducted with an EM device to estimate soil salinity at farm scale in the Khorezm region [26,32] demonstrated that this device can accurately map the spatial distribution of soil salinity and consequently monitor soil salinity dynamics as a basis for the evaluation of alternative land reclamation and land management strategies in the Aral Sea Basin. The cost of using EM over a large area of 6400 ha, which comprises about 1/3 of a district in the highly saline province of Khorezm, Uzbekistan, equals 3.75 \$/ha, compared to 146.42 \$/ha using a conventional survey involving analyses of 43,200 samples [28].

### 3.3. The Process—Team Formation

The formation of the interdisciplinary team proved to be an interesting process in itself. It took almost one year before the team could confirm its final active membership, and garner collective interest in pursuing the innovation. Initially, the members of the group were specialists engaged in water and salinity topics and others who nominated themselves during the FTI training conducted in May 2008. These members comprised three core members or experts of salinity assessment, groundwater and hydrology, and five support members from allied disciplines. During team formation, the members opted for the key scientific expert from the discipline of the innovation to lead the team and process [4,5]. The group leader followed an informal approach of seeking ideas, advice, and inputs from other members verbally and taking responsibility for incorporating these into the planning processes, and then sharing the draft planning documents with the group members. This in consequence led to opaqueness that then had to be discussed.

In the team’s own assessment, for an initial period of almost a year, the FTI process was driven by a one-man team comprising the team leader, as other members would tend to simply agree to what he would propose. The team leader questioned the rationale of continuing FTI as there was a lack of interest from other team members. The ideas for withdrawing this innovation from the FTI process were exchanged with the FTI team members, FTI coordinator, and the project management as well. The team leader realized at that stage that he had misunderstood FTI as a straightforward extension type of exercise rather than a process of interaction, dialogue, and joint research with stakeholders.

On the other hand, it was hard to speed up the process as rapport building with stakeholders was very important but time consuming. The challenges that the team were struggling with were clarified with the FTI and project coordinators, as outlined in Box 1. During an internal FTI review workshop, held in May 2009, it was decided that the FTI facilitator would join the team to support the process with his expertise as well as an expert on groundwater, who knew the local stakeholders well, would get actively involved in the group more directly (Box 1).

**Box 1.** Group Dynamics—Excerpt of Minutes.

Date: 13 May 2009  
 Location: Project office  
 Participants: FTI team leader, FTI facilitator, FTI assistant, water specialist, project coordinator

Background:  
 The meeting was a follow up of discussions at an internal FTI review (April 2009). The team leader felt like “one-man” team as his team members tend to agree to everything proposed. In his view, the team had not made much progress since November 2008, and thus triggered opinions during the FTI review that this innovation should be shelved on account of lack of interest by members. At the same time, a number of potential stakeholders were identified, and several showed keen interest in the innovation.

Outcome:  
 The following roadmap was agreed on:

- (a) Team leader will write a brief description of the innovation for the stakeholders;
- (b) FTI facilitator will join the team as a member and visit potential stakeholders together with the team leader to bring the potential of the innovation to the attention of these organizations;
- (c) If stakeholder interest was not high enough, a final documentation would be prepared describing the results of this FTI effort and explaining why stakeholders were not interested;
- (d) If any potential stakeholder is interested, there will be a follow-up, depending on the interest.

Based on these discussions, a road map was drafted indicating activities, responsibilities, and timelines as illustrated in Figure 2.

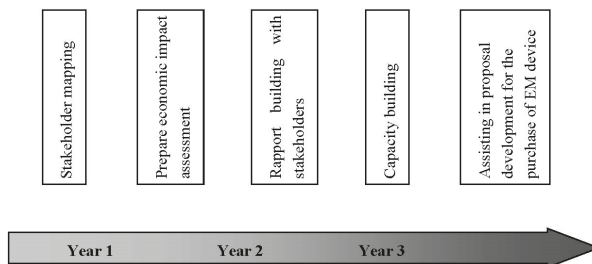


**Figure 2.** Roadmap of the Salinity Assessment Team.

### 3.4. Stakeholder Selection

A list of potential stakeholders was initially assembled by the collective knowledge of the team members, and shared across many others for the inclusion of additional potential stakeholders. Once listed, the team then prepared a matrix with stakeholders' mandates, jurisdiction, location, and perceived interest in the innovation, based on the advantages the innovation offered. A split was made based on the differences between the stakeholders directly using tools to measure in practice (implementing institutions) and those who educated and trained others on how to use tools to measure soil salinity (educational institutions).

In the following these stakeholders are coded as follows: Stakeholder 1 is a research organization, Stakeholder 2 is a salinity mapping organization, Stakeholder 3 is an educational institution, Stakeholder 4 represents an administrative unit with salinity mitigation mandate, and Stakeholder 5 is an applied research institute.

The suitability of the presented innovation needed to be assessed by the stakeholders and their interest confirmed in terms of their needs and financial constraints. After the stakeholders' interest was verified, the team expected to work with a delegated specialist/person from the stakeholder's institution.

Out of 11 potential stakeholders the team discerned five key stakeholders using the following criteria: (a) direct mandate to assess and map soil salinity, (b) dependence of ongoing activities on soil salinity assessment, and (c) promotion of innovative methods in natural resource management. While the project staff itself also carried out soil salinity assessments using EM, direct involvement of the selected stakeholders in the project's on-going measurements was found to be complicated because most stakeholders were located far from Khorezm. The possibility to bring the stakeholders to the project site in Urgench would not be as useful as to let them use EM in practice during their field work. Therefore, based on an analysis of stakeholder mandates, the following stakeholder-specific engagement strategies were outlined:

- Visit on-going Stakeholder 1's soil survey expeditions in the Khorezm region at their site to show and use the equipment;
- Collaborate with Stakeholder 2 because of their direct mandate to assess and map salinity and location within the same city as that of the project's location;
- Conduct training on the use and calibration of EM to selected educational institutions;
- Discuss with Stakeholder 5 the possible calibration of EM;
- While some institutions had the capacity and experience of initiating and funding projects, other institutions lacked that capacity. Demand from interested stakeholders could be pooled together to organize and initiate a collaborative funding proposal for the purchase of EM.

## 4. Results and Discussion

### 4.1. Process Implementation

The initial steps, i.e., roadmap writing and stakeholder mapping, were employed as planning tools, while remaining flexible for refining the roadmap based on the stakeholder engagements and their interests.

For the interactions with the potential stakeholders, a brief description of the device and its use was prepared in Uzbek and Russian languages that included key results of the correlation of the device readings with soil salinity data measured in the laboratory. Additionally, the device was taken along for demonstration. A number of activities were undertaken by team members in 2009 and 2010 towards initiating the transdisciplinary processes with potential stakeholders in 2009 (Table 1).

**Table 1.** Steps taken during 2009–2010.

#	Activity	Time
1	Roadmap preparation	15 January 2009
2	Land management program secretariat visited	10 March 2009
3	Seminar organized by an international agricultural research center	23 March 2009
4	Team internal discussion (e-mail)	4 May 2009
5	Internal discussion about future plans	18 May 2009
6	Discussion with Stakeholder 1 regarding survey in the region	19–20 May 2009
7	Stakeholder 1 letter for joint experimentation	22 May 2009
8	Collaboration with Stakeholder 1 to join EM survey with their soil survey in the region	28–30 May 2009
9	Initial meeting with Stakeholder 2	13 June 2009
10	Initial meeting with Stakeholder 3	29 June 2009
11	Initial meeting with Stakeholder 4	30 June 2009
12	Meeting with Stakeholder 1	7 July 2009
13	Meeting with Stakeholder 5	3 August 2009

#### 4.2. Stakeholder 1

Stakeholder 1's primary mandate is research in soil science and also providing support in soil surveys to state organizations. Initial contact with a managerial-level staff was positive, who showed keen interest in the innovation as it would ease their job related to salinity mapping, though the need for sampling based analyses would still remain, as the organization could not change the standard procedures. The FTI team undertook EM measurements when the stakeholder's field team implemented their soil survey in Khorezm region during spring 2009. The purpose was to (a) interact with field staff, (b) demonstrate EM at work on their site, and (c) prepare maps to present at the Stakeholder 1 meeting. Follow up was to be decided based on reactions from Stakeholder 1 staff after the presentation. A letter from Stakeholder 1 expressing interest in collaboration and inviting the project staff to undertake an EM survey in parallel with their routine soil survey was received in May 2009 confirming their interest. The FTI field assistant joined the Stakeholder 1 team for 3 days to jointly conduct a salinity survey. The FTI team leader visited the site for backstopping and meeting with the Stakeholder 1 team and to explain the purpose of the EM measurements. Several questions ranging from the working principles of the instrument and influencing factors to the device readings to the practical use of EM for the purpose of soil surveys were explored. The soil survey team leader had reservations due to different working principles that led to suspicions about the accuracy of its measurements. The fact that the device was of foreign origin, and not yet certified by agencies in Uzbekistan might have caused further objections. During the discussions, Stakeholder 1 was mainly concerned about the high price, the necessity to carry and walk to map large areas in addition to their main work load of soil profile descriptions, and the detailed laboratory analyses they routinely do to obtain salinity types and ion compositions regardless of the express methods that Stakeholder 1 owns to measure soil salinity. The Stakeholder 1 team leader mentioned that the existing express methods based on electric conductivity to measure soil salinity, which were already certified and were in use by some other salinity assessing organizations within Uzbekistan, were rarely used by his organization. This in part implied that the organization was relatively conservative in their approach and thus was reluctant in making use of innovative approaches.

Results from EM surveys conducted by the FTI team were shared with Stakeholder 1 for comparison. However, lengthy soil survey expeditions in other regions, and the time required for laboratory analyses of the soil samples collected were presented by Stakeholder 1 as the main reasons for a lack of their progress in comparing the two methods. Several attempts from the FTI team to inquire about the progress later on did not yield much. Consequently, the FTI team decided not to pursue with Stakeholder 1 unless the stakeholder addressed the project out of the stakeholder's interest. After this, there was no further follow-up on collaboration from either side.

#### 4.3. Stakeholder 2

The primary responsibility of Stakeholder 2 is to monitor salinity within the stakeholder's respective province. These maps are then sent to their national superior office. The FTI team saw that since Stakeholder 2's mandate was closer to what the innovation could deliver and because the organization was located within Khorezm province, the discussions proceeded faster and a high level of enthusiasm for partnership about testing the innovation was observed. The chief technical-level staff was approached for the first contact, who had a reputation of an expert interested in modern methods. The interaction gave an initial impression that the stakeholder would be interested in partnering with FTI. Despite an initial warm response and enthusiasm, as the process dynamics in Box 2 show, staff change, busy schedule and the need of confirmation from the managerial-level of Stakeholder 2, resulted in the engagement with the stakeholder being on hold during the entire 2009–2010.

**Box 2.** Initial Meeting with Stakeholder 2—Excerpt of Minutes.

Date: 11 June 2009  
Location: Office of Stakeholder 2, Urgench  
Participants: 2 technical-level staff of Stakeholder 2, FTI team leader, FTI coordinator, FTI groundwater specialist

As a routine, Stakeholder 2 selects three farms per season per district to estimate salinity, and these selected farms are rotated every year. The soil salinity surveys are carried out during the autumn period. Soil samples are taken and analyzed in Stakeholder 2's laboratory in the provincial capital, Urgench. Stakeholder 2 seems to be open to the innovation, as they have already tested alternative methods which they found suitable for moist conditions while not accurate for dry soils.

Also, they have often been called by government agencies to provide quick estimates of soil salinity in fields which puts additional pressure on Stakeholder 2's lean staff capacity. Furthermore, farmers often ask for advice on the salinity levels (distinguishing between not saline, moderate or highly saline) of their fields. The demand for speedy results from interested agencies and farmers seemed to be the main advantage of EM for the stakeholder. Stakeholder 2 staff asked for the manual in Uzbek or Russian languages to familiarize themselves. Additionally, the FTI team suggested conducting measurements with EM during Stakeholder 2's salinity survey on farms, as well as presentations to interested staff and farmers on the use of EM, working principle, and maps generated using EM readings in July. The FTI team also promised to make a small write-up in Uzbek language on the use of EM, which could then be expanded into a guide book. The Stakeholder 2's representative agreed to appraise the team on a suitable date for presentation and further discussions.

However, the Stakeholder 2 did not keep its promise of appraising the FTI team on their interest further. The team leader called a few times and learnt that the chief technical specialist had been transferred to another organization.

#### 4.4. Stakeholder 3

The discussions with Stakeholder 3, which has primarily a teaching mandate, led the team to believe that while such institutions might be more interested in testing and validation, the use of the innovation by such institutions would not necessarily result in wide scale adoption if successfully verified, because the innovation would remain in the realm of an educational facility. Besides, academic testing of the innovation had already been undertaken by the ZEF project and any replication would not add value to the innovation, unless it was undertaken in the stakeholder's real-life situation. The collaboration was therefore not pursued further.

#### 4.5. Stakeholder 4

Additionally, Stakeholder 4, responsible for land rehabilitation, and inspired by a TV interview with the stakeholder's managerial level on methods for salinity assessment, was contacted (Box 3).

**Box 3.** Meeting with Stakeholder 4—Excerpt of Minutes.

Date: 30 June 2009

Location: Office of Stakeholder 4, Tashkent

Participants: Managerial-level of Stakeholder 4, FTI team leader, FTI facilitator

The host expressed interest in the innovation and its capacities as well as attached costs and suggested to meet with the managerial-level staff responsible for the respective department in the Ministry of Agriculture and Water Resources, to discuss possible implementation. Additionally, the host promised that he would present the innovation to its board and if approved, would let us know to discuss and proceed further.

In a follow-up phone call the stakeholder nevertheless confirmed his interest in the service itself, but not the use of the tool by his institution. With this the potential for joint experimentation ceased. Furthermore, the project team contacted several internationally funded projects and donor agencies dealing with salinity mitigation. The dialogues with these stakeholders nevertheless indicated that they were interested in purchasing the services of well-equipped and scientifically valid service providers for covering large-scale as well as in trainings for the use of EM, but not interested in working with the innovation itself or in a transdisciplinary, joint experimentation and validation of the tool together with the project.

*4.6. Stakeholder 5*

The FTI team thought that Stakeholder 5 would be potentially interested in the innovation due to its mandate on both, research and implementation aspects of salinity assessment. Besides, Stakeholder 5 in the past had been engaged in the local assembly and the use of different express methods of soil salinity assessment using electrical conductivity. Furthermore, other stakeholders had voiced their interest in working with institutions simply providing the service of EM-based salinity assessment. From a project perspective, Stakeholder 5 seemed potentially to be this service provider. As outlined in Box 4, the technical-level stakeholder representative during the first meeting showed interest in validating and potentially outscaling the tool. This was then followed up with a meeting with the managerial-level for full approval and support for the further transdisciplinary process.

**Box 4.** Initial Meeting with Stakeholder 5.

Date: 30 June 2009

Location: Office of Stakeholder 5, Tashkent

Participants: Technical-level of Stakeholder 5, FTI team leader, FTI coordinator

As conventional soil salinity analyses and the classifying categories used are not accurate, Stakeholder 5 analyses large amounts of data to improve accuracy of salinity EC probes within given soil moisture ranges. Most of the work is done for research purposes and the upscaling of the results remains a practical challenge. The FTI team indicated the accuracy of the EM calibration ranged from mainly 60% to 80% which seemed low to the host. During the meeting the participants agreed that the stakeholder's laboratory would calibrate EM on their study area. The project would support the work during this calibration period with transport, field assistants, and other necessary inputs. The laboratory would prepare a formal 'statement of record' with the results of calibration. This calibration would be a first milestone for further planning.

The interest of the stakeholder was further confirmed in a meeting with the managerial-level (Box 5), where a tentative roadmap of collaborative innovation testing was discussed, prepared, and formally agreed through a partnership agreement.

**Box 5. Meeting to Confirm Collaboration.**

Date: 3 August 2009

Location: Office of Stakeholder 5, Tashkent

Participants: Managerial- and technical-levels of Stakeholder 5, FTI team leader, FTI facilitator

The host was supportive of the initiative and formally delegated the technical-level contact person. The participants agreed that a draft agreement would be initiated by the project, and then the stakeholder would modify it. A 2-step approach in calibration and dissemination was agreed on. The Stakeholder would calibrate the EM on their site in Khorezm region in parallel with soil survey and analysis by one of their staff. The necessary support in conducting this calibration work would be provided by the project.

The next step would be taken depending on the results of calibration and include training to the staff of Stakeholder 2, who would then impart regular training to other salinity assessment organizations from all the regions, which is part of the mandate of Stakeholder 2, and is already supported financially by the Ministry of Agriculture and Water Resources of Uzbekistan. A training module of 1-day including 2-hour lecture and probably demonstration if the EM device could be included in these regular trainings.

The partners moved quickly into action, and field activities were commenced within two weeks (Table 2).

**Table 2.** Steps taken during 2009–2010 with Stakeholder 5.

#	Activity	Time
1	Meeting for gauging interest	30 June 2009
2	Reaching an agreement	29 August 2009
3	Collaborative field testing of EM	19–22 September 2009
4	Data analyses for draft report	11 December 2009
5	Meeting—revisiting goals of collaboration	15 December 2009
6	Draft report submitted	14 January 2010
7	Participatory monitoring and evaluation	December 2010–January 2011

The main conclusion of the draft report submitted by Stakeholder 5 (Activity 6 in Table 2) and the “statement record” (Box 6) was that EM could be considered for a rough/ approximate estimation of soil salinity level. Additionally, the results of the calibration work were summarized by Stakeholder 5 in two articles.

**Box 6.** Summary of salient points from the “Statement Record” issued by Stakeholder 5 after completion of the Calibration Study.

1. Interpretation of results was complicated due to the influence of many factors including the variation of the groundwater table, pronounced soil textural difference laterally and vertically. Results indicate that at least 3–4 factors influence device readings (porosity, texture, moisture, and layering) which result in approximate salinity level assessments only.
2. Shallow groundwater table increases salinity in the 0–60 cm soil layer. Device readings tended to be higher where groundwater table was shallow, perhaps due to salinity of the groundwater.
3. Correlation analyses with several factors measured were weak.
4. Splitting surveyed locations into two groups based on soil moisture (above or below 20%) of 0–60 cm soil layer showed very high correlation between device readings and electrical conductivity measured in the laboratory. However, such interpretation would require data on soil moisture.
5. Classification of device readings into salinity levels was better when based on correlation with sodium content.
6. It is necessary to conduct the calibration study in other conditions, on more uniform soils where groundwater influence is low. Once completed, the method could be introduced to other organizations.

As a follow up of the calibration work conducted together in Khorezm in 2009, there was a formal request letter from Stakeholder 5 to borrow the EM-tool to use in other regions (letter 01/338 from

9 August 2010). Stakeholder 5 organized a trip to these regions in September 2010 in which the FTI team leader together with the device joined in and jointly conducted the calibration work.

#### 4.7. Stakeholder 5 Innovation Evaluation

The primary evaluation criteria of Stakeholder 5 were influenced by three key interests: (a) possibility of speedy monitoring; (b) acceptable (and low) initial cost; and at the same time (c) increased accuracy of the information regarding salinity distribution. Thus, EM was tested in terms of its reliability and applicability on diverse natural and soil-hydro-geological conditions of Uzbekistan.

According to the stakeholder, the draft report and the “statement of record” provided by the stakeholder’s specialist were sufficient proof of the innovation being validated. Out of the perspective of the project nevertheless a joint final evaluation, a participatory monitoring and evaluation of the pros and cons of the innovation in the real-life setting of a salinity mapping institution in Uzbekistan seemed necessary and eventually Stakeholder 5 agreed to such an exercise. Thus, 15 evaluation criteria were jointly formulated (Table 3), focusing on the validation of the tool, as well as, but secondary on its potential outscaling. There was a consensus to compare the performance of the innovation with TDS as well as with EC meters. The stakeholder chose three grades for scoring, “0”, “1”, and “2”, which corresponded to no or negligible, intermediate, and yes or high, respectively for each formulated criteria. Finally, the conducted matrix ranking consisted of 15 criteria and three salinity assessment techniques.

**Table 3.** Participatory evaluation of alternative salinity assessment methods.

Rank	Criteria	Evaluation/Score			
		Destructive Method		Non-Destructive Method	
		Total Dissolved Solids (TDS)	Electric Conductivity Meter (EC)	Electromagnetic (EM)	
Validation	1	Availability and affordability of the instrument	1	2	0
	2	Availability of trained staff and accessories	2	1	1
	3	More information to generate salinity spatial distribution	0	1	2
	4	Operational efficiency of obtaining information	0	1	2
	5	Level of field worker qualification (and necessity of special training)	1	1	0
	6	Savings in expenses in laboratory analysis, instruments, chemicals	0	1	2
	7	Convenience in the use (technological simplicity)	0	1	2
	8	Labor costs—field	0	0	1
	9	Labor costs—laboratory	0	1	2
	10	Current costs at field work stage (i.e., auger, equipment)	1	1	0
	11	Level of detail of information—layers	2	2	0
	12	Level of detail of information—further analyses for chemical composition	2	1	0
Outscaling	13	Popularity and acceptability of the method	2	1	0
	14	Readiness of practitioners to use	2	1	0
	15	No need for promotion and training	2	1	0

\* 0—no/negligible; 1—intermediate; 2—yes/high.

The ranking of the criteria was done by Stakeholder 5 and the top 5 included access to hardware (criterion 1) and skills required for calibration and conducting survey using any of the methods (criteria 2 and 5). The other two included criteria pertinent to the method; that is, the accuracy and operational efficiency (criteria 3 and 4). If the former three criteria (1, 2, 5) from the top 5 can be solved by providing hardware and upgrading skills of the staff the latter two criteria are critical, both methods, TDS and EC, cannot provide as good as EM.

Various costs included in several criteria were not as important as the convenience or simplicity of the method, awareness about the method and the readiness and interest of the practitioners to work

with it. The least important criteria were detailed information about the salinity within particular soil layers, and about the chemical composition of salts in the soil.

In Table 3 criteria 1–12 are related to the validation dimension of the tool, while the remaining three (criteria 13–15) focus on the potential for outscaling.

The sum of scores accrued by each method is illustrated in Table 4. EC and EM scored higher than TDS with regard to the validity of the tool and method. Regarding the potential for outscaling, the TDS scored higher than EC and EM. This is mainly explained by the fact that TDS is already in use and therefore does not require any change to the system in place. On the other hand, despite the EM tool scoring high in terms of validity, it requires the availability of the equipment and trained staff, training of field specialists of the concerned organizations as a precondition to any form of adoption or outscaling.

**Table 4.** Comparison of criteria categorized into validation and outscaling dimensions.

Criteria	Total Dissolved Solids (TDS)	Electric Conductivity Meter (EC)	Electromagnetic (EM)
validation	9	13	12
outscaling	6	3	0

Although quantitative information from a number of stakeholders would be ideal to formulate conclusions, the real-world case dictates different conditions where the number of stakeholders was limited to start with. There was a small number of stakeholders who have a mandate to provide either methodological or operational soil salinity assessment. These were state supported and mandated organizations that were approached, and only one had experience with different innovations in soil salinity assessment and was open to suggested innovation. Experiences and opinions drawn in this study were therefore based on the process that involved identification and mapping of eleven stakeholders, engaging with seven, interacting with five and finally testing the innovation with only a few.

## 5. Challenges Faced and Lessons Learned

The above outline of a transdisciplinary process of innovation research in post-Soviet Uzbekistan illustrated a number of challenges faced and lessons to be learned from these. In the following, we discuss these as shaped by the three interacting spheres: (a) the innovation itself and its specific characteristics, (b) the stakeholders' specific situations and (c) the project staff, interests and perspectives on the process.

With regard to the innovation itself, most of the stakeholders perceived the innovation as a new promising tool to provide exactly the same detailed analyses at a higher accuracy as obtained by sampling methods and laboratory analyses. Communicating the potential value in a trade-off between high accuracy and scale, at a better resolution and in less time posed a challenge. This was further enhanced by the costs for the device and the complexity involved in the adoption of a new approach and method, altering the existing way of doing things. Most stakeholders initially contacted, were especially concerned about the precision in measurements under different environments, such as different moisture levels and varying soil textures, affecting the readings of the equipment. This was compared to the advantages, such as the ability to assess salinity without destroying the soils, time saving, as well as the capacity of the device to provide high resolution and thus better accuracy of the soil salinity variation.

It consequently became obvious during the different interaction processes that the innovation itself only covers part of the mandate of most implementation stakeholders, and thus either will need to be improved in a way that it not only can map salinity quickly, but also can split up the results into related parameters and sub-components, such as ionic composition of salts. For Stakeholder 1 it might create operational difficulties due to the specifics of the surveys conducted. For example, the benefit of the use of EM is counter-balanced by other issues such as the travelling distance, the cost of additional

numbers of equipment per survey group, walking distance, and burden of carrying the device. While potentially useful, it seemed that the EM device does not fit into the routine soil survey work, where soil samples should be taken anyway, because any salinity mapping exercise by Stakeholder 1 that is not accompanied by detailed soil profiling is unacceptable on quality aspects for Stakeholder 1.

Perhaps, the expectation of the FTI team that the device would be well accepted by staff that undertook the survey was too high, or more time was needed for Stakeholder 1's staff to familiarize themselves with the tool and digest the information before on-field testing, so that they were prepared to field test and then discuss the implementation. On the other hand, the contact person of Stakeholder 1 belonged to the managerial-level of the institute, which initially speeded up the collaboration, but prematurely left the operationalization of collaboration to technical level staff to make further progress. It seems that unless the managerial-level and other lead staff pursue the collaboration regarding innovation with zeal and zest, the innovation is not accepted by technical specialists within the organization, who rely more on their well-practiced methods.

Despite, and possibly even due to the technical aspects of this innovation, which have been researched and reported in Western peer reviewed publications, the additional calibration work initiated and conducted by Stakeholder 5 was crucial for developing the required level of confidence and ownership. As the discussion above showed, the stakeholder subsequently took initiatives to use the device in other areas of Uzbekistan.

This characteristic of the innovation being a technical device, tool and method produced and commonly used in Western countries nevertheless also contributed to what we called the 'salesman-challenge'. The team, and especially the team leader, at times felt like a salesman trying to 'convince' stakeholders of 'his' device, while in fact he was mainly interested in finding one actually interested stakeholder who would be willing to test and validate the device in the stakeholder's real-life setting of everyday salinity mapping in Uzbekistan. It seemed that this especially came into play, when interacting with the managerial-level first, often focusing on the limitations and constraints of the tool, rather than on the potential. Later interactions suggested, that cooperating with technical-level staff first, gauging actual technical interest, and only later involving the managerial level might be more fruitful in certain settings. Furthermore, the 'salesman-challenge' was partly overcome once Stakeholder 5 was identified and the collaboration taken a step further than the initial meetings with other stakeholders, simply raising awareness but not yielding follow-ups.

The earlier stakeholder interactions, or 'mini-FTIs', showed that while a local specialist as a person might very well like the innovation, it is no guarantee that he/she acts as an advocate, or a 'product champion' for the innovation within his/her organization. This might especially be true in hierarchically organized societies in which a sense of belonging to one or another informal network seems crucial for everyday life organization. From the perspective of the local project staff, this was perceived as people not wanting to spoil their relationships with their colleagues for 'outsiders'. It here also became obvious that the personality of each partner in the interaction process plays a crucial role in the outcome of the collaboration and is often far more decisive than the quality or potential to locally fit of the innovation itself.

Here the existence of strong path dependencies within implementation oriented organizations could be observed, meaning that the innovation in parts simply would demand too many changes to the existing system, and therefore make its adoption unlikely. For example in the case of Stakeholder 2, apart from the lack of incentives and motivation to improve the monitoring system, the poor staffing and strong hierarchical control seem to be withholding factors to look for innovative ways for fulfilling their mandate. For the education oriented organizations, such as Stakeholder 3, the interest in the innovation is only limited to its application and use as an alternative tool for postgraduate students research, and does therefore not directly, but possibly indirectly, lead to an uptake by any of the potential users. For the demand by the donor supported projects, who count on service providers and need one or more of the implementation organizations or NGOs to undertake the assignments within the specified areas of the chosen projects, the methods and tools chosen are of much less interest

compared to the information generated by the process of innovation testing and attempted diffusion. Stakeholder 5 nevertheless, and differently to the other stakeholders, may possibly act in the future as a catalyst for introducing salinity assessment innovations. A few years back, for instance, they started promoting EC probes, which are now at least accepted as an alternative to soil sampling. This combined with the attempts to gauge any other serious local interest in taking the innovation further, suggests that the best route of EM being implemented in Uzbekistan is via Stakeholder 5, upon which the FTI team has already embarked. One can turn to Page [33] quoting an old Bostonian rhyme “I eat my peas with honey. I’ve done it all my life. It makes ‘em taste quite funny, but it keeps them on the knife” as a metaphor to explain that some start out eating their peas with knives and honey, and never move on to the fork or spoon, while others actually do. Page [33] looks at path dependence to understand why some countries succeed and some not and argues, that it “requires a build-up of behavioral routines, social connections, or cognitive structures around an institution”.

Yet, besides challenges posed by the local environment and the socio-political and cultural context of the stakeholders, we also encountered challenges induced by the project team involved in the process. Here it became quite obvious that the selected innovation required a subject specialist who at the same time possessed a high level of understanding of innovation development processes, transdisciplinary research tools, and participatory methods as well as other soft skills for interacting with the stakeholders, while at the same time also documenting and analyzing the process. While this posed an immense challenge for the team, it also made the team members go beyond their own disciplines, learn alternative approaches to research, and consider verbal conversation with stakeholders as “data”. As a learning process we nevertheless realized that a lot more time for learning within the project team should have been allocated, especially for those teams with mainly natural science backgrounds. For improved joint learning and research in a transdisciplinary team, feedback cycles of mutual learning and critical reflection of how to theoretically and practically work in a transdisciplinary manner turned out to be crucial and not to be underestimated.

All practical concerns for actually using the tool in the local context were discussed on an equal footing and eye-level between researchers and soil salinity assessment stakeholders. The tool was tested and the practices of testing commonly conducted by the stakeholders were adjusted in ways that EM as a tool was taken on by those potential end users and became theirs. As such, the transdisciplinary process assured not only the adjustment of the tool according to the local contexts, needs and considerations, but also that the joint dialogue structured around the use of the tool in Uzbekistan setting served as a learning and exchange platform for all involved.

**Acknowledgments:** This study was funded by the German Ministry for Education and Research [BMBF; project number 0339970A].

**Author Contributions:** All authors substantially contributed in conceiving and designing of the approach and realizing this manuscript. Akmal Akramkhanov led the process of stakeholder interaction and documentation. Muhammad Mehmood Ul Hassan provided backstopping and guidance throughout the study. Anna-Katharina Hornidge conceptualized approach and innovation development. All authors have read and approved the final manuscript.

**Conflicts of Interest:** The authors declare no conflict of interest.

## References

1. Bucknall, L.; Klytchnikova, I.; Lampietti, J.; Lundell, M.; Scatista, M.; Thurman, M. *Irrigation in Central Asia. Social, Economic and Environmental Considerations*; World Bank: Washington, DC, USA, 2003.
2. Akramkhanov, A.; Ibrakhimov, M.; Lamers, J.P.A. Managing Soil Salinity in the Lower Reaches of the Amudarya Delta: How to Break the Vicious Circle (Case Study 8–7). In *Case Studies in Food Policy for Developing Countries*; Pinstруп-Andersen, P., Cheng, F., Eds.; Cornell University Press: Ithaca, NY, USA, 2010; p. 13.

3. Forkutsa, I. Modeling Water and Salt Dynamics under Irrigated Cotton with Shallow Groundwater in the Khorezm Region of Uzbekistan. Ph.D. Thesis, Rheinische Friedrich-Wilhelms-Universität Bonn, Bonn, Germany, 2006.
4. Hornidge, A.-K.; Ul Hassan, M.; Mollinga, P. *Follow the Innovation—A Joint Experimentation and Learning Approach to Transdisciplinary Innovation Research*; ZEF Working Paper Series; Zentrum für Entwicklungsforschung: Bonn, Germany, 2009; Volume 39.
5. Hornidge, A.-K.; Ul Hassan, M.; Mollinga, P. Transdisciplinary innovation research in Uzbekistan—One year of ‘Following the Innovation’. *Dev. Pract.* **2011**, *21*. [[CrossRef](#)]
6. Waring, T.M.; Goff, S.H.; McGuire, J.; Moore, Z.D.; Sullivan, A. Cooperation across organizational boundaries: Experimental evidence from a major sustainability science project. *Sustainability* **2014**, *6*, 1171–1190. [[CrossRef](#)]
7. Ul Hassan, M.; Hornidge, A.-K. ‘Follow the Innovation’—The Second Year of a Joint Experimentation and Learning Approach to Transdisciplinary Research in Uzbekistan; ZEF Working Paper Series; Zentrum für Entwicklungsforschung: Bonn, Germany, 2010; Volume 63.
8. Chambers, R.; Jiggins, J. *Agricultural Research for Resource-Poor Farmers: A Parsimonious Paradigm*; IDS Discussion Paper 220; IDS: Brighton, UK, 1986.
9. Rogers, E. *Diffusion of Innovations*, 5th ed.; The Free Press: New York, NY, USA, 2003.
10. Douthwaite, B.; de Haan, N.C.; Manyong, V.; Keatinge, D. Blending “hard” and “soft” science: The “follow-the-technology” approach to catalyzing and evaluating technology change. *Conserv. Ecol.* **2001**, *5*, 13. [[CrossRef](#)]
11. Mollinga, P.; Martius, C.; Lamers, J. Work package 710, implementing, improving and adapting with target groups: “Follow the Innovation” (FTI). In *Economic and Ecological Restructuring of Land and Water Use in the Region Khorezm (Uzbekistan), Project Phase II: Change-Oriented Research for Sustainable Innovation in Land and Water Use (2007–2010)*; Martius, C., Lamers, J.P.A., Khamzina, A., Mollinga, P., Müller, M., Ruecker, G., Sommer, R., Tischbein, B., Conrad, C., Vlek, P.L.G., Eds.; Center for Development Research: Bonn, Germany, 2006.
12. Hall, A.; Nahdy, S. *New Methods and Old Institutions: The Systems Context of Farmer Participatory Research in National Agricultural Research Systems, The Case of Uganda*; Network Paper 93; ODI Agricultural Research and Extension Network: London, UK, 1999.
13. Wiesmann, U.; Biber-Klemm, S.; Grossenbacher-Mansuy, W.; Hirsch Hadorn, G. Enhancing transdisciplinary research: A synthesis in fifteen propositions. In *Handbook of Transdisciplinary Research*; Hirsch Hadorn, G., Hoffmann-Riem, H., Biber-Klemm, S., Grossenbacher-Mansuy, W., Joye, D., Pohl, C., Wiesmann, U., Zemp, E., Eds.; Springer: Dordrecht, The Netherlands, 2008; pp. 433–441.
14. Pohl, C.; Hirsch Hadorn, G. Core terms in transdisciplinary research. In *Handbook of Transdisciplinary Research*; Hirsch Hadorn, G., Hoffmann-Riem, H., Biber-Klemm, S., Grossenbacher-Mansuy, W., Joye, D., Pohl, C., Wiesmann, U., Zemp, E., Eds.; Springer: Dordrecht, The Netherlands, 2008; pp. 427–432.
15. Stock, P.; Burton, R.J.F. Defining terms for integrated (multi-inter-trans-disciplinary) sustainability research. *Sustainability* **2011**, *3*, 1090–1113. [[CrossRef](#)]
16. Häberli, R.; Bill, A.; Grossenbacher-Mansuy, W.; Thompson Klein, J.; Scholz, R.W.; Welti, M. Synthesis. In *Transdisciplinarity: Joint Problem-Solving among Science, Technology, and Society. An Effective Way of Managing Complexity*; Thompson Klein, J., Grossenbacher-Mansuy, W., Häberli, R., Bill, A., Scholz, R.W., Welti, M., Eds.; Birkhäuser Verlag: Basel, Switzerland, 2011; pp. 6–22.
17. Hoffmann-Riem, H.; Biber-Klemm, S.; Grossenbacher-Mansuy, W.; Hirsch Hadorn, G.; Joye, D.; Pohl, C.; Wiesmann, U.; Zemp, E. Idea of the handbook. In *Handbook of Transdisciplinary Research*; Hirsch Hadorn, G., Hoffmann-Riem, H., Biber-Klemm, S., Grossenbacher-Mansuy, W., Joye, D., Pohl, C., Wiesmann, U., Zemp, E., Eds.; Springer: Dordrecht, The Netherlands, 2008; pp. 3–17.
18. Gibbons, M.; Limoges, C.; Nowotny, H.; Schwartzmann, S.; Scott, P.; Trow, M. *The New Production of Knowledge—The Dynamics of Science and Research in Contemporary Societies*; Sage Publications: London, UK, 1994.
19. Nowotny, H. *Es ist so. Es könnte auch anders sein. Über das veränderte Verhältnis von Wissenschaft und Gesellschaft*; Suhrkamp Verlag: Frankfurt a.M., Germany, 1999.
20. Nowotny, H.; Scott, P.; Gibbons, M. *Re-Thinking Science, Knowledge and the Public in an Age of Uncertainty*; Polity Press: Cambridge, UK, 2001.

21. Elzinga, A. Participation. In *Handbook of Transdisciplinary Research*; Hirsch Hadorn, G., Hoffmann-Riem, H., Biber-Klemm, S., Grossenbacher-Mansuy, W., Joye, D., Pohl, C., Wiesmann, U., Zemp, E., Eds.; Springer: Dordrecht, The Netherlands, 2008; pp. 345–359.
22. Andrén, S. *A Transdisciplinary, Participatory and Action-Oriented Research Approach—Sounds Nice but What Do you Mean?* Working Paper, Human Ecology Division; Lund University: Lund, Sweden, 2010.
23. Cleaver, F. Paradoxes of participation: Questioning participatory approaches to development. *J. Int. Dev.* **1999**, *11*, 567–612. [[CrossRef](#)]
24. Shutt, C. Power in aid relations: A personal view. *IDS Bull.* **2006**, *37*, 79–87. [[CrossRef](#)]
25. Mosse, D. *Social Analysis in Participatory Rural Development, Critical Reflections from Practice. Sustainable Agriculture Programme*; PLA Notes No. 24; IIED: London, UK, 1995.
26. Akramkhanov, A.; Brus, D.J.; Walvoort, D.J.J. Geostatistical monitoring of soil salinity in Uzbekistan by repeated EM surveys. *Geoderma* **2014**, *213*, 600–607. [[CrossRef](#)]
27. Akramkhanov, A.; Lamers, J.P.A.; Martius, C. Conversion factors to estimate soil salinity based on electrical conductivity for soils in Khorezm region, Uzbekistan. In *Sustainable Management of Saline Waters and Salt-Affected Soils for Agriculture, Proceedings of the Second Bridging Workshop, Aleppo, Syria, 15–18 November 2009*; Qadir, M., Wichelns, D., Oster, J., Jacobsen, S.-E., Basra, S., Choukr-Allah, R., Eds.; ICARDA: Aleppo, Syria, 2010; pp. 19–25.
28. Rhoades, J.D.; Chanduvi, F.; Lesch, S.M. *Soil Salinity Assessment: Methods and Interpretation of Electrical Conductivity Measurements*; Irrigation and Drainage Paper; FAO: Rome, Italy, 1999; Volume 57.
29. Wraith, J.M. Time domain reflectometry. In *Methods of Soil Analysis*; Dane, J.H., Topp, G.C., Eds.; SSSA Book Series 5; Soil Science Society of America: Madison, WI, USA, 2002; Volume 4, pp. 1289–1296.
30. Hendrickx, J.M.H.; Baerends, B.; Raza, Z.I.; Sadig, M.; Chaudhry, A.M. Soil salinity assessment by electromagnetic induction of irrigated land. *Soil Sci. Soc. Am. J.* **1992**, *56*, 1933–1941. [[CrossRef](#)]
31. Bennett, D.L.; George, R.J.; Ryder, A. *Soil Salinity Assessment Using the EM38: Field Operating Instructions and Data Interpretation*; Miscellaneous Publication 4/95; Department of Agriculture: Kensington, Western Australia, 1995.
32. Akramkhanov, A. *The Spatial Distribution of Soil Salinity: Detection and Prediction*. Ph.D. Thesis, Rheinische Friedrich-Wilhelms-Universität Bonn, Bonn, Germany, 2005.
33. Page, S.E. Path dependence. *Q. J. Polit. Sci.* **2006**, *1*, 87–115. [[CrossRef](#)]



© 2018 by the authors. Licensee MDPI, Basel, Switzerland. This article is an open access article distributed under the terms and conditions of the Creative Commons Attribution (CC BY) license (<http://creativecommons.org/licenses/by/4.0/>).



MDPI  
St. Alban-Anlage 66  
4052 Basel  
Switzerland  
Tel. +41 61 683 77 34  
Fax +41 61 302 89 18  
[www.mdpi.com](http://www.mdpi.com)

*Water* Editorial Office  
E-mail: [water@mdpi.com](mailto:water@mdpi.com)  
[www.mdpi.com/journal/water](http://www.mdpi.com/journal/water)





MDPI  
St. Alban-Anlage 66  
4052 Basel  
Switzerland

Tel: +41 61 683 77 34  
Fax: +41 61 302 89 18

[www.mdpi.com](http://www.mdpi.com)



ISBN 978-3-03897-853-4